Number 3 Volume 18 1954

BULLETIN

of the

Academy of Sciences of the USSR

- Physical Series -

(Izvestiia Akademii Nauk SSSR)
(Seriia fizicheskaia)

Reproduction rights reserved

by

Columbia Technical Translations
5 Vermont Avenue
White Plains, New York

Single Issues

$20

Annual Subscription

$110

VLADIMIR KONSTANTINOVICH ARKAD'YEV (June 21, 1884-Dec. 1, 1953)

- K. M. Polivanov

V. K. Arkad'yev must be credited with many outstanding theoretical and experimental researches fundamental to present-day theory of the behavior of ferromagnetic substances in varying fields. He also conducted many important investigations in allied fields: researches on the generation and propagation of electromagnetic waves and experiments having to do with the diffraction of light and the beaming of short radio waves through dielectrics with subsequent recording of the images formed.

V. K. Arkad'yev's very first independent study, carried out in the laboratory of P. N. Lebedev in 1907, attracted wide attention and earned the young scientist a prize bestowed by the Moscow Society of the Friends of Science. In measuring the reflection of waves by Hertz gratings Arkad'yev discovered that the ferromagnetic properties of such gratings "vanished"in the range of frequencies of the order of 10^{10} cycles.

In his next investigation (1911), Arkad'yev determined the ferromagnetic properties of wires by means of absorption measurements. Arkad'yev reported on his work in December, 1911, at the sessions of the Physics Section of the Second Mendeleev Conference meeting in St. Petersburg. These reports subsequently appeared in the Journal of the Russian Physico-Chemical Society in 1913 (Ref. 1). The same Journal (Ref. 2) also carried a paper by Arkad'yev on the theory of the magnetization process under dynamic conditions, taking into account magnetic viscosity and the possibility of oscillatory processes, leading to resonance. These contributions attracted the notice of scientists both in Russia and abroad. In a letter dated June 20, 1913, P. S. Ehrenfest wrote to Arkad'yev: "Yesterday I told Weiss and Einstein about your work on magnetism. Both evinced great interest in your experiments and in your idea."

Having studied ferromagnetic effects over a wide range of frequencies, Arkad'yev evolved a theory of passive magnetic spectra and introduced the concept of complex magnetic permeability

$$\mu' = \mu - j\rho'. \qquad (1)$$

Proceeding from general phenomenological postulates regarding the motion of elementary magnets, Arkad'yev derived equations for the variation of magnetic permeability with frequency:

a) For the case of motion characterized by relaxation (viscosity):

$$\mu'(\omega) = \mu - j\rho' = m + \frac{m_1}{1+\nu^2}, \qquad (2)$$

or

$$\mu = m + \frac{m_1}{1+\nu^2} \quad \text{and} \quad \rho' = \rho'_1 + \frac{m_1}{1+\nu^2},$$

where $m + m_1 = \mu(0)$ is the permeability at low frequency

Digitized by the Internet Archive
in 2024

https://archive.org/details/russian-academy-of-sciences-physics-bulletin_1954_18_3

($\omega \to 0$); $m = \mu(\infty)$ is the permeability at high frequency ($\omega \to \infty$); $\nu = T_u/T$ (here T is the period of the forced oscillations; $T_u = 2\pi\tau_u$, and τ_u is the time constant of the relaxation law); ρ_1' is the minimum component of the permeability at the low frequency ($\omega \to 0$), corresponding to the hysteresis losses.

b) For the case of oscillatory motion:

$$\mu'(\omega) = m + \frac{m_1}{1 - \nu^2 + j\theta\nu}, \tag{3}$$

or

$$\mu = m + \frac{m_1(1-\nu^2)}{(1-\nu^2)^2 + \theta^2\nu^2} \quad \text{and} \quad \rho' = \frac{m_1\theta\nu}{(1-\nu^2)^2 + \theta^2\nu^2},$$

where $\nu = \lambda_0/\lambda$ (λ_0 is the wavelength in free space, corresponding to the natural frequency of oscillation of the elementary magnets and λ is the wavelength in free space, corresponding to forced oscillations); θ is the measure of viscosity (according to the terminology used by Arkad'yev) or a factor equal to the reciprocal of the quality of the oscillating system (with $\lambda = \lambda_0$); m and m_1 are as defined under Case a) above.

Analyzing his experimental results, Arkad'yev was the first to discover the existence of magnetic resonance; the experimentally determined frequency characteristic showed satisfactory agreement with the theoretical curves, computed on the assumption that the motion of the magnetic moment carriers was oscillatory.

Arkad'yev's early experiments were carried out at a time when only the most primitive equipment for microwave work was available; however, his results have been fully confirmed by all subsequent experiments.

The curves constructed by Arkad'yev for iron and nickel (Refs. 3 and 4) are reproduced in Figure 1.

As may be seen from these curves, the permeability approaches unity (the susceptibility drops to zero) at a wavelength of the order of 1 cm in the case of iron and of the order of 3 cm in the case of nickel. The theoretical curves are plotted on the assumption of oscillatory motion of the magnetic moment carriers [equation (3)] for the following values:

for Ni: $\theta = 3.2$ and $\lambda_0 = 7.4$
for Fe: $\theta = 1.6$ and $\lambda_0 = 6.0$.

After the Revolution, Arkad'yev was able to expand the scope of his civic and scientific activities; he organized one of the most progressive scientific laboratories at Moscow University. In this laboratory, under Arkad'yev's direction, A. A. Glagoleva-Arkad'yeva, using electromagnetic spark oscillators, was the first to obtain the very short waves that fall between the longer heat waves and the shortest radio waves (Ref. 5). This brilliant achievement received worldwide recognition.

Arkad'yev and his colleagues published over 200 works devoted to the thoery of magnetic spectra and associated problems of the dynamics of magnetization. The most detailed and extensive discussion of these problems to be found anywhere in scientific literature is given in the two-volume monograph (Ref. 4), published in 1934-1936, in which Arkad'yev summarizes the results of all investigations carried out in

this field both in the USSR and abroad, in the symposiums edited by Arkad'yev (Ref. 6) and in a number of his later articles.*

Throughout his life Arkad'yev continued his investigations in the field of magnetic spectroscopy; thus, in an article published in 1947 (Ref. 7) he again analyzed the experimentally determined variation of the magnetic permeability of nickel and iron (Fig. 2) and reiterated his conclusion that the closest agreement with theory is obtained in the case where oscillatory motion of the molecular magnets is assumed. Arkad'yev showed, on the basis of experimental data, that for iron one must assume the existence of three types of oscillating particles characterized by different values of λ_o, m_1 and θ:

λ_o	= 3	10	14 cm
m_1	= 0.13	0.8	3.7
θ	= 1.0	0.7	1.33

accordingly, the last term on the right side of equation (3) should be replaced by the sum of the three terms.

In the case of nickel, the best agreement of theoretical values with experimental data is obtained if we take λ_o = 3 cm, m = m_1 = 1, and θ = 0.9.

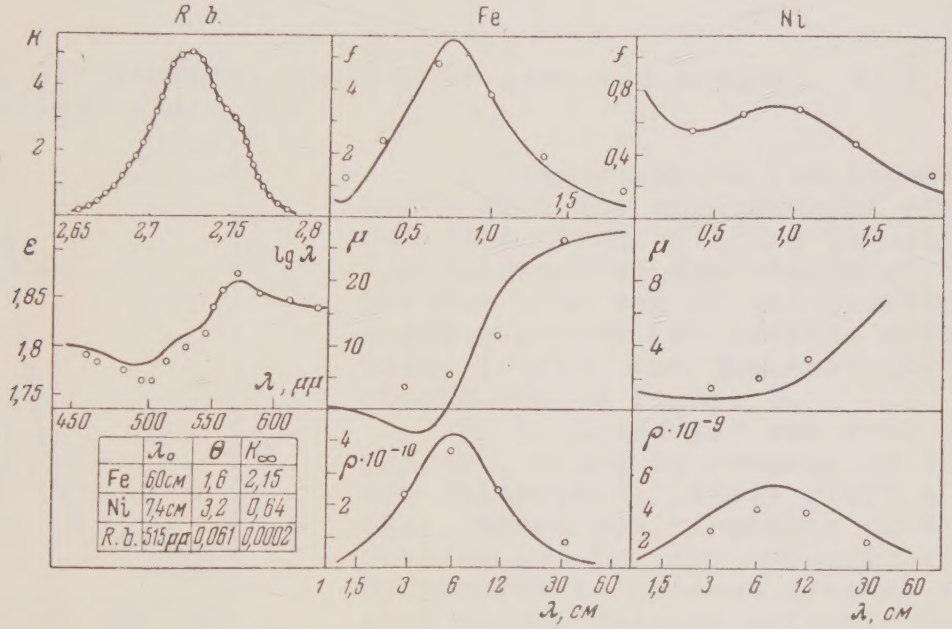

Fig. 1. Electric and magnetic spectra of iron and nickel (at left: electric spectrum of Bengal-Rose dye, in the region of optical frequencies). Solid lines plotted on the basis of theory by V. K. Arkad'yev. (Refs. 3 and 4).

Since ferromagnetic resonance was first observed by E. K. Zavoiski (Ref. 8) in the USSR and J. Griffiths in the U.S.A. (Refs. 9 and

---

* The monograph (Ref. 4) and the symposiums (Ref. 6) contain extensive bibliographies, listing earlier works.

10), the phenomenon has been widely studied (Ref. 10). There have also been very many investigations during the last decade devoted to magnetic spectra in the region of lower frequencies. In all these investigations, - even when no specific reference is made to Arkad'yev's publications - extensive use has been made of the methods of analysis and the basic theory of spectral characteristics developed by him.

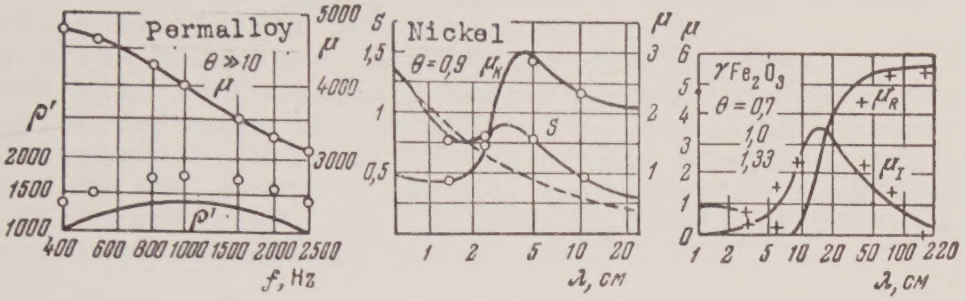

Fig. 2. Magnetic spectra of iron and nickel: V. K. Arkad'yev (Ref. 7).

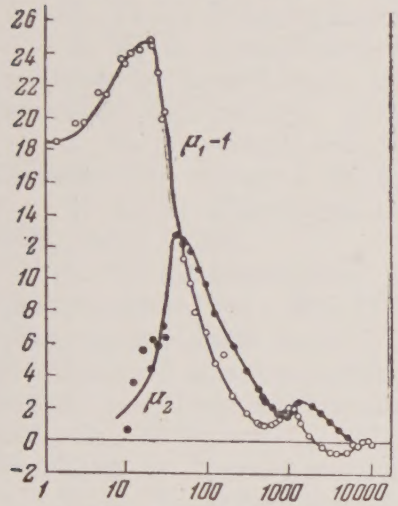

Fig. 3. Magnetic spectrum of ferrite in demagnetized state. (G. Rado - Ref. 10)

A comparison of the latest test results with the experimental and theoretical data cited by Arkad'yev clearly shows the fundamental importance of his investigations. By way of illustration, the resonance curves for ferrite obtained by Rado, Wright, and Emmerson (Ref. 10) are reproduced in Figure 3.

V. K. Arkad'yev was ever a Soviet patriot, quick to respond to the needs of our Fatherland. While still a student in 1911, Arkad'yev, together with a group of progressive faculty members, left Moscow University in protest against the arbitrary acts of the Tsarist police. During the First Imperialist World War, Arkad'yev organized a laboratory for studying methods of defense against poison gases (Ref. 11).

Teaching at Moscow University and heading various scientific laboratories, Arkad'yev built up a large following in the field of magnetism; a number of now famous Soviet physicists began their scientific work under Arkad'yev's supervision. Arkad'yev was also active in the communal sphere: he organized a number of scientific meetings and conferences (Ref. 12) at which not only theoretical subjects but practical problems connected with the application of ferromagnetic substances were considered.

Despite his poor health, Arkad'yev energetically developed new ideas and planned bold experiments to the last days of his life. One of the last experiments, executed in accordance with his suggestions,

was concerned with observing the behavior of a magnet "floating" above a superconducting surface (Ref. 13). On the basis of this essentially new interaction of forces, Arkad'yev advanced a hypothesis regarding the influence of similar forces in interstellar space; some of his writings published in 1950-1953 are devoted to problems of astrophysics (Ref. 14). Although already very ill, early in 1953, Arkad'yev in a report read at a session of the Learned Council of the Physics Department of Moscow State University, dedicated to "Radio Day", suggested a new and original method of generating millimeter and centimeter waves.

A brief biography, a selected bibliography and a chronicle of his work will be found in a book on Arkad'yev published by the Academy of Sciences of the USSR (Ref. 15). An account of his life and achievements, written by one of his students, Prof. N. N. Malov, appeared in the journal, Uspekhi fizicheskikh nauk (Progress of Physical Sciences) (Ref. 16); another in memoriam article was published in Electrichestvo (Electricity) (Ref. 17).

Bibliographic References

1. V. K. Arkad'yev. ZhRF-KhO (Journ. Russ. Phys.-Chem. Soc.) Physics Section, 45, 54, 103 (1913).

2. V. K. Arkad'yev, ibid. 45, 32 (1913).

3. V. K. Arkad'yev, in symposium "Sovremennye problemy magnetizma" (Current problems in magnetism), commemorating the tenth anniversary of the Moscow Magnetism Laboratory, p. 45 GNTI. M-L. 1931.

4. V. K. Arkad'yev, Elektromagnitnye protsessy v metallakh (Electromagnetic processes in metals) ONTI, M-L. Part I - 1934. Part II - 1936.

5. A. A. Glagoleva-Arkad'yeva, Sborn. trudov (Collected works), Acad. Sc. USSR. M-L. 1948.

6. V. K. Arkad'yev, Editor: a) Issledovanie po elektromagnetizmu (Studies in electromagnetism), NTO VSNKh, Pt. I -1925; Pt. II - 1926; b) Sovremennye problemy elektromagnetizma (see 3. above); c) Problemy elektrotekhnicheskogo metalla (Problems of electrotechnical metal). Acad. Sc. USSR. M-L. 1938; d) Prakticheskie problemy elektromagnetizma (Practical problems of electromagnetism), Acad. Sc. USSR. M-L. 1939; e) Problemy ferromagnetizma i magnetodinamiki (Problems of ferromagnetism and magnetodynamics), Acad. Sc. USSR, M-L. 1946.

7. V. K. Arkad'yev, Dokl. AN SSSR, 56, 8, 803 (1947).

8. E. K. Zavoiski, Journ. of Phys. USSR, 10, 197 (1946); Zhur. eksp. i teor. fiz. 17, 883 (1947).

9. J. Griffiths, Nature, 158, 670 (1946).

10. Ferromagnitnyi rezonans (Ferromagnetic resonance), symposium edited by S. V. Vonsovski, IL, M. 1952.

11. V. K. Arkad'yev, Nauchno-tekhnicheskie osnovy gazovoi bor'by (Scientific and technical fundamentals of gas warfare), lectures to instructors in gas defense. 2nd ed. 1915, 4th ed. 1917.

12. V. K. Arkad'yev, Izv. AN SSSR. Ser. fiz. 12, 493 (1948).

13. V. K. Arkad'yev, Priroda, 2, 50 (1945), Journ. of Phys. USSR, 9, 2, 148 (1945); Nauka i zhizn', 1, 20 (1947); Nature, 160, 4062, 330 (1947).

14. V. K. Arkad'yev, Dokl. AN SSSR, 71, 5, 843 (1950); 88, 2, 225 (1953).
15. "V. K. Arkad'yev", a brief biography and sketch of his scientific activity. Materials for the bibliography of USSR scientists. Ser. Phys. Issue 5, Acad. Sc. USSR. M-L. 1950.
16. "V. K. Arkad'yev" (In memoriam), Usp. fiz. nauk, 52, 3, 459 (1954).
17. "V. K. Arkad'yev" (In memoriam), Elektrich. 3, 91 (1954).

* * *

CERTAIN PROBLEMS CONNECTED WITH THE QUANTUM-MECHANICAL THEORY OF FERROMAGNETISM OF FERRITES AND ANTIFERROMAGNETISM

Part 1. A Critical Survey of Present Theory

- S. V. Vonsovski

1. In the classification of ferromagnetic materials, ferrites (crystalline products, having the general formula $MeO \cdot Fe_2O_2$, where Me is a bivalent metal ion) may be placed in a separate group of substances, characterized by a number of specific attributes. Among the attributes, which differentiate ferrites from ferromagnetic metals and alloys and, in a certain sense, relate them to antiferromagnetic substances, we may note the following:

a) The presence of an antiferromagnetic coupling between the magnetoactive ions of the crystal (i.e. between the electron spins of the ions of the metal and of the iron). This coupling, which is highly characteristic of ferrites*, leads to a net spontaneous magnetization of the crystal differing from zero only because of the "non-equivalence" of the magnetic moments of the ions, i.e. the magnetization is a differential effect. The difficulties encountered in determining the ground state of an antiferromagnetic substance and in subdividing a crystal into a system of magnetic sublattices are associated with this characteristic of ferrites.

b) The indirect nature of the exchange coupling between the magnetoactive ions, a coupling in which an important part is played by the magnetically neutral O^{--} ions, which participate in the exchange coupling through the outer part of their electron shells. This indirect exchange (= superexchange. Translator) is an example of strong coupling between the electron spins of next-to-nearest neighbor ions (of the second coordinational domain), rather than between nearest neighbor ions. In this case the transition of electrons between neighboring lattice sites, as well as the exitation of the electron states begins to be important. This type of exchange coupling is common to all ferrites as well as to all antiferromagnetic compounds.

c) The semiconductor character of the electric conductivity of ferrites. Ferrite crystals display a peculiar type of ion lattice, in which the positive ions are ions of metallic elements of the transition groups. Since conductivity electrons are absent in the normal

---

* As a rule, possible ferromagnetic coupling plays a secondary role.

state, ferrites should be classed as semiconductors; however, the presence of ions with incomplete shells and possibility of electronic ordering of ions of different valence result in a number of distinctive features where the semiconducting properties of ferrites are concerned.

Obviously, these three characteristics do not exhaust the list of the distinctive properties of ferrites; however, these are the specific attributes which lead to serious difficulties in any attempt to evolve a consistent atomic theory of the ferromagnetism of ferrites, difficulties over and above those encountered in elaborating a quantum-mechanical theory of the ferromagnetism of ordinary metals and alloys. Some of these difficulties are also inherent in the quantum theory of antiferromagnetism. Hence, it is of interest to analyze these difficulties and explore possible ways of resolving them.

2. Let us first turn to the problem of indirect exchange. It may be useful to recall the general crystallometric relationships for a typical representative of ferromagnetic ferrites, having a crystal structure of the $X^{++}Y_2^{+++}O_4^{--}$ spinel type, i.e. so-called 2-4 spinel (the prototype of such crystals is formed by the $MgAl_2O_4$; X^{++} and Y^{+++} are bi- and trivalent metal ions, Y^{+++}, in this case, being Fe^{+++}). The negative oxygen ions form a dense face-centered cubic lattice. Between these "large" negative ions there remain "narrow" inter-sites for the "small" positive metal ions. There are two types of intersites: Type A or tetrahedral, in the center of the elementary cells (the number of these intersites is equal to twice that of the O^{--} ions; i.e. to eight per cell; each is surrounded by four O^{--} ions) and Type B or octahedral, in the middle of the edges and in the center of the elementary cell (the number of these intersites equals the number of O^{--} ions, i.e. four per cell; they are surrounded by six O^{--} ions). In a spinel lattice the elementary cell has a double edge, since not all intersites are occupied by metal ions; i.e. in the case of tetrahedral (Type A) intersites only eight of the 64 sites available per 32 O^{--} ions are occupied by Y^{+++} ions, while in the case of octahedral (Type B) intersites, only 16 of the 32 sites are occupied, half by X^{++} and half by Y^{+++} ions. This distribution of the X and Y ions corresponds to the invert structure of spinel:

Y^{+++}	$(X^{++}Y^{+++})$	O_4^{--}
8	16	32
A	B	

(in the case of normal structure we have $X^{++}(Y^{+++}Y^{+++})O_4^{--}$). There arises a strong indirect exchange coupling, through the intermediate O^{--} ions, between the metal ions in the type A and B intersites.

Kramers (Ref. 1) pointed out that there can be an exchange spin-coupling in which the intermediate non-magnetic ions participate. He assumed that a substantial part in this exchange is played by the "excited" states of the intermediate ions, states in which these ions become paramagnetic. A simple example of such exchange coupling is furnished, for instance, by the antiferromagnetic ionic $Mn^{++}O^{--}$ crystals (rock salt type lattice). Aside from the purely ionic state, here one

must take into account an "admixture" of states in which at least one of the p-electrons from the O^{--} ion goes over into the d- or s-state on the Mn^{++} ion, which changes its valence (to Mn^{+}), while the O^{--} ion becomes paramagnetic and, hence, can participate in "magnetic" (for example, exchange) interactions. There are two possible configurations of the O^{--} ion and the two neighboring Mn^{++} ions: in the first, all three ions are located along one straight line (Fig. 1a); in the second, the lines connecting the Mn^{++} ions with the O^{--} ion forma right angle (Fig. 2b). Although the minimum distance ($a\sqrt{2}$) between the two Mn^{++} ions occurs in the second configuration, indirect exchange, as will be shown below, is effected by interaction between the next-to-nearest neighbors (from the second coordinational domain) rather than between the nearest neighbors. As follows from gyromagnetic relationships, the orbital moments in the crystals are "frozen". It may be assumed that in the normal state, two electrons in the O^{--} ion form a closed p-shell with a dumbbell-like distribution of electron density (Fig. 2a) about the axis along which all three atoms are located in the first configuration.

Anderson (Ref. 2), using Serber's generalization of the Dirac vector model (Ref. 3), investigated the perturbed problem for a four-electron system of three ions. Together with the ground state (Fig. 2a) in which in addition to two p-electrons on the O^{--} ion there are, also, two electrons, d_1 and d_2, in the d-orbits of the Mn^{++} ions, Anderson considered one excited state. In view of the distance between the Mn^{++} ions there is virtually no overlap between the d_1- and d_2-state wave functions. However, in view of the overlapping of the dumbbell cloud of the p-electrons with electron cloud of the Mn^{++} ions, strong interaction between the electrons of the O^{--} and the Mn^{++} ions is possible. That is, there is a finite probability that one of the p-electrons from the O^{--} ion will go over into some d_1' state on the Mn^{++} ion (Fig. 2b). In this case it must be assumed that the p-electron, becoming transformed into a d_1'-electron in consequence of the jump, will be coupled to the d_1-electron already on the Mn^{++} ion by some strong interaction, depending on the spin. In other words, there can take place exchange interaction, leading to splitting of the energy level, i.e. the energies of the $d_1 + d_1'$ pair in the singlet and triplet states may be different:

$$E_{\uparrow\downarrow}(d_1, d_1')_{sing} \neq E_{\uparrow\uparrow}(d_1, d_1')_{trip}.$$

It is now simple to describe qualitatively the process determining the indirect exchange. To the ground state of the four-electron system only two spin-states are available: a singlet (resultant spin equal to zero) and a triplet (resultant spin equal to unity), since the spins of the two electrons in the p-state on the O^{--} ion are always antiparallel. Let us assume, for example, that the p-electron, jumping on to the Mn^{++} ion, has a spin antiparallel to that of the d_1-electrons on the ion; then in the excited state of the four-electron system there is also only a singlet and a triplet (in the general case there may be two singlet states, three triplet states,

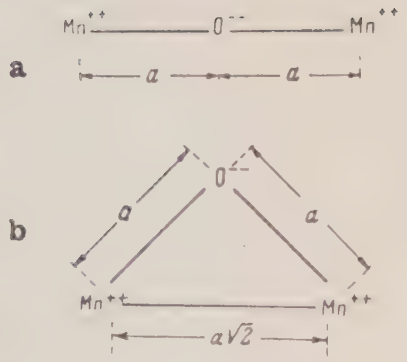

Fig. 1. Possible configuration of O^{--} and Mn^{++} ions in lattice of antiferromagnetic $Mn^{++}O^{--}$ crystal: a) all ions in line; b) lines connecting Mn^{++} ions to O^{--} ion form right angle.

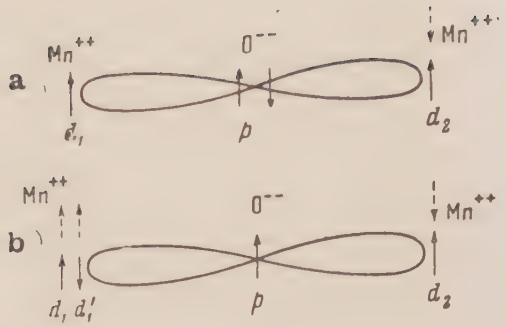

Fig. 2. Distribution of electron densities in $Mn_2^{++}O^{--}$ molecules: a) case of taking into account two magnetic electrons (d_1 and d_2), dash-lines indicate possible transition of one of these to excited state; b) case of transfer of one of the p-electrons from the O^{--} to the Mn^{++} ion (d_1' state).

and one state with spin 2). In the ground state, there is no splitting between the singlet and triplet states inasmuch as the O^{--} ion has a closed shell, while the Mn^{++} ions, being far apart, do not interact. In contrast, in the excited state of the system there can be splitting between the singlet and triplet spin configurations, since in this case there can be an appreciable exchange interaction between the p-electrons remaining on the O^{--} ion and the d_2-electron on the second Mn^{++} ion. The wave function of the system, in first approximation, has the form of a linear combination of the functions of the ground (Ψ_{gr}) and excited (Ψ_{ex}) states:

$$\psi^{1.3} = a\psi_{gr}^{1.3} + b\psi_{ex}^{1.3}; \qquad (1)$$

here, in view of the known selection rules, the singlet "1" and triplet "3" states are not combined. As a result of the solution of the perturbation problem for a four-electron system, there is obtained in the expression for the energy, along with the quasiclassical electrostatic interaction, an exchange term:

$$W = -2A_{indi}\,(\hat{S}_{d_1} \cdot \hat{S}_{d_2}), \qquad (2)$$

depending on the relative orientation of the spins of the Mn^{++} ion electrons. Here

$$A_{indi} = \left[E_{\uparrow\downarrow}^{-2} - E_{\uparrow\uparrow}^{-2}\right] \rho^{2} J, \qquad (3)$$

where $E_{\uparrow\downarrow}$ and $E_{\uparrow\uparrow}$ are the energies of the singlet and triplet states of the d_1 and d_1' electrons, respectively,

$$\rho = \int \psi_{d_1}(\mathbf{r})\, \hat{H}\, \psi_{p}(\mathbf{r})\, d\mathbf{r}$$

is the integral of electron transition from O^{--} to Mn^{++}, and

$$J = \int \psi_{d_1}(\mathbf{r}_1)\, \psi_{p}(\mathbf{r}_2)\, \hat{H}\, \psi_{d_1}(\mathbf{r}_2)\, \psi_{p}(\mathbf{r}_1)\, d\mathbf{r}_1 d\mathbf{r}_2$$

is the normal integral of exchange between the electrons on the O^- and Mn^{++} ions.

Thus, from equation (2) it is clear that the indirect exchange is an energy correction of the third order.

The above schematic interpretation of indirect exchange apparently correctly, if only qualitatively, characterizes this type of interaction in a crystal; however, from the quantitative standpoint it is wholly inadequate in view of its grossly approximate nature. There have been attempts to achieve greater accuracy by taking into account the fact that there are actually more (magnetically) active electrons on the metal ions than is assumed in the above-mentioned method of analysis (see, for example, Ref. 4). However, up to now indirect exchange has not been successfully taken into account in any consistent multiple-electron treatment of antiferromagnetism and ferromagnetism. In all multiple-electron calculations the negative ions are virtually ignored, and their presence in the crystal lattice is allowed for only by means of a certain "constant", i.e. the indirect exchange integral. This is due to the great mathematical difficulties encountered in attempting to extend the multiple-electron analysis to the case of antiferromagnetics (not pure metals) and ferromagnetic ferrites The primary problem, the solution of which would open the way to evolving a consistent multiple-electron theory, is the problem of a crystal in which all or a certain group of lattice sites are occupied by atoms having closed electron shells. The results of the calculations for such a model together with the conventional calculations based on the theory of ferromagnetism (for the open shells at the remaining sites) should make it possible to construct a more consistent multiple-electron model of crystals with indirect exchange. The most promising and rigorous line for such a generalization is indicated in the general method of treating the multiple-electron problem given by Bogolyubov and Tyablikov (Ref. 6).

3. As mentioned above, it is difficult to determine the grounds state energy in the quantum-mechanical theory of ferrites and antiferromagnetic substances. In the case of ordinary ferromagnetic materials, there is no such difficulty inasmuch as here the ground state is characterized by the maximum possible magnetic saturation, i.e. complete parallelism of the spin moments (if one neglects the minor perturbing influence of magnetic interaction between electrons). The difficulty of determining the ground-state energy of ferrites and antiferromagnetics stems from the fact that so far it has not been proved conclusively that the state of ideal antiferromagnetic ordering in the crystal lattice corresponds to the minimum energy condition. In the final analysis, this difficulty is one of justifying the introduction, into the theory, of the concept of magnetic sublattices in

ferrites and antiferromagnetic substances. The present writer already remarked on this difficulty back in 1940 (Ref. 6) in a critical appraisal of Bitter's contribution (Ref. 7) on the theory of ferromagnetic alloys. A similar criticism was also offered by Rudnitski (Ref. 8).

Within the framework of the spin-wave (or ferromagnon) theory the difficulty resides in the fact that it remains obscure why the antiferromagnons can be "linked" only to one sublattice. The question has been discussed in the most logical, but, unfortunately, very abbreviated, fashion by Bogolyubov and Tyablikov (Ref. 9), who showed that subdivision into magnetic sublattices is allowable only when the absolute value of the exchange integral between adjacent lattice sites is small compared to the exchange integral for two neighboring sites of the same sublattice. In the case of lattices with non-magnetic ions, naturally, the problem of subdivision into sublattices is closely associated with the problem of indirect exchange (see under 2 above).

It should be noted that despite the fact that rigorous proof for the magnetic sublattice hypothesis is lacking, experiments appear to confirm the existence of an antiferromagnetic spin-moment arrangement (neutron diffraction experiments reported in Ref. 10). Also, the results of theoretical calculations based on the sublattice hypothesis show close agreement with experimental data (Ref. 4).

Anderson (Ref. 11), reasoning from basic concepts, has shown that the true ground state energy, E_g, of an antiferromagnetic substance is lower than the value $-1/2\ NzJs^2$ obtained from the magnetic sublattice hypothesis where N is the number of sites per unit volume, J is the exchange integral, z is the coordinational number of the lattice (nearest neighbor number), and s is the spin quantum number of the magnetic ion. In addition, Anderson determined the lower energy limit, which differs by a factor of $(1 + \frac{1}{zs})$. Thus, we have the inequalities

$$-\tfrac{1}{2}NzJs^2 \quad E_g \quad -\tfrac{1}{2}NzJs^2\left(1+\tfrac{1}{zs}\right). \qquad (4)$$

From (4), it will be seen that the error in determining the ground state energy on the basis of the sublattice hypothesis is not great. For instance, in the particular case where z = 8 and s = 5/2, the error amounts to only 5%. Anderson discusses this question in more detail in a later article (Ref. 12), in which he approximates the ground state energy in the light of the antiferromagnon theory and making allowance for the fact that the magnetic moment (spin) of the lattice is not an integral of the motion,

Despite this, it cannot be said that we have a rigorous solution to the problem of the ground and weakly excited states of even pure antiferromagnetic materials, to say nothing of ferrites and antiferromagnetic substances with indirect exchange.

Yet another troublesome point arises in connection with the above-mentioned difficulty inherent in the quantum-mechanical theory of ferrites and antiferromagnetic materials. Even in the case of the conventional theory of ferromagnetism there has been some difficulty with divergences in computing thermodynamic values (for instance, the resultant magnetization of the lattice) for one-dimensional and two-

dimensional lattices. In the case of two-dimensional lattices this difficulty disappears if magnetic interaction is allowed for. The physical cause of these divergences is to be found in the quantum effect of "zero (neutral) oscillations" which automatically disrupt the magnetic order. In the case of antiferromagnetic substances these difficulties are aggravated: divergences in computing thermodynamic values crop up in the case of three-dimensional lattices as well. Hence, strictly speaking, the problem of antiferromagnetism cannot, in principle, be considered solely in the light of isotropic electrical interactions: it is essential also to take into account anisotropic magnetic interaction. So far no one had developed a consistent treatment for a multiple-electron system, taking into account simultaneously both electric and magnetic interaction.

One further remark regarding the quantum-mechanical theory of spin-waves for ferrites and antiferromagnetic materials is in order. The fact is that in the transition from the case of ordinary ferromagnetic substances to ferrites and antiferromagnetics the very character of the spin waves changes. Mathematically, this is evinced by the fact that for weak excitations of the lattice spin-systems the dispersion law - i.e. the connection between the energy and the quasi-impulse of the elementary excitations - is different for ferromagnons as compared with antiferromagnons. In the case of ferromagnons the relationship between the frequency (energy) and the wave number (quasi-impulse) is quadratic (for small quasi-impulses), while for antiferromagnons the dependence is linear (to the same approximation). This difference in the dispersion laws results in a difference between the temperature dependences of the static and kinetic macroscopic properties of ferromagnetics and of antiferromagnetics. A very clear explanation of the difference of the dispersion laws applying to ferromagnetic and to antiferromagnetic crystals has recently been given by Keffer, Kaplan, and Yafet (Ref. 13) who showed that this difference is due to phase differences between neighboring precessing spins at small deviations from complete saturation and in the presence of two almost saturated sublattices. It would be of interest to generalize this explanation to include the ferrites having both sublattices and net magnetization (at temperatures below the Curie point).

4. No one, so far, has investigated the electric properties of antiferromagnetic materials. Where ferrites are concerned, we know of only preliminary attempts at a theoretical treatment of their electric properties on the basis of the one-electron model, which is unsuitable for investigating their ferro- and antiferromagnetic properties (see survey in Ref. 14). Yet a comprehensive investigation of both the electric and magnetic properties of these substances, based on a single unified multiple-electron model, would be of undoubted interest. Investigators should note that among the antiferromagnetics there are metals of the transition groups (for example, chromium and, apparently, manganese). Hence, it may be desirable to apply the model of interacting outer and inner electrons of transition metals to this type of antiferromagnetics (Ref. 15). Antiferromagnetic compounds and most ferrites are semiconductors, although there are among them certain substances (for example, magnetite) which cannot be regarded as typical of this class. We still have no unified

treatment of the semiconductor and magnetic properties of these materials, with the exception of the preliminary attempt at such treatment by the author and Agrafonova (Ref. 16). A detailed study of the electric properties of ferrites and the relationship of these with the magnetic properties constitutes an extremely complex problem, yet an extremely important one as regards both the theory of ferrites and their practical application.

Among the very interesting characteristics of ferrites is the so-called phenomenon of electron ordering which results in an orderly arrangement of ions of different valence in lattice sites of a single type. Specifically, we have convincing proof of this phenomenon in magnetite (see editor's note in Ref. 17). It would also be worthwhile to investigate the electric properties of ferrites with the aid of the generalized crystal model according to Bogolyubov and Tyablikov (Ref. 5).

Physics of Metals Institute,
Urals Branch of the Academy
of Sciences of the USSR

Received:
3 May 1954

Bibliographic References

1. H. A. Kramers, Physica, 1, 182 (1933).
2. P. W. Anderson, Phys. Rev. 79, 359 (1950).
3. R. Serber, Phys. Rev. 45, 461 (1934).
4. J. H. Van Vleck, Jour. de phys. et rad., 12, 262 (1951).
5. N. N. Bogolyubov & S. V. Tyablikov, Zhur. eksp. i teor. fiz. 19, 251(1949); Bogolyubov, Lektsii z kvantovoi statistiki (Lectures on quantum statistics) - in Ukrainian - Kiev, 1949.
6. S. V. Vonsovski, Dokl. AN SSSR, 26, 564 (1940); Zhur. tekh. fiz. 18, 131 (1948).
7. F. Bitter, Phys. Rev. 54, 79 (1938).
8. V. E. Rudnitski, Zhur. eksp. i teor. fiz. 192, 256 (1949).
9. N. N. Bogolyubov & S. V. Tyablikov, Zhur. eksp. i teor. fiz. 19, 256 (1949).
10. C. G. Shull & J. S. Smart, Phys. Rev. 76, 1256 (1949).
11. P. W. Anderson, Phys. Rev. 83, 1260 (1951).
12. P. W. Anderson, Phys. Rev. 86, 694 (1952).
13. F. Keffer, H. Kaplan & Yafet, Amer. Jour. Phys. 21, 250 (1953).
14. G. Bush, UFN, 47, 258 (1952).
15. S. V. Vonsovski, Zhur. eksp. i teor. fiz. 16, 981 (1946); S. V. Vonsovski & E. A. Turov, Zhur. eksp. i teor. fiz. 24, 419 (1953).
16. S. V. Vonsovski & E. N. Agafonova, article in Symposium in honor of 70th anniversary of A. F. Ioffe, p. 92, Acad. Sc. USSR. M-L. 1950.
17. Ia. Snoek, Issledovaniya v oblasti novykh ferromagnitnykh materialov (Investigations in the field of new ferromagnetic materials), pp. 190-194, IL, Moscow, 1949.

CERTAIN PROBLEMS CONNECTED WITH THE QUANTUM-MECHANICAL THEORY OF FERROMAGNETISM OF FERRITES AND ANTIFERROMAGNETISM

Part II. The Quantum-Mechanical Theory of Ferromagnetic Ferrites

- S. V. Vonsovski and Iu. M. Seidov

1. The principal characteristics of ferromagnetism in ferrite type materials were described in the first part of this report (Ref. 1). The present part is devoted to the results of a quantum-mechanical treatment of the ferromagnetism of ferrites in the region of low temperatures (ferromagnon approximation). As our basic model we have selected the most consistent multiple-electron system, suggested by Bogolyubov and Tyablikov (Ref. 2). Ferromagnetic ferrites have a crystal lattice of the spinel type. The negative, magnetically neutral O^{--} ions form a face-centered cubic lattice, while the positive bi- and trivalent ions of metals of the transition group occupy lattice inter-sites of two types: tetrahedral (Type A) and octahedral (Type B). Below we will consider only the structure of invert spinel, in which the tetrahedral inter-sites, numbering eight per elementary cell, are occupied by trivalent ions while the sixteen octahedral inter-sites are taken up half by Fe^{+++} ions and half by bivalent ions of the transition metal, Me^{++}.

As was indicated in Part I, for a rigorous solution of the problem, the basic model should take into account the active role played by the O^{--} ions in indirect exchange. However, for our first approximation, in order not to complicate the calculations we will simply accept the fact that indirect exchange exists. Hence, the electrons of the closed shells of the O^{--} ions will not be explicitly provided for in our equations; they will be taken into account implicitly by the indirect exchange integrals introduced in the development.

The energy operator $\hat{H}$ of a system of N interacting electrons, moving in a field of N positive ions, in coordinate representation has the form:

$$\hat{H} = -\frac{\hbar^2}{2m}\sum_{j=1}^{N}\Delta_j + \sum_{n_k,\,j}^{N} G(\mathbf{q}_j - \mathbf{n}_k) + \sum_{j<j'}^{N} V(|\mathbf{q}_j - \mathbf{q}_{j'}|), \qquad (1,1)$$

where m is the electron mass, $2\pi\hbar$ is the action quantum, Δ_j is the Laplace operator of the jth electron, $\mathbf{q}_j$ and $\mathbf{n}_k$ are the radius vectors of the jth electron and the kth ion, respectively, $G(\mathbf{q}_j - \mathbf{n}_k)$ is the interaction potential of the electron j with the ion k and $V(|\mathbf{q}_j - \mathbf{q}_{j'}|)$ is the interaction potential of electrons j and j'. In requantized form (1,1) becomes (Refs. 2 and 3):

$$\hat{H} = U_0 + \sum_{f,f',\sigma} L(f, f')\hat{a}^{+}_{f\sigma}\hat{a}_{f'\sigma} + \frac{1}{2}\sum_{f_1 f_2 f_1' f_2',\,\sigma_1\sigma_2} F(f_1 f_2; f_1' f_2')\hat{a}^{+}_{f_1\sigma_1}\hat{a}^{+}_{f_2\sigma_2}\hat{a}_{f_2'\sigma_2}\hat{a}_{f_1'\sigma_1}. \qquad (1,2)$$

Here U_0 is an additive constant (ion energy); f are the numbers of the one-electron states; σ is the spin variable equal to $\pm 1/2$; $\hat{a}^{+}_{f\sigma}$, $\hat{a}_{f\sigma}$ are Fermi requantization operators, $L(f, f')$ and $F(f_1 f_2; f_1' f_2')$ are the matrix elements of the additive and binary parts, respectively, of

the operator (1,1) in the initial system of single-particle functions. The matrix elements $F(f_1 f_2; f_1' f_2')$ include indirect exchange integrals. The indices of f run through three rows of different values: N/3 tetrahedral inter-sites $t_1, \ldots, t_i, \ldots, t_{N/3}$, occupied by Fe^{+++} ions: N/3 octahedral inter-sites $r_1, \ldots, r_i, \ldots, r_{N/3}$, occupied by Fe^{+++} ions and N/3 octahedral inter-sites $s_1, \ldots, s_i, \ldots, s_{N/3}$, occupied by Me^{+++} ions. Further, let us introduce the condition of "quasi-homeopolarity":

$$\sum_{(\sigma)} \hat{a}^{+}_{f\sigma} \hat{a}_{f\sigma} = 1, \qquad (1,3)$$

i.e. assume that there is one electron participating actively in the ferromagnetism at each of the above-enumerated types of sites.* Utilizing condition (1,3) and Bogolyubov's perturbation theory (Ref. 3), we can effect a transition from Fermi-amplitudes to Bose amplitudes of spin deviation (Ref. 6), it being assumed that the tetrahedral and octahedral inter-sites of the ferrite lattice form two magnetic sublattices, which in the ground state ($0^{\circ}K$) are spontaneously magnetized to saturation: since the ferrite sublattices are not equivalent (there are two octahedral inter-sites for each tetrahedral inter-site), the lattice as a whole will have a net spontaneous magnetization differing from zero (in contrast to antiferromagnetic lattices characterized by equivalent sublattices).

As is known, the equations for transformation from Fermi operators to Bose operators have the form:

$$\hat{a}^{+}_{t_i,-\frac{1}{2}} \hat{a}_{t_i,\frac{1}{2}} = (2s)^{\frac{1}{2}} f(\hat{n}_{t_i}) \hat{b}_{t_i}, \qquad \hat{a}^{+}_{r_i,-\frac{1}{2}} \hat{a}_{r_i,\frac{1}{2}} = (2s)^{\frac{1}{2}} \hat{c}^{+}_{r_i} f(\hat{n}_{r_i}),$$

$$\hat{a}^{+}_{t_i,\frac{1}{2}} \hat{a}_{t_i,-\frac{1}{2}} = (2s)^{\frac{1}{2}} \hat{b}^{+}_{t_i} f(\hat{n}_{t_i}), \qquad \hat{a}^{+}_{r_i,\frac{1}{2}} \hat{a}_{r_i,-\frac{1}{2}} = (2s)^{\frac{1}{2}} f(\hat{n}_{r_i}) \hat{c}_{r_i},$$

$$\hat{a}^{+}_{t_i,\frac{1}{2}} \hat{a}_{t_i,\frac{1}{2}} = \frac{1}{2}(1 - s + \hat{n}_{t_i}), \qquad \hat{a}^{+}_{r_i,\frac{1}{2}} \hat{a}_{r_i,\frac{1}{2}} = \frac{1}{2}(1 + s - \hat{n}_{r_i}), \qquad (1,3')$$

$$\hat{a}^{+}_{t_i,-\frac{1}{2}} \hat{a}_{t_i,-\frac{1}{2}} = \frac{1}{2}(1 + s - \hat{n}_{t_i}); \qquad \hat{a}^{+}_{r_i,-\frac{1}{2}} \hat{a}_{r_i,-\frac{1}{2}} = \frac{1}{2}(1 - s + \hat{n}_{r_i});$$

(for tetrahedral inter-sites) (for octahedral inter-sites occupied by Fe^{+++} ions)

$$\left.\begin{aligned} \hat{a}^{+}_{s_i,-\frac{1}{2}} \hat{a}_{s_i,\frac{1}{2}} &= (2s)^{\frac{1}{2}} \hat{c}^{+}_{s_i} f(\hat{n}_{s_i}), \\ \hat{a}^{+}_{s_i,\frac{1}{2}} \hat{a}_{s_i,-\frac{1}{2}} &= (2s)^{\frac{1}{2}} f(\hat{n}_{s_i}) \hat{c}_{s_i}, \\ \hat{a}^{+}_{s_i,\frac{1}{2}} \hat{a}_{s_i,\frac{1}{2}} &= \frac{1}{2}(1 + s - \hat{n}_{s_i}), \\ \hat{a}^{+}_{s_i,-\frac{1}{2}} \hat{a}_{s_i,-\frac{1}{2}} &= \frac{1}{2}(1 - s + \hat{n}_{s_i}), \end{aligned}\right\} \qquad (1,4'')$$

(for octahedral inter-sites occupied by Me^{++} ions)

---

* This is, of course, an approximation since the Fe^{+++} and Me^{++} ions have a different number (in the general case ≠ 1) of magnetoactive electrons. Furthermore, these ions have different electron configurations. However, there is reason to assume that taking these factors into consideration would have little effect on the final result of the calculations. In this connection we call attention to Serber's article (Ref. 4) and the report by Kondoski and Pakhmov (Ref. 5).

where s is the spin quantum number of the ion,

$$\hat{n}_{t_i} = \hat{b}^+_{t_i}\,\hat{b}_{t_i}, \quad \hat{n}_{r_i} = \hat{c}^+_{r_i}\,\hat{c}_{r_i}, \quad \hat{n}_{s_i} = \hat{c}^+_{s_i}\,\hat{c}_{s_i} \tag{1,5}$$

are the spin deviation operators at sites t_i, r_i and s_i, while

$$f(\hat{n}) = \left[1 - \frac{\hat{n}}{2s}\right]^{\frac{1}{2}};$$

for weak excitations of the system (near 0^oK), it may be assumed that

$$f(\hat{n}) \approx 1 \tag{1,6}$$

Effecting the transformation to Bose operators and making use of (1,6), instead of (1,2), we get

$$\begin{aligned}\hat{H} = \hat{H}_0 &+ s\sum_{t_i<t_{i'}} J_{t_i t_{i'}}(\hat{b}^+_{t_i}\,\hat{b}_{t_{i'}} - \hat{b}^+_{t_i}\,\hat{b}_{t_i}) + s\sum_{r_i<r_{i'}} J_{r_i r_{i'}}(\hat{c}^+_{r_i}\,\hat{c}_{r_{i'}} - \hat{c}^+_{r_i}\,\hat{c}_{r_i}) + \\ &+ s\sum_{s_i<s_{i'}} J_{s_i s_{i'}}(\hat{c}^+_{s_i}\,\hat{c}_{s_{i'}} - \hat{c}^+_{s_i}\hat{c}_{s_i}) + \frac{s}{2}\sum_{t_i,\,r_i} J_{t_i r_i}[(\hat{b}_{t_i}\hat{c}_{r_i} + \hat{b}^+_{t_i}\,\hat{c}^+_{r_i}) + \\ &+ (\hat{b}^+_{t_i}\,\hat{b}_{t_i} + \hat{c}^+_{r_i}\,\hat{c}_{r_i})] + \frac{s}{2}\sum_{t_i,\,s_i} J_{t_i s_i}[(\hat{b}_{t_i}\hat{c}_{s_i} + \hat{b}^+_{t_i}\hat{c}^+_{s_i}) + (\hat{b}^+_{t_i}\,\hat{b}_{t_i} + \hat{c}^+_{s_i}\hat{c}_{s_i})] + \\ &+ \frac{s}{2}\sum_{r_i,\,s_j} J_{r_i s_i}[(\hat{c}^+_{r_i}\,\hat{c}_{s_i} - \hat{c}^+_{r_i}\,\hat{c}_{r_i}) + (\hat{c}^+_{r_i}\hat{c}_{s_i} - \hat{c}^+_{s_i}\,\hat{c}_{s_i})],\end{aligned} \tag{1,7}$$

where $\hat{H}_o$ contains all terms independent of the $\hat{b}$ and $\hat{c}$ operators, and

$$J_{t_i t_i},\ J_{r_i r_i},\ J_{s_i s_i},\ J_{t_i r_i},\ J_{t_i s_i},\ J_{r_i s_i}$$

are the exchange integrals between the corresponding sites in the sublattices and between the sublattices.

Let us perform one more unitary transformation of the Hamiltonian (1,7) and pass over to operators which are the Fourier components of the operators $\hat{b}$ and $\hat{c}$:

$$\left.\begin{aligned}\hat{b}_{t_i} &= \left(\frac{3}{N}\right)^{\frac{1}{2}}\sum_{\lambda} e^{-i(\mathbf{k}_\lambda\cdot\mathbf{R}_{t_i})}\hat{b}_\lambda, \\ \hat{c}_{r_i} = \left(\frac{3}{N}\right)^{\frac{1}{2}}\sum_{\lambda} e^{-i(\mathbf{k}_\lambda\cdot\mathbf{R}_{r_i})}\hat{c}_\lambda, &\quad \hat{c}_{s_i} = \left(\frac{3}{N}\right)^{\frac{1}{2}}\sum_{\lambda} e^{-i(\mathbf{k}_\lambda\cdot\mathbf{R}_{s_i})}\hat{c}_\lambda.\end{aligned}\right\} \tag{1,}$$

Introducing abridged notation, we get

$$\left.\begin{aligned}A_\lambda &= -N^{-1}s\left\{\sum_{t_i<t_{i'}} J_{t_i t_{i'}}[1-\exp i\mathbf{k}_\lambda(\mathbf{R}_{t_i}-\mathbf{R}_{t_{i'}})] - \frac{1}{2}\sum_{t_i,\,r_i} J_{t_i r_i} - \frac{1}{2}\sum_{t_i,\,s_i} J_{t_i s_i}\right\}, \\ B_\lambda &= -N^{-1}s\left\{\frac{1}{2}\sum_{t_i,\,s_i} J_{t_i s_i}\exp i\mathbf{k}_\lambda(\mathbf{R}_{t_i}-\mathbf{R}_{s_i}) \quad \frac{1}{2}\sum_{t_i,\,r_i} J_{t_i r_i}\exp i\mathbf{k}_\lambda(\mathbf{R}_{t_i}-\mathbf{R}_{r_i})\right\},\end{aligned}\right\} \tag{1,9}$$

$$D_\lambda = -N^{-1/2}\left\{\sum_{r_i<r_{i'}} J_{r_i r_{i'}}[1-\exp i\mathbf{k}\,(\mathbf{r}_i-\mathbf{R}_{r_{i'}})]+\sum_{s_i<s_{i'}} J_{s_i s_{i'}}[1-\exp i\,\mathbf{k}_\lambda(\mathbf{R}_{s_i}-\right.$$
$$\left.-\mathbf{R}_{s_{i'}})]+\sum_{r_i s_i} J_{r_i s_i}[1-\exp i\,\mathbf{k}_\lambda(\mathbf{R}_{r_i}-\mathbf{R}_{s_i})]-\frac{1}{2}\sum_{t_i r_i} J_{t_i r_i}-\frac{1}{2}\sum_{t_i s_i} J_{t_i s_i}\right\}. \qquad (1,9)$$

Then the energy operator of the system (1,7), in the abridged notation, will be

$$\hat{H}=\hat{H}_0+\sum_\lambda A_\lambda \hat{b}_\lambda^+\hat{b}_\lambda+\sum_\lambda B_\lambda \hat{b}_\lambda\hat{c}_\lambda+\sum_\lambda B_\lambda^*\hat{b}_\lambda^+\,\hat{c}_\lambda^++\sum_\lambda D_\lambda\hat{c}_\lambda^+\,\hat{c}_\lambda. \qquad (1,10)$$

In order to find the energy spectrum of the elementary excitations (ferromagnons) the operator (1,10) must be diagonalized. To this end we effect another unitary transformation, to Hermitean operators $\hat{Q}_\lambda$, $\hat{P}_\lambda$, $\hat{R}_\lambda$ and $\hat{S}_\lambda$:

$$\hat{b}_\lambda=\frac{1}{\sqrt{2}}(\hat{Q}_\lambda+i\hat{P}_\lambda),\quad \hat{c}_\lambda=\frac{1}{\sqrt{2}}(\hat{R}_\lambda+i\hat{S}_\lambda). \qquad (1,11)$$

It can readily be shown that the transposition relationships for the new operators will have the form:

$$\hat{Q}_\lambda\hat{P}_{\lambda'}-\hat{P}_{\lambda'}\hat{Q}_\lambda=i\delta_{\lambda\lambda'},\quad \hat{R}_\lambda\hat{S}_{\lambda'}-\hat{S}_{\lambda'}\hat{R}_\lambda=i\delta_{\lambda\lambda'}. \qquad (1,12)$$

Then the new operator (1,10) (accurate to the additive constant) will be written

$$\hat{H}=\text{const}-\frac{1}{2}\sum_\lambda(A_\lambda+D_\lambda)+\frac{1}{2}\sum_\lambda A_\lambda(\hat{Q}_\lambda^2+\hat{P}_\lambda^2)+$$
$$+\sum_\lambda B_\lambda(\hat{Q}_\lambda\hat{R}_\lambda-\hat{P}_\lambda\hat{S}_\lambda)+\frac{1}{2}\sum_\lambda D_\lambda(\hat{R}_\lambda^2+\hat{S}_\lambda^2). \qquad (1,13)$$

To complete the diagonalization of (1,13) we must carry out a final unitary transformation to operators $\hat{q}_{1\lambda}$, $\hat{p}_{1\lambda}$ and $\hat{q}_{2\lambda}$, $\hat{p}_{2\lambda}$:

$$\left.\begin{aligned}\hat{Q}_\lambda&=(1+)^{-1}(w\hat{q}_{1\lambda}+\hat{q}_{2\lambda}), & \hat{R}_\lambda&=(1+w)^{-1}(\hat{q}_{1\lambda}+w\hat{q}_{2\lambda}),\\ \hat{P}_\lambda&=(1-w)^{-1}(-w\,\hat{p}_{1\lambda}+\hat{p}_{2\lambda}), & \hat{S}_\lambda&=(1-w)^{-1}(\hat{p}_{1\lambda}-w\hat{p}_{2\lambda}),\end{aligned}\right\} \qquad (1,14)$$

where the parameter w will be selected below. Substituting (1,14) in (1,15), we obtain:

$$\hat{H}=\text{const}-\frac{1}{2}\sum_\lambda(A_\lambda+D_\lambda)+\frac{1}{2}\sum_\lambda\{(A_\lambda w^2+D_\lambda+2B_\lambda w)\times$$
$$\times[(1+w)^{-2}\hat{q}_{1\lambda}^2+(1-w)^{-2}\hat{p}_{1\lambda}^2]+(A_\lambda+D_\lambda w^2+2B_\lambda w)\times$$
$$\times[(1+w)^{-2}\hat{q}_{2\lambda}^2+(1-w)^{-2}\hat{p}_{2\lambda}^2]\}. \qquad (1,15)$$

Thus, we have reduced the operators of the electron system to an additive sum of the operators of harmonic oscillators, which represent the elementary excitations of the system: the ferromagnons.

The parameter w is determined from the quadratic equations:

$$w^2\pm(A_\lambda-D_\lambda)w-A_\lambda D_\lambda+B_\lambda^2=0. \qquad (1,16)$$

The eigen-values of the energy operator (1,15) will be

$$E = \text{const} - \frac{1}{2}\sum_{\lambda}\left[A_\lambda + D_\lambda - \sqrt{(A_\lambda + D_\lambda)^2 - 4B_\lambda^2}\right] + \\ + \frac{1}{2}\sum_{\lambda} n_{1\lambda}\left[D_\lambda - A_\lambda + \sqrt{(A_\lambda + D_\lambda)^2 - 4B_\lambda^2}\right] + \\ + \frac{1}{2}\sum_{\lambda} n_{2\lambda}\left[A_\lambda - D_\lambda + \sqrt{(A_\lambda + D_\lambda)^2 - 4B_\lambda^2}\right]. \qquad (1,17)$$

2. Let us now find the dispersion law for ferrites, i.e. connection between the ferromagnon energy and the quasi-impulse k_λ. To this end we expand the abridged notation of (1,9), using the nearest neighbor approximation for the exchange integrals J and assuming that the quasi-impulses of the ferromagnons (at low temperatures) are small; we obtain

$$\left.\begin{aligned} A_\lambda &= -\frac{s}{6}\left[J_{tt}(a_1 k_\lambda)^2 - z_{tr} J_{tr} - z_{ts} J_{ts}\right], \\ B_\lambda &= -\frac{s}{12}\left[\frac{1}{2} J_{ts}(a_2 k_\lambda)^2 + \frac{1}{2} J_{tr}(a_3 k_\lambda)^2 - z_{ts} J_{ts} - z_{tr} J_{tr}\right], \\ D_\lambda &= -\frac{s}{6}\left[J_{rr}(a_4 k_\lambda)^2 + J_{ss}(a_5 k_\lambda)^2 + J_{rs}(a_6 k_\lambda)^2 - z_{tr} J_{tr} - z_{ts} J_{ts}\right]. \end{aligned}\right\} \qquad (2,1)$$

Here a_i (i = 1, 2, 3, 4, 5, 6) are the distances between nearest neighbor inter-sites of different types (tt, ts, tr, rr, ss, rs); z_{tt}, z_{ts}, z_{rr}, z_{ss}, z_{tr} and z_{rs} are the corresponding nearest neighbor numbers. We introduce the following abbreviated notation:

$$\left.\begin{aligned} \alpha &= -\frac{s}{6}(J_{rr} l_4^2 + J_{ss} l_5^2 + J_{rs} l_6^2), & \alpha + \beta' &= u, \\ \beta' &= -\frac{s}{6} J_{tt}, & \alpha - \beta' &= v, \\ b &= -\frac{s}{3}(z_{tr} J_{tr} + z_{ts} J_{ts}), & 2b(c-u) &= d, \\ c &= -\frac{s}{6}(J_{ts} l_2^2 + J_{tr} l_3^2), & l_i &= \frac{a_i}{a_1}, \quad (i = 2, 3, 4, 5, 6). \end{aligned}\right\} \qquad (2,2)$$

Then, instead of (1,17) we obtain

$$E = \text{const} - \frac{1}{2}\sum_{\lambda}\left[u(a_1 k_\lambda)^2 - b - (a_1 k_\lambda)\sqrt{(u^2 - c^2)(a_1 k_\lambda)^2 + d}\right] + \\ + \sum_{\lambda} n_{1\lambda}\hbar\omega_{1\lambda} + \sum_{\lambda} n_{2\lambda}\hbar\omega_{2\lambda}, \qquad (2,3)$$

where

$$\left.\begin{aligned} \omega_{1\lambda} &= \frac{1}{2\hbar}\left[v(a_1 k_\lambda)^2 + (a_1 k_\lambda)\sqrt{(u^2 - c^2)(a_1 k_\lambda)^2 + d}\right], \\ \omega_{2\lambda} &= \frac{1}{2\hbar}\left[-v(a_1 k_\lambda)^2 + (a_1 k_\lambda)\sqrt{(u^2 - c^2)(a_1 k_\lambda)^2 + d}\right]. \end{aligned}\right\} \qquad (2,4)$$

Thus we see that the dispersion law in the case of ferrites is different from this law for ordinary ferromagnetics and antiferromagnetics. It can be seen, however, that in particular cases the dispersion equation (2,4) may become identical with the law for ferro-

and antiferromagnetic materials. Thus, in the case of ordinary ferromagnetics, when there are not two sublattices (for instance, when only tt type terms remain), we have $\alpha = 0$, $b = 0$, $c = 0$, $d = 0$ and $u = -v$ and, hence, instead of (2,4) we get

$$\omega_\lambda = \frac{1}{2h} u (a_1 k_\lambda)^2, \tag{2,5}$$

i.e., the law for ordinary ferromagnetics.

In the case of antiferromagnetic materials the two sublattices are equivalent and the interaction only between the sublattices is taken account of ($J_{tr} = J_{ts}$, while $J_{tt} = J_{ss} = J_{rr} = J_{rs} = 0$); hence, in (2,2) $\alpha = \beta' = 0$, $u = v = 0$ and with k_λ small, we obtain instead of (2,4) the familiar dispersion law for antiferromagnetics (Ref. 8):

$$\left.\begin{aligned} \omega_{1\lambda} &= \frac{1}{2h} \sqrt{d}\,(a_1 k_\lambda), \\ \omega_{2\lambda} &= \frac{1}{2h} \sqrt{d}\,(a_1 k_\lambda). \end{aligned}\right\} \tag{2,6}$$

Thus, the present analysis may be viewed as one of the possible generalizations of the theory of ordinary ferromagnetism and antiferromagnetism.

3. Let us now calculate the temperature dependence of the spontaneous magnetization of ferrites. To this end we must determine the phase sum as a function of the external magnetic field. To the energy of the system (1,17) must be added the energy in the external field (since we require this energy only to compute the spontaneous magnetization, it is permissible to neglect the internal magnetic interactions which cause magnetic anisotropy, magnetostriction and a small departure from absolute saturation with the external field $H = 0$); as a result of simple operations, instead of (1.17), we obtain

$$\begin{aligned} E(H) = &-\frac{1}{2}\sum_\lambda \left[A_\lambda^{(H)} + D_\lambda^{(H)} - \sqrt{(A_\lambda^{(H)} + D_\lambda^{(H)})^2 - 4B_\lambda^2} \right] + \\ &+ \frac{1}{2}\sum_\lambda n_{1\lambda} \left[D_\lambda^{(H)} - A_\lambda^{(H)} + \sqrt{(A_\lambda^{(H)} + D_\lambda^{(H)})^2 - 4B_\lambda^2} \right] + \\ &+ \frac{1}{2}\sum_\lambda n_{2\lambda} \left[A_\lambda^{(H)} - D_\lambda^{(H)} + \sqrt{(A_\lambda^{(H)} + D_\lambda^{(H)})^2 - 4B_\lambda^2} \right] + \frac{N}{3} g_1^3 s H, \end{aligned} \tag{3,1}$$

where

$$A_\lambda^{(H)} = A_\lambda + g_1^3 H, \quad D_\lambda^{(H)} = D_\lambda - 2g_1^3 H. \tag{3,2}$$

Here the values of A_λ and D_λ are determined, as previously, from (1,9), while B_λ is independent of the field H. Substituting (3,1) in the expression for the phase sum,

$$Z = \sum_{n_{1\lambda}, n_{2\lambda}} \exp\left(-\frac{E(H)}{kT}\right),$$

and using the conventional calculations, we obtain

$$\ln Z = \frac{N}{3} g\beta sH - \sum_\lambda \frac{1}{2kT}\left[A_\lambda^{(H)} + D_\lambda^{(H)} - \sqrt{(A_\lambda^{(H)} + D_\lambda^{(H)})^2 - 4B_\lambda^2}\right] +$$
$$+ \sum_\lambda \ln\left\{1 - \exp\left[-\frac{1}{2kT}\left(D_\lambda^{(H)} - A_\lambda^{(H)} + \sqrt{(A_\lambda^{(H)} + D_\lambda^{(H)})^2 - 4B_\lambda^2}\right)\right]\right\} +$$
$$+ \sum_\lambda \ln\left\{1 - \exp\left[-\frac{1}{2kT}\left(A_\lambda^{(H)} - D_\lambda^{(H)} + \sqrt{(A_\lambda^{(H)} + D_\lambda^{(H)})^2 - 4B_\lambda^2}\right)\right]\right\}. \qquad (3,3)$$

In order to evaluate the spontaneous magnetization of ferrite we must determine the magnitude of $kT\left(\frac{\partial \ln Z}{\partial H}\right)_{H=0}$, which, in view of (3,3), equals

$$kT\left(\frac{\partial \ln Z}{\partial H}\right)_{H=0} = \frac{N}{3} g\beta s - \frac{1}{2} g\beta \sum_\lambda \left[\frac{A_\lambda + D_\lambda}{\sqrt{(A_\lambda + D_\lambda)^2 - 4B_\lambda^2}} - 1\right] -$$
$$- \frac{3}{2} g\beta \sum_\lambda \left\{\exp\left[\frac{1}{2kT}\left(D_\lambda - A_\lambda + \sqrt{(A_\lambda + D_\lambda)^2 - 4B_\lambda^2}\right)\right] - 1\right\}^{-1} +$$
$$+ \frac{3}{2} g\beta \sum_\lambda \left\{\exp\left[\frac{1}{2kT}\left(A_\lambda - D_\lambda + \sqrt{(A_\lambda + D_\lambda)^2 - 4B_\lambda^2}\right)\right] - 1\right\}^{-1} -$$
$$- \frac{1}{2} g\beta \sum_\lambda \left\{(A_\lambda + D_\lambda)\left[(A_\lambda + D_\lambda)^2 - 4B_\lambda^2\right]^{-\frac{1}{2}} \times \right.$$
$$\left. \times \left[\exp\frac{1}{2kT}\left(D_\lambda - A_\lambda + \sqrt{(A_\lambda + D_\lambda)^2 - 4B_\lambda^2}\right) - 1\right]^{-1}\right\} +$$
$$+ \frac{1}{2} g\beta \sum_\lambda \left\{(A_\lambda + D_\lambda)\left[(A_\lambda + D_\lambda)^2 - 4B_\lambda^2\right]^{-\frac{1}{2}} \times \right.$$
$$\left. \times \left[\exp\frac{1}{2kT}\left(A_\lambda - D_\lambda + \sqrt{(A_\lambda + D_\lambda)^2 - 4B_\lambda^2}\right) - 1\right]^{-1}\right\}. \qquad (3,4)$$

Utilizing (2,1) and the abbreviated notation of (2,2), invoking the assumption that the ferromagnon quasi-impulse is very small and going over from sums to integrals, as is commonly done in the theory of ferromagnetism, we obtain, instead of (3,4) the following expression for the spontaneous magnetization:

$$M_s(T) = kT\left(\frac{\partial \ln Z}{\partial H}\right)_{H=0} =$$
$$= M_0 - \frac{1}{2}\left(\frac{La_1}{2\pi}\right)^3 g\beta \int\left[\frac{u(a_1k_\lambda)^2 - b}{a_1k_\lambda\sqrt{(u^2 - c^2)(a_1k_\lambda)^2 + d}} - 1\right] d\mathbf{k}_\lambda -$$
$$- \frac{3}{2}\left(\frac{La_1}{2\pi}\right)^3 g\beta \int\left\{\exp\left[\frac{s}{2kT}\left(v(a_1k_\lambda)^2 + a_1k_\lambda\sqrt{(u^2 - c^2)(a_1k_\lambda)^2 + d}\right)\right] - 1\right\}^{-1} d\mathbf{k}_\lambda +$$
$$+ \frac{3}{2}\left(\frac{La_1}{2\pi}\right)^3 g\beta \int\left\{\exp\left[\frac{s}{2kT}\left(-v(a_1k_\lambda)^2 + \right.\right.\right.$$
$$\left.\left.\left. + a_1k_\lambda\sqrt{(u^2 - c^2)(a_1k_\lambda)^2 + d}\right)\right] - 1\right\}^{-1} d\mathbf{k}_\lambda - \frac{1}{2}\left(\frac{La_1}{2\pi}\right)^3 g\beta \times$$
$$\times \int \frac{[u(a_1k_\lambda)^2 - b]\, d\mathbf{k}_\lambda}{a_1k_\lambda\sqrt{(u^2 - c^2)(a_1k_\lambda)^2 + d}\left\{\exp\left[\frac{s}{2kT}\left(v(a_1k_\lambda)^2 + a_1k_\lambda\sqrt{(u^2 - c^2)(a_1k_\lambda)^2 + d}\right)\right] - 1\right\}} -$$
$$- \frac{1}{2}\left(\frac{La_1}{2\pi}\right)^3 g\beta \times$$
$$\times \int \frac{[u(a_1k_\lambda)^2 - b]\, d\mathbf{k}_\lambda}{a_1k_\lambda\sqrt{(u^2 - c^2)(a_1k_\lambda)^2 + d}\left\{\exp\left[\frac{s}{2kT}\left(-v(a_1k_\lambda)^2 + a_1k_\lambda\sqrt{(u^2 - c^2)(a_1k_\lambda)^2 + d}\right)\right] - 1\right\}}, \qquad (3,5)$$

where $M_0 = \frac{N}{3} g\beta s$ is the maximum value of the magnetization and $(La_1)^3$ is the volume of the specimen. The integrals comprised in (3,5) are readily computed (see Appendix); hence, we finally obtain for the temperature dependence of the spontaneous magnetization of ferrite:

$$M_s(T) = M_0\left[1 - \frac{0{,}04}{s} - \frac{1}{40\,s^2}\left(\frac{T}{\theta}\right)^2\right], \qquad (3,6)$$

where

$$\theta = \frac{|c|}{k} \qquad (3,7)$$

Two important conclusions may be drawn from (3,6):

First, the temperature dependence of the spontaneous magnetization of ferrites at low temperature is different from that of ordinary metallic ferromagnetics; to wit, instead of the well-known $T^{3/2}$ law holding for the latter, we find a T^2 law for the former.

From a judicious evaluation of the indirect exchange integral we have

$$|c| \sim 10^{-26}\text{-}10^{-28} \text{ erg};$$

assuming that $s \sim 1$, it follows from (3,6) and (3,7) that

$$M_s(T) = M_0[1 - \gamma_1 - \gamma_2 T^2], \qquad (3,8)$$

where $\gamma_1 \sim 10^{-2}$ degree^{-2} and $\gamma_2 \sim 10^{-4}\text{-}10^{-6}$ degree^{-2}. Equation (3,8) is in close agreement with the experimental data reported by Pauthenet (Ref. 7); specifically, the latter obtained the following temperature dependences for nickel ($NiO \cdot Fe_2O_3$), cobalt ($CoO \cdot Fe_2O_3$) and iron ($FeO \cdot Fe_2O_3$) ferrites:

$$M_s(T)/M_0 = 1 - 1{,}121 \cdot 10^{-6} \cdot T^2,$$

$$M_s(T)/M_0 = 1 - 1{,}576 \cdot 10^{-6} \cdot T^2,$$

$$M_s(T)/M_0 = 1 - 8{,}26 \cdot 10^{-7} \cdot T^2.$$

Only for manganese ferrite ($MnO \cdot Fe_2O_3$) was the ordinary $T^{3/2}$ law found to hold, i.e. $M_S(T)/M_O = 1 - 5.75 \cdot 10^{-5} \cdot T^{3/2}$. It may be that for the last case, the lowest temperature used by Pauthenet (20.4°K) was not low enough. The magnitude of the numerical coefficients in the T^2 terms is in close agreement with the theoretically evaluated values for γ_2 in equation (3,8).

Second, in addition to the temperature dependent term, there appears in our equation (3,8) a term γ_1, which does not depend on the temperature, and, hence, violates the simple additivity rule for partial magnetizations of ferrite sublattices (Ref. 8). It is apparent from the evaluation of this term, however, that the resultant departure from the simple additivity rule is not great, which is also in good agreement with Pauthenet's observations (Ref. 7).

Hence, the present development of the quantum-mechanical theory of ferrites may be regarded as an acceptable first approximation for a description of the magnetic behavior of ferrites in the region of low temperatures.

Appendix: Evaluation of integrals comprised in equation (3,5)

1. The first integral in the right member of (3,5) is

$$I_1 = \frac{(La_1)^3 g\beta}{2(2\pi)^3} \int \left[\frac{u(a_1 k_\lambda)^2 - b}{a_1 k_\lambda \sqrt{(u^2 - c^2)(a_1 k_\lambda)^2 + d}} - 1 \right] d\mathbf{k}_\lambda. \qquad \text{(I)}$$

It can readily be seen that in the case of ordinary ferromagnetic materials this integral is equal to zero. Inasmuch as we are interested only in the case of low temperatures, we can neglect all terms in (I) with the quasi-impulse to the second power. Then, after integration, we get

$$I_1 = \frac{(La_1)^3 g\beta}{4\pi^2} \int_0^\pi \left[\frac{|b|}{a_1 k_\lambda \sqrt{2|b|(|c| + u)}} - 1 \right] k_\lambda^2 \, dk_\lambda =$$
$$= \frac{N}{2} g\beta \left[\frac{|b|}{2\sqrt{2|b|(|c| + u)}} - \frac{\pi}{3} \right].$$

Further, bearing in mind that $u \ll |c|$, since the interaction between more remote neighbors is relatively weaker, using equations (2,2) and noting that for typical ferrites with an invert spinel structure $l_2 = l_3 = \sqrt{11/8}$ and $z_{ts} = z_{tr}$, we find that

$$\frac{|b|}{|c|} = \frac{128}{11} \qquad \text{(II)}$$

Whence, we get

$$I_1 = M_0 \frac{0.04}{s} \qquad \text{(III)}$$

2. In the assumed approximation the second and third integrals of the right half of (3,5) are equal in absolute magnitude but opposite in sign. Consequently, their net contribution to the magnetization is zero.

3. The fourth and fifth integrals, to the same approximation, are also equal in absolute magnitude, but have the same sign. Hence, through elementary calculations we find

$$I_4 + I_5 = \frac{(La_1)^3 g\beta}{2\pi^2 a_1 |d|} \int_0^\infty \frac{k_\lambda dk_\lambda}{\exp\left(\frac{s|d|}{2kT} a_1 k_\lambda\right) - 1} = \frac{2Ng\beta\lambda^2}{3\pi^2 s^2 d^2 l_1} T^2 \Gamma(2) \zeta(2).$$

Replacing the gamma-function and the Riemann zeta-function by their respective values 2! and $\pi^2/6$, applying equation (II), and neglecting u ($\ll |c|$), we obtain

$$I_4 + I_5 \approx M_0 \frac{k^2}{40 s^2 |c|^2} T^2. \qquad \text{(IV)}$$

Physics of Metals Institute

Received 8 June 1954

Bibliographic References

1. S.V.Vonsovski, preceding article in the present Bulletin.
2. N.N.Bogoliubov & S.V.Tiablikov, Zhur. eksp. i teor.fiz.,19,251,256 (1949).
3. N.N.Bogoliubov, Lektsii z kvantavoi statistiki (Lectures on quantum statistics) - in Ukranian - Kiev 1949.
4. R.Serber, Phys. Rev., 45, 461 (1934).
5. E.I.Kondorski & A.S.Pakhomov, Dokl. AN SSSR, 93, 431 (1953).
6. T.Holstein & H.Primakoff, Phys. Rev., 58, 1098 (1940).
7. R.Pauthenet, Ann. de phys., 7, 710 (1952).
8. L.Néel, Ann. de phys., 3, 137 (1948).

CERTAIN PROBLEMS CONNECTED WITH THE QUANTUM-MECHANICAL THEORY OF FERROMAGNETISM OF FERRITES AND ANTIFERROMAGNETISM

Part III. The Antiferromagnetism of Transition Metals

- A. A. Berdyshev and S. V. Vonsovski

1. In transition metals the totality of their physical and chemical properties is determined not only by the valence electrons but also by the former inner electrons of the incomplete layers of the electron shell. Consequently, in constructing a multiple-electron theory for transition metals it is necessary to take account of the existence of two groups of electrons, one of which primarily determines electric conductivity phenomena while the other affects the magnetic properties. An appropriate model has been suggested by one of the present authors (Ref. 1) and developed in Refs. 2 and 3. In the present paper the results of these investigations are extended to the case of antiferromagnetic metals of the transition groups.

As has by now been clearly established, in metals of the transition groups a strong electrostatic exchange interaction between the inner electrons, when the sign of the exchange integral is negative, leads to the appearance of antiferromagnetism (see, for instance, Ref. 4). Below a certain critical temperature θ_{af} (the antiferromagnetic Curie point) an antiparallel arrangement of the inner electron spins is established in the crystal lattice of such metals. The lattice may be broken up into a number (depending on the type of lattice) of "magnetic" sublattices, in each of which the spins of the inner electrons are parallel. In the case of a simple cubic or body-centered cubic lattice, this subdivision amounts to separating out two sublattices with antiparallel magnetization, so that the electron spins at each site of one sublattice are surrounded by antiparallel spins at the nearest neighbor sites of the other sublattice. In the case of a face-centered cubic lattice and lattices of other types, one must invoke a large number of magnetic sublattices. Neutron diffraction experiments (Ref. 5) have clearly confirmed the antiparallel alignment of electron spins in antiferromagnetic crystals. For the transitions metals the existence of antiferromagnetism has been rigorously proved in chromium and manganese (Ref. 6).

2. According to equation (6) from Ref. 2 and formula (2,6) from Ref. 3, the energy operator of a system of interacting inner and outer electrons in requantized form may be written

$$\hat{H} = U_0 + \sum_{\mathbf{k},\sigma} E_{\mathbf{k}}\, \hat{a}^{+}_{\mathbf{k},\sigma}\, \hat{a}_{\mathbf{k},\sigma} - \frac{1}{2} \sum_{\mathbf{n}_1 \neq \mathbf{n}_2;\ \sigma_1,\sigma_2} J(\mathbf{n}_1, \mathbf{n}_2)\, \hat{a}^{+}_{\mathbf{n}_1,\sigma_1}\, \hat{a}_{\mathbf{n}_1,\sigma_1}\, \hat{a}^{+}_{\mathbf{n}_2,\sigma_2}\, \hat{a}_{\mathbf{n}_2,\sigma_2} -$$

$$- \frac{1}{N_d} \sum_{\mathbf{n},\ \mathbf{k}_1,\ \mathbf{k}_2,\ \sigma_1,\ \sigma_2} e^{i(\mathbf{k}_2 - \mathbf{k}_1)\mathbf{n}}\, I(\mathbf{k}_1, \mathbf{k}_2)\, \hat{a}^{+}_{\mathbf{n},\sigma_1}\, \hat{a}^{+}_{\mathbf{n},\sigma_2}\, \hat{a}^{+}_{\mathbf{k}_1,\sigma_2}\, \hat{a}_{\mathbf{k}_2,\sigma_1} +$$

$$+ \frac{1}{2} \sum_{\mathbf{k}_1, \mathbf{k}_2, \mathbf{k}'_1, \mathbf{k}'_2, \sigma_1, \sigma_2} F(\mathbf{k}_1, \mathbf{k}_2, \mathbf{k}'_1, \mathbf{k}'_2)\, \hat{a}^{+}_{\mathbf{k}_1,\sigma_1}\, \hat{a}^{+}_{\mathbf{k}_2,\sigma_2}\, \hat{a}_{\mathbf{k}'_1,\sigma_1}\, \hat{a}_{\mathbf{k}'_2,\sigma_2}, \qquad (1)$$

where U_0 is the constant energy of interaction of the "stationary" ions of the lattice; $E_{\mathbf{k}}$ is the ordinary translational energy of a conductivity electron, $J(\mathbf{n}_1, \mathbf{n}_2)$ is the exchange integral relating to the two inner electrons at sites $\mathbf{n}_1$ and $\mathbf{n}_2$, $I(\mathbf{k}_1, \mathbf{k}_2)$ is the exchange

integral relating to the inner and outer electrons; k_1 and k_2 are the quasi-impulses of the outer electrons; $\hat{a}_{n,\sigma}$ and $a_{k,\sigma}$ are the Fermi operators of requantization for the inner and outer electrons respectively. The matrix element $F(k_1, k_2, k_1', k_2')$ determines the interaction energy of the outer electron pairs.

Our problem is to isolate the elementary excitations both in the system of conductivity electrons and in the system of inner electrons. In deriving equation (1) we made use of the quasi-homeopolar approximation for inner electrons (see equation (5) in Ref. 2 or (2,4) in Ref. 3), i.e. assumed that there is always one inner electron near each lattice site. Here, in contrast to the case of ferromagnetics, discussed in Ref. 2, we will assume that the integral relating to the exchange between electrons is negative: $J(n_1, n_2) < 0$, since this is the necessary condition for antiferromagnetism (Refs. 4 and 7).

Let us assume that we are dealing with either a simple or a body-centered cubic lattice. In this case the crystal lattice can be divided into two magnetic sublattices with antiparallel spontaneous magnetizations. To differentiate between these two sublattices we will employ the subscripts n and m below. Let us replace the inner electron Fermi operators in equation (1) by the spin-vector component operators $\hat{S}_n^{(x)}$, $\hat{S}_n^{(y)}$, $\hat{S}_n^{(z)}$ (utilizing equations (5) and (10) from Ref. 2 to this end). We obtain

$$\hat{H} = U_0 - \frac{1}{4}\sum_{n_1 \neq n_2} J(n_1, n_2) + \sum_{k,\sigma} E_k \hat{a}^+_{k,\sigma}\hat{a}_{k,\sigma} - \frac{1}{4S^2}\sum_{n_1 \neq n_2} J(n_1, n_2)\hat{S}_{n_1}\hat{S}_{n_2} -$$

$$- \frac{1}{2SN_d}\sum_{n, k_1, k_2} e^{i(k_2 - k_1)n} J(k_1, k_2)\Big[(S - \hat{S}_n^{(z)})\hat{a}^+_{k_1, \frac{1}{2}}\hat{a}_{k_2, \frac{1}{2}} +$$

$$+ (\hat{S}_n^{(x)} - i\hat{S}_n^{(y)})\hat{a}^+_{k_1, \frac{1}{2}}\hat{a}_{k_2, -\frac{1}{2}} + (\hat{S}_n^{(x)} + i\hat{S}_n^{(y)})\hat{a}^+_{k_1, -\frac{1}{2}}\hat{a}_{k_2, \frac{1}{2}} +$$

$$+ (S + \hat{S}_n^{(z)})\hat{a}^+_{k_1, -\frac{1}{2}}\hat{a}_{k_2, -}\Big] +$$

$$+ \frac{1}{2}\sum_{k_1, k_2, k_1', k_2', \sigma_1, \sigma_2} F(k_1, k_2, k_1', k_2')\hat{a}^+_{k_1, \sigma_1}\hat{a}^+_{k_2, \sigma_2}\hat{a}_{k_2', \sigma_2}\hat{a}_{k_1', \sigma_1}. \qquad (2)$$

Assuming that near 0°K both sublattices are close to magnetic saturation,* we can effect another transformation of the energy operator, expressing the spin component operators through Bose-amplitudes, according to the following equations:

$$\left.\begin{aligned} \hat{S}_n^{(x)} + i\hat{S}_n^{(y)} &= (2S)^{\frac{1}{2}}\hat{f}_n\hat{b}_n, & \hat{S}_m^{(x)} + i\hat{S}_m^{(y)} &= (2S)^{\frac{1}{2}}\hat{c}_m^+\hat{f}_m, \\ \hat{S}_n^{(x)} - i\hat{S}_n^{(y)} &= (2S)^{\frac{1}{2}}\hat{b}_n^+\hat{f}_n, & \hat{S}_m^{(x)} - i\hat{S}_m^{(y)} &= (2S)^{\frac{1}{2}}\hat{f}_m\hat{c}_m, \\ \hat{S}_n^{(z)} &= S - \hat{b}_n^+\hat{b}_n, & \hat{S}_m &= -(S - \hat{c}_m^+\hat{c}_m), \end{aligned}\right\} \qquad (3)$$

---

* Strictly speaking, this should be proved; however, we have not succeeded in obtaining such proof. See Ref. 8.

where $\hat{b}_n^+ \hat{b}_n = \hat{n}_n$, $\hat{c}_m^+ \hat{c}_m = \hat{n}_m$, $\hat{n}_m$, $\hat{n}_n$ are spin deviation operators, S is the maximum value of the spin quantum number for a sublattice site and

$$\hat{f}_n = \left(1 - \frac{\hat{n}_n}{2S}\right)^{\frac{1}{2}}, \quad \hat{f}_m = \left(1 - \frac{\hat{n}_m}{2S}\right)^{\frac{1}{2}}. \tag{4}$$

In the case of low temperatures (almost complete saturation of the sublattices) we can assume, with negligible error, that $\langle \hat{f}_{n,m} \rangle = 1$; then (2) is simplified to

$$\begin{aligned}
\hat{H} = \hat{H}_0 + \sum_{k,\sigma} E_{k,\sigma} \hat{a}^+_{k,\sigma} \hat{a}_{k,\sigma} - \frac{1}{2S} \sum_{n,m} J(n,m) (\hat{b}_n^+ \hat{b}_n + \\
+ \hat{c}_m^+ \hat{c}_m + \hat{b}_n \hat{c}_m + \hat{b}_n^+ \hat{c}_m^+) - \\
- \frac{1}{2SN_d} \sum_{n,k_1,k_2} I(k_1, k_2) \Big\{ e^{i(k_2 - k_1)n} \Big[\hat{n}_n \hat{a}^+_{k_1,\frac{1}{2}} \hat{a}_{k_2,\frac{1}{2}} + \\
+ (2S)^{\frac{1}{2}} \hat{b}_n^+ \hat{a}^+_{k_1,-\frac{1}{2}} \hat{a}_{k_2,\frac{1}{2}} + (2S)^{\frac{1}{2}} \hat{b}_n \hat{a}^+_{k_1,\frac{1}{2}} \hat{a}_{k_2,-\frac{1}{2}} + \\
+ (2S - \hat{n}_n) \hat{a}^+_{k_1,-\frac{1}{2}} \hat{a}_{k_2,-\frac{1}{2}} \Big] + e^{i(k_2 - k_1)m} \Big[(2S - \hat{n}_m) \hat{a}^+_{k_1,\frac{1}{2}} \hat{a}_{k_2,\frac{1}{2}} + \\
+ (2S)^{\frac{1}{2}} \hat{c}_m \hat{a}^+_{k_1,-\frac{1}{2}} \hat{a}_{k_2,\frac{1}{2}} + (2S)^{\frac{1}{2}} \hat{c}_m \hat{a}^+_{k_1,\frac{1}{2}} \hat{a}^+_{k_2,-\frac{1}{2}} + \hat{n}_m \hat{a}^+_{k_1,-\frac{1}{2}} \hat{a}_{k_2,-\frac{1}{2}} \Big] \Big\} + \\
+ \frac{1}{2} \sum_{k_1,k_2,k_1',k_2',\sigma_1,\sigma_2} F(k_1, k_2, k_1', k_2') \hat{a}^+_{k_1,\sigma_1} \hat{a}^+_{k_2,\sigma_2} \hat{a}_{k_2',\sigma_2} \hat{a}_{k_1',\sigma_1'}.
\end{aligned} \tag{5}$$

where

$$\hat{H}_0 = U_0 - \frac{1}{4} \sum_{n,m} J(n,m).$$

To bring the operator (5) to diagonal form we must apply another unitary transformation, from the Bose operators to Hermitean operators:

$$\begin{aligned}
\hat{b}_n &= \frac{1}{2}(\hat{Q}_n + i\hat{P}_n), & \hat{c}_m &= \frac{1}{2}(\hat{R}_m + i\hat{S}_m), \\
\hat{b}_n^+ &= \frac{1}{2}(\hat{Q}_n - i\hat{P}_n), & \hat{c}_m^+ &= \frac{1}{2}(\hat{R}_m - i\hat{S}_m),
\end{aligned} \tag{6}$$

and expand these in Fourier series:

$$\left.\begin{aligned}
\hat{Q}_n &= \left(\frac{2}{N}\right)^{\frac{1}{2}} \sum_l e^{il n} \hat{Q}_l, \\
\hat{P}_n &= \left(\frac{2}{N}\right)^{\frac{1}{2}} \sum_l e^{-il n} \hat{P}_l, \\
\hat{R}_m &= \left(\frac{2}{N}\right)^{\frac{1}{2}} \sum_l e^{il m} \hat{R}_l, \\
\hat{S}_m &= \left(\frac{2}{N}\right)^{\frac{1}{2}} \sum_l e^{-il m} \hat{S}_l.
\end{aligned}\right\} \tag{7}$$

Then operator (5) will become

$$\hat{H} = \hat{H}_0 + \hat{H}_d + \hat{H}_{sd} + \hat{H}_s, \tag{8}$$

where

$$\hat{H}_d = \frac{ZJ}{8S}\sum_{\mathbf{l}}[\hat{Q}_{\mathbf{l}}^2 + \hat{P}_{\mathbf{l}}^2 + \hat{R}_{\mathbf{l}}^2 + \hat{S}_{\mathbf{l}}^2 + 2\gamma_{\mathbf{l}}(\hat{Q}_{\mathbf{l}}\hat{R}_{\mathbf{l}} - \hat{P}_{\mathbf{l}}\hat{S}_{\mathbf{l}})], \tag{9a}$$

$$\hat{H}_{sd} = -\frac{1}{8SN_d}\sum_{\mathbf{k}_1,\,\mathbf{k}_2,\,\mathbf{l}_1,\,\mathbf{l}_2} I(\mathbf{k}_1,\,\mathbf{k}_2)\,[(\hat{Q}_{\mathbf{l}_1}\hat{Q}_{\mathbf{l}_2} + \hat{P}_{\mathbf{l}_1}\hat{P}_{\mathbf{l}_2}) -$$

$$-(\hat{R}_{\mathbf{l}_1}\hat{R}_{\mathbf{l}_2} + \hat{S}_{\mathbf{l}_1}\hat{S}_{\mathbf{l}_2})]\,(\hat{a}^{+}_{\mathbf{k}_1,\,\frac{1}{2}}\hat{a}^{+}_{\mathbf{k}_2,\,\frac{1}{2}} - \hat{a}^{+}_{\mathbf{k}_1,\,-\frac{1}{2}}\hat{a}_{\mathbf{k}_2,\,-\frac{1}{2}})\,\delta(\mathbf{k}_2 -$$

$$-\mathbf{k}_1 + \mathbf{l}_2 - \mathbf{l}_1) - \frac{1}{4\sqrt{SN_d}}\sum_{\mathbf{k}_1,\,\mathbf{k}_2,\,\mathbf{l}} I(\mathbf{k}_1,\,\mathbf{k}_2)\Big[(\hat{Q}_{\mathbf{l}} - i\hat{P}_{\mathbf{l}})\,\hat{a}^{+}_{\mathbf{k}_1,\,-\frac{1}{2}}\hat{a}_{\mathbf{k}_2,\,\frac{1}{2}} \times$$

$$\times\,\delta(\mathbf{k}_2 - \mathbf{k}_1 - \mathbf{l}) + (\hat{Q}_{\mathbf{l}} + iP_{\mathbf{l}})\,a^{+}_{\mathbf{k}_1,\,\frac{1}{2}}\,a_{\mathbf{k}_2,\,-\frac{1}{2}}\,\delta(\mathbf{k}_2 - \mathbf{k}_1 - \mathbf{l}) +$$

$$+(\hat{R}_{\mathbf{l}} + i\hat{S}_{\mathbf{l}})\,\hat{a}^{+}_{\mathbf{k}_1,\,-\frac{1}{2}}\,\hat{a}_{\mathbf{k}_2,\,\frac{1}{2}}\,\delta(\mathbf{k}_2 - \mathbf{k}_1 + \mathbf{l}) +$$

$$+(\hat{R}_{\mathbf{l}} - i\hat{S}_{\mathbf{l}})\,\hat{a}^{+}_{k_1,\,\frac{1}{2}}\,\hat{a}_{\mathbf{k}_2,\,-\frac{1}{2}}\,\delta(\mathbf{k}_2 - \mathbf{k}_1 - \mathbf{l})\Big], \tag{9b}$$

$$\hat{H}_s = \sum_{\mathbf{k},\,\sigma}\varepsilon_{\mathbf{k}}\hat{n}_{\mathbf{k},\sigma} + \frac{1}{2}\sum_{\mathbf{k}_1,\,\mathbf{k}_2,\,\mathbf{k}_1',\,\mathbf{k}_2',\,\sigma_1,\,\sigma_2} F(\mathbf{k}_1,\,\mathbf{k}_2,\,\mathbf{k}_1',\,\mathbf{k}_2')\,\hat{a}^{+}_{\mathbf{k}_1,\,\sigma_1}\hat{a}^{+}_{\mathbf{k}_2,\,\sigma_2}\hat{a}_{\mathbf{k}_2',\,\sigma_2}\hat{a}_{\mathbf{k}_1',\,\sigma_1}, \tag{9c}$$

where $\delta(\mathbf{k}_i - \mathbf{k}_j \pm \mathbf{l})$ are ordinary delta functions, taking account of the conservation laws relating to the quasi-impulses $\mathbf{k}_i$ and $\mathbf{l}$;

$$\varepsilon_{\mathbf{k}} = E_{\mathbf{k}} - I(\mathbf{k}_1,\,\mathbf{k}_2) \tag{10}$$

is the translational energy of the outer electron, allowing for the influence of the s-d exchange;

$$\hat{n}_{\mathbf{k},\,\sigma} = \hat{a}^{+}_{\mathbf{k},\sigma}\,\hat{a}_{\mathbf{k},\sigma}$$

is the number of conductivity electrons in the $(\mathbf{k},\,\sigma)$ state; $\gamma_{\mathbf{l}}$ is determined from the relationship

$$\gamma_{\mathbf{l}} = \frac{1}{Z}\sum_{\rho=1}^{Z} e^{i(\mathbf{e}_\rho a\mathbf{l})} \approx 1 - \frac{a^2\mathbf{l}^2}{2}; \tag{11}$$

here, a is the lattice constant, Z is the coordinational (nearest neighbor) number; the summation in (11) is limited to the nearest neighbors; J is the inner electron exchange integral for nearest neighbor sites.

Let us isolate the diagonal part $(\mathbf{k}_1 = \mathbf{k}_2,\ \mathbf{l}_1 = \mathbf{l}_2)$ of operator (9b):

$$-\frac{1}{8SN_d}\sum_{\mathbf{k},\,\mathbf{l}} I(\mathbf{k}_1,\,\mathbf{k}_2)\,[(\hat{Q}_{\mathbf{l}}^2 + \hat{P}_{\mathbf{l}}^2) - (\hat{R}_{\mathbf{l}}^2 + \hat{S}_{\mathbf{l}}^2)], \tag{12}$$

and introduce, temporarily, the following abbreviated notation:

$$\Delta = \frac{1}{ZJN_d}\sum_{\mathbf{k}} I(\mathbf{k}_1,\,\mathbf{k}_2)\,\left(\hat{n}_{\mathbf{k},\,\frac{1}{2}} - \hat{n}_{\mathbf{k},\,-\frac{1}{2}}\right). \tag{13}$$

Up to now only the isotropic electric interaction between electrons has been taken account of in the energy operator relating to the

system; hence, the orientation of the resultant spin of the magnetic sublattices in the crystal remains indeterminate, i.e. spatial degeneracy obtains. Actually, each lattice has one or more preferred axes, along which the spontaneous magnetization of the sublattices is aligned. The number and direction of these axes are determined by the internal magnetic interaction between electrons, participating in the exchange interaction. To remove spatial degeneracy we must introduce into the energy operator a term taking account of the magnetic interaction. Inasmuch as in the discussion below we are not interested specifically in the magnetic properties of antiferromagnetic materials, we can take into account the presence of magnetic interaction phenomenologically by introducing a magnetic anisotropy energy operator, in the form used, for example, in Ref. 8:

$$H_{\text{anis}} = -K\left(\sum_{n} \hat{S}_{n}^{(z)^2} + \sum_{m} \hat{S}_{m}^{(z)^2}\right), \tag{14}$$

where K is the effective magnetic anisotropy constant. Let us apply the transformation to operators (6) in equation (14) and introduce the notation:

$$\beta = K\frac{8S^2}{ZJ}. \tag{15}$$

Using the first summand of (9c) and formulas (9a), (12), (13), (14), and (15) and temporarily dropping the H_o term, we obtain the following expression for the operator relating to the energy of the system, disregarding the energy of interaction between the outer electrons (see second summand in (9c)) and the non-diagonal part of (9b) (i.e. the s-d interaction):

$$\sum_{k,\sigma} \varepsilon_k \hat{n}_{k,\sigma} + \frac{ZJ}{8S}\sum_{l}\Big[(1+\beta+\Delta)\,(\hat{Q}_l^2+\hat{P}_l^2) + (1+\beta-\Delta)\,(\hat{R}_l^2+\hat{S}_l^2) +$$

$$+ 2\gamma_l\,(\hat{Q}_l\hat{R}_l - \hat{P}_l\hat{S}_l)\Big] = \sum_{k,\sigma}\varepsilon_k n_{k,\sigma} + \frac{ZJ}{8S}\sum_{l}\Phi_l. \tag{16}$$

To find the eigen-values of the operator (16), which are equal to the energy of the elementary excitations of the investigated system, we effect a further unitary transformation from operators $\hat{Q}_l$, $\hat{P}_l$, $\hat{R}_l$, and $\hat{S}_l$ to new operators $\hat{q}_{1l}$, $\hat{q}_{2l}$, $\hat{p}_{1l}$ and $\hat{p}_{2l}$:

$$\hat{Q}_l = \frac{\hat{q}_{1l} + w\hat{q}_{2l}}{1-w}, \qquad \hat{R}_l = \frac{w\hat{q}_{1l} + \hat{q}_{2l}}{1+w},$$

$$\hat{P}_l = \frac{\hat{p}_{1l} + w\hat{p}_{2l}}{1-w}, \qquad \hat{S}_l = \frac{-w\hat{p}_{1l} + \hat{p}_{2l}}{1-w}. \tag{17}$$

The parameter w will be determined below. It can readily be seen from (17) that the operator Φ_l from (16) will assume the form

$$\Phi_1 = [(1+\beta+\Delta) + w^2(1+\beta-\Delta) + 2\gamma_1 w]\left(\frac{\hat{q}_{11}^2}{(1+w)^2} + \frac{\hat{p}_{11}^2}{(1-w)^2}\right) +$$
$$+ [(1+\beta+\Delta)w^2 + (1+\beta-\Delta) + 2\gamma_1 w]\left(\frac{\hat{q}_{21}^2}{(1+w)^2} + \frac{\hat{p}_{21}^2}{(1-w)^2}\right) +$$
$$+ 2[2(1+\beta)w + \gamma_1(1+w^2)]\left(\frac{\hat{q}_{11}\hat{q}_{21}}{(1+w)^2} - \frac{\hat{p}_{11}\hat{p}_{21}}{(1-w)^2}\right). \qquad (18)$$

We invoke the condition

$$2(1+\beta)w + \gamma_1(1+w^2) = 0 \qquad (19)$$

to determine w. From (18) and (19) it will be seen that we are dealing with energy operators of oscillators with natural frequencies of

$$\hbar\omega_1 = \frac{1+w}{1-w}. \qquad (20)$$

Eliminating the parameter w with the aid of (19), we obtain the following expression for the eigen-values of operator (16) (into which we replace H_0):

$$E = H_0 \sum_{k,\sigma} \varepsilon_k n_{k,\sigma} + \frac{ZJ}{4S}\sum_1 \left\{\left[-\Delta + \sqrt{(1+\beta)^2-\gamma_1^2}\right]\left(n_{11}+\frac{1}{2}\right) +\right.$$
$$\left. + \left[\Delta + \sqrt{(1+\beta)^2-\gamma_1^2}\right]\left(n_{21}+\frac{1}{2}\right)\right\}; \qquad (21)$$

here n_{11} and n_{21} are the quantum numbers of the oscillators (antiferromagnons), equal to 0, 1, 2, 3,..., of the first and second magnetic sublattices, respectively. Let us isolate the terms in (21) corresponding to the operator (12); taking into account the abbreviated notation of (13), we get

$$-\frac{ZJ}{4S}\sum_1\left[\frac{1}{ZJN_d}\sum_k I(\mathbf{k}_1, \mathbf{k}_2)\left(n_{k,-\frac{1}{2}} - n_{k,\frac{1}{2}}\right)\left(n_{11}+\frac{1}{2}\right) -\right.$$
$$\left. - \frac{1}{ZJN_d}\sum_k I(\mathbf{k}_1, \mathbf{k}_2)\left(n_{k,-\frac{1}{2}} - n_{k,\frac{1}{2}}\right)\left(n_{21}+\frac{1}{2}\right)\right] =$$
$$= -\frac{1}{4SN_dJ}\sum_k I(\mathbf{k}_1, \mathbf{k}_2)\left(n_{k,-\frac{1}{2}} - n_{k,\frac{1}{2}}\right)\sum_1\left[\left(n_{11}+\frac{1}{2}\right) - \left(n_{21}+\frac{1}{2}\right)\right] = 0. \qquad (22)$$

Thus we see that, within the bounds of accuracy determined by the fluctuation of the numbers of antiferromagnons in the two equivalent sublattices, the energy fraction due to the s-d exchange interaction is reduced to zero. Hence, to this approximation, we find that the energy of the system is equal to the sum of the energies of the two types of elementary excitations: of the conductivity electrons (the translational energy of which changed due to the s-d coupling - see equation (10):

$$\sum_{k,\sigma} \varepsilon_k n_{k,\sigma} \qquad (23)$$

and of the antiferromagnons of the two equivalent sublattices:

$$\sum_1\left[\varepsilon_{11}\left(n_{11}+\frac{1}{2}\right) + \varepsilon_{21}\left(n_{21}+\frac{1}{2}\right)\right]; \qquad (24)$$

the energy of an antiferromagnon being equal to

$$\varepsilon_{11} = \varepsilon_{21} = \frac{ZJ}{2}\sqrt{(1+\beta)^2 - \gamma_1^2}. \tag{25}$$

From (25) it will be seen that when the anisotropy energy is vanishingly small ($\beta \to 0$), in view of (11), the energy of an antiferromagnon becomes

$$\varepsilon_1 \approx \frac{ZJ}{2} al. \tag{26}$$

Hence, the dispersion law is characterized by a linear dependence of the energy of an antiferromagnon on its quasi-impulse **l** in the case of the s-d exchange model of antiferromagnetism as well.

3. Let us now proceed to an evaluation of the additional electric resistance of an antiferromagnetic metal, due to collisions between the conductivity electrons and the antiferromagnons. These collisions are described by equation (9b). We return to the Fourier operator components of the initial Bose-operators; invoking equations (6), we get

$$\hat{H}_{sd} = \hat{H}_{sd}^{\text{inela}} + \hat{H}_{sd}^{\text{ela}}, \tag{27}$$

$$\hat{H}_{sd}^{\text{inela}} = -\frac{1}{4\sqrt{SN_d}} \sum_{\mathbf{k}_1,\mathbf{k}_2,\mathbf{l}} I(\mathbf{k}_1, \mathbf{k}_2) [\hat{b}_{\mathbf{l}}^{+} \hat{a}_{\mathbf{k}_1,-\frac{1}{2}} \hat{a}_{\mathbf{k}_2,\frac{1}{2}} \delta(\mathbf{k}_2 - \mathbf{k}_1 - \mathbf{l}) +$$

$$+ \hat{b}_{\mathbf{l}} \hat{a}_{\mathbf{k}_1,\frac{1}{2}} \hat{a}_{\mathbf{k}_2,-\frac{1}{2}} \delta(\mathbf{k}_2 - \mathbf{k}_1 + \mathbf{l}) + \hat{c}_{\mathbf{l}} \hat{a}_{\mathbf{k}_1,-\frac{1}{2}} \hat{a}_{\mathbf{k}_2,\frac{1}{2}} \delta(\mathbf{k}_2 - \mathbf{k}_1 + \mathbf{l}) +$$

$$+ \hat{c}_{\mathbf{l}}^{+} \hat{a}_{\mathbf{k}_1,\frac{1}{2}} \hat{a}_{\mathbf{k}_2,-\frac{1}{2}} \delta(\mathbf{k}_2 - \mathbf{k}_1 - \mathbf{l})], \tag{27a}$$

$$\hat{H}_{sd}^{\text{ela}} = -\frac{1}{8SN_d} \sum_{\mathbf{k}_1,\mathbf{k}_2,\mathbf{l}_1,\mathbf{l}_2} I(\mathbf{k}_1, \mathbf{k}_2) (\hat{b}_{\mathbf{l}_1}^{+} \hat{b}_{\mathbf{l}_2} - \hat{c}_{\mathbf{l}_1}^{+} \hat{c}_{\mathbf{l}_2}) (\hat{a}_{\mathbf{k}_1,\frac{1}{2}}^{+} \hat{a}_{\mathbf{k}_2,\frac{1}{2}} -$$

$$- \hat{a}_{\mathbf{k}_1,-\frac{1}{2}}^{+} \hat{a}_{\mathbf{k}_2,-\frac{1}{2}}) \delta(\mathbf{k}_2 - \mathbf{k}_1 + \mathbf{l}_2 - \mathbf{l}_1). \tag{27b}$$

First, let us examine the effect of inelastic collisions. Applying standard operations (see, for example, Ref. 8), we obtain the kinetic equation for the conductivity electron number partition function

$$\frac{eF_x}{\hbar} \cdot \frac{N_d \hbar}{2\pi} \cdot \frac{\partial\left(n_{\mathbf{k},\frac{1}{2}} + n_{\mathbf{k},-\frac{1}{2}}\right)}{\partial k_x} =$$

$$= \sum_{\mathbf{l}} I(\mathbf{k}\ \ \mathbf{k}+\mathbf{l})|^2 \left\{ \left[n_{\mathbf{k}+\mathbf{l},\frac{1}{2}} \left(1 - n_{\mathbf{k},-\frac{1}{2}}\right)(n_{\mathbf{l}}+1) - \right.\right.$$

$$\left. - n_{\mathbf{k},-\frac{1}{2}} \left(1 - n_{\mathbf{k}+\mathbf{l},\frac{1}{2}}\right) \right] \delta(\varepsilon_{\mathbf{k}} + \varepsilon_{\mathbf{l}} - \varepsilon_{\mathbf{k}+\mathbf{l}}) +$$

$$+ \left[n_{\mathbf{k}+\mathbf{l},-\frac{1}{2}} \left(1 - n_{\mathbf{k},\frac{1}{2}}\right) n_{\mathbf{l}} - n_{\mathbf{k},\frac{1}{2}} \left(1 - n_{\mathbf{k}+\mathbf{l},-\frac{1}{2}}\right)(n_{\mathbf{l}}+1) \right] \times$$

$$\left. \times \delta(\varepsilon_{\mathbf{k}} - \varepsilon_{\mathbf{l}} - \varepsilon_{\mathbf{k}+\mathbf{l}}) \right\}. \tag{28}$$

As we saw under 2. above, the energy of a conductivity electron ε_k is not dependent on the orientation of its spin (to the order of accuracy determined by the fluctuation of the magnetization of the inner electrons in the sublattices); hence, all physical conditions for electrons with both orientations of the spin projection will be identical and we may assume that there is no spontaneous magnetization in the system of outer electrons and that

$$n_{k,\frac{1}{2}} = n_{k,-\frac{1}{2}} = \frac{1}{2} n_k,$$

where n_k is the sought electron partition function; $n_l = (e^{\frac{\varepsilon_l}{kT}} - 1)^{-1}$ is the antiferromagnon equi-partition function, N_d is the number of inner electrons of the crystal; the delta-function of the last term takes into account the law of the conservation of energy in collisions; e is the elementary charge and F_x is the intensity of the electric field directed along the X-axis. We seek a solution of (27a) in the conventional form

$$n_k = n_k^0 + \psi_k, \tag{29}$$

and changing to a continuum in quasi-impulse space, we obtain for (28):

$$\begin{aligned} -eF_x \frac{N_d}{\pi\Omega_0}\left(\frac{2\pi}{G}\right)^3 \frac{\partial n_k^0}{\partial k_x} = \\ = \int_0^{l_m} l^2\, dl \int_0^{2\pi} d\varphi \int_0^{\pi} \sin\vartheta\, d\vartheta\, |I(\mathbf{k},\ \mathbf{k}+\mathbf{l})|^2 \{[\psi_{k+1}(n_l + 1 - n_k^0) - \\ - \psi_k (n_{k+1} + n_l)]\, \delta(\varepsilon_{k+1} - \varepsilon_k - \varepsilon_l) + \\ + [\psi_{k+1}(n_k^0 + n_l) - \psi_k (n_l + 1 - n_{k+1})]\, \delta(\varepsilon_{k+1} - \varepsilon_k + \varepsilon_l)\}, \end{aligned} \tag{30}$$

where ϑ and φ are polar angles in k-space and Ω_0 and G are, respectively, the volume and number of the elementary cells. The conductivity electron equi-partition function has the usual form:

$$n_k^0 = e^{\left(\frac{\varepsilon_k - \mu}{kT} + 1\right)^{-1}} \tag{31}$$

The maximum impulse of the antiferromagnons l_m is determined from the antiferromagnetic Curie point $\Theta_{a\phi}$. Invoking the presence of the delta-function under the integral in the right-hand member of (30), we integrate over the angle ϑ, and obtain, instead of (30):

$$\begin{aligned} \frac{d\varepsilon_k}{dk} eF_x \frac{N_d}{\pi\Omega_0}\left(\frac{2\pi}{G}\right)^3 \frac{\partial n_k^0}{\partial k_x} = \\ = \int_0^{l_m} l\, dl \int_0^{2\pi} d\varphi\, |I(\mathbf{k},\ \mathbf{k}+\mathbf{l})|^2 \{[\psi_{k+1}(n_l + 1 - n_k^0) - \\ - \psi_k (n_{k+1}^0 + n_l)]_{\varepsilon_{k+1} = \varepsilon_k + \varepsilon_l} + \\ + [\psi_{k+1}(n_k^0 + n_l) - \psi_k (n_l + 1 - n_{k+1}^0)]_{\varepsilon_{k+1} = \varepsilon_k + \varepsilon_l}\}. \end{aligned} \tag{32}$$

We seek the perturbation term of the electron equi-partition function in the form:

$$\psi_{\mathbf{k}} = k_{\mathbf{k}}\chi(\varepsilon_{\mathbf{k}}). \tag{33}$$

Substituting (33) in (32) and integrating over φ, we obtain:

$$\frac{d\varepsilon_{\mathbf{k}}}{dk}\cdot\frac{eF_x}{2\pi^2 k_x}\cdot\frac{N_d}{\Omega_0}\left(\frac{2\pi}{G}\right)^3\frac{\partial n^0_{\mathbf{k}}}{\partial k_x} =$$

$$= \int_0^{l_m} l\,dl\,n_1 |I(\mathbf{k};\mathbf{k}+\mathbf{l})|^2 \left\{\left[\left(1+\frac{l}{k}\cos\vartheta_1\right)\chi(\varepsilon_{\mathbf{k}}+\varepsilon_1)\frac{n^0(\varepsilon_{\mathbf{k}})}{n^0(\varepsilon_{\mathbf{k}}+\varepsilon_1)} - \right.\right.$$

$$-\chi(\varepsilon_k)\frac{n^0(\varepsilon_{\mathbf{k}}+\varepsilon_1)}{n^0(\varepsilon_{\mathbf{k}})}e^{\frac{\varepsilon_1}{kT}}\Big] + \Big[-\chi(\varepsilon_{\mathbf{k}})\frac{n^0(\varepsilon_{\mathbf{k}}-\varepsilon_1)}{n^0(\varepsilon_{\mathbf{k}})} +$$

$$\left.\left. +\left(1+\frac{l}{k}\cos\vartheta_2\right)\chi(\varepsilon_{\mathbf{k}}-\varepsilon_1)\,e^{\frac{\varepsilon_1}{kT}}\frac{n^0(\varepsilon_{\mathbf{k}})}{n^0(\varepsilon_{\mathbf{k}}-\varepsilon_1)}\Big]\right\}, \tag{34}$$

where

$$l\cos\vartheta_{1,2} = \pm\frac{\varepsilon_1 - I(\mathbf{k},\mathbf{k})}{d\varepsilon_{\mathbf{k}}/dk} - \frac{l^2}{2k}.$$

We seek a solution of (34) in the form

$$\chi(\varepsilon_{\mathbf{k}}) = -\zeta\frac{dn^0(\varepsilon_{\mathbf{k}})}{d\varepsilon_{\mathbf{k}}} + \eta_l(\varepsilon_{\mathbf{k}}), \tag{35}$$

where, in this case,

$$|\eta_l| \ll \left|\zeta\frac{dn^0(\varepsilon_{\mathbf{k}})}{d\varepsilon_{\mathbf{k}}}\right|.$$

As a result of substituting (35) in (34) and simple transformations, we obtain

$$\frac{d\varepsilon_{\mathbf{k}}}{dk}\cdot\frac{eF_x}{2\pi^2 k_x}\cdot\frac{N_d}{\Omega_0}\left(\frac{2\pi}{G}\right)^3\frac{\partial n^0_{\mathbf{k}}}{\partial k_x} +$$

$$+\zeta\int_0^{l_m} l\,dl\,n_1|I(\mathbf{k},\mathbf{k}+\mathbf{l})|^2\left\{\frac{l}{k}\cos\vartheta_1\frac{n^0(\varepsilon_{\mathbf{k}})}{n^0(\varepsilon_{\mathbf{k}}+\varepsilon_1)}\cdot\frac{dn_0(k_{\mathbf{k}}+\varepsilon_1)}{d\varepsilon_{\mathbf{k}}} + \right.$$

$$\left. +\frac{l}{k}\cos\vartheta_2\frac{n^0(\varepsilon_{\mathbf{k}})}{n^0(\varepsilon_{\mathbf{k}}-\varepsilon_1)}\frac{dn^0(\varepsilon_{\mathbf{k}}-\varepsilon_1)}{d\varepsilon_{\mathbf{k}}}e^{\frac{\varepsilon_1}{kT}}\right\} =$$

$$= \int_0^{l_m} l\,dl\,|I(\mathbf{k},\mathbf{k}+\mathbf{l})|^2\left\{\left[\eta_l(\varepsilon_{\mathbf{k}}+\varepsilon_1)\frac{n^0(\varepsilon_{\mathbf{k}})}{n^0(\varepsilon_{\mathbf{k}}+\varepsilon_1)} - \right.\right.$$

$$-\eta_l(\varepsilon_{\mathbf{k}})e^{\frac{\varepsilon_1}{kT}}\frac{n^0(\varepsilon_{\mathbf{k}}+\varepsilon_1)}{n_1(\varepsilon_{\mathbf{k}})}\Big] + \Big[-\eta_l(\varepsilon_{\mathbf{k}})\frac{n^0(\varepsilon_{\mathbf{k}}-\varepsilon_1)}{n^0(\varepsilon_{\mathbf{k}})} +$$

$$\left.\left. +\eta_l(\varepsilon_{\mathbf{k}}-\varepsilon_1)e^{\frac{\varepsilon_1}{kT}}\frac{n^0(\varepsilon_{\mathbf{k}})}{n^0(\varepsilon_{\mathbf{k}}-\varepsilon_1)}\Big]\right\}. \tag{36}$$

Integrating over the energy $\varepsilon_{\mathbf{k}}$ from $-\infty$ to $+\infty$, we obtain for evaluating ζ (the terms with η drop out in the accepted approximation):

$$-\int_{-\infty}^{+\infty}\frac{eF_x}{2\pi^3 k_x}\cdot\frac{N_d}{\Omega_0}\left(\frac{2\pi}{G}\right)^3\frac{\partial n_k^0}{\partial k_x}\cdot\frac{d\varepsilon_k}{dk}\,d\varepsilon_k=$$

$$=\zeta\int_0^{l_m} l\,dl\,n_l\int_{-\infty}^{+\infty}d\varepsilon_k\,|I(\mathbf{k},\,\mathbf{k}+\mathbf{l})|^2\times$$

$$\cdot\times\left\{\left[\frac{\varepsilon_1-I(\mathbf{k},\,\mathbf{k})}{k\dfrac{d\varepsilon_k}{dk}}-\frac{l^2}{2k^2}\right]\frac{n^0(\varepsilon_k+\varepsilon_l)}{n^0(\varepsilon_k)}\,e^{\frac{\varepsilon_l}{kT}}\frac{dn^0(\varepsilon_k)}{d\varepsilon_k}+\right.$$

$$\left.+\left[-\frac{\varepsilon_1-I(\mathbf{k},\,\mathbf{k})}{k\dfrac{d\varepsilon_k}{dk}}-\frac{l^2}{2k^2}\right]\frac{n^0(\varepsilon_k-\varepsilon_l)}{n^0(\varepsilon_k)}\cdot\frac{dn^0(\varepsilon_k)}{d\varepsilon_k}\right\}. \qquad (37)$$

We change over to new variables

$$\frac{\varepsilon_k-\mu}{kT}=e,\ \frac{\varepsilon_l}{kT}=\frac{ZJ}{2kT}\sqrt{2\beta+a^2l^2}=x,\quad l_m=\frac{\theta_{a\Phi}}{T}. \qquad (38)$$

Upon integrating over ε_k, instead of (37), we have

$$\frac{eF_x}{4\pi^3}\cdot\frac{N_d}{\Omega_0}\left(\frac{2\pi}{G}\right)^3\left[\frac{1}{k}\left(\frac{d\varepsilon_k}{dk}\right)^2\right]_{\varepsilon_k=\mu}=$$

$$=\zeta\int_0^{\frac{\theta_{a\Phi}}{T}}\left(\frac{2kT}{ZaJ}\right)^2 x\,dx\,n(x)\int_{-\infty}^{+\infty}\frac{dn^0(\varepsilon)}{d\varepsilon}\times$$

$$\times\left\{|I_1(\mathbf{k},\,\mathbf{k}+\mathbf{l})|^2\left[\frac{\varepsilon_1-I(\mathbf{k},\,\mathbf{k})}{k\dfrac{d\varepsilon_k}{dk}}-\frac{l^2}{2k^2}\right]\frac{e^{\varepsilon}+1}{e^{\varepsilon+x}+1}e^{x}+\right.$$

$$\left.+|I_2(\mathbf{k},\,\mathbf{k}+\mathbf{l})|^2\left[-\frac{\varepsilon_1-I(\mathbf{k},\,\mathbf{k})}{k\dfrac{d\varepsilon_k}{dk}}-\frac{l^2}{2k^2}\right]\frac{e^{\varepsilon}+1}{e^{\varepsilon-x}+1}\right\}, \qquad (39)$$

where from formula (25) in Ref. 2, we have

$$I_{1,2}(\mathbf{k},\,\mathbf{k}+\mathbf{l})=\alpha+\beta(2k^2+l^2+2kl\cos\vartheta_{1,2});$$

α and β are the s- and d-electron exchange integrals for a single lattice site and for two neighboring sites, respectively; we can neglect the difference between $|I_1(\mathbf{k},\,\mathbf{k}+\mathbf{l})|^2$ and $|I_2(\mathbf{k},\,\mathbf{k}+\mathbf{l})|^2$, since this is determined by corrections of the second order; hence, we finally obtain

$$\zeta=\frac{\dfrac{eF_x}{\pi^2\alpha^3}\cdot\dfrac{N_d}{\alpha^2\Omega_0}\left(\dfrac{2\pi}{G}\right)^3\left[\dfrac{1}{k}\left(\dfrac{d\varepsilon_k}{dk}\right)^2\right]_{\varepsilon_k=\mu}}{J_4\left(\dfrac{T}{\theta_{a\Phi}}\right)^4-2\beta\,J_2\left(\dfrac{T}{\theta_{a\Phi}}\right)^2}; \qquad (40)$$

here

$$J_m \equiv J_m\left(\frac{\theta_{a\Phi}}{T}\right) = \int_0^{\frac{\theta_{a\Phi}}{T}} \frac{y^m dy}{(e^y - 1)(1 - e^{-y})} = m! \sum_{\rho=1}^{\infty} \frac{1}{\rho^m}$$

for m = 2, 4, and the approximate assumption that $|I(\mathbf{k}, \mathbf{k}+\mathbf{l})|^2 \approx \alpha$.

(Translator's note: Subscript aΦ = antiferromagnetic).

From (40) it can readily be seen that the specific conductivity fraction due to inelastic collisions between conductivity electrons and antiferromagnons has the following temperature dependence:

$$\sigma_{\text{inela}} = a_1\left(\frac{T}{\theta_{a\Phi}}\right)^{-2} + a_2\left(\frac{T}{\theta_{a\Phi}}\right)^{-4}. \qquad (41)$$

In view of the fact that one of the factors comprised in a_1 is the anisotropy constant β, which is small, the dominant part in (41) may well be played by the term with T^{-4}.

The fraction of the electric conductivity due to elastic collisions between the conductivity electrons and the antiferromagnons is readily evaluated according to the precedure outlined in our earlier work (Ref. 3). We will not repeat the calculations here but simply note that their end result shows that the temperature dependence of this component of the conductivity is given by

$$\sigma_{\text{el}} = b_1\left(\frac{T}{\theta_{a\Phi}}\right)^{-4} + b_2\left(\frac{T}{\theta_{a\Phi}}\right)^{-6}. \qquad (42)$$

Hence, together both types of collisions give

$$\sigma_{a\Phi} = a_1\left(\frac{T}{\theta_{a\Phi}}\right)^{-2} + (a_2 + b_1)\left(\frac{T}{\theta_{a\Phi}}\right)^{-4} + b_2\left(\frac{T}{\theta_{a\Phi}}\right)^{-6}. \qquad (43)$$

It should be noted that the coefficient b_1 in (42) contains the magnetic anisotropy constant β and, consequently, at very low values of this constant the predominant role may be assumed by the T^{-6} term. Thus, it may be predicted that the specific fraction of the electric conductivity of an antiferromagnetic transition metal in the case of strong anisotropy will be characterized by

$$\sigma_{a\Phi\,(\beta\neq 0)} \approx a_1\left(\frac{T}{\theta_{a\Phi}}\right)^{-2} + b_1\left(\frac{T}{\theta_{a\Phi}}\right)^{-4}, \qquad (43a)$$

while in the case of very weak anisotropy ($\beta \to 0$),

$$\sigma_{a\Phi\,(\beta\neq 0)} \approx a_2\left(\frac{T}{\theta_{a\Phi}}\right)^{-4} + b_2\left(\frac{T}{\theta_{a\Phi}}\right)^{-6}. \qquad (43b)$$

Unfortunately, the present state of the theory is such that we cannot give a reasonably accurate quantitative evaluation of the numerical coefficients in the above conductivity formulas. Experimental data regarding the low-temperature variation of the resistance of the substances in question is also lacking. We can only note that the temperature law described by (43) differs substantially from the accepted law

for the "background" conductivity fraction (T^{-5}). Where a comparison with the portion of the resistance due to electron collisions is concerned, this, as was shown in our earlier investigation (Ref. 3), varies with the temperature according to the following formula:

$$\sigma_{elec} = d_1 T^{-2} + d_2 T^{-3};$$

hence, there is, in principle, the possibility of distinguishing it from (43).

Despite the serious shortcomings of this investigation, - the impossibility of obtaining a quantitative evaluation of the coefficients we feel that our analysis is of interest in that it indicates the potentiality of certain unique characteristics in the temperature dependence of the electric resistance of antiferromagnetic metals of the transition groups in the region of low temperatures.

Ural State University

Received
3 May 1954

Bibliographic References

1. S.V.Vonsovski, Zhur. eks. i teor. fiz., 16, 981 (1946).
2. S.V.Vonsovski & E.A.Turov, Zhur. eksp. i teor. fiz., 24,419 (1953).
3. S.V.Vonsovski & A.A.Berdyshev, Zhur.eksp. i teor. fiz.,25,723 (1953).
4. S.V.Vonsovski, Sovremennoe uchenie o magnetizme (Modern teachings on magnetism), Section 13e. Gostekhizdat, M.-L. 1953.
5. C.G.Shull & J.S.Smart, Phys. Rev., 76, 1256 (1949).
6. C.G.Shull and others, Rev. Mod. Phys., 25, 100 (1953).
7. N.N.Bogoliubov & S.V. Tiablikov, Zhur. eksp. i teor. fiz.,19,256 (1949).
8. R.Kubo, Phys. Rev., 87, 568 (1952).

* * * * *

A CONTRIBUTION TO THE THEORY OF ANTIFERROMAGNETISM

- K. B. Vlasov

As is known, many materials designated as antiferromagnetic exhibit certain specific characteristics. Thus, the temperature dependence of the magnetic susceptibility of antiferromagnetics differs from the temperature dependence characteristic of paramagnetic substances, i.e., the temperature-susceptibility curve for antiferromagnetics has a maximum at the so-called antiferromagnetic Curie point T_c. Near this point, too, anomalies are observed in the variation of the specific heat, the electric resistance, the thermal expansion coefficient and other attributes. To explain this phenomenon the hypothesis was advanced (and subsequently confirmed by neutron diffraction experiments - see Ref. 1) that there is established in antiferromagnetics at temperatures below T_c a long-range order in which the magnetic moments are oriented antiparallel to each other.

The credit for the first step in developing the theory of antiferromagnetism belongs to L. D. Landau (Ref. 2). Further development of the theory of the magnetic properties of antiferromagnetics is due primarily to Néel (Ref. 3) and Van Vleck (Ref. 4) who utilized the molecular field method. In the present paper an attempt is made to develop the theory by the method of energy centers of gravity.

1. We select the energy operator relating to the system in the form:

$$H = H_1 + H_2 + H_3 + H_4 = -\frac{\hbar}{2m}\sum_q \Delta_q + \sum_{q<q'} V_{qq'}(|r_q - r_{q'}|) +$$

$$+ \sum_{\alpha, q} G_\alpha(|r_q - r_\alpha|) + \sum_{q \neq q'} \frac{e^2}{2m^2c^3} \cdot \frac{(\sigma_q \sigma_{q'})\, r_{qq'}^2 - 3(\sigma_q r_{qq'})(\sigma_{q'} r_{qq'})}{r_{qq'}^5}, \qquad (1)$$

where H_1 is the electron kinetic energy operator, H_2 is the energy operator relating to the electrostatic interaction of the electrons, H_3 is the energy operator relating to the electrostatic interaction between the electrons and the ions of the lattice, H_4 is the operator relating to the energy of the magnetic spin-spin interaction, σ_q is the spin operator relating to the q-th electron (Pauli matrix), $r_{qq'}$ is the electron spacing and $r_q - r_\alpha (= r_{\alpha q})$ is the distance between the q electron and the α ion of the lattice.

In the case of antiferromagnetic metals the wave function Ψ of the system of interacting electrons may be taken in the form of the sum of the antisymmetric products of the atomic functions $\varphi_q(r)$. In the case of non-metallic antiferromagnetics, which are chemical compounds, the wave function will be more complex (it must include the wave functions of the non-metallic ions, as well as the wave functions of the excited states). As examples of the treatment of such more complex systems one may cite the calculations of Van Vleck (Ref. 4) and Anderson (Ref. 5), based on the so-called indirect (super-) exchange concept. It is interesting to note that the final expression for the part of the energy depending on the magnetization, derived in these calculations, has exactly the same form as in the case where ordinary exchange interaction (rather than indirect exchange interaction) is assumed. Hence, there is reason to suppose that taking into account the magnetic interaction in non-metallic antiferromagnetics

will lead to results qualitatively equivalent to those obtained in the case of metallic antiferromagnetics. However, this argument still lacks rigorous proof.

Let us agree, then, that the wave function for a system of interacting magnetoactive electrons may be selected in the form of a sum of the antisymmetric products of the atomic functions. Then the mean value of the energy of the system $E = \int \Psi H \Psi^* d\Phi$ will be (Ref. 6):

$$E(h_1, \ldots, h_r) = \varepsilon - \frac{1}{2}\sum_{q \neq q'} A_{q_h q'_h} - \frac{1}{2}\sum_{q \neq q'} A_{q_k q'_k} + \sum_{q,\, q'} B_{q_h q'_k}, \tag{2}$$

where

$$A_{qq'} = -D_{qq'} + \varepsilon^z_{qq'} + J_{qq'} + I_{qq'} - J^z_{qq'}, \quad B_{qq'} = A_{qq'} - I_{qq'}, \tag{3}$$

with

$$\left.\begin{aligned} D_{qq'} &= \beta \int r_{qq'}^{-3} \varphi_q^2(\mathbf{r}) \varphi_{q'}^2(\mathbf{r}')\, d\mathbf{r}\, d\mathbf{r}', \\ \varepsilon^z_{qq'} &= 3\beta \int |z_{qq'}|^2 r_{qq'}^{-5} \varphi_q^2(\mathbf{r}) \varphi_{q'}^2(\mathbf{r}')\, d\mathbf{r}\, d\mathbf{r}', \\ I_{qq'} &= \int [G_\alpha(\mathbf{r}') + G_\beta(\mathbf{r})]\, \varphi_q(\mathbf{r}) \varphi_{q'}(\mathbf{r}') \varphi_q(\mathbf{r}') \varphi_{q'}(\mathbf{r})\, d\mathbf{r}\, d\mathbf{r}', \\ J_{qq'} &= \beta \int r_{qq'}^{-3} \varphi_q(\mathbf{r}) \varphi_{q'}(\mathbf{r}') \varphi_q(\mathbf{r}') \varphi_{q'}(\mathbf{r})\, d\mathbf{r}\, d\mathbf{r}', \\ J^z_{qq'} &= 3\beta \int |z_{qq'}|^2 r_{qq'}^{-5} \varphi_q(\mathbf{r}) \varphi_{q'}(\mathbf{r}') \varphi_q(\mathbf{r}') \varphi_{q'}(\mathbf{r})\, d\mathbf{r}\, d\mathbf{r}'. \end{aligned}\right\} \tag{4}$$

The numbers $h_1, \ldots h_r$ refer to the r lattice sites at which are located the electrons having "right" spin, whereas $k_1, \ldots k_u$ refer to the u sites at which are located the electrons having "left" spin; $D_{qq'}$ and $\varepsilon^z_{qq'}$ are integrals representing the quasi-classical magnetic interaction, the integral $I_{qq'}$ represents the electric exchange interaction and the integrals $J_{qq'}$ and $J^z_{qq'}$ represent the magnetic exchange interaction and ε is the part of the energy not dependent on the distribution of the spins over the lattice sites.

Equation (2) may be written in vector representation, according to Dirac:

$$E = \varepsilon - \sum_{qq'} A'_{qq'} \vec{s}_q \vec{s}_{q'}, \tag{5}$$

where

$$A'_{qq'} = A_{qq'} + B_{qq'} = I_{qq'} - 2D_{qq'} + 2\varepsilon^z_{qq'} + 2J_{qq'} - 2J^z_{qq'}. \tag{6}$$

Let us consider the lattice of an antiferromagnetic as being composed of two sublattices, magnetized in opposite directions; let us tentatively assume that of the N_1 magnetoactive electrons belonging to the first lattice r_1 have "right" spin, while of the N_2 magnetoactive electrons belonging to the second lattice u_2 have "left" spin. This division into sublattices is not rigorous, since the magnetizations of the sublattices and, consequently, the values of r_1 and u_2, as may be shown from the commutation relationship for the moment of momentum and the energy operators, are not integrals of motion. However, Anderson (Ref. 5) has shown that the exact energy of

the ground state must be close to the energy of a system consisting of two sublattices. Hence, the errors associated with the approximate description of the phenomenon, based on the introduction of the two-lattice concept, are apparently not as great as the errors involved in the use of the energy centers of gravity approximation for describing the behavior of antiferromagnetic materials at temperatures below the Curie point.

In accordance with the quasi-classical approximation, in our subsequent calculations we will regard the $\bar{\sigma}_q$ variables not as operators but as unit vectors. Averaging over the various spin alignments, corresponding to the given magnetizations in the sublattices and taking into account the energy in the external magnetic field, we obtain the following expression for the part of mean energy of the system, depending on the magnetization of the sublattices:

$$\overline{E}(m_1, m_2) = -\frac{1}{2}\left[\frac{2m_1^2}{N_1^2}\sum_{qq'}^{N_1} A'_{qq'} + \frac{4m_1 m_2}{N_1 N_2}\sum_{qj}^{N_1 N_2} A'''_{qj} + \frac{2m_2^2}{N_2^2}\sum_{jj'}^{N_2} A''_{jj'}\right] - 2\mu_0 H(m_1 + m_2), \quad (7)$$

where

$$m_1 = r_1 \frac{N_1}{2}, \quad m_2 = u_2 - \frac{N_2}{2},$$

μ_0 is the Bohr magnetron and $A'_{qq'}$, $A''_{jj'}$, and A'''_{qj} are the sums of the type (6) integrals for the electrons of the first sublattice, of the second sublattice and of both sublattices, respectively.

Let us assume that all the atoms in the sublattices are identical and that each is situated with respect to all the others in the same way as any other. Then the double sums may be expressed through simple ones, referred, respectively, to an arbitrary atom q', j', q or j:

$$\left.\begin{aligned} &\sum_{q\neq q'}^{N_1} A'_{qq'} = N_1 \sum_{q(\neq q')}^{N_1} A'_{qq'}, \quad \sum_{j\neq j'}^{N_2} A''_{jj'} = N_2 \sum_{j(\neq j')}^{N_2} A''_{jj'}, \\ &\sum_{q,j}^{N_1 N_2} A'''_{qj} = N_1 \sum_{j}^{N_2} A'''_{qj} = N_2 \sum_{q}^{N_1} A'''_{qj}. \end{aligned}\right\} \quad (8)$$

Let us now determine the angular dependence of the $\sum_{q(\neq q')} A_{qq'}$ terms. To do this we must consider the specific type of lattice involved. First let us examine the case of a tetragonal type lattice. Let us orient the Z-axis in the direction of magnetization of the sublattices and tie our coordinate system $\bar{x}$, $\bar{y}$, $\bar{z}$ to the crystal axes; then

$$z_{qq'} = \cos\gamma_1 \cdot \bar{x}_{qq'} + \cos\gamma_2 \bar{y}_{qq'} + \cos\gamma_3 \cdot \bar{z}_{qq'}. \quad (9)$$

Substituting (9) in (8), carrying out the summation, taking into account the conditions of symmetry in accordance with which terms containing $\bar{x}_{qq'}$, $\bar{y}_{qq'}$ and $\bar{z}_{qq'}$ to the first power will cancel each other, considering the corresponding integrals containing $\bar{y}^2_{qq'}$ and $\bar{z}^2_{qq'}$ to be equal (the tetragonal axis is aligned with the $\bar{x}$ axis), invoking the

trigonometric identity $\cos^2\gamma_2 + \cos^2\gamma_3 = 1 - \cos^2\gamma_1$ and grouping the summands depending on and those independent of the angle $\gamma_1 = \gamma$, we obtain

$$\left.\begin{aligned} \sum_{q\,(\neq q')}^{N_1} A'_{qq'} = P + P'\cos^2\gamma, \quad \sum_{j\,(\neq j')}^{N_2} A''_{jj'} = R + R'\cos^2\gamma, \\ \sum_{j}^{N_2} A'''_{qj} = Q + Q'\cos^2\gamma, \end{aligned}\right\} \tag{10}$$

where P, Q and R are the sums of the integrals characterizing the value of the electric and magnetic interaction, while P', Q' and R' are the sums of the integrals characterizing the magnetic interaction of the electrons of the first, the second and both sublattices, respectively. In the case of a hexagonal crystal lattice, we obtain expressions analogous to (10).

2. To determine the free energy of the system we must evaluate the phase sum, which in this case is equal to

$$Z = \sum_{m_1=-\frac{N_1}{2}}^{\frac{N_1}{2}} \sum_{m_2=-\frac{N_2}{2}}^{\frac{N_2}{2}} \binom{N_1}{\frac{N_1}{2}+m_1} \binom{N_2}{\frac{N_2}{2}+m_2} e^{-\frac{\bar{E}}{kT}} \tag{11}$$

In this sum the predominant role is played by the terms for which m_1 and m_2 are close to the mean values $\bar{m}_1$ and $\bar{m}_2$. Hence, the summation in (11) may be removed and the corresponding means values $\bar{m}_1$ and $\bar{m}_2$ substituted for m_1 and m_2. Substituting (7) in (11) while taking into account (8) and (10), invoking Stirling's formula, $\ln n! = n(\ln n - 1)$, and introducing mean values of the magnetizations of the sublattices $y_1 = 2\bar{m}_1/N_1$ and $y_2 = 2\bar{m}_2/N_2$ for the part of the free energy that depends on the magnetization, we obtain

$$\begin{aligned} \Phi(y_1, y_2, H, \gamma) = -kT\ln Z = \frac{N_1}{2}kT\left[(1+|y_1|)\ln(1+|y_1|) + \right. \\ \left. + (1-|y_1|)\ln(1-|y_1|)\right] + \frac{N_2}{2}kT\left[(1+|y_2|)\ln(1+|y_2|) + \right. \\ \left. + (1-|y_2|)\ln(1-|y_2|)\right] - \frac{N_1}{4}y_1^2(P + P'\cos^2\gamma) - \\ - \frac{N_1}{2}(y_1, y_2)(Q + Q'\cos^2\gamma) - \frac{N_2}{4}y_2^2(R + R'\cos^2\gamma) - \\ - 2\mu_0 H\left(y_1\frac{N_1}{2} + y_2\frac{N_2}{2}\right). \end{aligned} \tag{12}$$

In antiferromagnetics, the sublattices are equivalent, i.e. $N_2 = N_1 = N_1/2$, R = P and R' = P'. In the absence of a magnetic field and in the presence of negative exchange interaction between the sublattices, the sublattice magnetization vectors will orient themselves antiparallel (as will be seen below, a necessary condition for this is

$(P - Q) + (P' - Q')\cos^2\gamma > 0$), i.e. $y_1 = -y_2 = y$. When $(P' - Q') > 0$, the minimum value of the energy occurs for $\gamma = 0$ (the sublattice magnetization vectors coincide with the direction of the tetragonal or hexagonal axis; this will hereinafter be referred to as the direction of preferred magnetization). If $(P' - Q') < 0$, the energy will be minimal for $\gamma = 90^\circ$ (magnetizations in the sublattices aligned antiparallel in the plane normal to the tetragonal or hexagonal axis).

In the presence of a magnetic field, oriented at any arbitrary angle to the tetragonal or hexagonal axis, the sublattice magnetization vectors will be oriented as shown in Figure 1 (D identifies the axis and direction of preferred magnetization; the orientation of the field relative to this direction will be designated through the angle β). The angles between the magnetization vectors and the direction of the field will be $(\Psi - \alpha_1)$ and $(180 - \Psi - \alpha_2)$, while the absolute magnitudes of the vectors will change due to application of the field by $(\Delta y_1)_\Psi$ and $(\Delta y_2)_\Psi$, i.e.

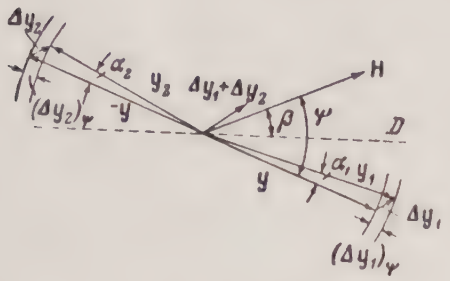

Fig. 1. Diagram showing the relative positions of the sublattice magnetization vectors in an antiferromagnetic for a given orientation of the external field and preferred magnetization direction.

$$|y_1| = |y| + (\Delta y_1)_\psi \qquad \& \qquad |y_2| = |y| - (\Delta y_2)_\psi.$$

Since the magnetic interaction energy determining the magnitude of the angle $\gamma = \Psi - \beta$ is by some 3-4 orders smaller than the electric exchange interaction energy determining the angles α_1 and α_2 and the increments $(\Delta y_1)_\Psi$ and $(\Delta y_2)_\Psi$, we can assume that the former will be small compared to Ψ and the latter small compared to y; hence, to the first approximation we can take $\alpha_1 = \alpha_2 = \alpha$, $(\Delta y_1)_\Psi = (\Delta y_2)_\Psi = \Delta y$ and $\Delta y_1 = \Delta y_2 = \frac{y_1 + y_2}{2}$. Then the expression for the free energy of the antiferromagnetic will assume the form

$$\begin{aligned}\Phi = {} & \frac{NkT}{4}[(1+y+\Delta y)\ln(1+y+\Delta y) + (1-y-\Delta y)\ln(1-y-\Delta y) + \\ & + (1+y-\Delta y)\ln(1+y-\Delta y) + (1-y+\Delta y)\ln(1-y+\Delta y)] - \\ & - \frac{N}{2}(y^2+\Delta y^2)[P + P'\cos^2(\psi-\beta)] + \\ & + \frac{N}{2}(y^2-\Delta y^2)(1-2\alpha^2)[Q + Q'\cos^2(\psi-\beta)] - \\ & - N\mu_0 H(\alpha y\sin\psi + \Delta y\cos\psi). \end{aligned} \tag{13}$$

We find the equilibrium values for y, Δy, α and Ψ from the minimum conditions:

$$\frac{\partial\Phi}{\partial y} = 0, \tag{14a}$$

$$\frac{\partial\Phi}{\partial\Delta y} = 0, \tag{14b}$$

$$\frac{\partial\Phi}{\partial\alpha} = 0, \tag{14c}$$

$$\frac{\partial\Phi}{\partial\psi} = 0. \tag{14d}$$

Neglecting the α and Δy terms in (14a), we obtain the following equation for the temperature dependence of y:

$$y = \operatorname{tgh} y \frac{T_c}{T}, \tag{15}$$

where

$$T_c = \frac{(P-Q) + (P'-Q')\cos^2(\psi-\beta)}{k} \tag{16}$$

is the antiferromagnetic Curie point, above which antiferromagnetism vanishes.

Neglecting α^2 in (14b) and expanding $\ln \frac{(1+y+\Delta y)(1-y+\Delta y)}{(1-y-\Delta y)(1+y-\Delta y)}$ into a series in Δy in the neighborhood of (1 + y) and (1 - y), we obtain

$$\Delta y = \frac{\mu_0 H (1-y^2)\cos\psi}{k[T+\theta(1-y^2)]}, \tag{17}$$

where

$$\theta = -\frac{(P+Q) + (P'+Q')\cos^2(\psi-\beta)}{k}. \tag{18}$$

Neglecting the Δy^2 term in (14c) and invoking (16) and (18), we obtain

$$\alpha = \frac{\mu_0 H \sin\psi}{yk(T_c+\theta)}. \tag{19}$$

The magnitude of the resultant magnetization, in accordance with (17) and (18), will be given by

$$I = N\mu_0 \Delta y \cos\psi + N\mu_0 \alpha y \sin\psi = (\chi_{\parallel}\cos^2\psi + \chi_{\perp}\sin^2\psi)H, \tag{20}$$

where

$$\chi_{\parallel} = \frac{N\mu_0^2(1-y^2)}{k[T+\theta(1-y^2)]} \tag{21}$$

and

$$\chi_{\perp} = \frac{N\mu_0^2}{k(T_c+\theta)}, \tag{22}$$

while the equilibrium value of Ψ is found from

$$\operatorname{tg} 2\psi = \frac{\sin 2\beta}{\cos 2\beta - \frac{H^2}{H_0^2}}, \tag{23}$$

where

$$H_0^2 = \frac{N(P'-Q')}{\chi_{\perp}} \cdot \frac{y^2}{1-\frac{\chi_{\parallel}}{\chi_{\perp}}} = H_0(0)\frac{y^2}{1-\frac{\chi_{\parallel}}{\chi_{\perp}}}, \tag{24}$$

which is obtained from (14d), if we neglect Δy^2 and $2\alpha^2$ and take into account (17), (19), (21) and (22).

[Translator's note: In order to facilitate typing, X will be used as the equivalent of chi to denote the susceptibility in the text below.]

From (20) and (23) it follows that the dependence of the net magnetization on the field is non-linear. Hence, in the case of

antiferromagnetics, we must distinguish between the differential susceptibility χ_{diff} and the full or total susceptibility χ_{π}:

$$\chi_{diff} = \frac{dI}{dH} \quad \text{and} \quad \chi_{\pi} = \frac{I}{H} = \frac{1}{H}\int_0^H \chi_{diff}\, dH. \tag{25}$$

In experimental work the quantity usually measured is the full susceptibility, which from (25) and (20) equals

$$\chi_{\pi} = \chi_{\parallel}\cos^2\psi + \chi_{\perp}\sin^2\psi. \tag{26}$$

The expression for the differential susceptibility may be obtained either from the definition of (25) or by differentiating (20):

$$\chi_{diff} = \chi_{\pi} + H\frac{d\chi_{\pi}}{dH}. \tag{27}$$

Equations (26), (21), (22), (24) and (15) determine the functional dependence of the full susceptibility of an antiferromagnetic on the absolute magnitude of the magnetic field and its orientation relative to the crystallographic axes and on the temperature when $T < T_c$. At $T > T_c$ these relationships - with the exception of (24), are no longer valid, inasmuch as at these higher temperatures Δy can no longer be considered small compared to $y(y = 0)$ and, hence, the susceptibility will obey the Curie-Weiss law

$$\chi = \frac{N\mu_0^2}{k(T+\theta')}, \tag{28}$$

where θ' is the paramagnetic Curie point, determined from

$$\theta' = -\frac{(P+Q)}{k}. \tag{29}$$

3. Let us analyze the significance of (26) in greater detail, turning first to the field-dependence of the susceptibility. Let the external field be applied in the direction perpendicular to that of the preferred magnetization, i.e. $\beta = 90^o$. In this case, according to (23), for all field strengths, $\Psi = 90^o$ and the full susceptibility, from (26), equals the perpendicular susceptibility as well as the differential susceptibility.

Let the field be applied in the direction of preferred magnetization, i.e. $\beta = 0$. In this case, according to (23), $\Psi = 0$ when $H < H_o$ and $\Psi = 90^o$ when $H > H_o$, where H_o is the critical field as determined from (24). Thus, according to (26) the full susceptibility X_{π} is equal to the parallel susceptibility $X_{\parallel}$ when $H < H_o$; at $H = H_o$, X_{π} jumps to a value equal to the perpendicular susceptibility $X_{\perp}$ and with $H > H_o$ remains constant and equal to $X_{\perp}$. The differential susceptibility for the same field strength intervals will equal $X_{\parallel}, \infty$, and $X_{\perp}$, respectively.

For any arbitrary orientation of the applied field, defined by β, the functional dependence of the full susceptibility on the field will be more complex: i.e., with increasing field strength X_{π} will increase continuously from $X_{\pi} = X_{\parallel}\cos^2\beta + X_{\perp}\sin^2\beta$ at fields $H \ll H_o$ to $X_{\pi} = X_{\perp}$ at fields $H \gg H_o$. The magnitudes of $X_{\parallel}$ and H_o in any given case will depend on the temperature. When $T \to 0^oK$, $X_{\parallel} \to 0$, $H_2 \to H_o(0)$ and the

substances as FeO and FeF_2; specifically, according to the data cited in Ref. 11, at temperatures $T > 1/2T_c$ the susceptibility in $FeF_2(\theta/T_c = 1.48)$ falls more rapidly with decreasing temperature than in $FeO(\theta/T_c \cong 2.9)$, even if the curves are shifted to intersect at 0^oK. However, it must be noted that in substances characterized by a relatively high magnitude of the θ/T_c ratio, such as MnO ($\theta/T_c = 5$) the prediction fails to hold.

As noted above, the value of the critical field should depend on the temperature. This conclusion is confirmed in the results of investigations of $CuCl_2 \cdot 2H_2O$ monocrystals. Although this substance has a rhombic bipyramidal type structure, rather than a tetragonal one, it does exhibit a preferred magnetization direction and consequently one may expect qualitative agreement of experimental data with the dependence deduced from theory. Thus, according to Refs. 12 and 13, the value of the critical field, as expected, increases with the temperature: specifically, $H_o = 6500$ oersteds at 1.57^oK and 7460 oersteds at 3.02^oK. However, this increase is somewhat smaller than might be expected from the curve of Figure 2.

Investigations of proton resonance in $CuCl_2 \cdot 2H_2O$, reported in Refs. 12 and 14, make it possible to determine the temperature dependence of the mean magnetization of the ions from the magnitude of the splittings of the resonance lines, i.e., essentially to determine the magnetization of the sublattices; also, from the variation in symmetry of the resonance line polar diagrams (variation of the resonance line frequency with the orientation of the field relative to the crystallographic axes) it is possible to establish the antiferromagnetic Curie point with great accuracy.

These experiments indicate that up to 4^oK the observed temperature dependence of the magnetization is in close agreement with that found from equation (15), if we assume $T_c = 4.5^oK$. At higher temperatures the magnetization drops more sharply than predicted by equation (15). The divergence may, presumably, be explained by the influence of the short-range order.

In Ref. 14 it is shown that the antiferromagnetic Curie point in $CuCl_2 \cdot 2H_2O$ depends on the strength of the field applied during measurement: when the field is applied in a direction perpendicular to that of preferred magnetization, increasing the field from 0 to 9000 oersteds ($H > H_c$) causes a drop of less than 0.002^oC in the Curie point temperature; when the field is applied in the preferred magnetization direction, increasing the field produces a marked change in T_c, from $T_{c_1} = 4.33^oK$ with $H < H_o$ to $T_{c_2} = 4.29^oK$ with $H > H_o$ in conformity with the prediction based on the theory.

The change in Curie point may be due either directly to the influence of the magnetic field (see discussion in Ref. 15) or to the change in the orientation of the lattice magnetizations in a field equal to the critical one.

According to Ref. 15, the critical field H_{cr} leading to destruction of the antiferromagnetic ordering at 0^oK in the substance investigated is $H_{cr} = kT_c/\mu_o = 63{,}000$ oersteds which is one order of magnitude higher than the critical field H_o producing reorientation in the lattice magnetizations. Hence, there is reason to affirm that the marked alteration in the value of T_c in fields approximating H_o is due to a change in the orientation of lattice magnetizations.

From (30) and (24) it follows that the following relationship holds between the change in Curie point temperature T_c, the critical field at $0^\circ K$, $H_0(0)$, and the perpendicular susceptibility:

$$H_0^2(0) = \frac{Nk\Delta T_c}{\chi_\perp}. \qquad (31)$$

Substituting the value of the perpendicular susceptibility $170 \cdot 10^{-6}$ measured at $T < T_c$ (Ref. 10) in (31), we obtain $H_0(0) = 10{,}600$ oersteds. The perpendicular susceptibility can also be evaluated from the Curie-Weiss law (28) by substituting the experimental values $\theta' = 5^\circ K$ and $T = T_c = 4.3^\circ K$ therein. In this case, $X_\perp = X(T_c) = 280 \cdot 10^{-6}$ while $H_0(0)$ from (31) equals 6450 oersteds. In both cases we obtain satisfactory qualitative (and in the latter case, also, quantitative) agreement of theoretically predicted with experimental values. However, it must be noted that the reason for the disparity between the two computed values for the perpendicular susceptibility is, as yet, not clear.

5. In conclusion, the principal results of our calculations may be summarized as follows:

1) There has been deduced an expression for the susceptibility of antiferromagnetic monocrystals, taking account of the susceptibility anisotropy, for the region of relatively high temperatures (up to the antiferromagnetic Curie point).

2) There has been obtained an expression for the temperature dependence of the criticalfield, above which this anisotropy should vanish. (Author's note in preparing the manuscript for publication: Ref. 16 appeared subsequent to the presentation of this report at the Conference on Magnetism; the authors derive an equation identical with (24) and cite experimental data confirming its validity.)

3) There has been deduced an expression describing the anisotropy of the antiferromagnetic Curie point.

4) It has been shown that a well-defined relationship exists between the square of the critical field measured at $0^\circ K$, the magnitude of the change in the Curie point temperature in a field equal to the critical field and applied in the direction of preferred magnetization and the value of the perpendicular susceptibility.

5) It has been shown that the character of the temperature dependence of the susceptibility and the critical field should vary with the magnitude of the ratio of the paramagnetic to the antiferromagnetic Curie point.

6) It has been shown that the susceptibility anisotropy, the critical field and the Curie point anisotropy are determined solely by the dependence of the energy of the antiferromagnetic on the orientation of the elementary magnetic moments relative to the crystal axes, which, in turn, is determined by the quasi-classical magnetic and exchange interaction.

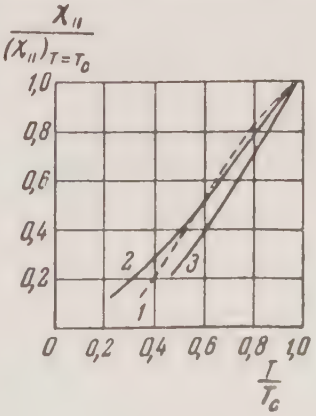

Fig. 3. Comparison of experimental curves of the temperature dependence of the parallel susceptibility for MnF_2 (Curve 2) and FeF_2 (Curve 3) with the theoretical curve (Curve 1).

Physics of Metals Institute,
Ural Branch of the Academy
of Sciences of the USSR

Received
3 May 1954

Bibliographic References

1. R.P.Ozerov, Usp. fiz. nauk, 47, 445 (1952).
2. L.Landau, Sow. Phys., 4, 675 (1933).
3. L.Neel, Ann.de phys.,18, 5 (1932); 5, 232 (1936); 3, 1937 (1948).
4. J.H.Van Vleck, J.Chem.Phys., 9,85 (1941); J. de phys.et rad.,12,262 (1951).
5. P.W.Anderson, Phys. Rev., 83, 1260 (1951).
6. S.V.Vonsovski, Zhur.eksp. i teor.fiz.,10, 762 (1940); S.V.Vonsovski and Ia.S.Shur, Ferromagnetizm (Ferromagnetism). GITTL, M.-L. 1948.
7. J.W.Stout & L.M.Matarrese, Rev. Mod. Phys., 25, 338 (1953).
8. W.J. de Haas,B.H.Schultz & J.Koolhaus, Physica, 7, 57 (1940).
9. H.Bisette & B.Tsai, C.R., 212, 119 (1941).
10. J.Van den Handel, H.M.Gijsman & N.J.Poulis, Physica, 18, 862 (1952).
11. H.Bisette, Ann. de phys., 1, 233 (1946).
12. C.J.Gorter, Rev. Mod. Phys., 25, 332 (1953).
13. N.J.Poulis & G.E.G.Hardeman, Physica, 18, 315 (1952).
14. N.J.Poulis & G.E.G.Hardeman, Physica, 18, 429 (1952).
15. C.G.B.Garret, J.Chem.Phys., 19, 1154 (1951).
16. N.J.Poulis & G.E.G.Hardeman, Physica, 20, 7 (1954).

* * * * * * *

ROTATION OF THE PLANE OF POLARIZATION OF CENTIMETER WAVES BY A FERRITE DISC

- K. M. Polivanov, Ia. N. Kolli and M. B. Khasina

The rotation of the plane of polarization of centimeter waves by longitudinally magnetized ferromagnetic materials is generally analogous to the Faraday effect in the optical wavelengths, but differs from the latter 1) as regards intensity and 2) in that, in the case of microwaves, the thickness of the rotation-producing layer may be of the same order of magnitude as the wavelength.

Rotation of the plane of polarization can find a number of applications in microwave technology, for example, in the design of current actuated antenna switches, modulating and controlling the radiated power, isolating a generator from waves reflected by the load, etc. (Refs. 1-4). Investigation of this effect may also be helpful in gaining an understanding of the physics of magnetization processes in high-frequency fields and in the development of new magnetic materials.

In the investigation covered by the present report we observed the rotation of the plane of polarization produced by Grade 0-400 nickel-zinc ferrite* and deduced the fundamental equations for a simple system (plane wave in an infinite plate of finite thickness), equations which permit determining the possible effect of a number of factors, not always taken into account.

Experimental Procedure

The experimental set-up employed was an analog of the Faraday optical system and was similar to the set-up described by Hogan (Refs. 1 and 2). Two rectangular waveguides were joined by a transition piece, the center section of which was a circular waveguide containing the ferrite disc. The ferrite disc was held in a special mount (Fig. 2), inserted at the middle joint of the circular waveguide. The mounting permitted rotating one of the rectangular sections relative to the other, with provision for accurate reading of the relative angle. The circular

---

* The authors are indebted to the laboratory headed by N. N. Shol'ts for preparing the specially shaped specimens of ferrite used in the investigation.

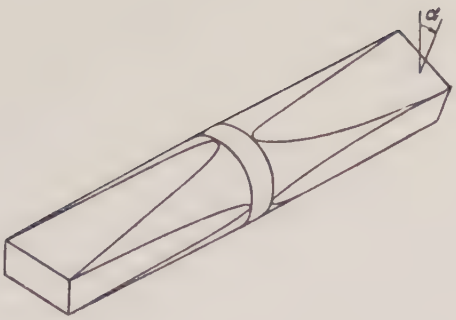

Fig. 1. Schematic sketch of two rectangular waveguides separated by a transition piece comprising a circular waveguide section; α - angle of rotation of one rectangular waveguide relative to the other.

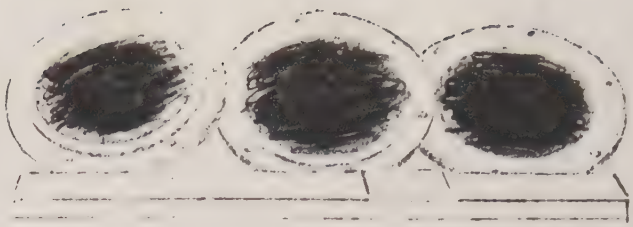

Fig. 2. Ferrite discs inserted in central section of the circular waveguide.

waveguide was surrounded by a coil to magnetize the ferrite disc in a direction parallel to the axis of the waveguide.

The cross section of the rectangular waveguides was such that it would support only TE modes, with the E vector directed perpendicular to the long side of the section. Suitable devices were inserted in the transition sections to absorb other modes.

The angle of rotation of the plane of polarization was measured in the following manner. A linearly polarized wave entering the circular section from the waveguide coupled to the oscillator, changes its angle of polarization and in passing through the ferrite disc is transformed into an elliptically polarized wave (see discussion below). A detector located in the second rectangular waveguide is connected to a suitable measuring instrument, by means of which the electric field strength in this second waveguide could be measured. As the second waveguide was rotated relative to the first, the indications of the instrument varied, reaching a maximum when the linearly polarized wave coincided with the major axis of the polarization ellipse. When the rectangular waveguide was turned $\pm 90^{\circ}$ from this position, the reading of the instrument reached a minimum; at this point the transmitted wave corresponded to the magnitude of the minor axis of the polarization ellipse. The ellipticity of the waves leaving the ferrite disc can be determined from the ratio of the field strengths at the two positions of the waveguide. The ellipse of polarization may be characterized by the ellipticity in decibels:

$$d = 10 \log \frac{E_{max}}{E_{min}}$$

where E_{max} is the electric field intensity along the major axis of the ellipse and E_{min} is the intensity along the minor axis. Obviously, in accordance with this definition, true circular polarization will be characterized by $d = 0$, while linear polarization will be characterized by $d \to \infty$. For an ellipticity $d = 20$ db, the ratio of the field intensities in the two mutually perpendicular directions (in one of which the intensity is maximum) will be equal to 100.

Test Results

The principal experimental results - in the form of the variation of the angle of rotation of the plane of polarization with the magnetic field strength - are shown in Fig. 3.

An analysis of these results shows that the dependence of the angle of rotation on the thickness of the discs is non-linear: the ratio of the angle of rotation for the 10.5 mm thick disc to that for the 7 mm thick disc is 1.64 ± 0.03 at a frequency of 3040 mc and 2.0 ± 0.1 at a frequency of 2560 mc, whereas the ratio of the two thicknesses is 1.5. The decrease in the angle of rotation at lower frequencies may be explained by a reduction of the effective electrical length of the disc.

Figure 4 shows the dependence of the ellipticity of the polarization on the magnetic field. The decrease in ellipticity with increasing field strength is evidence that one of the circularly polarized components approaches gyromagnetic resonance.

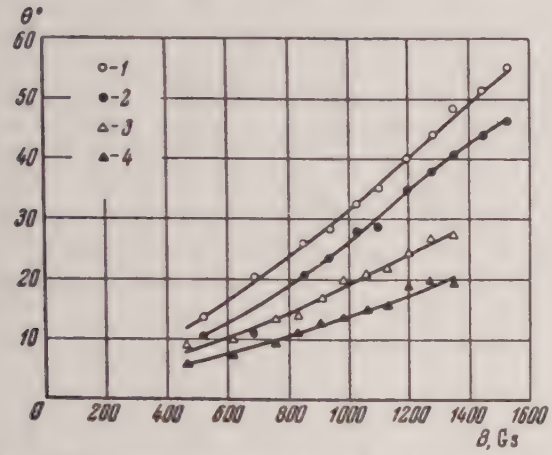

Fig. 3. Dependence of the angle of rotation of the major axis of the ellipse of polarization on the strength of the magnetic field parallel to the waveguide axis. Abscissa scale - mean values of the flux density at the surface of the discs. Curves 1 and 2 are for the 10.5 mm thick discs at frequencies of 3240 and 2560 mc, respectively. Curves 3 and 4, same for 7 mm thick discs.

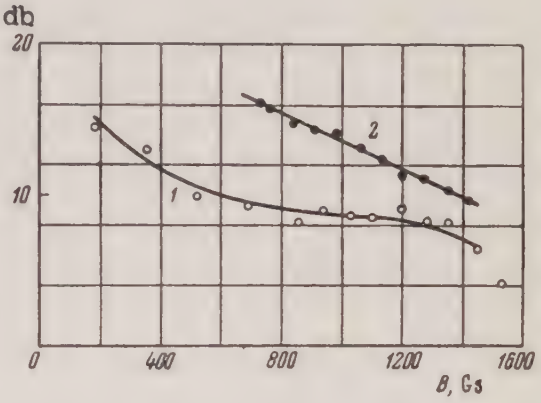

Fig. 4. Variation of the ellipticity coefficient d with the flux density at the surface of the discs: 1) curve for disc of thickness b = 10.5 mm; 2) curve for disc of thickness b = 7 mm.

Rotation of the plane of polarization by a plate of infinite extent and finite thickness

Let us analyze the case of a plane wave being propagated in the direction of the Z-axis through a plate or slab of finite thickness b, bounded by parallel walls, normal to Z. We assume the static magnetic field to be directed along the Z-axis. This field $B_0 = B_z$ produces magnetic gyrotropy of the medium.

Using the conventional method of complex quantities, the relationship between the varying components of the induction and of the magnetic field strength can be described by the following equalities:

$$\left.\begin{aligned} \frac{1}{\mu_0}\dot{B}_x &= \mu\dot{H}_x + i\mu_r\dot{H}_y, \\ \frac{1}{\mu_0}\dot{B}_y &= -i\mu_r\dot{H}_x + \mu\dot{H}_y, \\ \frac{1}{\mu_0}\dot{B}_z &= \dot{H}_z. \end{aligned}\right\} \qquad (1)$$

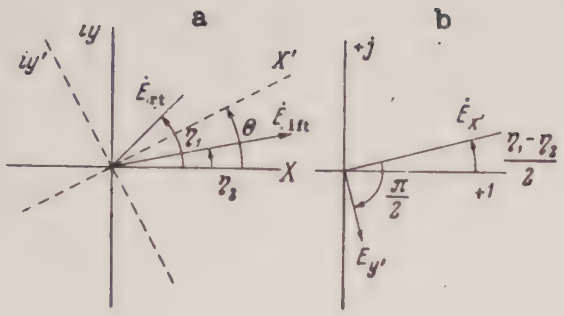

Fig. 5. Diagram for determining the direction of the principal axes of the polarization ellipse (x',y') for any given complex components of right and left circular polarization ($\dot{E}_{rt}$ and $\dot{E}_{lft}$) (a is the spatial and b is the temporal complex plane.) The arguments of the corresponding complex quantities indicate the phase at the initial instant (t = 0). The spatial components of the vector **E** at t = 0 are shown in the spatial plane (a).

where μ and μ_r are complex permeabilities; their imaginary components characterize the losses present; μ_r may be termed the gyrotropic permeability; μ_o is a constant, equal to $4\cdot10^{-9}$ H cm^{-1} in practical units. In converting from complex quantities to instantaneous values, we assume, in conformity with the usual rules, that the instantaneous value is obtained as the real part of $H_x = H_x e^{j\varphi x}$ multiplied by $e^{j\omega t}$, i.e., that

$$H_x(t) = \mathrm{Re}\,(\dot{H}_x e^{j\omega t}) = H_x \cos(\omega t + \varphi_x), \qquad (2)$$

or

$$2H_x(t) = \dot{H}_x e^{j\omega t} + \dot{H}^*_x e^{-j\omega t}. \qquad (3)$$

The asterisk * indicates a complex conjugate quantity.

In considering a plane wave, having components H and E lying in the plane X,Y (Fig. 5), it is convenient to regard this plane as a complex plane and represent the vectors as complex quantities. In this case the instantaneous value of the vector may be represented by an equation of the form

$$\mathrm{H}(t) = H_x(t) + iH_y(t), \qquad (4)$$

which does not preclude the possibility of expressing the instantaneous values through complex numbers in accordance with (2) and (3). Thus, if $\dot{H}_x = H_x e^{j\varphi x}$ and $\dot{H}_y = H_y e^{j\varphi y}$, we have

$$\mathrm{H}(t) = \frac{1}{2} H_x \left[e^{i(\omega t+\varphi_x)} + e^{-i(\omega t+\varphi_x)}\right] + i\frac{1}{2} H_y \left[e^{i(\omega t+\varphi_y)} + e^{-i(\omega t+\varphi_y)}\right] \qquad (5)$$

or after appropriate grouping of the terms:

$$\mathrm{H}(t) = \dot{H}_{rt} e^{i\omega t} + \dot{H}_{lft} e^{-i\omega t}, \qquad (6)$$

where

$$2\dot{H}_{rt} = \dot{H}_x + i\dot{H}_y \quad \text{and} \quad 2\dot{H}_{lft} = \dot{H}^*_x + i\dot{H}^*_y \qquad (7)$$

are the complex amplitudes of the right and left circularly polarized waves; they coincide with the corresponding components of the space vectors at the initial instant (t = 0).

From equation (7), it is clear that the time-dependence of the x and y components can be expressed in terms of ordinary complex quantities according to the equations:

$$\dot{H}_x = \dot{H}_{rt} + \dot{H}^*_{lft} \quad \text{and} \quad i\dot{H}_y = \dot{H}_{rt} - \dot{H}^*_{lft}. \qquad (8)$$

It must be emphasized that in the expressions for $\dot{H}_x$ and $\dot{H}_y$ the argument is equal to the phase only at t = 0 and does not represent the angle of rotation of the vector in the X,Y plane.

The sinusoidally varying magnitudes of the magnetic-induction, electric-field-intensity and electric-displacement vectors can be represented in the same fashion.

Thus, from (1) and (7), we find

$$\dot{B}_{rt} = (\mu + \mu_r)\mu_0 \dot{H}_{rt} \quad \text{and} \quad \dot{B}_{lft} = (\mu - \mu_r)\mu_0 \dot{H}_{lft}. \tag{9}$$

Applying Maxwell's equations to the vectors of an electromagnetic field in a gyrotropic medium (we assume that as regards electrical properties the medium is isotropic and characterized by a complex dielectric constant ξ) and resolving the vectors into components with left and right circular polarization, we obtain

$$\frac{d^2\dot{H}_{rt}}{dz^2} = \gamma_1^2 \dot{H}_{rt} \quad \text{and} \quad \frac{d^2\dot{H}_{lft}}{dz^2} = \hat{\gamma}_2^2 \dot{H}_{lft} \tag{10}$$

where

$$\gamma_{1,2} = i\frac{2\pi}{\lambda_0}\sqrt{\varepsilon(\mu \pm \mu_r)} = i\alpha_{1,2} + \beta_{1,2}. \tag{11}$$

The symbol $\hat{}$ in (10) designates the conjugate value of the corresponding complex variable; i.e.,

$$\hat{\gamma}_2 = -i\frac{2\pi}{\lambda_0}\sqrt{\hat{\varepsilon}(\hat{\mu} - \hat{\mu}_r)}. \tag{12}$$

The solution of (10) is obviously

$$\left.\begin{aligned} \dot{H}_{rt} &= \dot{A}_1 e^{\gamma_1 z} + \dot{B}_1 e^{-\gamma_1 z}, \\ \dot{H}_{lft} &= \dot{A}_2 e^{\hat{\gamma}_2 z} + \dot{B}_2 e^{-\hat{\gamma}_2 z}. \end{aligned}\right\} \tag{13}$$

The first and second terms on the right in the last equations are readily interpreted as the magnetic field vectors of waves propagated in the - or + direction along z and, accordingly, right or left circularly polarized.

From Maxwell's first equation we can readily find the expression for the vectors of the electric field intensity:

$$\left.\begin{aligned} \dot{E}_{rt} &= i\zeta_1(\dot{A}_1 e^{\gamma_1 z} - \dot{B}_1 e^{-\gamma_1 z}), \\ \dot{E}_{lft} &= i\hat{\zeta}_2(\dot{A}_2 e^{\hat{\gamma}_2 z} - \dot{B}_2 e^{-\hat{\gamma}_2 z}); \end{aligned}\right\} \tag{14}$$

here

$$\zeta_{1,2} = 120\pi\sqrt{\frac{\mu \pm \mu_1}{\varepsilon}} \quad \text{(in ohms)} \tag{15}$$

Equations (12) and (15) show that both the propagation constant and the wave impedance in a gyrotropic medium are different for right as against left circularly polarized waves.*

In investigating the propagation of electromagnetic waves in a gyrotropic medium it may be advantageous to use the mean (in time) value of the Umov-Poynting vector, expressed in terms of the right and left polarized components introduced by equations (5), (6) and (7):

$$Y_Z = \mathrm{Im}\,(\dot{E}^*_{rt}\dot{H}_{rt} + \dot{E}^*_{lft}\dot{H}_{lft}) \tag{16}$$

---

* The fact that the wave impedance, too, is different is often forgotten.

field dependence of the full susceptibility conforms to the relationship deduced by Neel (Ref. 3).

We now turn to the temperature dependence of the full susceptibility. In the case of weak fields $H \ll H_0$, $\Psi = \beta$ and the temperature dependence of the full susceptibility, as given by (25), is wholly determined by the temperature dependence of $X_{\parallel}$ and $X_{\perp}$. In the case of strong fields ($H \gg H_0$), $X_{\pi} = X_{\perp}$.

The perpendicular susceptibility, according to (23) should not depend on the temperature, while the parallel susceptibility, according to (21), should increase with increasing temperature from 0 at $T = 0^{\circ}K$ to $X_{\parallel} = X_{\perp}$ at $T = T_c$.

This last conclusion is in accord with deductions based on the theory of Néel and Van Vleck (Refs. 3 and 4). Moreover, as it follows from (21), the form of the $T - X_{\parallel}$ curve should be determined by the magnitude of the ratio of the paramagnetic Curie point θ' to the antiferromagnetic Curie point T_c; the smaller the ratio, the steeper should be the gradient of the curve (slope relative to the temperature axis) near T_c.

The dependence of the differential susceptibility on the field or temperature can readily be determined from (27) and the corresponding dependence of X_{π}. Obviously, $X_{diff} \geqslant X_{\pi}$, since in the range of field strengths in question (i.e. fields for which the conditions $\Delta y \ll y$ and $\alpha \ll \Psi$ are satisfied), $X_{\pi} > 0$ and $\partial X/\partial H > 0$.

According to (24), the value of the critical field H_0 should increase with the temperature, from $H_0(0) = \left[\frac{N(P'-Q')}{\chi_{\perp}}\right]^{1/2}$ at $T = 0^{\circ}K$ to $H_0(T_c) = \left[\frac{3}{2}\left(1 + \frac{\theta}{T_c}\right)\right]^{1/2} H_0(0)$ at $T = T_c$. This increase should depend on the magnitude of the ratio θ/T_c. The variation of the relative critical field $H_0/H_0(0)$ with the relative temperature T/T_c predicted by theory for the case when $\theta = T_c$ is shown in Figure 2.

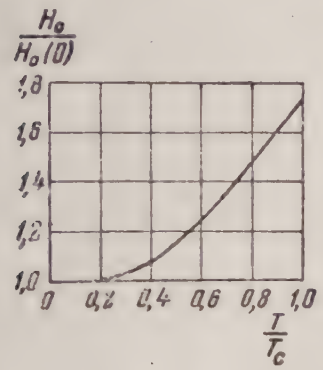

Fig. 2. Variation of the relative strength of the critical field with the relative temperature as predicted by theory.

An important conclusion that may be drawn from the above calculations is that, according to (16), the antiferromagnetic Curie point should depend on the magnitude of the angle between the direction of magnetization in the sublattices and the direction of preferred magnetization.

In this connection it must be noted that in the case of ferromagnetic materials the concept of a Curie point has validity only when the external field $H = 0$, since in such materials the field establishes a ferromagnetic ordering above the Curie point as well; in the case of antiferromagnetics, on the other hand, the external field cannot establish an antiferromagnetic ordering. Hence, it is meaningful to speak of an antiferromagnetic Curie point not only when $H = 0$ but also in the presence of an external field (generally speaking, a relatively weak field for which the conditions $\Delta y \ll y$ and $\alpha \ll \Psi$ are fulfilled, since with stronger fields destruction of the antiferromagnetic ordering by the field is possible). Accordingly, the

effect of the direction of magnetization on the Curie point may be evaluated as follows. Assume a field applied in the direction of preferred magnetization ($\beta = 0$). In this case if $H < H_0$, then $\Psi = 0$ and the Curie point, according to (16), equals $T_{c_1} = \frac{(P - Q) + (P' - Q')}{k}$; if $H > H_0$, then $\Psi = 90^\circ$ and $T_{c_2} = \frac{(P - Q)}{k}$; i.e., the antiferromagnetic Curie temperature should be reduced by

$$\Delta T_c = T_{c_1} - T_{c_2} = \frac{P' - Q'}{k}; \qquad (30)$$

In the case of polycrystalline materials in a field $H > H_c$ instead of a Curie point, it is more correct to speak of a Curie temperature range $T_{c_1} > T > T_{c_2}$, within which the differently oriented crystals go over into the antiferromagnetic state at different temperatures.

4. Let us compare the functional dependences deduced above with experimental data.

First, it must be noted that we cannot expect close quantitative agreement inasmuch as the method of energy centers of gravity is valid essentially only in the region of temperatures above the Curie point and applicable only with certain reservations in the vicinity of the Curie point. Moreover, the subdivision of antiferromagnetics into magnetic sublattices near the Curie point may be less legitimate than such subdivision near absolute zero. However, bearing in mind that in the case of ferromagnetics theoretical functional dependences deduced by the method of energy centers of gravity are in fairly close agreement with experimental data, we may reasonably expect at least satisfactory qualitative agreement in the case of antiferromagnetics.

The temperature dependence of the parallel and perpendicular susceptibility is given in Ref. 7. Figure 3* shows comparative curves for the theoretical dependence of parallel susceptibility (dash line) and the experimentally determined dependence for MnF_2 and FeF_e. The agreement is fairly satisfactory, particularly in view of the considerations outlined above. The perpendicular susceptibility according to the same investigators (Ref. 7) increases in MnF_2 and decreases in FeF_2 with decreasing temperature, whereas theory predicts that $X_\perp$ should remain constant. The discrepancy may be due to inadequacy of the theory or it may be due to the fact that the investigators themselves measured only the difference $X_\parallel - X_\perp$ and obtained the temperature dependence of the two susceptibilities by computation, utilizing data on the resultant susceptibility in a polycrystal reported by other authors (Refs. 8 and 9), which procedure could lead to erroneous results. In fact, this is not improbable since other investigators (Ref. 10), who measured the perpendicular susceptibility in $CuCl_2 \cdot 2H_2O$ ($T_c = 4.3^\circ K$) directly, showed that $X_\perp$ is virtually temperature independent. These investigators also report that, with fields $H > H_0$, the susceptibility measured in different crystallographic directions becomes equal to $X_\perp$, which is in accord with the theory.

The prediction of the theory that the form of the temperature dependence curve of the parallel susceptibility (and, consequently, for polycrystals, of the resultant susceptibility, as well) is determined by the magnitude of the ratio θ/T_c is confirmed experimentally for such

---

* See page 45.

In particular, application of this expression to the solutions (13) and (14) confirms the interpretation of the right and left polarized components as being proper to the direct and return waves, respectively.

Returning to our problem of the rotation of the plane of polarization by a plate of infinite extent and finite thickness b (Fig. 6), let us subdivide all space into three regions, where regions I and III are filled with air, while region II (the plate) is filled with a gyrotropic medium. Having written the general expressions for all the components of the electric and magnetic field intensities, let us specify continuity of the corresponding components at the surfaces of separation. This is the commonly accepted procedure in solving the problem of the refraction or reflection of plane waves in an isotropic medium. The distinguishing feature in our case is that in a gyrotropic medium (region II) the values of the wave impedance and of the propagation constant differ for right and left polarized waves.

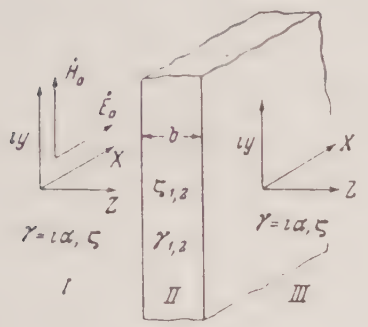

Fig. 6. Diagram for the determination of the rotation of the plane of polarization by a plate of infinite extent and finite thickness b.

In the table below, we give expressions for all the components, comprising in all 12 constants (parameters). Obviously, from the conditions at the two boundary surfaces we can derive eight equations. Consequently, for the solution of our problem (if the parameters of the medium and the thickness of the plate are known) we must be given the values of four constants. These values are determined by the specific attributes or conditions of the system. The conditions closest to those obtaining with the set-up described above are the following.

In region I, we have a known direct (incident) linearly polarized wave; its amplitude at the surface of the plate (z = 0),

$$\dot{E}_{x,+} = \dot{E}_{\text{пл},+} + \dot{E}^{*}_{\text{отр},+} = -i\zeta_0 (\dot{P}_1 - \dot{P}_2) = \dot{E}_0 \quad (17)$$

can readily be related to the field intensity produced by the oscillator. To do this, however, we must know the conditions of excitation of the waveguide and the value of the x component of the return (reflected) wave, characterized by the parameters $\dot{R}_1$ and $\dot{R}_2$. These are readily expressed through the constants $\dot{P}$.

Components of the electromagnetic waves in the three regions

Region	Field Vectors	Right, +	Right, −	Left, +	Left, −
III	H				
	E				
II	H				
	E				
I	H				
	E				

In accordance with the excitation conditions, the direct wave has no y component in region I, i.e.,

$$\dot{E}_{y+} = -\zeta_0(\dot{P}_1 + \dot{P}_2) = 0. \tag{18}$$

Since we are free to select the initial instant, we can, from (17) and (18), set

$$\dot{P}_1 = -\dot{P}_2 = P = \frac{i}{2\zeta_0}\dot{E}_0 = \frac{1}{2}\dot{H}_0. \tag{19}$$

We note that condition (18) does not imply the absence of a reflected wave with a y component; however, the absorbing device inserted in the transition piece between the waveguides absorbs this wave without reflection.

Applying the boundary conditions separately for the right and the left polarized components, we obtain the sought system of equations. Thus, for continuity of $\dot{E}$ and $\dot{H}$ at the boundary between regions I and II, we have for the right polarization components

$$\left.\begin{aligned} P - \dot{R}_1 &= \zeta_1' (\dot{F}_1 - \dot{G}_1), \\ P + \dot{R}_1 &= \dot{F}_1 + \dot{G}_1, \end{aligned}\right\} \tag{20}$$

where

$$\zeta_1' = \frac{\zeta_1}{\zeta_0}. \tag{21}$$

For a complete solution of our problem, we must know the conditions at the end of region III, which would enable us to establish the relation between A_1 and B_1, and A_2 and B_2. Such conditions might be those of a short circuit ($\dot{E}_{1ft} = \dot{E}_{rt} = 0$) at a known distance from the surface of the plate, the absence of the reflected y component of the field intensity together with a short circuit at a known distance for the x component, or other conditions consonant with the design of the experimental set-up in question. In the following example, we will assume the absence of reflected waves:

$$\dot{B}_1 = \dot{B}_2 = 0 \tag{22}$$

In this case at the boundary between regions II and III, where $z = b$ and z_3 may conveniently be taken equal to zero, we have the following conditions for the components with right polarization:

$$\left.\begin{aligned} \dot{A}_1 &= \zeta_1' (\dot{F}_1 e^{-\gamma_1 b} - \dot{G}_1 e^{\gamma_1 b}), \\ \dot{A}_1 &= (\dot{F}_1 e^{-\gamma_1 b} + \dot{G}_1 e^{\gamma_1 b}). \end{aligned}\right\} \tag{23}$$

From these equations we can readily find

$$\dot{F}_1 = \dot{A}_1 \frac{1+\zeta_1'}{2\zeta_1'} e^{\gamma_1 b} \quad \text{and} \quad \dot{G}_1 = -\dot{A}_1 \frac{1-\zeta_1'}{2\zeta_1'} e^{-\gamma_1 b}, \tag{24}$$

and from (20)

$$2P = (1+\zeta_1')\dot{F}_1 + (1-\zeta_1')\dot{G}_1. \tag{25}$$

Substituting the values of F_1 and G_1 from (24) in (25) and transposing as necessary, we get

$$\dot{E}_{rt} = -i\zeta_0 \dot{A}_1 = \frac{-i2\zeta_1\zeta_0^2 P}{(\zeta_0^2 + \zeta_1^2)\operatorname{sh}\gamma_1 b + 2\zeta_1\zeta_0 \operatorname{ch}\gamma_1 b}. \tag{26}$$

Analogously, for the left polarization, we find

$$\dot{E}_{1ft} = -i\zeta_0 \dot{A}_2 = \frac{-i2\hat{\zeta}_2\zeta_0^2 P}{(\zeta_0^2 + \hat{\zeta}_2^2)\operatorname{sh}\hat{\gamma}_2 b + 2\hat{\zeta}_2\zeta_0 \operatorname{ch}\hat{\gamma}_2 b}. \tag{27}$$

Now let

$$\dot{E}_{rt} = E_1 e^{i\eta_1} \quad \text{and} \quad \dot{E}_{1ft} = E_2 e^{i\eta_2} \tag{28}$$

In this case the major axis of the ellipse of polarization of the E(t) vector is rotated through an angle

$$\theta = \frac{1}{2}(\eta_1 + \eta_2) \tag{29}$$

relative to the X-axis, lying in the plane of polarization of the incident wave. The ratio of the major to the minor axis of the ellipse is

$$K = \left|\frac{E_1 + E_2}{E_1 - E_2}\right|; \tag{30}$$

the ellipticity (in decibels)

$$d = 10 \log K \tag{31}$$

The above assertions are readily verified: taking a new system of coordinates in which the axes x' and y' are displaced by θ relative to the x and y (Fig. 5), we find that in the new system

$$\left.\begin{aligned} \dot{E}_{rt} &= E_1 e^{i(\eta_1 - \theta)} = E_1 e^{i\left(\frac{\eta_1 - \eta_2}{2}\right)} \\ \dot{E}_{1ft} &= E_2 e^{i(\eta_2 - \theta)} = E_2 e^{-i\left(\frac{\eta_1 - \eta_2}{2}\right)} \end{aligned}\right\} \tag{32}$$

Consequently, according to (8), in this new system

$$\left.\begin{aligned} \dot{E}_{x'} &= (E_1 + E_2) e^{i\frac{\eta_1 - \eta_2}{2}}, \\ \dot{E}_{y'} &= (E_1 - E_2) e^{i\left(\frac{\eta_1 - \eta_2}{2} - \frac{\pi}{2}\right)}. \end{aligned}\right\} \tag{33}$$

We note again that the arguments of (33) represent the phase only at the initial instant (t = 0) of the corresponding sinusoidal functions

$$\left.\begin{aligned} E_{x'}(t) &= (E_1 + E_2)\cos\left(\omega t + \frac{\eta_1 - \eta_2}{2}\right), \\ E_{y'}(t) &= (E_1 - E_2)\sin\left(\omega t + \frac{\eta_1 - \eta_2}{2}\right). \end{aligned}\right\} \tag{34}$$

The deduced expressions for E_{rt} and E_{1ft} characterize the dependence of the rotation of the plane of polarization on the parameters of the medium $\zeta_{1,2}$ and $\gamma_{1,2}$ and on the thickness of the plate. This dependence is rather complicated and cannot be expressed simply in terms of a numerical constant, dimensioned in degrees rotation per centimeter path length through the gyrotropic medium.

That is, a numerical value can be derived for any particular case, but it will be determined not only by the properties of the plate (disc) but also by its thickness. The above treatment of the problem shows that in the general case the rotation of the polarization also depends on the conditions obtaining in front (region I) and back (region III) of the plate.

In some cases the effect produced by changes in the "in front" and "in back" conditions is scarcely noticeable either because the newly reflected waves are comparatively weak or because the resultant additional

rotation is virtually the same for both the $\dot{E}_{rt}$ and $\dot{E}_{lft}$ vectors. Thus, in the experiments referred to above, changes in the position of the short-circuiting piston produced no apparent difference in the results.

From our solution of the problem it is obvious that the waves propagated through the plate are elliptically rather than linearly polarized; pure rotation of the plane of polarization will occur only in the case where the moduli of $\dot{A}_1$ and $\dot{A}_2$ are equal.

In the case of a feeble gyrotropic effect, such as is observed in paramagnetic materials in the form of Faraday rotation, the last condition is virtually satisfied. Thus, for paramagnetic media with a low value of gyrotropic permeability, we can assume

$$\left.\begin{aligned} &\zeta_1 \approx \zeta_2 \approx \zeta_0, \\ &\gamma_1 \approx i\alpha_1 = i(\alpha_0 - \theta), \\ &\gamma_2 \approx -i\alpha_2 = -i(\alpha_0 + \theta). \end{aligned}\right\} \qquad (35)$$

Then, from (26) and (27), we have

$$\left.\begin{aligned} \dot{E}_{rt} &= \tfrac{1}{2}\,\zeta_0 P e^{-i\left[(\alpha_0-\theta)b+\frac{\pi}{2}\right]}, \\ \dot{E}_{lft} &= \tfrac{1}{2}\,\zeta_0 P e^{i\left[(\alpha_0+\theta)b+\frac{\pi}{2}\right]}. \end{aligned}\right\} \qquad (36)$$

Obviously, with the above values of $\dot{E}_{rt}$ and $\dot{E}_{lft}$ we will obtain a linearly polarized wave with the plane of polarization rotated through an angle Θb relative to the plane of polarization of the incident wave ($P_1 = -P_2 = P$). Multiplying $\dot{E}_{rt}$ by $e^{i\omega t}$ and $\dot{E}_{lft}$ by $e^{-i\omega t}$, we obtain a vector quantity (in the complex plane) representing the instantaneous value of the electric field intensity at the plate boundary and in region III:

$$E(t) = \zeta_0 P \frac{e^{i\left(\omega t-\alpha_0 b-\frac{\pi}{2}\right)} + e^{-i\left(\omega t-\alpha_0 b-\frac{\pi}{2}\right)}}{2} e^{i\theta b} = E_0 \cos\left(\omega t - \alpha_0 b - \frac{\pi}{2}\right) e^{j\theta b}. \qquad (37)$$

This vector will always be directed at an angle Θb relative to the X-axis and, hence, the rotation of the plane of polarization, in this case, will be directly proportional to the thickness of the plate. Obviously, Θ is an algebraic quantity and the angle of rotation can be negative as well as positive. In particular, when the direction of the magnetic field is positive ($B_0 = B_z = \text{const}$), μ_r is positive and the angle $\alpha_1 = \alpha_0 - \theta > \alpha_2 = \alpha_0 + \theta$ as follows from (11).

Moscow Energetics Institute
Imeni V. M. Molotov

Received
16 May 1954

Bibliographic References

1. C.L.Hogan, Bell System Tech. Journ., 31, 1 (1952).
2. C.L.Hogan, Rev. Mod. Phys., 25, 253 (1953).
3. F.F.Roberts, Journ. de phys. et rad., 12, 305 (1951).
4. N.G.Sakiotis & H.N.Chait, Proc. IRE, 41, 87 (1953).

ON MEASURING PARAMAGNETIC RESONANCE ABSORPTION BY THE STANDING WAVE METHOD IN THE CENTIMETER WAVE BAND

- N. N. Neprimerov

1. Theoretical Considerations

Paramagnetic resonance absorption has been the subject of numerous studies in recent years; the two methods commonly employed in investigating absorption are the one based on measuring the power of waves transmitted through a resonance cavity containing the investigated substance and the method based on measuring the power of the waves reflected from the substance. In addition to these two, there is yet a third method, based on measuring the parameters of standing waves in a waveguide. This method was suggested by Birks (Ref. 1) for the study of ferromagnetic resonance and was subsequently perfected by Lazukin (Ref. 2) and Shekhtman (Ref. 3). The principal advantage of this method is that it permits determining a rigorous theoretical relationship between the investigated characteristics of the substance and the measured parameters of the rf network. Thus, if we consider the plane, monochromatic wave transmitted through the waveguide together with the wave reflected from the short circuit in front of which is located a layer of the substance being investigated, we can deduce a general expression for the dependence of the complex dielectric constant and magnetic permeability on the displacement of the minimum Δ and the voltage standing wave ratio r. We will not reproduce the general expression here (see Refs. 2 and 4), but will only give the formulas derived for the imaginary and real parts of the complex magnetic susceptibility $X = X' - j X''$,* for the particular case when it is permissible to neglect the quadratic terms relating to X and to assume that the dielectric constant ε is not dependent on the applied external magnetic field:

$$\chi'' \approx \frac{\lambda^2}{\pi\varepsilon\lambda_B dr} = \frac{C}{r} \qquad (1)$$

and

$$\frac{\operatorname{tg} 2\pi\left(\frac{d}{\lambda}\sqrt{\varepsilon(1+4\pi\chi')-\left(\frac{\lambda}{\lambda_K}\right)^2}\right)}{\frac{d}{\lambda}\sqrt{\varepsilon(1+4\pi\chi')-\left(\frac{\lambda}{\lambda_K}\right)^2}} = \frac{\lambda_B}{d}\operatorname{tg} 2\pi\left(\frac{\Delta+d}{\lambda_B}\right), \qquad (2)$$

where λ is the wavelength in free space, λ_B is the wavelength in the guide and λ_K is the cut-off wavelength. Taking advantage of the fact that X' is negligibly small, (2) can be greatly simplified and reduced to

$$\chi' = D + E\Delta, \qquad (3)$$

where D and E, like C in (1), are constants, dependent on the values of ε, d, λ, λ_B and λ_K.

Equations (1) and (2) are similar to the ones deduced in Ref. 2; it follows from these equations that the paramagnetic absorption coefficient X'' [i.e. the imaginary part of the high-frequency susceptibility] is essentially proportional to the change in r, while the dispersion of susceptibility is linearly related to the displacement of the minimum.

---

* Translation editor's note: Here, and in the next article, as in the preceding "antiferromagnetism" article, to facilitate typing, X will be used as the equivalent of chi in the text.

In the conventional methods of resonance investigation, the paramagnetic absorption coefficient X" is obtained as a function of the applied magnetic field in relative units. Up to the present, absolute measurements of paramagnetic resonance absorption have been made only for eight salts as reported in Refs. 5 and 6. In addition Rivkind (Ref. 7), working at a frequency of 10^7 mc made absolute determinations of the coefficient X" in the absence of an external magnetic field. The method of standing waves also permits of working out a procedure for making absolute determinations of the coefficient X". To this end, in view of the constant character of the load, which varies only under the influence of the external magnetic field, we can equate the ratio of the power of the incident to the power of the reflected wave to the ratio of the squares of their amplitudes and, by carrying out the appropriate transformations, bring this equality to a form convenient for experimental work:

$$\frac{W_{ref}}{W_{inc}} = \left(\frac{r - 1}{r + 1}\right)^2 = \gamma \qquad (4)$$

Having the attenuation coefficient γ, one can easily find the part of the high-frequency energy absorbed by the substance. Let the power emitted by the generator be unity, then

$$1 - \gamma = \sigma \qquad (5)$$

and to determine the purely magnetic loss, we need only find the difference

$$\sigma_{total} - \sigma_{diel} = \varkappa \qquad (6)$$

where σ_{total} = the total loss and σ_{diel} = the dielectric loss, determined at the maximum intensity of the magnetic field when, it may be assumed, magnetic-dipole transitions are wholly absent. Obviously, the apparent losses, caused by reflection from the load when this is mismatched, will distort the absolute values of σ_{total} and σ_{diel}, but since they figure equally in the expressions for both, the net effect on the difference will be virtually nil.

The value of $\varkappa$ computed from (6) characterizes the mean value of the high-frequency magnetic field energy absorbed per cycle; hence, the product of $\varkappa$ times the frequency ν will determine the absorption coefficient $A_{(sec)}$, for which theory yields the following expression (Ref. 8):

$$A_{(sec)} = 16\pi^2\chi''\nu = \varkappa\nu. \qquad (7)$$

The sought value of X" is found from (7); converted to cm^3 per ion dimensions:

$$\chi'' = \frac{1}{2} \cdot \frac{\varkappa M v}{16\pi^2 N P n}, \qquad (8)$$

where M is the molecular weight of the substance, v is the volume, P is the weight of the investigated salt, N is the number of ions per mole, n is the number of ions per molecule; the constant 1/2 is introduced in view of the fact that the wave passes through the sample twice.

2. Description of set-up and measuring procedure

The experimental set-up employed consisted of a reflection oscillator (Klystron), an attenuator, a measuring line with a movable probe and detector, a matching device and a short-circuited waveguide section into which the investigated salt was placed in the form of a plane-parallel layer. The Klystron anode was supplied from an electronic stabilizer; the heaters and reflector plate were powered from storage batteries, as was the electromagnet. The magnetic field was measured by a fluxmeter with an accuracy of ±2%.

To minimize errors due to reflection from the probe and deviations of the crystal detector characteristic from the square law, the values of r and Δ were measured at the level of double the minimum of the standing wave. In this case the theory of measurement at microwave frequencies (see Ref. 4) gives the following expression for the standing wave ratio:

$$r^2 = 1 + \cos^2\left\{\frac{\pi(x-y)}{\lambda_B}\right\} \approx \frac{1}{\left\{\frac{\pi(x-y)}{\lambda_B}\right\}^2}, \qquad (9)$$

where x and y are the measured coordinates of the probe at double the minimum level. The approximate equation (9) involves an error of less than 1% when $r \geqslant 1.33$ and hence may be regarded as an exact equality.

The use of a reducing gear and a special indicating device made it possible to measure x and y to within 0.0005 cm.

In addition to matching by means of a tuning stub, all tests were run using specimens of half-wave thickness in order to insure better matching of the load (Ref. 9). The value of the dielectric constant, needed to determine the wavelength in the substance, was found experimentally on the same set-up.

The theoretical basis for determining ε is a graphic solution of (2), in which the term in parentheses under the square root can be set equal to unity by virtue of the fact that X' is very small. However, the values of ε so obtained are not the dielectric constants of the paramagnetic salts proper but of a mixture of these salts with air and are, therefore, strongly dependent on the packing. To find the true dielectric constants we made use of the following equation for dielectric mixtures, suggested in Ref. 10:

$$\log |\varepsilon_c| = v \log |\varepsilon| - (1 - v) \log \varepsilon_o \qquad (10)$$

where the subscript $_c$ refers to the mixture, while the subscript $_o$ refers to the solvent or diluent. In our particular case ε_c refers to air, while the last term can be neglected. The applicability of (10) was checked by comparing the computed values with measurements made on monocrystals. Thus, for example, for a crystal of $CuSO_4 \cdot 5H_2O$, the average of measurements at three different thicknesses d was $\varepsilon_{monocr} = 6.50 \pm 0.15$. For powdered specimens, the average for three thicknesses was $\varepsilon_{powd} = 4.30 \pm 0.50$, while the value computed from equation (10) was $\varepsilon = 6.60 + 0.15$.

The values of ε for the investigated salts are listed in the last column of Table 1.

Experimental results

The results of our measurements for thirteen different salts of Cr, Mn, Fe and Cu are summarized in Table 1.

The measured values of the coefficient X''_{max} at maximum absorption are given in column 2. For purposes of comparison, the theoretical values of this coefficient computed according to the following equation from Ref. 11:

$$\chi'' = \chi_0 \frac{\sqrt{\pi}}{2} \cdot \frac{\nu}{\nu_i} \left\{ e^{-\left(\frac{\nu-\nu_0}{\nu_i}\right)^2} + e^{-\left(\frac{\nu+\nu_0}{\nu_i}\right)^2} \right\}. \qquad (11)$$

are listed in column 3.

As may be seen from the figures, agreement in most cases is satisfactory, the divergence between theoretical and experimental values being within the limits of the experimental error. The greatest deviations occur in the cases of $CrCl_3$ and $MnSO_4(NH_4)_2SO_4 \cdot 6H_2O$; they are, apparently, due to deviation of the curves from the Gaussian distribution (see Figs. 3 and 4).

As Al'tshuler notes (Ref. 12), some investigators have used a simplified equation for the absorption coefficient, differing from (11) by the absence of the second exponential term, but having a coefficient double that in (11) in the first term. In the case of very high frequencies, when it may be assumed that $\nu \gg \nu_i$ (i.e. for $\nu \gtrsim 10^{10}$ mc), the second term is negligibly small and consequently the value of X''_{max} obtained from (11) will be only half that computed according to the simplified equation. A comparison of the data in columns 2 and 3 indicates that the values computed according to the equation given by Al'tshuler, Zavoiski and Kozyrev (Ref. 11) are the correct ones.

Our experimental data were checked by means of the integral relationship between the paramagnetic absorption and the static susceptibility established by Al'tshuler (Ref. 12):

$$\chi_0 - \chi'(0) = \frac{\pi}{2} \int_0^\infty \frac{F(H_1)}{H_1} dH_1 = \chi_{0\,exp}, \qquad (12)$$

where

$$F(H_1) = \chi''(H_1) - \chi''(0) \frac{e^{-\left(\frac{\nu+\nu_0}{\nu_i}\right)^2}}{e^{-\left(\frac{\nu}{\nu_i}\right)^2}}. \qquad (13)$$

It will be noted that X'(O), i.e., the value of the magnetic susceptibility in the absence of an external magnetic field, enters into (12). This can be computed according to the following equation, derived by Shaposhnik (Ref. 13) and experimentally verified by Rivkin (Ref. 7):

$$\chi'(0) = \frac{\chi_0 \rho_s \nu}{1 + \rho_s^2 \nu^2}. \qquad (14)$$

Here ρ_s is the spin-spin relaxation time, which is of the same order of magnitude as $1/\nu_i$. It can readily be seen that at the high frequencies used in our experiments, X'(O) will amount to less than 1% of X_o and, hence, can be disregarded. The values of $X_{o\,exp}$, computed according to (12) are given in column 4 of the table. In the next column are known, measured values of the static susceptibility. Divergences between the two sets of values, in most cases, do not exceed 5-15%. The agreement may be considered satisfactory, particularly in view of the fact that the accuracy of the experimental data is known not to be high.

Cummerow, Holliday and Moore (Ref. 5) and Lacroix and Exterman (Ref. 14)* used the following semi-empirical equation to check their results.

---

* Lacroix and Exterman referred their relative measurements of X" to the absolute value at the maximum given by Cummerow, Holliday and Moore (Ref. 5).

Table 1

Paramagnetic resonance absorption in Cr, Mn, Fe and Cu salts

(All values of χ'' and χ_0 in 10^{-25} cm^3/ion.)

Substance	χ''_{exp}	χ''_{theor}	χ_{0exp}	χ_0	σ'	σ''	ε
$CrCl_3$	1,40±0,15	2,0	0,12 ± 0,01	0,117	160±15	240±15	13,5±0,3
CrF_3	0,32±0,05	0,31	0,07 ± 0,01	0,074	660±30	770±30	13,7±0,3
$MnSO_4$	1,10±0,15	1,0	0,22 ± 0,03	0,24	660±30	860±30	8,4±0,2
$MnSO_4.H_2O$	2,20±0,2	2,1	0,25 ± 0,03	0,24	310±20	400±20	9,90±0,2
$MnSO_4\{NH_4\}_2SO_4.6H_2O$	1,10±0,15	0,60	0,28 ± 0,03	0,24	1200±50	1400±50	7,7±0,2
$MnCl_2.4H_2O$	0,40±0,04	0,39	0,20 ± 0,03	0,24	1820±50	1860±50	9,6±0,25
$MnCO_3$	1,10±0,1	1,0	0,25 ± 0,03	0,24	640±25	800±25	12,8±0,3
$Fe_2\{SO_4\}_3\{NH_4\}_2SO_4.24H_2O$	0,90±0,08	0,80	0,20 ± 0,02	0,24	740±25	880±50	4,3±0,3
$Ca_3Fe_2\{SO_4\}_3$	1,50±0,3	1,70	0,10 ± 0,02	0,14	220±20	260±20	—
$CuSO_4.5H_2O$	0,30±0,03	0,26	0,024 ± 0,003	0,026	300±20	360±20	6,6±0,15
$Cu(NO_3)_2.6H_2O$	0,40±0,05	0,38	0,028 ± 0,005	0,028	200±15	360±15	5,0±0,2
$Cu\{NH_3\}_4SO_4.H_2O$	0,70±0,09	0,65	0,028 ± 0,005	0,024	100±20	200±20	7,0±0,2

$$\chi_o = \frac{2S}{\pi H_{res}} \qquad (15)$$

Lacroix and Exterman (Ref. 14) obtained an area S under the resonance absorption curve 20% smaller than that reported in Ref. 5. They explain the difference as being due to the effect of the rotation of the plane of polarization on the form of the absorption curve.

We measured the Faraday rotation at centimeter wave frequencies (Ref. 15) and from our results it is apparent that with the orientation of the high-frequency and static magnetic fields obtaining in the set-up used by Cummerow, Holliday and Moore the rotation of the plane of polarization is negligibly small. The distortion of the absorption curve should rather be attributed to the influence of the dispersion of susceptibility and efflorescence of the salts (see below). We recalculated the curves given by these authors, using equation (12). The results are shown in Table 2, where the values for $\chi_{o\ exp}$ from Refs. 5 and 14, determined according to equation (14) are given in columns 2 and 3, while the corresponding values recalculated by us according to (12) are listed in columns 4 and 5. As will be seen, the recalculated values are in closer agreement with data derived from the static susceptibility.

Table 2

Results of recalculation of paramagnetic resonance absorption measurements reported by other authors

(all values of χ_o in 10^{-25} $cm^3 ion^{-1}$)

Substance	$\chi_{o\ exp}$ from Ref. 5	$\chi_{o\ exp}$ from Ref. 14	Ref. 5 values recalc. accord. to (12)	Ref. 14 values recalc. accord. to (12)	χ_o
$MnCl_2 \cdot 4H_2O$	0.32	-	0.21	-	0.25
$MnSO_4 \cdot 4H_2O$	0.30	0.25	0.26	0.23	0.25
$CuSO_4 \cdot 5H_2O$	0.024	-	0.024	-	0.024

The values of δ " shown in Table 1 are half-widths of the paramagnetic resonance absorption curves. In some cases our values differ appreciably from those reported by other authors. Thus, Ting and Williams (Ref. 16) obtained δ " = 610 oersteds from $CrCl_3$. Bagguly and others (Ref. 17) report a value of 50 oersteds for the same salt. Our value of δ " = 160 oersteds, which agrees with the data in Ref. 18 and the results given in Refs. 7, 19 and 20, may be regarded as the more dependable one, since it is based on absolute determinations and has been verified by the methods outlined above. The value obtained by a group of Japanese investigators (Ref. 6 and 21) for $MnSO_4(NH_4)_2SO_4 \cdot 6H_2O$ -- about 70 oersteds - is also doubtful. Not only is this value at variance with our result - 1200 oersteds but it is inconsistent with the structural character of the line.

An interesting conclusion regarding the half-width of the absorption curves can be drawn for the case of manganese sulfate. The numerous determinations of paramagnetic resonance in this salt, made both for the

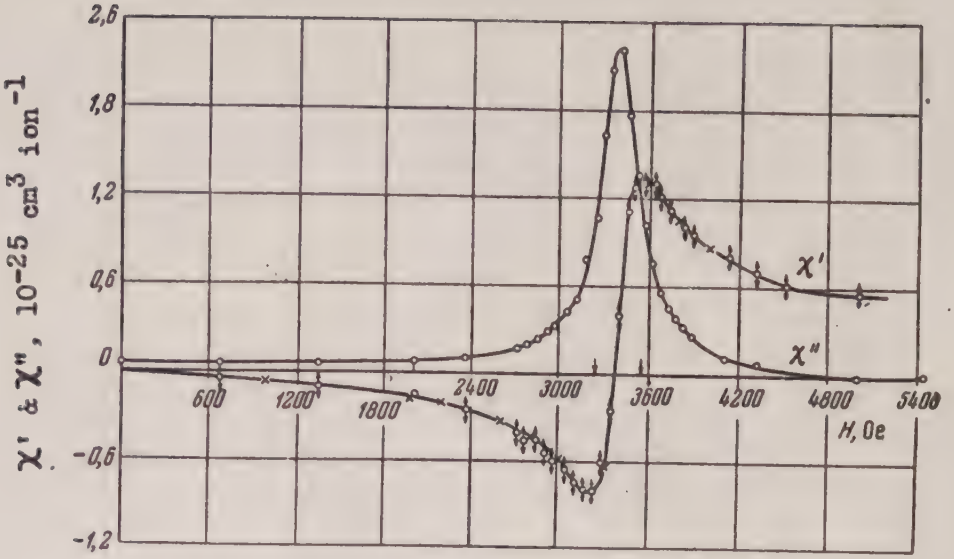

Fig. 1. Paramagnetic resonance absorption curve (X") and dispersion curve (X') for $MnSO_4 \cdot H_2O$.

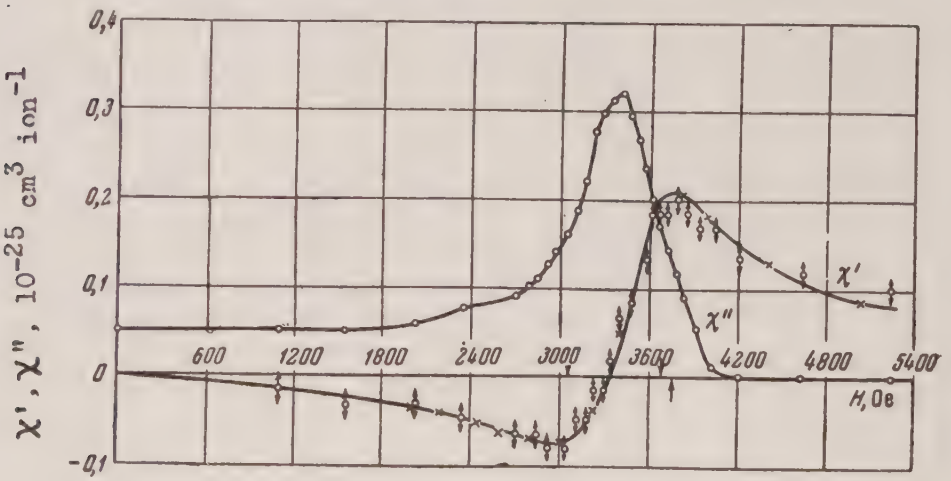

Fig. 2. Paramagnetic resonance absorption curve (X") and dispersion curve (X') for CrF_3.

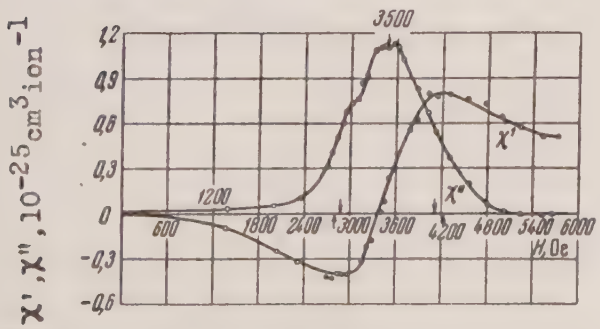

Fig. 3. Paramagnetic resonance absorption curve (X") and dispersion curve (X') for $MnSO_4(NH_4)_2SO_4 \cdot 6H_2O$.

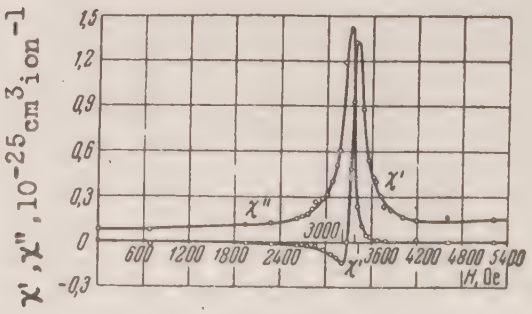

Fig. 4. Paramagnetic resonance curve (X") and dispersion curve (X') for $CrCl_3$.

anhydrous salt (Refs. 7, 18 and 20) and for the tetrahydrate (Refs. 5, 14 and 22) yielded values of δ'' lying in the interval from 300 to 500 oersteds, which is in the neighborhood of the value of 340 oersteds for the monohydrate. Our value of 660 oersteds for anhydrous $MnSO_4$ (the sample was roasted at 250° immediately before measurement), which agrees with the value given in Ref. 6, and the value of $\delta'' = 1140$ oersteds reported for $MnSO_4 \cdot 4H_2O$ in Refs. 6 and 21 would appear to indicate that the monohydrate form of manganese sulfate is the most stable one.

In addition to absorption, the dispersion of susceptibility (in relative units) in perpendicular fields was measured for all the salts listed above. Knowing the form of the absorption line, the dispersion of susceptibility curves can be computed by means of the following integral equation given by Al'shuler (Ref. 12):

$$\chi_0 - \chi'(H) = \frac{1}{\pi}\int_0^\infty \frac{F(H+H_1) - F(H-H_1)}{H_1}\, dH_1, \qquad (16)$$

Such curves were obtained for low frequencies ($\nu \approx 10^8$ mc) by Romanov (Ref. 19), while at high frequencies, one such curve has been determined by Kozyrev, Salikhov and Shamonin (Ref. 18).

We carried out the appropriate calculations for $MnSO_4 \cdot H_2O$ and CrF_3. The computed dispersion curves (χ') are plotted in Figs. 1 and 2, together with the paramagnetic resonance absorption curves (χ''). Experimental data, with the relative values referred to the point, corresponding to the maximum value of χ', have been plotted as circles with arrows, the lengths of which are proportional to the experimental error. As may be seen from the diagrams, the agreement is satisfactory. In view of this, in Figs. 3 and 4 we have plotted the dispersion curves (χ') with all relative values referred to the one point for which the magnitude of χ' was computed according to equation (16).

From the experimental results obtained, within the limits of experimental error, one can draw the following conclusions:

1) The difference δ' between the intensities of the magnetic field corresponding to the maximum and minimum values of χ' is greater than δ'', the half-width of the absorption curve.

2) The difference between the maximum and minimum values of χ' as a function of H equals the magnitude of χ''_{max}.

3) At values of H_{res} corresponding to χ''_{max}, the χ' curve is close to χ_0; a deviation is observed in cases of asymmetry of the absorption curve.

4) At $H = 2H_{res}$, the value of χ' is close to $2\chi_0$.

Kazan' State University
Imeni V. I. Ul'yanov-Lenin

Received
3 May 1954

Bibliographic References

1. J.B.Birks, Proc. Phys. Soc.,60, 282 (1948).
2. V.N.Lazukin, Izv.(Bulletin) AN SSSR,Ser.fiz.,16,510 (1952).
3. I.A.Shekhtman, Izv.(Bulletin) AN SSSR,Ser.fiz.,16, 498 (1952).
4. Tekhnika izmerenii na santimetrovykh volnakh (Microwave measurement techniques). Pub.by "Soviet Radio", M. 1949.
5. R.L.Cummerow, D.Holliday & G.E.Moore, Phys. Rev., 72, 1233 (1947).
6. H.Kumagai & others, Phys. Rev., 82, 954 (1951).
7. A.I.Rivkin, Izv. (Bulletin) AN SSSR,Ser.fiz.,16,541 (1952).
8. C.Gorter, Paramagnetnaia relaksatsiia (Paramagnetic relaxation), M. 1949.
9. I.V.Grebenshchikov, Prosvetlenie optiki (Coating lenses),M.-L. 1946.

10.K.Lichtenecker, Phys. ZS., 19, 374 (1918).
11. S.A.Al'tshuler, Zavoiski & Kozyrev,Zhur.eksp.i teor.fiz.,17,1122 (1947).
12. S.A.Al'tchuler, Zhur. eksp. i teor. fiz., 20, 1047 (1950).
13. I.G.Shaposhnikov, Thesis, FIAN, 1949.
14. R.Lacroix & R.Exterman, Physica, 17, 427 (1951).
15. N.N.Neprimerov, Zhur.eksp. i teor. fiz., 26, 4, 511 (1954).
16. Y.Ting & W.D.Williams, Phys. Rev., 82, 507 (1951).
17. Bagguly & others, Proc. Phys. Soc., 61, 551 (1948).
18. B.M.Kozirev, Salikhov & Shamonin, Zhur.eksp.i teor.fiz.,22, 56 (1952).
19. I.M.Romanov, Thesis, Kazan' State University, 1950.
20. Iu.Iu.Samitov, Zhur. eksp. i teor. fiz., 23, 734 (1952).
21. H.Kumagai & others, Phys. Rev., 83, 1077 (1951).
22. Lancaster & Cordy, J. Chem. Phys., 19, 1181 (1951).

* * * * * * *

ROTATION OF THE PLANE OF POLARIZATION IN PARAMAGNETIC SUBSTANCES AND FERRITES

- N. N. Neprimerov

A recent survey by Mikaelian (Ref. 1) of what is known about the rotation of the plane of polarization of radio waves (one might also mention a similar survey by Sokolov (Ref. 2), devoted to rotation effects in the optical region of the spectrum) is concerned mainly with discussion of the Faraday effect in ferromagnetic materials. Yet the effect at radio frequencies was originally discovered (Ref. 3) in paramagnetic materials and the first theory (Ref. 4) as well as later theoretical advances (Ref. 5) stemmed from experimental investigations (Refs. 6-8) of the effect in paramagnetics. Unfortunately, researches in this field have not, as yet, yielded any definite results. This is explained not so much by the weakness of the effect in paramagnetics as by the inadequacies of the experimental procedure: paramagnetic resonance absorption (hereinafter referred to as PRA) is also relatively weak, yet it has been investigated in greater detail than ferromagnetic resonance absorption.

The experimental methods employed hitherto in studying rotation of the plane of polarization both in paramagnetic (Refs. 3, 6, 7 and 8) and in ferromagnetic materials (Ref. 9 and 10) utilize, for radio waves, the basic arrangement borrowed from optics. However, the qualitative change in frequencies has led to a quantitative change in experimental technique. The fact that at radio frequencies the wavelengths used are commensurate with the dimensions of the specimen and the response of the analyzer resulted in large errors and a considerable loss of sensitivity, yet this very commensurability makes it feasible to develop bridge circuits for detecting the rotation, circuits which have no analogs in optics and which are extremely sensitive. Such experimental installations, one variant of which will be described below, not only permit direct investigation of paramagnetic resonance rotation (hereinafter referred to as PRR) but can also be used for the study of ferromagnetic materials in very thin layers and high magnetic dilutions, which, in conjunction with large external magnetic fields, should be useful in developing the pertinent theory.

The present article is devoted to the part of our investigation of a "gyrobicomplex" paramagnetic medium, concerned with the rotation of the plane of polarization. The other part of the investigation, devoted to measurements of the complex magnetic susceptibility and the complex dielectric constant of the same substances, is reported on in a separate article (Ref. 11 - the preceding article in the present Bulletin).

1. Measuring Procedure

The principal unit of the experimental set-up designed by us for investigating rotation of the plane of polarization is comprised by a complex 12-terminal waveguide assembly, possessing a high degree of symmetry. The assembly consists of two crossed rectangular waveguides connected to a circular waveguide so that the axis of the latter is parallel to the narrow sidewalls of the rectangular guides (see Fig. 1).

The theory of high-frequency transmission lines (Ref. 12) gives a dissipation matrix for such a waveguide assembly, on the basis of which one can establish a number of its properties; among these the following were utilized in designing the experimental set-up:

1) In some band of frequencies the assembly branches can be matched by means of three variable parameters, installed in the form of coaxial stubs in the bottom of the rectangular waveguides at the axis of the circular one.

2) In the matched condition, the power W entering through arm 1 will be distributed at the junction point so that half the power will enter the circular waveguide, while the other half will be equally divided between the arms 2 and 3. No power at all will flow into arm 4. Since arms 2 and 3 are connected parallel to arm 1, in the planes formed by the narrow sides of the waveguides 1 and 4 the phases of both waves (incident and reflected) will be equal, and in the case when the arms 2 and 3 are short circuited and equal in length the two reflected waves will coincide in phase at the junction point, while the reflected power will be distributed equally between arms 1 and 4. No power will enter the circular waveguide since the waves in it will have opposite polarizations and will cancel each other.

3) If one of the side arms is longer than the other by one-quarter the wavelength in the guide, the waves reflected from both arms will be 180° apart in phase at the junction point and the polarization produced by them in the circular waveguide will coincide with the axis of the short-circuited arms. In this case there will be propagated through the circular waveguide two waves, equal in amplitude but polarized at right angles to each other.

A block diagram of the set-up developed is shown in Fig. 2.

The bridge details are milled of brass angle members; all surfaces are finish lapped and silvered. The circular waveguide has a choke-flange joint and is removable. The two matched crystal detectors, connected to the instrument panel, are located in arms 2 and 3 at equal distances from the central junction point (see Fig. 3). All arms are shorted by non-contacting pistons; in one of the arms the piston can be displaced by means of a micrometer screw with a vernier scale reading to 5μ. The linear dimensions of the bridge were held to within 0.01 mm of the design specifications, while the angles were machined to Class I precision.

The magnetic field (maximum strength - 6000 oersteds) along the axis of the circular waveguide is applied by means of an electromagnet,

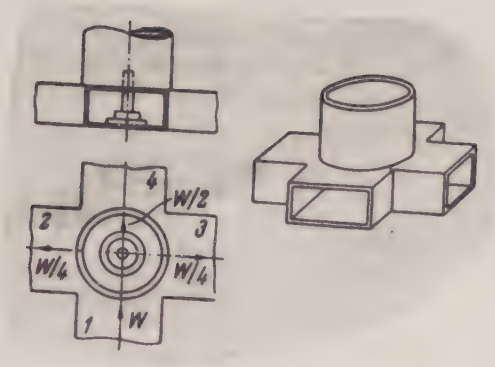

Fig. 1. Diagram and sketch of the 12-terminal waveguide assembly

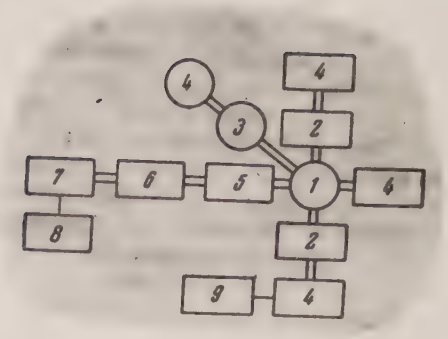

Fig. 2. Block diagram of set-up: 1- bridge, 2- detector, 3- specimen, 4- short circuit, 5- phase shifter, 6- attenuator, 7- oscillator, 8- power supply, 9- small displacements vernier-indicator.

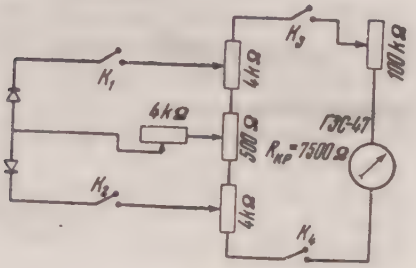

Fig. 3. Diagram of detector bridge. All resistances except 100 kΩ are wire resistors. Switches K_1, K_2, K_3 and K_4 are interlocked. The circuit is electrically and magnetically shielded.

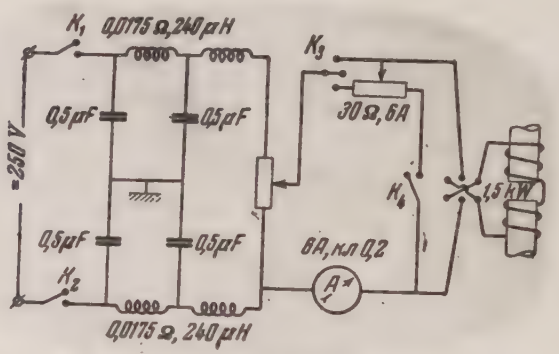

Fig. 4. Electromagnet power supply circuit. Roller type rheostat permits continuous adjustment. Ammeter scale has 3X optical magnifier. All parts and conductors after the filters have electric and magnetic shielding.

the power circuit for which is shown in Fig. 4. The magnet control was graduated according to a fluxmeter and subsequently calibrated with reference to paramagnetic resonance (accuracy approximately ±1.5%). The investigated paramagnetic salt or ferrite, suspended in paraffin, was placed in the form of a plane-parallel plate in front of the shorting piston in the circular waveguide. The thickness of the specimens in all cases was such that the "optical" length of the circular guide equalled exactly half the wavelength in the guide. The dielectric constant (required to compute the wavelength in the specimen) was determined experimentally at the same frequency (Ref. 11).

The microwave power W from the oscillator is fed through the buffer-attenuator and the phase shifter into arm 1 of the assembly (Fig. 2). In accordance with the second property of the assembly noted above, half the accepted power, W/2, enters the circular waveguide, is reflected from the short circuit (thus passing twice through the specimen) and arrives at the junction point in counterphase with the incident wave. In conformity with the reciprocity rule and the second property of the assembly, half this reflected power will go into arm 4 (Fig. 1), while the other half will be divided equally between the arms 2 and 3. With

the pistons in the waveguides suitably positioned, a standing wave pattern is established in the system. If the side arms are equal in length, the currents set up by the detectors in the arms of the balanced bridge circuit (Fig. 3) will be equal and the galvanometer will show a zero reading. It is worth emphasizing that despite the presence of absorption and dispersion in the specimen and, in fact, even in case of power or frequency drift the detector bridge remains balanced. This was checked in practice by varying the input power by 20-30 db and shifting the phase 180° and, also, by applying an external field perpendicularly to the axis of the circular waveguide. In such cases the detector in arm 4 indicated the presence of PRA, but the bridge remained in balance.

An entirely different pattern emerges when a magnetic field is applied parallel to the axis of the circular waveguide. The resultant rotation of the plane of polarization through an angle φ is equivalent to the appearance of a component polarized at right angles to the plane of polarization of the original wave. In this case the detector in one of the arms (2 or 3 depending on the sign of the rotation) will receive an additional amount of power equal to half that of the rotated component (in accordance with the second property of the assembly, as outlined above). The bridge will be unbalanced and the galvanometer will show a deflection proportional to the angle of rotation. However, in this case the remarks made above regarding the balanced bridge are no longer valid: the deflection of the galvanometer will be affected by both dispersion and absorption, although to a lesser degree than in other methods of measurement (Refs. 6-10).

This is where the linear dependence of the Faraday rotation on the field comes to our aid (as is known, dispersion and absorption do not depend on the direction of the field). All experimental curves are obtained as the half-sums of the commutated curves. This simple expedient not only makes it possible to eliminate the influence of dispersion and absorption almost entirely, but also provides an automatic check on the operation of the bridge.

The transition from purely qualitative determinations to quantitative measurements is made on the basis of the third property of the waveguide assembly. The unbalanced bridge can be brought back into balance by moving the piston in one of the arms: the angle of rotation is proportional to the linear displacement of the piston and can be computed from the equation

$$\varphi = \frac{\pi x}{\lambda_s} \qquad (1)$$

where x is the displacement of the piston and λ_s is the wavelength in the guide. Computing the rotation per unit length (thickness) then presents no difficulty.

The reproducibility of the absorption measurements and the accuracy of the calculations may be judged from the curve for $CuSO_4 \cdot 5H_2O$ reproduced in Fig. 5. The different points correspond to measurements made at different sensitivities, on different specimens and with an interval of several months between determinations. A further criterion of the dependability of the developed set-up and procedure is furnished by a comparison of our data with that cited by other authors.

The PRR curve for $MnCO_3$ is shown in Fig. 6. Here the points obtained by Gozzini are indicated by crosses; our points, by circles. The distortion of the curve and scattering of the points obtained by the earlier method are obvious.

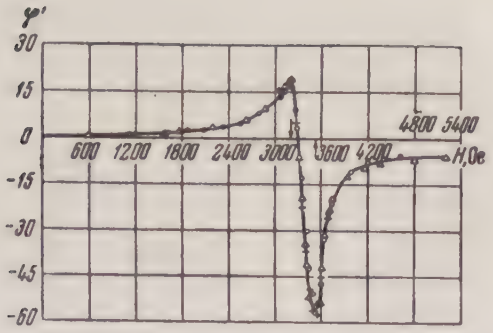

Fig. 5. PRR (rotation) curve for $CuSO_4 \cdot 5H_2O$. The differently plotted points correspond to three different determinations.

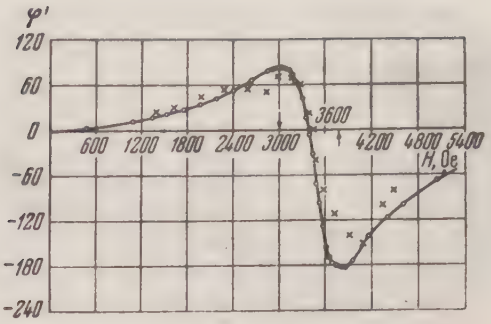

Fig. 6. PRR curve for $MnCO_3$. Crosses are values reported by Gozzini (Ref. 8); circles represent our data.

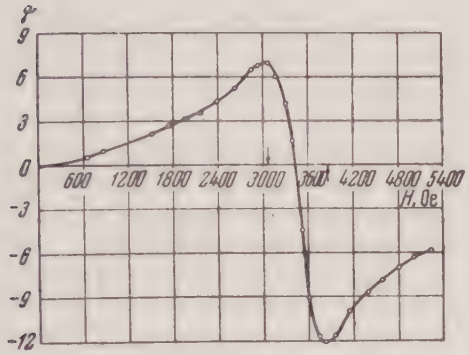

Fig. 7. PRR curve for $Cr_2(SO_4)_3 \cdot 18H_2O$.

The sensitivity of our set-up is clearly demonstrated by the curve for $Cr_2(SO_4)_3 \cdot 18H_2O$ reproduced in Fig. 7. The total rotation - i.e. the sum of the absolute values of the positive and negative angles of rotation - for this salt is about 19' The total swing of the galvanometer light spot corresponding to this angl was about 600 graduations, with a fluctuation of about one division on the scale. It follows that the approximate sensitivity of the set-up (i.e., the value of a graduation) is 2". Of course, the sensitivity shoul not be confused with the accuracy of measurement, which depends on the errors in determining the wavelength in the wave guide, λ_g, the displacement of the piston, x, the weight of the specimen, P, and the density of the material, d.

2. Results for Paramagnetic Materials

We made paramagnetic resonance absorption (PRR) determinations for twelve salts of the iron group. Specimens were prepared in the form of a homogeneous, finely ground powder, suspended in paraffin and were placed directly in the waveguide. When the specimen was truly plane-parallel full symmetry of the bridge was attained; this condition could readily be checked by rotating the circular waveguide about its axis.

The results of the tests with Cr^{+++}, Mn^{++}, Fe^{+++}, and Cu^{++} indicate that all substances having PRA also exhibit PRR. At the same time tests run at the extreme frequency adjustments of the Klystron, as well as the single curve, obtained at λ = 10 cm, given in Ref. 7, show that the dependence of the rotation, like that of paramagnetic absorption, on the frequency is quadratic.

The free ions of trivalent chromium are in the $^4F_{3/2}$ state; the g- factor determined for these ions from the PRA is close to 2, which is confirmed by the absorption characteristics. The rotation curves are distinctly asymmetric, with the negative rotation predominating

over the positive. The distance between extreme values is greater than the half-width δ'', determined from the absorption. Our measurements show that CrF_3 exhibits a somewhat greater rotation than might normally be expected: whereas the coefficient X" for CrF_3 is smaller than that for $CrCl_3$ by a factor of 1:5 (Ref. 11), the rotation is smaller by a factor of only 1:2 1/2.

For the Mn^{++} ions, which were investigated in greater detail, the g-factor is also close to 2, since these ions are in the $^6S_{5/2}$ state and their magnetism is due solely to the spin of the free electrons. The angles of rotation observed for some manganese salts are the largest found for any of the investigated materials. In contrast to the curves for salts of the other elements, the rotation curves for Mn^{++} salts, as a rule, are symmetric relative to a center line which lies in the region of negative angles and at the same time marks the point of resonance. With some approximation it may be said that the angles of rotation corresponding to strong fields tend toward a mean value of about 50'. In view of the isotropism of the g-factor for most bivalent manganese compounds, it may be assumed that the symmetry of the PRR curve could serve as an index to or criterion for this isotropism. Where comparison with the data of other authors is concerned, the choice of anhydrous $MnSO_4$ and $MnSO_4 \cdot 4H_2O$ for purposes of measurement is unfortunate, since, as was shown in the preceding article (Ref. 11), with the exception of the monohydrate, these salts tend to be very unstable as regards the water of crystallization; hence, measurements cannot fairly be referred to a definite form (hydrate). For example, in all probability the measurements reported in Ref. 6 were made not on the tetrahydrate but on a monohydrate specimen, as is apparent from the magnitude of the rotation and the half-width of the absorption curve reported. Gozzini's (Ref. 8) curve lies between our curves for the anhydrate and monohydrate. A more dependable basis for comparison is furnished by the data for $MnCO_3$ (see Fig. 7 above).

Only one trivalent iron salt (ions also in the $^6S_{5/2}$ state) - ammonium ferric alum - was investigated. Like the Mn^{++} salts, this salt exhibits a large total rotation. Whereas the PRA curve for this salt shows indications of structure, the rotation curve is smooth.

While for manganese salts, as noted above, symmetry of the rotation curve appears to indicate isotropism of the g-factor, the contrary would seem to be the case for the Cu^{++} salts investigated. X-ray analysis shows that these salts (Table 1) have two magnetic ions per elementary cell (Ref. 13). In spite of the polycrystalline character of the specimens, this apparently leads to signs of structure in the absorption curve (Ref. 11) and asymmetry of the rotation curve. By analogy one may assume that the asymmetry of the rotation curves for CrF_3 and $CrCl_3$ is due to anisotropy of the g-factor. Another possible cause for the asymmetry may be the influence of exchange forces.

So far, in our discussion of the experimental results, we have not touched upon the question of the nature and cause of the rotation. The PRR curves reproduced in Figs. 5-9 show that the rotation of the plane of polarization as a function of the external magnetic field has extreme values to both sides of the resonance point. The location of these extremums and the character of the dispersion curve give reason to think that there may be a deep-seated connection between the dispersion of magnetic susceptibility and paramagnetic resonance rotation. To facilitate qualitative comparison, we have assembled data characterizing

Table 1

Dispersion of magnetic susceptibility in salts of elements of the iron group

№ п/п	Grnd State	Substance	$\chi_0 \cdot 10^6$ (cm³/ion)	χ^-/χ^+	δ'	χ', 10^{-25} cm³/ion		$\frac{2\chi'}{\chi'(2H_{res})}$
						H_{res}	$2H_{res}$	
1	$^4F_{3/2}$	$CrCl_3$	1,45	$\frac{0,15}{1,30}=0,1155$	240	0,10	0,14	$\frac{2,90}{0,14}=20,7$
2	»	CrF_3	0,33	$\frac{0,11}{0,22}=0,5$	770	0,05	0,10	$\frac{0,66}{0,1}=6,6$
3	»	$Cr_2(SO_4)_3.18H_2O$						
4	$^6S_{5/2}$	$MnSO_4$	1,05	$\frac{0,45}{0,60}=0,75$	860	0,20	0,43	$\frac{2,10}{0,43}=4,9$
5	»	$MnSO_4.H_2O$	2,10	$\frac{0,80}{1,30}=0,62$	400	0,25	0,50	$\frac{4,20}{0,50}=8,4$
6	»	$MnSO_4(NH_4)_2SO_4.6H_2O$	1,20	$\frac{0,40}{0,80}=0,5$	1400	0,2	0,50	$\frac{2,40}{0,50}=4,8$
7	»	$MnCl_2.4H_2O$	0,50	$\frac{0,13}{0,37}=0,35$	1860	0,13	0,25	$\frac{1,0}{0,25}=4$
8	»	$MnCO_3$	1,0	$\frac{0,30}{0,70}=0,43$	800	0,20	0,32	$\frac{2,0}{0,32}=6,25$
9	$^6S_{5/2}$	$Fe_2(SO_4)_3(NH_4)_2SO_4.24H_2O$	0,83	$\frac{0,30}{0,53}=0,566$	880	0,16	0,30	$\frac{1,66}{0,30}=5,55$
10	»	$Fe_2Ca_3(SiO_4)_3$	1,50	$\frac{0,50}{1,00}=0,5$	260	0,25	0,32	$\frac{3,0}{0,32}=9,4$
11	$^2D_{5/2}$	$CuSO_4.5H_2O$	0,33	$\frac{0,08}{0,25}=0,32$	360	0,1	0,05	$\frac{0,66}{0,05}=13,2$
12	»	$Cu(NO_3)_2.6H_2O$	0,38	$\frac{0,14}{0,24}=0,580$	360	0,1	0,05	$\frac{0,76}{0,05}=15,2$
13	»	$Cu(NH_3)_4SO_4.H_2O$	0,64	$\frac{0,17}{0,47}=0,36$	200	0,1	0,075	$\frac{1,28}{0,075}=17,8$

respective curves in Tables 1 and 2. The absolute values of the overall dispersion of susceptibility and of the total rotation are shown in the respective fourth columns of the tables. With the exception of one salt (copper ammine) a certain correlation is traceable between corresponding values. The distances between the extreme values (extremums) or the half-widths δ^φ and δ' of the curves (δ^φ - the half-width of the PRR curve; δ' - the half-width of the PRA curve) coincide to within the experimental error; the coincidence of the extreme points is equally close.

What may be termed the characteristic of the symmetry of the curves - the ratio of the positive to the negative parts of the curves - is given in the next (5th) column. Despite the wide range of values (0.3 to 0.7), there is fairly close agreement in all cases. The correlation between the angle of rotation and the dispersion of susceptibility is further confirmed by the similarity in the relative locations of the points corresponding to H_{res} and $2H_{res}$ (see columns 7 and 8). The figures in the last columns provide a means for evaluating the intensity of the effect (extent of the absorption and rotation) relative to the values of X_0 and φ_0. The meaning of φ_0 will be explained in the next section.

Table 2

Paramagnetic resonance rotation in salts of elements of the iron group

№ п/п	Grnd State	Substance	φ'	φ^+/φ^-	δ	$\varphi'(H_{res})$	$\varphi'(2H_{res})$	$\frac{2\varphi}{\varphi(2H_{res})}$
1	$^4F_{3/2}$	$CrCl_3$	264	$\frac{28}{236}=0,1186$	280	5	20	$\frac{528}{20}=26,4$
2	»	CrF_3	103	$\frac{28}{75}=0,375$	780	5	20	$\frac{206}{20}=10,3$
3	»	$Cr_2(SO_4)_3.18H_2O$	18,9	$\frac{6,8}{12,1}=0,56$	800	1,5	6	$\frac{39,8}{6}=6,6$
4	$^6S_{5/2}$	$MnSO_4$	205	$\frac{85}{120}=0,71$	840	40	55	$\frac{410}{55}=7,5$
5	»	$MnSO_4.H_2O$	330	$\frac{138}{192}=0,72$	420	20	60	$\frac{660}{60}=11$
6	»	$MnSO_4(NH_4)_2SO_4.6H_2O$	107	$\frac{32}{75}=0,43$	1500	15	45	$\frac{214}{45}=4,75$
7	»	$MnCl_2.4H_2O$	42	$\frac{13}{29}=0,45$	1840	4	20	$\frac{84}{20}=4,2$
8	»	$MnCO_3$	264	$\frac{82}{182}=0,45$	800	18	60	$\frac{528}{60}=8,8$
9	$^6S_{5/2}$	$Fe_2(SO_4)_3(NH_4)_2SO_4.24H_2O$	185	$\frac{75}{110}=0,68$	840	30	35	$\frac{370}{35}=10,6$
10	«	$Fe_2Ca_3(SiO_4)_3$						
11	$^2D_{5/2}$	$CuSO_4.5H_2O$	72	$\frac{17}{55}=0,31$	320	15	7	$\frac{144}{7}=20,6$
12	«	$Cu(NO_3)_2.6H_2O$	80	$\frac{25}{55}=0,45$	400	0	7	$\frac{160}{7}=22,8$
13	»	$Cu(NH_3)_4SO_4.H_2O$	39	$\frac{10}{29}=0,34$	180	4	3	$\frac{78}{3}=26$

3. Comparison of Experimental Results with Theory

The theory of the rotation of the plane of polarization stems from the well-known Fresnel equation:

$$\frac{\varphi}{e}=\frac{\pi}{\lambda}(n^- - n^+), \qquad (2)$$

which gives the most general expression for the dependence of the angle of rotation on the indices of refraction for the right and left circularly polarized waves. As the first step toward providing a basis for comparing our results with theory, let us make the reasonable assumption that in a paramagnetic material the dielectric constant ε is independent of the applied external field H. In this case (2) can be simplified by applying the appropriate elementary transformations and brought to the form

$$\frac{\varphi}{e}=\frac{2\pi^2\sqrt{\varepsilon}}{\lambda}\mathrm{Re}\,\chi^{\mp}, \qquad (3)$$

where the ± sign refers to the variation of the magnetic quantum number m, the rule for the selection of which is $\Delta m = \pm 1; 0$. Utilizing the calculations made by Al'tshuler (Ref. 14) for the magnetic susceptibility

and corrections to the real part introduced by Romanov (Ref. 15), we can write the expression for the angle of rotation of the plane of polarization in the form:

$$\varphi(\nu) = \frac{2\pi^2 e \nu_0 \sqrt{\varepsilon}}{c} \chi_0 \left\{ 1 + \frac{\nu_0}{\nu} \left[e^{-\left(\frac{\nu-\nu_0}{\nu_i}\right)^2} \int_0^{\frac{\nu-\nu_0}{\nu_i}} e^{x^2} dx - e^{-\left(\frac{\nu+\nu_0}{\nu_i}\right)^2} \int_0^{\frac{\nu+\nu_0}{\nu_i}} e^{x^2} dx \right] \right\}, \quad (4)$$

where

$$\nu = \frac{g\beta H}{h}, \quad \nu_0 = \frac{g\beta H_{res}}{h}, \quad \nu_i = \frac{g\beta H_i}{h},$$

χ_0 is the static susceptibility, β is the Bohr magneton, h is Planck's constant and H_i is the internal magnetic field.

Strictly speaking, equation (4) is only a first approximation since assumptions made in its derivation are rigorously valid only for paramagnetic gases. However, in spite of this, it gives a fairly accurate description of the experimental results. Thus for high frequencies $\nu \geqslant 10^9$ mc, introducing the notation $\varphi_0 = \frac{2\pi^2 e \nu_0 \sqrt{\varepsilon}}{c} \chi_0$,

we have $\varphi(0) = 0$, $\varphi(H_{res}) = \frac{3}{4}\varphi_0$, $\varphi(2H_{res}) = \frac{5}{3}\varphi_0$ and, lastly, $\varphi(\infty) = \varphi_0$.

For a quantitative comparison we will use the experimental data for the dispersion of susceptibility and the values of the dielectric constant from Ref. 11 (the preceding article). The requisite data are assembled in Table 3.

Table 3

Quantitative comparison of the dispersion of magnetic susceptibility and paramagnetic resonance rotation

№ п/п	Substance	M	d	ε	ε''	Total susceptibility $\chi' \times 10^{-25}$ cm^3 ion^{-1}	$\varphi' = \frac{2\pi^2\sqrt{\varepsilon}}{\lambda} \cdot \frac{\chi' Na}{M}$	$\varphi = \frac{2\lambda}{\lambda_g (u^2_{mn} - n^2)}$	φ' wvgd
1	$CrCl_3$	158,38	2,757	13,5	32,4	1,45	117	118	264
2	CrF_3	109,01	3,80	13,7	2,46	0,33	51,5	47	103
3	$MnSO_4$	151,00	3,25	8,4	0,37	1,05	80,5	92	205
4	$MnSO_4.H_2O$	169,00	2,95	9,9	0,26	2,10	152	150	330
5	$MnSO_4(NH_4)_2SO_4.6H_2O$	391,24	1,831	7,7	0,15	1,20	19,2	48,5	107
6	$MnCl_2.4H_2O$	197,91	2,01	9,6	0,43	0,50	19,3	18,8	42
7	$MnCO_3$	114,94	3,125	12,8	1,79	1,0	120	120	264
8	$Fe_2(SO_4)_3(NH_4)_2SO_4.24H_2O$	962,42	1,719	7,2	0,25	0,83	5	84	185
9	$CuSO_4.5H_2O$	249,69	2,286	6,6	0,19	0,33	9,75	32,3	72
10	$Cu(NO_3)_2.6H_2O$	295,65	2,074	5,0	0,15	0,38	6,6	36,2	80
11	$CuSO_4(NH_3)_4.H_2O$	245,74	1,81	7,0	0,63	0,64	15,5	17,7	39

The experimental values of the angle of rotation given in Table 1 and Figs. 5-9 cannot be compared directly with the calculated values since they are obtained for conditions in a waveguide, which conditions are different from those in free space. The necessary correction may be approximated by means of the following equation from Ref. 16:

$$\varphi = \varphi_{wvgd} \frac{2\lambda}{(u^2_{mn} - n^2)\lambda_B}, \quad (5)$$

where for the mode employed $TE_{mn} = TE_{11}$ and u_{11} is the first root of the first derivative of the first Bessel function $J_1'(x)$. Substituting its value (from Ref. 17) gives us the correction coefficient of $\varphi = 0.438\varphi_{wvgd}$ for our set-up.

The corrected values of the angles of rotation together with the values computed according to (4) are listed in Table 3. Considering the large number of experimentally determined quantities comprised in equation (4), the agreement for most salts may be regarded as good. The apparent anomaly as regards the rotation in CrF_3 is now explained. However, it will be noted that now there is no quantitative agreement for four salts. The initial assumption that the divergences in the cases of these salts are due to the inapplicability of equation (5) in view of the large dielectric losses involved proved not to be justified since measurement of the dielectric loss tangents for these salts showed even smaller values than for the other salts.

4. Results of Measurements for Ferrites

The applicability of the developed procedure to ferrites was verified by measurements on two ferrites. Determination of the rotation of the plane of polarization in the vicinity of resonance was of particular interest. The ferrite samples were prepared in the form of a finely dispersed powder suspended in paraffin, the concentration ratio being 1:10. The real and imaginary parts of the magnetic susceptibility of the ferrite specimens were also investigated. The three curves for nickel-zinc ferrite are reproduced in Fig. 8; the curves for the manganese-zinc ferrite, in Fig. 9. From the shape of the real part of the susceptibility curves, it will be seen that the observed variation is consistent with that noted in Ref. 11 (preceding article) for the dispersion of susceptibility in paramagnetic materials:

1) the half-width of the curve, determined from the dispersion of susceptibility, is greater than the half-width of the absorption peak ($\delta' = 1.13\delta''$);

2) at the resonance value of the field, the dispersion curve passes through μ_o,

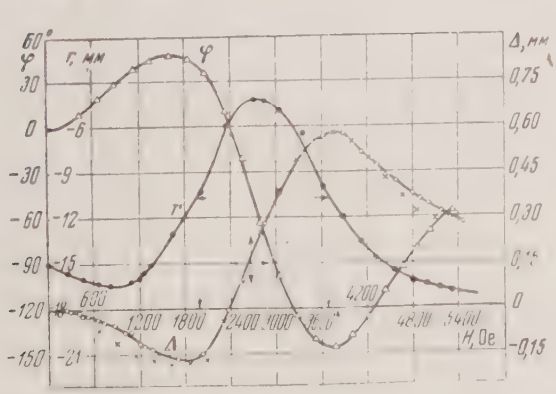

Fig. 8. Real and imaginary parts of the magnetic susceptibility and rotation of the plane of polarization for $NiO \cdot ZnO \cdot Fe_2O_3$ ferrite. (Composition: 25-25-50).

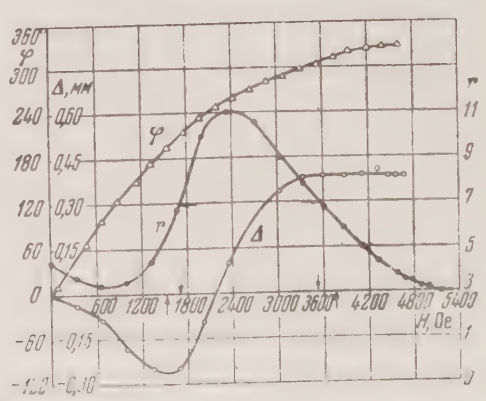

Fig. 9. Curves as in Fig. 8 but for $MnO \cdot ZnO \cdot Fe_2O_3$ ferrite. (Composition: 30-20-50)

3) when the field equals $2H_{res}$, the real part of the susceptibility is close to $2\mu_o$.

The rotation curves for the two investigated ferrites are different, whereas the curve for the nickel-zinc ferrite roughly parallels the dispersion of susceptibility curve, that for the manganese-zinc ferrite has the form common to ferrite curves found by other authors (Refs. 9 and 10), in spite of the fact that it passes through a point of resonance. A possible reason for the difference between the curves may be that while one of the ferrites was sintered, the other was not.

Principal Conclusions

1. We developed and tested in practice a new method for measuring the rotation of the plane of polarization; this method is based on the fact that the specimen, the analyzer and the wavelengths involved are of the same order of magnitude and has a number of advantages over earlier methods, to wit:

a) variations of the power and frequency of the incident wave do not affect the determination;

b) the method gives the angle of rotation as a function of the field H, virtually eliminating the influence of the dispersion of susceptibility and the absorption;

c) in the new method mechanical measurement of the angle of rotation is replaced by measurement of linear displacement, which increases the sensitivity to 2" and insures good reproducibility of results;

d) by taking advantage of the linearity of the effect, it permits measuring double the angle of rotation, thus increasing the accuracy;

e) it permits replacing the solenoid producing the external field in earlier set-ups by a conventional electromagnet with a narrow gap.

2. As a result of measurements on twelve salts of the iron group, we have established that all substances exhibiting paramagnetic resonance absorption also exhibit paramagnetic resonance rotation.

3. We found that there is a qualitative and quantitative relationship between the dispersion of susceptibility and the rotation of the plane of polarization.

4. We have deduced a semi-macroscopic formula for the dependence of the angle of rotation on the external magnetic field which approximately describes the experimental results.

5. The developed experimental method is applicable to measurement of the rotation of the plane of polarization in ferrites.

Kazan' State University
Imeni V. I. Ul'yanov-Lenin

Received
3 May 1954

Bibliographic References

1. A.L.Mikaelian, Usp. fiz. nauk, 51 205 (1953).
2. A.V.Sokolov, Usp. fiz. nauk, 50, 161 (1953).
3. Wilson and Hull, Phys. Rev., 74, 711 (1948).
4. A.Kastler, C.R., 228, 1640 (1949).
5. W.Opehowski, Rev. Mod. Phys., 25, 264 (1953).
6. R.Lacroix, Rytter & Exterman, Hevtca Phys. Acta, 23,539 (1950).
7. Soutif-Guicherd & Lambert, C.R., 231, 1460 (1950).
8. A.Gozzini, Nuovo Cimento, 8, 928 (1951).
9. F.F.Roberts, Journ. Phys. Rad. 12, 305 (1951).

10. C.L.Hogan, Bell System Tech. Jour., 31, 1 (1952).
11. N.N.Neprimerov, Preceding article in this issue of the Bulletin.
12. Teoriia linii peredachi sverkhvysokikh chastot (Theory of ultra-high frequency transmission lines). Pub. "Soviet Radio", M. 1951.
13. C.A.Beevers & H.Lipson, Proc. Royal Soc., A-146, 570 (1934).
14. S.A.Al'tshuler, Zhur. eksp. i teor. fiz., 17, 572 (1950).
15. I.M.Romanov, Zhur.eksp. i teor. fiz., 20, 572 (1950).
16. H.Suhl & Z.R.Walker, Phys. Rev., 86, 122 (1952).
17. N.Watson Theory of Bessel Functions (Russian ed.) Vol.II, M. 1949

* * * * * * *

INVESTIGATION OF THE FARADAY EFFECT IN FERRITES AT CENTIMETER WAVELENGTHS

- N. A. Smol'kov

The method of investigating the Faraday effect at microwave frequencies is analogous to that employed in optics. Instead of the Nichols prisms used as polarizer and analyzer at optical frequencies, rectangular waveguides are employed at centimeter wave frequencies, while the investigated specimen is placed in a circular waveguide, separating the rectangular ones and surrounded by a solenoid.

A block diagram of the basic set-up used at microwave frequencies is shown in Fig. 1.

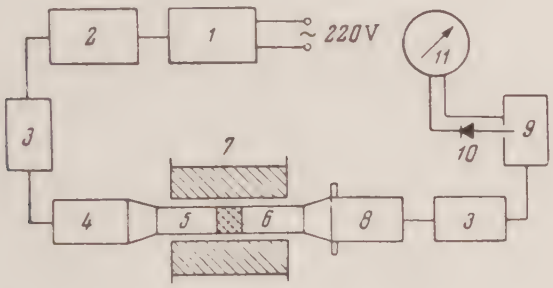

Fig. 1. Block diagram of set-up: 1) regulated rectifier, 2) Klystron, 3) adjustable attenuators, 4) polarizer, 5) circular waveguide, 6) specimen, 7) solenoid, 8) analyzer with angle scale, 9) detecting head (probe), 10) detector, 11) galvanometer.

A TE_{10} mode is excited in the rectangular waveguide which serves as the polarizer (see Fig. 2, a, where the electric field is designated by solid lines and the magnetic field by dash lines). This mode goes over into the circular guide, where it is transformed into the dominant TE_{11} mode, as shown in Fig. 2, b. As the wave passes through the section of the circular guide with the investigated substance, which is magnetized by the longitudinal field of the solenoid, its plane of polarization is rotated through an angle φ, as shown in Fig. 2, c. From the circular guide the wave enters the second rectangular guide, serving as the analyzer, where the TE_{11} mode is transformed into the TE_{10} mode. The power of the high frequency oscillations accepted by the analyzer will be a maximum when the latter is also turned through an angle φ relative to the first rectangular guide, as shown in Fig. 2, d.

Theoretically, the angle φ is determined from a simultaneous solution of the magnetodynamic equation of Landau and Lifshits:

$$\frac{\partial \mathbf{M}}{\partial t} = \gamma [\mathbf{M}\mathbf{H}_i] - \frac{\gamma\delta}{M} [\mathbf{M}[\mathbf{M}\mathbf{H}_i]] \qquad (1)$$

together with Maxwell's equations:

$$\left.\begin{aligned} \operatorname{rot} \mathbf{H} &= \frac{\partial \mathbf{D}}{\partial t}, \\ \operatorname{rot} \mathbf{E} &= \frac{\partial \mathbf{B}}{\partial t}, \end{aligned}\right\} \tag{2}$$

where $\gamma = g\frac{e}{2mc}$ is the gyromagnetic ratio, i.e. the ratio of the magnetic to the mechanical moment of an electron; g is the Landé splitting factor and δ is a parameter characterizing the damping of the precessing magnetic moments M about the direction of the internal field H_i.

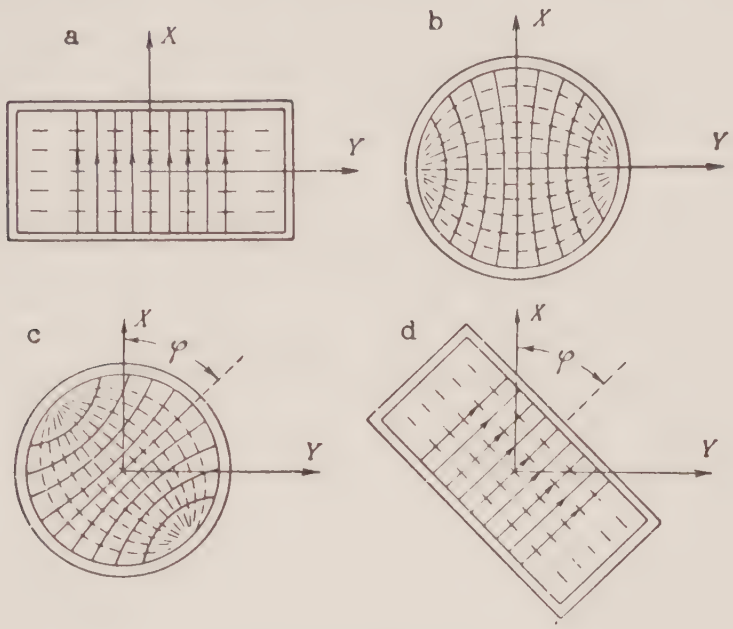

Fig. 2. Modes in waveguide assembly: a) in first rectangular guide (polarizer), b) in circular guide, c) rotation of plane of polarization through an angle φ incident to transmission through specimen, d) in second rectangular guide (analyzer) when this is turned through the angle φ.

It follows from equation (1) that the relationship between the high-frequency magnetic induction and the high-frequency internal field is not scalar, as is commonly assumed, but a tensor relationship: i.e.,

$$\mathbf{b} = T_{ij}\mathbf{h}^i, \tag{3}$$

where

$$T_{ij} = \begin{vmatrix} \mu & -ik & 0 \\ ik & \mu & 0 \\ 0 & 0 & 1 \end{vmatrix} \tag{4}$$

In other words, the components of the vector b have the form

$$\left.\begin{aligned} b_x &= \mu h_x^i - ikh_y^i, \\ b_y &= ikh_x^i + \mu h_y^i, \\ b_z &= h_z^i. \end{aligned}\right\} \tag{5}$$

The quantities μ and k are complex:

$$\mu = \mu_1 - i\mu_2, \tag{6}$$

$$k = k_1 - ik_2, \tag{7}$$

where

$$\mu_1 = 1 + \frac{[\gamma^2 H_z^2 (1+\delta^2) - \omega^2][M_z \gamma^2 H_z (1+\delta^2)] + 2\gamma^2\omega^2\delta^2 H_z M_z}{[\gamma^2 H_z^2 (1+\delta^2) - \omega^2]^2 + 4\gamma^2\omega^2\delta^2 H_z^2}, \tag{8}$$

$$\mu_2 = \frac{M_z \gamma\delta\omega [\gamma^2 H_z^2 (1+\delta^2) + \omega^2]}{[\gamma^2 H_z^2 (1+\delta^2) - \omega^2]^2 + 4\gamma^2\omega^2\delta^2 H_z^2}, \tag{9}$$

$$k_1 = \frac{M_z \gamma\omega [\gamma^2 H_z^2 (1+\delta^2) + \omega^2]}{[\gamma^2 H_z^2 (1+\delta^2) - \omega^2]^2 + 4\gamma^2\omega^2\delta^2 H_z^2}, \tag{10}$$

$$k_2 = \frac{2\gamma^2\omega^2\delta H_z M_z}{[\gamma^2 H_z^2 (1+\delta^2) - \omega^2] + 4\gamma^2\omega^2\delta^2 H_z^2}; \tag{11}$$

here, ω is the cyclic frequency of the high-frequency field

$$h = h_0 e^{i\omega t - \gamma_0 l},$$

where $\gamma_0 = \alpha + i\beta$ is the propagation constant (α is the attenuation constant and β is the phase factor).

Solving Maxwell's equations for the case of a plane wave being propagated through a ferromagnetic medium in the direction of the static magnetic field H_0 and bearing in mind that b_x, b_y and b_z are determined by (5), we obtain two values for the propagation constant:

$$\gamma_{0\pm} = \frac{i\omega}{c}\sqrt{(\mu \pm k)\varepsilon}, \tag{12}$$

indicating that the linearly polarized wave is resolved into two circularly polarized components, having different propagation constants.

The plus sign applies to the right polarized wave; the minus sign, to the left polarized wave.

The phase velocities of the two components can be determined from equations (8)-(12) and from these, in turn, one can find the angle of rotation:

$$\varphi = \frac{\beta_- - \beta_+}{2} l, \tag{13}$$

where l is the path length through the material (i.e., the thickness of the specimen).

The theoretical analysis of the Faraday effect in ferromagnetic materials at microwave frequencies, summarized above, has been carried out by Polder (Ref. 2) and Hogan (Ref. 3), who base their treatment on the assumption that the high-frequency dielectric constant does not change with variations of the external field H_0, comprised in the field H_i. However, our experiments (Ref. 4) have shown that the dielectric constant ε is a function of the field H_0 in the case of ferromagnetic resonance in ferrites. Hence, the present theory of the Faraday effect at microwave frequencies in ferrites and other non-metallic magnetic semiconductors requires modification or further development.

Employing the above-described method we investigated the Faraday rotation in the ferrites $Ni_\delta Cd_{1-\delta}Fe_2O_4$ and $(Ni_{0.5}Cu_{0.5}Fe_2O_4)_{0.85}(BaO)_{0.15}$

at a wavelength of 3.15 cm. The samples were prepared in the form of cylinders, one 9.8 mm in length, the other, 5.0 mm. The diameter of both was such as to completely fill the internal cross section of the circular guide.

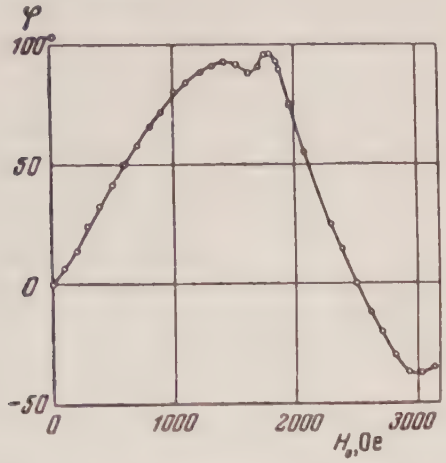

Fig. 3. Dependence of the angle of rotation in the $Ni_{\delta}Cd_{1-\delta}Fe_2O_4$ ferrite on the external magnetic field H_o. Length (thickness) of specimen - 9.8 mm.

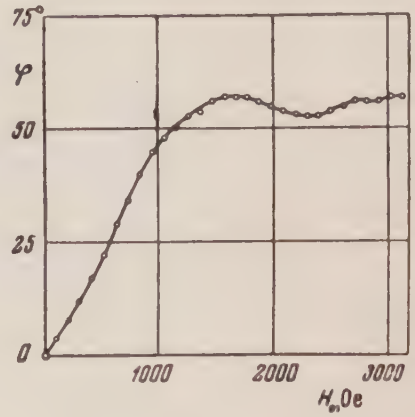

Fig. 4. Dependence of the angle of rotation in the $(Ni_{0.5}Cu_{0.5}Fe_2O_4)_{0.85}(BaO)_{0.15}$ ferrite. Length (thickness) - 5.0 mm.

The curve showing the variation of φ with the external field H_o for the first specimen is reproduced in Fig. 3. It will be seen that up to about H_o = 1000 oersteds the angle of rotation is proportional to the field strength; above this point the proportionality breaks down: apparently the material becomes saturated magnetically. At H_o = 1670 oersteds there is a small dip in the curve, which, according to Hogan, can be attributed to skin effect. The region of ferromagnetic resonance begins at H_o = 1800 oersteds and at H_o = 2500 oersteds φ goes through zero and becomes negative.

Fig. 4 shows the rotation curve for the second specimen, the region of resonance for which occurs at values of the field above 3000 oersteds. This curve, also exhibits a minimum, though in this case the dip is less pronounced, which may be attributed to the influence of the shape of the specimen.

Conclusions

1. In the Faraday rotation in ferrites there is observed a skin effect ahead of the region of resonance.

2. At the resonance point the angle of rotation of the plane of polarization changes sign.

The writer desires to express his thanks to E . I. Kondorski for his advice and counsel in the preparation of this report.

Moscow State University
Imeni M. V. Lomonosov

Received
3 May 1954

Bibliographic References

1. L.D.Landau & E.M.Lifshits, Sow. Phys., 8, 153 (1935).
2. D.Polder, Phil. Mag., 40, 300, 99 (1949).
3. C.L.Hogan, Bell System Tech. Journ.,31,1 (1952);Rev.Mod.Phys.,1,253 (1953).
4. E.I.Kondorski & N.A.Smol'kov, Dokl. AN SSSR, 93, 2, 237 (1953).

FERRITE DISC IN A COAXIAL LINE

- Ia. N. Kolli and E. M. Polivanov

Measuring Procedure and Processing of Results

1. Open- and short-circuit method

The relatively simple and commonly employed method of determining the four parameters of a doubly-complex medium ($\mu = \mu_1 - i\mu_2$ and $\varepsilon = \varepsilon_1 - i\varepsilon_2$), filling a section of coaxial line, consists of measuring the input impedances with the line containing the specimen (obstacle) terminated 1) by a short circuit (impedance Z_k) and 2) by an open circuit (impedance Z_x).

The input impedance can be determined using the familiar method of measuring the travelling /standing?/ wave ratio and the displacement of the minimum point.

Denoting with primed letters the normalized values of the input impedances, i.e., the values of the input impedances divided by the characteristic impedance of the line without the obstacle, we have:

$$Z'_к = Z'_c \operatorname{th} \gamma' l \quad \text{and} \quad Z'_x = \frac{Z'_c}{\operatorname{th} \gamma' l}, \tag{1}$$

whence

$$Z'_c = \sqrt{\frac{\mu}{\varepsilon}} = \sqrt{Z'_к Z'_x} \tag{2}$$

and

$$\operatorname{th} \gamma' l = \operatorname{th} (\beta l + i\alpha l) = \sqrt{\frac{Z'_к}{Z'_x}} = Te^{i\tau}, \tag{3}$$

here T and τ are the modulus and phase angle, respectively, of the complex hyperbolic tangent.

Knowing T and τ, we can compute the complex argument of the hyperbolic tangent. For our purposes, it is convenient to use the following equations:

$$\left.\begin{aligned} \operatorname{tg} 2\alpha l &= \frac{2T \sin \tau}{1 - T^2}, \\ \operatorname{th} 2\beta l &= \frac{2T \cos \tau}{1 + T^2}. \end{aligned}\right\} \tag{4}$$

Once the values α and β are obtained (the length of the line with the obstacle is assumed here to be known), we find

$$\sqrt{\mu\varepsilon} = \gamma' = \frac{\beta + i\alpha}{i\alpha_0}, \tag{6}$$

where

$$\alpha_0 = \frac{2\pi}{\lambda_0} \tag{7}$$

is the propagation constant of the line without the obstacle.

From (2) and (6) we can readily determine

$$\mu = \gamma' Z'_c \quad \text{and} \quad \varepsilon = \frac{\gamma'}{Z'_c}. \tag{8}$$

The adjustable line method described has the following serious shortcomings: 1) to determine the positions of the piston corresponding to a short circuit and open circuit at the end of the line, it is necessary to calibrate the line with the piston; 2) the values of μ and

are determined on the basis of only two measurements: one at open circuit, the other at short circuit.

2. Method of three reactive loads

The above shortcomings are eliminated in the method of three reactive loads.* This method comprises the following steps.

a) Construction of a Circle Diagram. The input impedances Z' are determined for a number of piston positions. All the determined values Z' should lie on the circumference of a circle, since the varying load remains purely reactive. In practice, the experimentally derived values of Z' are plotted in the complex plane and a circle is drawn through them.

The radius R of the circle and the coordinates of its center

$$x_0 + iy_0 = a \angle \varphi \tag{9}$$

are then computed.

The equation of the circle diagram for the input impedance (see Appendix 1 for derivation) has the form:

$$Z' = Z'_x + \frac{Z'_н - Z'_x}{1 + i\dfrac{X'_н}{Z'_x}}. \tag{10}$$

Here

$$X'_н = \operatorname{tg} \alpha_0 x \tag{11}$$

is the impedance of the reactive load connected at the output of the line with obstacle; x is the distance from the obstacle to the short-circuiting piston.

The functional relationship between the three parameters of the circle diagram and the values Z'_k and Z'_x is readily deduced; it is described by:

$$x_0 + iy_0 = Z'_x + Z'_x \frac{Z'_н - Z'_x}{2R'_x}, \tag{12}$$

$$R = \left| Z'_x \frac{Z'_н - Z'_x}{2R'_x} \right| = \left| \frac{(Z'_c)^2 - (Z'_x)^2}{2R'_x} \right|, \tag{13}$$

where $R'_x = \mathrm{Re}(Z'_x)$.

Thus, by plotting a circle diagram on the basis of a series of measurement at various piston positions, we can evaluate the extent to which the values of Z'_x and Z'_k, selected for further computation, are consistent with the other measurements of the series.

For example, assume we have an obstacle 0.413 cm in length in a transverse magnetic field H = 1225 oersteds and that at a wavelength λ_0 = 10.8 cm, observation yields:

$$Z'_k = 0.59 + i0.535 = 0.795 \angle 42^\circ 10';$$

$$Z'_x = 0.14 - i0.19 = 0.235 \angle -53^\circ 30'.$$

---

* V. Iu. Lomonosov participated in the development of this method.

The center of the circle plotted from a series of measurements has the coordinates

$$x_o + iy_o = 1.03 \angle -10^o35' = 1.015 - i\ 0.19$$

and a radius

$$R = 0.87$$

On the other hand, the coordinates and the radius, computed according to equations (12) and (13), are respectively:

$$x_o + iy_o = 0.865 \angle -8^o47' = 0.855 - i\ 0.132 \quad \text{and} \quad R = 0.715$$

The discrepancy permits, first, to evaluate the accuracy of the results, and second, to correct the plotted circle or the values of Z'_x and Z'_k so as to bring them into agreement.

b) Determination of the Characteristic Impedance from Measurements with Three Reactive Loads. The three parameters of the circle diagram are in themselves (when Z'_x and Z'_k are unknown) not sufficient to determine the values of the four desired parameters (μ_1, μ_2, ε_1 and ε_2). However, these parameters can be found by supplementing the circle diagram with the value of the characteristic impedance Z'_c of the line with the obstacle.

The value of Z'_c can be found if three values of the input impedance Z'_1, Z'_2 and Z'_3, corresponding to three consecutive positions of the piston separated by equal displacements Δx, are known. It is not necessary to know the distance between the piston and obstacle; we need only know the relative position of the piston for the three measurements: x for the first measurement, $x + \Delta x$ for the second, and $x + 2\Delta x$ for the third.

The characteristic impedance is computed from the three measured input impedances by means of the following equation (see Appendix 2 for derivation):

$$(Z'_c)^2 = \frac{(tZ'_2)^2 - 2rstq - (Z'_1 s - Z'_3 r)^2 q^2}{t^2 + 2rstq - (s-r)^2 q^2}, \tag{14}$$

where

$$q = i \operatorname{ctg}(\alpha_0 \Delta x), \quad r = Z'_1 - Z'_2, \quad s = Z'_2 - Z'_3, \quad t = Z'_3 - Z'_1. \tag{15}$$

Equation (14) can be replaced by an equivalent formula, in which the impedances and differences between impedances are replaced by admittances and differences between admittances, namely:

$$(Z'_c)^2 = \frac{p^2 - 2mnpq - (m \pm n)^2 q^2}{(pY'_2)^2 + 2mnpq - (Y'_3 m - Y'_1 n)^2 q^2}, \tag{16}$$

where q has the same value as before, and

$$Y'_i = \frac{1}{Z'_i}, \quad m = Y_1 - Y'_2, \quad n = Y'_2 - Y'_3, \quad p = Y'_3 - Y'_1. \tag{17}$$

If a series of measured input-impedance values (satisfying the requirement that the piston displacements be equal) are available, Z'_c can be computed repeatedly for each set of three equal-displacement readings. Thus, the computation formulas given here permit determining the characteristic impedance on the basis of a series of measurements for obtaining which it is not necessary to know the distance from the end of the obstacle to the piston.

In practice, it is convenient to verify the assumed open-circuit and short-circuit positions of the piston by making measurements at these points and also at the half-way point. In this case, $Z_1' = Z_k'$, $Z_3' = Z_x'$ and $\Delta x = \lambda/8$ and $q = 1$.

Applying equation (14) to this case, we get

$$(Z_c')^2 = \frac{(tZ_2')^2 - i2rst + (Z_1 s - Z_3 r)^2}{t^2 + i2rst + (s-r)^2}, \qquad (14a)$$

The computed result should equal the product of Z_x' by Z_k', i.e., $Z_1'Z_3'$. Agreement indicates that the piston positions have been properly selected, i.e. that the first position corresponds to an open circuit and the third position corresponds to a short circuit.

c) Determination of the Propagation Constant from Circle Diagram with Characteristic Impedance Known. Knowing the characteristic impedance Z_c' and the parameters a, φ, and R of the circle diagram, it is possible to determine the propagation constant of the line with the obstacle, and consequently the parameters of the obstacle (specimen) itself.

To derive computation formulas, we must express Z_k' and Z_x' in terms of the line parameters

$$Z_k' = Z_c' \operatorname{th} \gamma l \quad \text{and} \quad Z_x' = Z_c' \operatorname{cth} \gamma l \qquad (18)$$

and substitute these values in equation (10)

$$Z_{in}' = Z_c' \operatorname{cth} \gamma l + Z_c' \frac{\operatorname{th} \gamma l - \operatorname{cth} \gamma l}{1 + i \frac{X_H'}{Z_c'} \operatorname{th} \gamma l}, \qquad (19)$$

where X_H' is the load impedance [reactance].

Appropriate transformation of this equation (see Appendix 3) yields the following relationships between the line parameters and those of the circle diagram:

$$\operatorname{ch} 2\beta l = \frac{a}{R} \cdot \frac{\cos(\delta_c - \varphi)}{\cos \delta_c}, \qquad (20)$$

$$\cos 2\alpha l = \frac{a}{R} \cdot \frac{\sin(\delta_c - \varphi)}{\sin \delta_c}, \qquad (21)$$

$$R = \frac{|Z_c|}{\operatorname{sh} 2\beta l \cos \delta_c + \sin 2\alpha l \sin \delta_c}. \qquad (22)$$

Here

$$\delta_c = \arg Z_c'.$$

The first two equations permit determining the attenuation constant β and the phase factor α of the line with obstacle. The last equation (22) serves as a check on the accuracy of computation.

When Z_c' and $\gamma' = \frac{\alpha}{\alpha_0} - i\frac{\beta}{\alpha_0}$ have been found, the values of μ and ε can be computed from equation (8).

In the case of specimens with high attenuation, the values of Z_x' and Z_k' measured in making determinations by the open- and short-circuit

method differ little from each other. In this case th γl ($\tanh \gamma l$) approaches unity and the accuracy in determining αl and βl from (4) and (5) is greatly reduced. For the sake of higher accuracy it is preferable to determine Z_c' from (2) and make use of the circle diagram and equations (20) and (21) to compute αl and βl.

On the other hand, in cases of low attenuation or whenever $\frac{\mu_2}{\mu_1} \approx \frac{\varepsilon_2}{\varepsilon_1}$, the angles δ_c and φ tend to approach zero and the error involved in using (21) becomes great. In this case, it is preferable to use the open- and short-circuit method and to utilize (20) and (21) only for checking purposes.

Experimental results

We used the above-described method and procedure in investigating, at a wavelength of about 10 cm, the parameters of a disc of Grade 0-400 ferrite placed in static magnetic fields directed parallel (Fig. 1) and perpendicular to the axis of the coaxial line.

The results of the input impedance measurements at various values of the applied field are shown in Figs. 2 through 5 (points 1). The normalized (relative) characteristic impedances of the disc were computed on the basis of these measurements. The computations were made for three series of points: those corresponding to open- and short circuit conditions (points 2), those obtained by the three-reactive-loads method, the two end points corresponding to the open and the short circuit with $\Delta x = \lambda/8$ (points 3) and points obtained by the same method but with $\Delta x \neq \lambda/8$ (points 4).

The results are given in Table 1 below.

Results of measurements on Grade 0-400 Ferrite disc 0.37 cm thick in parallel and perpendicular fields

Parameter	Zero field	In transverse field	In longitudinal field		
H oersteds	0	2020	1770	2020	3700
Z_c' by open- and short-circuit method	0.39 $\angle -42^\circ 10'$	0.38 $\angle -0^\circ 40'$	0.77 $\angle -53^\circ 50'$	0.93 $\angle 55^\circ 05'$	0.25 $\angle 4^\circ 30'$
Z_c' by three-reactive-loads method with $x=\lambda/8$	0.37 $\angle -58^\circ 09'$	0.46 $\angle -0^\circ 31'$	0.63 $\angle -63^\circ 20'$	1.18 $\angle -55^\circ 35'$	0.50 $\angle -1^\circ 58'$
with $x \neq \lambda/8$	0.45 $\angle -42^\circ 05'$	0.47 $\angle -3^\circ 14'$	- -	0.89 $\angle -55^\circ 42'$	- -
Δx	2.00	0.20	-	2.00	-
R_{exp}	0.33	2.37	0.13	0.14	1.29
R_{comp}	0.35	2.72	0.19	0.49	3.54
$\frac{R_{comp}-R_{exp}}{R_{exp}}$	0.06	0.147	0.492	2.50	1.74

(Note: Field intensities given in the table and in the curves below are values measured in the absence of the disc.)

In addition to the measurements with reactive loads, two direct measurements of Z_c' were made in a field parallel to the axis of the line and equal to 1770 and 2020 oersteds. For this purpose another disc, 6 mm thick, was inserted on the load side of the investigated disc. This damped out the reflected wave completely, and the input impedance of the disc did not vary with the piston position. In this case, it can be assumed that the measured input impedance is approximately equal to Z_c' of the disc. These values of Z_c' are identified in Figs. 3 and 4 by $\otimes$. It will be noted that they lie outside the circle diagram plotted for a reactive load; this is in conflict with the theory of symmetric four-terminal networks.

It also follows from an analysis of the table that the discrepancy between the radius of the circle, obtained from the circle diagram (R_{exp}) and that computed from equation (13) (R_{comp}) is much greater in the case of a parallel field than in the cases of a zero field and of a transverse field. This suggests that the theory of symmetric lines or symmetric four-terminal networks is inapplicable to a ferrite disc in the presence of gyromagnetic effects.

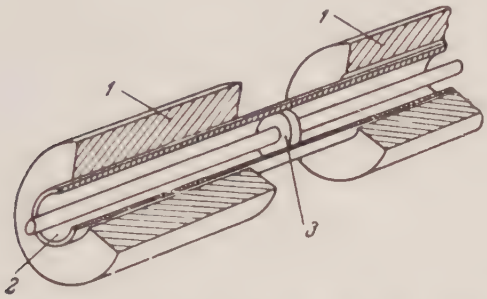

Fig. 1. Coaxial line with obstacle and with polepieces of magnet, when the applied magnetizing field is parallel to the axis of the line: 1) polepieces, 2) coaxial line, 3) ferrite disc.

Yet in many investigations (Refs. 3-5) the waveguide open- and short-circuited method has been employed without prior verification of its applicability to gyrotropic magneto-dielectrics.

In the case of a field perpendicular to the axis of the line (Fig. 5) the determinations made by the different methods are in closer agreement: the relative error in the determination of R_{comp} does not exceed 15%. This percentage is determined by the accuracy of the initial data (within 1-3%) and the cumulative error introduced by the approximations of the computation formulas.

The variation of the characteristic impedance and the propagation constant with the field is shown in Figs. 6 and 7.

The change in attenuation can be evaluated from the variation in the radius of the circle diagram: a smaller radius means that the influence of the load on the input impedance is diminished, i.e. that the attenuation is increased. A comparison of the circle diagrams of Figs. 2 and 5 shows that the application of a transverse field reduced the attenuation, while from Figs. 2, 3 and 4 it follows that the application of a longitudinal field increases the attenuation. In view of the disagreement between the observed results in the case of transverse field and the theory of four-terminal networks, it is questionable whether any useful purpose is served in determining αl, βl and Z_c' by conventional methods for this case.

We computed the values of μ and ε in the case of a transverse field with $\lambda = 10.25$ cm and $\alpha_0 = 0.616$ on the basis of the determined magnitudes of Z_c' and γ, using (6) and (8). The variation of μ and ε with the field intensity is shown in Fig. 8.

For fields from 0 to 1700 oersteds, the dependence of the attenuation on the field is approximately linear (Fig. 6). This region is

suitable for the operation of adjustable microwave attenuators. When the field exceeds 3000 oersteds $\mu_1 \leqslant 1$ and μ_2 and ε_2 are small (Fig. 8). In such fields the ferrite behaves as a low-loss dielectric: the loss tangent equals approximately 0.06-0.001. In fields between 1000 and 2000 oersteds, there is appreciable scattering of the points for ε, so that the values of ε_2 given for this region cannot be regarded as reliable. In any case, there is observed an apparent increase in ε_2 in this region. It will be noted from Fig. 7 that there is a corresponding change in the sign of the phase angle of the characteristic impedance at about 1700 oersteds, indicating that the dielectric loss begins to exceed the magnetic loss.

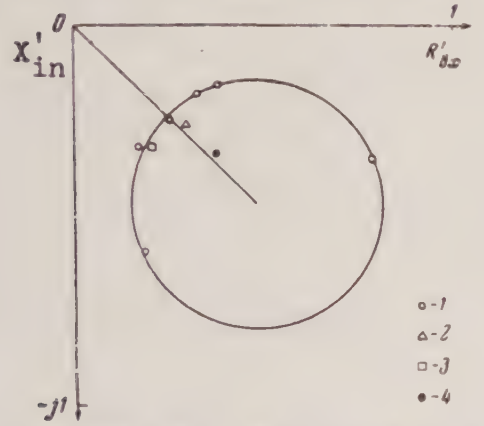

Fig. 2. Circle diagram for zero static magnetic field. 1) experimentally determined values of the input impedance Z'_c; 2) values of Z'_c computed using the open- and short-circuit method; 3) Z'_c computed using the method of three-reactive-loads with $\Delta x = \lambda/8$; 4) the same as 3, but with $\Delta x \neq \lambda/8$.

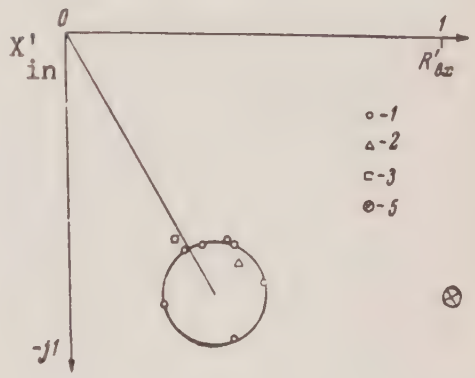

Fig. 3. Circle diagram for a static magnetic field, H = 1700 oersteds, parallel to axis of the line; 1 through 4) same as in Fig. 2; 5) Z'_c measured directly.

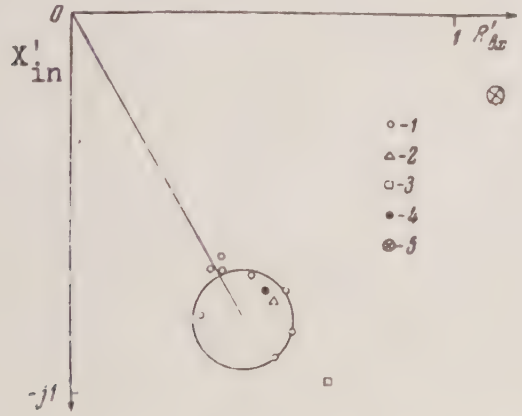

Fig. 4. Circle diagram for a static field, H = 2020 oersteds, parallel to the axis of the line. Number references as in Figs. 2 and 3. Identifying figures as in Figs. 2 and 3.

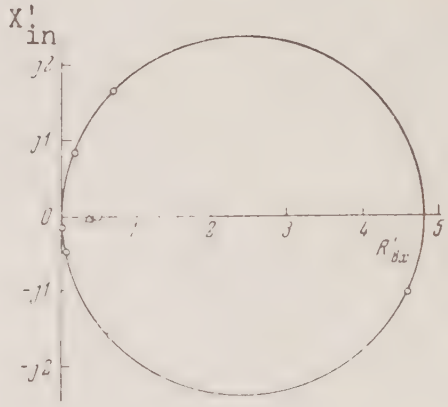

Fig. 5. Circle diagram for a static field H = 2020 oersteds, perpendicular to axis of line; scale 1/5th that in Figs. 2-4; identifying figures as in Fig. 2.

The values of μ and ε given in Fig. 8 are actually equivalent parameters rather than true values of the permeability and dielectric constant of the material since when a transverse magnetic field is applied, the angle between the alternating and constant components of the magnetic field differs at different points in the disc. This naturally makes for different values of μ at different points. Moreover, the methods discussed above do not take into account the gyrotropic components of the permeability.

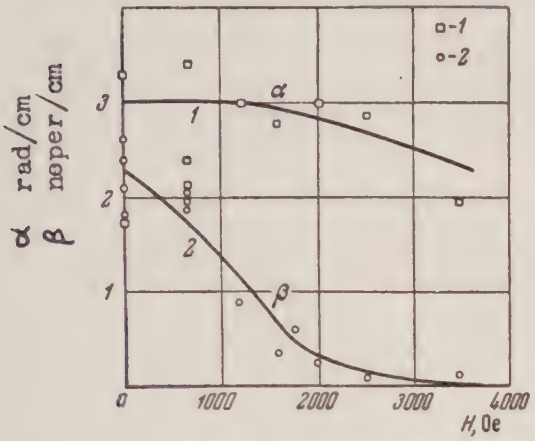

Fig. 6. Dependence of the propagation constant on the magnetic field perpendicular to the axis of the line: 1) $\alpha = \mathrm{Im}(\gamma)$; 2) $\beta = \mathrm{Re}(\gamma)$.

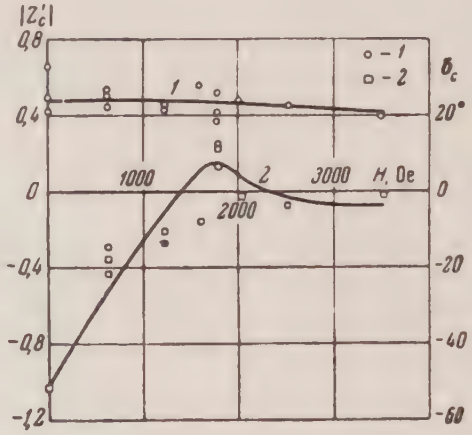

Fig. 7. Dependence of the characteristic impedance on the magnetic field perpendicular to axis of line: 1) $|Z'_c|$; 2) $\delta_c = \arg Z'_c$.

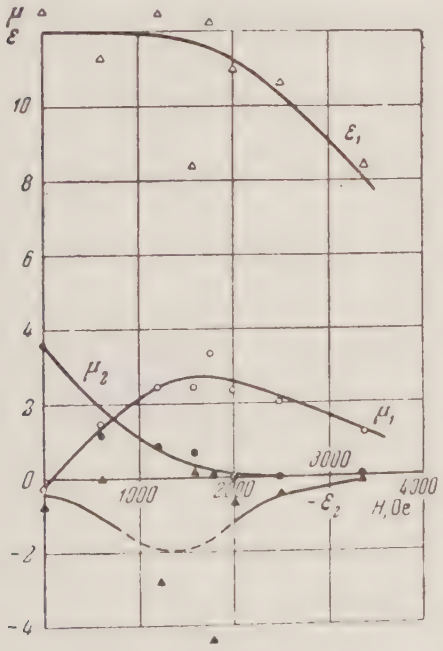

Fig. 8. Dependence of permeability and dielectric constant on the intensity of a magnetic field perpendicular to the axis of the line.

Hence, the determined values of ε and μ are essentially the values of ε and μ for an equivalent homogeneous disc in which gyromagnetic effects are absent.

Such "averaging" results in an apparent dependence of the equivalent dielectric constant on the applied magnetic field, although actually the dielectric constant of the material is probably independent of the magnetic field.

Conclusions

The familiar adjustable line method can be extended by supplementing it with the plotting of a circle diagram and by replacing the measurements made at two positions of the shorting piston with measurements made at three piston positions (the method of three-reactive-loads). Agreement of the end results of the different computations can serve as a check on the applicability of the symmetrical-line or symmetrical four-terminal network theory. No such internal check was available with the earlier open- and short-circuit method.

The results of our experiments make it questionable whether a section of line filled with a magneto-dielectric can be regarded as a section of a conventional uniform line in the presence of a longitudinal static field. An explanation of the divergence from theory must be sought through a rigorous analysis of the electrodynamic problem.

In the presence of a transverse static field, a section of line containing a magneto-dielectric retains the properties of a conventiona four-terminal network, but the permeability and dielectric constant measured in this case must not be identified with the intrinsic permeability and permittivity of the material inasmuch as the magnetic permeability of the disc varies from point to point (due to differences in the angle between the directions of the static and alternating magnetic fields).

Where no static field is present, the conventional adjustable-line method can be used to determine the permeability and dielectric constant of a magneto-dielectric material, and an extension of the method proposed in this article can be utilized for verifying the accuracy of the results.

Appendix 1

Equations relating the parameters of the circle with the open- and short-circuit impedances

From the equations for a four-terminal network

$$\left.\begin{aligned}\dot{U}_1 &= \dot{U}_2 A + \dot{I}_2 B = \dot{I}_2 (Z_н A + B),\\ \dot{I}_1 &= \dot{U}_2 C + \dot{I}_2 D = \dot{I}_2 (Z_н C + D)\end{aligned}\right\} \qquad (1.1)$$

we derive the familiar expression for the input impedance

$$Z_{in} = \frac{\dot{U}_1}{\dot{I}_1} = \frac{AZ_н + B}{CZ_н + D}, \qquad (1.2)$$

where Z_H is the alternating load.

Dividing algebraically and separating out A/C as a constant quality, we get

$$Z_{in} = \frac{A}{C} + \frac{\frac{B}{D} - \frac{A}{C}}{1 - \frac{Z_н}{D/C}}. \qquad (1.3)$$

It is evident from (1.1) and (1.2) that

$$\frac{A}{C} = Z_x, \quad \frac{B}{D} = Z_н, \quad \frac{D}{C} = Z_{in\ rev} \qquad (1.4)$$

where $Z_{in\ rev}$ is the impedance looking into the output terminals with the input terminals open.

In our case the four-terminal network is symmetrical

$$Z_x - Z_{in\ rev} \qquad (1.5)$$

and the load impedance is purely reactive

$$Z_н = iX_н. \qquad (1.6)$$

In this case, (1.3) takes the form

$$Z_{in} = Z_x + Z_x \frac{Z_н - Z_x}{Z_x - iX_н}. \tag{1.7}$$

Invoking the equation

$$\frac{1}{1 + i\,\mathrm{tg}\,\psi} = \frac{1}{2}(1 - e^{-i2\psi}) \tag{1.8}$$

and modifying the variable part of the second term of (1.7), we obtain

$$Z_{in} = Z_x + Z_x \frac{Z_н - Z_x}{2R_x}(1 + e^{-i2\psi}), \tag{1.9}$$

where

$$\psi = \mathrm{arc\,tg}\,\frac{X_н + X_x}{R_x}. \tag{1.10}$$

If ψ is the variable, equation (1.9) describes a circle. After dividing by the proper power of Z_{c0} (the characteristic impedance of line without without the obstacle) i.e., after converting to normalized values, we obtain the radius of the circle:

$$R = \left| \frac{Z'_x (Z'_н - Z'_x)}{2R'_x} \right| = \left| \frac{(Z'_c)^2 - (Z'_x)^2}{2R'_x} \right| \tag{1.11}$$

and the coordinates of the center of the circle:

$$x_0 + iy_0 = Z'_x + \frac{Z'_x (Z'_н - Z'_x)}{2R'_x} = Z'_x + \frac{(Z'_c)^2 - (Z'_x)^2}{2R'_x}. \tag{1.12}$$

Appendix 2

Derivation of equations (14) and (16), expressing the characteristic impedance in terms of three input impedances *

The system under consideration contains: 1) a line with an obstacle (specimen) of length l, having an unknown characteristic impedance Z_c and an unknown propagation constant γ, and 2) a load line, connected in series with the obstacle, having known values of Z_{c0} and $\gamma_0 = i\alpha_0$ and short-circuited by a piston at a certain distance from the obstacle.

Let the input impedances of the line with the obstacle correspond to the following distances between the end of the obstacle to the short circuit: $x_0 - \Delta x$, x_0, and $x_0 + \Delta x$. The value of x_0 is assumed to be unknown, while that of Δx is assumed to be an accurately measured quantity.

The load of the line can be expressed by the following equation:

$$Z_н = iZ_{c0}\,\mathrm{tg}\,\alpha_0 x. \tag{2.1}$$

In this case the input impedance of the specimen line with the obstacle can be characterized by

$$Z = Z_c \frac{Z_{c0}\, i\,\mathrm{tg}\,\alpha_0 x\,\mathrm{ch}\,\Gamma + Z_c\,\mathrm{sh}\,\Gamma}{Z_{c0}\, i\,\mathrm{tg}\,\alpha_0 x\,\mathrm{sh}\,\Gamma + Z_c\,\mathrm{ch}\,\Gamma}. \tag{2.2}$$

---

* The derivation was suggested by V. Iu. Lomonosov.

Changing to normalized impedances (dividing all impedances by Z_{c0}), we get

$$Z' = Z'_c \frac{i \operatorname{tg} \alpha_0 x \operatorname{ch} \Gamma + Z'_c \operatorname{sh} \Gamma}{i \operatorname{tg} \alpha_0 x \operatorname{sh} \Gamma + Z'_c \operatorname{ch} \Gamma}, \tag{2.3}$$

or

$$Y' = \frac{\theta i \operatorname{tg} \alpha_0 x \operatorname{sh} \Gamma + \operatorname{ch} \Gamma}{i \operatorname{tg} \alpha_0 x \operatorname{ch} \Gamma + \frac{1}{\theta} \operatorname{sh} \Gamma}. \tag{2.4}$$

Here

$$\theta = Y'_c \quad \text{and} \quad \Gamma = \gamma l. \tag{2.5}$$

Let us denote the input admittances* at the three different values as follows:

$$\left.\begin{aligned} Y'_1 &= Y'(x_0 - \Delta x) = c - a, \\ Y'_2 &= Y'(x_0) = c, \\ Y'_3 &= Y'(x_0 + \Delta x) = c + b. \end{aligned}\right\} \tag{2.6}$$

Solving (2.4) with respect to $\operatorname{tg} \alpha_0 x$ with $x = x_0$, and consequently with $Y' = c$, we get

$$\operatorname{tg} \alpha_0 x_0 = \frac{\operatorname{ch} \Gamma - \frac{c}{\theta} \operatorname{sh} \Gamma}{ic \operatorname{ch} \Gamma - i\theta \operatorname{sh} \Gamma}. \tag{2.7}$$

This equation will be used to eliminate the unknown x_0.

Let us represent the tangent of a sum as:

$$\operatorname{tg} \alpha_0 (x_0 \pm \Delta x) = \frac{\operatorname{tg} \alpha_0 x_0 \operatorname{ctg} \alpha_0 \Delta x \pm 1}{\operatorname{ctg} \alpha_0 \Delta x \mp \operatorname{tg} \alpha_0 x_0}. \tag{2.8}$$

We introduce the following designation for the value of the known cotangent in the above equation:

$$q = i \operatorname{ctg} \alpha_0 \Delta x, \tag{2.9}$$

and invoke equation (2.7) to express the unknown tangent. We thus get

$$\operatorname{tg} \alpha_0 (x_0 \pm \Delta x) = \frac{q\left(\operatorname{ch} \Gamma - \frac{c}{\theta} \operatorname{sh} \Gamma\right) \mp (c \operatorname{ch} \Gamma - \theta \operatorname{sh} \Gamma)}{iq (c \operatorname{ch} \Gamma - \theta \operatorname{sh} \Gamma) \mp i\left(\operatorname{ch} \Gamma - \frac{c}{\theta} \operatorname{sh} \Gamma\right)}. \tag{2.10}$$

Taking $x = x_0 \pm \Delta x$ in (2.4), and using the notation of (2.6), we get

$$\left.\begin{matrix} c + b \\ c - a \end{matrix}\right\} = \frac{i\theta \operatorname{sh} \Gamma \operatorname{tg} \alpha_0 (x \pm \Delta x) + \operatorname{ch} \Gamma}{i \operatorname{ch} \Gamma \operatorname{tg} \alpha_0 (x \pm \Delta x) + \frac{1}{\theta} \operatorname{sh} \Gamma}, \tag{2.11}$$

and upon substituting for the tangent as per (2.10) and changing to functions of twice the angle**:

$$\left.\begin{matrix} c + b \\ c - a \end{matrix}\right\} = \frac{\pm (\theta^2 - 1) \operatorname{ch} 2\Gamma \pm \left(\frac{c}{\theta} - \theta c\right) \operatorname{sh} 2\Gamma \mp (\theta^2 + 1) + 2qc}{\pm \left(\frac{c}{\theta^2} - c\right) \operatorname{ch} 2\Gamma \pm \left(\theta - \frac{1}{\theta}\right) \operatorname{sh} 2\Gamma \mp \left(c + \frac{c}{\theta^2}\right) + 2q}. \tag{2.12}$$

---

* As usual, it is assumed throughout that $Y_i = 1/Z_i$.

** According to the equations: $\operatorname{sh} \Gamma \operatorname{ch} \Gamma = \frac{1}{2} \operatorname{sh} 2\Gamma$; $\operatorname{sh}^2 \Gamma = \frac{1}{2} (\operatorname{ch} 2\Gamma - 1)$; $\operatorname{ch}^2 \Gamma = \frac{1}{2} (\operatorname{ch} 2\Gamma + 1)$.

After grouping the coefficients of the hyperbolic functions, the two equations (2.12) lead to the following system:

$$\left.\begin{aligned} A_1 \operatorname{ch} 2\Gamma + B_1 \operatorname{sh} 2\Gamma = D_1, \\ A_2 \operatorname{ch} 2\Gamma + B_2 \operatorname{sh} 2\Gamma = D_2, \end{aligned}\right\} \tag{2.13}$$

with

$$\left.\begin{aligned} A_1 &= (1-\theta^2)\left(1 + c\frac{c+b}{\theta^2}\right), \\ B_1 &= -(2c+b)(1-\theta^2)\frac{1}{\theta}, \\ D_1 &= -2bq - (1+\theta^2)\left(1 - c\frac{c+b}{\theta^2}\right), \\ A_2 &= -(1-\theta^2)\left(1 + c\frac{c-a}{\theta^2}\right), \\ B_2 &= (2c-a)(1-\theta^2)\frac{1}{\theta}. \\ D_2 &= 2aq + (1+\theta^2)\left(1 - c\frac{c-a}{\theta^2}\right). \end{aligned}\right\} \tag{2.14}$$

The determinant of the system (2.13) is:

$$\Delta = A_1 B_2 - A_2 B_1 = \frac{(1-\theta^2)^2}{\theta}(a+b)\frac{c^2-\theta^2}{\theta^2}. \tag{2.15}$$

The auxiliary determinants are:

$$\Delta_1 = D_1 B_2 - B_1 D_2 = \frac{1-\theta^2}{\theta}\left[Rq + (1+\theta)(a+b)\left(1+\frac{c^2}{\theta^2}\right)\right], \tag{2.16}$$

where

$$R = 4(ab - bc + ca), \tag{2.17}$$

and

$$\Delta_2 = A_1 D_2 - A_2 D_1 = (1-\theta^2)\left[Qq + 2c\frac{(1+\theta^2)(a+b)}{\theta^2}\right], \tag{2.18}$$

where

$$Q = 2\left[a - b + c\frac{c(a-b) + 2ab}{\theta^2}\right]. \tag{2.19}$$

Since

$$\operatorname{ch}^2 2\Gamma - \operatorname{sh}^2 2\Gamma = 1, \tag{2.20}$$

we can write

$$\Delta_1^2 - \Delta_2^2 - \Delta^2 = 0 \tag{2.21}$$

(here it is naturally assumed that $\Delta \neq 0$). We substitute (2.15), (2.16) and (2.18) into (2.21), and cancel the factor $1 - \theta^2$, common to all determinants, assuming that

$$1 - \theta^2 \neq 0 \tag{2.22}$$

(thereby excluding the roots $\theta = \pm 1$ from the solution). As a result we obtain, grouping the coefficients of the q^n terms:

$$Z'_{in} = Z'_c \operatorname{cth} \gamma l + Z'_c \frac{\operatorname{th} \gamma l - \operatorname{cth} \gamma l}{1 + i \frac{X'_H}{Z'_c} \operatorname{th} \gamma l} . \qquad (3.2)$$

Expression (3.2) is the equation of a circle diagram, of the form:

$$Z'_{in} = Z'_x + \frac{Z'_H - Z'_x}{1 + if(X'_H)} . \qquad (3.3)$$

Further computations require an expression for the radius of a circle diagram. For this purpose let us recast circle-diagram equation (3.2) in the following form:

$$Z'_{in} = Z'_x + R(1 + e^{i2\psi}), \qquad (3.4)$$

where Ψ is a function of X'_H and **R** is a vector whose modulus equals the radius of the circle.

To find suitable expressions for **R** and Ψ, let us effect the following transformations: let $\operatorname{th} \gamma l = te^{i\theta}$. We multiply and divide the second term of (3.2) by $e^{i\theta}$:

$$Z'_{in} = Z'_c \operatorname{cth} \gamma l + Z'_c \frac{t - \frac{1}{t} e^{-i2\theta}}{e^{-i\theta} + i \frac{X'_H t}{Z'_c}} . \qquad (3.5)$$

Let us make the substitution $e^{-i\theta} = \cos\theta - i \sin\theta$ and re-write the last equation in the following form:

$$Z'_{in} = Z'_c \operatorname{cth} \gamma l + Z'_c \frac{t^2 - e^{-i2\theta}}{t \cos\theta} \cdot \frac{1}{1 - i \frac{\sin\theta - (X'_H t / Z'_c)}{\cos\theta}} . \qquad (3.6)$$

We put

$$\left.\begin{aligned} 2R &= Z'_c \frac{t^2 - e^{-i2\theta}}{t \cos\theta} , \\ \operatorname{tg}\psi &= \frac{\sin\theta - (X'_H t / Z'_c)}{\cos\theta} . \end{aligned}\right\} \qquad (3.7)$$

Substituting (3.7) in (3.6) and using Euler's equation for tg Ψ,

$$\operatorname{th} 2\beta l = \frac{Z'_c}{a} ,$$

we obtain an equation of the same form as (3.4):

$$Z'_{in} = Z'_c \operatorname{cth} \gamma l + R(1 + e^{i2\psi}). \qquad (3.8)$$

The location of the center of the circle is determined by the vector sum:

$$OO_1 = Z'_c \operatorname{cth} \gamma l + R.$$

After carrying out the vector addition, we get:

$$OO_1 = \frac{Z'_c (|\operatorname{th} \gamma l|^2 + 1)}{2 \operatorname{Re} (\operatorname{th} \gamma l)} . \qquad (3.9)$$

It follows from (3.9) that the center of the circle lies on the real axis. From (3.2) we have:

1) in case of a short circuit ($X'_H = 0$) [H stands for Load]

$$Z'_{in} = Z'_c \operatorname{th} \gamma l = Z'_c t e^{i\theta}, \tag{3.10}$$

2) in case of an open circuit ($X'_H = \infty$)

$$Z'_{in} = Z'_c \operatorname{cth} \gamma l = Z'_c \frac{e^{-i\theta}}{t}, \tag{3.11}$$

i.e., the lines Z_k and Z_x [$Z_{shortc.}$ and $Z_{open\ c.}$] are symmetrical with respect to the real axis (Fig. 9).

From the familiar geometric theorem concerning the tangent OC and secant OD we have: $OC^2 = OB \cdot OD = OA \cdot OD$. The segments OB and OA are equal because the angles AOO_1 and DOO_1 are equal. Therefore, we get:

$$OC^2 = Z'_c |\operatorname{th} \gamma l| \cdot Z'_c |\operatorname{cth} \gamma l| = (Z'_c)^2$$

and

$$OC = Z'_c.$$

To determine the attenuation constant of the line let us substitute for $\operatorname{th} \gamma l$ in (3.9) the following equations:

$$|\operatorname{th} \gamma l|^2 = \frac{\operatorname{sh}^2 2\beta l + \sin^2 2\alpha l}{(\operatorname{ch} 2\beta l + \cos 2\alpha l)^2} \tag{3.12}$$

and

$$\operatorname{Re}(\operatorname{th} \gamma l) = \frac{\operatorname{sh} 2\beta l}{\operatorname{ch} 2\beta l + \cos 2\alpha l}. \tag{3.13}$$

Substituting (3.12) and (3.13) in (3.9), and denoting $|OO_1| = a$, we get:

$$a = Z'_c \frac{\frac{\operatorname{sh}^2 2\beta l + \sin^2 2\alpha l}{(\operatorname{ch} 2\beta l + \cos 2\alpha l)^2} + 1}{\frac{2 \operatorname{sh} 2\beta l}{\operatorname{ch} 2\beta l + \cos 2\alpha l}}.$$

From this we find that

or

$$a = Z'_c \operatorname{cth} 2\beta l$$

$$\operatorname{th} 2\beta l = \frac{Z'_c}{a}. \tag{3.14}$$

Using the relationships:

$$\operatorname{sh} x = \frac{\operatorname{th} x}{\sqrt{1 - \operatorname{th}^2 x}}, \quad \operatorname{ch} x = \frac{1}{\sqrt{1 - \operatorname{th}^2 x}}, \quad (Z'_c)^2 = a^2 - R^2,$$

other expressions can be given for βl

$$\operatorname{sh} 2\beta l = \frac{Z'_c}{R} \tag{3.15}$$

and

$$\operatorname{ch} 2\beta l = \frac{a}{R}. \tag{3.16}$$

General Case

We assume the wave impedance of the line is complex: $Z'_c = |Z'_c| e^{i\delta_c}$.

In this case, (3.2) can be rewritten:

$$Z'_{in} = Z'_c \operatorname{cth} \gamma l + |Z'_c| e^{i\delta_c} \frac{te^{i\theta} - \frac{1}{t} e^{-i\theta}}{1 + i \frac{X'_H t}{|Z'_c|} e^{-i(\delta_c - \theta)}}. \qquad (3.17)$$

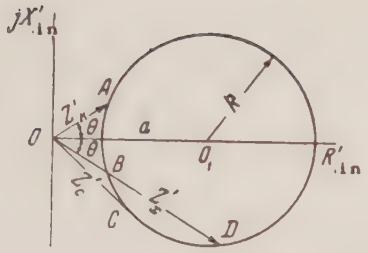

Fig. 9. Circle diagram with active (purely resistive) characteristic impedance

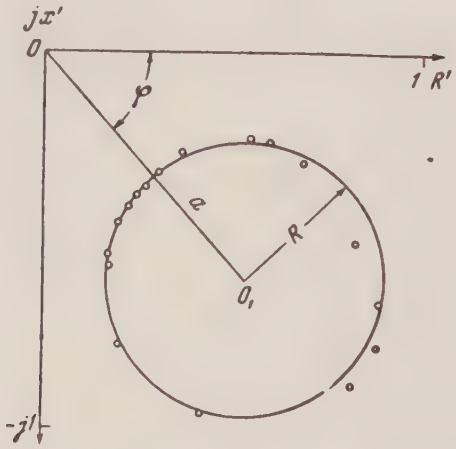

Fig. 10. Circle diagram with complex characteristic impedance

To bring this expression into the same form as (3.4), we multiply and divide the second term by $e^{i(\delta_c - \theta)}$:

$$Z'_{in} = Z'_c \operatorname{cth} \gamma l + |Z'_c| e^{i2\delta_c} \frac{t - \frac{1}{t} e^{-i2\theta}}{e^{i(\delta_c - \theta)} + i \frac{X'_H t}{|Z'_c|}}.$$

Let us make the following substitution:

$$e^{i(\delta_c - \theta)} = \cos(\delta_c - \theta) + i \sin(\delta_c - \theta)$$

and transform

$$Z'_{in} = Z'_c \operatorname{cth} \gamma l + |Z'_c| e^{i2\delta_c} \frac{t^2 - e^{-i2\theta}}{t \cos(\theta - \delta_c)} \times \frac{1}{1 - i \frac{\sin(\theta - \delta_c) - (X'_H t / |Z'_c|)}{\cos(\theta - \delta_c)}}. \qquad (3.18)$$

Let us put:

$$2R = |Z'_c| e^{i2\delta_c} \frac{t^2 - e^{-i2\theta}}{t \cos(\theta - \delta_c)}, \qquad (3.19)$$

$$\operatorname{tg} \psi = \frac{\sin(\theta - \delta_c) - (X'_H t / |Z'_c|)}{\cos(\theta - \delta_c)}. \qquad (3.20)$$

Substituting (3.19) and (3.20) into (3.18), and carrying out exactly the same transformation as in the particular case described above, we obtain:

$$Z'_{in} = Z'_c \operatorname{cth} \gamma l + R(1 + e^{i2\psi}), \qquad (3.20a)$$

where R and ψ are now determined from (3.19) and (3.20).

Let us find the radius vector that determines the location of the center of the circle (Fig. 10):

$$OO_1 = Z_c' \operatorname{cth} \gamma l + \mathbf{R} = \frac{|Z_c'|(t^2 e^{i2\delta_c}+1)}{2t\cos(\theta-\delta_c)}. \qquad (3.21)$$

Equating (3.21) to $ae^{i\varphi}$ we finally get:

$$ae^{i\varphi} = \frac{|Z_c'|(t^2 e^{i2\delta_c}+1)}{2t\cos(\theta-\delta_c)}. \qquad (3.22)$$

Equating the real and imaginary parts of (3.22) we obtain two equations, which together with the expression for the modulus of **R** yield three equations for the four unknowns Z_c, t, δ_c and θ.

$$R = |Z_c'| \frac{\sqrt{t^4 - 2t^2\cos 2\theta + 1}}{2t\cos(\theta-\delta_c)}, \qquad (3.23)$$

$$a\cos\varphi = |Z_c'| \frac{t^2\cos 2\delta_c + 1}{2t\cos(\theta-\delta_c)}, \qquad (3.24)$$

$$a\sin\varphi = |Z_c'| \frac{t^2\sin 2\delta_c}{2t\cos(\theta-\delta_c)}. \qquad (3.25)$$

If Z_c is known from another experiment, this system permits solving for β and α.

Solution of System of Equations (3.23) - (3.25). We invoke the relationships:

$$t^2 = \frac{\operatorname{ch} 2\beta l - \cos 2\alpha l}{\operatorname{ch} 2\beta l + \cos 2\alpha l}, \qquad (3.26)$$

$$t\cos\theta = \operatorname{Re}(\operatorname{th}\gamma l) = \frac{\operatorname{sh} 2\beta l}{\operatorname{ch} 2\beta l + \cos 2\alpha l}, \qquad (3.27)$$

$$t\sin\theta = \operatorname{Im}(\operatorname{th}\gamma l) = \frac{\sin 2\alpha l}{\operatorname{ch} 2\beta l + \cos 2\alpha l}. \qquad (3.28)$$

Substituting (3.26) - (3.28) into (3.23) we get

$$R = \frac{|Z_c'|}{\operatorname{sh} 2\beta l\cos\delta_c + \sin 2\alpha l\sin\delta_c} \qquad (3.29)$$

if $\delta_c = 0$, we have sh $2\beta l = Z_c'/R$, which is identical with (3.15). Transformation of (3.24) yields

$$2a\cos\varphi = |Z_c'| \frac{2\operatorname{ch} 2\beta l\cos^2\delta_c + 2\cos 2\alpha l\sin^2\delta_c}{\operatorname{sh} 2\beta l\cos\delta_c + \sin 2\alpha l\sin\delta_c}. \qquad (3.30)$$

From (3.25) we find that

$$2a\sin\varphi = |Z_c'| \frac{(\operatorname{ch} 2\beta l - \cos^2\alpha l)\sin 2\delta_c}{\operatorname{sh} 2\beta l\cos\delta_c + \sin 2\alpha l\sin\delta_c}. \qquad (3.31)$$

Substituting from (3.29) in (3.30) and (3.31):

$$a\cos\varphi = R(\operatorname{ch} 2\beta l\cos^2\delta_c + \cos 2\alpha l\sin^2\delta_c), \qquad (3.32)$$

$$a\sin\varphi = R(\operatorname{ch} 2\beta l\cos\delta_c\sin\delta_c - \cos 2\alpha l\cos\delta_c\sin\delta_c). \qquad (3.33)$$

When $\varphi = \delta_c = 0$, we obtain from (3.32):

$$\operatorname{ch} 2\beta l = \frac{a}{R},$$

which is identical with (3.16). From (3.32) we have:

$$a\cos\varphi = R(\operatorname{ch} 2\beta l - \cos 2\alpha l)\cos^2\delta_c + R\cos 2\alpha l. \qquad (3.34)$$

Multiplying (3.33) by ctg δ_c and subtracting (3.34) from the product:

$$a\sin\varphi\operatorname{ctg}\delta_c - a\cos\varphi = -R\cos 2\alpha l.$$

Hence:

$$\cos 2\alpha l = \frac{a}{R}\cdot\frac{\sin(\delta_c - \varphi)}{\sin\delta_c}. \qquad (3.35)$$

Now, let us rewrite (3.32) as follows:

$$a\cos\varphi = R[\operatorname{ch} 2\beta l - (\operatorname{ch} 2\beta l - \cos 2\alpha l)\sin^2\delta_c]. \qquad (3.36)$$

Multiplying (3.33) by tg δ_c and adding the product to (3.36):

$$a\sin\varphi\operatorname{tg}\delta_c + a\cos\varphi = R\operatorname{ch} 2\beta l.$$

From which we get

$$\operatorname{ch} 2\beta l = \frac{a}{R}\cdot\frac{\cos(\delta_c - \varphi)}{\cos\delta_c}. \qquad (3.37)$$

Equations (3.35) and (3.37) are identical with (21) and (20), the equations used to determine the propagation constant from the circle diagram and the argument of the complex characteristic impedance.

Moscow Energetics Institute
Imeni V. M. Molotov

Received
3 May 1954

Bibliographic References

1. Izmereniia na sverkhvysokikh chastotakh (Measurements at Ultra-High Frequencies). In Russian Translation, edited by V.B.Steinshleiger. Pub. by "Soviet Radio", M. 1952.
2. J.B.Birks, Proc. Phys. Soc., 60, 282 (1948).
3. W.H.Hewitt, Phys. Rev., 73, 1118 (1948).
4. A.J.E.Welch & others, Phys. Rev., 77, 403 (1950) [Refs. 2, 3 & 4 are cited in Russian translation in "Ferromagnitnyi rezonans" (Ferromagnetic Resonance), edited by S.V.Vonsovski, Moscow 1952]
5. V.N.Lazukin, Izv. (Bulletin) AN SSSR,Ser.fiz., 16, 4, 510 (1952).

TEMPERATURE DEPENDENCE OF THE ELECTRIC RESISTIVITY OF FERRITES

- A. P. Komar and V. V. Kliushin

Purpose of the Investigation

It is known that in pure metals ferromagnetic transitions are transitions of the second order, but even in metallic alloys there can already be cases when the manifestation of ferromagnetic properties is connected with transitions of the first order.

Ferromagnetic transitions are accompanied by anomalies of the thermal, galvanometric and other properties of the material. Some of these anomalies have also been investigated in the new ferromagnetic materials: ferrites. Ferrites are known to exhibit a specific heat anomaly (Ref. 1) and an anomaly of the coefficient of linear expansion (Ref. 2). These anomalies indicate that in ferrites, ferromagnetic transitions are transitions of the second order. In metallic ferromagnetics there is also observed a marked alteration of the temperature dependence of the electric resistivity at the Curie point. Detection of a similar effect in ferrites, which are semiconductors, would be of undoubted interest. The temperature dependence of the electric resistivity of ferrites is described by an equation of the form $R = Ae^{\Delta E/kT}$ (Ref. 3) where the values of A and E change little in the narrow range of temperatures within which the resistivity is commonly measured. In the vicinity of the Curie point, however, A and E may undergo a sudden change in connection with the disappearance of spontaneous magnetization. This is a distinct possibility in view of the fact that the short-range order of the metallic ions of different valences changes at the Curie temperature.

The purpose of the present investigation was to determine the temperature dependence of the electric resistivity of ferrites in the range of ferromagnetic-transition temperatures.

Measurement Procedure

The ferrites investigated included nickel, copper and manganese ferrites with molar proportions of the oxides amounting to 50:50, 50:50 and 45:50 respectively, and a number of mixed nickel-zinc ferrites of different compositions. The specimens were in the shape of cylinders 8 mm in diameter and up to 50 mm in length.

The temperature dependence of the resistivity was determined by the compensation method with the use of probes. The contacts were formed by the application of silver at 850°C. The temperature range of measurement for the simple ferrites was 300 to 1000°K; the range for the nickel-zinc ferrites was 200 to 500°K.

To prevent the true temperature dependence of the resistivity from being obscured by the magnetocaloric effect and various other transition processes, the ferrite specimens were cooled slowly and heated in stages. The resistance was measured at each set temperature only after complete temperature equilibrium between the specimen and the surrounding medium had been established. This method insured coincidence of the temperature-resistivity curves obtained both in heating and in cooling.

A special thermal chamber was constructed for making measurements above 0°C.

The principal experimental error was due to temperature fluctuations. The temperature was maintained constant within 1° in measuring the resistivity of the simple ferrites and within 0.2° of the set point in the case of the mixed ferrites. The percentage error in measurement did not exceed 7%.

Data regarding the Curie points of the simple ferrites were taken from Refs. 3 and 4. The Curie points of the mixed ferrites were determined experimentally.

Experimental Results

The results of the investigations showed that there is a break in the $\log\rho = f(1/T)$ line in the vicinity of the Curie point and that above the Curie point the $R = Ae^{\Delta E/kT}$ law, characteristic of semiconductors, holds for ferrites.

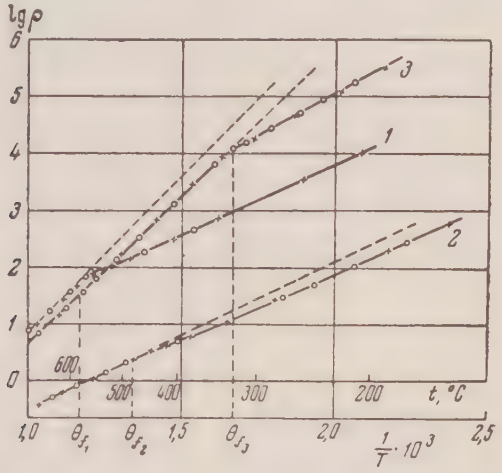

Fig. 1. Temperature dependence of the electric resistivity of simple ferrites: 1) nickel, 2) copper, 3) manganese ferrites.

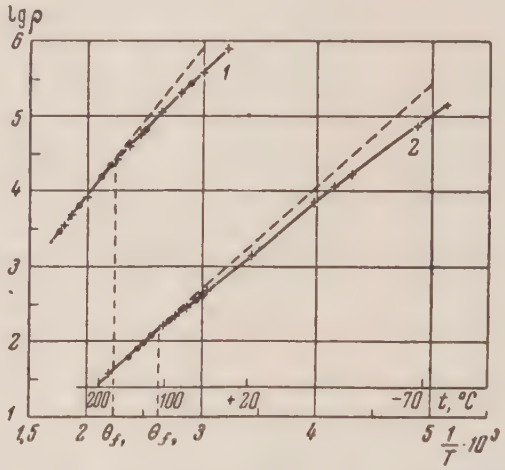

Fig. 2. Temperature dependence of the resistivity of nickel-zinc ferrites: 1) specimen having a 170°C Curie point, 2) specimen having a 105° Curie point.

The break in the curve for nickel ferrite (Fig. 1) comes at 595±5°C. According to data in the literature the Curie point temperature for this ferrite is Θ_f = 590°C. For copper ferrite the break is observed at 480±5°C (Θ_f = 480°C) and for manganese ferrite, at 335±5°C (Θ_f = 315°C). The Curie point for manganese ferrite obtained from resistivity measurements is lower than that given in the literature, due to its deviation from the stoichiometric composition.

A change in the temperature dependence of the resistivity in the vicinity of the Curie point is observed in the case of nickel-zinc ferrites as well. The experimental results for nickel-zinc ferrites with Curie points at 100° [105° under Fig. 2!] and 170° are shown in Fig. 2. In order to obtain more dependable results (i.e. additional points for the curves) the resistivity measurements on the nickel-zinc ferrites were extended into the region below 0°C. It will be noted that the effect in nickel-zinc ferrites is weak. Hence, it is not surprising that Smolenski (Ref. 3), in view of the inadequate accuracy of his measurements, failed to note the resistivity anomaly, although he did deduce the correct law for the variation of the resistivity with temperature. Thus, we have definitely established that

the temperature dependence of the resistivity of the investigated ferrites does change at the Curie point.

Before attempting to connect this change with the appearance of spontaneously magnetized domains, we must make sure the observed results are not simply a consequence of spontaneous magnetostriction. In order to evaluate the influence of magnetostriction, $\rho = f(T)$ measurements were made on nickel ferrite specimens of different shapes. The temperature dependence of the resistivity proved to be the same regardless of shape. The influence of strictive changes in the dimensions of the specimens was evaluated by simple calculations for nickel ferrite, since this ferrite exhibits considerable volumetric striction. For the calculation we used the magnetostriction at 20°C; at this temperature $\Delta l/l = -1.28 \cdot 10^{-3}$ (Ref. 2). The calculations showed that the change in resistivity due to strictive changes of the dimensions of the specimen is less than 1%, whereas the observed changes in resistivity below the Curie point were of the next higher order of magnitude.

Discussion of Experimental Results

The noticeable change in the temperature dependence of the electric conductivity in the vicinity of the Curie point indicates that in this temperature region there is a change in the conditions governing the appearance and continued existence of conductivity electrons. The decrease in the value of the energy term in the exponent of $Ae^{\Delta E/kT}$ shows that the availability of free electrons is increased; an increase in the magnitude of A is connected only with a change in the ordering of the metallic ions of different valence in the ferrite lattice. This change in the ordering can be manifested in a change in the degree of inversion of the ferrite structure or in the valence of the ions located at the different lattice sites.

The exact nature of the changes can be determined only through X-ray analysis.

Conclusions

1. An investigation of the variation of the electric resistivity of ferrites with temperature above and below the Curie point showed that the $R = Ae^{\Delta E/kT}$ holds both above and below this point, which is in conflict with the data of Bochirol (Ref. 5) but in agreement with the findings of Smolenski for nickel-zinc ferrites (Ref. 3).

2. It was also found that the magnitudes of A and E change in the vicinity of the Curie point.

In conclusion, the writer wishes to thank N. M. Reinov for his help in the investigation.

Physico-Technical Institute of the
Academy of Sciences of the USSR

Received
3 May 1954

Bibliographic References

1. L. Bochirol, C.R., 232, 1474 (1951).
2. L. Weil, C.R., 231, 122 (1950).
3. G.A.Smolenski, Izv.(Bulletin) AN SSSR,Ser.fiz., 16, 728 (1952).
4. A. Michel, Chaudron & Benard, Jorn. phys. et rad., 12, 189 (1951).
5. L. Bochirol, C.R., 233, 736 (1951).

А. П. КОМАР и В. В. КЛЮШИН

ЭФФЕКТ ГОЛЬДГАММЕРА—ТОМСОНА В ФЕРРИТАХ

THE GOL'DGAMMER-THOMSON EFFECT IN FERRITES

- A. P. Komar and V. V. Kliushin

In ferromagnetic metals and in certain alloys the variation of the electric resistivity - the so-called Gol'dgammer-Thomson effect (Translator's note: See last article in this Bulletin) - with technical magnetization has different signs in transverse and in longitudinal fields. In the region of the para-process the resistivity of ferromagnetic materials always decreases. For most ferromagnetics the dependence of the Gol'dgammer-Thomson effect on the magnetization is quadratic. The purpose of the present study was to investigate the effect in ferrites and to determine whether there is any connection between the variation of electric resistivity with the magnetic field and the magnetization.

Experimental Procedure

Specimens of nickel, copper and nickel-zinc ferrites in the form of cylindrical rods 8 mm in diameter and 20 to 50 mm in length were investigated; the resistivity measurements were made by the compensation (bridge) method with the use of probes. The applied magnetic field was varied from 0 to 10,000 oersteds. The measurement error in the 200-400 oersted field range did not exceed 10-15%; in stronger fields the probable error was 5-8%.

In addition to the Gol'dgammer-Thomson effect, the magnetization of the ferrite specimens in the section between the probes was determined by the ballistic method.

Experimental Results

The results of the measurements for nickel ferrite, shown in Fig. 1, indicated that in this ferrite the sign of the effect is negative both in transverse and in longitudinal fields. Analogous results were obtained for the copper and nickel-zinc ferrites.

Thus, Akulov's second rule of even effects, according to which the transverse and longitudinal effects in the region of technical magnetization differ in sign and are related by the proportion $\frac{\Delta\rho_\perp}{\rho} = -\frac{1}{2}\frac{\Delta\rho_\parallel}{\rho}$ does not hold for these ferrites. The identity of sign for alloys has already been observed by Komar and Portiagin (Ref. 1). Similar results for a chromium-tellurium alloy were reported by Fakidov, Grazhdankina and Kikoin (Ref. 2). An explanation of these results, based on taking into account the higher-power terms in Akulov's anisotropy law, has been given by Vonsovski (Ref. 3).

In general, departures from the second rule of even effects are possible in the following cases:

1) in the presence of volumetric effects; in this case, as has already been noted, it is necessary to take into account not only the second power terms but also the higher even-power terms in Akulov's expression for even effects:

$$\frac{\Delta a}{a} = K_1 \sum_{i=1,2,3} s_i^2 g_i^2 + K_2 \sum_{i \neq j} s_i s_j g_i g_j + K_3 \sum_{i \neq j} s_i^2 s_j^2 + \ldots,$$

in this case, too, the third anisotropy constant $K_3 \neq 0$;

2) in case the para-process exerts a strong effect;

3) in case the specimen exhibits structure.

The investigated specimens showed no structure, hence the last alternative could be eliminated. In order to determine which of the first two causes was primarily responsible for the departure from Akulov's second rule, we investigated the dependence of the galvanomagnetic effect in question on the temperature. Comparative curves for the variation of $\Delta\rho/\rho$ as a function of the field H in nickel ferrite at 20° and 140°C are reproduced in Fig. 1. It will be noted that the absolute magnitude of both the transverse and longitudinal effects decreases with increasing temperature.

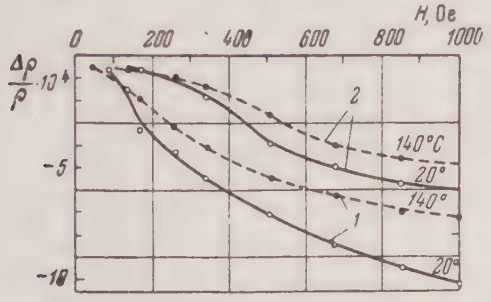

Fig. 1. Dependence of the resistivity of nickel ferrite on the field intensity and on temperature: Curve 1 - longitudinal field; Curve 2 - transverse field.

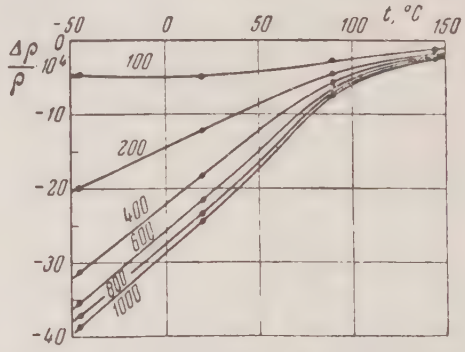

Fig. 2. Dependence of the galvanomagnetic effect on temperature in nickel-zinc ferrite (Curie point, Θ_f = 150°C).

Similar measurements were made for nickel-zinc ferrite at different temperatures up to the Curie point (Θ = 150°C). The results, depicted in Fig. 2, show that the magnitude of the effect is very small near the Curie point. The $\Delta\rho/\rho$ curves for ferrites show no maximum such as that exhibited by the curves for invar type alloys investigated by Belov (Ref. 4). This indicates that the part played by the para-process is insignificant. The maximum of the even effect in invar alloys was observed to occur in consequence of a strong para-process; Belov holds that the deviation from the second rule of even effects in the case of invar alloys is due to the influence of the para-process. Inasmuch as in ferrites the influence of the para-process is negligible while the spontaneous volumetric magnetostriction is appreciable (Ref. 5) it may be concluded that the principal reason for the departure from the second rule of even effects is the influence of magnetostriction. It will be noted that in Akulov's anisotropy law the factor determining the magnitude of the third constant, $K_3 \neq 0$, is precisely the magnetostriction.

In addition to measuring the galvanomagnetic effect, we also obtained the basic magnetization curves for the specimens for the purpose of determining the nature of the connection between the Gol'dgammer-Thomson effect and the magnetization. Both the negative sign of the effect (the decrease with increasing field intensity), characteristic of ferromagnetic materials (Fig. 1) and the evident approach of the magnitude of the effect to a saturation value with increasing field strengths (Fig. 2) prove that some such connection exists. In the range of technical magnetization the variation of $\Delta\rho/\rho$ with the magnetization is complicated, conforming neither to the I^2 nor to the I^4 law.

As the applied field is increased up to 10,000 oersteds the sign of both the transverse and longitudinal effects remains negative for all the investigated ferrites. In nickel ferrite the magnitude of $\Delta\rho/\rho$ approaches a saturation value as the field is increased (Fig. 3). In very strong fields the dependence of the galvanomagnetic effect on the magnetization approaches the quadratic law (Fig. 4).

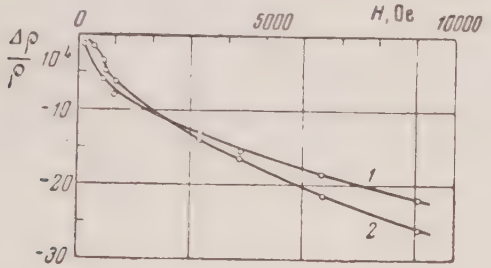

Fig. 3. Dependence of electric resistivity of nickel ferrite on the field intensity in the case of magnetization in a strong field: Curve 1) longitudinal field; Curve 2) transverse field.

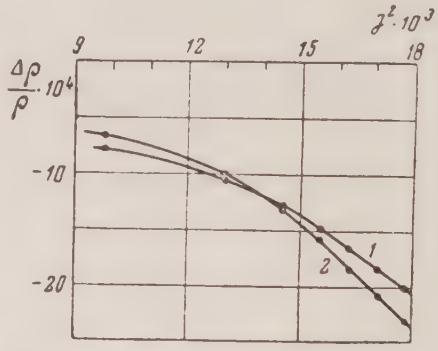

Fig. 4. Dependence of the galvanomagnetic effect in nickel ferrite on the degree of magnetization: 1) longitudinal effect; 2) transverse effect.

Conclusions

1. In ferrites the sign of both the transverse and the longitudinal Gol'dgammer-Thomson effects is negative (i.e. both effects decrease with increasing field intensity).

2. In view of the minor influence of the para-process, the departure from Akulov's second rule of even effects is apparently due primarily to volumetric magnetostriction.

3. The variation of the galvanomagnetic effect as a function of the technical magnetization is complicated (i.e. follows no single consistent law).

Physico-Technical Institute of the
Academy of Sciences of the USSR

Received
3 May 1954

Bibliographic References

1. A.P.Komar & I.I.Portiagin, Doklady AN SSSR, 60, 569 (1948).
2. I.G.Fakidov, N.P.Grazhdankina & A.K.Kikoin, Dokl.AN SSSR,68,491 (1949).
3. S.V.Vonsovski, Zhur. tekh. fiz., 18, 145 (1948).
4. K.P.Belov, Doklady AN SSSR, 71, 261 (1950).
5. L.Weil, C.R., 231, 122 (1950).

А. П. КОМАР, Н. М. РЕЙНОВ и С. С. ШАЛЫТ

ИССЛЕДОВАНИЕ ТЕМПЕРАТУРНОЙ ЗАВИСИМОСТИ САМОПРОИЗВОЛЬНОЙ НАМАГНИЧЕННОСТИ НЕКОТОРЫХ ФЕРРИТОВ ПРИ НИЗКИХ ТЕМПЕРАТУРАХ

AN INVESTIGATION OF THE TEMPERATURE DEPENDENCE OF THE SPONTANEOUS MAGNETIZATION OF CERTAIN FERRITES AT LOW TEMPERATURES

- A. P. Komar, N. M. Reinov and S. S. Shalyt

At the present time there is a great deal of scientific interest in the physical properties of a special class of ferromagnetic semiconductors: ferrites.

The object of our investigation was to determine experimentally the temperature dependence of spontaneous magnetization of ferrites at low temperatures, i. e. in the temperature range in which ferrites most clearly evince their semiconductor characteristics.

The theoretical aspects of the problem were investigated by Vonsovski and Agofonova (Ref. 1). Their treatment, based on a polar model of ferromagnetic semiconductors, taking into account excitons, leads to a temperature dependence of the spontaneous magnetization in the vicinity of absolute zero having the form:

$$J = J_0\left[(1 - \alpha T^{3/2}) - \alpha' T^{3/2} e^{-\frac{\gamma}{kT}} + e^{-\frac{\Delta E}{kT}}(1 - \alpha'' T^{3/2})\right],$$

where the first term is the usual dependence for the exchange model, the second term is a correction due to the admixture of polar states and the third term results from taking into account the excitons ($\triangle$E is the excitation energy of an exciton).

Hence, according to this theory, if the magnetic moments in ferromagnetic semiconductors are determined to any appreciable extent by the excited states, i.e. the excitons, then in the region of sufficiently low temperatures the J(T) curves for such materials must differ markedly from the analogous curves for ordinary metallic ferromagnetics; that is, such materials should exhibit two Curie points: the ordinary Curie point at a relatively high temperature, and another at a low temperature.

The experimental investigation of the magnetic properties of a large number of different types of simple and mixed ferrites in the temperature range from the Curie points to 20°K, carried out by Pauthenet (Ref. 2), disclosed no anomalies which could be attributed to magnetization due to excitons.

In view of this, it appeared worthwhile to extend the investigation of spontaneous magnetization into the range of the lowest attainable temperature.

Experimental Procedure

The magnetic moments of the ferrite specimen, which had the shape of an ellipsoid (a = 12 mm and b = 5 mm), were measured by the ballistic method. To this end two pairs of flat coaxial coils (r_1 = 50 mm, r_2 = 120 mm), with the windings (n_1 = 400 turns, n_2 = 160 turns) connected in opposition to compensate for fluctuations in the electromagnet supply current, were mounted directly on the polepieces of the electromagnet. The specimen holder was located in a glass Dewar, inserted into a second, larger Dewar (Fig. 1). The inner Dewar was filled successively with liquid nitrogen, hydrogen and helium. When helium was used in the inner flask, the outer Dewar was filled with liquid nitrogen. The temperature of the specimen was determined on the basis of the liquid used and the vapor pressure above it. For temperatures above room temperature an electric heater was installed between the polepieces instead of the Dewars. A special mechanical device (shown in Fig. 1) was provided for withdrawing the specimen from the system of ballistic coils so as to insure that the withdrawal time would be constant and much shorter than the period of the galvanometer. The specimen holder of nonmagnetic material terminated at its upper end in a toothed rack which engaged a gear wheel by means of which the specimen and holder were lowered into the center of the system of coaxial coils. Lowering the specimen and holder compressed a helical spring. The specimen was retained in the down position by a catch. When the catch was released the spring quickly pulled the specimen out of the system of coils, the return (withdrawal) time for each successive measurement of the magnetic moment being constant within the limits of the required accuracy.

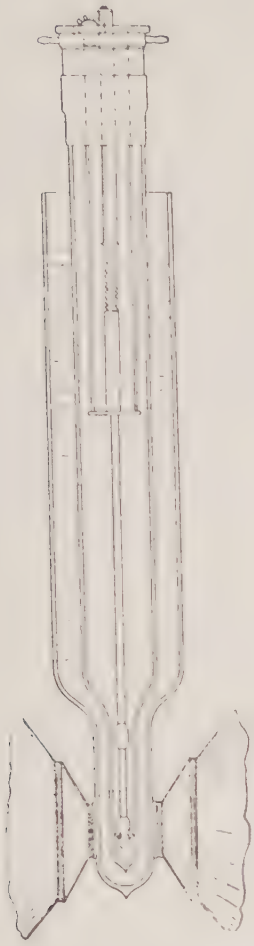

Fig. 1. Set-up for measuring magnetic moments

The magnetic field inside the system of coils was calibrated by the ballistic method by means of a special induction coil with a known area of turns and a standard solenoid. To permit allowing for the effect of magnetic reflection in the iron polepieces, the variation of the sensitivity of the ballistic system with the intensity of the magnetic field was determined. For this purpose a coil having a known area of turns and the geometric dimensions of the specimen was mounted in the holder in place of the specimen. Passing a known current through this coil provided a "standard" magnetic moment whose magnitude was independent of the external field. This "standard" coil was used to calibrate the ballistic system of coaxial coils to permit determining the absolute magnitude of the magnetic moments of the investigated specimen.

Results

The experimentally determined magnetization curves for a nickel-zinc ferrite specimen (Composition: Fe_2O_3-0.6, NiO-0.4, ZnO) at

different temperatures are shown in Fig. 2. After forming, the specimen was roasted at 1350°C and then cooled slowly to room temperature over a period of six hours. As may be seen from the curves, saturation was attained at external field intensities of H_e = 3000-5000 oersteds (the magnetization of the specimen is scaled along the Y-axis in arbitrary units).

The temperature dependence of the saturation magnetization for nickel-zinc ferrite in the temperature range from the Curie point down to 1.3°K is shown in Fig. 3. Here the relative temperature - i.e., the ratio of the absolute temperature of the specimen to the Curie temperature - is laid off along the X-axis. The Curie points were taken from Pauthenet's data (Ref. 2). For the investigated nickel-zinc ferrite the Curie temperature is 618°K. The Y-axis in Fig. 3 is laid off in ratios of the magnetization of saturation at the given temperature to the saturation magnetization at 0°K. The latter was determined by extrapolating the experimental curves to absolute zero. The curve in the upper part of the figure shows the variation of saturation magnetization with the absolute temperatures in the vicinity of 0°K.

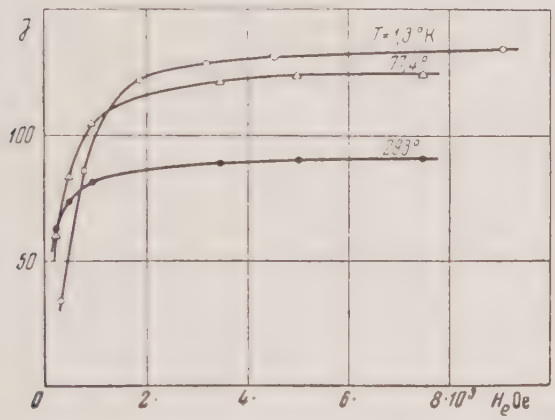

Fig. 2. Magnetization curves for $Fe_2O_3$00.6 NiO-0.4 ZnO ferrite at different temperatures

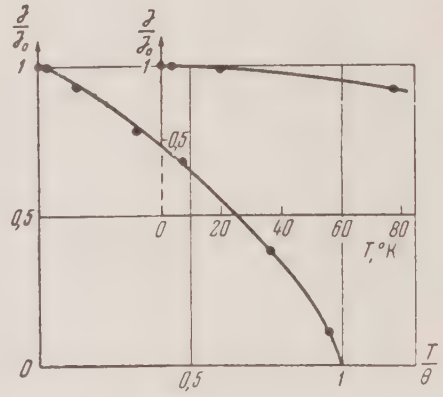

Fig. 3. Temperature dependence of saturation magnetization of the same ferrite (as in Fig. 2) in the temperature range from Curie point (618°K) to 1.3°K. Top curve: saturation vs absolute temperature in the vicinity of 0°K.

The results of preliminary measurements on a nickel-zinc ferrite specimen, having a low nickel content (Fe_2O_3-0.1 NiO-0.9 ZbO), indicate that for this ferrite, too, the saturation magnetization increases monotonously with decreasing temperature down to 1.3°K.

Conclusions

The results of our investigation show that the variation of the spontaneous magnetization of nickel-zinc ferrites with temperature is normal down through the temperature range from the Curie point to 1.3°K, i.e., there is no evidence of a decrease in the saturation magnetization at very low temperatures.

Physico-Technical Institute of the
Academy of Sciences of the USSR

Received
3 May 1954

Bibliographic References

1. S.V.Vonsovski & E.N.Agafonova, in Symposium dedicated to the 70th anniversary of Academician A.F.Ioffe, p.92. Pub.by the AN SSSR, M.-L. 1950.
2. R. Pauthenet, Ann. de phys., 7, 710 (1952).

* * * * * * *

DETERMINATION OF THE TEMPERATURE DEPENDENCE OF THE ELECTRIC RESISTANCE OF NICKEL-ZINC FERRITES

- A. L. Frumkin and S. D. Kholodnyi

The absolute magnitude and the temperature dependence of the electric resistance are important characteristics of ferrites. That the resistance of ferrites is connected with or influenced by their other properties is indicated by the fact that both the resistance and the magnetic properties change simultaneously at low temperatures (Ref. 1), by the equality of the values of the activation energy determined from the temperature dependence of the resistance and from the dielectric constant (Ref. 2) and by other observed data. In practical applications the resistance itself is an important characteristic inasmuch as it determines the eddy-currents loss.

The resistance of ferrites, like that of certain other semiconductors, depends on their composition, the method of sintering and cooling and the medium in which the thermal treatment is carried out. Thus, an increase in the proportion of FeO leads to a decrease in the resistance. Rapid cooling results in a ferrite with low specific resistance and a low activation energy: the activation energy of a quickly cooled specimen may be half that of a slowly cooled specimen of the same composition (Ref. 2), while the resistance may be two orders of magnitude lower (Ref. 3).

All investigators report that the variation of the resistance with temperature is an exponential function in a wide temperature range. The resistance-temperature curves for both increasing and decreasing temperatures coincide up to 200-250°C. The conductivity of ferrites is electronic in character (Ref. 4).

Measurement of the resistance of ferrites presents some difficulty due to contact effects. To obtain a good contact the surface of the ferrite must be metallized by cathodic deposition in a vacuum, by burning-in or by a combination of cathodic and electrolytic deposition of a noble metal.

In the laboratory of the Department of the Theoretical Bases of Electrical Technology of the Moscow Energetics Institute, Imeni Molotov, we measured the specific DC resistance of Grade 0-1000 and 0-2000 ferrites and determined the variation of the resistance temperature.

Our specimens Nos. 1001, 1002, 2001 and 2002, received from the N. N. Shol'ts Laboratory, were in the form of square-section (10 x 10 mm) rods, 30 mm in length. Measurements on the first three were made in the temperature interval from 20 to 70°C; those on No. 2002 extended over the 20-150° interval.

The results given below were obtained by the potentiometer method of resistance measurement. At the same time, in order to compare the quality of different electrodes, we also measured the resistance by the ammeter-voltmeter method.

The error in measuring by the potentiometer method did not exceed 5%; the principal source of error was the non-uniform distribution of current over the specimen which is most noticeable in the case of short specimens. The possibility of any appreciable errors due to incomplete heating through of the specimen, to heating of the specimen by the measuring current or to inhomogeneity of the temperature field of the thermostat may be discounted.

The functional dependence of the resistance of the specimens on the temperature was found to have the form common to semiconductors;

$$\rho = \rho_0 e^{\frac{E}{k}\left(\frac{1}{T} - \frac{1}{T_0}\right)}.$$

This is in agreement with the data given in Ref. 1.

At 19°C the measured resistances were 32,000 ohm·cm for specimen No. 1001, 3450 ohm·cm for No. 1002 and 1400 ohm·cm for Nos. 2001 and 2002.

For all samples the value of the activation energy E was close to 0.23 eV, the value of B (=E/K), close to 2800°C and the magnitude of the temperature coefficient, close to 0.03.

With weak currents - i.e. when the power dissipated in the specimen did not exceed 10 m W cm^{-3} - the specimens gave no indication of non-linearity. With heavier currents non-linearity, due to heating, appears and the V-i curve falls off. Resistance measurements on other ferrite specimens, having a higher resistance, showed no departure from linearity up to potential gradients of 1 kV cm^{-1}.

We also measured the thermoelectromotive power of sample No. 1002 with respect to copper and found this to be $1 \cdot 10^{-4}$ V/°C. This indicates that the conductivity is electronic, which is in agreement with Smolenski's data (Ref. 4).

In using the potentiometer method we became convinced that in applying this method it is essential to use "probes" making contact with the entire periphery of the specimen rather than just touching it at one or more points, as is the case when knife-edge probes (contacts) are employed. Use of peripheral contacts minimizes the influence of non-uniform current distribution over the specimen.

In determining the temperature dependence of the resistance of several specimens, placed side-by-side in the thermostatic chamber, there is no need to have special potentiometer clamps for each specimen: we successfully used contact wires wrapped around each specimen. The method of processing the results eliminated the necessity of accurately measuring the distance l between the potentiometer probes (clamps) for each observation. The procedure consisted in obtaining a number of temperature dependence curves for each specimen, differing from each other by constant multiples of the roughly determined value of l and then reducing these to a single curve passing through the accurately determined resistance at some known temperature.

Although the resistance can be determined by the potentiometer method which eliminates the influence of current contacts, the matter of providing high-quality electrodes (contacts) is extremely important for other measurements (for example, for measuring the dielectric constant).

The electrode-ferrite resistance depends on two factors: 1) the actual metal-to-ferrite-surface contact resistance, whose magnitude stems from the fact that the contacting surfaces are not ideal planes and 2) the resistance of the ferrite surface layer, which, presumably,

forms during thermal treatment. The resistance of this surface layer is very high. Thus, the resistance of a specimen as measured by the ammeter-voltmeter method dropped to less than one hundredth the initial value after removal of the surface layer. Hence, it can be asserted that good contact with the material proper cannot be secured by metallizing the ferrite surface unless the surface layer is removed beforehand.

Most methods of metallizing are rather complicated and require special equipment. We were able to obtain a good covering of the ferrite surface with a relatively low specific resistance by the following procedure. A layer of copper was first deposited on the ferrite electrolytically, then this coating was tinned and finally the wire lead was soldered to it. However, it is virtually impossible to deposit a uniform layer of copper on specimens, having high specific resistance.

When great accuracy is not required, satisfactory results may be obtained by coating the contacting surfaces of the ferrite specimen with a suspension of graphite or acetylene black in some suitable liquid, such as glycerin. With a properly prepared suspension the error will not exceed 30% and may be considerably smaller. However, such coatings can only be used at temperatures which preclude rapid vaporization or carbonization of the liquid.

Other methods of metallizing, such as silvering, for example, do not always yield satisfactory results. Hence, when metallizing is employed it is essential to check the quality of the contacts. One possible check is to test the specimen for non-linearity, since ferrite itself apparently does not exhibit non-linearity. The check test should be carried out using weak currents to avoid the appearance of non-linear effects due to heating. The quality of the contacts may also be checked by comparative tests on specimens of different lengths.

In attempting to copper plate the No. 1002 ferrite specimen (ρ = 3450 ohm·cm), we discovered that the copper was being deposited in spots rather than in a uniform layer. When the plating was repeated after cleaning and grinding the ferrite surface with an emery stone the spots reappeared at the same locations. The process was repeated several times and the overall spot-pattern was found to change little, if at all.

Possibly ferrite is a macroscopically inhomogeneous material, having regions of different conductivity. This supposition is supported by the fact that exploration of the surface of the specimen with a contact needle discloses areas of different conductivity.

The question of the possible macro-inhomogeneity of ferrites unquestionably merits further investigation.

Our investigation was carried out at the suggestion and under the supervision of K. M. Polivanov. We were constantly helped by Ia. N. Kolli and S. N. Andreev.

Moscow Energetics Institute
Imeni V. M. Molotov

Received
16 May 1954

Bibliographic References

1. Ia.G.Dorfman, Izv.(Bulletin) AN SSSR,Ser.fiz., 16, 412 (1952).
2. Kan-ichi Kamiyoshi, Phys. Rev., 84, 374 (1951).
3. L.Bochirol, C.R., 233, 736 (1951).
4. G.A.Smolenski, Izv. (Bulletin) AN SSSR, Ser.fiz.,16, 728 (1952).

INFLUENCE OF A HIGH-FREQUENCY FIELD ON THE ELECTRIC RESISTANCE OF FERROMAGNETIC MATERIALS

- R. A. Dautov

Introduction

It is known that spontaneous magnetization may have an appreciable influence on the temperature dependence of the electric, magnetic and other properties of ferromagnetic materials. Furthermore, the properties of a ferromagnetic substance may be affected (through changes in the magnetization) by the external magnetic field, by external mechanical forces and, in the case of alloys, by the degree of ordering (Ref. 1).

Russian and Soviet physicists have long studied these peculiar properties of ferromagnetics. Thus, Gol'dgammer, back in 1889 (Ref. 2), noted that the electric resistance of metals in the ferromagnetic state (at $T < \Theta$, where Θ is the Curie point) varies as the square of the spontaneous magnetization.

The most thorough investigation of the Hall-Kikoin transverse galvanomagnetic effect in ferro- and paramagnetic materials has been made by Kikoin (Ref. 3), who established that the Hall voltage is determined not by intensity of the applied external field but by the degree of magnetization of the metal. Not long ago evidence was found of a break at the Curie point in the photoelectric current - temperature curve for ferromagnetics (Ref. 4).

The physical nature of these "anomalies" in the behavior of ferromagnetic materials has been clarified by the theory developed by Vonsovski and his colleagues (Ref. 5), who base their treatment on the s-d-exchange interaction model.

According to the calculations of these authors, the intensity of the Gol'dgammer effect (change in resistance with magnetization) among others, should vary directly as the square of the magnetization of the specimen; this theoretical deduction is in good agreement with experimental data.

On the other hand, studies of para- and ferromagnetic resonance carried out by Zavoiski (Ref. 6) and others (Ref. 7) have established that the magnetization of paramagnetic and ferromagnetic materials is altered when both a high-frequency magnetic field and a static field perpendicular or parallel to it are applied simultaneously.

For instance, in the case of a spherical ferromagnetic specimen in a high-frequency field and a static field perpendicular to the h-f field, the component of the magnetization in the direction of the static field is described by

$$M_z = \frac{M_0}{1 + \frac{1}{2}\gamma^2 H_1^2 T_1 T_2 \frac{\omega_0^2 + \omega^2}{4\omega^2 + T_2^2(\omega_0^2 - \omega^2)^2}},$$

where ω is the frequency and H_1 the amplitude of the high-frequency field, M_0 is the saturation value of the magnetization, γ is the gyromagnetic ratio, T_1 is the spin-lattice relaxation time, T_2 is a quantity characterizing the width of the resonance line and ω_0 is the electron spin precession frequency.

It will be seen from this equation that, in the presence of a high-frequency magnetic disturbance of large amplitude, the magnetization of the specimen does not remain constant and equal to M_0.

It may, therefore, be assumed that through its effect on the magnetization a high-frequency field will produce changes in the non-magnetic properties of the material, i.e., that the ohmic resistance,

the transverse e.m.f. /Hall voltage/, the photoelectric current and other properties displayed by the ferromagnetic material will depend in some manner on the characteristics of the high-frequency magnetic field.

The purpose of the present study was to investigate the dependence of the longitudinal and transverse Gol'dgammer effects on the high-frequency magnetic field.

Experimental Procedure and Specimens

The experimental set-up consisted of a push-pull oscillator designed about a 6N7 tube. The oscillator output coil, with the specimen inside it, was located in the gap of the electromagnet which was capable of producing a static field of up to 2000 oersteds. The oscillator was supplied from storage batteries. The frequencies of the field produced by the oscillator were $4.33 \cdot 10^7$ and $3.07 \cdot 10^7$ cycles; the amplitude of the high-frequency field was of the order of 7 oersteds. The relative change of the electric resistance was measured by means of the unbalanced bridge circuit described by Vilbig (Ref. 8) and utilized for the same purpose by Fedenev (Ref. 9). The alternating magnetic field was oriented in the plane of the specimen; the static field was perpendicular to the direction of the current for measurement of the transverse effect and parallel to the current for measurement of the longitudinal effect.

The measurements were made on polycrystalline specimens of silicon steel (about 4% Si) and dynamo grade steel (1% Si) in the form of thin rectangular section plates 27 x 2.5 x 0.09 mm and on one specimen of manganese-zinc ferrite (30% Mn, 20% Zn) in the shape of a disc 1.5 mm thick and 8 mm in diameter.

Prior to measurement the specimens were thoroughly demagnetized by the method of DC reversals. Next the variation of the resistance in a static field only was observed, the data being obtained for both directions of the field and of the current flow. Reversing the field made it possible to discount any apparent changes in the resistance due to the Hall voltage. Reversal of the current made it possible to eliminate the influence of the thermoelectromotive force and contact-potential differences.

After these preliminary measurements the specimen was again demagnetized before being placed in the h-f coil. The measurements in the presence of the h-f field were initiated only after thermal equilibrium was established and were carried out at room temperature, to the same accuracy and in the same manner as described above (i.e., for both directions of the static magnetic field and current flow).

Results and Conclusions

The observed variations of the relative electric resistance with the intensity of the static magnetic field are shown in Figs. 1 through 4. Curves 1 in Fig. 1-3 characterize the static Gol'dgammer effect. Curves 2 represent the dynamic Gol'dgammer effect due to the simultaneous influence of mutually perpendicular alternating and static magnetic fields.

As may be seen from the curves, in both the static and dynamic cases the electric resistance varies rather rapidly with the field strength in the range of relatively weak fields. This range corresponds to technical magnetization of the specimen. As the field strength [illegible] the rate of change of the resistance falls off.

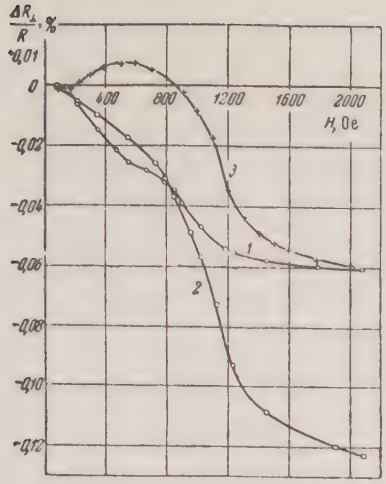

Fig. 1. Dependence of Gol'dgammer effect on transverse static field for silicon steel (~4% Si): 1) static effect in static field only, 2) dynamic effect in mutually perpendicular static and oscillating fields, 3) difference.

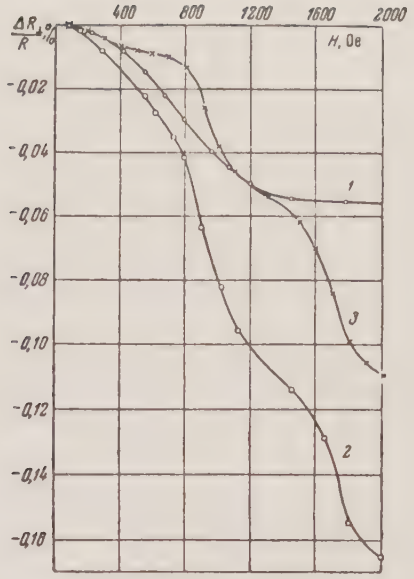

Fig. 2. Same as Fig. 1 but for dynamo steel (1% Si).

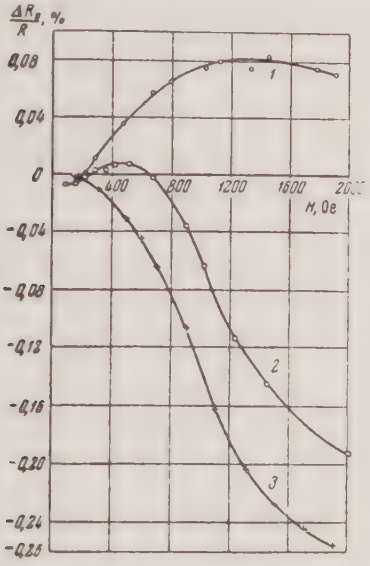

Fig. 3. Dependence of Gol'dgammer effect on longitudinal field for silicon steel (~4% Si): 1) static effect, 2) dynamic effect in mutually perpendicular fields, 3) difference.

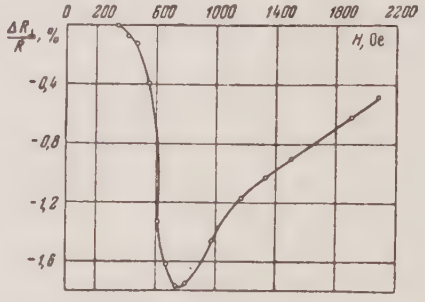

Fig. 4. Dependence of Gol'dgammer effect on transverse static field for manganese-zinc ferrite (30% MnO - 20% ZnO - 50% Fe_2O_3)

The variation of the relative resistance $\Delta R_\perp/R$ is more rapid under the influence of a high-frequency field as compared with a static field; in the case of the longitudinal effect the functional dependence even changes sign from plus to minus.

Curves 3 in Figs. 1-3 represent the difference between the dynamic and static effects at different values of the static field. These curves characterize the change in the component of the magnetization of the specimen in the direction of the static field, due to the influence of the high-frequency field.

A non-ferromagnetic metal, specifically, electrolytic copper, was subjected to the same tests. In this case there were no noticeable changes in the resistance with application of the high-frequency and

static magnetic fields, which shows that the effect in question is clearly apparent only in ferromagnetics.

In view of the low value of the electric conductivity of ferrites the depth of penetration of the alternating electromagnetic field is appreciable so that a relatively large volume of the specimen participates in the process. Hence, determination of the variation in $\Delta R_{\perp}/R$ and $\Delta R_{\parallel}/R$ in ferrites should be of particular interest.

We had available for test purposes a piece of polycrystalline manganese-zinc ferrite (30% MnO, 20% ZnO and 50% Fe_2O_3) from which a specimen in the form of a disc was prepared (initial resistance: 11.1 ohms). This shape was selected to facilitate determining the distribution of the current through the specimen. To insure good contact for the current leads the surfaces of the disc were metallized by silvering in a vacuum. Only weak currents were used to minimize heating effects.

The mutually perpendicular high-frequency and static fields were oriented parallel to the plane surfaces of the disc while the current flow was perpendicular to both fields. Thus, what we observed was the transverse Gol'dgammer effect. Measurements on the ferrite disc were made at a frequency of $3.07 \cdot 10^7$ cycles. It was found that in the absence of a static field the resistance of the ferrite dropped rather rapidly under the influence of the high-frequency field. It was found that with the application of the high-frequency field the resistance fell to about 30% of the initial value; this drop was taken into account in the subsequent measurements. With the application of the static field there was observed a further decrease in resistance, with the resultant curve showing a distinct resonance-type dip. The dynamic effect curve, i.e., the relative resistance plotted against the magnetization in the transverse static field - is reproduced in Fig. 4. The variation in resistance proved to be large, so that measurements could be made with a less sensitive instrument: specifically, we used a conventional Type MD-6 double bridge for determining the dynamic values of $\Delta R_{\perp}/R$ for the ferrite specimen.

We have not yet been able to compare the observed data for either the ferrite or the steel specimens with corresponding ferromagnetic absorption data.

It may be concluded as a result of our investigation that the electric resistance of ferromagnetic materials is definitely influenced by an applied high-frequency magnetic field.

Kazan' State Pedagogical Institute

Received
13 May 1954

Bibliographic References

1. S.V.Vonsovski, Sovremennoe uchenie o magnetizme (Modern teachings on magnetism), Gostekhizdat, M.-L. 1953.
2. D.I.Gol'dgammer, Uchenye zapiski Moskovskogo universiteta (Scientific Notes of the University of Moscow), 8, 1, (1889).
3. I.K.Kikoin, Sow.Phys., 9,1 (1936);Zhur.eksp. i teor.fiz.,10,1242 (1940).
4. A.B.Cardwell, Phys. Rev., 76, 125 (1949).
5. S.V.Vonsovski, Zhur. eksp. i teor.fiz., 16,981 (1946); Vonsovski, Kobelev & Rodionov, Izv.(Bulletin) AN SSSR, Ser.fiz., 16, 569 (1952).
6. E.K.Zavoiski, Thesis, FIAK 1944.
7. R.W.Damon, Rev. Mod. Phys., 25, 239 (1953).
8. F.Vilbig, Archiv f. Elektrotechnik, 22, 194 (1929).
9. D.R.Fedenev, Zhur. tekh. fiz., 23, 828 (1953).

Bulletin of the Academy of Sciences of the USSR - Physical Series
Vol. 18, No. 3, 1954 - Conference on Ferrites (1-5 Feb. 1954)

TABLE OF CONTENTS

	Page Trans.	Orig.
Vladimir Konstantinovich Arkad'yev (1884-1953) - K.M.Polivanov	1	307
Certain problems connected with the quantum-mechanical theory of ferromagnetism of ferrites and antiferromagnetism. Part I. A critical survey of present theory - S.V.Vonsovski	6	312
Certain problems connected with the quantum-mechanical theory of ferromagnetism of ferrites and antiferromagnetism. Part II. The quantum-mechanical theory of ferromagnetic ferrites - S.V.Vonsovski and Iu.M.Seidov	14	319
Certain problems connected with the quantum-mechanical theory of ferromagnetism of ferrites and antiferromagnetism. Part III. The antiferromagnetism of transition metals - A.A.Berdyshev & S.V.Vonsovski	23	328
A contribution to the theory of antiferromagnetism.- K.B.Vlasov	35	339
Rotation of the plane of polarization of centimeter waves by a ferrite disc - K.M.Polivanov, Ia.N.Kolli and M.B.Khasina	46	350
On measuring paramagnetic resonance absorption by the standing wave method in the centimeter wave band - N.N.Neprimerov	55	360
Rotation of the plane of polarization in paramagnetic substances and ferrites - N.N.Neprimerov	63	368
Investigation of the Faraday effect in ferrites at centimeter wavelengths - N.A.Smol'kov	74	378
A ferrite disc in a coaxial line - Ia.N.Kolli & K.M.Polivanov	78	382
The temperature dependence of the electric resistivity of ferrites - A.P.Komar and V.V.Kliushin	96	400
The Gol'dgammer-Nikolson effect in ferrites - A.P.Komar & V.V.Kliushin	99	403
An investigation of the temperature dependence of the spontaneous magnetization of certain ferrites at low temperatures - A.P.Komar, N.M.Reinov and S.S.Shalyt	102	406
Determination of the temperature dependence of the electric resistance of nickel-zinc ferrites - A.L.Frumkin and S.D.Kholodnyi	105	409
Influence of a high-frequency field on the electric resistance of ferromagnetic materials - R.A.Dautov	108	142

Translated in 1955 by
Columbia Technical Translations
5 Vermont Ave., White Plains, N.Y.

Single issues: $20 each.
Individual articles: $8 each.

MAGNETIC SPECTRA DUE TO THE MACROSCOPIC STRUCTURE OF THE MATERIAL

- N. G. Katkov and K. M. Polivanov

1. Introduction

In developing the theory of magnetic spectra, Arkad'ev introduced not only the now commonly accepted concepts of permeability of the substance and permeability of the body but also the concept of the permeability of the material (Ref. 1, p. 121), i.e. of the apparent permeability of a body or specimen having a composite structure, as, for example, a core consisting of a stack of steel laminae. Another and perhaps more important example of a ferromagnetic to which the concept of complex permeability of the material should be applied is furnished by artificial magneto-dielectrics: conglomerates composed of a ferromagnetic powder bonded in an insulating base. The permeability of such composite materials is determined to an appreciable extent by their macroscopic structure. It is conceivable that the magnetic spectrum of ferrites also depends on their structural inhomogeneity.

Borrowing from the terminology of optics, the frequency-dependence of the permeability may be termed dispersion. Then, in view of the different physical processes that affect this dependence, we must distinguish between 1) dispersion of the substance (or medium), 2) dispersion of the form (or body) and 3) dispersion of the structure (or material, or body of complicated shape).

Dispersion of the substance is determined by the dynamics of polarization, dependent upon the properties of the elementary magnetic moment carriers (gyromagnetic resonance - Ref. 2), by the statistical laws governing transitions from one equilibrium state to another (see Editorial note No. 8 in Russian translation of Smythe's book - Ref. 3), by the inertia of magnetic domain boundary displacements (Refs. 2 and 4), by the rise of eddy currents, accompanying domain boundary displacements (Refs. 2, 4 and 5), by diffusion processes, i.e. atomic rearrangements incident to domain boundary displacements (Ref. 3) and by a number of other, similar processes, most of which were described in general terms by Arkad'ev (Ref. 1).

Magnetic dispersion of the substance may be characterized by damping (anomalous dispersion) or by resonance (normal dispersion).

The simplest instance of dispersion of the form is furnished by the influence of skin effect on the mean or apparent magnetic permeability. The influence of skin effect depends both on the electromagnetic characteristics of the material and on the form of the body (the shape of the specimen) introduced into the alternating field.

Thus, for a long rod of rectangular cross section in a longitudinal alternating field the apparent magnetic permeability is given by (Ref. 6)

$$\bar{\mu} = \bar{\mu}_1 - j\bar{\mu}_2 = \mu\left[1 - 0{,}657 \sum_{m,\,n} \frac{1}{m^2 n^2 \left[1 + \frac{\pi^2}{4}\left(\frac{m^2}{a^2} + \frac{n^2}{b^2}\right)\frac{1}{\Gamma^*}\right]}\right], \qquad (1.1)$$

where m and n are series of odd integers, 2a and 2b are, respectively, the thickness and width of the rod,

$$\Gamma^* = j\omega\mu\mu_0\sigma - \left(\frac{\omega}{c}\right)^2 \varepsilon\mu, \qquad (1.2)$$

ω is the circular frequency, μ_0 is an electrodynamic constant, dependent upon the system of units employed, c is the speed of light, μ is the magnetic permeability and ε the dielectric constant of the substance, and σ is the electric conductivity.

If the second term in (1.2) is neglected, we obtain the usual expression for the apparent magnetic permeability of a rod in the presence of skin effect. In this case the dispersion of form will be characterized by damping (with several damping constants).

In the case of ferrites, the second term in the expression for Γ^* may turn out to be the dominant one, especially at high frequencies. In this case the dispersion of form curve will exhibit resonance characteristics (with a series of natural frequencies). The attenuation of the natural frequencies of the rod, which in this case may be likened to a cavity resonator, will be determined by the imaginary components of the dielectric constant and permeability of the substance.

When $b \gg a$, (1.1) reduces to the familiar expression for the skin effect in a thin plate:

$$\mu = \mu \frac{\operatorname{th} a\sqrt{\Gamma^*}}{a\sqrt{\Gamma^*}}. \tag{1.3}$$

Dispersion of the form for a conducting sphere in a homogeneous alternating field was exhaustively investigated by Divil'kovski in 1939 (Ref. 7). The same problem is treated in a somewhat different manner by Smythe (Ref. 8); the equations given by Smythe are more convenient for direct determination of the equivalent permeability of such a sphere. Thus, according to Smythe, in the case of a sphere in an external homogeneous field H_0, the radial and tangential components of the field in the region outside the sphere are given by*

$$\left.\begin{aligned} \dot{H}_\theta &= -\dot{H}_0\left(1 - \frac{D}{2r^3}\right)\sin\theta, \\ \dot{H}_r &= \dot{H}_0\left(1 + \frac{D}{r^3}\right)\cos\theta, \end{aligned}\right\} \tag{1.4}$$

where

$$D = \frac{(2\mu+1)\,v I_{-1/2}(v) - (1+v^2+2\mu)\,I_{1/2}(v)}{(\mu-1)\,v I_{-1/2}(v) + (1+v^2-\mu)\,I_{1/2}(v)}\,a^3 = \frac{(2\mu+1)\,v - (1+v^2+2\mu)\operatorname{th} v}{v(\mu-1) + (1+v^2-\mu)\operatorname{th} v}\,a^3. \tag{1.5}$$

Here $v^2 = j\omega\gamma\mu\mu_0 a^2$, a is the radius of the sphere and the other letters are as defined above.

Under static conditions ($\omega \to 0$), the field intensity components due to a sphere in a homogeneous external field (in the region outside the sphere) are given by the familiar expressions:

$$\left.\begin{aligned} H_\theta &= -H_0\left(1 - \frac{\mu-1}{\mu+2}\cdot\frac{a^3}{r^3}\right)\sin\theta, \\ H_r &= H_0\left(1 + \frac{\mu-1}{\mu+2}\cdot\frac{2a^3}{r^3}\right)\cos\theta. \end{aligned}\right\} \tag{1.6}$$

Comparing (1.4) and (1.6), we find that the sphere produces a field such as though there were no eddy currents in the sphere, but has an equivalent permeability, defined by the proportion

$$\frac{\mu_{equi}-1}{\mu_{equi}+2}\,a^3 = \frac{D}{2}. \tag{1.7}$$

This value of the equivalent permeability,

---

* We have made some changes in the notation employed by Smythe to conform with the common usage in our (Soviet) electrotechnical literature: · over capital letter to designate complex expressions for sinusoidally varying quantities.

/Translator's note: To permit photographic reproduction, we are retaining the modified (Soviet) notation./

$$\mu_{equi} = 2\mu \frac{v - \operatorname{th} v}{v^2 \operatorname{th} v - (v - \operatorname{th} v)} \qquad (1.8)$$

is the one that should be taken as the apparent value of the complex permeability, due to dispersion of the form.

2. Structural dispersion in artificial magneto-dielectrics

The structure of the most common type of artificial dielectrics may be described as a system of spheres of equal radius a, separated from each other by an insulating medium. Derivations of the equations for the mean permeability of such composite materials in static fields will be found in Ollendorf (Ref. 9) and Kondorski (Ref. 10). Ollendorf treats the system of spheres as a system of randomly distributed dipoles and, in conformity with the argument of Lorentz and Debye, assumes that the influence of nearest neighbors is absent. As the result of his calculations, Ollendorf arrives at the following equation for the permeability of the material (under static conditions):

$$\bar{\mu} = \frac{1 + \left[p + \frac{1}{3}(1-p)\right](\mu - 1)}{1 + \frac{1}{3}(1-p)(\mu - 1)}, \qquad (2.1)$$

where p is the filling factor (Füllfaktor), i.e., the ratio of the volume occupied by the ferromagnetic substance to total volume of the conglomerate.

The magnitude of the permeability computed according to Ollendorf's equation usually turns out to be lower than the actual value for most magneto-dielectrics. Thus, from (2.1) for p = 0.5 we get $\bar{\mu} = 4$ even for $\mu \to \infty$, while experiments yield generally higher values of $\bar{\mu}$ and indicate a stronger influence of the permeability of the ferromagnetic phase on the permeability of the conglomerate.

It must be noted that Ollendorf's assumptions are valid only for low values of the filling factor.

In his treatment, Kondorski (Ref. 10) proceeds from the assumption that the ferromagnetic particles, having a permeability μ, are surrounded by a medium characterized by a permeability equal to the mean permeability of the material ($\bar{\mu}$). In this case the permeability of the material

$$\bar{\mu} = \frac{1}{4}[2 - 3p + \mu(3p-1)] + \sqrt{\frac{1}{16}[2 - 3p + \mu(3p-1)]^2 + \frac{1}{2}\mu}. \qquad (2.2)$$

In contrast to Ollendorf's equation, (2.2) gives an exaggerated value of the permeability and yields satisfactory results only in cases where the permeability of the ferromagnetic phase itself is relatively low.

The comparative values of the mean permeability of the material ($\bar{\mu}$) as a function of the filling factor, computed according to the equations of Kondorski (2.2), Lichtenecker (2.6) and Ollendorf (2.1) are shown in graphic form in Fig. 1.

The same value of the permeability of the ferromagnetic phase, μ, chosen to make the Lichtenecker equation curve pass through the available experimental points, was used in plotting curves K_1, L and O_1.

It is impossible to make an analogous selection of μ for the Ollendorf equation (2.1), since even with $\mu \to \infty$, the theoretical Ollendorf curve (Curve 2 in Fig. 1) lies well below the curve through the experimental points.

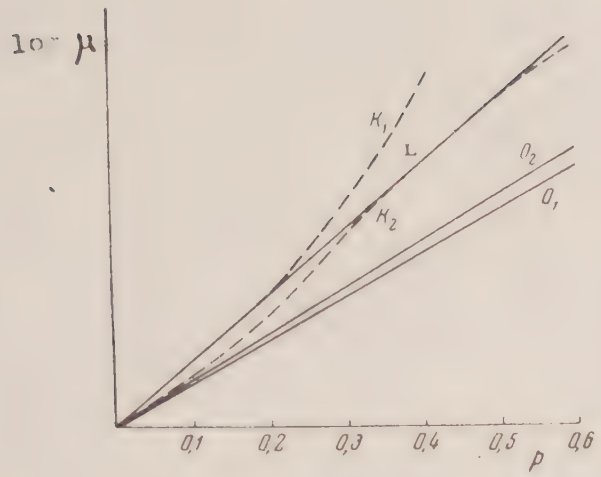

Fig. 1. Dependence of the computed mean permeability ($\bar{\mu}$) of an artificial magneto-dielectric on the filling factor, Curves K_1 and K_2 computed according to Kondorski's equation (2.2); Curve L, according to Lichtenecker's equation (2.6); Curves O_1 and O_2, according to Ollendorf's equation (2.1). By design, experimental values virtually coincide with curve L. The same values of the permeability of the substance, selected to make the curve L, based on (2.2), pass through the experimental points, were used in computing K_1, L and O_1. For curve K_2 the value of the permeability was reduced to make the values from (2.2) agree with experimental data for $p \approx 0.5$; curve O_2 was computed assuming $\mu \to \infty$.

Curve K_2 is plotted according to (2.2), using a value of μ such that the resultant theoretical Kondorski curve is in agreement with the experimental data in the region of $p \approx 0.5$. In this case the magnitude of μ must be reduced to 0.415 of the value determined on the basis of the Lichtenecker curve [i.e., to make curve L pass through the experimental points]. To evaluate the degree to which Kondorski (2.2) and Lichtenecker's (2.6) equatio agree with experimental data we must know the true values of the permeabili of the substance. Unfortunately, experimental determination of the permeability of the substance composing the fine ferromagnetic particles, is extremely difficult, so that in most cases the true value of this permeability remains unknown.

It must be noted that while the experimentally determined values of the mean permeability $\bar{\mu}$ of the materia lie on or close to the Lichtenecker curve as plotted, the value of the per meability of the substance which must be assumed to obtain this agreement is much lower than the permeability prope to the same ferromagnetic substance, a determined for large specimens. This is presumably to be explained by a decrease in the permeability of the substance with reduction in particle size

Fradkin (Ref. 11), in his treatment of the problem of the frequency dependence of the permeability of artificial dielectrics, assumes that each of the minute spheres is magnetized in accordance with Divil'kovski's equation, and replaces the actual applied external field by the field defined by Ollendorf's or Kondorski's equations. (Electrodynamic calculations for determining the properties of artificial magneto-dielectrics have also been carried out by Levin ((Ref. 12)). However, Levin's final equation is identical with Ollendorf's equation ((2.1)), given above, if Levin's μ is replaced by μ_{eqiv}, as defined in ((1.8)). Thus, Levin's result is a particular case of Fradkin's general calculations.)

The expressions, derived by Fradkin, have the form

$$\bar{\mu} = 2\left[\frac{3}{2 - p(v + j\omega)} - 1\right] \qquad (2.3)$$

(if Ollendorf's equation is used) or

$$\bar{\mu} = 1 + \frac{3(v + j\omega) - \frac{2}{p} + \sqrt{(v + j\omega)^2\left(9 - \frac{8}{p}\right) + (v + j\omega)\frac{4}{p} + \frac{4}{p^2}}}{\frac{4}{3} \cdot \frac{1}{p}[2 - (v + j\omega)]} \qquad (2.4)$$

(when Kondorski's formula is employed). In both expressions

$$v + jw = \frac{(2\mu + 1)\left(\frac{1}{x^2} - \frac{1}{x}\operatorname{ctg} x\right) - 1}{(\mu - 1)\left(\frac{1}{x^2} - \frac{1}{x}\operatorname{ctg} x\right) + 1}, \qquad (2.5)$$

where $x = j\sqrt{j\frac{4\pi\omega}{c^2}\sigma\mu a}$.

These equations already characterize the dispersion of the structure, rather than simply the dispersion of the form.

Obviously, the value of the permeability of the substance (μ) entering into (2.3)-(2.5) is a complex quantity and depends on the frequency.

Generalizing the above deductions, one might introduce the concept of a structural demagnetizing factor N_{str}, whose value, instead of being computed theoretically, would be determined experimentally in a static field. The dependence of $\bar{\mu}$ on the frequency could then be determined, on the assumption that N_{str} is constant, by substituting the value of μ_{equi} from (1.8) for the static-field value of μ.

Just as in magnetization of an ellipsoid the limiting value of the permeability is termed the permeability of the form, the limiting value of the permeability of a conglomerate may be called the permeability of the structure or the structural permeability.

A method for determining the mean permeability of a conglomerate, based on a fundamentally different line of reasoning, is given by Lichtenecker (Ref. 13), who extends the earlier calculations of Maxwell and Rayleigh. According to Lichtenecker the permeability ($\bar{\mu}$) of a material formed of a mixture of substances a and b, having permeabilities μ_a and μ_b, is given by the following equation:

$$\log \mu = p \log \mu_a - (1 - p)\log \mu_b \qquad (2.6)$$

where p is the ratio of the volumes of a and b. Numerous tests (Refs. 14 and 15) have shown that Lichtenecker's formula is valid in many instances.

Applying (2.6) to our magneto-dielectrics, we set $\mu_a = \mu$ and $\mu_b = 1$. Then

$$\bar{\mu} = \mu^p. \qquad (2.7)$$

In alternating fields the mean permeability $\bar{\mu}$ (or the permeability of the material) and the permeability of the substance μ must be regarded as complex quantities:

$$\bar{\mu} = |\bar{\mu}| \cdot e^{-j\bar{\delta}} \quad \text{and} \quad \mu = |\mu| e^{-j\delta}. \qquad (2.8)$$

In this case it follows from Lichtenecker's equation that

$$|\bar{\mu}| = |\mu|^p \qquad (2.9)$$

and

$$\bar{\delta} = p\delta. \qquad (2.10)$$

Instead of the last equality, Birks (Ref. 14) assumes

$$\operatorname{tg}\bar{\delta} = p \operatorname{tg}\delta. \qquad (2.11)$$

Equation (2.10) and (2.11) are equivalent for small values of δ; however, only the former is rigorously justified. As Arkad'ev showed,

Maxwell's equations and derivations therefrom can be applied to a medium with complex parameters; hence insofar as (2.7) is valid, equations (2.8)-(2.10) are also valid.

Utilizing the concept of the equivalent permeability of a sphere - equation (1.8) - introduced above, the application of Lichtenecker's equation can be extended not only to the simple case of an alternating field in a magneto-dielectric with a complex permeability of the ferromagnetic phase but also to cases in the range of frequencies where the skin effect in each individual minute sphere must be taken into account; this is done by using μ_{equi} instead of the ordinary permeability of the substance μ.

In view of the above, the complex permeability of an artificial magneto-dielectric consisting of uniform ferromagnetic spheres insulated from each other may be described by the following equation:

$$\bar{\mu} = \bar{\mu}_1 - j\bar{\mu}_2 = \mu_{equi}^p = \mu^p \left[2 \frac{v - \operatorname{th} v}{v^2 \operatorname{th} v - (v - \operatorname{th} v)} \right]^p, \qquad (2.12)$$

where [illegible]; p is the filling factor, μ is the permeability, σ is the conductivity and a, the radius of each individual sphere.

In like manner we can derive an expression for the complex permeability of a magneto-dielectric composed of spheres of two different radii a and b, for which the filling factors are p_a and p_b, respectively:

$$\bar{\mu} = \bar{\mu}_1 - j\bar{\mu}_2 = (2\mu)^p \left[\frac{v_a - \operatorname{th} v_a}{v_a^2 \operatorname{th} v_a - (v_a - \operatorname{th} v_a)} \right]^{p_a} \cdot \left[\frac{v_b - \operatorname{th} v_b}{v_b^2 \operatorname{th} v_b - (v_b - \operatorname{th} v_b)} \right]^{p_b}. \qquad (2.13)$$

Here

$$v_a = \sqrt{j\omega\mu\mu_0\bar{\sigma}}\, a, \quad v_b = \sqrt{j\omega\mu\mu_0\bar{\sigma}}\, b, \quad p = p_a + p_b. \qquad (2.14)$$

In the above equation the permeability of the substance and the conductivity of all the spheres are assumed to be the same. However, a similar equation for a mixture of spheres having different conductivities and permeabilities can readily be deduced.

In the case of a mixture of spheres of different radii, the sum in (2.6) should be replaced by an integral.

In applying the above equation, particularly in the region of very high frequencies, one should take into account the dependence of the permeability of the substance (μ) on the frequency. In the case of small particles, the permeability of the substance will also depend on the particle size (radius); obviously direct determination of the permeability of minute particles is fraught with great difficulty.

The above formulas, (2.12) - (2.14), still require extensive experimental verification; however, there is reason to assume that they characterize the structural dispersion of artificial magneto-dielectrics better than all other, previously employed equations.

It must be noted that in investigating artificial magneto-dielectrics there is the problem of determining not only $\bar{\mu}$ but also $\bar{\varepsilon}$. However, even at very high frequencies the dielectric constant of the material remains virtually independent of the frequency (provided the dielectric constant of the insulating substance does not vary) and depends only on the filling factor.

The problems touched upon in the present section have been extensively discussed in the scientific literature of recent years. We have space here to mention only a few of the more interesting publications. One of the most thorough treatments of the theoretical and experimental aspects of the subject will be found in a contribution by Pistoulet (Ref. 15). A detailed discussion is also contained in Prache's article

(Ref. 16). The results of measurements at low frequencies and interesting calculations are given in Refs. 17 and 18. The above-mentioned articles contain further bibliographic material.

3. Structural dispersion of a stack of steel laminae

At relatively low frequencies the magnetic permeability of a transformer core, composed of a number of ferromagnetic laminations, is determined by the skin effect in the individual laminae as such and by the filling factor; i.e., in this case the stacking factor. However, at high frequencies and when the insulating laminae separating the ferfomagnetic sheets are very thin, it may be necessary to treat the core as a composite body and seek a simultaneous solution of the equations for the metal laminae and for the insulating layers.

This is because there is a distinct possibility that the distribution of eddy currents in the laminae may be influenced by displacement currents between the laminations. The question was originally raised by Kondorski during the discussion of reports on the high-frequency characteristics of thin steel sheets, presented at the Second Conferenc on Magnetism (1951).

An analysis made by the present writers indicates that in view of recent developments in the technology of transformer core manufacture (progressive reduction in the thickness of the steel laminae and the insulating layers) the question is a timely one.

The problem of the structural dispersion of a laminated core, as discussed here, has much in common with the problem of a coaxial cable having an outer sheath and central conductor consisting not of solid metal but of thin metal laminae separated by insulation.

The parameters of such a cable (i.e. its dispersion characteristics) are also determined not only by the substance and form of the conductors, but by their structure as well (see abstracts of articles by Clockston and others in Ref. 19).

Before proceeding to a mathematical solution of the problem, we must point out that there are a number of different ways of viewing the processes taking place in a laminated core.

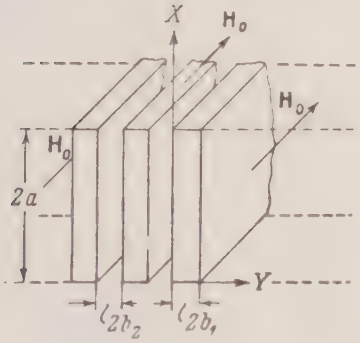

Fig. 2. Stack of steel laminae, unlimited in extent along the Y axis, regarded as an inhomogeneous ferromagnetic body with anisotropic properties.

First, a stack of steel laminae may be regarded as an inhomogeneous body with anisotropic characteristics; i.e., a conductor along the X axis and a dielectric along the Y axis (Fig. 2). In this case the field distribution in the core may be regarded as dependent upon both the x and y coordinates.

Second, the laminations of the core may be treated as a series of flat waveguides through which waves are transmitted from the two open ends along the ±X axis, with losses present both in the ferromagnetic walls of the waveguide and in the imperfect insulation between the metal laminae. At moderate frequencies or with very thin ferromagnetic laminae the walls of the waveguides must be considered to be semitransparent.

In this treatment, the electromagnetic field along the Y axis varies periodically, with the same field pattern repeating in each successive lamination. The solution holds more closely to the "guide" picture. It must be noted that in both cases analysis points to the possibility of resonance effects.

The equation to be solved has the form

$$\nabla^2 \dot{H} - \gamma_k^2 \dot{H} = 0. \tag{3.1}$$

The values of the propagation constant are different for the metal and for the insulating layers:
for the metal:

$$\gamma_1^2 = j\omega\mu\mu_0\sigma_1, \tag{3.2}$$

for the insulating layers:

$$\gamma_2^2 = j\omega\mu_0\sigma_2^*. \tag{3.3}$$

In both equations μ and ε are complex quantities. The conductivit of the insulating layers σ_2^* is the full complex conductivity ($\sigma_2 - j\omega\varepsilon\varepsilon_0$
The boundary conditions which our solution must satisfy are

$$\begin{aligned} &\dot{H} = \dot{H}_0 && \text{when } x = 0 \text{ and } x = 2a \\ &\dot{H} = \dot{H}_{bou_i}(x) && \text{when } y = 0 \text{ and } y = 2b_k \end{aligned} \tag{3.4}$$

The solution of (3.1), satisfying the conditions of (3.4) is

$$\dot{H} = \sum_m \left[D_{i-1} \frac{\operatorname{sh} l_m y}{\operatorname{sh} l_m 2b_k} - D_i \frac{\operatorname{sh} l_m (y - 2b_k)}{\operatorname{sh} l_m 2b_k} \right] \cdot \sin \frac{m\pi}{2a} x +$$

$$+ \frac{16}{\pi^2} \dot{H}_0 \sum_{m,n} \frac{1}{mn} \frac{\gamma_{mn}^2}{\gamma_{mn}^2 + \gamma_k^2} \cdot \sin \frac{m\pi}{2a} x \cdot \sin \frac{n\pi}{2b_k} y, \tag{3.5}$$

where m and n are series of odd integers; $l_m = \sqrt{\left(\frac{m\pi}{2a}\right)^2 + \gamma_k^2}$ and D_i is define below.

In view of the equipollence of the y-boundaries and the symmetry of the problem, the field intensities at all boundaries are equal; hence,

$$D_{i-1} = D_i = \ldots = D_k = -\frac{4\dot{H}_0}{m\pi} C'_m. \tag{3.6}$$

In this case (3.5) assumes the form

$$\dot{H} = -\sum_m \frac{4\dot{H}_0}{m\pi} C'_m \frac{\operatorname{ch} l_m (y - b_k)}{\operatorname{ch} l_m b_k} \sin \frac{m\pi}{2a} x +$$

$$+ \frac{16}{\pi^2} \dot{H}_0 \sum_{m,n} \frac{1}{mn} \cdot \frac{\gamma_{mn}^2}{\gamma_k^2 + \gamma_{mn}^2} \cdot \sin \frac{m\pi}{2a} x \cdot \sin \frac{n\pi}{2b_k} y. \tag{3.7}$$

Determining the tangential components of the electric field to both sides of the boundary between the laminae and equating them,

$$E_x = \frac{1}{\sigma_1} \cdot \frac{\partial H_1}{\partial y}\bigg|_{y_{bou}} = \frac{1}{\sigma_2^*} \cdot \frac{\partial H_2}{\partial y}\bigg|_{y_{bou}}, \tag{3.8}$$

we find the expression for the coefficient C'_m in (3.7):

$$C'_m = \frac{\dfrac{\gamma_1^2 \operatorname{th} l_{m_1} b_1}{\sigma_1 l_{m_1}} + \dfrac{\gamma_2^2 \operatorname{th} l_{m_2} b_2}{\sigma_2^* l_{m_2}}}{\dfrac{l_{m_1} \operatorname{th} l_{m_1} b_1}{\sigma_1} + \dfrac{l_{m_2} \operatorname{th} l_{m_2} b_2}{\sigma_2^*}}. \tag{3.9}$$

Averaging the field in the ferromagnetic lamina,

$$\dot{H}_{av} = \frac{1}{2a(2b_1+2b_2)}\int_0^{2a}\int_0^{2b_1}\dot{H}\,dx\,dy = -\frac{8}{\pi^2}\dot{H}_0 p\sum_m \frac{C'_m}{m^2}\cdot\frac{\operatorname{th} l_{m_1}b_1}{l_{m_1}b_1} + \\ + p\dot{H}_0 - \frac{64}{\pi^4}\dot{H}_0 p\sum_{m,n}\frac{1}{m^2n^2}\cdot\frac{\gamma_1^2}{\gamma_1^2+\gamma_{mn}^2}, \qquad (3.10)$$

we find the expression for the apparent magnetic permeability of the medium:

$$\bar{\mu} = \frac{\mu\dot{H}_{av}}{\dot{H}_0} = \mu\left[1-\frac{64}{\pi^4}\sum_{m,n}\frac{\gamma_1^2+\gamma_{n_1}^2 C'_m}{\gamma_1^2+\gamma_{mn_1}^2}\right]p. \qquad (3.11)$$

Solution (3.11) is the most general one and includes all the particular cases that might be encountered in practice.

In some cases a laminated core may be regarded, from the electrodynamic viewpoint, as a honogeneous body with equivalent structural parameters.

The possible appearance of an appreciable inductive capacity among the structural electromagnetic parameters is connected with the shunting effect of the non-ferromagnetic layers on the eddy current distribution in the ferromagnetic laminae.

The structural electric parameters of an equivalent homogeneous medium prove to be dispersive even in the case when the electric parameters through which they are expressed (manifested) are independent of the frequency. That is, the dispersion of the said parameters is structural in character. However, the parameters of the medium, both electric and magnetic, can, naturally, depend on the frequency. Hence, dispersion of these parameters should be taken into account only when the necessity for doing so is obvious.

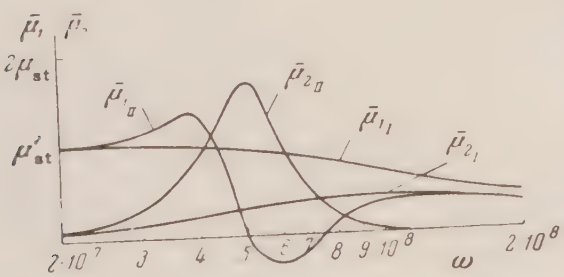

Fig. 3. Frequency-dependence of the apparent permeability of a core of thin laminae: $\bar{\mu}_{1_I}$ and $\bar{\mu}_{2_I}$ - apparent permeability of a single strip (lamina); $\bar{\mu}_{1_{II}}$ and $\bar{\mu}_{2_{II}}$ - same for laminae in a stack; μ_{st} - static value of permeability. The curves are computed on the basis of the following dimensions and parameters of the medium (see Fig. 2): $2b_1=3\cdot10^{-4}$ cm, $2b_2=0.15\cdot10^{-4}$ cm, $\sigma_1=10^4$ mho/cm, $\sigma_2=10^6$ mho/cm, $\mu_1=10^4$, $\varepsilon_2=5$.

The results of our analysis show that there may be a resonance peak in the curve for the apparent magnetic permeability of a core composed of thin laminae. As a consequence of this resonance effect, the magnetic properties of a core (stack of laminations) may vary more rapidly than in the case of an isolated ferromagnetic sheet of the same thickness.

Fig. 3 shows the variation of the apparent magnetic permeability of a laminated core of ferromagnetic material with the frequency.

It will be seen that the resonance peak is flattened by the superimposed structural dispersion of the magnetic permeability. The values for the frequency-dependence curves were computed according to the following equation, for the case when the dispersion of the form of the composite body and of the individual ferromagnetic lamina overlap:

$$\bar{\mu} = \mu\frac{2}{b_1^2}\sum_n\frac{1}{\gamma_1^2+\left(\frac{n\pi}{2b_1}\right)^2}\cdot\frac{2}{a^2}\sum_m\frac{1}{\lambda_2^2+\gamma_m^2}\,p. \qquad (3.12)$$

This equation shows the feasibility of reducing a non-plane wave (which is what we to an equivalent plane wave by introducing

the structural permeability,

$$\mu_{str} = \mu \frac{2}{b_1^2} \sum_n \frac{1}{\gamma_1^2 + \gamma_{n_1}^2} p = \mu \frac{\operatorname{th} \gamma_1 b_1}{\gamma_1 b_1} p \qquad (3.13)$$

and the structural conductivity of an equivalent homogeneous medium,

$$\sigma^*_{str} = \frac{b_1 \sigma_1 \sigma_2^*}{b_1 \sigma_2^* \frac{\mu_{str}}{\mu_1} + b_2 \sigma_1}. \qquad (3.14)$$

into equation (3.1). The modified equation (3.1) will then characterize the propagation of the wave through the whole composite body. Consequently, a core of thin laminae may be regarded as a homogeneous ferromagnetic body with anisotropic electromagnetic properties, which can be expressed in terms of the structural parameters of a fictitious (equivalent) homogeneous medium. As is made evident by the analysis, these parameters may be characterized by dispersion of structural origin.

Having determined the dispersive electromagnetic parameters of the equivalent homogeneous anisotropic medium:

$$\sigma_{xx} = \sigma_x = \sigma_1 \frac{b_1}{b_1 + b_2}, \quad \sigma^*_{yy} = \sigma^*_y = \sigma^*_{str}, \quad \mu_{zz} = \mu_z = \mu_{str},$$

our problem resolves itself into the conventional one of the propagation of electromagnetic waves through an anisotropic medium.

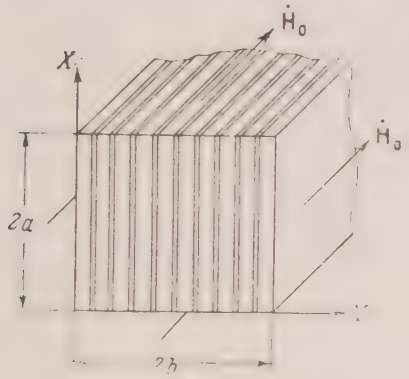

Fig. 4. Stack of steel laminae, having a finite thickness along the Y-axis, regarded as a homogeneous ferromagnetic body with anisotropic properties.

In particular, inasmuch as the properties of the medium in the two directions of propagation of the waves (along the X and Y axes) are known, the problem of the propagation of an electromagnetic disturbance in a laminated core, having a cross section of finite dimensions, can be readily solved.

Thus, let us assume that we have a core the extent of which along the Y axis is limited (Fig. 4) and that the core is being magnetized along the Z axis. The expression for the propagation of the electromagnetic disturbance in this case will be

$$\sigma_x \frac{\partial^2 H_z}{\partial x^2} + \sigma^*_y \frac{\partial^2 H_z}{\partial y^2} = \mu_z \mu_0 \sigma_x \sigma^*_y \frac{\partial H_z}{\partial t}. \qquad (3.15)$$

Substituting for the independent variables in the above from

$$x_1 = \frac{xK}{\sqrt{\sigma_x}} \quad \text{and} \quad y_1 = \frac{yK}{\sqrt{\sigma^*_y}}, \qquad (3.16)$$

we obtain

$$\frac{\partial^2 H_z}{\partial x_1^2} + \frac{\partial^2 H_z}{\partial y_1^2} = \mu_z \mu_0 \frac{\sigma_x \sigma^*_y}{K^2} \cdot \frac{\partial H_z}{\partial t}. \qquad (3.17)$$

Taking

$$K^2 = \sigma_x,$$

we get

$$\frac{\partial^2 H_z}{\partial x_1^2} + \frac{\partial^2 H_z}{\partial y_1^2} = \mu_z \mu_0 \sigma^*_y \cdot \frac{\partial H_z}{\partial t}, \qquad (3.18)$$

where x_1 and y_1 are related to the initial coordinates by

$$x_1 = x \quad \text{and} \quad y_1 = y\sqrt{\frac{\sigma_x}{\sigma_y^*}}. \tag{3.19}$$

It will readily be noted that through the transformation of coordinates (3.19) we deform the coordinate space along the Y axis, thereby changing the corresponding dimension of the core section (2b) and at the same time - as follows from the propagation equation (3.18) - replace our initial homogeneous anisotropic medium by a homogeneous and isotropic medium, having an equivalent conductivity:

$$\sigma_{equi} = \sigma_y^*. \tag{3.20}$$

The above transformation is to some extent similar to that applied by Netushil (Ref. 20) in his analysis of quasi-static electric fields in anisotropic media.

Thus, our problem is reduced to seeking a solution of the equation (3.18) for a deformed core (Fig. 5) with isotropic properties, satisfying the boundary condition:

$$H_z = H_0 \quad \text{when} \quad \begin{cases} x_1 = 0 & \text{and} \quad x_1 = 2a \\ y_1 = 0 & \text{and} \quad y_1 = 2b\sqrt{\dfrac{\sigma_x}{\sigma_y^*}} \end{cases}. \tag{3.21}$$

The sought solution has the form

$$\dot{H}_z = \frac{16}{\pi^2}\dot{H}_0 \sum_{m,n} \frac{1}{mn} \cdot \frac{\lambda_{mn}^2}{\lambda_1^2 + \lambda_{mn}^2} \sin\frac{m\pi}{2a}x \cdot \sin\frac{n\pi}{2b\sqrt{\dfrac{\sigma_x}{\sigma_y^*}}}y_1; \tag{3.22}$$

here

$$\lambda_1^2 = -\omega^2\mu_z\mu_0\varepsilon_y\varepsilon_0 + j\omega\mu_z\mu_0\sigma_y = j\omega\mu_z\mu_0\sigma_y^*$$

is the propagation constant of the electromagnetic disturbance in the equivalent isotropic medium, while

$$\lambda_{mn}^2 = \left(\frac{m\pi}{2a}\right)^2 + \left(\frac{n\pi}{2b\sqrt{\dfrac{\sigma_x}{\sigma_y^*}}}\right)^2$$

Averaging the solution (3.22) over the cross-section of the core and determining the mean (i.e. apparent) permeability of the core, we obtain

$$\bar{\mu}_z = \mu_z\left[1 - \frac{64}{\pi^4}\sum_{m,n}\frac{1}{m^2n^2} \cdot \frac{\lambda_1^2}{\lambda_1^2 + \lambda_{mn}^2}\right] \tag{3.23}$$

or

$$\bar{\mu}_z = \mu_z\left[1 - \frac{64}{\pi^4}\sum_{m,n}\frac{1}{m^2n^2} \cdot \frac{j\omega\mu_z\mu_0\sigma_y^*}{j\omega\mu_z\mu_0\sigma_y^* + \left(\frac{m\pi}{2a}\right)^2 + \left(\frac{n\pi}{2b}\right)^2\frac{\sigma_y^*}{\sigma_x}}\right]. \tag{3.24}$$

The results noted above follow from the last equation as particula cases. Specifically, when $2b \to \infty$, which corresponds to the case of a "plane" wave (Fig. 2), we obtain

$$\bar{\mu}_z = \mu_z\left[1 - \frac{8}{\pi^2}\sum_{m}\frac{1}{m^2} \cdot \frac{j\omega\mu_z\mu_0\sigma_y^*}{j\omega\mu_z\mu_0\sigma_y^* + \left(\frac{m\pi}{2a}\right)^2}\right] = \mu_z\frac{\operatorname{th}\lambda_2 a}{\lambda_2 a}, \tag{3.25}$$

In the particular case when $2a \to \infty$, we get

$$\bar{\mu}_z = \mu_z\left[1 - \frac{8}{\pi^2}\sum\frac{1}{n^2} \cdot \frac{j\omega\mu_z\mu_0\sigma_x}{j\omega\mu_z\mu_0\sigma_x + \left(\frac{n\pi}{2b}\right)^2}\right]. \tag{3.26}$$

Equation (3.25) indicates that the frequency dependence curve of the apparent magnetic permeability may exhibit a resonance peak due to structural conductivity σ^*_y, as was pointed out above (p. 121).

Equation (3.26) indicates that, inasmuch as the structural conductivity, σ_x, along the X axis is real, the frequency dependence curve of the apparent permeability of the core will be characterized by attenuation (falling characteristic). It follows that the transition to a core with a finite dimension along the Y axis (Fig. 4) leads to a relative weakening of the resonance effect.

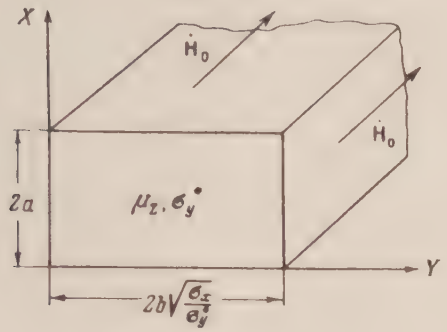

Fig. 5. Deformed core with isotropic properties, equivalent electromagnetically to an anisotropic stack of thin steel laminae.

The results of our analysis may be useful in interpreting the nature of the electromagnetic spectra of technical ferrites and explaining the high values of their dielectric constants, inasmuch as polycrystalline ferrite material may be regarded as a conglomerate of ferromagnetic grains separated by thin layers of a low-conductivity non-ferromagnetic substance. A number of authors give an analogous interpretation of the structure of semiconductors (see, for example, Refs. 21 and 2

Moscow Energetics Institute
Imeni V. M. Molotov

Received
26 July 1954

Bibliographic References

1. V.K.Arkad'ev, Elektromagnitnye protsessy v metallakh (Electromagnetic processes in metals). GEI, M. Part I 1934; Part II 1936.
2. S.V.Vonsovski, Sovremennoe uchenie o magnetizme (Modern teachings on magnetism). GTTI, M.-L. 1952.
3. J.L.Snoek, Issledovaniia v oblasti novykh ferromagnitnykh materialov. IL, M. 1949. (Prob.: New Developments in Ferromagnetic Materials. Amst.1947).
4. S.V.Vonsovski, Ferromagnitnyi rezonans (Ferromagnetic resonance): collection of translated articles, edited by Vonsovski. IL, M. 1952.
5. K.M.Polivanov, Izv. (Bulletin) AN SSSR, Ser.fiz., 16, 449 (1952).
6. K.M.Polivanov, Sb. trudov MEI im.Molotova (Collected reports of the imeni Molotov Moscow Energetics Institute), 14, M.-L. 1953.
7. M.A. Divil'kovski, Zhur. tekh. fiz., 9, 5 (1939).
8. W.R.Smythe, Static and Dynamic Electricity (in Russ. trans., M. 1954).
9. F.Ollendorf, Potentialfelder der Electrotechnik, Berlin 1939.
10. E.I.Kondorski, Izv.(Bulletin) AN SSSR, Ser.fiz., 16, 398 (1952).
11. B.M.Fradkin, Izv. (Bulletin) AN SSSR, Ser. fiz., 16, 481 (1952).
12. L.Levin, Sovremennaia teoriia volnovodov(Modern waveguide theory).M.1952.
13. L.Lichtenecker, Phys. ZS, 27, 115 (1926).
14. J.B.Birks, Proc. Phys. Soc., 60, 282 (1948).
15. M.Pistoulet, Ann. de telecommunications, 27, 85, 127 (1952).
16. P.Prache, Cables et transmission, 1, 22 (1952).
17. M.Kharadly & W.Jackson, Proc. IEE, p.III, 100,66, 199 (1953).
18. J.Lucas, Frequentz, 7, 10, 289 (1953).
19. Usp. fiz. nauk, 49, 325 (1953).
20. A.V.Netushil, Elektrichestvo, 3 (1950).
21. G.Möltgen, ZS ang. Phys., 4, 6, 216 (1952).
22. G.Pearson, Haynes & Shokley, Phys. Rev., 78, 295 (1950).

FERRITES IN PULSE CIRCUITS

- N. G. Katkov

1. Recent developments in microwave engineering impose certain stringent requirements on the materials used in the fabrication of many parts and assemblies of high-frequency equipment. In many cases, the material must be highly transparent to electromagnetic waves.

In this connection certain new ferromagnetic materials--the ferromagnetic oxides known collectively as ferrites--present considerable interest. Together with a high initial permeability (400-2500) and high specific resistivity (10^2-10^8 ohm-cm) they have a very considerable dielectric constant ($\varepsilon = 10^2 - 10^5$). Their high transparency to electromagnetic waves permits the use of ferrites as core materials for pulse transformers, particularly those intended for short-pulse operation (Ref. 1).

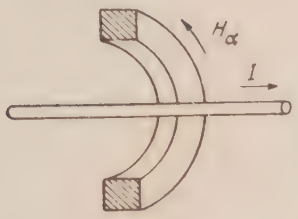

Fig. 1. Toroidal ferrite core, magnetized by a current pulse flowing in the central conductor.

This article is devoted to a theoretical and experimental investigation of the dynamics of magnetization of ferrite cores.

2. Let us examine the case of a toroidal ferrite core of rectangular cross section, magnetized by a current pulse flowing through a central conductor encircled by the core (Fig. 1).

The magnetic field produced by this current has a single component H_α at the surface of the core. The wave equation for this component is

$$\frac{\partial^2 H_\alpha}{\partial r^2} + \frac{1}{r}\cdot\frac{\partial H_\alpha}{\partial r} + \frac{\partial^2 H_\alpha}{\partial z^2} + \left(\lambda^2 - \frac{1}{r^2}\right) H_\alpha = 0, \qquad (1)$$

where $\lambda^2 = -\lambda_1^2 = -p^2\mu\mu_0\varepsilon\varepsilon_0 - p\mu\mu_0\sigma$, with λ_1 being the propagation constant.

It is assumed that the parameters μ, ε, and σ of the core material are independent of the frequency, that the medium is linear and that the hysteresis losses are negligible. These assumptions are justified for the case of weak fields; this is postulated to be the case in the discussion below.

We seek a solution of (1) satisfying the following boundary condition at the contour of the core cross section:

$$l_k \to H_\alpha = \frac{Iw}{2\pi r}, \qquad (2)$$

where I is the magnetizing current, w is the number of turns in the magnetizing winding, r is the radius (distance between the point in question on the core cross section contour and the axis of the central conductor). The solution is given by

$$H = -\frac{Iw}{2\pi r} - \frac{Iw}{2\pi}\sum_{mn}\frac{4}{m\pi}\cdot\frac{4}{l_n}\cdot\frac{Z_0(x_k) - Z_0(x_{k+n})}{r_1^2 Z_0^2(x_{k+n}) - r_0^2 Z_0^2(x_n)}\times$$
$$\times\frac{\lambda_1^2}{\lambda_1^2 + \lambda_{mn}^2}\left[I_1(l_n r) - \frac{I_1(x_k)}{N_1(x_k)}N_1(l_n r)\right]\sin\frac{m\pi}{2a}z. \qquad (3)$$

This expression, satisfying equation (1) and boundary condition (2), determines the strength of the magnetic field at any point on the core cross section.

In view of the fact that in practice ferrite toroids are used as cores for coils and transformers, constituting electric network components, let us consider suitable equivalent circuits for cores. Three

equivalent circuits are possible. First, we have a series circuit. The impedance introduced by the core into the magnetizing-current circuit can be found as follows: the voltage drop in the core winding due to the magnetic flux induced in the core is

$$U = p\mu\mu_0 SH_{av} = p\mu\mu_0 S \frac{1}{2a \cdot 2b} \int_0^{2a} \int_{r_0}^{r_1} H \, dz \, dr = I \frac{8}{\pi^2} \sum_{mn} \frac{1}{m^2} \cdot \frac{\lambda_{mn}^2}{\lambda_1^2 + \lambda_{mn}^2} \psi_n p\mu\mu_0, \qquad (4)$$

where

$$\psi_n = \frac{w^2}{2\pi} \cdot \frac{2}{bl_n} S \frac{[Z_0(x_k) - Z_0(x_{k+n})]^2}{r_1^2 Z_0^2(x_{k+n}) - r_0^2 Z_0^2(x_k)},$$

and S is the cross sectional area of the core. Dividing the numerator and denominator of each term in the series by the numerator, we obtain:

$$Z(p) = \frac{U}{I} = \sum_{mn} \frac{1}{\frac{1}{pL_{mn}} + \frac{1}{R_{mn}} + pC_{mn}}, \qquad (5)$$

where

$$L_{mn} = \frac{8}{\pi^2} \mu\mu_0 \frac{\psi_n}{m^2}, \quad C_{mn} = \frac{\pi^2}{8} \varepsilon\varepsilon_0 \frac{m^2}{\psi_n \lambda_{mn}^2}, \text{ and } R_{mn} = \frac{8}{\pi^2} \cdot \frac{1}{\sigma} \frac{\psi_n \lambda_{mn}^2}{m^2}. \qquad (5a)$$

It follows from (5) that the core in a magnetizing-current circuit may be replaced by a ladder network, each mesh of which consists of three parallel branches: an inductive, a capacitive, and a resistive.

Expression (5a) for the parameters of the equivalent series network for a ferrite core is the most general one, and covers the following particular cases:

1) core, having a large center-line radius r_{cl},

$$\lambda_{mn} = \sqrt{\left(\frac{m\pi}{2a}\right)^2 + \left(\frac{n\pi}{2b}\right)^2}, \quad \psi_n = \frac{8}{\pi^2} \frac{1}{n^2} \frac{w^2 S}{2\pi r_{cl}};$$

2) flattened core, having a large center-line radius r_{cl} (flat ring)

$$\lambda_{mn} = \lambda_m = \frac{m\pi}{2a}, \quad \psi_n = \frac{w^2 S}{2\pi r_{cl}};$$

3) flattened core, having small center-line radius,

$$\lambda_{mn} = \lambda_m = \frac{m\pi}{2a}, \quad \psi_n = \frac{w^2 S}{2\pi \frac{2b}{\ln \frac{r_1}{r_0}}};$$

4) strip core,

$$\lambda_{mn} = \lambda_n = \frac{n\pi}{2b}, \quad \psi_n = \frac{w^2 S}{2\pi r}.$$

Inversion of the series circuit for the core leads to the second possible equivalent circuit: a parallel circuit. For the case of a plane wave in the core, inversion yields

$$Y(p) = \frac{1}{L_1 p} + \sum_{k=1}^{\infty} \frac{1}{L_1 p \frac{R_k \frac{1}{C_k p}}{R_k + \frac{1}{C_k p}}}, \qquad (6)$$

where

$$L = \frac{\mu\mu_0 w^2 S}{2\pi r_{cl}}, \quad L_1 = \frac{1}{2} L, \quad R_k = \frac{k^2 \pi^2 w^2 S}{\sigma \pi r_{cl} (2a)^2} \text{ and } C_k = \frac{\varepsilon\varepsilon_0 \pi^2 r_{cl} (2a)^2}{k^2 \pi^2 w^2 S}. \qquad (6a)$$

Where a plane wave is propagated in the core, a third equivalent circuit variant is possible: a long line terminated in a short circuit.

The length of the line equals half the thickness of the core lamination, and its parameters per unit length are given by the following equations:

$$L_0 = \frac{\mu\mu_0\omega^2 S}{2\pi r_{c1}} \cdot \frac{1}{a}, \quad C_0 = \frac{\varepsilon\varepsilon_0 2\pi r_{c1}}{\omega^2 S} a, \quad G_0 = \frac{\sigma 2\pi r_{c1}}{\omega^2 S} a. \tag{7}$$

The line is short circuited at the end because, from considerations of symmetry, the electric vector passes through zero at the center of the lamination.

All three circuits are equally applicable and whichever happens to be more convenient may be used for analysis in any given case.

If the ferrite core is used in a pulse transformer, any of the circuits described above can be used in lieu of the magnetizing branch element in the equivalent T-network of the transformer.

The equivalent circuits for metal cores are but particular cases of the above circuits, lacking the capacitive branches.

In Ref. 2 there is a description of an equivalent parallel circuit to replace a laminated metal core. The described circuit corresponds to the second of the equivalent circuits considered above, but without the capacitive branch. The theory of metal-core pulse transformers is based on this circuit.

In the case of ferrite cores, however, it is impossible to neglect capacitance in the equivalent network.

The presence of capacitance leads to the possibility of resonance effects, associated with the formation of standing electromagnetic waves in the core section, at certain frequencies (Ref. 3).

The rise of such effects, when ferrite cores are used in pulse transformers, is extremely undesirable, for it may lead to waveform distortion of the output signal. The fact that the frequency characteristics of the permeability and dielectric constant of actual ferrites are not ideal, which makes for the cores being low-Q resonators, does permit of damping of these resonance effects by suitable choice of the core cross section.

3. The frequency dependence of the permeability and dielectric constant is influenced by micro- and macro-structural polarization processes. This fact was first noted by Arkad'ev in 1913 (Ref. 4). Consideration of the nature of the processes of magnetic and electric polarization leads, in the simplest case, to the following operator equations for the permeability and the dielectric constant:

$$\mu(p) = \frac{B(p)}{H(p)} = \frac{\lambda_1}{k_1} + \frac{\lambda_2}{k'p + k_2} \quad \text{and} \quad \varepsilon(p) = \frac{D(p)}{E(p)} = \frac{\lambda_1'}{k_1'} + \frac{\lambda_2'}{k''p + k_2'}. \tag{8}$$

The above are the simplest operator equations. Actual materials may have other frequency spectra; however, operator expressions for the permeability and dielectric constant can always be derived from the observed spectra and, hence, an appropriate equivalent network constructed.

In practice there is no point in further complicating the equivalent circuits in order to allow for the influence of the magnetic and electric polarization processes. The relaxation frequencies and, consequently, the parameters of the simple circuits should be selected so that their transient functions will coincide as closely as possible with those for the actual spectra.

In seeking to take account of the effect of dispersion of the core parameters, we arrive at circuits such as those pictured in Fig. 2. These are comparatively complicated and differ from those described

above in that they do not incorporate resistances, determined through the DC conductivity of the material. This is allowable due to the low conductivity of ferrites.

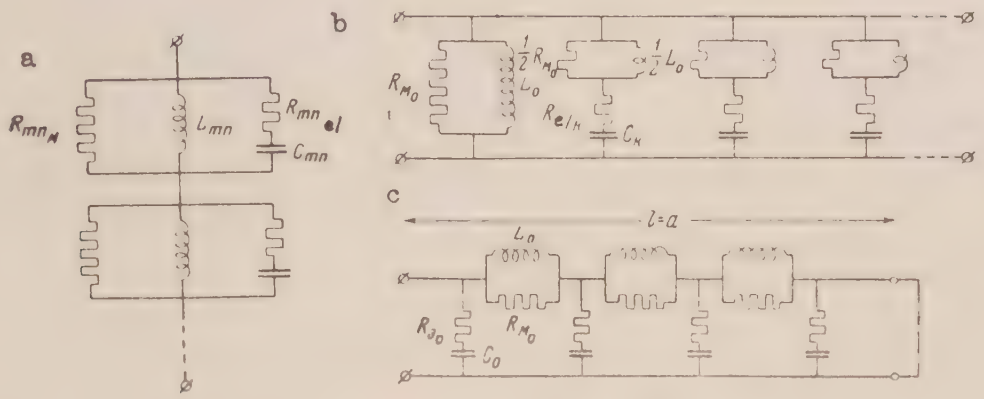

Fig. 2. Equivalent circuits for ferrite cores with dispersive electromagnetic parameters: a) series, b) parallel, c) in the form of a long line.

In the case of conventional metal cores there was no need to take into account the influence of polarization, since due to the high conductivity of such cores dispersion of the form generally lies in a lower range of frequencies than dispersion of the parameters of the core material.

This is the factor which made it feasible to base the theory of pulse transformers with metal cores on the above-mentioned, relatively simple, equivalent circuit, in which no account is taken of the frequenc dependence of the electromagnetic parameters of the material.

From the equivalent circuits for coils with ferrite cores deduced above, it follows that such coils behave as inductances only at relatively low frequencies. At higher frequencies, i.e. above the frequency range of attenuation of dispersion of the form and polarization, "inductance of the core" loses its conventional significance. Consequently, design of a core for operation in this higher frequency range on the basis of the static inductance will lead to unsatisfactory results.

As may be seen from inspection of the above equivalent circuits, dispersion of the form in ferrite cores can be eliminated by satisfying the following condition:

$$R_{2\,mn_M} \ll R'_{2mn_{el}}, \tag{9}$$

which can be rewritten as:

$$(\mu_{st}\mu_0 2\pi f_{u_M})(\varepsilon_{st}\varepsilon_0 2\pi f_{u_{el}}) \ll \lambda^2_{mn}. \tag{9a}$$

Here μ_{st} and ε_{st} are the static values of the permeability and dielectri constant of the core material and are the respective relaxation frequencies and λ_{mn} has the same meaning as above.

The inequality (9a) signifies that the resonant properties of the core depend on the frequency characteristics of the core-material parameters. The greater the width of the characteristic curves, the more pronounced the resonant properties of the core, and vice versa.

4. Our experimental investigation of pulse-magnetization processes was carried out by placing ring-shaped specimens in a coaxial line. A diagram of the set-up is shown in Fig. 3.

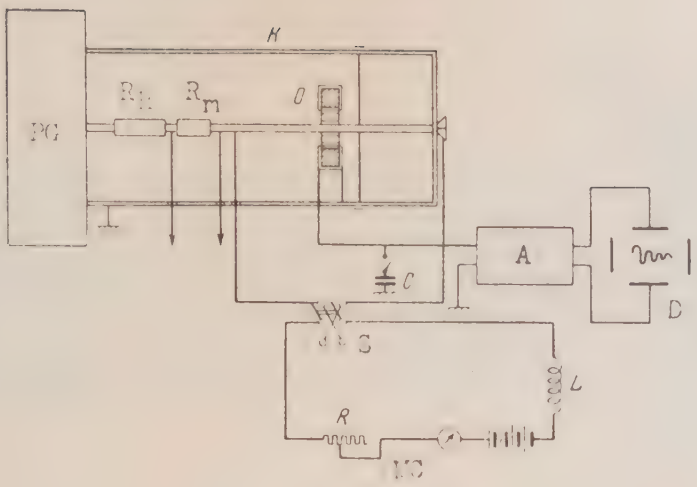

Fig. 3. Diagram of the experimental set-up: PG) pulse generator, K) coaxial line, O) toroidal ferrite specimen, MC) magnetizing circuit, A) amplifier, D) oscilloscope and deflecting system, C) additional capacitance, R_H) generator load resistance, R_m) measuring resistance, S) switch.

The short-circuited coaxial line was fed from a pulse generator. The diameter of the inner conductor of the line was 0.5 cm, and that of the sheath was 15 cm. A load resistance R_H = 2000 ohms and a measuring resistance R_m = 56 ohms were connected to the inner conductor on the pulse-generator side.

The toroidal specimens were suspended inside the line sheath, and encircled the inner conductor. One layer of fine wire (0.071 mm dia.) was wound directly on the specimen to form a measuring winding. The ends of the winding were brought outside by means of leads and connected either directly to the oscilloscope amplifier or to a cathode follower which in this case acted as an intermediate link between the winding and the amplifier.

The sweep of the amplifier was synchronized with the pulse generator and graduated with time markers at $0.5 \cdot 10^{-6}$ sec. intervals. The total sweep period was $20 \cdot 10^{-6}$ sec. The maximum resistance introduced by the specimen in the magnetizing current-pulse circuit does not exceed the magnetic-viscosity resistance, which is of the order of only some tens of ohms. Hence, it may be assumed that magnetization of the specimen is fully effected by the current source. The equivalent circuit of the set-up is shown in Fig. 4.

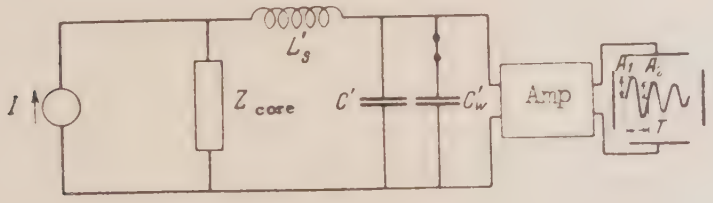

Fig. 4. Equivalent circuit of experimental set up. The pulse generator and the load resistance are replaced by a current source.

When the specimen is acted upon by a current pulse having the form shown in the oscillogram of Fig. 5, there will be an emf induced in the measuring coil. The variation of the voltage across the coil terminals will depend on the nature of the processes occurring in the core. If the process in the core is aperiodic, the transient voltage at the output of the measuring coil resembles an exponential curve. A superposition of aperiodic transient functions correspondingly spaced in time produces a resultant output voltage curve such as that shown in Fig. 6. The curve pictured was recorded with the measuring coil wound on a core of permalloy strip. The analogous oscillogram for a ferrite core is shown in Fig. 7.

The shape of the aperiodic output-voltage trace obtained with a metallic core can be explained with the aid of the equivalent circuit

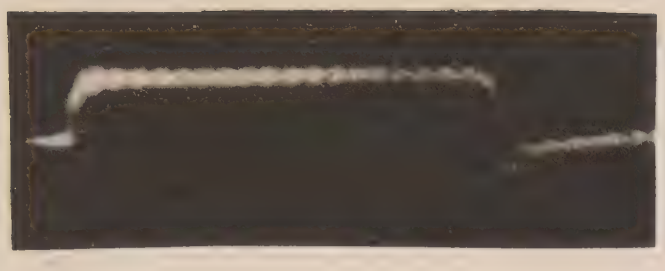

Fig. 5. Magnetizing current pulse. Interval between markers equals $0.5 \cdot 10^{-6}$ sec.

Fig. 6. Aperiodic output voltage trace obtained with permalloy strip core.

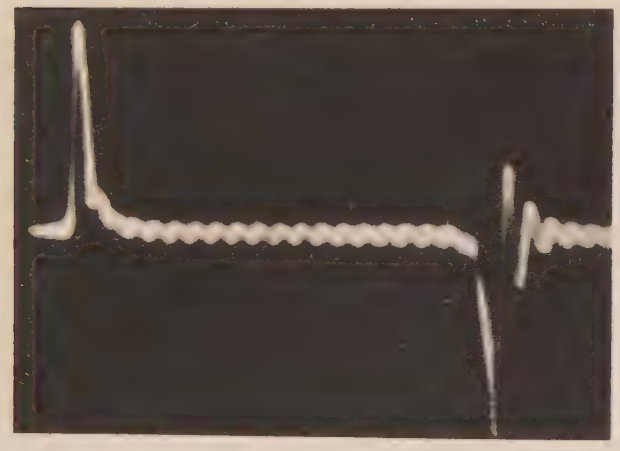

Fig. 7. Aperiodic output voltage trace obtained with ferrite core.

Fig. 10. Trace of damped sinusoidal oscillations obtained in recording the frequency characteristics of a pulse-magnetized ferrite core.

for a metallic core. The equivalent circuit contains no capacitive branches, since these are well shunted by the resistances due to the DC conductivity. When the laminae of the metal core are sufficiently thin, these resistances are of the same order of magnitude as the magnetic-viscosity resistances. Hence, the hysteresis lag, i.e., the time lag in the build-up of flux density and, consequently, the trailing edges of the output voltage trace can be attributed to eddy currents as well as to magnetic viscosity.

The nature of the observed viscosity can be explained by analyzing the equivalent circuit of the metal core. If the skin effect is strong, the exact equivalent circuit of the metal core can be reduced to a simplified two-stage series circuit (Fig. 8a) by approximating the transient function.

In case of a weak skin effect, when $R_1 \gtrsim R_{1M}$, the equivalent circuit assumes a different form (Fig. 8b).

It is easy to obtain oscillations in the case of ferrite cores and cores built up of thin laminae, for in these cases the magnetic-viscosity resistances shunting the elements in the equivalent series circuit are sufficiently large. The Q of these elements is high in this case, and the resultant oscillations are virtually sinusoidal. In the case of metal cores with pronounced dispersion of the form, the described procedure may be unsuitable, inasmuch as the DC resistances in the equivalent-circuit elements are small and, therefore, effectively shunt the measuring circuit and insure aperiodic operation.

The measurement method is based on the fact that the measuring-winding circuit has virtually no effect on the operation of the power source. The roots of the characteristic transient equation are therefore determined from the expression:

$$Z(p) + L_s' p + r' + \frac{1}{C_{N_1}' p} = 0, \qquad (11)$$

where Z(p) is the operator impedance of the core, L_s' is the reduced scattering inductance of the measuring winding, r' is the reduced resistance of the measuring winding, and $C_{N_1}' = C_N' + C'$ (C_N' is the known and C' is the parasitic capacitance of the measuring circuit).

The frequency and the damping of the oscillations produced were recorded on oscillograms. Such an oscillogram is shown in Fig. 10. Substituting the roots, determined from the oscillogram,

$$p_k = -\alpha_k + j\omega_k, \qquad (12)$$

into (11) and bearing in mind that $\alpha_k \ll \omega_k$ and, also, that the scattering inductance introduces a constant error, we get:

$$\bar{\mu}_1 = \frac{l_{av}}{\mu_0 w_1^2 S} \cdot \frac{1}{C_{N_1}'} \cdot \frac{1}{\omega_k^2} \quad \text{and} \quad \bar{\mu}_2 = 2\mu_1 \frac{\alpha_k}{\omega_k} = \frac{l_{av}}{\mu_0 w_1^2 S} \cdot \frac{r'}{\omega_k}. \qquad (13)$$

The order of magnitude of the parasitic capacitance of the measuring circuit can be evaluated from the expressions:

$$C' = \frac{C_{N_1}' - kC_{N_2}'}{k-1}, \quad k = \left(\frac{\omega_2}{\omega_1}\right)^2, \qquad (14)$$

where ω_1 and ω_2 are two close frequencies, and C_{N_1} and C_{N_2} are the values of the known capacitance corresponding to these frequencies.

During the measurements, capacitances $C_{N_1}' \geqslant C'$ were connected into the circuit. It follows from (13) that at low frequencies the losses in the measuring windings affect the measured value of the $\bar{\mu}_2$ component.

The frequency characteristics of the apparent permeability of cores obtained by this method are for a minor reversible cycle of pulse-magnetization and differ from the conventional frequency characteristics obtained with bridges and lines. This follows from the fact that the magnetizing current pulse throws the indicating spot into the center of the reversible cycle, while the sinusoidal current of the measuring winding causes a symmetrical movement of the spot along the reversible magnetization cycle. As a result of the equality of the induced currents the base of the cycle lies on the ordinate axis of the I-B coordinate system, while the location of the peak is determined by the double amplitude of the magnetizing current pulse (Fig. 11).

The frequency characteristics thus obtained are, therefore, suitable for analyzing the operation of cores magnetized by a double-amplitude pulse current.

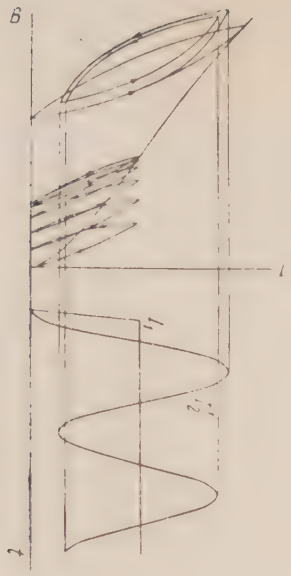

Fig. 15. Formation of a dynamic minor cycle of pulse magnetization in the process of recording the frequency characteristics.

Analysis of the applicability of this method, under the assumption that the core exhibits weak resonant properties, leads to the following expression for the frequency of the induced oscillations:

$$\omega = \sqrt{\frac{\Delta C'}{L_{st}(C'_{N_1\,cr} + \Delta C')^2}}, \qquad (15)$$

$$\Delta C' = C'_{N_1} - C'_{N_1\,cr},$$

$$C'_{N_1\,cr} = \tau_M^2 / 4L_{st},$$

where L_{st} is the static inductance of the specimen, and τ_M is the magnetic-viscosity time constant. The maximum frequency occurs when $\Delta C' = C'_{N_1\,cr}$, and equals:

$$\omega_{max} = \frac{1}{\tau_M} = \omega_{u_M}, \qquad (16)$$

i.e., it equals the relaxation frequency of the permeability of the material. If ferrites really had a permeability frequency characteristic with a single discrete relaxation frequency, the last result would provide means of determining this relaxation frequency. Actually this is not the case and, therefore, the obtained result serves only to establish the existence of a limiting frequency, above which measurements cannot be made. This maximum frequency equals the permeability relaxation frequency of the core material only in the simplest case.

The lower frequency limit is determined by technical considerations, namely, the duration of the magnetizing current pulse, the values of the required capacitances, and the gain of the amplifier. There are no particular [limiting] requirements where the length of the wavefront of the magnetizing current pulse is concerned.

The described procedure permits rapid and simple recording of the frequency characteristic of the apparent permeability of ferrite and magneto-dielectric cores and of cores made of thin ferromagnetic laminations; these measurements can be made in the frequency band of interest from the point of view of operating the core in pulsed magnetizing circuits. The procedure was used to record the frequency characteristics of the apparent permeability of nickel-zinc ferrite cores of different cross sections and characterized by diverse magnetic properties.

A series of curves showing the static and dynamic magnetic properties of one nickel-zinc ferrite specimen are reproduced in Figs. 12-16.

Fig. 12. Normal magnetization curve and largest hysteresis loop of a toroidal Ni-Zn ferrite core.

The core was a ring of rectangular cross section - 0.8 x 1.1 cm - and a 2.2 cm center line radius. Fig. 12 shows the static characteristics of the specimen under symmetric magnetization, i.e., the normal magnetization curve and the largest hysteresis loop. Fig. 13 shows the static characteristic for unipolar magnetization, namely, the curve representing the locus of the end points of the quasi-static minor reversible cycles. One of the minor cycles, with the peak identified by the coordinates ΔH and ΔB, is shown in the figure.

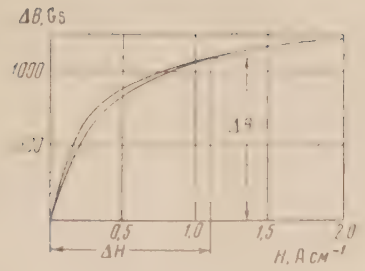

Fig. 13. Static pulse-magnetization curve for the same core.

The solid curve in Fig. 14 shows the dependence of the quasi-static permeability for unipolar magnetization on the amplitude of the field H; the dash-line shows the variation of the quasi-static permeability with the amplitude of the field H (in terms of ampere turns) with concurrent static magnetization aw_o = 10 A.* In Fig. 15 the solid lines represent portions of the frequency characteristic of the apparent permeability of the core in the absence of concurrent magnetization while the dash lines are the probable extrapolations of the curves into the region of low frequencies. The corresponding portions of the apparent permeability characteristics with concurrent aw_o = 10A magnetization are shown in Fig. 16, with the extrapolations into the low-frequency regions being indicated by dash lines.

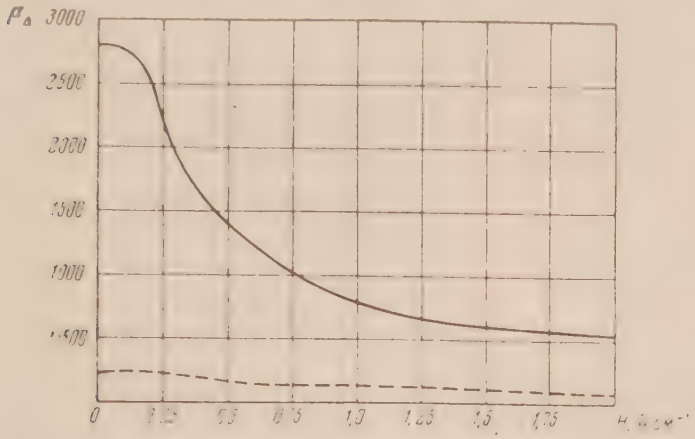

Fig. 14. Solid curve: dependence of the quasi-static pulse-magnetization permeability of the same core on the field amplitude; dash-line: quasi-static pulse permeability as a function of the field amplitude with a concurrent static magnetization aw_o = 10 A.

It will be noted that there is a resonance peak in the curves for the real part of the apparent permeability. Magnetization of the specimen displaces the peak in the direction of higher frequencies.

Other Ni-Zn ferrite specimens (initial permeability - 400, cross section - 0.6 x 0.5 cm and initial permeability - 1000, cross section 0.8 x 1.1 cm) also exhibited a resonance peak in the real apparent permeability vs frequency curve.

The resonance effect is presumably associated with dispersion of the form. This is indicated by the noted displacement of the resonance peak in the direction of high frequencies in the case of static magnetization and is confirmed by calculations of the order of magnitude of the frequency corresponding to the extreme point value of the real part of the apparent permeability. Magnetization with a field of only 1-2 oersteds can hardly influence the gyromagnetic resonance frequency, consequently the resonance effect noted is not of gyromagnetic origin.

No resonance peak was observed in the case of thin specimens. It is possible, however, that this is to be explained not by absence of dispersion of the form but simply by the scattering of the observed characteristics for the individual specimens.

5. The equivalent circuits for ferromagnetic cores derived above, taking into account the frequency dependence of the electromagnetic parameters of the core material, can be utilized directly for the analysis of transient phenomena in pulse transformers. Both the theory and design of ferrite pulse transformers and chokes can be based only on such equivalent circuits.

---

* Presumably aw_o stands for ampere turns. Translator.

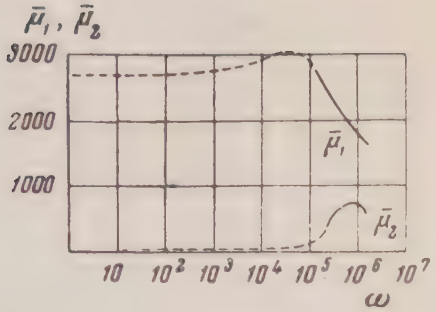

Fig. 15. Frequency dependence of the real ($\bar{\mu}_1$) and imaginary ($\bar{\mu}_2$) components of the apparent permeability of the Ni-Zn ferrite core in the absence of concurrent magnetization.

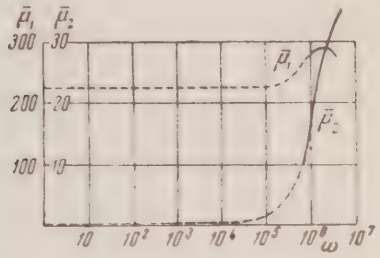

Fig. 16. Frequency dependence of the real and imaginary components of the apparent permeability of the same core with concurrent magnetization with aw_0=10 A.

To make use of these circuits for practical design purposes one must know the frequency dependence of the permeability and permittivity of the core material. According to the nature of this dependence and the cross section dimensions of the proposed core, it is possible to simplify the full equivalent circuits, in some cases to the point of using the simple equivalent circuit for purely magnetic polarization.

It must be noted, however, that so far no separate determinations of the frequency characteristics of the permeability and the dielectric constant have been made.

The general suitability of a ferrite core for use in a particular pulse circuit component (for example, in voltage, current or differentiating transformers) can be ascertained by recording the frequency characteristic of the apparent permeability of the material in the appropriate frequency band, i.e. in the band between the limits

$$\frac{1}{10\ T_p} \geq \omega \geq \frac{10}{\tau_f}$$

where τ_f is the required pulse-form front at the transformer output and T_p is the pulse duration.

The measuring procedure described above permits of simple and rapid determination of the required frequency characteristics.

The present investigation was carried out in the Theoretical Bases of Electrical Engineering Department of the Moscow Energetics Institute, at the suggestion and under the guidance of K. M. Polivanov, to whom the author wishes to express his profound gratitude.

Moscow Energetics Institute
Imeni V. M. Molotov

Received
20 July 1954

Bibliographic References

1. National Bureau of Standards, Tech. News Bulletin, 36, 5, 78 (1952).
2. F.V.Ludkin, Radiotekhnika (Radio Engineering), 2, 4 (1947).
3. K.M.Polivanov, Izv. (Bulletin) AN SSSR, Ser. fiz., 16, 451 (1952).
4. V.K.Arkad'ev, Elektromagnitnye protsessy v metallakh (Electromagnetic processes in metals). Parts I and II, ONTI, M.-L. 1934-1936.

ON WAVES IN A GYROTROPIC MEDIUM

- M. A. Gintsburg

1. Propagation of electromagnetic waves in a plane gyrotropic layer

The angle of rotation Ψ of the plane of polarization of electromagnetic waves propagated through a medium in an external magnetic fiel depends on the intensity H_0 of this field and on the distance d traversed by the wave. Media in which rotation of the plane of polarization occurs are called gyrotropic. If reflection from the boundaries of the gyrotropic medium is neglected and the magnetic field is assumed to be weak, the dependence of Ψ on H_0 and d is given by Faraday's law: $\Psi = \text{const} \cdot H_0 d$.

However, reflection from the medium boundaries perpendicular to th direction of propagation does have an appreciable influence on both the strength and polarization of the waves. A new, additional effect appears incident to transmission through the gyrotropic layer: an additional Faraday rotation, which has a complex, non-linear dependence on the thickness d, and an augmented ellipticity of both the reflected and refracted waves, connected with the reflection rather than absorption.

Let us assume that the wave is propagated along the OZ axis and that the field H_0 is parallel to this axis. The tensors of the dielectric constant ε_{ik} and of the magnetic permeability μ_{ik} will then have the following form:

$$\left.\begin{aligned} \varepsilon_{xx} = \varepsilon_{yy} = \varepsilon_1, \quad \varepsilon_{yx} = -\varepsilon_{xy} = i\varepsilon_2, \quad \varepsilon_{zz} = \varepsilon_3, \\ \mu_{xx} = \mu_{yy} = \mu_1, \quad \mu_{yx} = -\mu_{xy} = i\mu_2, \quad \mu_{zz} = \mu_3. \end{aligned}\right\} \qquad (1)$$

For ferrites in the microwave frequency range $\varepsilon_2 = 0$ and $\mu_2 \neq 0$; for dielectrics in the range of optical frequencies $\varepsilon_2 \neq 0$ and $\mu_2 = 0$.

Let us investigate the case of normal incidence of a plane wave $E_{1y}^{+} = 0$, $E_{1x}^{+} = 2\exp i(kz - \omega t)$ on a plane gyrotropic layer II ($0 < z < d$), located between two isotropic media I ($z < 0$) and III ($z > d$).

As noted, H_0 is parallel to the OZ axis. In medium I, $\varepsilon = \varepsilon^{(1)}$; $\mu = \mu^{(1)}$; in medium III, $\varepsilon = \varepsilon^{(3)}$, $\mu = \mu^{(3)}$; medium II is characterized by tensors ε_{ik} and μ_{ik} of type (1).

Let us represent the incident wave in the form of a sum of two circularly polarized waves:

$$\bar{E}_{1y}^{+} = i\bar{E}_{1x}^{+}, \quad \bar{E}_{1x}^{+} = \exp i(\bar{k}z - \omega t) \text{ and } \bar{\bar{E}}_{1y}^{+} = -i\bar{\bar{E}}_{1x}^{+}, \quad \bar{\bar{E}}_{1x}^{+} = \exp i(\bar{\bar{k}}z - \omega t).$$

It is not difficult to find $\bar{k}$ and $\bar{\bar{k}}$ as well as the impedance $Z = E_x/H_y$ of media I, II and III for the two circularly polarized waves, from Maxwell's equations:

$$\bar{k} = \frac{\omega}{c}[(\varepsilon_1 + \varepsilon_2)(\mu_1 + \mu_2)]^{1/2}, \quad \bar{\bar{k}} = \frac{\omega}{c}[(\varepsilon_1 - \varepsilon_2)(\mu_1 - \mu_2)]^{1/2},$$

$$\bar{Z}_2 = \left(\frac{\mu_1 + \mu_2}{\varepsilon_1 + \varepsilon_2}\right)^{1/2}, \quad \bar{\bar{Z}}_2 = \left(\frac{\mu_1 - \mu_2}{\varepsilon_1 - \varepsilon_2}\right)^{1/2}. \qquad (2)$$

The complex amplitudes of these normal waves are readily determine from the condition of continuity of the tangential components of the E and H vectors at the interfaces z = 0 and z = d. Having E_x, E_y, $\bar{E}_x$ and $\bar{E}_y$ in each of the three media, we find the ratio (Ref. 1):

$$\frac{E_{3y}}{E_{3x}} = M_3 = i\,\frac{(1 + Z_{13})[\cos\bar{k}d - \cos\bar{\bar{k}}d] + i(\bar{Z}_{12} + \bar{Z}_{23})\sin\bar{k}d - i(\bar{\bar{Z}}_{12} + \bar{\bar{Z}}_{23})\sin\bar{\bar{k}}d}{(1 + Z_{13})[\cos\bar{k}d + \cos\bar{\bar{k}}d] - i(\bar{Z}_{12} + \bar{Z}_{23})\sin\bar{k}d - i(\bar{\bar{Z}}_{12} + \bar{\bar{Z}}_{23})\sin\bar{\bar{k}}d}, \qquad (3)$$

which determines the polarization of the transmitted wave. Separating

(weakly-gyrotropic medium approximation; see Ref. 1) equation (3) is greatly simplified:

$$\frac{E_{3y}}{E_{3x}} = M_3 = \frac{1}{2} \cdot \frac{i\alpha R\,(e^{i2k_0 d} - 1) - \beta k_0 d\,(1 + R^2 e^{i2k_0 d})}{1 - R^2 e^{i2k_0 d}}, \qquad (6)$$

where R^2 is the reflection coefficient and k_0 is the propagation constant for $H_0 = 0$; $\alpha = \frac{\mu_2}{\mu_1} - \frac{\varepsilon_2}{\varepsilon_1}$; $\beta = \frac{\mu_2}{\mu_1} + \frac{\varepsilon_2}{\varepsilon_1}$. From (6) it follows that when $d = \frac{2n+1}{4}\lambda$, $\psi = \psi_0 \frac{1-R^2}{1+R^2}$, while when $d = \frac{n\lambda}{2}$, $\psi = \psi_0 \frac{1+R^2}{1-R^2}$ and $\vartheta = 0\left(\psi_0 = -\frac{1}{2}\beta k_0 d\right)$, i.e. in quarter-wave ferrite plates the effect of reflection is to reduce the rotation and increase the ellipticity, while in plates an integral number of half-waves thick, reflection increases the rotation without introducing additional ellipticity. Hence, we conclude that one effective method of reducing the ellipticity in practice is to make the ferrite plate thickness equal to an integral number of half-waves. The other method of reducing ellipticity is through suitable selection of the electric parameters of the isotropic media I and III.

We obtain the corresponding condition by equating $E_{3x} = \bar{E}_{3x}$:

$$[(1 + Z_{13})^2 - (\bar{Z}_{12} + \bar{Z}_{23})^2]\cos^2 \bar{k}d - [(1 + Z_{13})^2 - (\bar{\bar{Z}}_{12} + \bar{\bar{Z}}_{23})^2]\cos^2 \bar{\bar{k}}d =$$
$$= [(\bar{\bar{Z}}_{12} + \bar{\bar{Z}}_{23})^2 - (\bar{Z}_{12} + \bar{Z}_{23})^2]. \qquad (7)$$

In the "weakly gyrotropic" approximation, it follows from (6) that ϑ also equals zero when $R_0 = 0$; i.e., that in order to maintain linear polarization it is sufficient to place plate II in an isotropic medium, having the same impedance as the material of the plate II would have in the absence of an external magnetic field.

Rayleigh (Ref. 5) proposed a one-way optical system, consisting of two Nicol prisms with their planes of acceptance at 45° degrees to each other and a gyromagnetic plate between them, also rotated through 45°. In order for the Rayleigh light valve to operate the plate must not only rotate the plane of polarization through 45° but it must also maintain linear polarization. From (3) it follows that the second condition is, in general, not satisfied with $\varepsilon^{(1)} = \mu^{(1)} = \varepsilon^{(3)} = \mu^{(3)} = 1$ (gyrotropic plate in air). Hence, it is desirable to modify the Rayleigh system somewhat by placing isotropic plates I and III, having appropriate values of ε and μ, on both sides of the gyrotropic plate II. Such modification is essential in the radio-frequency region. Putting $\psi = 45°$ and $\vartheta = 0$, we obtain from (3) the requisite values of Z_1 and Z_3:

$$Z_{1,3} = \frac{1}{A}\{M \pm \sqrt{M^2 - AN}\}, \qquad (8)$$

where

$$M = (\bar{Z}^2 - \bar{Z}_2^2)\sin \bar{k}d \cdot \sin \bar{\bar{k}}d, \quad A = \bar{Z}_2 \sin 2\bar{k}d + \bar{\bar{Z}}_2 \sin 2\bar{\bar{k}}d,$$
$$N = \bar{Z}_2 \bar{\bar{Z}}_2 (\bar{Z}_2 \sin 2\bar{k}d + \bar{\bar{Z}}_2 \sin 2\bar{\bar{k}}d). \qquad (9)$$

In the "weakly gyrotropic" approximation, we have $\vartheta = 0$ not only with $R = 0$, but also for $d = n\lambda/2$; that is, to realize the Rayleigh one-way system the thickness of plate II should be made equal to an integral number of half-waves.

Let us now turn to the case when the propagation of the electromagnetic waves is perpendicular to the field H_0. Assuming $\mathbf{H}_0 \| OY$, then $\varepsilon_{xx} = \varepsilon_{zz} = \varepsilon_1$, $\varepsilon_{xz} = -\varepsilon_{zx} = i\varepsilon_2$, $\varepsilon_{yy} = \varepsilon_3$; $\mu_{xx} = \mu_{zz} = \mu_1$, $\mu_{xz} = -\mu_{zx} = i\mu_2$, $\mu_{zz} = \mu_3$ [ε_i and μ_i have the same values as in (1)]. It follows from Maxwell's equations that

two types of plane waves are possible in this system:

$$\left.\begin{aligned}
&1)\ \text{E-waves:}\quad E_x \neq 0,\ E_z = i\frac{\varepsilon_2}{\varepsilon_1}E_x,\ H_y = -\frac{\omega}{k\cdot c}(\varepsilon_1 E_x + i\varepsilon_2 E_z),\\
&\qquad E_y = H_x = H_z = 0;\\
&\qquad \bar{k}^2 = \frac{\omega^2}{c^2}\cdot\frac{\mu_3}{\varepsilon_1}(\varepsilon_1^2 - \varepsilon_2^2);\ Z = \left[\frac{\varepsilon_1\mu_3}{\varepsilon_1^2 - \varepsilon_2^2}\right]^{\frac{1}{2}};\\
&2)\ \text{H-waves:}\quad H_z = i\frac{\mu_2}{\mu_1}H_x,\ E_y = \frac{\omega}{c\cdot\bar{k}}(\mu_1 H_x + i\mu_2 H_z),\\
&\qquad H_y = E_x = E_z = 0;\\
&\qquad \bar{k}^2 = \frac{\omega^2}{c^2}\cdot\frac{\varepsilon_3}{\mu_1}(\mu_1^2 - \mu_2^2);\ Z = \left[\frac{\mu_1^2 - \mu_2^2}{\mu_1\varepsilon_3}\right]^{\frac{1}{2}}.
\end{aligned}\right\} \qquad (10)$$

We find the complex amplitudes of the two normal waves and their ratio in the refracted wave from the boundary conditions at $\bar{\bar{z}} = 0$ and $\bar{\bar{z}} = d$:

$$M = \frac{E_{3y}}{E_{3x}} = \frac{(1 + Z_{13})\cos\bar{k}d - (\bar{Z}_{12} + \bar{Z}_{23})\,i\sin\bar{k}d}{(1 + Z_{13})\cos\bar{\bar{k}}d - (\bar{\bar{Z}}_{12} + \bar{\bar{Z}}_{23})\,i\sin\bar{\bar{k}}d}\cdot\frac{E_{1y}^{+}}{E_{1x}^{+}}. \qquad (11)$$

We can then determine the angle of rotation and the ellipticity:

$$\operatorname{tg} 2(\psi - \alpha) = \frac{2\operatorname{Re} M}{1 - |M|^2} \quad \text{and} \quad \sin 2\vartheta = \frac{2\operatorname{Im} M}{1 + |M|^2}\cdot\frac{1}{i}$$

(α is the angle between the incident wave vector and the field H_0. In practice it is desirable to obtain a gyrotropic layer with a zero reflection coefficient. For this we must have

$$\bar{Z} = \bar{\bar{Z}} = 1,\ \text{i.e.,}\ \varepsilon_1\mu_3 = \varepsilon_1^2 - \varepsilon_2^2,\ \mu_1\varepsilon_3 = \mu_1^2 - \mu_2^2.$$

If reflection is neglected, (11) becomes $E_{3y}/E_{3x} = \exp(\bar{\bar{k}} - k)d \times \frac{E_{1y}^{+}}{E_{1x}^{+}}$.

With $(\bar{\bar{k}} - \bar{k})d = \pi(n + 1/2)$, we obtain a quarter-wave plate (maximum ellipticity), while with $(\bar{\bar{k}} - \bar{k})d = \pi n$, we have a half-wave plate (transmitted wave linearly polarized). If the angle between the E_1 vector of the incident wave and H_0 is $(+\alpha)$, then with $(\bar{\bar{k}} - \bar{k})d = \pi(2n + 1)$, the vector of the refracted wave will be at an angle $(-\alpha)$ to H_0, i.e. the plane of polarization will be rotated through an angle $\psi = 2\alpha$. If the external field, H_0, be rotated about the OZ axis (with its magnitude remaining constant), the E_3 vector will rotate with the field, but through twice the angle. Thus, through appropriate rotation of the applied field the plane of polarization of the electromagnetic waves can be made to turn in any prescribed manner.

Let us consider the influence of reflection at the boundaries in the case of isotropic substances whose natural ability to produce rotation is due to molecular asymmetry. In such substances (Ref. 2):

$$D_x = \varepsilon E_x - i\tau E_y,\quad B_x = H_x + \frac{a\tau}{k}E_x,\quad D_y = \varepsilon E_y + i\tau E_x,\quad B_y = H_y + \frac{a\tau}{k}E_y,$$

where $a = -i\omega/c$ and τ is a constant, dependent upon the structural asymmetry of the molecules. Equations (3)-(6) hold in such media, with the difference that the propagation constants and the impedances have other values:

$$\bar{k}^2 = (\varepsilon + 2\tau)\cdot\frac{\omega^2}{c^2},\quad \bar{\bar{k}}^2 = (\varepsilon - 2\tau)\cdot\frac{\omega^2}{c^2},\quad \bar{Z} = \frac{\sqrt{\varepsilon + 2\tau}}{\varepsilon + \tau},\quad \bar{\bar{Z}} = \frac{\sqrt{\varepsilon - 2\tau}}{\varepsilon - \tau};$$

and, in the "weakly gyrotropic" approximation $\bar{R} = \bar{\bar{R}} = R_0$, $\bar{k} = k_0(1 + \alpha)$, $\alpha = \frac{\tau}{\varepsilon}$, i.e.,

$$M_3 = \frac{E_{3y}}{E_{3x}} = -\alpha k_0 d \frac{1 - R^2 e^{i2k_0 d}}{1 + R^2 e^{i2k_0 d}};$$

that is, in this approximation, refraction at the first (z = 0) boundar does not introduce ellipticity.

2. Space-time analogy between waves in a gyrotropic medium and the oscillation of coupled systems

Let us consider the case of plane waves in a gyrotropic medium (1). Eliminating the H_x and H_y components from Maxwell's equations, we obtain

$$\ddot{E}_x + n_1^2 E_x - \rho_1 E_y = 0, \quad \ddot{E}_y + n_2^2 E_y - \rho_2 E_x = 0, \tag{12}$$

where $n_1^2 = n_2^2 = \mu_1\varepsilon_1 + \mu_2\varepsilon_2$, $\rho_2 = -\rho_1 = i\frac{\omega^2}{c^2}(\varepsilon_1\mu_2 + \mu_1\varepsilon_2)$; and the dots indicate differentiation with respect to z. Equations (12) remain invariant for all directions of propagation relative to the field H_0, only n_1^2 and n_2^2 must be expressed in terms of all twelve components of the ε_{ik} and μ_{ik} tensors.

The equations for small-amplitude oscillations of a system of two pendulums coupled by a spring (or any other linear system with two degrees of freedom) are similar. Let φ_1 and φ_2 be the angular deviations of the first and second pendulums from the equilibrium position. Then

$$\ddot{\varphi}_1 + n_1^2\varphi_1 - \rho_1\varphi_2 = 0, \quad \ddot{\varphi}_2 + n_2^2\varphi_2 - \rho_2\varphi_1 = 0 \tag{13}$$

here the dots indicate differentiation with respect to the time t and n_1^2 and n_2^2 are constants, determined by the mass and geometry of the pendulums and the connecting spring.

Inasmuch as (12) and (13) are analogous we can regard the componen of the H and E vectors as generalized coordinates [analogous to φ_1 and φ_2 in (13)] and apply the methods and results of the classical treatment of linear oscillations to the propagation of electromagnetic waves the only difference being that in this case the independent variable will be the spatial coordinate z, rather than the time t.

The general solution of (13) is sought in the form of a superposition of normal oscillations:

$$\varphi_1 = A_1 e^{i\Omega_1 t} + A_2 e^{i\Omega_2 t}, \quad \varphi_2 = A_1 p_1 e^{i\Omega_1 t} + A_2 p_2 e^{i\Omega_2 t}.$$

In like manner, we seek the solution of (12) in the form of a supe position of normal waves:

$$E_x = A_1 e^{i\bar{k}z} + A_2 e^{i\bar{\bar{k}}z}, \quad E_y = A_1 p_1 e^{i\bar{k}z} + A_2 p_2 e^{i\bar{\bar{k}}z}.$$

Substituting these expressions in (12), we find A_1/A_2, $\bar{k}$, $\bar{\bar{k}}$, p_1 and p_2. The character of the coupling between E_x and E_y and the nature of the gyrotropic effect are determined by the "coupling" of the partia systems: $\Lambda = \rho_1\rho_2/(n_1^2 - n_2^2)$ (the concept of "coupling" ["connectedness"] was originally introduced by L. I. Mandel'shtam). The case of a transverse field, $H_0 \| OY$, corresponds to $\rho_1 = \rho_2 = 0$ ($\Lambda = 0$: no coupling). In contrast, in a longitudinal field, $H_0 \| OZ$, we have the case of extreme coupling: $n_1^2 = n_2^2$, $\Lambda = \infty$.

In this analogy, the Faraday effect corresponds to "spatial beats" for just as in beats, energy is periodically transferred from one of th

"coupled systems", E_x, to the other, E_y. The beat frequency is equal to the half-difference of the normal frequencies. By analogy, the rotation per unit path length equals the half-difference between the propagation constants of the two waves: $\psi = \frac{1}{2}(\bar{k} - \bar{k})$.

3. Gyrotropic waveguides

Let us also investigate the case of inhomogeneous waves in a gyrotropic medium. In our analysis we will follow the reasoning and keep the notation originally given in Ref. 6.* We turn first to the case of a longitudinal field parallel to the OZ axis. Eliminating E_x, E_y, H_x and H_y from Maxwell's equations, we obtain partial equations of the fourth order in E_z and H_z:

$$\left.\begin{aligned} \Delta^2 E_z + a_1 \Delta E_z + a_2 E_z = 0, \\ \Delta^2 H_z + a_1 \Delta H_z + a_2 H_z = 0 \end{aligned}\right\} \qquad (14)$$

(a_1 and a_2 are as defined in Ref. 6).

Thus, in a gyrotropic medium, Maxwell's equations reduce to one fourth-order equation in one unknown function. This deduction is genera and valid for all anisotropic media; it also follows from the character of the boundary conditions. A fourth order equation is the "natural" equation for a waveguide; although electrodynamics has until now dealt primarily with boundary conditions characterized by second order equations (and, accordingly, TE and TM modes) it must be emphasized that these are merely particular cases in which it is feasible to set E_z or H_z equal to zero (thereby reducing Maxwell's equations to a single equation because of the isotropy of the medium. This is confirmed by the very nature of the boundary conditions, i.e., by the fact that there are always two such conditions ($E = E_z = 0$ or $E_{x,y} = E_z = 0$, etc.), corresponding to a fourth order, rather than a second order equation (a second order boundary value equation involves only one boundary condition).

In the general case, in anisotropic media neither of the longitudinal components (neither H_z nor E_z) vanishes, which fact is reflected in the order of the equations.

Let us take another case - that of a waveguide filled with a medium characterized by symmetric ε_{ik} and μ_{ik} tensors ($\varepsilon_{xx} = \varepsilon_1$, $\varepsilon_{yy} = \varepsilon_2$; $\varepsilon_{zz} = \varepsilon_3$; $\mu_{xx} = \mu_1$, $\mu_{yy} = \mu_2$, & $\mu_{zz} = \mu_3$; one of the principal axes of the tensors coincides with the OZ axis of the wave guide). Eliminating the other components from Maxwell's equations, we obtain for E_z:

$$\left\{\left(\varepsilon_1\mu_2\frac{\partial^2}{\partial x^2} + \varepsilon_2\mu_2\frac{\partial^2}{\partial y^2} + \varepsilon_2\mu_3\frac{\partial^2}{\partial z^2} - \frac{1}{c^2}\varepsilon_1\varepsilon_2\mu_2\mu_3\frac{\partial^2}{\partial t^2}\right)\left(\mu_1\varepsilon_2\frac{\partial^2}{\partial x^2} + \right.\right.$$

$$\left.\left. + \mu_2\varepsilon_2\frac{\partial^2}{\partial y^2} + \mu_2\varepsilon_3\frac{\partial^2}{\partial z^2} - \frac{1}{c^2}\cdot\frac{\partial^2}{\partial t^2}\mu_1\mu_2\varepsilon_2\varepsilon_3\right) + \frac{\partial^2}{\partial x^2}\cdot\frac{\partial^2}{\partial z^2}(\varepsilon_2\mu_3 - \varepsilon_3\mu_2)(\varepsilon_1\mu_2 - \mu_1\varepsilon_2)\right\} E_z = 0. \qquad (15)$$

Let us determine the normal waves in a rectangular, anisotropic waveguide bounded by conducting walls at $x = 0$, $y = 0$, $x = x_1$ and $y = y_1$. We seek a solution in the form: $\sin k_x x \cdot \sin k_y y \cdot \exp[i(kz - \omega t)]$. We obtain a fourth degree equation in k:

* While Refs. 1 and 6, representing condensed versions of parts of our thesis (Ref. 7), were at the printers awaiting publication, there appeared in foreign literature a series of articles (Refs. 8-12) on gyrotropic waveguides which partially duplicate Ref. 6.

$$k^4 - A_1 k^2 + A_2 = 0,$$

where

$$A_1 = \frac{1}{\varepsilon_3 \mu_3}\left[k_x^2(\varepsilon_1\mu_3 + \mu_1\varepsilon_3) + k_y^2(\mu_2\varepsilon_3 + \mu_3\varepsilon_2) - \frac{\omega^2}{c^2}\varepsilon_3\mu_3(\varepsilon_1\mu_2 + \mu_2\varepsilon_1)\right],$$

$$A_2 = \frac{1}{\varepsilon_3\mu_3}\left[\varepsilon_1\mu_1 k_x^4 + \varepsilon_2\mu_2 k_y^4 + k_x^2 k_y^2(\mu_1\varepsilon_2 + \mu_2\varepsilon_1) - \frac{\omega^2}{c^2}\left[\varepsilon_1\mu_1(\mu_2\varepsilon_3 + \varepsilon_2\mu_3)k_x^2 + \varepsilon_2\mu_2(\varepsilon_1\mu_3 + \mu_1\varepsilon_3)k_y^2\right] + \frac{\omega^4}{c^4}\varepsilon_1\mu_1\varepsilon_2\mu_2\right];$$

$$k_x = \frac{\pi m}{x_1}, \quad k_y = \frac{\pi n}{y_1}, \quad m, n = 0, 1, 2, 3, \ldots$$

The above equation has two roots, $k^2 = k^2_{1,2}$, corresponding to the two systems of normal waves. Knowing E_z one can readily find the other E and H components from Maxwell's equations. It appears that when $k_x \neq 0$ and $k_y \neq 0$ in both normal wave systems, both longitudinal components will differ from zero, i.e. neither E_z nor H_z will vanish. As noted above, equation (13) for the $E_z(x, y)\exp i(kz - \omega t)$ wave is an equation of the fourth order.

It is often convenient to expand the differential operators of (14) and (15) into products of operators of the second order. Thus, the former can be expanded into

$$L = \Delta^2 + a_1\Delta + a_2 = (\Delta + k_{c_1}^2)(\Delta + k_{c_2}^2)$$

($k_{c_1}^2$ and $k_{c_2}^2$ are the roots of the characteristic equation $k_c^4 + a_1 k_c^2 + a_2 = 0$), and the solution sought as the sum of the solutions of the second order equations $(\Delta + k_{c_1}^2)E_z = 0$ and $(\Delta + k_{c_2}^2)E_z = 0$. For example, for a circular waveguide the first equation yields $E_{z_1} \sim J_n(k_{c_1}r)$; the second, $E_{z_2} \sim J_n(k_{c_2}r)$. We must emphasize, however, that under the conditions of the given boundary problem the $J_n(k_{c_1}r)$ and $J_n(k_{c_2}r)$ "waves" have no physical meaning: the boundary conditions are satisfied only by a certain superposition of these "waves"; i.e., only $E = A_n J_n(k_{c_1}r) + B_n J_n(k_{c_2}r)$ represents a normal wave.

For waves propagated between the two planes x = 0 and $x = x_1$, we again seek a solution of (14) in the form of a sum of the solutions of separate second order equations:

$$E_z = [A_1 \sin k_{c_1}x + A_2\cos k_{c_1}x + A_3 \sin k_{c_2}x + A_4\cos k_{c_2}x]\exp i(kz - \omega t).$$

From the boundary conditions at 0 and x_1, we obtain a system of four homogeneous linear equations for the four unknown amplitudes A_i. Setting the determinant of this system equal to zero, we find the transcendental equation defining the propagation constant.

The solution of (14) for the case of a circular waveguide was discussed in Ref. 6. Hence, here we will only give an additional equation determining the cutoff frequencies of a gyrotropic waveguide. This equation follows from (8) in Ref. 6 and has the form:

for H_{gyro} waves (TE mode) for E_{gyro} waves (TM mode)

$$\frac{dJ_n(k_{c_1}R)}{dR} = \pm n\frac{\varepsilon_2}{\varepsilon_1}\cdot\frac{1}{R}J_n(k_{c_1}R) \qquad J_n(k_{c_2}R) = 0, \qquad (16)$$

where

$$k_{c_1}^2 = \frac{\omega^2}{c^2}\cdot\frac{\mu_3}{\varepsilon_1}(\varepsilon_1^2 - \varepsilon_2^2) \quad \text{and} \quad k_{c_2}^2 = \frac{\omega^2}{c^2}\cdot\frac{\varepsilon_3}{\varepsilon_1}(\mu_1^2 - \mu_2^2).$$

The plus sign applies to the $\exp i(n\varphi - kz - \omega t)$ wave and the minus sign applies to the $\exp i(-n\varphi - kz - \omega t)$ wave.

Equations (16) indicate the possibility of adjusting the wave transmission factor of a gyrotropic layer in a waveguide by regulating the

---

*In a later paper in Zhur. Tekh. Fiz., the author states that the term, $+\varepsilon_1\varepsilon_2\varepsilon_3\mu_1\mu_2\mu_3$, was left out of the right hand member of this equation. Translator.

external magnetic field, inasmuch as varying the applied field changes the values of the ε_{ik} and μ_{ik} components and the differences $\varepsilon_1^2 - \varepsilon_2^2$ and $\mu_1^2 - \mu_2^2$.

It may also be of interest to give the expressions for the field components in a circular waveguide:

$$H_z = M_1 J_n(k_{c_1} r) + B_{n,m} M_2 J_n(k_{c_2} r),$$

$$E_r = \frac{1}{D}\left\{ \frac{inc}{r} b_1 E_z + a b_2 \frac{dE_z}{dr} + \frac{ina}{r} b_3 H_z + a b_4 \frac{dH_z}{dr} \right\},$$

$$E_\varphi = \frac{1}{D}\left\{ \frac{inb_2}{r} E_z + \frac{c}{r} b_1 \frac{dE_z}{dr} + \frac{ina}{r} b_4 H_z + a b_3 \frac{dH_z}{dr} \right\},$$

where

$$M_{1,2} = \frac{\mu_1 \varepsilon_1 k_{c_{1,2}}^2 - a^2 \varepsilon_1 \varepsilon_3 (\mu_1^2 - \mu_2^2) - \gamma^2 \mu_1 \varepsilon_3}{\gamma^2 i a (\varepsilon_1 \mu_2 + \varepsilon_2 \mu_1)},$$

$$b_1 = \gamma^2 - a^2 (\varepsilon_1 \mu_1 + \varepsilon_2 \mu_2), \quad b_2 = a^2 i (\varepsilon_1 \mu_2 + \varepsilon_2 \mu_1),$$

$$b_3 = i [\mu_2 \gamma^2 + a^2 \varepsilon_2 (\mu_1^2 - \mu_2^2)], \quad b_4 = \mu_1 \gamma^2 - a^2 \varepsilon_1 (\mu_1^2 - \mu_2^2),$$

$$D = [\gamma^2 - a^2 (\varepsilon_1 + \varepsilon_2)(\mu_1 + \mu_2)][\gamma^2 - a^2 (\varepsilon_1 - \varepsilon_2)(\mu_1 - \mu_2)], \quad a = -i\frac{\omega}{c}$$

H_φ and Hr are found from the equations for E_φ and E_r by replacing E_z by H_z, H_z by E_z, ε_{ik} by μ_{ik}, μ_{ik} by ε_{ik} and a by $-a$.

4. Excitation of gyrotropic waveguides

Let us investigate the excitation of a waveguide filled with a gyrotropic medium by wall currents of known density. In our analysis we will use the method proposed by Vainshtein for an isotropic waveguide (Ref. 13).

We seek a solution of Maxwell's equations

$$\operatorname{rot} \mathbf{H} = a\mathbf{D} + \frac{4\pi}{c}\mathbf{j}_e, \quad \operatorname{rot} \mathbf{E} = -a\mathbf{B} - \frac{4\pi}{c}\mathbf{j}_m, \tag{17}$$

where $a = -i\frac{\omega}{c}$, and $\mathbf{j}_e$ and $\mathbf{j}_m$ are, respectively, the electric and magnetic wall-current densities.

The boundary conditions may be formulated as follows: there exists a certain cylindrical surface within which the entire field is concentrated. On this surface $E = H = 0$.

The ε_{ik} and μ_{ik} tensors of the medium filling the waveguide can be expressed by any piecewise-continuous function of x and y. We specify the OZ axis to be coincident with the waveguide axis and the magnetic field parallel to OZ. We seek a solution of (17) in the form of a series of eigenfunctions of the homogeneous equations $\operatorname{rot} \mathbf{H} = a\mathbf{D}$ and $\operatorname{rot} \mathbf{E} = -a\mathbf{B}$. The Lorentz lemma is generally used to determine the coefficients of this series.

However, the principle of reciprocity does not apply in a gyrotropic medium and the Lorentz lemma cannot be used. Instead, in a similar manner, we obtain the relation

$$\oint_S ([\mathbf{E}'\mathbf{H}''] - [\mathbf{E}''\mathbf{H}'])\mathbf{n}\, dS = -2\frac{\omega}{c}\int_V (\mu_2 [\mathbf{H}'\mathbf{H}''] - \varepsilon_2 [\mathbf{E}'\mathbf{E}''])\mathbf{l}\, dv$$

$$-\frac{4\pi}{c}\int_V (\mathbf{j}_e'\mathbf{E}'' - \mathbf{j}_e''\mathbf{E}' + \mathbf{j}_m'\mathbf{H}'' - \mathbf{j}_m''\mathbf{H}')\, dv, \tag{18}$$

relating the E' and E'' fields due to the two systems of electric and magnetic currents j'_e, j'_m and j''_e, j''_m. Equation (18) generalizes the Lorentz lemma to include the case of a gyrotropic waveguide.

Applying (18) to the normal waves of the gyrotropic waveguide, we obtain the orthogonality relation between them:

$$\int_{S_p} \left\{ [\mathbf{E}_m \mathbf{H}_{m'}] - [\mathbf{E}_{m'} \mathbf{H}_m] - \frac{2\omega/c}{\gamma_m + \gamma_{m'}} (\varepsilon_2 [\mathbf{E}_m \mathbf{E}_{m'}] - \mu_2 [\mathbf{H}_m \mathbf{H}_{m'}]) \right\} \mathbf{l}\, dS = 0,$$

(here $\mathbf{l} \parallel OZ$, $|l| = 1$).

For the norm N_m we select

$$N_m = \frac{c}{4\pi} \int_S ([\mathbf{E}_m \mathbf{H}_{-m}] - [\mathbf{E}_{-m} \mathbf{H}_m]) \mathbf{l}\, dS = 0. \qquad (19)$$

Expression (19) can be simplified. As may readily be shown, if the Maxwell equations for a gyrotropic medium admit of a particular solution in the form of normal waves $\mathbf{E}_m(E_{x,m}, E_{y,m}, E_{z,m})$; $\mathbf{H}_m(H_{x,m}, H_{y,m}, H_{z,m})$ with a phase factor $\exp(\gamma_m z - i\omega t)$, , then the $\mathbf{E}_{-m}(-E_{x,m}, -E_{y,m}, E_{z,m})$; $\mathbf{H}_{-m}(H_{x,m}, H_{y,m}, -H_{z,m})$ vectors also generate a solution with a phase factor $\exp(-\gamma_m z - i\omega t)$. Hence, (19) can be rewritten: $N_m = \frac{c}{2\pi} \int_{S_p} [\mathbf{E}_m \mathbf{H}_m] \mathbf{l}\, dS$; i.e. this is the complex power delivered by both waves - $\exp \gamma_m z$ and $\exp(-\gamma_m z)$ - through the cross section S_p.

These results open the way to a solution of our gyrotropic waveguide problem.

Let us assume the sources to be located in the region $z_2 \leqslant z \leqslant z_1$. Then only $\mathbf{E}_{-m}$ waves are propagated to the left of the sources (i.e., $E = \sum \alpha_m \mathbf{E}_{-m}$); while to the right ($z > z_1$), $\mathbf{E} = \sum \alpha_m \mathbf{E}_m$. The complex amplitudes may be determined from (18). To this end, we use the total field $\sum \alpha_m \mathbf{E}_m$ or $\sum \alpha_{-m} \mathbf{E}_{-m}$, for $\mathbf{E}'$ in (18) and $\mathbf{E}_n$ or $\mathbf{E}_{-n}$ for the field $\mathbf{E}''$. We then obtain

$$\alpha_n = \frac{1}{N} \int_{z_2}^{z_1} (\mathbf{j}_e \mathbf{E}_{-n} - \mathbf{j}_m \mathbf{H}_{-n})\, dV, \quad \alpha_{-n} = \frac{1}{N_n} \int_{z_2}^{z_1} (\mathbf{j}_e \mathbf{E}_n - \mathbf{j}_m \mathbf{H}_n)\, dV. \qquad (20)$$

Let us now determine the field in the region occupied by the sources. We seek a solution of (17) in the form

$$\left.\begin{aligned} \mathbf{E} &= \sum \alpha_m \mathbf{E}_m + \sum \alpha_{-m} \mathbf{E}_{-m} + \mathbf{E}_{add}, \\ \mathbf{H} &= \sum \alpha_m \mathbf{H}_m + \sum \alpha_{-m} \mathbf{H}_{-m} + \mathbf{H}_{add}, \end{aligned}\right\} \qquad (21)$$

where $\mathbf{E}_{add}$ $\mathbf{H}_{add}$ is an additional field which will be determined below, while the coefficients α_m and α_{-m} have the form (21), with the difference that one of the limits of integration will be the coordinate value of z for the point at which the field is determined.

We make use of the method proposed by Vainshtein (Ref. 13) to determine $\mathbf{E}_{add}$ and $\mathbf{H}_{add}$: we remove the sources from the plane layer ($z - \delta$, $z + \delta$). The field inside such a cut will be defined by $\mathbf{E} = \sum \alpha_m \mathbf{E}_m + \sum \alpha_{-m} \mathbf{E}_{-m}$. However, by removing the sources from the layer, we change the actual field at every point of the volume, to wit 1) we interrupt the longitudinal currents $\mathbf{j}^l_e = j_{e,z} \mathbf{l}$ and $\mathbf{j}^l_m = j_{m,z} \mathbf{l}$; as a result surface charges, which do not tend to zero as $\delta \to 0$, form on the walls of the cut; 2) we eliminate the currents in the $z - \delta$, $z + \delta$ volume, but, inasmuch as the densities of these currents are finite, their field

approaches zero as $\delta \to 0$ and, hence, can be neglected. Therefore, we take account of only the first effect: the break in the longitudinal currents and the consequent formation of surface charges. These charges are equal in magnitude but opposite in sign on the opposite sides $z - \delta$ and $z \cdot \delta$ of the cut; hence, they give rise to electric and magnetic fields, directed along the OZ axis: $\mathbf{B}_{aux} \| OZ$, $\mathbf{D}_{aux} \| OZ$. Since in a longitudinal field the components $\varepsilon_{xz}, \varepsilon_{zx}, \varepsilon_{yz}, \varepsilon_{zy}; \mu_{xz}, \mu_{zx}, \mu_{yz}, \mu_{zy}$ equal zero, $\mathbf{E}_{add}$ and $\mathbf{H}_{add}$ will also be parallel to OZ.

Since the left-hand parts of the equations

$$\frac{\partial H_x}{\partial y} - \frac{\partial H_y}{\partial x} = aD_z + \frac{4\pi}{c} j_{ez} \text{ and } \frac{\partial E_x}{\partial y} - \frac{\partial E_y}{\partial x} = -aB_z - \frac{4\pi}{c} j_{mz}$$

are not changed by the interruption of the longitudinal currents (in view of the fact that $\mathbf{E}_{add} \| OZ$ and $\mathbf{H}_{add} \| OZ$), the additional fields (equivalent to the effect of the interrupted currents) will equal

$$\mathbf{D}_{aux} = -\frac{4\pi}{ac} \mathbf{j}_e^l \text{ and } \mathbf{B}_{aux} = -\frac{4\pi}{ac} \mathbf{j}_m^l. \qquad (22)$$

Passing to the limit with $\delta \to 0$, we obtain the final expressions for the electric and magnetic fields in the volume of the gyrotropic waveguide occupied by the sources:

$$E = \sum \alpha_n \mathbf{E}_n + \alpha_{-n} \mathbf{E}_{-n} + \frac{4\pi}{i\omega\varepsilon_3} j_{ez} \mathbf{l} \text{ and } H = \sum \alpha_n \mathbf{H}_n + \alpha_{-n} \mathbf{H}_{-n} + \frac{4\pi}{i\omega\mu_3} j_{mz} \mathbf{l} \qquad (23)$$

Equations (23) are also valid for a waveguide filled with a dielectric, characterized by symmetric ε_{ik} and μ_{ik} tensors.

5. Ferrite-loaded waveguide in a transverse magnetic field

A waveguide filled with a gyrotropic medium and situated in a transverse magnetic field (field parallel to OY) may be called a "traverse waveguide". Let us investigate the degenerate H-waves in such a waveguide, having a rectangular section. From Maxwell's equation for the $\mathbf{E}(x, y) \times \exp[\gamma z - i\omega t]$ wave:

$$\gamma E_y = a(\mu_1 H_x + i\mu_2 H_z), \quad \frac{dE_y}{dx} = a(i\mu_2 H_x - \mu_1 H_z),$$

$$\gamma H_x - \frac{dH_z}{dx} = a\varepsilon_3 E_y \qquad (24)$$

we find the field components

$$\left.\begin{aligned} E_y &= A_1 \sin k_2 x + A_2 \cos k_2 x, \\ H_x &= \frac{1}{a(\mu_1^2 - \mu_2^2)} \left[\mu_1 \gamma E_y + i\mu_2 \frac{dE_y}{dx}\right], \\ H_z &= \frac{1}{a(\mu_1^2 - \mu_2^2)} \left[i\mu_2 \gamma E_y - \mu_1 \frac{dE_y}{dx}\right], \end{aligned}\right\} \qquad (25)$$

where

$$k_2^2 = \gamma^2 - a^2 \varepsilon_3 \mu_1 \left(1 - \frac{\mu_2^2}{\mu_1^2}\right). \qquad (25')$$

It follows from (25) that the waves propagated in opposite directions (+z and -z) are characterized by different field distributions over the cross section of the waveguide. The normal waves of a "traverse waveguide" are mutually perpendicular. The corresponding orthogonality condition is

$$\int_{S_p} \left\{ ([\mathbf{E}_m \mathbf{H}_{m'}] - [\mathbf{E}\mathbf{H}_m]) \mathbf{l} + \frac{2a\gamma}{\gamma_m + \gamma_{m'}} (\mu_2 [\mathbf{H}_m \mathbf{H}_{m'}] - \varepsilon_2 [\mathbf{E}_m \mathbf{E}_{m'}]) \mathbf{j}_l^l \right\} dS = 0.$$

where E_m, H_m and $E_{m'}$, $H_{m'}$ are two different normal waves; $\mathbf{j} \| OY$ and $|\mathbf{j}| = 1$.

We can show that an infinite number of normal waves of different types may form at the boundary between an isotropic and a "traverse" waveguide. Let the region of the waveguide where $z < 0$ be filled with an isotropic medium (here $\varepsilon = \varepsilon_0$ and $\mu = \mu_0$ and we will denote the normal waves through E_m, H_m) and let the region $z > 0$ be filled with a gyrotropic medium in a transverse field (the normal waves of the "traverse waveguide" will be characterized by (25) and we will denote them through $\bar{E}_m$, $\bar{H}_m$). Resolving the field in regions I and II in conformity with the normal waves, we can write the boundary conditions at $z = 0$ as

$$\sum_{m=-\infty}^{m=+\infty} A_m E_{m,y} = \sum_{m=1}^{m=\infty} B_m \bar{E}_{m,y}, \qquad \sum_{-\infty}^{+\infty} A_m H_{m,x} = \sum_{1}^{\infty} B_m \bar{H}_{m,x} \tag{26}$$

($m < 0$ corresponds to the reflected wave and A_m and B_m are coefficients). Multiplying both sides of equalities (26) by $E_{p,y}$ and $H_{p,x}$, respectively, and integrating over the entire cross section, we obtain for the amplitudes A_m and B_m of the individual normal waves in the system of reflected (A^-) and (B^+) refracted waves the following infinite series of equations:

$$\left.\begin{aligned} (A_p^+ - A_p^-)\frac{\gamma_p}{\mu_0} &= B_p \cdot \frac{\mu_1}{\mu_1^2 - \mu_2^2}\bar{\gamma}_p + \frac{i\mu_2}{\mu_1^2 - \mu_2^2}\sum_{m \neq p} B_m \nu_{m,p}, \\ A_p^+ + A_p^- &= B_p^+, \end{aligned}\right\} \tag{27}$$

where $p = 1, 2, 3, \ldots$, and $\nu_{m,p} = \frac{2p^2}{m^2 - p^2}[(-1)^{m+p} - 1]$, $\frac{1}{x_1}$.

The transformation of wave types and formation of new wave types are effects characteristic of reflection from the gyrotropic layer or, in general, from any inhomogeneity in a waveguide.

Let us investigate the case of a waveguide only partially filled with a gyrotropic medium, i.e. in the section $x < d$; in the section $x > d$ the medium is isotropic; the width of the waveguide $x_1 = D$. We seek a solution for the gyrotropic section in the form

$$E_y = \alpha_2 \sin k_2 x, \quad H_z = \frac{\alpha_2}{a(\mu_1^2 - \mu_2^2)}(i\mu_2\gamma \cdot \sin k_2 x - \mu_1 k_2 \cos k_2 x). \tag{28}$$

And, for the isotropic section, in the form

$$E_y = \alpha_1(\sin k_1 x - \operatorname{tg} k_1 D \cdot \cos k_1 x), H_z = -\frac{1}{a\mu_0} \cdot \frac{dE_y}{dx}. \tag{29}$$

Equating (28) to (29) at $x = d$, we obtain a transcendental equation for the propagation constant:

$$\operatorname{tg} k_2 d \cdot [(\mu_1^2 - \mu_2^2) \cdot \frac{k_1}{\mu_0} - i\mu_2\gamma \cdot \operatorname{tg} k_1 d'] + \mu_1 k_2 \operatorname{tg} k_1 d' = 0 \tag{30}$$

where $k_1^2 = \gamma^2 - a^2\varepsilon_0\mu_0$, $d' = D - d$, while k_2 is determined from (25'). It is important to note that, as follows from (30), the phase velocities of the direct and inverse waves are different, i.e., the waveguide in question has unidirectional properties.

In general unidirectionality may be the result of 1) differences in dielectric and magnetic absorption (Ref. 14) and differences in the absorption of waves rotated in opposite directions in the presence of ferromagnetic resonance (Ref. 9), or 2) differences in the coefficients of reflection of the $\exp(\gamma z)$ and $\exp(-\gamma z)$ waves from the boundaries of the gyrotropic layer ($z = 0$ and $z = d$).

The reflection and refraction in a waveguide partially filled with a gyrotropic medium may be computed in an analogous fashion. By writing out the rather cumbersome expressions for the coefficients ν_m and ν_n, it can readily be shown that with $d \neq D/2$ the transmission factors for the direct and the inverse waves are different.

Received
24 June 1954

Bibliographic References

1. M.A.Gintsburg, Dokl. AN SSSR, 95, 753 (1954).
2. M.Born, Optika (Optics). Trans. from German. ONTI, M. 1937.
3. L.Goldstein, Lampert & Heney, Phys. Rev., 82, 956 (1951).
4. C.L.Hogan, Bell System Tech. Journ. 31, 1 (1952).
5. Rayleigh, Phil. Trans., 176, 343 (1885); Scienific papers, 2, 360.
6. M.A.Gintsburg, Dokl. AN SSSR, 95, 489 (1954).
7. M.A.Gintsburg, Thesis, MEI (Moscow Energetics Inst.) 1953.
8. H.Suhl & L.Walker, Phys. Rev., 86, 122 (1952).
9. M.L.Kales, Chait & Sakiotis, J. Applied Phys., 24, 816 (1953).
10. M.L.Kales, J. Applied Phys., 24, 604 (1953).
11. H.Gamo, Journ. Phys. Soc. Japan, 8, 176 (1953).
12. A.Van Trier, Appl. Scient. Research, Sec. B, 3, 305 (1953).
13. L.A.Vainshtein, Zhur. tekh. fiz., 23, 646, 654 (1953).
14. K.M.Polivanov, Dokl. AN SSSR, 95, 501 (1954).
15. K.M.Polivanov, Kolli & Khasina, Izv. AN SSSR,Ser. fiz., 18, 350 (1954) (English translation of Ref. 15 appears in the preceding issue of the BULLETIN on page 46.)

* * * * *

MEASUREMENT OF THE PERMEABILITY AND THE DIELECTRIC CONSTANT OF CERTAIN FERRODIELECTRICS AT CENTIMETER WAVELENGTHS

- S. G. Salikhov

1. Set-up for measuring μ'' in a resonant cavity by the transmission method and results of measurement

In our investigation of ferrodielectrics we use the sensitive set-up shown in block-diagram form in Fig. 1. The signal generator is crystal controlled, making it possible to maintain the output power constant. The signal goes through an attenuator before passing through the resonant cavity into which the investigated specimen is placed.

The real part of the magnetic permeability, μ', is determined by the resonant frequency displacement, the imaginary part μ'', by the Q-factor of the resonant cavity.

In the case of a ferromagnetic material the electric loss, due to the terminal resistivity of the substance, cannot be separated from the magnetic loss. It is convenient to place the specimen on the moving-end part of the resonant cavity.

A TE_{11} mode was excited in the cylindrical resonator. The generator was matched to the resonator by means of a circular slot, 6 mm in diameter. In addition, the resonator was also coupled through orifices to two rectangular waveguides. Tuning was accomplished by varying the resonator length through displacement of the upper and lower pistons (sic). The Q-factor was determined from the resonance curve. The measuring procedure was the following.

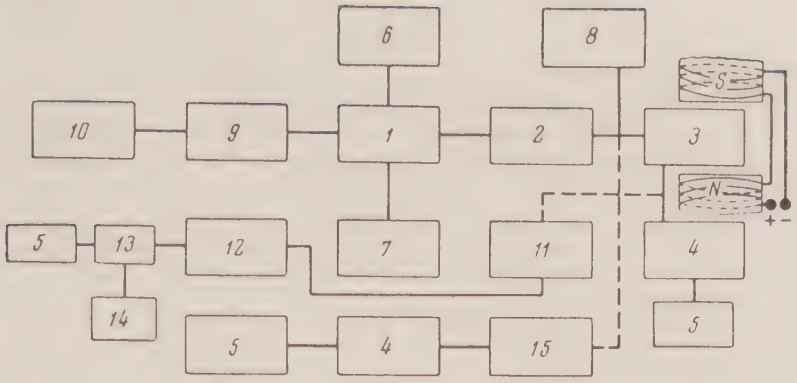

Fig. 1. Block diagram of set-up: 1) Klystron generator, 2) variable attenuator, 3) resonant cavity, 4) crystal detector, 5) meters, 6) power control, 7) resonance-frequency meter, 8) heterodyne frequency meter, 9) electronic regulator, 10) ferro-resonance regulator, 11) input attenuator, 12) thermistor chamber with thermistor unit, 13) bridge, 14) power source, 15) measuring line.

The resonator was tuned to the resonance frequency ω_0 of the circuit with the specimen in place, as indicated by maximum deflection of the meter pointer. The frequency was increased or decreased by an amount $\pm\Delta\omega_0$ to the point where the meter showed half the maximum deflection. The Q-factor was computed from

$$Q=\frac{\omega_0}{2|\Delta\omega_0|}. \qquad (1)$$

The transmission of parasitic modes through the resonator was negligible.

The resonator and waveguide assembly were located between the polepieces of the electromagnet.

If we regard the plane of the ferromagnetic wall as the XOZ plane, the alternating field was directed along the X axis and the static field along the Z axis. The polepieces of the magnet measured 100 x 100 mm; the gap was 45 mm. A current of up to 10 amperes at 120 volts could be sent through the magnet coils to produce a field of up to 10,000 oersteds.

Since the ferromagnetic resonance curves obtained are fairly wide, the often encountered difficulties connected with insuring a highly uniform field and maintaining its intensity constant did not arise in this case.

The specimens were prepared in the form of circular discs 2-3 mm in diameter and 0.1 mm thick and were mounted on the bottom of the resonator. The demagnetizing field was negligibly weak.

Curves for the ferromagnetic resonance absorption as a function of the field intensity were obtained by measurements at different values of the static field. In plotting the experimental points, the values of $C\mu''$ in relative (arbitrary) units (C is a proportionality factor) were laid off along the y-axis against field intensities H in oersteds along the x-axis. It is assumed that the major part in resonance absorption is played by μ'' and that the role of μ' is negligible.

The results of measurement for the different materials tested are shown in the form of $\mu''(H)$ curves in Figs. 2-6 and in tabular form in Table 1.

The spectroscopic splitting factor g was computed according to the Landau-Lifshits-Kittel equation given in Ref. 1:

$$\omega = \gamma (B \cdot H^*)^{1/2}, \qquad (2)$$

where $\gamma = ge/2m$, ω is the angular frequency, B is the saturation induction and H* is the intensity of the resonance field.

For the two Ni-Zn-ferrite specimens investigated (see curves 1 and 2 of Fig. 4), in addition to the usual peak in the region of strong fields we observed an anti-resonance dip at low values of the field. For a plane (disc) specimen the position of the anti-resonance minimum is given by

$$\omega_{min} = \gamma B, \qquad (3)$$

which we may compare with the expression (2) for the case of maximum permeability μ":

$$\omega_{max} = \gamma (B_z H^*)^{1/2}. \qquad (4)$$

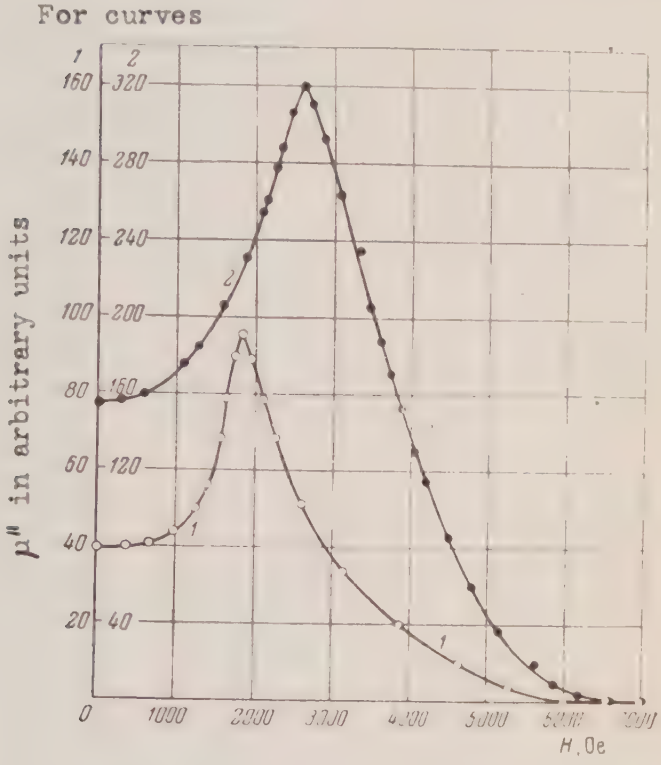

Fig. 2. Variation of μ" with the intensity of the static field for 1) FeS and 2) 95% Fe_3O_4 + 5% FeS_2. [Translator's note: The values of δ and g, given in the original under the curves, are omitted here, inasmuch as they appear in Table 1.]

Physically, the maximum μ" point corresponds to the case when var. $4\pi M_x$ equals H_x in magnitude but is opposite in direction, so that the high-frequency induction $B_x = 0$ (Ref. 2).

The difference between the resonance curves for different directions of the field relative to the axes of a single crystal of Fe_3O_4 (Fig. 6) illustrates the part played by crystallographic magnetic anisotropy.

The experimental results are summarized in Table 1.

The width of the resonance peaks for the ferrodielectrics tested depends on the structure and varies from 500 to 3000 oersteds.

The next to the last column of the table lists the g-factors, which vary between 2.38 and 2.10. The lower g-factor values given in Ref. 3 agree with our experimental values for many of the tested ferromagnetic materials. Appreciable zero-field absorption (i.e. absorption at H = 0) was observed for most ferrodielectrics. Zero-field absorption depends on the splitting of the levels under the influence of the intra-crystalline magnetic and electric fields.

2. Measurement of the permeability of ferromagnetic materials with low conductivity at centimeter wave frequencies

For these measurements a measuring waveguide section was connected into the set-up shown in Fig. 1 after the variable attenuator (see dash lines in Fig. 1). The introduction of this measuring section made it possible to measure the standing wave ratio over a frequency range of

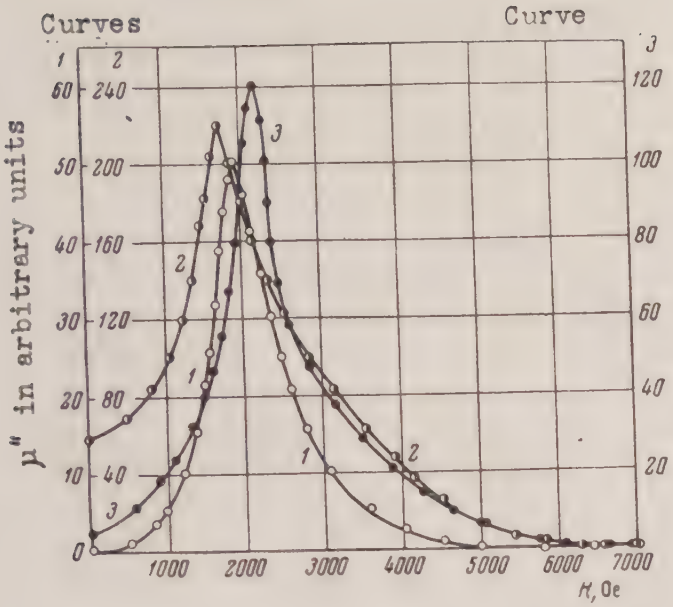

Fig. 3. Curves as in Fig. 2 but for 1) hematite Fe_2O_3, 2) ferrous ferrite $FeO \cdot Fe_2O_3$ and 3) $TiO_2 \cdot 2Fe_2O_3$.

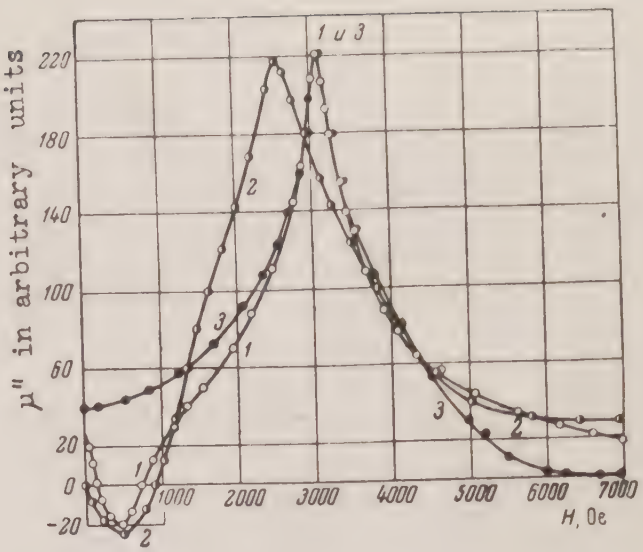

Fig. 4. Curves as in Fig. 2 but for the following ferrites:
1) 17% NiO + 33% ZnO + 50% Fe_2O_3,
2) 18% NiO + 33% ZnO + 49% Fe_2O_3,
3) 20% NiO + 30% ZnO + 50% Fe_2O_3.

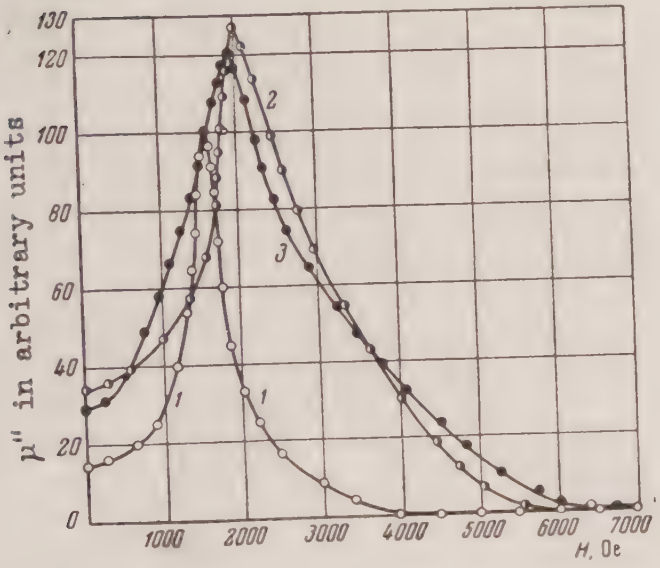

Fig. 5. Curves as in Fig. 2 but for the following ferrites: 1) 18% NiO + + 42% ZnO + 40% Fe_2O_3, 2) 25% MgO + + 25% ZnO + 50% Fe_2O_3, 3) No. 1 BCh (h.f.) ferrite (taken from induction coil core). [BCh = VCh].

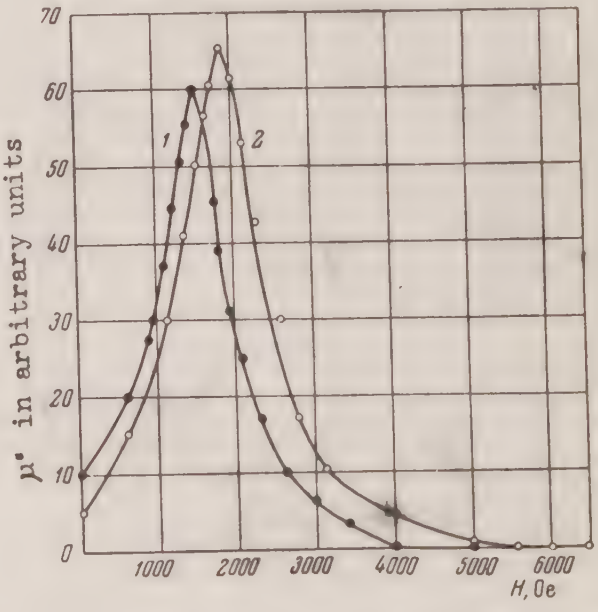

Fig. 6. Curves as in Fig. 2 but for single crystal of magnetite Fe_3O_4, cut in the form of a thin disc (3 mm dia., 0.1 mm thick), with different orientations of the disc relative to the external field: 1) (100) plane aligned wit with field; 2) (110) plane aligned with field.

Table 1

Characteristics of certain ferromagnetic materials obtained in measuring μ" as a function of the magnetic field

№	Material	Resonance field, H* oersteds	Saturation induction, B, gs	Width of resonance curves δ, oe.	Spectroscopic splitting factor g	Figure and curve
1	FeS	1850	4000	1500	2,33	2, *1*
2	Fe_2O_3	1950	4500	950	2,18	3, *1*
3	$FeO.Fe_2O_3$	1800	4500	1500	2,27	3, *2*
4	$FeO.Fe_2O_3$	2200	4100	850	2,17	—
5	25 % MgO + 25 % ZnO + 50 % Fe_2O_3	2000	4500	1400	2,17	5, *2*
6	20 % NiO + 30 % ZnO + 50 % Fe_2O_3	3100	3000	1400	2,13	4, *3*
7	17 % NiO + 33 % ZnO + 50 % Fe_2O_3	3100	3100	1200	2,10	4, *1*
8	18 % NiO + 33 % ZnO + 49 % Fe_2O_3	2600	3750	2500	2,10	4, *2*
9	15 % NiO + 35 % ZnO + 50 % Fe_2O_3	2400	3750	2000	2,16	—
10	18 % NiO + 42 % ZnO + 40 % Fe_2O_3	1650	4500	500	2,38	5, *1*
11	Single crystal $FeO.Fe_2O_3$ [100]	1550	4650	1000*	2,34	6, *1*
12	Single crystal $FeO.Fe_2O_3$ [110]	1850	4500	1250*	2,24	6, *2*
13	95 % Fe_3O_4 + 5 % FeS_2	2600	3450	3000	2,15	2, *2*
14	ВЧ = 1 (r.f.)	1950	2600	2000	2,17	5, *3*
15	$TiO_2.2Fe_2O_3$	2200	3900	850	2,17	3, *3*

*Values for 2δ, rather than δ.

$(8.1\text{-}12.8)\cdot 10^9$ cps. The error of measurement is not over 5%. Knowing the standing wave ratio we can readily determine the travelling wave ratio, since they are reciprocal. For our determinations of the high-frequency permeability and dielectric constant of low-conductivity ferromagnetics at a wavelength of 3.28 cm we employed the method of Birks and Lazukin (Ref. 3), based on measuring the waveguide impedance. While we used the method for ferrodielectrics it can be used with equal success for the investigation of ferromagnetic metals in the form of fine powders dispersed through a non-conducting medium.

The permeability and the dielectric constant may be determined from two parameters: the wave impedance Z of the medium (i.e. specimen) relative to the wave impedance in free space and the propagation constant (Ref. 4):

$$Z=\left(\frac{\mu}{\varepsilon}\right)^{1/2} \quad (5) \text{ and } \quad \gamma=i\frac{2\pi}{\lambda}(\mu\cdot\varepsilon)^{1/2}, \quad (6)$$

where λ, the wavelength in free space, determines the phase velocity (the imaginary component of γ). The real component of γ characterizes the attenuation constant. For lossy dielectrics, ε is a complex quantity:

$$\varepsilon=\varepsilon'-i\varepsilon''=|\varepsilon|e^{-i\delta_\varepsilon}, \quad (7)$$

where $\tan\delta_\varepsilon = \varepsilon''/\varepsilon'$ is the dielectric loss tangent.

Analogously, the magnetic loss for ferromagnetic materials at high-frequencies is characterized by

$$\tan\delta_\mu = \mu''/\mu', \quad (8)$$

termed the magnetic loss tangent.

If the measuring line is shorted at the output end by a metal plate and the probe is then displaced from its extreme position at the output end in towards the generator, the location of the first node can readily be determined. This is the location of the reference end of the line. In measuring the full impedance the distance to the first node (i.e. the next or first measurement node) should be reckoned from this reference end.

The circuit shown in Fig. 7 was assembled for making the measurements; it consists of an oscillator, an attenuator and a measuring line, connected at one end to the specimen chamber and at the other to a uniform line with a displaceable short circuiting piston.

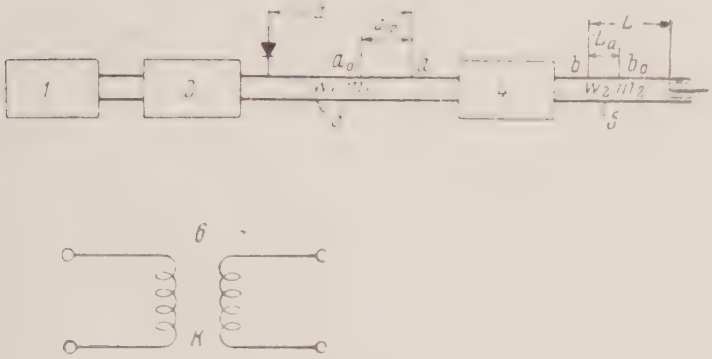

Fig. 7. Diagram illustrating method of determining the permeability and dielectric constant from measurements of Z_{sc} and Z_{op} in a waveguide: 1) oscillator, 2) attenuator, 3) measuring line, 4) specimen, 5) section with piston, 6) equivalent circuit.

If the specimen does not introduce distortion, displacement of the piston produces a corresponding equal displacement of the voltage nodes in the measuring line. On the other hand, if the specimen does introduce an inhomogeneity into the measuring line, the shift in the position of the nodes will not be equal to the piston displacement. The measurement method is based on this effect; the experimental procedure is the following.

Two arbitrary reference points a and a_o (Fig. 7) are selected on the measuring line and the two corresponding points b and b_o on the piston line are noted. The piston is then displaced various distances L from point b and the corresponding displacements of the node point x in the measuring line relative to point a are determined and recorded.

The ratio of the input impedance of the filled waveguide to the wave impedance of the empty waveguide was measured when the line was short circuited and when the line was connected to a shorted quarter-wave section, which is equivalent to an open circuit. The relative input impedances of a short circuit and open circuit are given by

$$Z_{sc} = \frac{k_2 \operatorname{tg} \frac{2\pi}{\lambda_0}(\Delta l_2 + d) - i}{\operatorname{tg} \frac{2\pi}{\lambda_0}(\Delta l_2 + d) - ik_2} \qquad (9)$$

and

$$Z_{op} = \frac{k_1 - i \operatorname{tg} \frac{2\pi}{\lambda_0}(\Delta l_1 + d)}{1 - ik \operatorname{tg} \frac{2\pi}{\lambda_0}(\Delta l_1 + d)}. \qquad (10)$$

In the above equations k_1 and k_2 are the travelling wave ratios when the specimen is placed at the node and at the antinode, respectively; Δl_1 and Δl_2 are the corresponding displacements of the node, λ_0 is the wavelength in the empty line, and d is the thickness of the absorbing impedance [obstacle]. Next the total impedance Z_0 of the line is determined in terms of the open and short circuit impedances (see Ref. 1, p. 231):

$$Z_0 = (Z_{sc} \cdot Z_{op})^{1/2}. \qquad (11)$$

From a solution of Maxwell's equations, we can express ε and μ of the substance, comprising the load impedance, in terms of Z_{sc} and Z_{op} and, consequently, through Δl and k:

$$|\mu| = \left| \frac{\lambda}{2\pi d} (Z_{sc} \cdot Z_{op})^{1/2} \right| \quad (12) \text{ and } \quad |\varepsilon| = \left| \frac{\lambda}{2\pi d} \cdot \frac{1}{(Z_{sc} \cdot Z_{op})^{1/2}} \right|. \quad (13)$$

Values of the dielectric constant and the permeability at room temperature for the different substances as functions of the specimen thickness, computed on the basis of the experimental data according to equations (12) and (13) are listed in Table 2.

Table 2

Moduli of the dielectric constant and the permeability of certain magnetic materials with different thicknesses of the specimen

№	Material	Thickness of specimen d_1, mm	$\|\mu\| = \|\mu' - i\mu''\|$	$\|\varepsilon\| = \|\varepsilon' - i\varepsilon''\|$	Thickness of specimen d_2, mm	$\|\mu\| = \|\mu' - i\mu''\|$	$\|\varepsilon\| = \|\varepsilon' - i\varepsilon''\|$
1	FeS	3,00	1,80	5,50	1,50	2,50	4,00
2	$FeO.Fe_2O_3$	2,10	3,15	2,00	1,00	5,50	5,00
3	$FeO.Fe_2O_3$	2,20	1,80	3,20	0,90	4,90	6,00
4	$TiO_2.2Fe_2O_3$	1,50	4,60	3,00	1,20	4,90	3,50
5	25 % MgO + 25 % ZnO + 50 % Fe_2O_3	1,70	3,10	3,10	0,80	6,60	6,60
6	20 % NiO + 30 % ZnO + 50 % Fe_2O_3	1,65	4,00	3,00	0,70	4,40	12,40
7	17 % NiO + 33 % ZnO + 50 % Fe_2O_3	1,20	5,60	4,60	0,80	4,25	10,00
8	18 % NiO + 33 % ZnO + 49 % Fe_2O_3	1,30	3,90	7,00	0,70	4,90	11,40
9	15 % NiO + 35 % ZnO + 50 % Fe_2O_3	1,20	3,80	7,20	0,60	3,80	20,00
10	18 % NiO + 42 % ZnO + 40 % Fe_2O_3	2,00	3,47	8,00	0,80	4,00	11,00
11	95 % Fe_3O_4 + 5 % FeS_2	1,50	3,00	4,50	1,00	3,00	5,00
12	ВЧ-1(h.f.)	4,50	1,50	1,80	1,00	2,50	7,00
13	Fe_2O_3	1,70	7,00	5,00	1,40	3,50	3,00

Table 3

Real and imaginary components of the permeability and dielectric constants and the values of the magnetic and dielectric loss tangents of certain magnetic materials

№	Material	Thickness d, mm	μ''	μ'	$tg\delta_\mu = \frac{\mu''}{\mu'}$	ε''	ε'	$tg\delta_\varepsilon = \frac{\varepsilon''}{\varepsilon'}$
1	FeS	3,00	1,66	0,71	67°	1,66	0,30	17
2	Fe_2O_3	1,70	6,70	2,25	71°	0,89	0,75	9
3	$FeO.Fe_2O_3$ I	2,10	2,47	0,95	69°	4,75	3,36	54
4	$FeO.Fe_2O_3$ II	2,20	3,00	0,98	72°	1,86	0,23	83°
5	$TiO_2.2Fe_2O_3$	1,50	0,20	1,40	8°	0,20	1,10	10°
6	95 % Fe_3O_4+5 % FeS_2	4,50	1,00	1,82	10°	3,80	4,75	38°
7	ВЧ-1 (h.f.)	1,70	1,00	1,00	45°	3,18	3,08	59°
8	25 % MgO + 25 % Zn + 50 % Fe_2O_3	2,00	2,44	1,60	57°	3,30	2,20	61°
9	18 % NiO + 42 % ZnO + 40 % Fe_2O_3	1,65	0,90	2,50	20°	2,10	1,00	78°
10	20 % NiO + 30 % ZnO + 50 % Fe_2O_3	1,20	1,93	2,10	41°	3,00	5,00	3°
11	17 % NiO + 33 % ZnO + 50 % Fe_2O_3	1,30	4,66	0,97	76°	6,30	8,50	51°
12	18 % NiO + 33 % ZnO + 49 % Fe_2O_3	1,20	1,44	3,10	25°	1,66	0,40	17°
13	15 % NiO + 35 % ZnO + 50 % Fe_2O_3	1,20	2,44	1,69	55°	2,03	0,34	80

The variation of the values of the dielectric constant and permeability with the thickness of the specimen is explained by the fact that the equations used for computing $|\varepsilon|$ and $|\mu|$ are inaccurate and give undue weight to the specimen thickness. The dielectric constant of nonmagnetic materials can be determined by the same method from measurements of Z_{sc}, Z_o and γ_o.

Data on the dielectric constant, magnetic permeability and magnetic and dielectric loss tangents of the same materials obtained by the open and short circuit method are given in Table 3; it will be noted that in general there is close agreement with the data of other investigators.

Many of the materials were never previously investigated.

Conclusions

1. We developed a method for investigating ferromagnetic resonance absorption in a resonator.

2. Values of the spectroscopic splitting factor g computed on the basis of our experimental data are in good agreement with the values given in scientific literature for certain ferrodielectrics.

3. In the case of two Ni-Zn ferrites, in addition to a resonance peak at high frequencies we observed an antiresonance minimum (in the μ'' curves) in the region of low frequencies.

4. Pronounced crystallographic anisotropy was observed for a crystal of $FeO \cdot Fe_2O_3$.

5. In the measurement in which the waves pass through the investigated substance, the imaginary component of the magnetic permeability μ'' can be separated from the real permeability μ' through control of the frequency shift.

6. We give a method for measuring the permeability μ and the dielectric constant ε.

7. The results of measurement of μ', μ'', ε', ε'' $\tan \delta_\mu$ and $\tan \delta_\varepsilon$ for thin specimens of certain ferrodielectrics show good agreement with the data in literature.

The writer wishes to express his thanks to S. V. Vonsovski for his helpful discussion of the experimental results.

Physico-Technical Institute of the
Kazan' Branch of the Academy of Sciences

Received
14 July 1954

Bibliographic References

1. Ferromagnitnyi rezonans (Ferromagnetic resonance). Collection of translated articles, edited by S.V.Vonsovski, IIL, M. 1952.
2. C.Kittel, Phys. Rev., 76, 743 (1949).
3. V.N.Lazukin, Izv. (Bulletin) AN SSSR, 16, 510 (1952).
4. J.B.Birks, Nature, 158, 671 (1946).

Note added in reprinting: The attention of the reader is called to the two insert pages following - pp. 154a & 154b. Col. Tech.Translations.

ELECTROMAGNETIC PROPERTIES OF OXIDE FERROMAGNETIC MATERIALS

- N. N. Shol'tz

Theoretical investigations of oxide ferromagnetics disclosing the exceptional electromagnetic properties of these new magnetic materials could not but attract the interest of the electrical and communications equipment industry which makes extensive use of various high-quality magnetic materials. In recent years we have witnessed the development, manufacture and successful application of a number of magnetic materials, consisting of solid solutions of ferrites, having different desirable electromagnetic characteristics and adapted to different purposes.

Some results of an investigation of a group of solid solutions of nickel-zinc ferrites of different composition in static magnetic fields are shown in Fig. 1. The investigation of the variation of the permeability, magnetization, specific resistance and Curie temperature with the molar composition was carried out on specimens prepared in a manner to insure optimum formation of the solid solution. As may be seen from the curves, the initial permeability is strongly dependent upon the proportion of the components: an increase of only a few per cent in the relative nickel ferrite content in the region of low nickel ferrite concentrations leads to a reduction of the permeability to half the initial maximum value. Both the magnetization in weak fields and the intensity of magnetization in the vicinity of saturation vary with the composition; the flux density in a 100 oersted field shows a maximum of about 4800 gauss for a composition close to the stoichiometric. The Curie point temperature, which at high nickel ferrite concentrations approaches 500°C (for pure nickel ferrite $T_C \approx 560°C$), drops sharply in the region of maximum initial permeability mixtures (low nickel concentrations). The specific resistance, which is indicated approximately by the dash line in Fig. 1, is lowest for materials having the highest initial permeability.

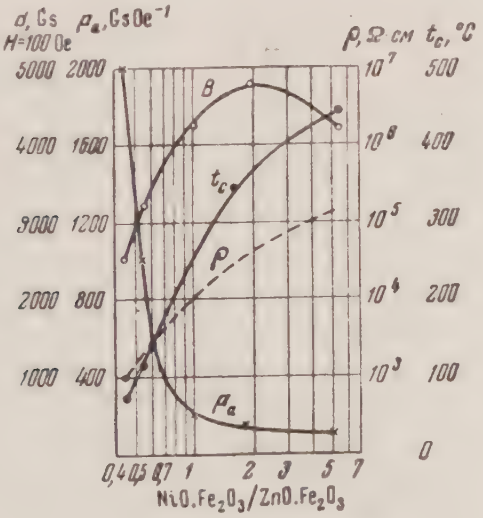

Fig. 1. Variation of the main electromagnetic properties of Ni-Zn ferrites in static fields with the molar composition.

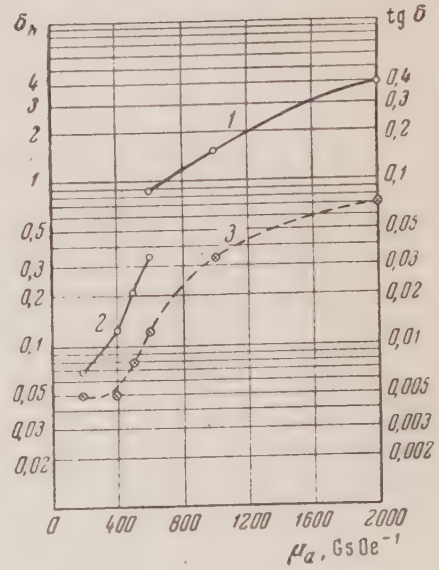

Fig. 2. Permeability dependence of the hysteresis coefficient at f = 100 kc and H_a = 1 oersted for specimens of varying composition sintered at 1350°C (Curve 1) and for specimens of the same composition sintered at 1250-1150°C (Curve 2); also permeability dependence of the loss tangent at 100 kc and H_a = 0 (Curve 3).

More detailed investigation of a number of nickel-zinc ferrites in alternating fields showed the best relation between the permeability and the hysteresis coefficient δ_h^* is obtained with incomplete formation of the solid solution of the given concentration. Apparently, in such cases there is present a non-magnetic or weakly magnetic phase whose effect is somewhat analogous to that of an air gap in a magnetic circuit: the relationship between the hysteresis coefficient and the permeability for magnetic circuits containing air gaps is quadratic. The more favorable relation between μ_a and δ_h is, naturally, obtainable only for ferrites with an initial permeability below the maximum for the given type of mixture. Curve 1 in Fig. 2 shows the relation between μ_a and δ_h in an alternating field having a frequency of 100 kc for specimens of different composition (see Fig. 1), sintered at 1350°C. Curve 2 applies to specimens of the same composition, sintered at 1250-1150°C (i.e. with the formation of the solid solution not going to completion). The total loss tangent at f = 100 kc and $H_a \rightleftharpoons 0$ decreases with the permeability at about the same rate regardless of whether the given initial permeability is obtained by varying the composition or the sintering temperature.

As the result of earlier research on solid solutions of nickel-zinc ferrites, four groups (ten types) of oxide ferromagnetics - known as oxyfers - having different electromagnetic characteristics are now in production. These new materials are already being widely used for the cores of high-frequency transformers employed in wire communication, radio and television, the cores of magnetic amplifiers, frequency converters, magnetic variometers, filter coils and chokes, as well as for certain components of meters and other test instruments; the commercial availability of these new ferrites has greatly expanded the application of magnetic materials and has made possible the development of many new and radically different circuits and types of equipment. The basic parameters of these oxyfers in static fields are listed in Table 1 and Fig. 3.

Oxyfers may be divided into four groups on the basis of their physical properties:

Group I comprises the oxyfers with the highest initial permeability: 2000-1000 gauss/oersted. Oxyfer 1000 has a higher Curie point than Oxyfer 2000. Because of the high specific resistance of oxyfers, eddy-current losses are negligible; consequently, the permeability in weak fields is constant over a wide range of frequencies and the loss tangent is small (Fig. 4). In stronger fields the permeability drops sharply with frequency, as may be seen from the curves for Oxyfers 2000 and 1000 shown in Fig. 5. It is interesting to note that the frequency losses increase sharply with rising temperature. Fig. 6 shows the temperature dependence of the loss tangent for several oxyfers; the values of the tangent were obtained by extrapolating the variation of loss tangent with field strength curves to $H_a \rightleftharpoons 0$. It is possible that the increase in frequency losses is connected to some extent with the large negative temperature coefficient of specific conductivity. The hysteresis loss tangent shows little change with temperature within the limits indicated in Fig. 6.

By exercising great care in fabrication (using highest purity raw materials, insuring accurate proportioning, guarding against contamination in the process of manufacture and making sure that the formation of the solid solution goes to completion) it is possible to obtain

---

* The hysteresis (loss) coefficient δ_h was determined from the change in the total loss tangent to 1.0 oersted (assumed to be linear) i.e. from the slope at 1 oersted.

Table 1

Electromagnetic properties of oxyfers in static fields

Oxyfer Group	Grade	μ_a, gauss per oersted	μ_{max}, gauss per oersted	H at μ_{max}, oersteds	H = 100 Oe: B, Gs	B_r, Gs	H_c, Oe	Maximum operating temp.* t_k, °C	Temp. coef. of permeability $\beta \cdot 10^6$ at H = 0	Specific resistance ρ, ohm cm	Temp. coef. of specific resistance	ϵ at f = 100 cps	Density, gr/cm^3
I	2000	1800÷2400	6000÷7000	0,15	2500	1200	0,10	70	+6000	~1·10^3	−20·10^{-3}	~1·10^3	5,0
	1000	800÷1200	3000÷3700	0,4	3200	1500	0,25	110	+4000	2·10^4	−20·10^{-3}	~2·10^4	5,0
II	600	550 : 600	1200÷1400	0,7	3100	1400	0,4	120	+3500				4,9
	500	500 : 550	1000÷1200	0,9	2800	1300	0,5	120	+3000				4,8
	400	360÷440	750÷850	1,0	2800	1200	0,8	120	+2000	5·10^5		~30	4,6
	200	180÷220	280÷330	2,0	1800	1000	1,5	120	+800	—			4,6
III	I-4	180÷220	750÷850	1,5	4200	2000	0,8	250	+3500	—			4,8
	I-5	135 : 165	650÷750	2,5	4800	2250	1,2	360	+3700	5·10^4	16·10^{-3}		5,0
IV	RCh-15	14÷16	35÷45	30	1850	1000	15	400	+500	5·10^6	−13·10^{-3}	~10	3,2
	RCh-10	9÷11	14 : 17	40	1400	400	25	400	+200	—	—		2,9

---

* t_k is not the Curie point but the temperature at which μ_a falls 20% below its room temperature value.

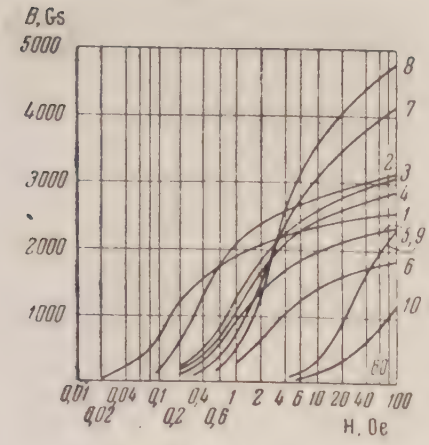

Fig. 3. Magnetization curves for different grades of oxyfers: 1) Oxyfer 2000, 2) Oxyfer 1000, 3) Oxyfer 600, 4) Oxyfer 500, 5) Oxyfer 400, 6)Oxyfer200, 7) I-4, 8) I-5, 9) RCh-15, 10) RCh-10.

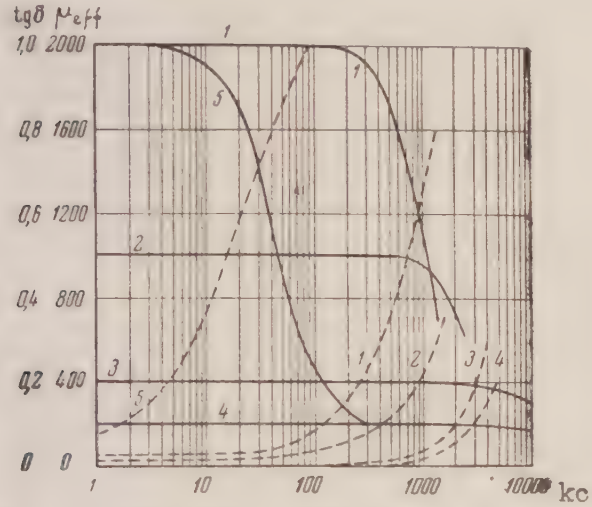

Fig. 4. Frequency dependence of the effective permeability (solid lines) and the loss tangent (dash lines) at $H_a = 0$ for 1)Oxyfer 2000, 2) Oxyfer 1000, 3) Oxyfer 400, 4) Oxyfer 200, 5) 50 NKhS ferro-nickel alloy, 0.1 mm thick.

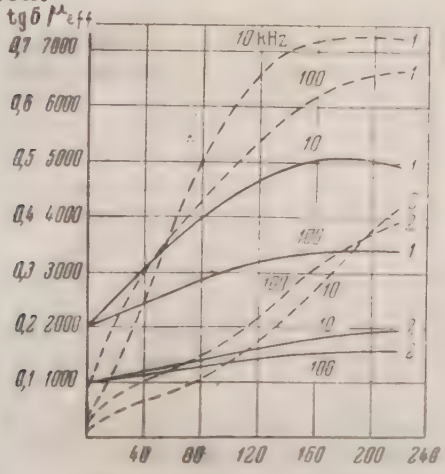

Fig. 5. Variation of effective permeability (solid lines) and loss tangent (dash lines) with field intensity H_a for 1) Oxyfer 2000 & 2) Oxyfer 1000.

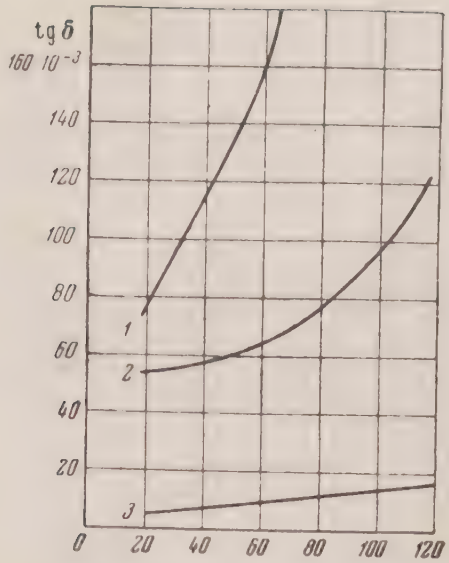

Fig. 6. Variation of loss tangent with temperature at 100 kc and $H_a = 0$ for 1)Oxyfer 2000, 2) Oxyfer 1000, 3) Oxyfer 400 and Oxyfer 200.

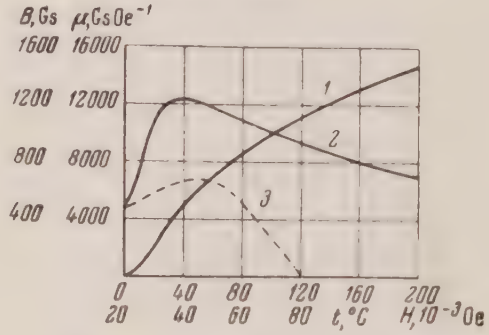

Fig. 7. Section of magnetization curve (1) and dependence of the permeability on field intensity (2) and on the temperature (3) for oxyfer sample with μ_a = 5000 gauss/oersted.

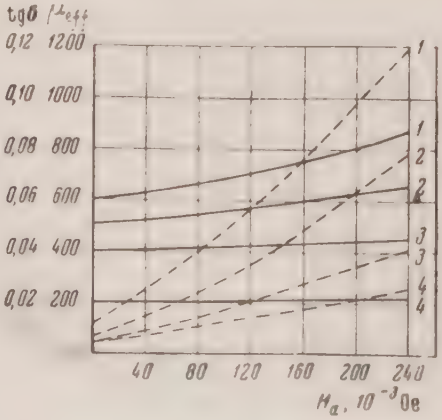

Fig. 8. Variation of effective permeability (solid lines) and loss tangent (dash lines) with field intensity at 100 kc for 1) Oxyfer 600, 2) Oxyfer 500, 3)Oxyfer 400, 4) Oxyfer 200 and I-4.

nickel-zinc ferrites having appreciably higher values of permeability and induction than those given in Table 1.

A section of the magnetization curve and the variation of the permeability with the field intensity and with the temperature for a specimen characterized by an initial permeability of 5000 gauss/oersted are reproduced in Fig. 7.

Oxyfers in Group II differ from those of Group I in having much lower losses in general and particularly a markedly lower hysteresis loss; investigations indicate that this is due to the use of lower temperatures in sintering the oxyfers in this group. The dependence of the permeability and loss tangent on the frequency and intensity of the magnetic field for Oxyfers 600, 500, 400 and 200 are shown in Figs. 4 and 8.

Where an even greater reduction of the hysteresis loss - and of losses in general - is required, recourse is had to open magnetic circuit core designs (shielded cores, Ш-shaped cores with an air gap, H-cores, cylindrical cores, etc.). The best material for such cores is Oxyfer 400; the hysteresis coefficient, the eddy currents and the effects of these in such cores will not be higher and in most cases will be appreciably lower than in cores of magnetodielectrics having the same initial permeability.

Group III comprises oxyfers with a high value of the saturation inductance and a high Curie point; as regards other parameters Oxyfers I-4 (И-4) and I-5 (И-5) differ little from Oxyfer 200.

Oxyfers of Group IV - the radiofrequency oxyfers [РЧ = r.f.] - are characterized by the fact that their loss tangent depends little on the frequency. Using these materials in a closed magnetic circuit design, one can obtain inductance coils having a Q-factor of about 200 in the megacycle band and a Q-factor of 50-100 in the 10^7-10^8 cycle range. Cores of these oxyfers show appreciably higher hysteresis losses than open magnetic circuit cores of Oxyfer 400 and, hence, can be used only in equipment where nonlinear distortion is not objectionable. The outstanding characteristic of the oxyfers in this group which distinguishes them from all other types of radiofrequency core materials (magnetodielectrics and Oxyfer 400 in open magnetic circuit cores) is the sharp change in their permeability with the application of a static magnetic field.

The rapid variation of the reversible permeability with external field intensity exhibited by oxyfers in a wide range of frequencies is a consequence of their exceptionally high specific resistance and the non-linearity of their magnetization curve; this characteristic is made advantageous use of in the design of magnetic amplifiers, variometers, frequency converters and similar equipment. The variation of the reversible permeability and the reciprocal of the loss tangent with the intensity of the magnetizing field for a number of commercial oxyfers and for thin-rolled permalloy strip at 100 kc is shown in Figs. 9 and 10. It is interesting to note that even for the 5μ thick lamina of special iron-nickel alloy, which in static fields shows a hysteresis loop approaching the rectangular, the reversible permeability at 100 kc drops off less sharply than for the oxyfers. This is explained by the breaking off of the permalloy magnetization curve, due partly to the cold hardening of the rolled metal (not fully relieved even by the most careful heat treatment) and partly by the effect of eddy currents. At much higher frequencies the drop in reversible permeability with increased field intensity is reduced for the oxide ferromagnetics in question as well, which may be taken as evidence of a break in their magnetization

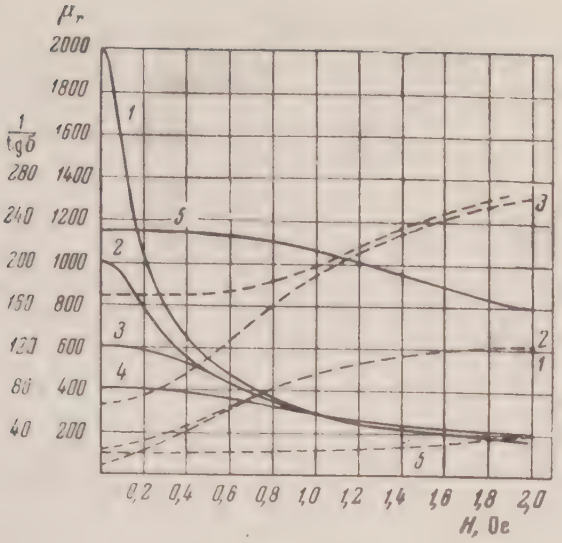

Fig. 9. Variation of the reversible permeability and of the reciprocal of the loss tangent (dash lines) with the field intensity at 100 kc and $H_a = 5 \cdot 10^{-3}$ oersteds for 1) Oxyfer 2000, 2) Oxyfer 1000, 3) Oxyfer 600, 4) Oxyfer 400, 5) 50 NP nickel-iron alloy, 5 μ lamination.

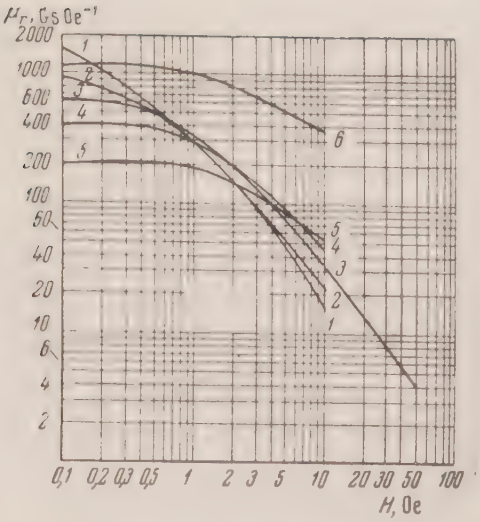

Fig. 10. Reversible permeability in strong fields (f = 100 kc): 1)Oxyfer 2000, 2) Oxyfer 1000, 3) Oxyfer 600, 4) Oxyfer 400, 5) Oxyfer I-5, 6) 50 NP nickel-iron alloy, 5 μ thick.

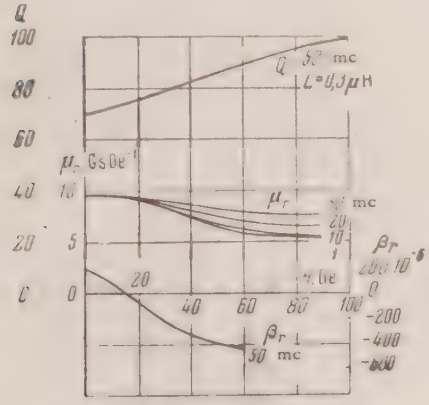

Fig. 11. Variation of the reversible permeability, the Q-factor and the temperature coefficient of the reversible permeability with field intensity for Oxyfer RCh-15.

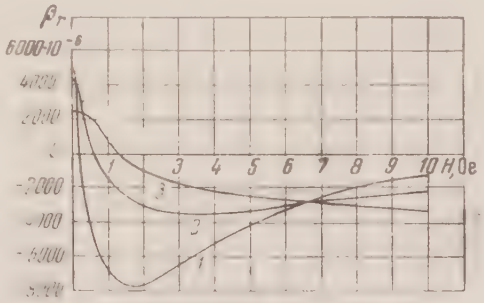

Fig. 12. Variation of the temperature coefficient of the reversible permeability at 100 kc for 1)Oxyfer 2000, 2) Oxyfer 1000, 3)Oxyfer 400.

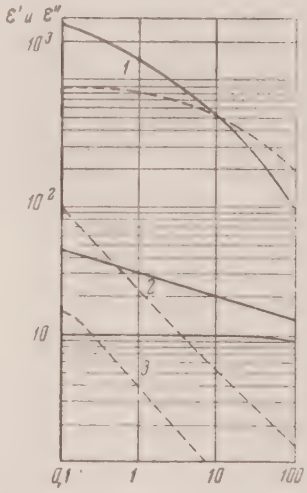

Fig. 13. Frequency dependence of the real (solid lines) and imaginary (dash lines) parts of the dielectric const. of 1)Oxyfer 1000, 2)Oxyfer 400, and 3) Oxyfer RCh.

[RCh stands for radio-frequency]

curves. As may be expected, the sharpest drop in reversible permeability is observed in the case of oxyfers with the steepest magnetization curve. For an oxide ferromagnetic specimen having an initial permeability of 5000 gauss/oersted when magnetized in a 10 oersted field at a frequency of 100 kc the reversible permeability changes by a factor of 1:250, i.e. double that for Oxyfer 2000 under similar conditions. In the 10^6-10^8 cps frequency range none of these magnetic materials is noticeably affected by a static magnetizing field. By virtue of a large internal demagnetization factor, magneto-dielectrics, which are used

primarily in this frequency range, have a rather flat magnetization curve and their reversible permeability remains virtually constant with increasing field intensities of up to hundreds of oersteds. The magnetization curve for the radiofrequency oxyfers is non-linear and the variation of the reversible permeability with field intensity is appreciable (Fig. 11).

The temperature coefficient of permeability of magnetically soft (susceptible) materials, which in weak alternating fields is positive, generally reflects the temperature dependence of magnetization processes in weak and strong fields and at a certain value of the field goes through zero, then becomes negative and after passing through a minimum (maximum absolute value), gradually decreases in absolute magnitude. In the case of the investigated oxyfers (see Figs. 11 and 12), the temperature coefficient of the reversible permeability goes through zero in the region of field intensities corresponding to the sharpest drop in the reversible permeability, which is highly important for certain applications.

Oxide ferromagnetics have a very high dielectric constant. The values of ε at a frequency of 100 kc are listed in Table 1. The dielectric properties of oxyfers depend on the frequency as may be seen from Fig. 13, where the variation of the real and imaginary parts of the dielectric constant with the frequency are plotted for Oxyfers 1000, 400 and RCh(r.f.). Assuming that there is a direct relation between the dielectric loss and the conductivity of semiconductors, the decrease in the imaginary part of the dielectric constant with increasing frequency may be regarded as decrease of specific resistance with frequency. If there really is a rapid drop in specific resistance with increasing frequency, which could be explained, for example, by structural inhomogeneity, then appreciable eddy currents may develop at high frequencies in these ferrites.

In the course of our investigation the need for a thorough and comprehensive theoretical study of this new group of non-metallic ferromagnetic materials became increasingly evident. It is essential to investigate the physics and mechanism of the formation of ferrite solid solutions and the manner in which the conditions of preparation affect the electromagnetic properties and the structure of these oxide products. No less important is the development of an adequate theory to explain the behavior of oxide ferromagnetics in both weak and strong alternating fields within a wide range of frequencies. Such investigations cannot but lead to the development of new materials even better suited for various special applications.

Received
3 May 1953

* * * * *

/The above article has no bibliography. The abbreviations used for Soviet journals in the bibliographic references are those employed by the Library of Congress. We are also using the Library of Congress transliteration system in rendering names, designations, etc./
C.T.T.

MAGNETIC FERRITES IN ALTERNATING FIELDS

- L. I. Rabkin

1. Introduction

In recent years ferrites have attracted the attention of many physicists, technicians and microwave engineers, both due to the possibilities they offer as regards the study of ferromagnetism in general and because of their great potentialities as magnetic materials for use in communications and other high-frequency equipment.

The electric and magnetic properties of ferrites have been investigated and reported on by Snoek, Smolenski, Shol'ts, Piskarev, Toporov, Freidenfel'd, Epshtein, Fomenko and Rabkin (Refs. 1 through 9) and many others.

The present contribution is concerned with certain results of an extensive investigation of ferrites carried out in 1952 in the LONIIS (Leningrad Oblast Communications Research Institute). The properties and characteristics of the ferrite specimens prepared at the Institute were determined using high-frequency bridge set-ups, an oscillographic ferrometer and other special test equipment.

2. Technology of preparation

There are three basic methods of preparing ferrites:

1. By sintering a compressed mixture of powdered oxides.

2. By sintering compressed hydroxides, obtained by precipitation with accurately proportioned amounts of alkali.

3. By sintering compressed mixtures of the appropriate oxides, obtained by thermal decomposition of the carbonates, oxalates, nitrates or sulfates of nickel, manganese, zinc, iron and other metals.

Comparing the three methods, we note that the product obtained by the simultaneous precipitation of hydroxides is the most homogeneous and active by virtue of the exceptionally large surface area of the precipitated material.

Second in order of chemical activity are the mixtures obtained by thermal decomposition of the metal salts.

The powdered oxides are the least active, since the potential energy available for chemical reaction is minimal in this case in view of the well defined crystal structure of the particles.

Toporov, Freidenfel'd, Epshtein and Rabkin have shown, however, that ferrites with virtually identical properties can be obtained by any of the listed methods (Ref. 6). The weaker activity of a batch prepared by mixing powdered oxides can be compensated for by modification of the synthesis conditions, i.e., by sintering for a longer time and/or at a higher temperature.

By way of illustration, we show in Fig. 1 the frequency dependence of the permeability and the loss tangent for ferrite cores of the same composition, but prepared in different ways. The solid lines are for specimens from a batch prepared by mixing powdered oxides, while the dash lines are for a batch prepared by precipitation of the hydroxides. ChDA grade raw materials were employed in both cases.

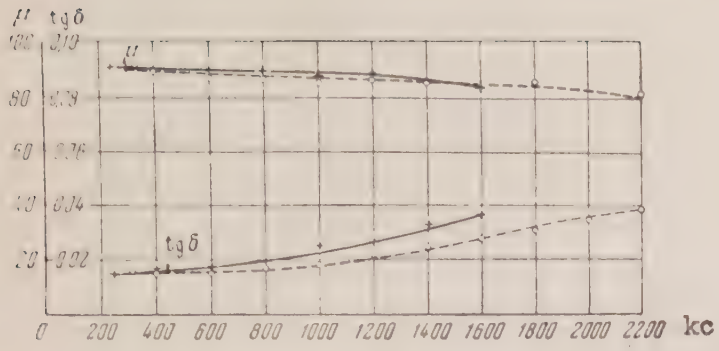

Fig. 1. Variation of permeability (μ) and loss tangent (tg δ) with the frequency for ferrites of the same composition, but prepared in different ways: solid lines - by mixing powdered oxides (specimen No. 280); dash lines - by precipitation of hydroxides (specimen No. 307).

It follows that the method of preparing the batch, provided it does not involve the introduction of additional impurities (the effect of these is usually to reduce the permeability and increase the loss tangent), is in itself not important as far as the ultimate magnetic properties are concerned. Of course, it must be borne in mind that in view of the kinetics of synthesis the mixtures of powdered oxides require longer roasting at a higher temperature.

From the point of view of the technology and economy of production, selection of the method of compounding the batches deserves careful consideration, since it is an important factor in determining the cost of the product. As compared with the other methods, the method of mixing oxides has the advantage that all of the reacting material turns into ferrite, whereas with the other two methods the weight of the final product is only a fraction of the weight of the raw material.

The conditions of synthesis, i.e. the temperature, the duration of heating and the medium in which the latter takes place, are very important where the ultimate magnetic properties of the ferrite are concerned. In general it may be stated that for greater values of the permeability, other conditions being equal, the sintering temperature must be higher and the heating time longer to insure complete ferritization and homogeneity of the solid solution.

In cases when good frequency characteristics into the 10-100 megacycle range are the primary consideration, while high permeability is secondary, satisfactory results can be obtained by incomplete sintering of the specimens under appropriate special conditions.

The frequency curves for a nickel-zinc ferrite specimen prepared from a batch compounded by mixing powdered oxides are shown in Fig. 2. It will be noted that ferrites compounded by this method and prepared by sintering in an atmosphere of oxygen have a satisfactory frequency characteristic into the 10-50 mc range at normal temperatures. These ferrites, which may be termed high-frequency ferrites, do not consist of a homogeneous solid solution; they are extremely porous and are characterized by a very considerable hysteresis loss. However, in most cases the operating conditions for magnetic materials in the 10^7 cps region are such that hysteresis losses are not an important consideration.

Tests of coils with toroidal cores of this material show that even at frequencies of about 40 megacycles it is possible to obtain a Q-factor of over 100 with a core volume of 1-1.5 cm^3.

In view of the fact that manganese exhibits different valences in oxidizing, the preparation of manganese-zinc ferrites calls for special processing conditions: the manganese must be present in the mixture in the form of bivalent ions. The basic method of controlling the valence of manganese in preparing ferrites is through appropriate selection of

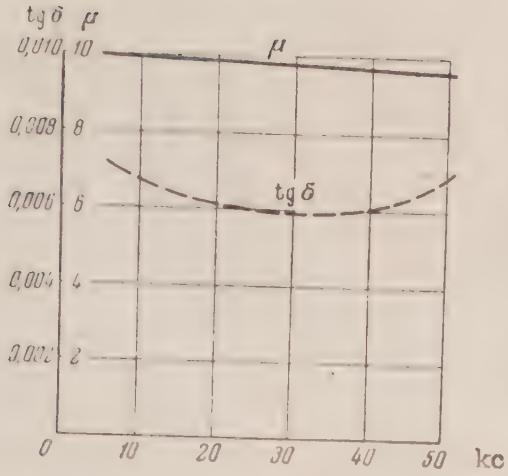

Fig. 2. Frequency dependence of μ and tan δ for NTs-10 [Nickel-Zinc] ferrite (specimen No. 759), prepared by sintering a mixture of powdered oxides in oxygen.

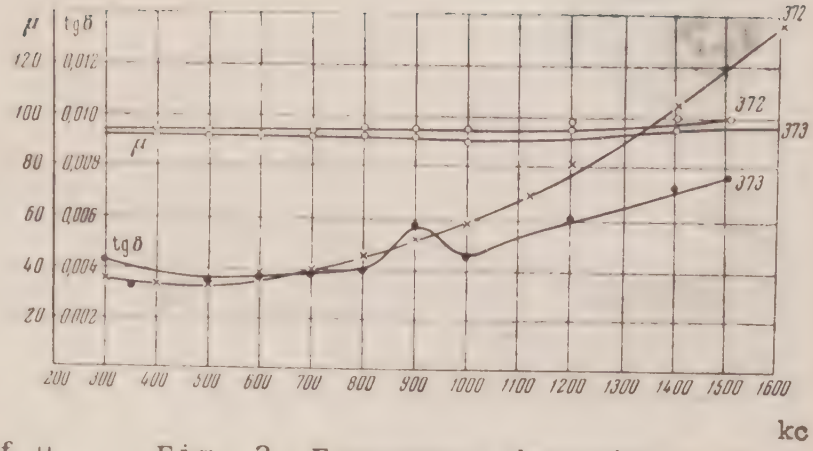

Fig. 3. Frequency dependence of μ and tan δ for two specimens (Nos. 372 and 373; latter described in the text) of MSh-100 manganese ferrite.

the sintering medium (see Ref. 7). The synthesis of magnetically "soft" manganese-zinc ferrites is best carried out in an inert medium. If this condition is observed it is feasible to obtain ferrites with a permeability of the order of 2000 gauss/oersted or higher. More attentions should be given to research and development work on manganese-zinc ferrites in view of their low hysteresis losses and the fact that manganese is comparatively inexpensive and in ample supply.

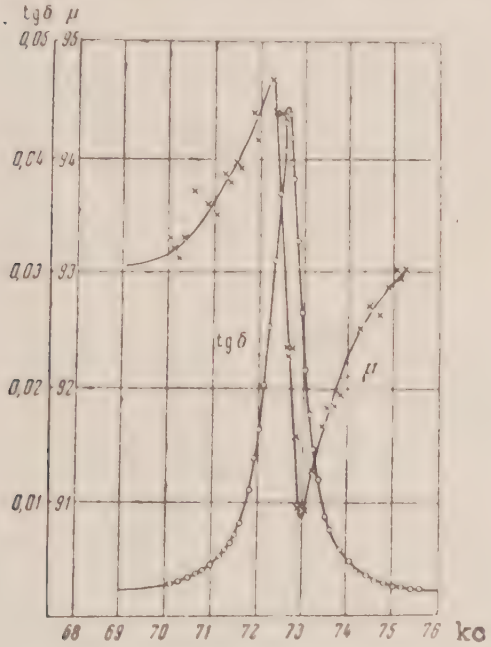

Fig. 4. Frequency dependence of μ and tan δ in the resonance region for an annular specimen (No. 373- described in text) of MSh-100 manganese ferrite.

It must be noted that not only solid solutions of magnetic and non-magnetic ferrites but also some solid solutions of manganese ferrite with iron oxides exhibit interesting characteristics. Thus, for example, ferrite, consisting of 65 mol% Fe_2O_3 and 35 mol% MnO, together with a permeability of the order of 100 gauss/oersted has a very small loss tangent at all frequencies ranging up to several megacycles (Fig. 3).

However, among other shortcomings, this material has a rather pronounced magnetic instability, in view of which it can be used in closed magnetic circuits only where variation of the permeability to the extent of several per cent is not objectionable. In open magnetic circuits the permeability is more constant. The material also exhibits strong resonance characteristics, with the resonance frequency depending on the dimensions of the specimen. Thus for an annular core of rectangular cross section, having an outside diameter of 2.72 cm, an inside diameter of 2.14 cm and a thickness of 0.51 cm, the resonance frequency is 72.5 kc (Fig. 4). As may be seen from the curves, the permeability changes from 95 to 90 gauss/oersted and the loss tangent varies between 0.0025 and 0.045 in the region of resonance.

3. Some characteristics of nickel-zinc ferrites

The basic technical characteristics of magnetic ferrites are usually given in the form of a family of curves showing the variation of the permeability and loss tangent with the frequency at different field intensities (Fig. 5). High-frequency magnetic materials are also characterized by three loss coefficients or factors, obtained from the curves for the variation of the loss tangent with the frequency and with the field strength. These factors are usually called the hysteresis (loss) coefficient, the eddy current loss factor and the secondary loss (eddy current aftereffect) coefficient. For engineering design purposes, in cases of a relatively narrow frequency range and weak fields, it is usually permissible to divide the losses in the same manner for ferrites, since it is more convenient to make design calculations using constant parameters (coefficients), rather than with reference to a family of curves. However, it must be remembered that in the case of ferrites the losses, whose tangent is pr[illegible]tional to the frequency, are due primarily to magnetic viscosity and only fractionally to eddy currents.

There is reason to assume that in metallic ferromagnetics and in magneto-dielectrics the component of the loss tangent proportional to the frequency also characterizes the total loss due to eddy currents and to magnetic viscosity. Hence, the equation for the loss tangent must have the form

$$\delta_c = \frac{R_c}{\omega L} = \delta_h H + \delta_{ef} + \delta_{is} \qquad (1)$$

where

$$\delta_e = \delta_{ec} + \delta_{hf}, \qquad (2)$$

R_c is the resistance connected with losses in the core, δ_c is the magnetic loss angle in the core, δ_h is the hysteresis loss coefficient, δ_e is the coefficient of the losses proportional to the frequency, δ_{ec} is the frequency dependent eddy current loss coefficient, δ_{hf} is the second ary high-frequency loss coefficient and δ_{is} is the initial secondary loss (eddy current aftereffect) coefficient.

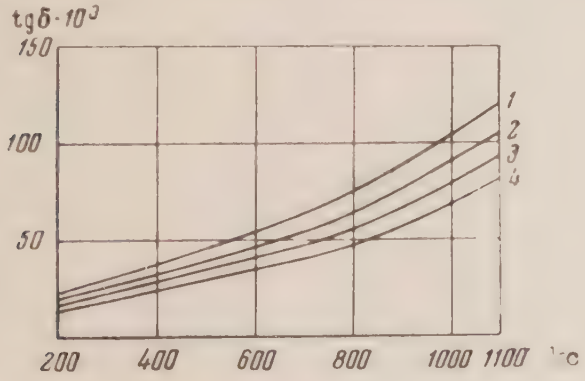

Fig. 5. Family of curves for the frequency dependence of the loss tangent (specimen No. 75) of NTs-250 ferrite (μ_o = 280; W = 50 turns) at different magnetic field intensities: 1) $80 \cdot 10^{-3}$, 2) $60 \cdot 10^{-3}$, 3) $40 \cdot 10^{-3}$, 4) $20 \cdot 10^{-3}$ oersteds.

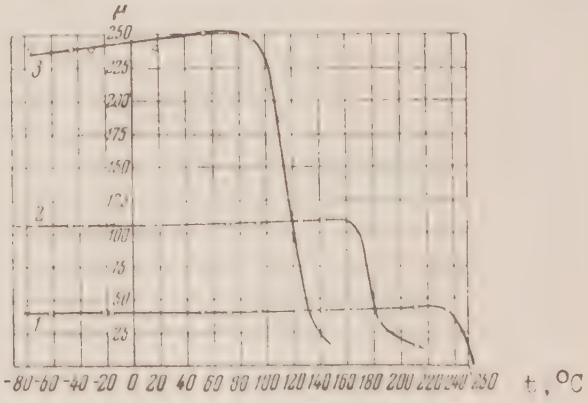

Fig. 6. Temperature dependence of μ for nickel-zinc ferrites: 1) NTs-40 (specimen No. 90); 2) NTs-100 (No. 130); $H_\sim$ = 10 milli-oersteds; f = 800 cps.

At frequencies of several hundred kilocycles the eddy current loss in ferrites is small. This has been proved by a number of experiments in which the losses for different cores of the same material but of different cross section were compared and by tests in which the losses in compact ferrite cores (cores of single ferrite with no additions) were compared with those in cores of ferrite magneto-dielectrics (i.e. cores consisting of a mixture of ferrite powder with a dielectric material).

The increase in the initial magnetic permeability, particularly in the case of high-permeability ferrites, is linear only in relatively weak fields.

This led certain investigators to conclude that Rayleigh's law does not hold for ferrites. Our repeated permeability measurements on many ferrites have shown, however, that there is always at least a small region near the beginning of the curve where the field-dependence of the permeability is linear.

Hence, in obtaining data for dividing the losses into components as mentioned above, the measurements must be made in very weak fields and at relatively low frequencies (i.e. in the region where the variation of the loss tangent with the frequency is linear).

The variation of the permeability of nickel-zinc ferrites with temperature is shown in Fig. 6. It will be seen from the curves that the permeability increases to a maximum value as the Curie point is approached and then, in the vicinity of the Curie point, falls off sharply. The temperature dependence is most pronounced for the initial permeability and the permeability in weak fields. As a rule, the higher the initial permeability of a ferrite, the lower its Curie point.

Determinations of the temperature dependence of NTs-2500 ferrite in different fields (10 to 350 milli-oersteds) have shown that the temperature coefficient goes as high as $+380 \cdot 10^{-5}$ in the 20-40°C interval.

Such high temperature coefficients make it feasible to use high-permeability ferrites in closed magnetic circuit cores only where a high degree of stability is not required (for example, in transformers and chokes). Low-permeability ferrites, such as NTs-250, NTs-100, etc., are superior in this respect: they have a higher Curie point and their initial permeability is less dependent on the temperature. The temperature coefficient of permeability of these ferrites in the -30 to +30°C range is comparable with that of ordinary magneto-dielectrics.

In the production of ferrites, even minor changes in the manufacturing procedure may result in appreciable alterations of the magnetic properties. Hence, the characterization of a particular type or grade of ferrite based on measurements on an individual specimen may be misleading; to obtain a representative picture one must average the data for a series of specimens from different production lots. Frequency dependence curves of the permeability and loss tangent for a number of standard type ferrites, based on such averaged data, are shown in Fig. 7. The dependence of the permeability on the field intensity at audio frequencies is given in Fig. 8.

4. Magnetic reversal loops and non-linear distortion in nickel-zinc ferrites

From the engineering point of view, it is most important to know the properties of ferrites in the region of high frequencies. For practical purposes it is desirable to investigate not only the frequency and field-intensity characteristics of the materials but also the specific magnetization characteristics at various peak field strengths and frequencies.

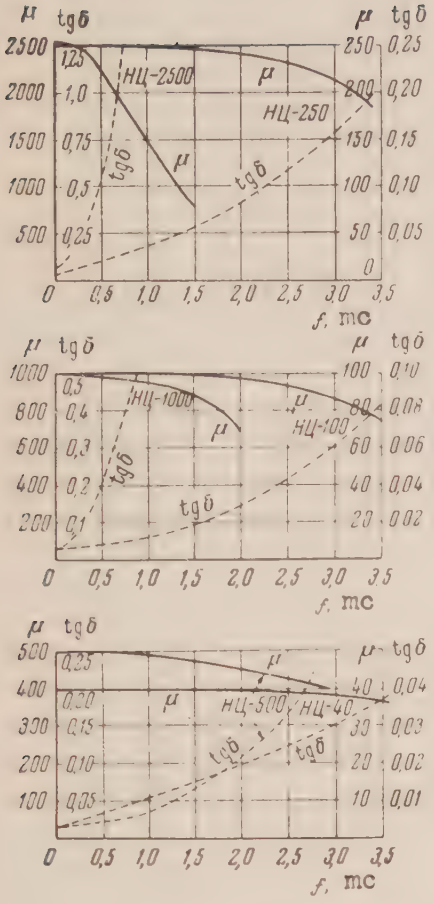

Fig. 7. Frequency dependence of μ and tan δ of typical ferrites in weak fields. Toroidal specimens, 0.5 x 0.3 in cross section. Curves plotted for averaged data obtained for a number of specimens from different lots.

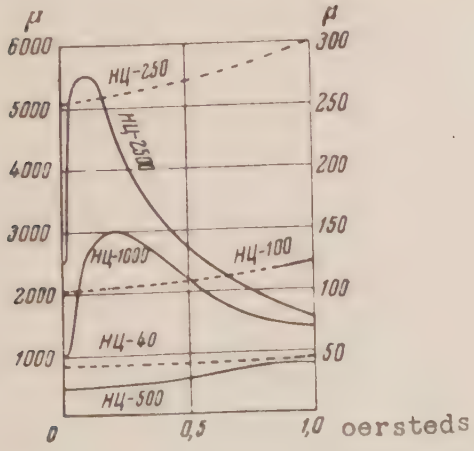

Fig. 8. Dependence of dynamic permeability of typical ferrites on the magnetic field intensity at audio frequencies.

IIII = NTs

Study of the magnetization characteristics is essential not only to ascertain the nature of the non-linear distortion introduced by the core but also to evaluate the possibility of using the various ferrites in the design of harmonic oscillators, magnetic amplifiers, and similar components.

Whereas the static loop is determined solely by the hysteresis loss, the dynamic magnetization loop derives not only from the hysteresis loss but also from the eddy current and the secondary (aftereffect) losses.

The dynamic magnetic reversal loops are determined by means of a ferrometer, an oscillographic instrument which permits observing, measuring and photographing the dynamic hysteresis loops (Fig. 9). All elements of the loop (the dynamic, maximum and residual induction, the retentivity and so on) are functions of the frequency and differ from the corresponding parameters for a static hysteresis loop.

Some of the magnetization loops recorded by us for standard nickel-zinc ferrites at different frequencies and field intensities are shown in Fig. 10.

The loop area in weak and moderate fields is given by

$$S = \pi H_c B_{max}, \qquad (3)$$

where H_c is the dynamic coercive force and B_{max} is the maximum induction.

In the case of weak fields, for purposes of evaluating non-linear distortion, one can use Rayleigh's equation:

$$B = \mu_1 H_1 \cos \omega t + \frac{8b}{3\pi} \sin \omega t - \frac{8b}{\pi} \cdot \frac{1}{1 \cdot 3 \ldots} \sin 3\omega t - \frac{8b}{\pi} \cdot \frac{1}{3 \cdot 5 \cdot 7} \sin 5\omega t - \ldots; \qquad (4)$$

where b is the residual induction of the hysteresis loop. Measurements of the third harmonic (the klirrfactor /distortion factor/ for which is greater than 97% of the general klirrfactor introduced by the ferromagnetic core) indicate that non-linear distortion at high frequencies is less than predicted by equation (4). After a certain frequency is reached, the non-linear distortion begins to decrease in connection with the gradual change in the form of the dynamic hysteresis loop: with increasing frequency the loop goes

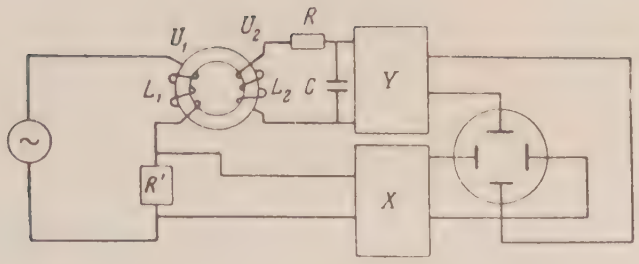

Fig. 9. Block diagram of a ferrometer with electric horizontal deflection.

over from a parabolic diangle to an ellipse (Fig. 11). The latter loop results in an induction vector displaced in phase relative to the magnetic field vector, but without additional harmonic components.

For long-range communications applications it is important to know the non-linear distortion characteristics of ferrites.

In the case of laminated metallic ferromagnetic materials, the magnetization loop approaches an ellipse with increasing frequency, which explains the lower non-linear distortion at high frequencies in designs employing these materials. In comparison, the magnetization loop of ferrites undergoes less modification and, in consequence, the non-linear distortion of ferrites shows less decrease with increasing frequency.

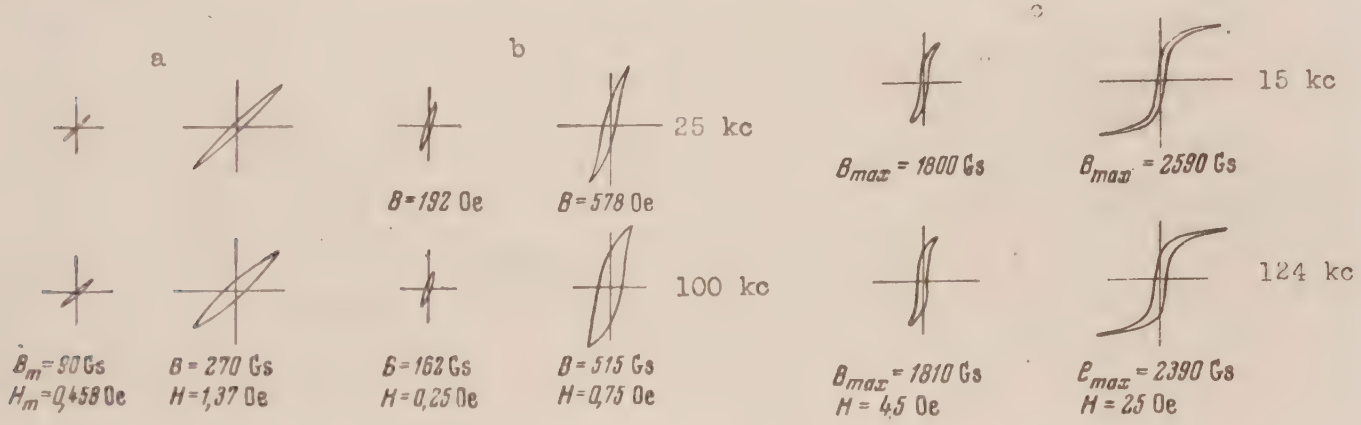

Fig. 10. Dynamic magnetization loops at different frequencies and field intensities (a and b--in weak fields; c--in moderate fields) for a) ferrite with an initial permeability μ_H = 200 gauss/oersted; b) NTs-500; c) NTs-250.

The values of the klirrfactor with respect to the different higher harmonics for NTs-250 ferrite at a basic frequency of 100 cps are shown in Fig. 12. It will be seen at even in a field of 1.3 oersteds the magnetic flux is comprised of a large number of harmonic components, the amplitude of which slowly decreases for higher harmonics.

In our tests 100 cps was selected as the basic frequency; however, because of the virtual absence of eddy currents in a wide frequency range and the consequent negligible secondary (aftereffect) losses, there is a close distribution of higher harmonics, which will also occur at higher basic frequencies of up to tens of kilocycles. Our investigations showed that the use of ferrites in fields of several oersteds intensity, like the use of thin laminated permalloy core materials, leads to appreciable harmonic distortion.

The non-linear distortion caused by a ferrite core with a closed magnetic circuit falls off sharply with reduced field intensity. However, in many cases the distortion still remains greater than is permissible in certain types of high-frequency equipment.

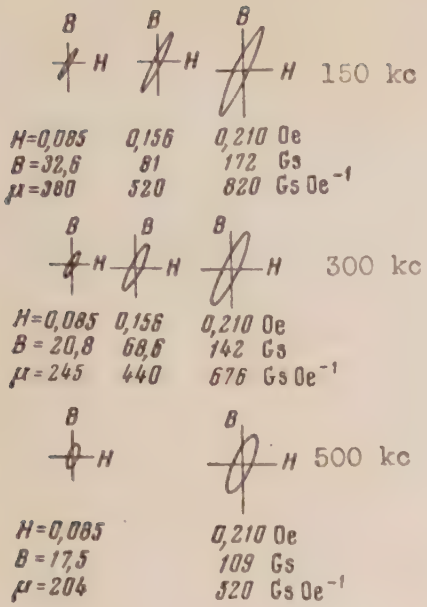

Fig. 11. Recorded dynamic magnetization loops for nickel-zinc ferrite core having an initial permeability of 350 gauss/oersted.

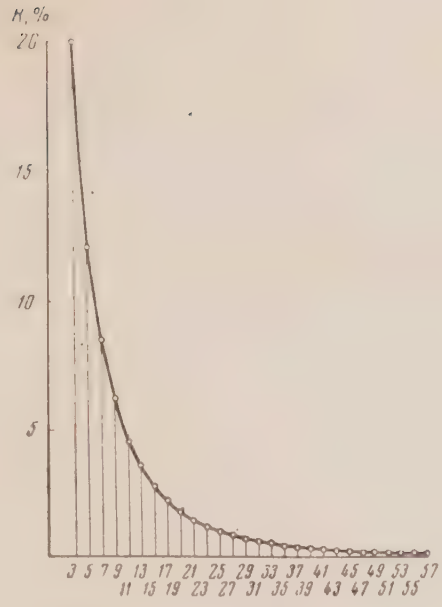

Fig. 12. Magnitude of harmonic components corresponding to numbers of harmonics for NTs-1000 ferrite (specimen No. 82) $H_{\sim}$=1.3 oe; f=100 cps.

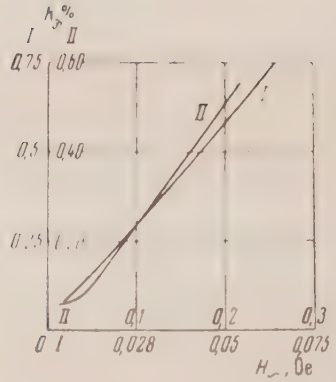

Fig. 13. Variation of third harmonic with strength of the alternating field at 330 kc for ferrites: I) NTs-100 (u_o=110 gauss/oersted); II) NTs-1000 (u_o=1000 gauss/oersted).

This observation applies particularly to the 100-1000 kc range; it must be noted that laminated metallic core materials (permalloy and VCh /ВЧ - h.f./ steel in 100-350 μ thick laminae), formerly used for components operated in this frequency range, introduce less distortion than do ferrite cores.

The non-linear distortion factors with respect to the third harmonic for two types of ferrite, as measured in weak fields at a basic frequency of 330 kc, are given in Fig. 13.

The harmonic distortion produced by ferrite cores can be effectively reduced by introducing non-magnetic gaps in the path of the magnetic lines of force or by employing open magnetic circuit designs for the cores.

5. Nickel-zinc ferrites in pulsating fields

In modern high-frequency equipment, magnetic materials often operate in a pulsating field, i.e., a field having both a static and an alternating component. Hence, it is important to investigate the variation of the pulse permeability of ferrites,

$$\mu_{\Delta} = \mu_r + \nu_r H_{\sim} = \mu_r(1 + \alpha_r H_{\sim}), \qquad (5)$$

with the intensity of the alternating, $H_{\sim}$, and the constant (static) components of the field. In (5) μ_r is the reversible permeability, ν_r is the Rayleigh coefficient for pulsating fields and α_r is the coefficient of permeability amplitude instability for magnetization in a static field.

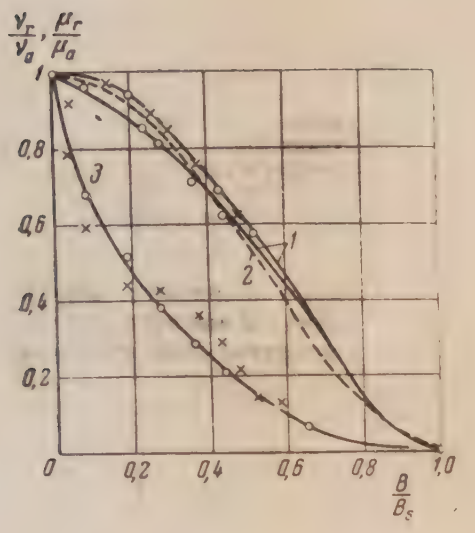

Fig. 14. Variation of the relative reversible permeability μ_r/μ_a and the ratio ν_r/ν_a with B/B_S for NTs-250 ferrite: 1) experimental curve for μ_r/μ_a; 2) theoretical curve for μ_r/μ_a; 3) curve based on values computed according to equation (7). Experimental curves drawn through test points.

Tests have shown that ferrites deviate somewhat from the theoretical law of Hans:

$$\frac{\varkappa_r}{3\varkappa_a} = \frac{1}{x^2} - \frac{1}{\sin^2 x}, \qquad \frac{I}{I_s} = \operatorname{ctg} x - \frac{1}{x}; \qquad (6)$$

the divergence between the theoretical and experimental values for low-permeability ferrites is of the same order of magnitude as for many metallic ferromagnetic materials, while for high-permeability ferrites it is appreciably higher. The variation of the relative reversible permeability μ_r/μ_a with B/B_S for a core of NTs-250 ferrite is shown in Fig. 14.

In order to determine the pulse permeability μ_Δ it is necessary to find the dependence of ν_r on the strength of the magnetizing field. The function $\nu_r(B/B_S)$ appears to be generally similar for most types of ferrites. It was found that the following empirical equation yields values of ν_r in close agreement with experimentally determined values:

$$\nu_r = \nu_a\left(1 - \sqrt{\frac{B}{B_s}}\right)\frac{\mu_r}{\mu_a}; \qquad (7)$$

As may be seen from the curves for ν_r/ν_a against B/B_S reproduced in Fig. 14, experimental values do not differ from computed values of this ratio by more than 20%.

Thus, making use of equation (7) we obtain the following computation equation for the pulse permeability of ferrites:

$$\mu_\Delta = \mu_a\psi + \nu_a\left[1 - \sqrt{\frac{B}{B_s}}\right]\psi H_\sim, \qquad (8)$$

where ψ is the value of μ_r/μ_a at the given value of B/B_S. For the case of weak and moderate fields ($B \leqslant 60\%\ B_S$), Arkad'ev proposed the equation (Ref. 10):

$$\frac{\mu_r}{\mu_a} = 1 - \frac{5}{3}\left(\frac{I}{I_s}\right)^2, \qquad (9)$$

from which one can derive the following approximate equation for the pulse permeability in weak and moderate fields:

$$\mu_\Delta = \mu_a\left[1 - \frac{5}{3}\left(\frac{B}{B_s}\right)^2\right] + \nu_a\left[1 - \sqrt{\frac{B}{B_s}}\right]\left[1 - \frac{5}{3}\left(\frac{B}{B_s}\right)^2\right]\cdot H_\sim. \qquad (10)$$

For practical engineering purposes it is also necessary to know the variation of the reversible permeability with the intensity of the static field. In our investigation we determined the variation of the reversible permeability for NTs-2500 ferrite at frequencies of 2, 25 and 200 kc at three different values of the alternating field. The 25 kc experimental curves are reproduced in Fig. 15 a. It will be seen that the reversible permeability of high-permeability ferrites is strongly dependent on the intensity of the static magnetizing field.

The dependence of the reversible permeability on the static field intensity (as well as on the frequency of the alternating field) is weaker for lower-permeability ferrites.

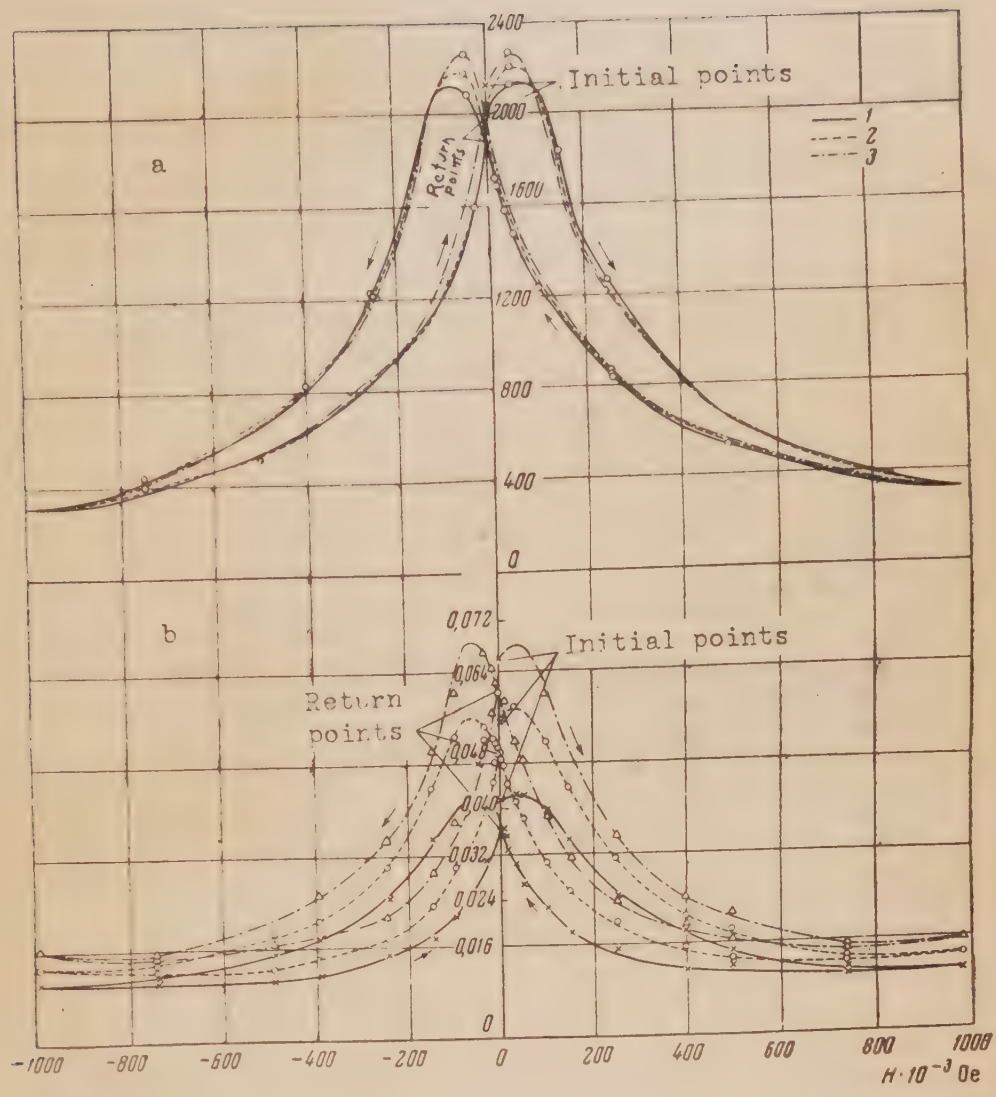

Fig. 15. Variation of the pulse permeability (a) and the loss tangent (b) of an NTs-2500 ferrite core with the intensity of the static magnetic field at a frequency of 25 kc for three different alternating field strengths: 1) $H_{\sim} = 7.4 \cdot 10^{-3}$ oersted; 2) $14.8 \cdot 10^{-3}$ oersted; 3) $22.1 \cdot 10^{-3}$ oersted.

Whereas the reversible permeability of ferrites in a certain frequency range is only weakly dependent on the frequency, the loss tangent is very strongly frequency dependent even for ferrites with a relatively low initial permeability. We carried out tests on NTs-2500 ferrite at frequencies of 2, 25 and 200 kc; the curves for the 25 kc measurements are shown in Fig. 15 b. It will be seen that the loss tangent in ferrites depends both on the static and on the alternating components of the magnetizing field as well as on the frequency.

Investigation of the variation of the temperature coefficient of the reversible permeability with the static component of a pulsating magnetic field (Fig. 16) showed that the temperature coefficient decreases with increasing static field intensity (over 10 permil per degree C for NTs-2500 ferrite).

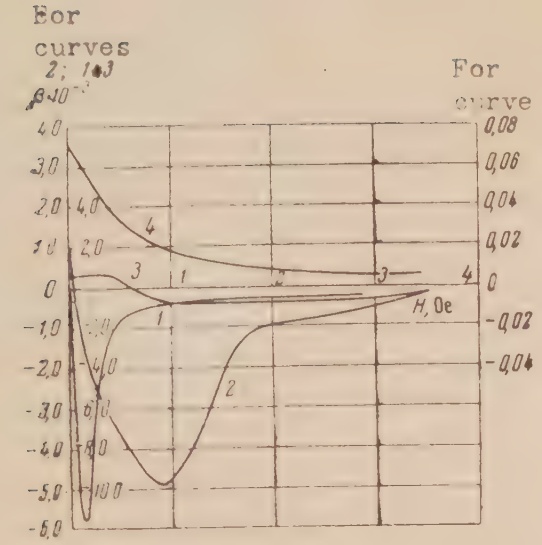

Fig. 16. Variation of temperature coefficients with strength of static component of pulsating magnetic field for typical zinc-nickel ferrites at f = 50 kc and $H_{\sim}$ = 0.005 oersted: 1) NTs-2500 (specimen No. 124); 2) NTs-1000 (specimen No. 119); 3) NTs-100 (specimen No. 147); 4) NTs-40 (specimen No. 471).

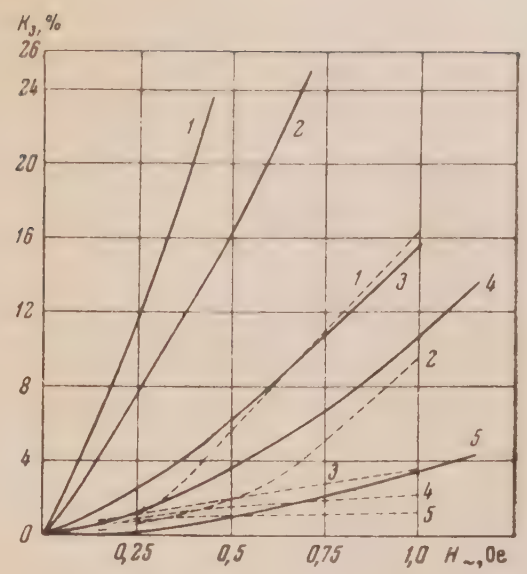

Fig. 17. Dependence of the magnitude of the second (solid lines) and third (dash lines) harmonics (K_2 and K_3) on the intensity of the alternating field $H_{\sim}$ in a static parallel field $H_{=}$ =0.8 oersted (f = 3 kc) for different nickel-zinc ferrites: 1) NTs-2000; 2) NTs-1000; 3) NTs-500; 4) NTs-250 5) NTs-40.

With further increase of the static field intensity the absolute magnitude of the temperature coefficient of the pulse permeability passes through a maximum and then decreases. It should be noted that in some cases the temperature coefficient of pulse permeability finally changes sign with increasing static field intensities, going from positive to negative values.

We also investigated the dependence of the second and third harmonics, K_2 and K_3, on the value of the alternating field at different intensities of the static field (0 to 0.8 oersted) for cores fabricated of different types of nickel-zinc ferrite. It was established that the application of a static magnetizing field leads to the appearance of even-number harmonics and to a change in the magnitude of the odd-number harmonics.

By way of illustration, the K_2 and K_3 vs alternating field strength curves for a number of ferrites in a constant field $H_{=}$ = 0.8 oersted (f = 3 kc) are reproduced in Fig. 17.

6. The dielectric properties of nickel-zinc ferrites

Ferrites belong to the group of doubly complex substances which in addition to distinctive magnetic properties possess dielectric characteristics and attributes. Where high-frequency applications are concerned, the dielectric properties of ferrites are extremely important since it has been experimentally established that the dielectric constant of ferrites is large and strongly dependent on the frequency. Thus, the dielectric constant of NTs-1000 ferrite at 5 kc is 1200

(Fig. 18). While in the case of low-permittivity ferrites the value of the constant is lower, it is still comparable to that of conventional dielectric materials (see table below).

Dielectric constant ε and dielectric loss tangent tan δ_ε of some nickel-zinc ferrites

Ferrite type	ε			tan δ_ε		
	frequency, kc			frequency, kc		
	5	50	500	5	50	500
NTs-1000	1335	190	30	1.5	2.3	1.87
NTs-500	225	65	35	1.7	0.7	0.35
NTs-100	107	78	48	0.32	0.31	0.31

The permittivity of all ferrites decreases with increasing frequency. It is also worth noting that the difference between the dielectric constants of different types of ferrites diminishes at higher frequencies.

Ferrites characterized by a higher magnetic permeability as a rule also have a larger dielectric loss tangent.

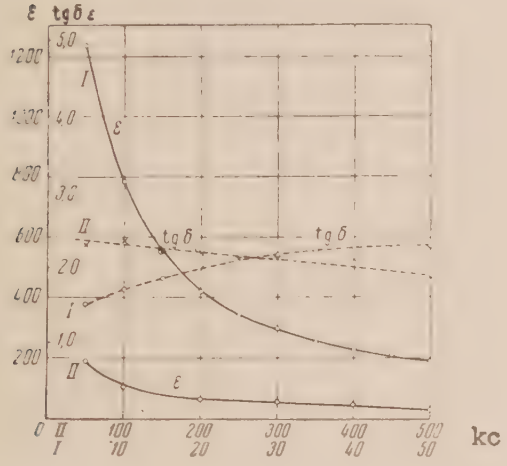

Fig. 18. Frequency dependence of the dielectric constant and the dielectric loss tangent for a plate of NTs-1000 ferrite (specimen No. 8-21) in two frequency ranges: I) 0 - 50 kc and II) 0 - 500 kc.

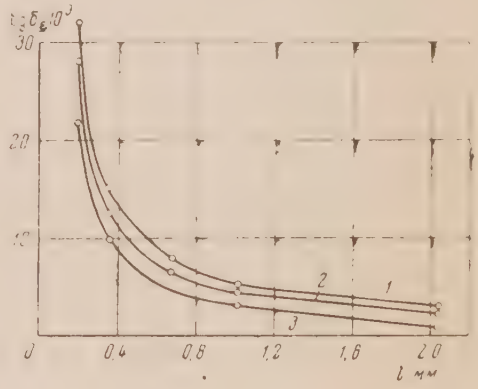

Fig. 19. Variation of dielectric loss tangent with the gap length in an annular core of NTs-1000 ferrite (specimen No. 190) at 1) 60 kc, 2) 40 kc, 3) 20 kc.

7. Engineering applications

As has been noted, ferrites are characterized by a high permeability in the region of high frequencies, the value of the permeability depending on the temperature, the intensity and nature of the magnetic field, the magnetic history of the specimen, etc. The fact that the permeability is not constant generally restricts the use of ferrites to components where variations of permeability are not objectionable,

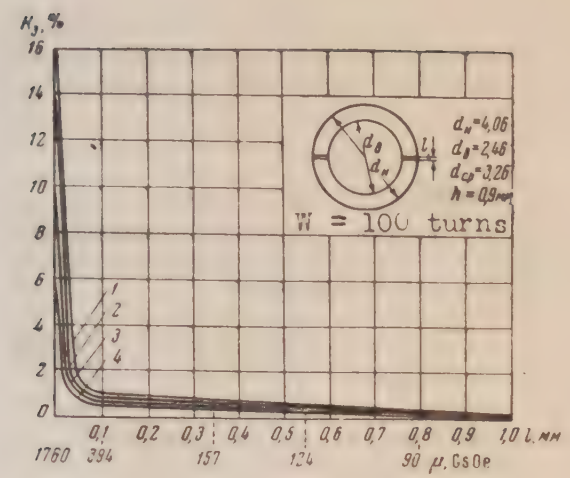

Fig. 20. Variation of the magnitude of the third harmonic with the gap length in an annular NTs-1000 ferrite core at different values of the alternating magnetic field, $H_{\sim}$: 1) 0.15; 2) 0.1; 3) 0.05; 4) 0.025 oersted (f = 1 kc).

provided its value does not fall below a certain specified level. Such components include the cores of many h.f. transformers, differentiating systems, some chokes, h.f. magnetic amplifiers, etc.

However, in high-frequency engineering extensive use is also made of various coils whose induction must not change appreciably under the influence of the various factors discussed above. Such constant inductances include various types of Pupin coils, oscillating circuit coils, and filter coils, operating at frequencies ranging from the audio region to hundreds of megacycles. Engineering specifications usually call for the induction of such coils to be constant within a fraction of a per cent, despite variations of the frequency, field, etc. Some engineers hold that ferrites are completely unsuitable for use as core materials for constant-induction coils. Our investigations have shown, however, that given proper aging of the ferrite material and suitable design of the magnetic circuit it is feasible to fabricate ferrite cores with very stable permeability characteristics, low non-linear distortion and a high Q-factor. One way of insuring constant permeability is by making the cores in the form of rings or the like with non-magnetic gaps in the flux path.

In many cases the introduction of a non-magnetic gap of some hundredths or tenths of a millimeter in a high-permeability ferrite core suffices to obtain a core, having a permeability of 100-200 gauss/oersted, with good stability and low losses. By way of illustration, the measured variation of the loss tangent with the gap length for a ring core of NTs-1000 ferrite is shown in Fig. 19.

Comparison of the losses in ferrite cores with gaps with the losses in magneto-dielectrics shows that, for the same permeability, ferrite cores are characterized by lower losses.

The introduction of a gap makes the permeability far less dependent on the intensity of the magnetizing field and sharply reduces the secondary effects due to the influence of the magnetization on the permeability and loss tangent. A gap also reduces the non-linear distortion, as may be seen from the curves in Fig. 20 where values of the third harmonic klirrfactor for an NTs-2500 ferrite core are plotted against gap length.

A Pupin coil for audio frequencies, designed about an NTs-1000 core with a gap, had a permeability of about 120 gauss/oersted and showed an overall instability (i.e. variation in permeability due to changes in temperature, field intensity and frequency as well as due to secondary effects) of less than 1%, with only minor non-linear distortion.

In cases where even more stable induction characteristics are essential, as in stabilizing circuits, the coils of quartz crystal filters and so on, coil designs with an even higher demagnetization factor

must be employed. For example, for crystal filter coils, where the induction must not vary by more than 0.1% at the most, satisfactory stability characteristics and a high Q are attainable with coaxial core designs. Lastly, at radio frequencies it is often advisable to use cylindrical cores with a relative permeability of only 2 to 5.

Conclusions

Comparison of the properties of ferrites, metallic ferromagnetics and magneto-dielectrics indicate that ferrites are the most promising materials for use in high-frequency equipment designed to operate in weak magnetic fields.

Ferrites offer a solution to a number of difficult design problems in the field of high-frequency engineering. It must be borne in mind, however, that in attempting to replace present materials by ferrites one must proceed cautiously and not fail to take into due account the specific electric, magnetic and other characteristics of ferrites.

Leningrad Branch of the
Central Communications Research Institute
of the Ministry of Communications of the USSR

Received
19 July 1954

Bibliographic References

1. J.L.Snoek, Issledovanie v oblasti novykh ferromagnitnykh materialov (Probably: New Developments in Ferromagnetic Materials), IL, M. 1947.
2. G.A.Smolenski & L.I.Rabkin, Vest. sviazi, 10 (1952).
3. G.A.Smolenski & L.I.Rabkin, Report presented at the Conference of Industrial Workers, Scientists and Engineers, Issue 74, 1951.
4. G.A.Smolenski, Dokl. AN SSSR, 78, 921 (1951).
5. N.N.Shol'ts & K.A.Piskarev, Izv. AN SSSR, Ser. fiz., 16, 6 (1952).
6. N.A.Toropov, Rabkin, Freidenfel'd & Epshtein, Zhur.tekh.fiz.,23,9 (1953).
7. Same authors, Zhur. prik. khim., 26, 9 (1953).
8. L.I.Rabkin & B.Sh.Epshtein, Radio (Radio), 10, (1952).
9. L.N.Fomenko, Zhur. eksp. i teor. fiz., 24, 3 (1953).
10. V.K.Arkad'ev, Elektromagnitnye protsessy v metallakh (Electromagnetic processes in metals). ONTI, M.-L. 1935.

/Translator's note: The ferrite designation transliterated in the article as NTs- is НЦ in Russian; these are the initial letters for nickel-zinc./

* * * * * * * * *

INVESTIGATION OF THE EFFECT OF SINTERING TEMPERATURE ON THE MECHANICAL, STRUCTURAL AND ELECTROMAGNETIC PROPERTIES OF OXYFER 2000

- A. A. Shvarts

1. Oxide ferromagnetic substances are extremely brittle materials and their mechanical properties cannot be determined by conventional testing methods.

Consequently, we made use of a special type of testing equipment, developed by Gofman (Ref. 1) and based on a new method of determining the modulus of elasticity and the ultimate strength of highly brittle materials. Analysis of measurements made by Gofman and his co-workers showed that variation of the sintering temperature within the 1150° to

1400°C range has virtually no effect on the modulus of elasticity of Oxyfer 2000 ($16 \cdot 10^3$-$22 \cdot 10^3$ kg/mm^2) while the tensile strength increases from 4.5-6.2 kg/mm^2 to 7.3-8.7 kg/mm^2 as the sintering temperature is raised.

Thus, it will be seen that the modulus of elasticity of this oxyfer is of the same order of magnitude as that of cast steel, while the ultimate strength is equal to the strength of certain types of glass.

2. The next step in the investigation of the mechanical properties of the oxyfer was measurement of its micro-hardness. These measurements were carried out by V. B. Sakhov and A. P. Erastova.

Microscopic examination of polished sections and hardness measurements showed that the section surfaces of specimens sintered at different temperatures differ in appearance and character. The polished section surface presents a pattern of irregular white and dark grey areas (Figs. 1 and 2); the micro-hardness of the dark areas is appreciably lower than that of the white ones. The ratio of the white and grey areas varies with changes in the sintering temperature: as may be seen from the figures, both the number and size of the grey areas decrease with increasing sintering temperature.

At first we assumed that the grey areas might be abrasions due to grinding and polishing. However, this was disproved by surface quality determinations made with a surface analyzer (IZP Profilograph) with a vertical enlargement of 4000 X and a horizontal magnification of 100 X. The dimensions of the grey areas were appreciably larger than the surface scratches disclosed by the analyzer. To make doubly sure that the grey areas were not cavities clogged with abrasive we etched one of the specimens in boiling hydrochloric acid. Both the appearance of the grey areas and the proportion of the surface occupied by them remained unaltered after etching. The absence of abrasive traces on the surface was confirmed by X-ray photographs taken by the reversal method with a CROSS-1 camera.

Fig. 1. Microsection of Oxyfer 2000 specimen sintered at 1150°C. Magnified 300 X.

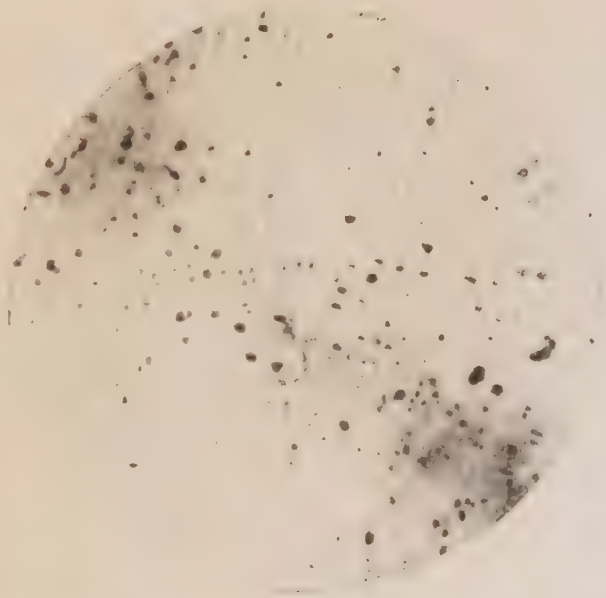

Fig. 2. Microsection of Oxyfer 2000 specimen sintered at 1340°C. Magnified 300 X.

There is good reason to assume that the dark areas consist of the same basic material but in a finely dispersed state. This assumption is supported by examination of the surface under a binocular microscope: it has the appearance of an alternation of rounded mounds and hollows, formed by the disintegration or crumbling out of fine-grain material of the same composition as the main mass.

Micro-hardness measurements showed that the hardness of the white areas varies little with changes in the sintering temperature and that the hardness of the dark grey areas, i.e. the areas where the material is in a finely dispersed state, is lower than that of the white areas. It must also be noted that the micro-hardness at the original surface of the specimen is always somewhat lower than at internal sections.

3. Appropriate X-ray studies were made in order to determine whether changes in the sintering temperature resulted in phase transformations in the oxyfer. The preparatory work and photographing were done by A. P. Erastova. The X-ray photographs were obtained with a VRS camera (D = 143.25 mm) with a divider, which permitted photographing two specimens simultaneously.

These studies showed that there is only one crystal phase present in Oxyfer 2000 and this phase has a spinel structure. Furthermore, X-ray photographs taken flush against specimens sintered at 1150° and 1200°C, 1200° and 1250°C, 1250° and 1300°C, 1300° and 1340°C and 1340° and 1400°C proved that the lattice constant remains the same for all sintering temperatures from 1150° to 1400°C.

However, with the same heat treatment but different initial compositions (for example, Oxyfer 2000 differs from Oxyfer 1000 by 0.5% in Fe_2O_3 content, 1% in ZnO content and 1.5% in NiO content) the resultant solid solutions have a different lattice constant: the relative displacement of the diffraction rings is clearly discernible in the photographs.

4. The magnetic properties of the oxyfer were investigated on toroidal specimens, forming induction coil cores.

The induction and losses were measured in the frequency range of 0.3 to 10 kc by means of a Maxwell bridge.

The influence of the sintering temperature on the permeability and on the character of the frequency dependence of the loss tangent is apparent from the curves of Figs. 3 and 4. The strong influence of the sintering temperature on the permeability and loss characteristics is surprising in view of the absence of phase transitions. It is but natural to seek a physical explanation of the phenomenon.

For purposes of analysis let us consider a model in which the actual structure of the ferromagnetic domains of the polycrystalline specimen is replaced by a simple structure consisting of alternate plane-parallel layers at 180° to each other and let us relate all the energy processes, accompanying motion of the boundary layers in this "equivalent" ferromagnetic material to energy changes at the layer boundaries.

Then to find an expression for the complex permeability of the substance in an alternating field, we must first derive an equation for the motion of the boundary layer. To derive this equation, we must know the character of the forces acting on the boundary layer.

Let us assume that the forces acting on the boundary layer when it is displaced from the position of equilibrium may be regarded as quasi-

elastic and that these forces are determined by the inhomogeneity of the internal stresses and by the presence of extraneous inclusions in the lattice.

In addition to these quasi-elastic forces, the boundary in the process of displacement will be acted upon by "frictional forces". If we assume that conductivity of the ferromagnetic material is equal to zero, these "frictional forces" reduce to two forces (Ref. 2):

$$F_1 = av$$

and

$$F_2 = \beta / b (1 - e^{-b/f}) v,$$

where v is the displacement velocity of the boundary layer, $a = \frac{\varepsilon}{e/mc \cdot J_s \delta}$ (Ref. 3), ε is a coefficient, characterizing the magnetic spin interaction, δ is the thickness of the boundary layer, f is the frequency of the magnetizing field, b is a coefficient, characterizing the quasi-elastic force, retaining the extraneous atoms in the given lattic position, and β is a coefficient whose magnitude depends on the distribution of the extraneous atoms and the structure of the ferromagnetic domains.

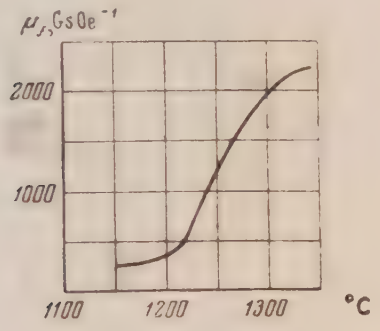

Fig. 3. Dependence of μ_f on the sintering temperature of Oxyfer 2000 (μ_f is the value of the permeability extrapolated for H = 0 at a frequency of 1 kc).

Knowing the forces acting on the shifting boundary layer, we can write the appropriate equations for the motion and from a solution of these find the expression for the mean reversible displacement of the boundary layer and from this, in turn, the expressions for the complex permeability and loss tangent.

In the case when the amplitude of the alternating field $\hat{H} \to 0$, the expression for the loss tangent, derived as outlined above, will be

$$\operatorname{tg} \delta_f \approx \frac{\alpha_2}{\alpha_1} S_1 \frac{f \cdot f_1}{1 - (f/f_1)^2} + \frac{f}{f_2} (\gamma - e^{-b/f}), \qquad (1)$$

where $f_1 = \frac{\alpha_1}{2\pi a}$, $f_2 = \alpha_2 \frac{b}{2\pi\beta}$, $\gamma = 1 + \frac{ab}{\beta}$,

α_1 is a coefficient, characterizing the quasi-elastic force due to the inhomogeneity of the internal stresses; α_2 is a coefficient, characterizing the quasi-elastic force due to the extraneous inclusions; S_1 is the relative area of a unit surface of the boundary layer on which the acting quasi-elastic forces are due almost exclusively to the inhomogeneity of the internal stresses.

Further, invoking certain theories regarding "inclusions" and "stresses", it can be shown that the values of

$$A = \frac{\alpha_2}{\alpha_1} S_1 f_1, \quad B = \frac{b}{f_2} \quad \text{and} \quad C = \frac{\gamma - 1}{f_2} \qquad (2)$$

will be proportional, respectively, to

$$(K + \lambda\sigma) S_1 \theta, \quad \frac{J_s}{\sqrt{(K + \lambda\sigma) \cdot \theta}} \quad \text{and} \quad \frac{1}{K + \lambda\sigma} \cdot \frac{1}{\theta}, \qquad (3)$$

where K is the magnetic anisotropy constant, λ is the magnetostriction at saturation, σ is the amplitude of the internal stresses, θ is the Curie point and J_s is the saturation magnetization.

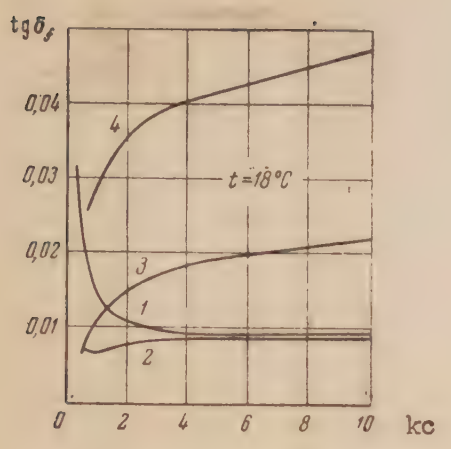

Fig. 4. Dependence of tan δ_f on the frequency of the magnetizing field for Oxyfer 2000 specimens sintered at different temperatures: 1) 1150°, 2) 1200°, 3) 1250°, 4) 1340°C (tg δ_f = values of the loss tangent extrapolated for H = 0 at the given frequency f).

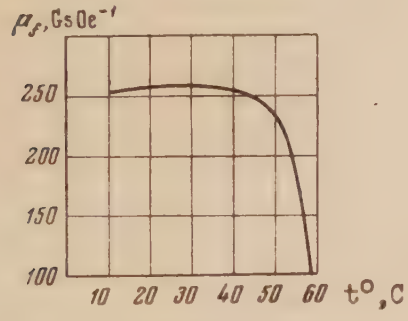

Fig. 5. Variation of μ_f with the temperature for an Oxyfer 2000 specimen sintered at 1150°C.

An examination of the curves of Fig. 4 will show that they can all be described by equations of the form of (1), using appropriate values of the parameters A, B and C. In view of the relation between the respective terms of (2) and (3), it may be asserted that all changes in the magnitude and nature of the frequency dependence of the oxyfer with increases in the sintering temperature may be attributed to decreases in the values of K, $\lambda\sigma$ and S_1.

If the above considerations are valid, then, taking into account the fact that K and λ are strongly dependent upon the temperature of the ferromagnetic material, we may expect to find an analogous variation of the frequency dependence of the loss tangent when the specimen is heated. The results of heating tests on a specimen sintered at 1150°C are shown in Figs. 5 and 6.

In the light of the above, it will be seen from the curves of Fig. 6 that up to 34° the change in the frequency dependence of the loss tangent is due primarily to the decrease in K and λ.

The nature of the frequency dependence of the tan δ_f observed at higher temperatures (45 - 55°) indicates that here, in addition to a continuing decrease of the anisotropy and magnetostriction constants, we also have a sharp drop in S_1. This may be explained by an appreciable increase in the thickness of the boundary layer (i.e. surface layer) with increasing temperature.

It may be assumed that with a certain correlation between the size of the extraneous inclusions and the distribution of the internal stresses, an increase in the thickness of the boundary layer to a depth comparable to the wavelength of the stresses may lead to a great increase in the influence of the quasi-elastic forces due to the inhomogeneity of the internal stresses, i.e. to an increase in S_1. The effect may be further strengthened by an increase in the internal stresses as a result of different rates of thermal expansion of the large-grain and finely dispersed crystal phases. The absence of a Hopkinson maximum in the temperature-dependence of permeability curve (Fig. 5) may be explained by the increased influence of the internal stresses as the Curie temperature is approached.

5. In view of what has been stated above, the nature of the physical processes leading to changes in the magnetic properties of Oxyfer 2000 when the sintering temperature is raised or the specimen is heated may be described as follows:

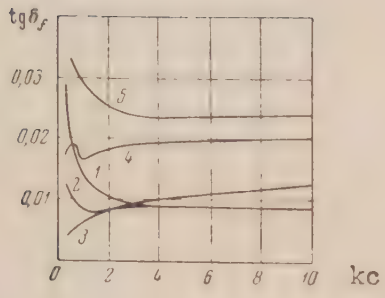

Fig. 6. Variation of the loss tangent with the frequency of the magnetizing field for an Oxyfer 2000 specimen sintered at 1150° at different temperatures: 1) 19°, 2) 27°, 3) 34°, 4) 45°, 5) 55°C.

Oxyfer 2000 sintered at 1150°C has a relatively large number of inclusions (regions) consisting of very fine crystals. The presence of these fine-grain inclusions makes for relatively large internal stresses. As the sintering temperature is increased the number of fine-crystal inclusions goes down while the size of the individual crystals increases, the material becomes more homogeneous and, as a result, internal stresses are reduced. This in turn leads to an increase in the initial permeability and a corresponding change in the character of the frequency-dependence of the losses.

If a specimen sintered at 1150° (hence, having a large number of fine-grain inclusions) is heated, at first the predominant part in the ensuing change of the frequency dependence of the loss tangent is played by the decrease in the anisotropy and magnetostriction constants: the falling section of the tan δ_f vs frequency curve becomes shorter and, for the specimen investigated, virtually vanishes at about 35°C. With a further rise in temperature, the influence of the internal stresses increases, due to an increase in the thickness of the boundary layer and the amplitude of the internal stresses; this leads to the reappearance of the falling section of the tan δ_f (f) curve.

In contrast, the number of fine-grain inclusions in specimens sintered at 1300-1400°C is small and consequently their influence is minor ($S_1 \approx 0$); as a result, the general character of the frequency-dependence of the loss tangent for such specimens is not affected by heating: the loss tangent vs frequency curves for different temperatures up to just below the Curie temperature have no falling section and differ from each other only as regards slope.

The writer wishes to thank N. N. Shol'ts for his valuable advice in connection with the preparation of the present report.

Received
13 May 1954

Bibliographic References

1. S.I.Gofman, Zhur. tekh. fiz., 23, 3 (1953).
2. A.A.Shvarts, Zhur. tekh. fiz., 21, 11 (1951).
3. L.D.Landau & E.M.Lifshits, Sow. Phys., 8, 153 (1935).

CHANGES IN THE CONDUCTIVITY OF CERTAIN FERRITES UNDER THE INFLUENCE OF GAMMA RAYS - N. V. Vol'kenshtein and A. N. Orlov

1. The present report is concerned with an investigation of the electric conductivity of certain ferrites which proved to be particularly sensitive to irradiation by gamma-rays. The results may be of some value in connection with studies of the behavior of semiconductors under the influence of hard radiation in general and may further our, as yet inadequate, understanding of the nature of conductivity in ferrites.

It has been shown experimentally that the temperature dependence of the conductivity of ferrites $\sigma(T)$ is characterized by the general law for semiconductors:

$$\sigma = Ae^{-B/T} \qquad (1)$$

However, knowledge of the activation energy Bk (k is the Boltzmann constant) is in itself insufficient to determine the energy spectrum of the electrons in the ferrite lattice which, in contrast to the lattices of many other, thoroughly studied oxide semiconductors, contains different types of transition-metal ions. It is not clear at present to what extent the zonal /energy-level/ theory is applicable to these mixed-oxide semiconductors.

Light may be shed on this problem by experiments in which it is possible to vary the number of electrons, participating in the electric current, as well as the number of lattice defects, forming local energy levels. Such variations occur when the specimen is irradiated by neutrons, heavy or light charged particles or relatively high-energy γ-quanta. Since the time rate of change of the number of excited electrons and that of the number of lattice defects are governed by different laws, depending on the mechanism of recombination, the form of the function $\sigma(t)$ during and after irradiation will depend upon which of these factors (the number of excited electrons or the number of lattice defects) is predominant where the conductivity is concerned.

2. In our investigation we used nickel-zinc ferrites of stoichiometric composition. These ferrites were selected because we were able to obtain specimens with a very low electric conductivity and it is known that the influence of gamma-ray radiation is strongest for lowest conductivity materials. The ferrite specimens were prepared from pure oxides and were sintered in the form of cylinders 20 mm in length and 6 mm in diameter.

The experimental procedure was the following. The specimens were placed in a double-walled chamber, connected by means of flexible, heat-insulated hose with an ultra-thermostat, designed to maintain the set temperature constant within 0.01°. After stabilization of the temperature, the specimen was exposed to radiation, the dosage being held constant at about 100 roentgen/min. The conductivity was measured at intervals of 10 minutes by the conventional voltmeter-ammeter method; during the measuring, the radiation was interrupted for about $t^{*}=30$ sec. The temperature was gaged by means of a copper-constantan couple (thermal e.m.f. = 4 millivolts per 100°C) connected to a multiflex galvanometer. The hot junction was welded to a conducting clamp attached directly to the specimen; the cold junction was kept at the temperature of melting ice.

The results of measurements at 30° and 36°C are given in Fig. 1. Here the time from the start of irradiation is laid off along the X-axis, while the Y-axis is scaled in arbitrary conductivity units (the same for both curves). The decrease in conductivity after cessation of irradiation is shown in Fig. 2.

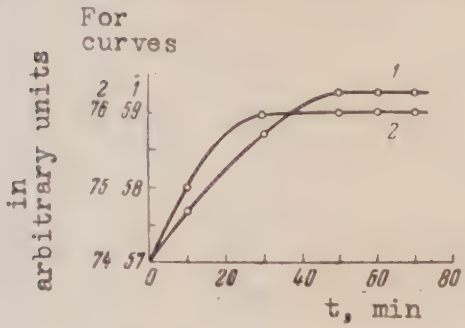

Fig. 1. Variation of the conductivity of a nickel-zinc ferrite with time of irradiation with gamma-rays at 1) 30°C, 2) 36°C.

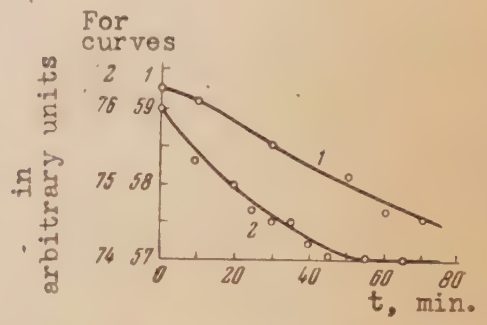

Fig. 2. Decrease in conductivity with time after cessation of irradiation at 1) 30°C, 2) 36°C.

As may be seen from the curves, the conductivity increases under the influence of continued radiation, leveling off at a maximum value: σ_{max}; after the radiation is cut off, the conductivity falls gradually back to the initial pre-irradiation level. The value of σ_{max} is lower for higher irradiation temperatures. The relative slopes of curves indicate that σ rises (and falls off) more rapidly at higher temperatures.

3. In order to explain these results let us investigate $\sigma(t)$ in the light of the zonal theory for the following model of a semiconductor (Fig. 3). In the initial state, i.e. before irradiation, there are N local levels W_2 per 1 cm^3 in the forbidden band (zone) of width u; at T = 0 these levels are occupied by N electrons (such levels may be associated, for example, with vacant oxygen sites, occupied at T = 0 by two electrons each and losing one electron each in case of excitation). During irradiation there form (due to the knocking out of O^{--} ions by secondary Compton electrons and photoelectrons) X additional lattice defects: W_2 local levels and as many W_1 levels (associated with the oxygen ion inter-sites) per 1 cm^3; in every case $W_2 < \varepsilon < W_1$, where ε is the Fermi surface.

At T = 0, n, the number of electrons at the W_1 levels, and n', the number of electrons in the conductivity zone, will equal zero, i.e.,

$$n = n' = 0 \qquad (\text{at } T = 0) \qquad (2)$$

Due to thermal agitation there will appear at the W_1 level $n = n_T$ electrons and $n' = n'_T$ electrons in the conductivity zone and simultaneously $p = p_T$ holes at the W_2 levels and $p' = p'_T$ holes in the ground zone.

During irradiation there may be a further increase in the numbers n and n' equal to αI, where I is the intensity of the radiation and α is a proportionality factor. Let us denote the numbers of these additional electrons through n_x and n'_x. Then

$$n = n_T + n_x, \quad n' = n'_T + n'_x, \quad p' = p'_T + p'_x \text{ and } p = p_T + p_x \qquad (3)$$

Inasmuch as in the general case the number of levels, X, depends on the irradiation time, t, all the variables in (3) also depend on t.[a)]

Simultaneously with irradiation, there will occur recombination of excited electrons and lattic defects. The mechanism of recombination may be monomolecular or bimolecular. In the first case,

$$dX = -bXdt \qquad (4)$$

where b is a proportionality factor, dependent on T. Examples of the operation of this mechanism of recombination are furnished by cases when the defects emerge to the surface of mosaic segments, grain boundaries or structural dislocations.

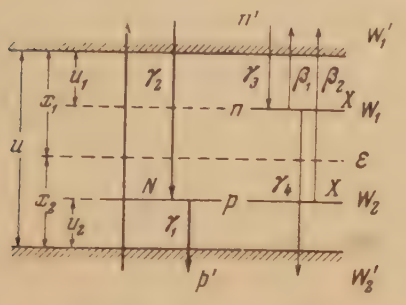

Fig. 3. Diagram of model used to explain the experimental results in the framework of the zonal theory of semiconductors.

In the second case, which occurs, for instance, in the recombination of imbedded ions and vacant sites,

$$dX = - cX^2dt \qquad (5)$$

In considering the recombination of excited electrons and holes, we must distinguish between two cases:

a) Instantaneous recombination, i.e. recombination time short compared to the interval t* (interval of interruption of irradiation for measuring purposes). In this case the additional number of electrons, n'_x, and holes, p'_n, will be present only during the irradiation time, but not during the measuring interval. To investigate the variation of $\sigma(t)$, which in this case will exhibit jumps at the instant the radiation is turned on and off, but will otherwise be determined by the function X(t), there is no need to know the mechanism of electron recombination in detail.

b) Excited electrons and holes recombine slowly. In this case to compute $\sigma(t)$ we must find $n'_x(t)$ and $p'_x(t)$, which can be done only by solving a system of kinetic equations in n, n', p and p', to write which we must know the nature of the mechanism of slow recombination. One step in this mechanism would presumably be a low-probability transition, insuring that the electron remains in the excited state for an appreciable time. One of the possible mechanisms, satisfying this condition, is suggested in Refs. 1 and 2 to explain the variation of photoconductivity with time in CdS crystals. Here, in the normal state of the crystal, the electrons occupy the "activator" levels. When an electron is knocked out of the ground state (in our case, of a normal O^{--} ion, for example) into the conductivity zone, the p'-hole formed is instantly filled by an electron from the W_2 level, where a p-hole is formed. The probability of the transition (capture) of an electron from the conductivity zone to the p-hole is low, consequently the electron may remain in the conductivity zone for a considerable time.

---

a) In view of the great difference between the masses of electrons and ions, $n'_x \gg X$; but if the recombination time of lattice defects is 10^3-10^4 times greater than that of electrons, the effect of the former will still be noticeable.

Thus, the possible recombination cases are:

Mechanism of ionic recombination is	Electrons combine
1a) monomolecular	instantaneously
1b) "	slowly
2a) bimolecular	instantaneously
2b) "	slowly

The general expression for the electric conductivity of a crystal in the assumed model has the form (Ref. 3):

$$\sigma = ev_n n' + v_p p', \tag{6}$$

where e is the absolute value of the charge of an electron and hole, v_n and v_p are the respective mobilities. Using the notation of Fig. 3 for the energy intervals, the number of electrons and the number of holes formed due to thermal agitation at a given temperature T, will be

$$n'_T = A_n e^{-x_1/kT} \quad \text{and} \quad p'_T = A_p e^{-x_2/kT}. \tag{7}$$

To the first approximation, we may assume

$$A_n \approx A_p \approx A \quad \text{and} \quad v_n \approx v_p \approx v. \tag{8}$$

Then from (3) and (6), according to Ref. 3, we have

$$\frac{\sigma}{evA} = \left[\left(\frac{1+(\nu+\zeta)\,e^{u_1/kT}}{1+\zeta e^{u_1/kT}}\right)^{1/2} + \left(\frac{1+\zeta e^{u_1/kT}}{1+(\nu+\zeta)\,e^{u_1/kT}}\right)^{1/2}\right] e^{-u/2kT} + \frac{n'_x + p'_x}{A}, \tag{9}$$

where

$$N/A = \nu, \quad X/A = \zeta. \tag{10}$$

In cases 1a and 2a, when n'_x and p'_x are virtually independent of t, the time-dependence of the conductivity is determined wholly by X(t). Let us determine the form of the latter function for the two above-mentioned mechanisms of the recombination of defects, for the case when radiation of intensity I is turned on at the instant t = 0.

In the case of monomolecular recombination, we have

$$dX = (aI - bX)\,dt, \tag{11}$$

where *a* is a proportionality factor. Assuming that the mobility of both types of defects is the same,

$$b = b_0 e^{-u_D/kT}, \tag{12}$$

where u_D is the activation energy of the diffusion of the defects. A solution of equation (11) may be found in the form

$$X = \frac{aI}{b}(I - e^{(-bt)}). \tag{13}$$

The maximum number of defects,

$$X_{max} = \frac{aI}{b} = \frac{aI}{b_0} e^{u_D/kT} \tag{14}$$

and decreases with increasing temperature.

In the case of a bimolecular mechanism, we have

$$dX = (aI - cX^2)\,dt, \tag{15}$$

whence

$$X = \sqrt{\frac{aI}{c}} \cdot \frac{e^{2\sqrt{acI}\,t} - 1}{e^{2\sqrt{acI}\,t} + 1}. \qquad (16)$$

The maximum value of X equals

$$X_{max} = \sqrt{\frac{aI}{c}} = \sqrt{\frac{aI}{c_0}}\, e^{(u_E/kT)}. \qquad (17)$$

Thus, with monomolecular recombination X_{max} is proportional to I, while with bimolecular recombination $X_{max} \approx \sqrt{I}$.

Substituting (13) or (16) in (9), we find $\sigma(t)$. The dependence is more complicated than for X(t) and cannot be described by any of the simple equations ordinarily characterizing the kinetics of mono- and bimolecular reactions. We note that at $X = X_{max}$, we have what may be termed "saturation" of the conductivity.

In cases 1b and 2b, when the electrons excited by irradiation recombine slowly, $\sigma(t)$ may be determined by solving a system of kinetic equations in n, n', p and p', which equations are more complicated than the formulae used in Ref. 1, since they contain the time-dependent variable X. Let us designate the concentration of electrons and holes at the W_1 and W_2 levels through n^o and p^o, respectively; then

$$n = n^\circ X, \quad p = p^\circ (N + X), \qquad (18)$$

and

$$1 - p^\circ = n_1^\circ \qquad (19)$$

is the concentration of electrons at the W_2 levels. Using this notation, the kinetic equations will have the form

$$\frac{dn'}{dt} = \alpha I (1 - p') + \beta_1 X n^\circ + \beta_2 (N + X)(1 - p^\circ) - \gamma_3 X (1 - n^\circ) n' - \gamma_2 (N + X) p^\circ n', \qquad (20)$$

$$-\frac{dp^\circ}{dt} = \gamma_2 n' p^\circ - \beta_2 (1 - p^\circ) - \gamma_1 (1 - p^\circ) p' \qquad (21)$$

with analogous equations for dn/dt and dp'/dt. The condition for neutrality of the crystal is that

$$n' + X n^\circ = (N + X) p^\circ + p'. \qquad (22)$$

Solution of this system of kinetic equations in the general case is possible only by numerical methods; comparison of the results with experimental data is hindered by the fact that the transition probabilities γ_i and β_i are unknown. However, we can draw certain deductions regarding the character of the $\sigma(t)$ curve without solving the system of equations. Specifically, we can show that there is a saturation value of the conductivity, σ_{max}, and can establish the temperature-dependence of σ_{max}. We note that at the instant of saturation there is established a stationary state, so that the derivatives in (20) and (21) go to zero. For purposes of illustration, let us consider only the simpler case when the presence of W_1 levels does not have an appreciable effect on the conductivity. In this case we need only consider the transitions between the W'_0, W_2 and W'_2 levels, indicated in Fig. 3 by heavy arrows. Introducing the notation N' = N + X, we obtain from (20) and (21),

$$\alpha I - \gamma_2 N' p^\circ n' = 0, \qquad (23)$$

$$\gamma_2 p^\circ n' - \gamma_1 (1 - p^\circ) p' = 0, \tag{24}$$

Condition (22) will now be written

$$n' = N' p^\circ + p', \tag{25}$$

hence, from (24) we have

$$\gamma_2 p^\circ n' - \gamma_1 (1 - p^\circ)(n' - N' p^\circ) = 0. \tag{26}$$

In order to solve the system of equations (23)-(26), we find from (26):

$$p^\circ = \frac{1}{2}\left[1 + \frac{\hbar'}{N'}(1 + \eta)\right] + \frac{1}{2}\sqrt{[1 + (1 + \eta) n'/N']^2 - 4n'/N'}, \tag{27}$$

where, in accordance with our assumption,

$$\eta = \gamma_2/\gamma_1 \ll 1. \tag{28}$$

Substitution of p° in (23) yields a cubic equation for n', attempts at a general solution of which lead to cumbersome expressions. Hence, let us investigate two cases when (27) can be simplified:

1) $n' \ll N'$ (almost all the W_2 levels occupied by electrons; $p^\circ \ll 1$). Expanding the root into a series in η and n'/N', we obtain

$$p^\circ = \frac{1}{2}\left(1 + \frac{n'}{N'}\right) \pm \frac{1}{2}\left(1 - \frac{n'}{N'}\right).$$

The root corresponding to the condition $n'/N' \ll 1$ is $p^\circ = n'/N$. Then from (23) we find

$$n' = n'_{\max} = \sqrt{\alpha I/\gamma_2}; \tag{29}$$

n'_{max} is independent of the number N' and is proportional to $\sqrt{I}$. The temperature dependence of n'_{max} is determined by the transition probability γ_2 which increases with the temperature. Thus n'_{max} goes down with rising temperature.

2) $n' \approx N'$ (almost all W_2 levels unoccupied; $p^\circ \lesssim 1$). We introduce the small quantity

$$\xi = 1 - \frac{n'}{N'}.$$

Then the expression under the square root in (27) equals $\gamma_1 + 0(\gamma_1^2)$ and

$$p^\circ = \frac{1 + \eta}{2} - \frac{1}{2}\xi \pm \sqrt{\gamma_1}.$$

To within the magnitude of the small quantities η and ξ

$$N' p^\circ = \frac{1}{2}(n' + N'). \tag{30}$$

Substitution of (30) in (23) gives

$$\alpha I - \frac{1}{2}\gamma_2 n'^2 - \frac{1}{2}\gamma_2 n' N' = 0,$$

whence

$$n' = -\frac{N'}{2} + \sqrt{\frac{N'^2}{4} + \frac{2\alpha I}{\gamma_2}}. \tag{31}$$

As the number of defects N' increases, the number of electrons n' in the conductivity zone goes down; when $N'^2 \gg 8\alpha I/\gamma_2$, $n' \sim (N')^{-1}$; when $N'^2 \ll 8\alpha I/\gamma_2$, $n' \sim \text{const} - N'$. However, in the vicinity of N' = 0, solution (31) is unacceptable since in this case $n'_{N' \to 0} \to \sqrt{2\alpha I/\gamma_2}$, while according to the assumed condition $n' \backsim N'$ should tend to zero.

As may be seen from (31), n' increases with I. The temperature dependence of n' is now determined both by the value of γ_2 and by the number of levels, N' = N + X.

If N + X is constant, n'_{max} will be functionally dependent upon γ_2 and as in the case of (29) will decrease with rising temperature. If the number N + X is increased by irradiation and the number of defects is great enough for solution (31) to be valid, the increase in N + X should lead to a reduction in the value n'_{max}.

Lastly, if N is affected by thermal agitation, the change must conform to the $N = N_0 e^{-u_c/kT}$ law, where u_c is the activation energy. In the range of N-values in question, an increase in temperature must also lead to a decrease in n'_{max}.

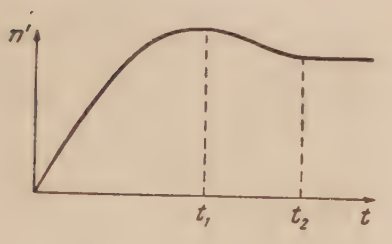

Fig. 4. Change in the number of electrons in the conductivity zone with irradiation time t.

If saturation is reached in the region where n' decreases with N + X, the n'(t) curve will have a maximum at the point t_1 (see Fig. 4), where n' reaches its maximum for the given N'(t). With continued irradiation N' will increase and n'_{max} will decrease with time until at a certain time t_2 the number of defects reaches its equiblibrium value for the given intensity of radiation. An analogous anomaly should be observed after the radiation is cut off, when n'(t) may reach a value below the equilibrium one for the given temperature (part of the electrons are retained at the "excess" local levels and become free after recombination). This form (maximum, followed by a decrease and levelling off) of the n'(t) curve - and, hence, of the $\sigma(t)$ curve - may be indicative of the formation of lattice defects in appreciable numbers under the influence of irradiation.

We note in conclusion that a noticeable change in the electric conductivity under the influence of irradiation was observed only for specimens having a low conductivity (of the order of 10^{-8} ohm·cm)*. In the light of the assumed model, such specimens are characterized by a small number of defects N. If this number is increased by X under the influence of radiation, the effect will be noticeable only if the initial value of N is commensurable with X.

Thus, the examined variants of the energy spectrum of a semiconductor help explain the gradual increase in the electric conductivity to σ_{max} when the specimen is exposed to radiation (and the return of σ to its initial value some time after the radiation is cut off). One cannot arrive at any definitive conclusions regarding the temperature dependence of σ_{max} in cases 1a and 2a without knowing the values of

---

* The activation energy Bk for these specimens, computed according to (1), on the basis of the $\sigma(T)$ curves recorded without irradiation, is 0.33 eV.

the energies u_1, u_2 . . . entering into equations (9), (12) and (17). In cases 1b and 2b (slow recombination of electrons), if we accept the simplifying assumptions made in deriving equations (23) and (26), the maximum value of the conductivity should decrease with increasing temperature. These deductions are in agreement with our experimental data.

Which of the suggested cases - 1a, 1b, 2a or 2b - corresponds most closely to the actual processes in the investigated ferrites and, in particular, how great the relative increase in the number of defects may be under the influence of radiation can be determined only on the basis of investigations of the properties of the ferrites, dependent primarily upon the presence of lattice defects (holes), rather than on the presence of free electrons (of such properties, for example, as the internal friction).

F. P. Shkliar participated in the experimental part of the present investigation.

Conclusions

1. Irradiation with gamma-rays produces a noticeable (several per cent) increase in the electric conductivity of certain ferrites.

2. The maximum increase in conductivity is greater at lower temperatures.

3. The electric conductivity relaxation time at room temperature is of the order of minutes.

4. The experimental results may be explained within the framework of the zonal theory for conventional semiconductors; they are in agreement with the hypothesis that the increase in the number of electrons in the conductivity zone is due to ionization, i.e. to internal photoelectric ionization. The observed data do not exclude the possibility, however, that radiation may result in the formation of lattice defects with a relaxation time τ_X appreciably exceeding the electron relaxation time τ_x.

Physics of Metals Institute of the
Ural Branch of the Academy of Sciences
of the USSR

Received
3 May 1954

Bibliographic References

1. J.Fassbender, Ann. de Phys., 5, 33 (1949).
2. E.I.Adirovich, Nekotorye voprosy teorii liuminestsentsii kristalov (Problems connected with the teory of the luminescence of crystals).M.-L.1951.
3. F.F.Vol'kenshtein, Elektroprovodnost' poluprovodnikov (The conductivity of semiconductors). M.-L. 1947.

A METHOD OF INVESTIGATING PHASE TRANSITIONS IN NON-METALLIC COMPOUNDS (FERRITES) AND IN METAL ALLOYS

- M. V. Dekhtiar, L. M. Dekhtiar and T. A. Iurina

Ferromagnetic materials obtained by sintering mixtures of certain non-magnetic oxides (Fe_2O_3, NiO, ZnO and others) - i.e., ferrites - are characterized by properties which set them apart from metallic ferromagnetics; ferrites are semiconductors and as such have a much higher specific resistance than metallic ferromagnetic materials.

The electric and magnetic properties of ferrites and their solid solutions are strongly dependent on the sintering conditions. The conductivity of the product may vary by several orders of magnitude and the magnetic permeability by at least one order as a result of changes in the temperature of sintering, the rate of heating and cooling and the nature of the medium in which these processes take place (Ref. 1).

Much still remains to be learned about the exact conditions required to obtain ferrites with a given set of electric and magnetic properties.

For investigating the sintering process it is desirable to make use of a procedure capable of disclosing the formation of both magnetic and non-magnetic ferrites as well as the presence of undissolved residues, i.e., uncombined non-magnetic oxides (Ref. 2).

The need for a similar procedure arises in studying the phase transitions of metal alloys, for example, various iron-base alloys. In the case of iron and other ferromagnetic alloys changes of phase are sometime evaluated on the basis of magnetic measurements. This method of investigation, however, often fails to give a complete picture of the processes involved, since in addition to the main para- to ferromagnetic transformation, certain non-ferromagnetic components may separate out (usually at other temperatures) to form inclusions in the paramagnetic matrix. Such separating out is not recorded by the magnetic method and, hence, remains undetected.

Even in simple Fe-C alloys and in Fe-C-base alloys it is impossible with the magnetic method to detect the formation of Fe_3C crystals in supercooled austenite in the temperature interval below the A_1 critical point and above the Curie point for the carbide crystals (220°C) or the rejection of this phase in hypereutectoid Fe-C alloys in the temperature interval between $A_3(A_{cm})$ and A_1. Nor can the magnetic method disclose the transformations of non-magnetic carbides in composite Fe-C alloys at high temperatures and other transitions of the same type.

In the present investigation of the sintering process and the formation of ferrites, we took advantage of the above-mentioned dependence of both the magnetic and the electric properties of ferrites on the conditions of processing (sintering) the oxides.

Our procedure for investigating the phase transitions in metallic and non-metallic alloys in a wide range of temperatures is based on an electric circuit developed earlier by one of the present authors (Refs. 3 and 4).

For purposes of observation, the specimen in the form of a hollow or solid sylinder (10 mm in diameter, 10 mm in length, with a wall thickness of 0.2-0.5 mm in the case of hollow specimens) is placed in an alternating field, produced by an electromagnet. The experimental procedure comprises measuring the change in the electric

resistance of the specimen in the direction perpendicular to the applied field and investigation of the magnetic state of the specimen while it is heated or cooled. The change in resistance is recorded by an inductive method. This not only eliminates the contact resistance factor but makes it feasible to carry out measurements at high temperatures and with the specimen in a vacuum or in any desired gaseous medium. Furthermore the inductive method excludes the possibility of errors due to diffusion of the contact electrode metal into the specimen at high temperatures.

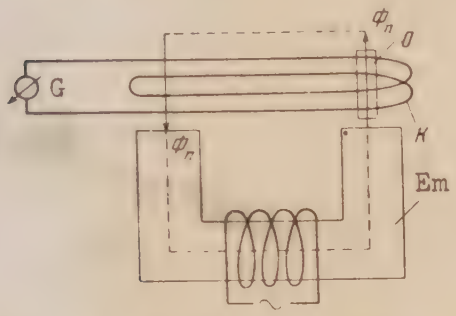

Fig. 1. Diagram of main unit of set-up: Em - electromagnet, K - coil, G - galvanometer, Φ_n - normal component of alternating magnetic flux.

A description of the experimental set-up may be of interest (also see Refs. 3 and 4). A long, narrow coil K (Fig. 1) is supported at its ends on the pole-pieces of a U-shaped electromagnet Em which produces an alternating field Φ_n of frequency ω. Since the flux passing through the right end of the coil is opposite in direction to that through the left end of the coil, two opposed emf's are induced in the coil; in the general case these emf's will not be equal. However, by displacing the coil horizontally, one can readily find the point at which the two emf's cancel; at this point the galvanometer in the circuit will indicate zero. Let us designate the emf induced in the coil K by the alternating flux passing through its right edge by E_r; then

$$E_r = Ir + j\omega LI, \qquad (1)$$

where r is the resistance and L is the self-inductance of the coil. With the coil in the neutral position, an equal but opposed emf, E_l, will be induced by the flux passing through the left edge of the coil.

Let us now put our hollow specimen (O in Fig. 1) inside the coil at, say, its right end. The specimen will then act as a closed conducting loop (shorted turn) in which the flux will induce an emf, giving rise to a current I_o. Let the coefficient of mutual induction between the coil K and the short-circuited loop-specimen be M.

With the introduction of the specimen, E_r of (1) will become

$$E'_r = Ir + j\omega LI + j\omega MI_o \qquad (2)$$

Since E_l will not be affected by the introduction of the specimen, the equality of the emf's will be disturbed, i.e. there will be a resultant emf,

$$\Delta E = E'_r - E_l = j\omega MI_o \neq 0 \qquad (3)$$

and a current will flow in the circuit, producing a corresponding deflection of the galvanometer.

The magnitude of I_o will depend on the electric resistance of the specimen, while M will be determined by the magnetic permeability of the specimen.

Phase transitions and ordering processes in non-magnetic alloys

as well as the solution or rejection of a non-magnetic Fe_3C phase in the non-magnetic austenite of Fe-C alloys do not affect M, but do produce changes in the resistance of the specimen, leading to a change in the value of E and, consequently, the current indicated by the galvanometer.

For example, in cases when in Fe-C alloys decomposition of the solid solution of non-ferromagnetic austenite is accompanied by the separating out of crystals of Fe_3C or other carbides (above the Curie point), the resistance decreases and, hence, the current I_o increases. When a magnetic phase forms, in addition to the increase in I_o there is an increase of the mutual induction M. This is evinced by an appreciable increase in ΔE, indicating the appearance of certain amounts of a new phase.

Heating of the specimens was accomplished by means of an electric "furnace", inserted through an appropriate aperture in the sheathing of coil K, located above one of the polepieces (Fig. 2). Heating of the coil K is obviated by a cooling jacket: a flow of water or compressed air through the jacket effectively insulates the windings of the measuring coil from the "furnace" and specimen.

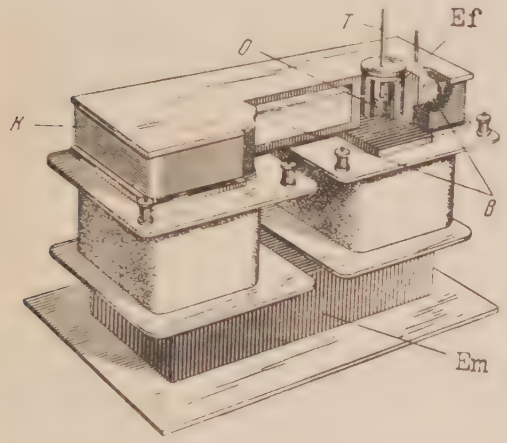

Fig. 2. Sectional view showing cooling jacket, heating element and measuring coil: Em - electromagnet, O - specimen, K - coil, B - cooling jacket, T - thermocouple, Ef - electric "furnace".

The sectional view of Fig. 2 shows the arrangement of the cooling jacket, electric "furnace", and the coil surrounding the jacket casing. The jacket and coil rest on the polepieces of the electromagnet and the whole coil-jacket assembly can be displaced to the right or left by means of lead screws (not shown in the drawing). The cooling jacket must be made of suitable non-conducting material in order not to interfere with the magnetic field. Furthermore, since one side of the four millimeter thick jacket wall is in contact with the hot "furnace" while the other side is cooled by flowing water at room temperature, the material for the jacket must be carefully selected to withstand this extreme temperature gradient.

The electric heating coil of the "furnace" must not introduce magnetic shielding; to this end the resistance winding is bifilar and is made of a material not subject to phase or magnetic transformations in the range of test temperatures.

The flux produced by the electromagnet must be stabilized. The effect of minor voltage fluctuations of the power source is automatically eliminated by the design of the unit, which insures that the flux through the two ends of the coil is equal in density and opposite in direction.

Fig. 3 shows a curve, obtained by means of the above described set-up, giving the change in ΔE in connection with the high-temperature decomposition of the β-phase of a copper-aluminum alloy (12.5% Al), previously investigated by Kurdiumov and his co-workers (Ref. 5). When rapidly cooled, the hot disordered solid solution, which has a face-centered cubic lattice, first undergoes a transition to the

ordered state, which transition is reflected in Fig. 3 by the increase in ΔE in the 510-330°C interval (section AB). Further cooling at tne same rate (about 100°C/min) leads to the formation of an acicular-structure martensite phase (section BC).

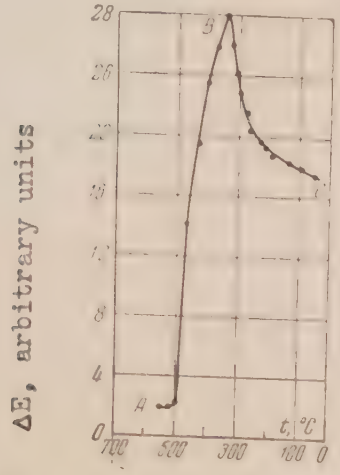

Fig. 3. Changes in the value of ΔE recorded during the cooling of a 12.5% Al copper-aluminum alloy at the rate of about 100°C/min (550 to 350°C).

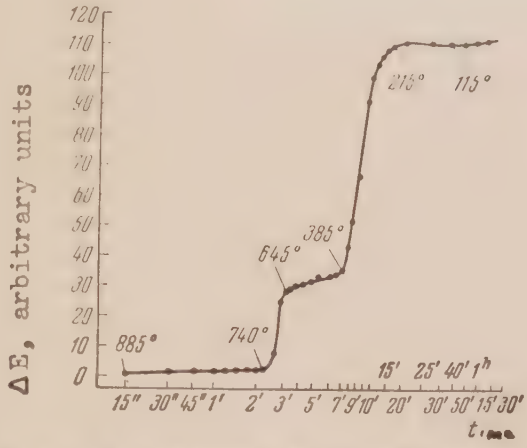

Fig. 4. Change in ΔE betraying decomposition of austenite during continuous cooling of tungsten steel (18% W).

The change in ΔE of a thin-walled tungsten steel (18% W) specimen due to decomposition of the solid austenite solution incident to continuous cooling is shown in Fig. 4. The horizontal time scale is logarithmic. The temperatures corresponding to the various change-of-slope points are indicated in the diagram in °C. The specimen was heated to 900° and held at this temperature for one hour before cooling; it will be noted that the ΔE curve shows clearly that the decomposition occurs in two stages.

The first stage, which with the cooling rate used in the experiments occurs at 740-645°C, consists of the rejection of excess components in the form of carbides (Fe_2W_2C and others), with a resultant increase in conductivity and rise in ΔE.

In the 645-385° temperature interval, the decomposition of austenite virtually stops. It is probable that crystalization centers appear in this interval, since the acicular martensite phase forms rapidly in the next, 385-215°C, interval under the given experimental conditions. In this 385-215° interval ΔE rises rapidly both as a result of the increase in conductivity due to the decomposition of austenite and in connection with the increase in permeability and, consequently, in the mutual induction M, incident to the formation of a magnetic component in the specimen.

Fig. 5 shows the ΔE-temperature curve recorded in heating and then cooling a compressed mixture of Fe_2O_3 and NiO; the oxide mixture was heated only up to 900°C in order to obviate the formation of ferrous oxide and magnetite (Ref. 4).

The mixture, consisting of 50 mols Fe_2O_3 and 50 mols NiO, was heated and cooled at the rate of 5°C per min. The sharp rise in ΔE (section BC, Fig. 5) is evidence of an intense reaction in the formed ferrite in the 775-570° interval during cooling (in air). As in the case of the decomposition of the solid solution of the copper-aluminum

alloy (Fig. 3), this change is doubtless connected with an ordering process: in this case the oxygen and metallic ions taking up positions in the ferrite lattice. The decrease in ΔE in cooling below 570° (section CD) is connected - see equation (3) - with the decrease in the mutual inductance (magnetic permeability), incident to the rejection of excess non-magnetic oxide in consequence of the reduction of the mutual solubility of the oxides with decreasing temperature.

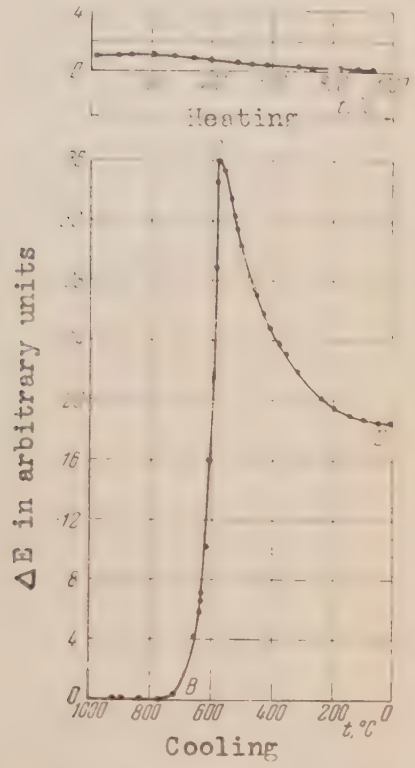

Fig. 5. Change in ΔE in the process of heating and cooling a compressed mixture consisting of 50 mols NiO and 50 mols Fe_2O_3. Rate of cooling - 5° per min.

Similar tests were made on compressed mixtures of Fe_2O_3 and ZnO. However, no reaction was observed for this mixture in cooling at the rate of 5° per min after heating to 900° (at the same rate). This may have been due to over-oxidation of the ferrite in cooling because of its porosity.* In order to eliminate porosity of the structure and prevent excessive oxidation of the $ZnO-Fe_2O_3$ system, these oxides were compressed with an admixture of silicon dioxide and aluminum oxide. As a precaution, a compressed sample of SiO_2 and Al_2O_3 alone was heated to 900°C and then cooled at the rate common to all our tests (5°/min). No reaction was noted.

According to the data available in literature, SiO_2 and Al_2O_3 do not react with ferric oxide in the range of temperatures employed in our tests (Ref. 6). It is reported that the formation of spinel in the $ZnO-Al_2O_3$ system begins above 900° (Ref. 7) to 975° (Ref. 8), while in the $ZnO-SiO_2$ system the formation of spinel is observed only when the mixture is held at 900° or higher over a period of days (Ref. 9).

In our tests the same specimen, formed by compressing an 85 mols Fe_2O_3 and 15 mols ZnO with an admixture of silicon dioxide and aluminum oxide, was heated, with intermediate cooling, successively to 200, 300, 450, 550, 600, 700 and 850°C. In every case the rate of heating and cooling was 5° per min. The recorded curves for ΔE are reproduced in Figs. 6-8.

According to the evidence of the curves, no reaction occurs in heating to 200 and 300° (Fig. 6a). Above 370°, Fe_2O_3 and ZnO in a mixture with the fillers mentioned above begin to combine actively. However, the ferrite formed in this temperature interval is unstable and decomposes partially in cooling down to 100° (section CD. Fig. 6b). In subsequent heating to 560° new portions of the oxides enter into the reaction, as evinced by the increase in ΔE (section EK, Curve 1, Fig. 7). At 470° the conductivity begins to drop (section KL), presumably in connection with transition of the ferrite into the disordered state. A reversible ordering process occurs during the subsequent cooling: the conductivity and hence ΔE increase (section BC). Section CD

---

* Snoek (Ref. 1) notes that the oxidation of certain ferrites can be prevented through elimination of porosity by the introduction of silicon dioxide.

of the curve indicates partial decomposition of the ferrite and rejection of the excess non-magnetic oxides.

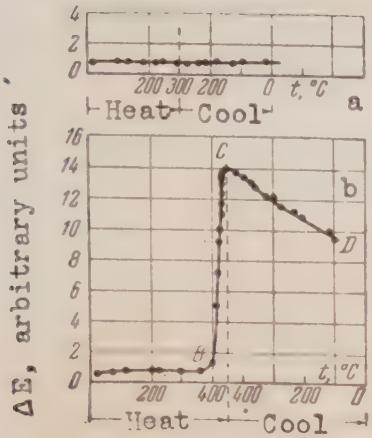

Fig. 6. Change in ΔE during heating and cooling of compressed mixtures of 85 mols Fe_2O_3 and 15 mols ZnO with an added amount of SiO_2 and Al_2O_3 at the rate of 5° per min. Heating, with intermediate cooling, to 200°, 300° and then 400°C.

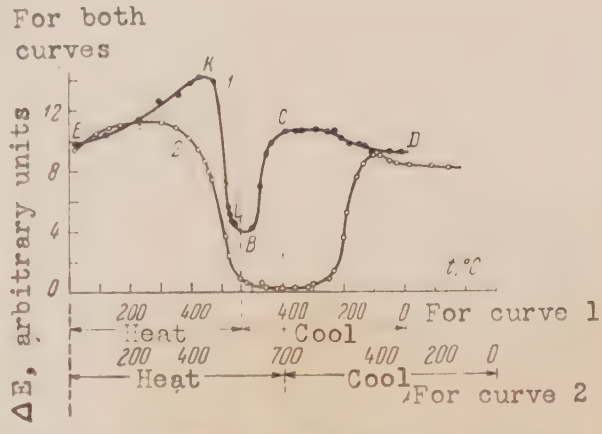

Fig. 7. Same as in Fig. 6 but for successive heating with intermediate cooling, to 580° (Curve 1) and then to 700° (Curve 2).

In the next heating of the specimen to 600° the rise in ΔE is noticeably smaller, since the amount of uncombined oxides in the mixture has been reduced as the result of the previous heatings. The composition of the ferrite is obviously altered and consequently the transition to the disordered state begins at a lower temperature: 420°. Heating from 420 to 600° appreciably reduces the conductivity of the ferrite; however, in cooling the conductivity is restored as a result of ordering.

The next heating - to 700° - does not introduce much change in the general form of the curve (Fig. 7, Curve 2). The ferrite formed during the preceding heat treatment begins to go over into the disordered state at under 350°. The reversible ordering process is again observed during the cooling from 700°.

An entirely different picture appears, however, where the cooling following the next heating - to 850° - is concerned (Fig. 8). The ferrite when cooled to room temperature (at the same rate as in the other tests) retains the high resistance developed in heating and in general undergoes little change in structure during the cooling.

An analogous series of tests was run on specimens having the following composition: 70 mols Fe_2O_3, 15 mols NiO and 15 mols ZnO. To minimize porosity a quantity of SiO_2 and Al_2O_3 was added to the mixture before compressing the specimens (Al_2O_3 and NiO react to form nickel aluminate only at 1000°C). The results of consecutive heatings, with intermediate cooling, of the same specimen to 200, 400, 600 and 900°C at the rate of 5° per min are shown in Figs. 9 and 10.

There is no evidence of reaction between these oxides when the compressed mixture is heated to 200° (upper curve, Fig. 9). When the specimen is reheated to 400°, reaction begins at about 350° (section AB, lower curve, Fig. 9). When the heating is stopped at 400° and the specimen is cooled at the same rate, the process of ferrite forma-

tion continues down to 372°C.* The reaction slows down rapidly in the 370-340° interval. Ordering begins at 340°, causing an additional increase in the electric conductivity and hence rise in ΔE. Below 220°, excess non-magnetic oxide separates out, resulting in a decrease in the mutual inductance and, accordingly, a decrease in ΔE. In the next heating test - to 600° - the reactions taking place are reversible (Curve 1, Fig. 10). As the temperature is raised above 400°, portions of the oxides that did not participate in the formation of complex nickel-zinc ferrite during preceding tests enter

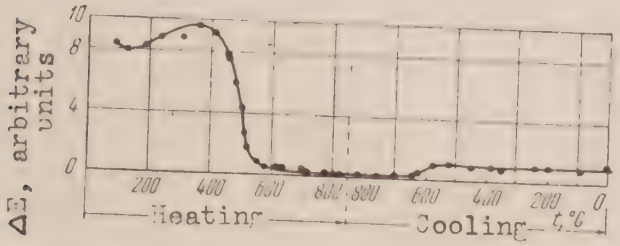

Fig. 8. Same as in Fig. 6 but for heating to and cooling from 850°C.

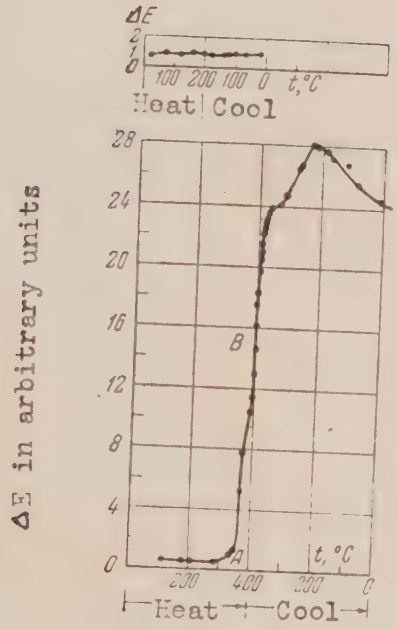

Fig. 9. Change in ΔE incident to successive heating and cooling a compressed mixture of Fe_2O_3, NiO and ZnO with an admixture of SiO_2 and Al_2O_3. a) to 200°, b) to 400°.

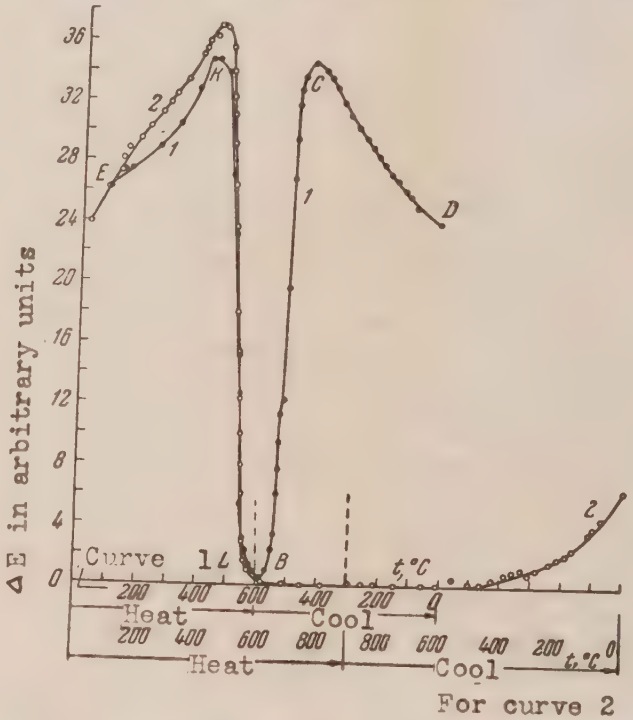

Fig. 10. Same as in Fig. 9 but in heating to 600° (Curve 1) and then to 900°C (Curve 2).

into the reaction. Transition to the disordered state occurs in the 460-600° interval; incident to this, the conductivity of the specimen and consequently ΔE, (section KL of the curve) fall off markedly. In cooling from 600° the processes are reversed: the section of the curve in the 600-450° interval corresponds to the disordered-to-ordered state transition in the ferrite, while the section in the 420-20° interval reflects the separating out of the excess non-magnetic oxide.

---

* As was pointed out in Ref. 11, a $NiO \cdot Fe_2O_3$ product with a spinel type lattice may form as a result of heating at 300-400° for half an hour; for instance, in the case of electrolytic nickel coatings on iron.

Lastly, in heating to 900° (Curve 2, Fig. 10), the processes of the preceding heating appear to repeat (resultant curve virtually duplicates the to-600° curve). However, the cooling in this case is completely different: as compared with cooling from lower temperatures, far less change in the structure of the mixed ferrite is observed. The ferrite becomes more "stable" and retains the low conductivity characterizing the heated mixture; in this case, apparently, no ordering process occurs in cooling.

Conclusions

For the purpose of investigating phase transitions in non-metallic compounds (ferrites) and metal alloys, we developed an experimental set-up by means of which it is feasible to keep track of structural changes in the specimen over a wide range of temperatures. Decomposition of the solid solution, the formation of a new phase and ordering processes are detected by the set-up if there is an accompanying change in the electric resistance or the magnetic permeability of the specimen. Changes in the resistance as well as in the permeability are gaged by the induction method by means of an electric circuit developed earlier (Refs. 3 and 4).

Deflections of the set-up galvanometer clearly indicate the various stages in the decomposition of austenite when the specimen is steadily cooled or held at a constant temperature as well as the occurrence of order-disorder transitions, such as the ordering process in a supercooled high-temperature β-phase of copper-aluminum alloy and the subsequent transformation of this phase into the acicular martensite phase.

We investigated the sintering of powdered oxides (Fe_2O_3, ZnO, and NiO with admixtures) and the reaction of ferrite formation. The measurements, which were made on compressed-powder specimens not subjected to heat treatment prior to testing, established that the actual formation of ferrites and their solid solutions is preceded by atomic diffusion starting at about 300° above room temperature.

In repeated heating to successively higher temperatures, with intermediate cooling, the course of the reactions occurring during the cooling changes markedly as the peak temperature is increased.

On the basis of our results one can conclude that the ferrites forming at low sintering temperatures (under our test conditions) undergo intensive ordering in the process of cooling (evinced by a marked increase in conductivity with cooling). The ferrites obtained from the same oxides by sintering at higher temperatures are more stable and undergo only minor structural changes in cooling; no evidence of an ordering process is observed during the cooling from high temperatures and the electric resistance of the ferrites remains high.

Physics Department
Imeni M. V. Lomonosov
Moscow State University

Received
13 May 1954

Bibliographic References

1. J.L.Snoek, Issledovanie v oblasti novykh ferromagnitnykh materialov (Probably: New Developments in Ferromagnetic Materials). IL, M. 1949.
2. N.A.Toropov & A.I.Borisenko, Dokl. AN SSSR, 63,705 (1948); 76, 85 (1951).
3. M.V.Dekhtiar, Uch. zap. Mosk Un., 76, Physics, 1944.
4. M.V.Dekhtiar, Certificate of authorship No. 67015, filed 6 Feb. 1941.

5. G.V.Kudriumov, Problemy metallovedeniia i fiziki metallov (Problems of metallurgy and the physics of metals). Metallurgizdat, M. 1949.
6. G.F.Hütting,ZS fur Elektrochimie, 41, 543 (1935).
7. O.Krause & W.Theil, ZS anorg. uhd allg. Chem., 203, 120 (1931).
8. W.Jander & W.Scheele, ZS anorg. u. allg. Chemie, 214, 61 (1933).
9. A.Pabst, ZS f. phys. Chemie, 142, 227 (1929).
10. W.O.Millikan & L. Merten, Jour. Phys. Chem., 50 467 (1946).
11. D.Dankov, Ignatov & Shishakov, Elektrograficheskie issledovaniia okisnikh i gidrookisnykh plenok na metallakh (Electrographic investigation of oxide and hydroxide films on metals). Pub. Acad. Sciences, M.L. 1953.

* * * * * *

ON THE FEASIBILITY OF INVESTIGATING MICROFIELDS IN MAGNETIC MATERIALS BY MEANS OF THE ELECTRON MICROSCOPE

- L. P. Soboleva

Experimental measurement of weak electric and magnetic fields of limited extent is difficult. Every test instrument indicates the value of the disturbed (by the test instrument) field averaged over some more or less appreciable volume (region). When the dimensions of the measuring instrument are commensurate with those of the investigated field, it is obviously impossible to ascertain the field distribution and consequently determine the sources producing the field.

At the same time in investigating the electric and magnetic properties of materials having dissipation fields (ferromagnetic and ferroelectric materials) it is often desirable to measure these fields, which are limited in extent and of low intensity.

A sensitive method of measurement, which does not introduce distortion or yield an averaged result, is based on the deflection of an electron beam passing through the investigated field. Inasmuch as the deflections in a weak field of limited length are necessarily small, it is desirable to have a means for "magnifying" them.

Such a measuring method may be realized by means of an appropriately modified electron microscope.

A parallel, monochromatic paraxial beam, passing through the magnetic lens of the microscope, is focused at a point on the axis of the system. In the case of a non-parallel beam (within the limits of paraxiality) one can readily determine the locus of the points of intersection of the rays with the axis of the system, from the laws of geometric optics.

In the particular case when the factor or agent, causing deflection of the rays from the direction parallel to the system axis, does not operate in the region of the focusing field, the distribution of the said points of intersection will depend only on the angles between the main optical axis and the individual trajectories. It follows that an electron microscope can be used for investigating weak and minute electric and magnetic fields.

The specimen, a section of which carries the field to be investigated (for instance, the dissipation field of a magnetic material with high remanence or the dissipation field of a magnetic domain) is placed on the stage of the electron microscope, in the plane conjugate with the plane of the fluorescent screen. Each ray of the parallel, mono-

chromatic (i.e. having the same speed) electron beam passes through a microfield of a certain intensity and is deflected accordingly.

The "indicator" component of the set-up is a fine-mesh, uniform grid, located between the focal point and the fluorescent screen. In the case of an undistorted (not deflected) beam, the grid is illuminated from the focus as from a point source. In this case we obtain an undistorted shadow image of the grid on the viewing screen of the microscope.

When the beam is deflected by the investigated field, the grid will be illuminated from a continuous series of point sources, each radiating in a certain direction. In this case we obtain a distorted shadow image of the grid on the microscope screen. From the nature of the image distortion one can judge of the spatial distribution of the investigated field.

Ref. 1 reports on the application of the outlined method to the investigation of the magnetic fields of sound-recording wire. The studied wire was 0.12 mm in diameter and was magnetized in alternate (opposed) regions 0.178 mm in length.

The same authors suggest in Ref. 2 that the method may be used for investigating the dissipation fields of ferromagnetic domains. Photographs showing distortion of the grid image in the neighborhood of a magnetized wire and at the edge of single cobalt crystal are reproduced in the reference.

We applied the described method to investigation of the microfields of polycrystalline cobalt, transformer steel and small-domain ferromagnetic powders. Moreover, in order to check and evaluate the experimental procedure we applied it to the investigation of a known field, the structure of which is similar to that of a dissipation field with a 180° neighbor (consequent pole) orientation of the spontaneously magnetized regions.

The specimens were mounted in the stage-space of the electron microscope, at a distance of 406 mm from the principal plane of the lens. During the tests, both the condenser lens, insuring a parallel electron beam, and the objective lens, forming the image, were switched on. The grid (mesh spacing s = 33 or 17 μ) was mounted between the objective lens and the fluorescent screen.

In order to determine the highest sensitivity and best resolving power the specimen-to-grid distance was varied between 5 and 20 mm.

Tests were made both with and without the internal polepieces of the objective lens in place. The specimen was located in the dissipation field of the objective lens.

The sensitivity of the method was evaluated by the possibility of observing and measuring the distortion of the grid shadow image. In the diagram of Fig. 1, a is the distance from the edge of the distorted image to the optical axis, νg is the corresponding distance from the edge of an undistorted image; hence, the image displacement, determining the distortion, will be $a - \nu g$, where ν is the magnification of the undistorted grid and g is the distance of the given grid filament from the optical axis.

The ratio $k = (a-\nu g)/\varphi'$, where φ' is the angle of deflection of the ray, can be taken as a measure of the sensitivity.

On the other hand, to bring out the structure of the field there must be at least a certain number, n, of grid meshes per single homogeneous region. In other words, a necessary condition for obtaining the true pattern of the field structure is

where β is the size of the individual region, s is the spacing of the grid filaments, μ is the magnification of the specimen and ν is the magnification of the grid; whence

$$\frac{\nu}{\mu} = \frac{\beta}{n\,s} \qquad (1)$$

It follows from the diagram of Fig. 1 that there is a simple relationship between k and ν/μ when $\mu \geqslant 1$, namely:

$$\frac{a - \nu g}{\varphi'} = \frac{\nu}{\mu}(B - \ell) \qquad (2)$$

where B is the distance between the principal plane of the lens and the plane of the screen and ℓ is the specimen-to-grid distance (in the electron microscope at our disposal B = 576 mm and ℓ = 5-20 mm).

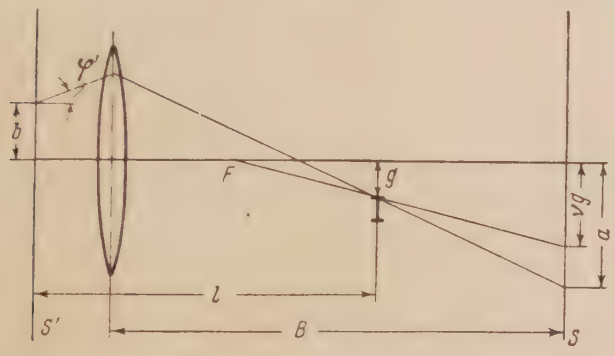

Fig. Optical diagram of set-up. F - focus, b - position of undistorted ray in plane, conjugate with plane of screen, S - fluorescent screen, S' - conjugate plane, φ' - angle of deflection of ray in investigated field, ℓ -distance of specimen from grid, B - distance between principal plane of lens and viewing screen, g - distance from optical axis to grid filament, a - distance of edge of distorted shadow image of grid from optical axis, ν - magnification of grid, νg - distance of undistorted shadow image of grid from optical axis.

Hence, the sensitivity - proportional to $(a - \nu g)/\varphi'$ - and the value of ν/μ, which determines the resolving power, are interdependent and cannot be established separately.

The purpose of the present study was to evaluate the applicability if the described method to the investigation of the microfields of ferromagnetic materials.

If we assume the linear dimensions of individual homogeneous magnetic regions to be approximately 10μ, then for a grid having a spacing s = 10μ, we obtain from (1):

$$\frac{10}{n \cdot 10} = \frac{1}{n}$$

That is, to bring out the individual homogeneous magnetization regions it is sufficient that the number of meshes per region be $n \geqslant 2$; then $\nu/\mu \leqslant 0.5$.

Substituting the latter value in (2) we find

$$k = \frac{a - \nu g}{\varphi'} \leqslant 280 \text{ mm}.$$

It remains to determine the strength and extent of the fields that can be detected under these conditions. Assuming that the angle of deflection φ' of an electron, having an initial velocity v_y perpendicular to the field, is proportional to the effective field B_{eff} and the effective path length ℓ_{eff} through the field and that the velocity perpendicular to the field remains unchanged, the expression

$$\varphi' = \frac{e}{m} B_{eff} \ell_{eff} \frac{1}{v_y} \qquad (3)$$

Then from (2) and (3) we obtain

$$(B_{eff}\ell_{eff})_{min} = \frac{v_y(a - \nu g)_{min}}{k_{max}} \cdot \frac{m}{e}$$

The minimum electron velocity with which one can still obtain a useful image corresponds to an accelerating potential of about 10 kV; i.e.,

$$v_y = 5.95 \cdot 10^5 \text{ m/sec}$$

$$\frac{m}{e} = 0.57 \cdot 10^{-11} \text{ kg coulomb}^{-1}.$$

In the present case, taking $a - \nu g = 0.5$, we get

$$B_{eff}\ell_{eff} = \frac{6 \cdot 10^7 \cdot 5 \cdot 10^{-4} \cdot 0.57 \cdot 10^{-11}}{28 \cdot 10^{-2}} = 0.6 \cdot 10^{-6} \text{ weber m}^{-1}$$

or

$$B_{eff}\ell_{eff} = 0.006 \text{ gauss} \cdot \text{meter}$$

i.e. with $\ell_{eff} = 10\mu$ the set-up will detect fields of $B_{eff} = 600$ gauss or with $\ell_{eff} = 100\mu$, fields of $B_{eff} = 60$ gauss.

For greater sensitivity in detecting minimal displacements of the shadow image, $(a - \nu g)_{min}$, the entire distorted image of the grid can be enlarged further, either photographically or by optical projection. The limiting enlargement in this case is the magnification at which irregularities and aberrational distortions of the grid are no larger than the minimal deflection of the shadow image.

Thus, in our case, assuming a 10 X magnification by a projection lens, $(a - \nu g)_{min} = 0.05$ mm and the effective sensitivity limit is $(B_{eff}\ell_{eff})_{min} = 0.6 \cdot 10^{-3}$ gauss meter, i.e. $B_{eff} = 60$ gauss for ℓ_{eff} 10μ or $B_{eff} = 6$ gauss for $\ell_{eff} = 100\mu$.

It will be seen, therefore, that when a fine-mesh grid is used the sensitivity of the method is adequate for the detection and observation of microscopic inhomogeneities of a magnetic material.

In order to explore the potentialities of the method and evaluate its sensitivity in practice we carried out a series of experiments with artificially produced fields. A stack of magnetized laminations of a hard magnetic material was assembled so that the poles of neighboring laminations would alternate; the direction of magnetization was parallel to the Z-axis, while the direction of the electron beam was in line with the Y-axis.

The effect of such a dissipation field on an electron ray may be characterized as follows. The alternate plates represent opposite poles; the resultant field pattern is as shown in Fig. 2. An electron beam directed downward, normal to the plane of the drawing at a point between a south pole on the left and a north pole on the right will be acted upon by an attracting force, while a downward beam between a north pole on the right and a south pole on the left will experience

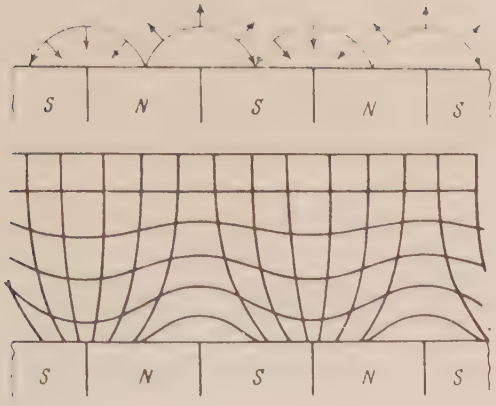

Fig. 2. Schematic representation of the forces of attraction and repulsion acting on an electron in the vicinity of a stack of magnetized laminations and the expected grid-image distortion pattern.

repulsion. Accordingly, the grid image at the edge of the specimen will be "pulled in" and contracted in the intervals between a south pole on the left and a north pole on the right, and "pushed out" and expanded in the intervals between a north pole on the left and a south pole on the right. The expected distortion pattern is pictured in the lower part of Fig. 2. The actual distortion pattern at the edge of a stack of magnetized laminations as recorded in the electron microscope is very close to the expected one (see Fig. 3 below).

The relation between the distortion of the grid, $a - \nu g$, and the entry angle φ' of the electron into the field of the lens, for a paraxial beam, can be derived from the laws of geometric optics:

$$a - \nu g = \varphi' \cdot C, \qquad (4)$$

where C is a coefficient, constant for the given experiment and dependent on the parameters of the microscope, the magnification and the location of the grid.

By making certain simplifying assumptions, we can establish a relationship between the field traversed by the electron and the deflection produced by the field.

We assume that the field of the stack is plane-parallel and is characterized by the components H_x and H_z. The error resulting from the distortion of the field at the edges can be minimized through proper selection of the assumed effective length of the field.

Inasmuch as the initial velocity of the electron v_y is much greater than the velocities v_x and v_z acquired in the field, we can neglect changes in the coordinates of the electron during the time of passage through the field. Actually the resultant error can be taken into account in processing the experimental data by comparing the values of the field at symmetrical points of two regions, in one of which the electron is displaced to the side of stronger fields and in the other, to the side of weaker fields.

On the basis of the above assumptions, we can say that an electron entering the field with a velocity v_y is acted upon by the field components H_x and H_z, which are assumed to be constant over the length of the electron's trajectory, and acquires corresponding angles of deflection φ'_x and φ'_z (the angles between the projections of the electron's trajectory on the XY and ZY planes and the optical axis); the equations defining these angles are

$$\varphi'_x = \frac{e}{m} B_z \frac{l}{v_y} \quad \text{and} \quad \varphi'_z = \frac{e}{m} B_x \frac{l}{v_y}. \qquad (5)$$

Since the horizontal filaments of the grid are aligned with the X-axis and the vertical filaments with the Z-axis, the angle φ'_x is given by the horizontal displacement of the image of the vertical filaments, $(a - \nu g)_x$, while φ'_z is given by the vertical shift of the image of the horizontal filaments $(a - \nu g)_z$.

Invoking (4) and (5), we obtain

$$H_x = (a - \nu g)_z \frac{v_y}{Cl} \cdot \frac{m}{e} \frac{1}{4\pi \cdot 10^{-7}} \text{ A/м} \quad \text{and} \quad H_z = (a - \nu g)_x \frac{v_y}{Cl} \cdot \frac{m}{e} \frac{1}{4\pi \cdot 10^{-7}} \text{ A/м}. \qquad (6)$$

Or under our experimental conditions

$$H_x = 10^3 (a - \nu g)_z \text{ A/м} \quad \text{and} \quad H_z = 10^3 (a - \nu g)_y \text{ A/м}. \qquad (7)$$

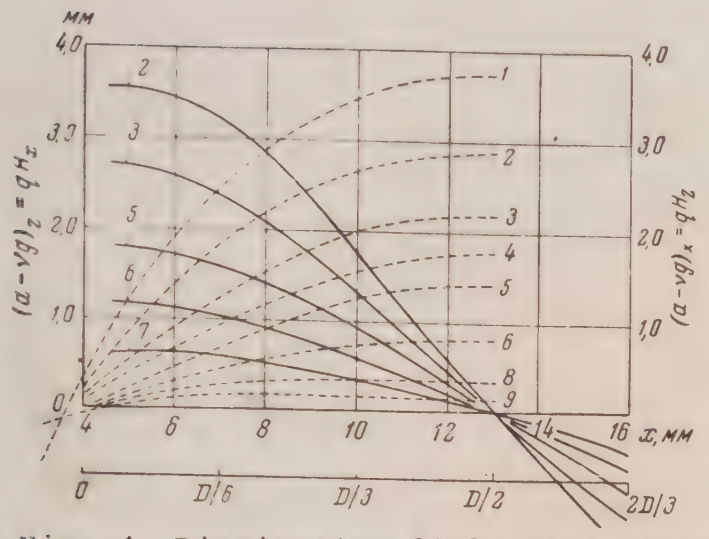

Fig. 4. Dissipation field of a stack of magnetized laminations, plotted on the basis of grid image distortion in Fig. 3. Solid lines - variation of $(a - \nu g)_z = qH_x$ with x; dash lines - variation of $(a - \nu g)_x = qH_z$ with x; 1) z=0.33D, 2) z=0.4D, 3) z=0.5D, 4) z=0.56D, 5) z=0.6D, 6) z=0.7D, 7) z=0.8D, 8) z=0.88D, 9) z=0.94D. $q = 10^{-3}$ A m·mm; D - size (linear dimension) of individual magnetic region.

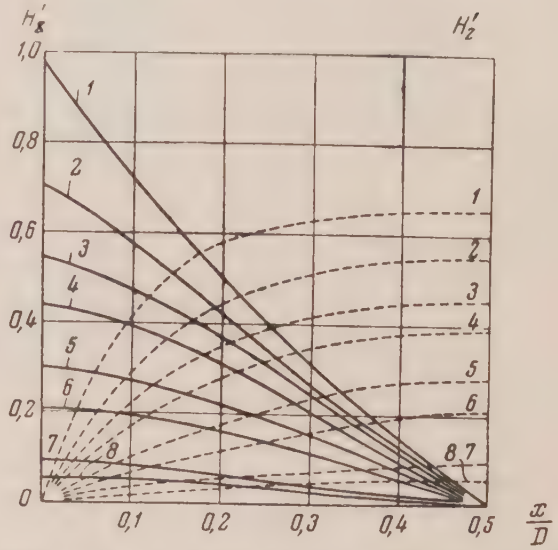

Fig. 5. Dissipation field of a stack of magnetized laminations, based on analytic computation. Solid lines - variation of H'_x with x/D; dash lines - variation of H'_z with x/D. 1) z=0.008D 2) z=0.16D, 3) z=0.22D, 4) z=0.29D, 5) z=0.4D, 6) z=0.5D, 7) z=0.7D, 8) z=0.9D.

The field in the vicinity of the magnetized stack, for the region over the midpoint of the stack, plotted on the basis of the distortion of the grid image in the photograph of Fig. 3, is shown in Fig. 4. The field in the neighborhood of such a stack, but plotted on the basis of values computed using equations derived by Polivanov, is given in Fig. 5.

From a comparison of the curves in the two figures it may be concluded that, in spite of the simplifying assumptions made above, the character of the field can be determined with reasonable accuracy by the outlined method.

Having the dissipation field, it is possible to determine the magnetization of the specimen.

The equation for the theoretical calculation of the field H' contains the intensity of magnetization, I, as a factor in the numerator; the value of I may be found by comparing the field H, obtained by the grid image distortion method, with the field H'.

Calculations based on experimental data for a series of points yielded values of $|I| \approx 5$ gauss, the computations for the different points being in close agreement.

In computing I on the basis of available data on the material of

tions were magnetized to saturation), we obtained a value of about 8 gauss.

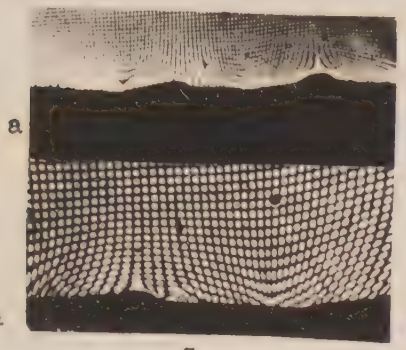

3

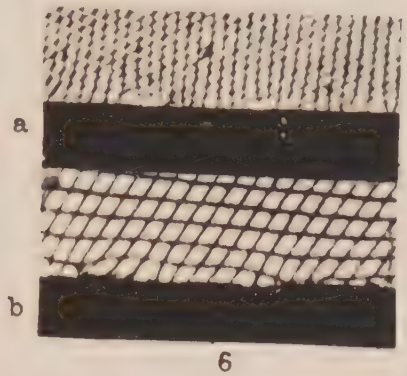

6

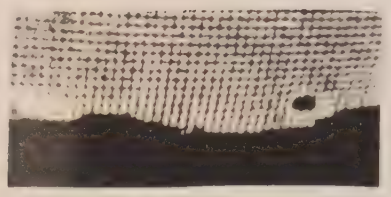

7

Fig. 3. Electron microscope photographs of the distortion of the grid image in the vicinity of a stack of magnetized laminations: a) Magnification 100 X, b) 200 X.

Fig. 6. Distortion of grid image at edge of specimen of a) pure cobalt, mag. 55 X, and b) transformer steel, mag. 70 X.

Fig. 7. Image of grid at edge of a piece of aluminum foil, mag. 70 X.

8

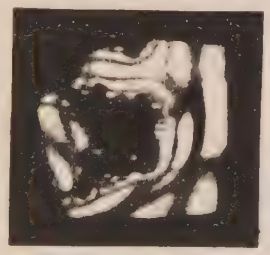

9

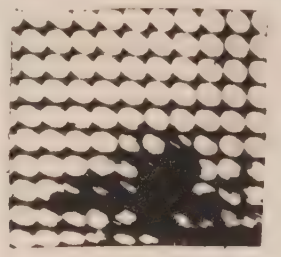

10

Fig. 8. Distortion of grid image in the vicinity of particles of manganese bismuthite: electron-optical magnification -- 200 X, anode voltage -- 16 kv, grid-to-specimen distance -- ℓ = 7 mm.

Fig. 9. Distortion of grid image in the vicinity of an iron carbonyl powder: electron-optical magnification -- 100 X; anode potential -- 10 kV; grid-to-specimen distance -- ℓ = 11 mm; photographic enlargement -- 4 X.

Fig. 10. Grid image in the vicinity of an aluminate powder: electron-optical magnification -- 170 X, photographic enlargement -- 4 X.

In view of the fact that the magnetization of neighboring laminations is reduced somewhat because of the effect of the dissipation field of the objective lens of the microscope, it may be asserted that the method permits of a fairly accurate quantitative evaluation of the intensity of magnetization of the specimen.

The field distribution pattern of the experimental stack proved similar to that of a section of magnetic material with a 180° neighbor (consequent pole) arrangement of spontaneously magnetized domains. It may be concluded, therefore, that the outlined method is suitable for the investigation of domain structure.

The applicability of the method to the study of dissipation fields due to magnetic inhomogeneity of the material was verified by examining polycrystalline specimens of pure cobalt and transformer steel. The specimens were prepared in the form of thin plates, of a size to cover half the specimen aperture of the electron microscope. In order to minimize the averaging effect of the fields on the beam, the thickness of the plates was made equal to the presumed domain dimensions (10 μ). After mechanical preparation, the specimens were annealed. Photographs of the grid image at the edge of the cobalt and transformer steel plates are reproduced in Fig. 6. For purposes of comparison, the grid image at the edge of a piece of aluminum foil is shown in Fig. 7. [Translator's note: The figure references in the original text are sadly scrambled; we are, accordingly, going by the numbers in the captions under the photographic plates.]

It is assumed that the distortion of the grid in the photographs is due primarily to 1) magnetization of the material in the field of the microscope lens, which leads to an overall skewing of the grid image and 2) irregularity of the edge or the presence of magnetic inhomogeneity, giving rise to N and S pole dissipation fields which produce minor distortions of the grid image at the edge of the specimen.

A careful study of the grid image patterns leads us to believe that the observed distortions are not connected with unevenness of the edge and that, consequently, the distortion must be attributed to magnetic inhomogeneity. In the case of transformer steel such inhomogeneity may be explained by the presence of impurities; in the case of pure cobalt, however, the magnetic inhomogeneity can only be structural. These conclusions, however, are only tentative and require further verification.

The magnetic inhomogeneities in the investigated polycrystalline specimens may be connected with the chaotic orientation of the individual crystals in the vicinity of the edge. Dissipation fields due to such inhomogeneity are much weaker than the dissipation fields of spontaneously magnetized domains. This should explain the weak and irregular character of the observed distortion. It should be on interest to investigate a specimen consisting of a single crystal of magnetic material in which the orientation of the domains can be accurately determined. A study of single crystals by this method is planned for the future.

The magnetic properties of ferromagnetic powders are usually investigated by means of the ballistic method, using specially prepared specimens, consisting of a mixture of the investigated powder and a viscous non-magnetic medium. Obviously, the test results in such cases are averaged values, characterizing the magnetic properties of the entire mixture and dependent upon the concentration and distribution of the powder in the binding or suspending medium. In many cases, however, it is desirable to know the magnetic characteristics of the individual particles and to analyze the dependence of the magnetic properties on the size, shape and grouping of the powder particles.

As a step in this direction we tried applying the electron microscope method to the determination of dissipation fields produced by individual particles and groups of particles.

By way of specimens for our preliminary investigation we chose high remanence powders of manganese bismuthite and soft iron carbonyl. To determine the form and size of the particles, the powders were first

examined microscopically with backlighting. The manganese bismuthite powder consisted of an unfractionated mixture of MnBi and particles of Bi and Mn.

The particles ranged from 1 to 20 μ in cross section and were extremely varied in shape.

The iron carbonyl particles were spherical, 0.4 to 1.2 μ in diameter.

When the powder is evenly distributed in a suitable lacquer, the individual particles can be distinguished; usually, however, the powder tends to clump. Sometime the particles link up to form chains.

The results of our investigations showed that the electron microscope method is applicable to the study of the dissipation fields surrounding individual particles and groups of particles of ferromagnetic powders.

Figs. 8 and 9 show the distortion of the grid image in the neighborhood of the two ferromagnetic powders investigated. For purposes of comparison a photograph of the undistorted grid image in the vicinity of a non-magnetic aluminate powder is reproduced in Fig. 10.

Individual particles and clumps of the powder as well as two grids may be seen in Fig. 8. The large undistorted grid /i.e. the black cross quartering the photograph/ supports the lacquer film in which the powder was suspended. The finer network is formed by the 17 μ mesh indicator grid and its distortion indicates the character of the dissipation field.

From a comparison of the photographs of the iron carbonyl and manganese bismuthite powders, making due allowance for the difference in magnification in the two cases, it may be concluded that the manganese bismuthite dissipation fields are somewhat stronger than those particular to iron carbonyl.

Different iron carbonyl powder clumps produce dissipation fields of different intensity. Obviously the configuration of the clump is an important factor in this respect. It is difficult to determine the field pattern of individual iron carbonyl particles, since the sensitivity of the method falls off at higher magnifications.

The degree of uniformity of an undistorted grid image in the absence of a dissipation field may be evaluated from the photographs of the aluminate powder. It is possible that some of the distortion of the grid image around the investigated powder particles and clumps is due not only to magnetic but also to electrostatic dissipation fields.

Our experimental investigations of the dissipation fields of a stack of magnetized laminations and specimens of cobalt and transformer steel indicate that the described electron-microscope method is suitable for the study of dimensionally minute fields, the determination of which by other methods is difficult or impossible.

Moscow Energetics Institute
Imeni V. M. Molotov

Received
19 August 1954

Bibliographic References

1. Z. Marton & S. Zachenbruch, Journ. Appl. Phys., 20, 1171 (1949).
2. Z. Marton & S. Zachenbruch, Journ. Appl. Phys., 20, 1258 (1949).

ON DETERMINING THE PHASE COMPOSITION OF FERRITES

- B. E. Levin

Serious difficulties are often encountered in determining the phase composition of ferrites in complex systems. Thus, when the system contains a number of ferrites with nearly identical lattice parameters, X-ray analysis is of little help in determining the phase composition. Nor can the problem be satisfactorily solved with the aid of chemical analysis. Hence, particularly in view of the ever increasing industrial use of complex ferrites, a reliable method for determining the phase composition of multiple component systems is urgently needed.

A method based on utilizing certain thermochemical characteristics of ferrites (Ref. 1) may prove useful in a number of instances. In simple cases (for example, for magnesium ferrite) the phase composition may be computed according to the law of additivity.

Thus, for a ferrite composed of 0.3 mols MgO and 0.7 mols Fe_2O_3, the phase composition of the equilibrium state is given by 0.3 $MgO \cdot Fe_2O_3$ + + 0.4 Fe_2O_3. It must be noted that this distribution of components obtains only when the magnesium ferrite formation reaction goes to completion. Whether this is the case is determined by the thermochemical characteristics of the process, of which more will be said below.

Analogously, in the case of a 0.6 mols MgO and 0.4 mols Fe_2O_3 ferrite, the phase composition may be characterized by 0.4 $MgO \cdot Fe_2O_3$ + + 0.2 Fe_2O_3.

This simple approach cannot be used in the case of systems comprising two (or more) ferrites.

Let us investigate the system: n Fe_2O_3, n_2CdO and n_1MgO, where $n_1 + n_2 + n = 1$. We note that two cases are possible: a) n_1MgO + + $n_2CdO < n\ Fe_2O_3$ and b) $n_1MgO + n_2CdO > n\ Fe_2O_3$.

In the first case the formula characterizing the phase composition will be $n_1MgO \cdot Fe_2O_3 + n_2CdO \cdot Fe_2O_3 + [n - (n_1 - n_2)] \cdot Fe_2O_3$.

Apparently, for a system of the above constituents in the equilibrium state, the last equation will be closely representative of the actual conditions obtaining.

Determination of the phase composition in the second case, when free metallic oxides are present in the system after the reaction, is more difficult. In this case the system will consist of $MgO \cdot Fe_2O_3$, $CdO \cdot Fe_2O_3$, MgO and CdO. Calculation of the amount of the free oxides of the bivalent metals presents a separate problem and can be accomplished by taking into account the thermochemical characteristics of the ferrites in question. Thus, for the particular system under discussion, the amount of MgO and CdO can be determined by solving the following system of equations.

Let us denote the concentration of MgO through x, that of CdO through y, that of $MgO \cdot Fe_2O_3$ through z and that of $CdO \cdot Fe_2O_3$ through v, we then have $x + z = n_1$, $y + v = n_2$ and $z + v = n$.

Further, knowing the free energy of the given ferrite-formation reactions we can obtain a fourth equation:

$$A = \frac{k_1}{k_2} = \frac{xv}{yz}$$

where k_1 and k_2 are the respective equilibrium constants of the reactions $MgO + Fe_2O_3 \rightleftarrows MgO \cdot Fe_2O_3$ and $CdO + Fe_2O_3 \rightleftarrows CdO \cdot Fe_2O_3$.

Approximate calculations of the heat of formation of a number of ferrites, carried out according to the method of Kubaschewski (Ref. 2), yielded the following values:

$FeO \cdot Fe_2O_3$: ΔH_{298}° = -7Kcal/mol; $MnO \cdot Fe_2O_3$: ΔH_{298}° = -7.7Kcal/mol;
$CoO \cdot Fe_2O_3$: ΔH_{298}° = -7.1Kcal/mol; $CdO \cdot Fe_2O_3$: ΔH_{298}° = -12.5Kcal/mol;
$NiO \cdot Fe_2O_3$: ΔH_{298}° = -14Kcal/mol; $MgO \cdot Fe_2O_3$: ΔH_{298}° = -2.5Kcal/mol.

When the heat of formation of the constituent ferrites is approximately the same, the amounts of the free oxides of the bivalent metals may be assumed to be proportional to the initial concentrations of the oxides. Where reliable thermochemical data are available, a general solution of the problem of determining the phase composition of ferrites can readily be deduced even for far more complex systems. In such cases the problem is reduced essentially to a solution of the system of equations determining the concentrations of the individual components.

In systems where the mutual solubility of the formed ferrites must be considered, the analysis becomes more complicated in view of the necessity of taking into account data derived from the structural and equilibrium diagrams for the system.

Conclusions

1. The suggested method of calculating the phase composition of ferrite system is based on utilization of their thermochemical characteristics.
2. The cited computation data on the values of the heat of formation of certain ferrites show that the heats in question lie between 7 and 14 Kcal/mol.
3. Complete solution of the general problem of determining the phase composition of ferrites is possible where reliable thermochemical data and dependable structural diagrams for the systems investigated are available.

Received
3 May 1954

Bibliographic References

1. V.P. Eliutin & B.E.Levin, Stal' (Steel), 10 (1947).
2. Q.Kubaschewski & H.E. Evans, Metallurgical Thermochemistry. London 1951.

BULLETIN of the Academy of Sciences of the USSR - Physical Series
Vol. 18, No. 4, 1954 - Conference on Ferrites (1-5 Feb. 1954)

TABLE OF CONTENTS

	Page Orig.	Trans.
Magnetic spectra due to the macroscopic structure of the material. - N.G.Katkov & K. M. Polivanov	419	113
Ferrites in pulse circuits. - N.G.Katkov	432	125
On waves in a gyrotropic medium. - M.A.Gintsburg	444	136
Measurement of the magnetic permeability and the dielectric constant of certain ferrodielectrics at centimeter wavelengths. - S.C.Salikhov	456	147
Electromagnetic properties of oxide ferromagnetic materials. - N.N.Shol'ts	465	155
Magnetic ferrites in alternating fields. -L.I.Rabkin	473	162
Investigation of the effect of sintering temperature on the mechanical, structural and electromagnetic properties of Oxyfer-2000. - A.A.Shvarts	489	175
Changes in the conductivity of certain ferrites under the influence of gamma rays. - N.V.Volkenshtein & A. N. Orlov	494	181
A method of investigating phase transitions in non-metallic compounds (ferrites) and in metal alloys. - M.V.Dekhtiar, I.M.Dekhtiar, and T.A.Iurina	502	189
On the feasibility of investigating microfields in magnetic substances by means of the electron microscope. - L.P.Soboleva	511	197
On determining the phase composition of ferrites. - B.E.Levin	519	205

Translated in 1955 by
Columbia Technical Translations,
5 Vermont Ave., White Plains, N.Y.

Price: $20 per copy.

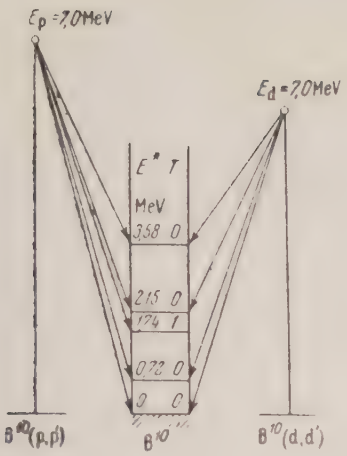

Fig. 5. Analysis of the isobaric spins of the excited states of B^{10} according to the (p,p') and (d,d') reactions.

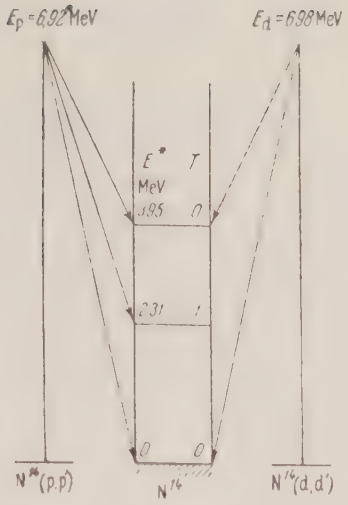

Fig. 6. Same as Fig. 5 but for N^{14}.

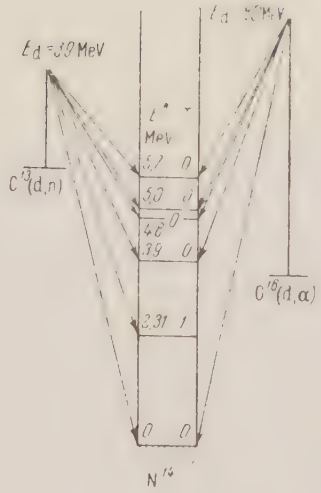

Fig. 7. Analysis of isobaric spins of the excited states of N^{14} according to the (d,n) and (d,α) reactions.

The isobaric spin of excited states of nuclei can be determined not only with reference to inelastic scattering but also through analysis of nuclear reactions.

Thus, (d,n) and (d,α) reactions leading to excited states of N^{14} are schematized in Fig. 7. The 2.31 Mev state of N^{14} is produced by the C^{13} (d,n) reaction but not through the O^{16}(d,α) reaction[56-58]; this is explained by the fact that the 2.31 Mev state has T = 1.

At the end of Section 4, we used the last example, together with the fact that this state is not observed in the N^{14}(d,d') reaction, to show that the isobaric spin of an α-particle is 0. This being the case, analogous examples can be found to help determine the isobaric spin of other individual states.

Excited states of nuclei with A odd. Mirror nuclei furnish good examples of nuclei for which the isobaric spin of excited states can be found through analysis of nuclear reactions. In most cases the spin can be determined through analysis of the (d,p) and (d,n) reactions, which with a target of the same material (usually with T = 0) lead to similar states of mirror nuclei with T = $\frac{1}{2}$. A typical example is furnished by the mirror pair B^{11}–C^{11} (see Fig. 8). For all the excited states of B^{11} and C^{11} investigated so far T = $\frac{1}{2}$.

It should be borne in mind, however, that the (d,p) and (d,n) reactions induced in nuclei with T = 0 yield only states with T = $\frac{1}{2}$. In order to find states with T = 3/2, one must investigate reactions of the $C^{13}(p,n)N^{13*}$ type (T = $\frac{1}{2}$ for the ground state of C^{13}).

Detection of the first state having T = 3/2 of ${}_ZM^{2Z+1}$ and ${}_{Z+1}M^{2Z+1}$ mirror nuclei would furnish a clue to the ground state mass of ${}_{Z-1}M^{2Z+1}$ and ${}_{Z+2}M^{2Z+1}$ nuclides, such as ${}_1H^5$ and ${}_4Be^5$, ${}_2He^7$ and ${}_5B^7$, ${}_3Li^9$ and ${}_6C^9$, ${}_4Be^{11}$ and ${}_7N^{11}$, ${}_5B^{13}$ and ${}_8O^{13}$, ${}_6C^{15}$ and ${}_9F^{15}$, ${}_7N^{17}$ and ${}_{10}Ne^{17}$, etc. Of the isotopes listed only Li^9, C^{15} and N^{17} have been observed to date.[52] Experimental determination of their masses indicate that the first excited levels with T = 3/2 of the mirror pairs Be^9–B^9, O^{15}–N^{15} and O^{17}–F^{17} have energy values of 15.0, 10.9 and 11.3 Mev, respectively (Fig. 9).

States with a high value of T. Experimental investigations of nuclear reactions are always carried out under conditions where isobaric spin of bombarding and emitted particles is either 0 (α-particles, deuterons) or $\frac{1}{2}$ (protons, neutrons, H^3 or He^3). In such reactions the isobaric spin cannot change by more than one unit.

ISOBARIC SPINS AND SIMILAR STATES OF ATOMIC NUCLEI

- B. S. Dzhelepov

1. Introduction

Within the last 2-3 years the concept of isobaric spin* has become firmly established in nuclear physics. A number of formerly puzzling facts have been elegantly explained with the aid of this concept; these include the non-occurrence of certain nuclear reactions, the unexpectedly low intensity of some γ-transitions, and the singular dependence of the photoexcitation and photodisintegration cross sections of some nuclei on the energy of γ-rays. It may be assumed that the number of branches of nuclear physics in which consideration of the isobaric spin concept will prove fruitful is destined to increase. Hence it is important that a wide circle of experimental physicists become familiar with the physical bases and the present applications of this concept. This report is aimed at such readers; in it the mathematical formalism of the theory has been reduced to a minimum. Readers desiring to acquaint themselves with the purely mathematical aspects of the question should consult the references and particularly the survey articles by Shapiro[3] and Zel'tser[4].

2. Comparison of the Forces of Interaction between Nucleons: n-n, n-p and p-p Forces

In 1932 the hypothesis was advanced that all atomic nuclei consist of protons and neutrons; soon thereafter the proton-neutron nuclear model became the universally accepted one. The appreciable binding energy, common to atomic nuclei, is due to the great forces of attraction between neutrons and protons. Thus there may be three types of nucleonic forces: n-n, n-p and p-p. There naturally arises the question: which of these forces is greatest for equal distances and identical relative orientations of the spins of these particles. A quantitative answer is suggested by an examination of the table of isotopes. Over most of the Mendeleev periodic system the number of protons and neutrons in the nuclei is about the same; only towards the end of the system of chemical elements does the number of neutrons become about 60% higher than the number of protons.

If the p-p forces were considerably greater than the others, one might expect the nuclei having more protons than neutrons to be more closely packed and hence more stable. In reality this is not the case. Analogously, if the n-n forces were appreciably stronger, one might expect stable nuclei to have more neutrons than protons; this supposition, too, is not upheld by experimental data.

Lastly, if the n-p forces were far more powerful than the others, isobars with equal or nearly equal numbers of protons and neutrons would be more tightly packed and have a much higher binding energy than other isobars in which the number of neutrons differs from the number of protons. Here again supporting evidence is lacking, as may be seen from Table 1 where, by way of illustration, the binding energies of six isobars with a mass number of 200 are compared.

It may be concluded, therefore, that under the conditions obtaining in nuclei no one of these interactions - n-n, p-p, and n-p - is vastly stronger than the others. Hence it must be assumed that these forces are of the same magnitude - or, perhaps, exactly equal to each other; we are not speaking here

---

*Up to 1952, the term "isotropic spin", introduced by Wigner[1] back in 1937, was commonly employed in scientific literature. However, since the values of this quantity prove to be the same for similar states of isobaric nuclei, in 1952 it was renamed "isobaric spin"; Wigner is in agreement with this change in nomenclature.[2]

Table 1

Binding energy of isobars with A = 200 (according to Kravtsov[6])

Isobar	Mass	Total nuclear binding energy, Mev
Au^{200}	200.0335	1579.7
Hg^{200}	200.0309	1581.4
Tl^{200}	200.0328	1578.8
Pb^{200}	200.0340	1576.9
Bi^{200}	200.0404	1553.5
Po^{200}	200.0438	1566.2

of electric and magnetic interactions, which, naturally, are different for the various pairs.

Thus, we have arrived at the hypothesis of the homology of the nuclear forces acting in the n-n, p-p and n-p pairs or, in currently accepted terminology, to the hypothesis of charge independence of nuclear forces. This hypothesis was, in part, suggested by Heisenberg[7] back in 1932, soon after discovery of the neutron. The basic ideas were subsequently formulated more clearly in 1935-1937 by Young[8], Wigner[1,9] and others[10]. Since then, investigators have brought to light many facts and arguments indicating that the nuclear forces acting in the n-n, p-p and n-p pairs are almost equal and, under some conditions, might be completely equal. We shall examine below four groups of such facts.

Nuclear forces evinced in n-p & p-p scattering

Of the three listed forms of interaction, two - n-p and p-p - can be studied experimentally, i.e. on the basis of data for neutron-proton and proton-proton scattering. This way of comparing the forces would seem to be the most direct. However, it must be noted that it comprises an intrinsic limitation: in consequence of the identity of particles in scattering of protons from protons with even values of ℓ, states with parallel spins are impossible, for they are forbidden by the Pauli principle. Hence investigation of p-p scattering can yield information only on the interaction of protons with antiparallel spins. This limitation does not exist for n-p scattering. Hence in comparing n-p with p-p scattering data, we must separate out from the n-p scattering data that part which relates to the scattering of particles with opposite spins, i.e., to "singlet scattering"; the other part, the part relating to scattering of particles with parallel spins, has no analogue with p-p scattering.

The scattering data should be compared for equal values of the energy of the scattered particles. In selecting the energy interval for purposes of comparison one must bear in mind the following: The energy must be sufficiently high so that the Coulomb forces, acting in p-p scattering, would not be predominant; otherwise the protons will not come close enough to each other to permit effective interaction of the nuclear forces.

On the other hand, since we are interested in the n-p and p-p forces acting between particles inside the nucleus, it is expedient to make the comparison at energies not exceeding the kinetic energy of intra-nuclear particles. The 2 to 20 Mev interval appears to be the most suitable.

Up to 1949 n-p and p-p scattering data were commonly processed in the following manner. An assumption was made regarding the character of the dependence of the potential energy of the colliding particles on the distance separating them, i.e., an assumption was made concerning the "form of the potential well". Two parameters were introduced into the relationship defining the dependence and the magnitudes of these were adjusted or selected to make the computed scattering curves coincide as closely as possible with the experimental ones.

The numerous contributions on the subject investigated a) a rectangular potential well of width R and depth U_0, b) an exponential well of the type $U(r) = \alpha e^{-\beta r}$, c) a Gaussian well of the type $M(r) = \alpha e^{-\beta r^2}$, d) the Yukawa potential: $U(r) = \frac{\alpha}{r} e^{-\beta r}$ and other forms.

It became apparent that through suitable choice of parameters the experimental data could be explained using any one of the potential well forms. Hence for the purpose of comparing the n-p and p-p forces it does not matter which form is selected; one need only compare the corresponding pairs of parameters. By way of illustration one might cite the data given by Fermi[11]. If the interaction be characterized by a rectangular potential well having a radius equal to the classical electron radius ($2.8 \cdot 10^{-13}$ cm), the depth of the well for n-p singlet scattering equals 11.5 Mev, while for p-p singlet scattering the depth is 10.5 Mev. The minor difference between the depths of the wells disappears if we introduce the necessary corrections for the Coulomb and magnetic forces, acting inside the potential well.

A shortcoming of the described method of analyzing n-p and p-p scattering stems from the arbitrary choice of the form of the potential well: as was noted above, by operating with two parameters one can readily obtain agreement with experimental data using divers forms of the potential well. In reality experimental investigation of the scattering of neutrons or protons with an energy inferior to 10 Mev cannot yield information on the dependence of nuclear forces on the distance. Hence the introduced parameters (R and U_0 or α and β) are of a purely arbitrary character.

The work of Landau and Smorodinskii[12&13], Schwinger[14], Bethe[15], Blatt and Jackson[16], and others[17-19] led to the development of a different system of two parameters to characterize the scattering: 1) The length of scattering a and 2) the effective range of nuclear forces r_0. By taking in turn all the above enumerated forms of potential and the appropriate values of the constants giving closest agreement with experimental results, and computing the corresponding values of a and r_0, one can readily show that these parameters have almost the same values for all forms of the potential. In other words, the parameters a and r_0 are less sensitive to the form of the potential well and hence are less "arbitrary" than R and U_0, α and β, etc. As such they are more suitable for comparison of the n-p and p-p forces. Average values of a and r_0 for singlet n-p and p-p scattering, based on data in the literature of the past few years, are listed in Table 2.

Table 2

Length of scattering a and effective range r_{0_s} of nuclear forces in scattering of nucleons with opposite spins (in 10^{-13} units)

Parameter	n-p	p-p
a	23.69 ± 0.06*	17.3 ± 1.0*
r_{0_s}	2.34 ± 0.17**	2.66 ± 0.07***

*Average values for two forms of potential (Ref. 20)

**Average values at different neutron energies (E_n = 4.75 Mev[21], E_n = 14 Mev[22] and $E_n < 5$ Mev[23]) for three forms of potential.

***Average values from the results of processing data on p-p scattering at under 3.6 Mev for four different forms of potential, according to Ref. 24.

It will be noted that the difference between the values for n-p and p-p interactions is not great, although it does exceed the limits of experimental error. At first glance this difference might be taken as proof that the hypothesis of the equivalence of n-p and p-p forces is invalidated. However, Schwinger[25] has pointed out that taking the magnetic interaction in n-p and p-p scattering into account reduces this difference. Hence the question of whether an actual difference exists still remains open.

The values compared above are, of course, for the scattering of neutrons with antiparallel spins. In view of the great difference between n-p and p-p scattering in the case of parellel spins, we must conclude that the results of our analysis of scattering allow only of qualitative deductions regarding the charge independence of nuclear forces.

Binding energy of mirror nuclei

In mirror nuclei of the first order there is always one extra proton or neutron in addition to the equal number of protons and neutrons. All the mirror nuclei of the first order known at present are listed in the first part of Table 3.

Without going into the question of what part of the binding energy is due to interaction between nucleons separated by long and short distances, we can state that in mirror nuclei of the ${}_{Z}M^{2Z+1}$ and ${}_{Z+1}M^{2Z+1}$ types there is an equal number of n-p pairs but a different number of interacting n-n and p-p pairs: in the first nucleus there are Z more n-n pairs, while in the second nucleus there are Z more p-p pairs. Hence, we could hope, by comparing the binding energy of mirror nuclei, to detect some effect due to this inequality of numbers if the n-n and p-p interactions should actually be unequal.

The atomic masses and total nuclear binding energies of the known mirror nuclei are given in Table 3.

However, the total binding energy of the nucleus reflects not only the nuclear forces holding the nucleons together but also the Coulomb forces, causing mutual repulsion of the protons. Hence, to evaluate the role of the nuclear forces in the total binding energy of the nucleus, one must add the Coulomb interaction energy to the total binding energy derived from experiment. This can only be done approximately, since the charge distribution in the nucleus is not known.

Assuming that the protons are distributed uniformly over the volume of a nucleus, having a radius $r_0 = 1.45 \cdot 10^{-13} A^{1/3}$ cm, we can compute the value of the Coulomb energy by means of the following equation:

$$E_{Coul} = 0.643 \cdot 10^{-3} \frac{Z(Z-1)}{A^{1/3}} \text{ amu} = 0.598 \frac{Z(Z-1)}{A^{1/3}} \text{ Mev}^{40} \qquad (1)$$

The computed values are entered in Column 4 of Table 3. It should be noted that like values of the Coulomb energy can be obtained starting with other assumptions regarding the charge distribution in the nucleus (for example, it may be assumed that the density of the charges decreases exponentially, that the density is constant up to a certain r and then falls following an exponential or Gaussian law[41&42], etc.). The expressions based on any of these assumptions can be reduced to equation (1) through a suitable choice of parameters; that equation (1) correctly characterizes the Coulomb energy follows directly from the experimental data reported by Dzhelepov[40].

Lastly, the values of the nuclear binding energy are listed in Column 5 of Table 3. An examination of the pairs of values shows that the binding energies for mirror nuclei are extremely close throughout the table. In no case does the difference exceed 1%, while in most cases it amounts to some tenths of a percent.

Almost the same agreement in binding energy values is found for mirror nuclei of the second order[43] (nuclei of the type ${}_{Z-1}M^{2Z}$ and ${}_{Z+1}M^{2Z}$) which are listed in the lower part of Table 3. These nuclei, too, have an equal number of interacting n-p pairs but different numbers of n-n and p-p nucleons.

The closeness of the binding energy values for mirror nuclei confirms the hypothesis that the n-n and p-p interaction forces are equal or nearly equal. However, one must proceed with circumspection in attempting to draw quantitative conclusions: the number of interacting pairs has only an indirect relation to the total binding energy, for nuclear forces fall off rapidly with the distance and do not bind neighboring nucleons and nucleons located at opposite sides of the nucleus to the same extent. Hence we cannot make quantitative deductions regarding the relative strength of the n-n and p-p forces on the basis of data for

Binding energy of mirror nuclei

Table 3

Mass number	Atomic mass	Total binding energy, Mev	Coulomb energy, Mev	"Nuclear" binding energy, Mev
	MIRROR NUCLEI OF THE FIRST ORDER			
3	H^3 = 3,017002 [26,27]	8,486	0	8,486
	He^3 = 3,016983	7,723	0,829	8,552
7	Li^7 = 7,018225	39,251	1,876	41,127
	Be^7 = 7,019153	37,606	3,751	41,357
11	B^{11} = 11,012796	76,209	5,378	81,587
	C^{11} = 11,014931	73,441	8,066	81,507
13	C^{13} = 13,007488	97,103	7,631	104,734
	N^{13} = 13,009877	94,097	10,683	104,770
15	N^{15} = 15,004877	115,49	10,19	125,68
	O^{15} = 15,007782	112,00	13,58	125,58
17	O^{17} = 17,004536	131,76	13,03	144,79
	F^{17} = 17,007508 [28,29]	128,21	16,75	144,96
19	F^{19} = 19,004454	147,78	16,14	163,92
	Ne^{19} = 19,007953 [30]	143,74	20,17	163,91
21	Ne^{21} = 21,000525	167,39	19,51	186,90
	Na^{21} = 21,004305	163,06	23,84	186,93
23	Na^{23} = 22,997094	186,54	23,13	209,67
	Mg^{23} = 23,00149 [31]	181,67	27,75	209,42
27	Al^{27} = 26,990088	224,97	31,10	256,07
	Si^{27} = 26,99504	219,57	36,28	255,85
29	Si^{29} = 28,985682	245,02	35,43	280,45
	P^{29} = 28,99102 [32]	239,27	40,88	280,15
31	P^{31} = 30,983588	262,92	39,98	302,90
	S^{31} = 30,98887	257,22	45,69	302,91
33	S^{33} = 32,981921	280,43	44,74	325,17
	Cl^{33} = 32,98753	274,42	50,70	325,12
37	A^{37} = 36,97844	315,57	54,92	370,49
	K^{37} = 36,98445	309,19	61,38	370,57
39	K^{39} = 38,97600	333,79	60,31	394,10
	Ca^{39} = 38,98260	326,87	67,01	393,88
41	Ca^{41} = 40,97516	350,53	65,91	416,44
	Sc^{41} = 40,98156	343,79	72,84	416,63
	MIRROR NUCLEI OF THE SECOND ORDER			
8	Li^8 = 8,025026 [33]	41,28	1,79	43,07
	Be^8 = 8,027 [34]	37,90	5,98	43,88
10	Be^{10} = 10,016717 [33]	64,97	3,33	68,30
	C^{10} = 10,02034 [33]	60,04	8,33	68,37
12	Be^{12} = 12,018172 [33]	79,57	5,23	84,80
	N^{12} = 12,02280 [33]	173,70	10,97	84,67
14	C^{14} = 14,007698 [33]	05,27	7,44	112,71
	O^{14} = 14,01305 [33,35]	198,73	13,90	112,63
18	O^{18} = 18,004888 [33]	139,79	12,78	152,57
	Ne^{18} = 18,0112 [36]	132,35	20,53	152,88
20	F^{20} = 20,006365 [28]	154,37	15,86	170,23
	Na^{20} = 20,0152 [34]	144,58	24,24	168,82
24	Na^{24} = 23,998608 [33]	193,50	22,81	216,31
	Al^{24} = 24,0075 [37]	183,65	32,35	216,00
28	Al^{28} = 27,990786 [33]	232,68	30,72	263,40
	P^{28} = 27,9994 [38,39]	223,10	41,35	264,45
32	P^{32} = 31,984056 [33]	270,85	39,55	310,40
	Cl^{32} = 31,9955 [38,39]	258,64	51,23	309,87
40	K^{40} = 39,97672 [33]	341,49	59,80	401,29
	Sc^{40} = 39,98604 [39]	331,25	73,44	404,69

Notes: 1) Atomic masses of the stable nuclides are taken from the table in Ref. 33. 2) The masses of radioactive nuclides, where no reference [ ] is given, are taken from Tables 1 and 2 of Ref. 40. Cases where new experimental data (published after 1 March 1952) are available are identified by reference brackets; the value shown in such cases is a weighted average based on all data. 3) In calculating the binding energies the following masses were assumed: n = 1,008,984,9 and p = 1,008,146,0 amu.

mirror nuclei until we have a much clearer picture of the actual structure of nuclei.

Binding energy of similar states: He^6-Li^{6*}, Be^{10}-B^{10*} and C^{14}-N^{14*}-O^{14}

A comparison of the "nuclear" binding energies of nuclei in similar states is of particular interest since they have different numbers of interacting n-n, p-p and n-p pairs. The values of the binding energy of nuclei in similar states are listed in Table 4.

Table 4

"Nuclear" binding energy of nuclei in similar states

Mass number	Atomic mass*	Total binding energy, Mev	Coulomb energy, Mev	"Nuclear" binding energy, Mev
6	He^6 = 6,02682	29,25	0,66	29,91
	3,572 MeV Li^{6**} = 6,020864	28,43	1,98	30,41
10	B^{10} = 10,016717	64,97	3,33	68,30
	1,74 MeV B^{10**} = 10,017986	63,01	5,52	68,52
	C^{10} = 10,02034	60,04	8,33	68,37
14	C^{14} = 14,007698	105,27	7,44	112,71
	2,31 MeV N^{14**} = 14,010012	102,34	10,42	112,76
	O^{14} = 14,01305	98,73	13,90	112,63

*See note to Table 3 regarding sources of atomic mass data.

**Hereinafter we shall indicate excited states of nuclei in this manner, putting the excitation energy before the designation of the nucleus.

The fact that Li^6, B^{10} and N^{14} have excited states with the same quantum characteristics as the ground states of He^6, Be^{10} and C^{14} and that the corresponding "nuclear" binding energies are nearly the same may be taken as an argument in favor of the approximate equality of n-n, n-p and p-p forces. Again, however, our deductions can only be qualitative, for the reasons already outlined at the end of the preceding subsection.

Neutron-neutron forces

Certain information regarding the n-n interaction forces can be gained from an analysis of the γ-spectrum in the capture of slow π^--mesons by deuterium: $\pi^- + d = n + n + \gamma$.

If as the result of the capture there were produced a bound system - a "dineutron" - the γ-rays would be monochromatic. On the other hand, if the neutrons scattered as non-interacting particles, the γ-spectrum would be continuous. Interaction between the neutrons gives the intermediate case: the spectrum should consist of a continuum and a line, whose relative intensity is dependent on the character of the n-n forces. Analysis[44&45] of the experimental γ-spectrum obtained by Panofsky, Aamodt and Hadley[46] leads to the conclusion that the n-n and p-p forces differ little as regards magnitude.

Summarizing the discussion of the present section, we may say that there exist a number of qualitative arguments in favor of the full or near equality of n-n, n-p

and p-p forces but that as yet we do not have sufficient reliable data to evaluate the difference or the upper bound of the difference between these forces. This approximate equality of the nucleonic forces is the physical basis for the isobaric spin concept which we shall examine below.

3. The Isobaric Spin Concept

Let us assume that the n-n, n-p and p-p forces are exactly equal and that the mass of a neutron is exactly the same as that of a proton. Then our system of protons and neutrons becomes similar to a system of particles identical in every way, except that some of them bear one type of marking while the rest bear a different marking. In fact, for the sake of simplicity let us refer to them as black and white particles. In classical physics the properties of such a system will, of course, be entirely independent of how many of the particles are black and how many are white, but will depend solely on the total number of particles present.

This is not the case in quantum mechanics. In view of the Pauli exclusion principle we must now differentiate between black and white particles, even if all their other attributes are exactly the same. The Pauli principle must be applied to the particles of each color separately. If both the black and white particles have a spin quantum number of $\frac{1}{2}$, they must obey the Fermi-Dirac statistical law. Hence we cannot locate more than two white particles at the same energy level, but we can have two white and two black particles occupying the same level.

It can readily be seen that the number of states forbidden by the Pauli principle will depend on the ratio between the number of black and white particles: in a system consisting of a given number of particles, there will be the greatest number of forbidden states when all particles are of the same color and the least number of forbidden states when we have an equal number of white and black particles.

By way of example let us investigate a hypothetical system consisting of four particles which have only two levels available to them. The possible distributions are shown in Fig. 1. If all four particles are of the same color, the only distribution consistent with the Pauli principle is two particles in the lower level and two particles in the upper level. It will be noted that this is the only state shown in the 4n and 4p columns of our chart. The total spin of the system is 0 (the spin is indicated in the first column of Fig. 1).

If we have three particles of one color and one of another (see the 3n+p and n+3p columns) the number of allowed states will be considerably greater.

In Fig. 1 we have shown all possible (allowed) distributions; actually some of them represent equivalent-energy states, but this need not concern us at the moment. First we must note the presence of states in which there are three particles in the lower level: we may reasonably expect that these states will be deeper-lying than the states of the 4n and 4p systems, consequently we have located them lower in the chart. These two new states will be of two types: with a spin number 0 or 1. We have provisionally located the state with the smaller spin number (more "balanced" state) lower. In the 3n+p and n+3p systems there can, of course, also be states in which two particles are in the upper level and two are in the lower level. We note certain differences between these states: in some the two different particles are in the upper level, while in others they are in the lower level. However, all these states have one trait in common: in each case the total spin at each level equals zero. These states cannot differ much as regards energy; they might be said to form a fine energy-state structure. Since we have no way of telling which is the higher-energy state, we have placed them on the same level in the chart.

Further, in the 3n+p and n+3p systems there can also be states having two particles at each level, but with uncompensated spins at one of the levels. These states with spin 1 have no counterparts in the systems of four identical particles. Presumably still higher on the energy scale, we will have the two groups of states in which there is one particle in the lower level and three in the upper level;

in one group the spin will be 0; in the other, 1. Thus, whereas the 4n and 4p systems have but a single state, in the case of the 3n+p and n+3p systems we can distinguish between at least seven groups of states.

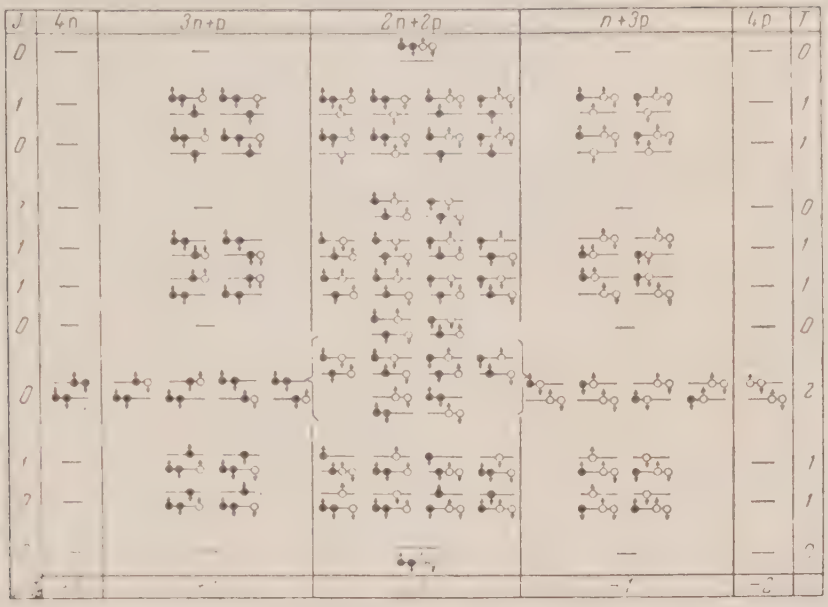

Fig. 1. Possible distributions of four nucleons in two energy levels: black dots = neutrons; light circles = protons.

The system consisting of two particles of each kind will be characterized by an even greater diversity of states (2n+2p column in Fig. 1). This system will have a new, even deeper-lying state in which all four particles occupy the lower level, a state with spin 2, and, finally a high-lying state in which all four particles occupy the higher level. None of these new states have counterparts in the previously examined systems.

The different columns of Fig. 1 characterize systems with the same total number of particles, i.e., isobaric nuclei, if the particles are understood to be protons and neutrons. Thus we see that if the forces of interaction between nuclear particles are exactly equal and the masses of these particles are also equal, but the protons and neutrons are not identical where the Pauli principle is concerned:

1) isobars must have similar states which are identical as regards energy;

2) the normal or ground states of isobars with more nearly equal numbers of protons and neutrons must lie deeper;

3) in going from isobars with the greatest to those with the least difference between the number of neutrons and protons we encounter new levels, not found in less symmetrical systems.

In drawing up the chart of Fig. 1 we used the simplest case of four particles and two levels. If there were more particles or levels, the diversity of states would be greater, but our three general deductions would still hold.

Let us turn to the state which is encountered in Fig. 1 for all five isobars. If the forces acting between the particles and the masses of the particles are equal, these five states of the isobaric nuclei are indistinguishable from each other; they become distinguishable only if and when it is necessary to take account of forces dependent upon the composition of the states.

One might ask whether we are not dealing here with five substates, five somewhat different forms of one and the same state, characterized by a certain distribution of the particles among the available levels and a certain orientation of their spins.

Not all the states shown in Fig. 1 have five substates: not all of them have

entries in all five columns. It will be noted that some states are encountered only in three columns and some only in one, the middle column.

Let us now introduce a new parameter characterizing nuclear states, namely, a number indicating in how many isobars (i.e., in how many columns of Fig. 1) the given state is encountered. Since similar states occur for one, three or five isobars - that is, always an odd number of isobars - it is convenient to characterize each state by a number T such that 2T+1 is the number of isobars in which the given state is encountered. The quantity T is called the isobaric spin. The term derives from its analogy to ordinary spin.

It has been shown in quantum mechanics that any isolated system of charges has a definite value of the total or net mechanical moment J, which remains constant in time as long as the system is not acted upon by external forces. In our case, however, we have 2J+1 substates which have the same energy and are indistinguishable in the absence of external forces. As soon as there is even a weak magnetic field, for example, differences between the substates at once become apparent: they all acquire different additional energies in a magnetic field. Hence, in quantum mechanics, in order to distinguish between these states an auxiliary quantum number, the magnetic quantum number m (which can have 2J+1 values, from +J to -J, through unity) is introduced.

Having introduced the isobaric spin T, we can immediately determine its value for all the states shown in Fig. 1: to this end we need merely count the number of isobars for which the given state occurs. We find T = 0, 1 and 2. The values of T for each line are given in the extreme right column. While the chart in Fig. 1 is for a system of four particles, we can readily elaborate a similar chart for a system with any number of particles. A system consisting of A particles can have A+1 isobars. For this system the values of T will range from 0 through A/2 if A is an even number, or from 1/2 through A/2 if A is odd. In the limiting case, when A = 1, we have only one nucleon which can be in two isobaric states, i.e., can be either a neutron or a proton. It follows from the above argument that we must assume T = 1/2 for a neutron or proton.

In Fig. 1 there is only one state where T = 2: the state which is encountered for all five isobars. If we want to distinguish between the five substates peculiar to these isobars we must find a way to number them, i.e., introduce a new quantity assuming the appropriate number of values: five in this case, or 2T+1 in the general case. By analogy with the magnetic quantum number, we can attribute numbers from +T, through unity, to -T to the various states in any given line of Fig. 1 (the direction of numeration is selected arbitrarily). This new quantity is commonly designated through T_z (or T_3) and is sometimes called the third component of isobaric spin.

It will readily be seen that for all the states listed in the middle column of Fig. 1 and, hence, relating to the isobar with an equal number of protons and neutrons $T_z = 0$. For all states of the 3n+p and n+3p isobars, $T_z = +1$ and -1, respectively; for the 4n and 4p isobars, $T_z = +2$ and $T_z = -2$, respectively. Accordingly, for A = 1, the neutron and proton have $T_z = +\frac{1}{2}$ and $T_z = -\frac{1}{2}$.

Hence, in the general case for a nucleus consisting of A nucleons, the value of T_z for an isobar having Z protons and N = A - Z neutrons is given by

$$T_z = \frac{N - Z}{2} .$$

Thus, investigating any given nucleus ${}_Z M^A$, we can readily find T_z for all states of the nucleus. Knowing T_z, we can determine the lower bound of possible values of T for any given nucleus. Thus, for example, for the nucleus ${}_{16}S^{36}$, $T_z = (20 - 16)/2 = 2$ and consequently for all states of this nucleus $T \geq 2$ and cannot be 0 or 1.

The ground and moderately excited states of light nuclei are characterized by low values of T and T_z; we first encounter T = 2 in the case of ${}_{16}S^{36}$. Towards the end of the periodic table, for heavy nuclei, in which the number of neutrons is considerably greater than the number of protons, T_z and, consequently, T are

appreciably greater than 2. Thus for lead, $_{82}Pb^{208}$, $T_z = 22$ and hence $T \geq 22$.

We must note in concluding, however, that the analogy of isobaric spin T with ordinary spin J should not be carried too far: the angular momentum is a vector in quantum mechanics while the isobaric spin, as follows from the definition given above, is simply an abstract number. Where the magnetic quantum number may be interpreted as the projection of J on the direction of the magnetic field, T_z, like T, is an abstract number.

4. Rules of Selection

The assumptions regarding the charge independence of nuclear forces and the equality of proton and neutron masses are essentially idealizing conventions which, theoretically, could be made even if neutrons and protons were known to be fundamentally different particles. However, another approach is possible: one may regard the neutron and proton as representing two states of the same particle (the nucleon), differing from each other only as regards the value of a supplementary coordinate: T_z (for a neutron, $T_z = \frac{1}{2}$ and $T = \frac{1}{2}$; for a proton, $T_z = -\frac{1}{2}$ and $T = \frac{1}{2}$).

Although the facts that the masses of neutrons and protons are nearly the same, that their spins are equal, that they obey the same statistical laws, that a neutron may be transformed into a proton and vice versa in the nuclear process of beta-decay and, finally, that the beta-transformation of a neutron into a proton has been observed cannot serve as definite proof of the "two states of a nucleon" hypothesis, they do speak in favor of it.

Having accepted the hypothesis, we can formulate it in mathematical terms.

Earlier, the behavior of neutrons and protons was described by the wave functions $\psi_n(\mathbf{r},\sigma)$ and $\psi_p(\mathbf{r},\sigma)$, where $\mathbf{r}$ denotes spatial coordinates and σ, the spin coordinate. Now, the behavior of each of these particles is described by the wave function $\psi(\mathbf{r},\sigma,t)$, where t is an isobaric coordinate, the different values of which ($+\frac{1}{2}$ or $-\frac{1}{2}$) indicate the "state" of the nucleon (proton or neutron). The variables σ and t, which can assume only two values ($+\frac{1}{2}$ or $-\frac{1}{2}$), are similar in a number of ways; this greatly facilitates investigation of the symmetry and other properties of these wave functions. Investigation of these properties in the light of the above assumptions regarding the equality of neutron-proton forces and masses has led to two important conclusions regarding the conservation or possible change of isobaric spin in various processes.

The first conclusion is that the isobaric spin, like ordinary spin, is conserved (i.e., remains unchanged) in all internal motions or transformations produced by forces independent of the charge, or, in mathematical terms: the isobaric spin is an integral of motion.

The second conclusion is that in nuclear reactions, β-decay, γ-emission and photoexcitation of nuclei, certain rules of selection for the isobaric spin obtain, violation of which must lead to a sharp decrease in the probability of the process. These selection rules have been deduced and established as the result of numerous investigations; although a detailed discussion of these rules lies beyond the scope of the present report, they are summarized in Table 5 below.

The first of these rules, established by Adair[47], is the law of the conservation of isobaric spin in reactions between heavy particles.

In the combination of nuclear systems, isobaric spins, like the values of the angular momentum, are added quantum mechanically. In adding the mechanical momenta of colliding systems one must take into account not only the spin momenta but also the orbital ones. Hence the net or total momentum depends on the characteristics of the relative motion of the system: on the velocity and collision parameter. In the case of isobaric spins, however, there is no analogue to the orbital momentum and this narrows the range of possible values of the total isobaric spin. Thus, if the colliding particles had isobaric spins T_1 and T_2 and $T_1 > T_2$, the resultant system can have one of $2T_2 + 1$ possible values of isobaric spin: from $T_1 + T_2$ to $T_1 - T_2$, through unity.

Table 5

Rules of selection for isobaric spin

1. NUCLEAR REACTIONS AND α-DECAY

$$\sum_{\substack{\text{quant.}\\ \text{mech.}}} T_i = \text{const.}$$

2. β-DECAY

For variants in which the rule for ordinary spin is....	Fermi ($\Delta J = 0$)	Teller ($J = 0, \pm 1$ (except $0 \rightarrow 0$)
Where the rule for the selection of isobaric spin is	$\Delta T = 0$	$\Delta T = 0, \pm 1$

3. γ-EMISSION

$$\Delta T = 0, \pm 1$$

except for the case $T_z = 0$, E1, when only $\Delta T = \pm 1$ is permitted; if in this case $\Delta T = 0$, the probability of gamma-radiation corresponds to M2 (approximately) rather than to E1.

Thus, for Be^8, in any combination of two α-particles ($T = 0$) only states with $T = 0$ can result. In the scattering of deuterons in helium only such states of Li^6 can be produced for which $T = 0$, just as $T = 0$ for the α-particle and the deuteron. In the capture of neutrons by H^2 and Li^6 there can result only states with $T = \frac{1}{2}$; in the capture of neutrons by $_8O^{18}$ ($T = 1$) only states with T equal to 1/2 or 3/2 can be formed.

It can be seen even from these few examples that the rule for the addition of isobaric spins in the combination of particles can be very useful for elucidating the isobaric spin of complex nuclei.

The spin addition rule can be applied in reverse to the dissociation of systems into two or more heavy particles. For instance, not all states of Be^8 and Li^6 can disintigrate into $\alpha + \alpha$ and α+d, respectively; the process can occur only in the case of states for which $T = 0$. For example, Li^6 in the state with an excitation energy of 3.58 Mev has $T = 1$ and sufficient energy for the α+d dissociation, but the process is forbidden by the conservation of isobaric spin principle. Many similar examples can be found in recent literature.

The above addition rule for isobaric spins can be applied regardless of the degree of stability or length of life of the resultant system. It is applicable, also to the formation and subsequent disintegration of intermediate states in nuclear reactions (to compound-nuclei). The addition rule can be applied directly to the initial and final systems, by-passing the intermediate-state stages. Thus, obviously, in reactions of the (α,d) and (d,α) type and in inelastic scattering (d,d') and (α,α'), the isobaric spins of the target nuclei and the product nuclei are equal; in the reactions (α,n), (α,p), (n,α), (p,α), (n,d), (d,n), (p,d) and (d,p), the isobaric spins of the target and product differ by $\frac{1}{2}$, while in the reactions (p,n) and (n,p) or (p,p') and (n,n') the isobaric spin can either remain the same or change by unity.

The selection rules for β-decay were established by Wigner[9,27 & 48]. For those variants of the theory of β-decay in which the ordinary spin selection rule is $\Delta J = 0, \pm 1$, the isobaric spin rule for allowed transitions is $\Delta T = 0, \pm 1$.

This isobaric selection rule is relatively "liberal", i.e., it forbids virtually no reactions. In all nuclei with $A<30$ and even, all the lower levels have $T = 0$ or 1 and all β-transitions between these levels are allowed; in nuclei with an odd number of nucleons, there are states with $T = 1/2$ or $3/2$ and again all β-transitions are allowed. In consequence it is difficult to check the operation of the selection rule in these cases.

For the variants in which the Fermi selection rule ($\Delta J = 0$) is applicable, the isobaric spin should be conserved ($\Delta T = 0$) in all allowed β-disintegrations. All the "purely Fermi" transitions known so far belong to the $+0 \rightarrow +0$ type. These are the transitions $C^{10} \rightarrow 1.74$ Mev B^{10}, $O^{14} \rightarrow 2.31$ Mev N^{14}, and $Cl^{34} \rightarrow S^{34}$. They all belong to the class of transitions between similar states[40]. Inasmuch as in similar states the isobaric spins are equal, ΔT in the decay process is zero and the isobaric selection rule is automatically observed.

The isobaric selection rules for γ-emission were established by Trainor[49] and Radicati.[50] In the case of nuclei having an unequal number of neutrons and protons ($T_z \neq 0$), ΔT must equal 0 or ± 1 for γ-emission to occur. Non-observance of this condition must lead to an appreciable decrease in the probability of radiation. In all light nuclei ($A<30$) the values of T for all the lower levels do not differ by more than unity ($T = 0$ or 1 for even values of A and $1/2$ or $3/2$ for odd values of A); hence the isobaric spin selection rule for γ-transitions introduces no new restrictions, i.e., does not forbid any transitions.

For nuclei having an equal number of protons and neutrons ($T_z = 0$) the selection rule remains the same as before for transitions of all types, except the E1, electric dipole, transition. For transitions of the E1 type, ΔT must equal ± 1. For cases when $\Delta T = 0$, the E1 type transition is forbidden and its probability is reduced by a factor of thousands or tens of thousands (i.e., approximately to the probability of an M2 transition). Since in nuclei with $T_z = 0$, many of the lower levels have $T = 0$, there are numerous cases where the γ-emission selection rule can be applied. Examples of such application are given below in Section 8.

Trainor[49] also established that in nuclei with an equal number of protons and neutrons transitions of the E1 type are forbidden between states having isobaric spins T and $T \pm 2k$, where k is any integer or zero. In the case when $k = 0$, this rule becomes identical with that listed in Table 5; while for $k>0$, the rule has no practical significance since so far no nuclei having states differing from each other by 2 or more as regards isobaric spin have been discovered.

5. Displacement of the Levels of Isobaric Nuclei Due to the Coulomb Energy of Nuclei and Difference in Mass Between Protons and Neutrons

The hypothesis of the equality of the n-n, n-p and p-p forces and of the n and p masses lead to the concept of similar states of isobaric nuclei, forming a "multiplet" [1,51] characterized by equal values of the isobaric spin T and energy E, the same spin J and the same parity.

The resultant "idealized" arrangement, tabulated in Fig. 1 is shown in a more familiar form in Fig. 2 (where the number of levels has been arbitrarily increased). Any level found in the "outer" isobars also occurs in the others and at the same height; the nearer an isobar is to the center of the diagram, the greater the number of available levels.

If the basic assumptions are not rigorously satisfied, the deduced consequences will also be only approximately fulfilled, i.e., 1) the various levels of the "multiplet" will be displaced relative to each other as regards energy and 2) the assignment of isobaric spin values T to each level will no longer be rigorous.

For example, taking account of a real or assumed inequality of the proton and neutron masses will lead to the displacement of each column in Figs. 1 and 2 downward by an amount $n - p$ relative to the neighboring column on the left. On

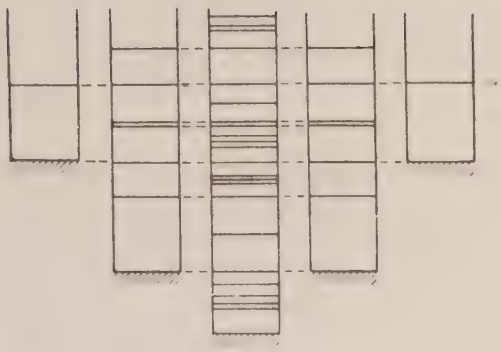

Fig. 2. Idealized diagram of energy levels of isobaric nuclei.

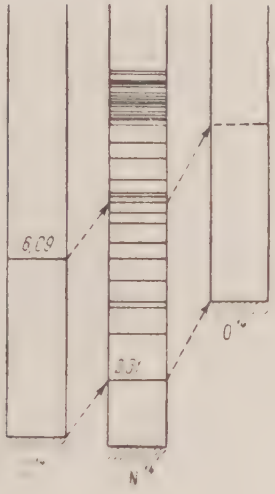

Fig. 3. Example of shifting of isobaric nuclei levels due to electrostatic interaction and the inequality of n and p masses.

the other hand, an additional electrostatic energy will shift the successive (left to right) columns in Figs. 1 and 2 upward. Since beginning with A = 4, the electrostatic displacement is greater than the n-p displacement, from A > 4 the levels of a multiplet are shifted upward as Z increases. The displacement ΔE_{Coul} gradually increases with increasing values of Z. In an earlier article[43] we showed on the basis of data on the ground states of mirror nuclei that

$$\Delta E_{Coul} = 1.196 \frac{Z-1}{A^{1/3}} \text{ Mev} \qquad (2)$$

and the total displacement

$$\Delta E = \Delta E_{Coul} - (n-p) = \left(1.196 \frac{Z-1}{A^{1/3}} - 0.781\right) \text{Mev}. \qquad (3)$$

As a result of this displacement the location of the levels in an isobaric multiplet departs from the "ideal" symmetrical arrangement relative to the central isobar Z^{M^2Z}.

The shift of levels is pictured in Fig. 3.

The displacement or energy difference ΔE defined above is linear with respect to Z. If with refinement in measuring techniques it can be shown that there is a systematic deviation from this linearity, this will indicate either that the nuclear forces between nucleons are not exactly equal or that the expression for the electrostatic energy of nuclei should include terms not proportional to Z(Z - 1), i.e., terms connected with exchange energy, changes in the distribution of the particle with changes in Z, etc.

Other possible consequences of the presence of Coulomb forces and the inequality of the neutron and proton masses will be examined in Section 7.

6. Isobaric Spins of Actual Nuclei

The states pictured in Fig. 1 have been arranged in the chart taking account of their structure in accordance with the commonly accepted view of the packing of nuclei. Thus on the basis of the accepted concept of this structure we were able to arrange the various states in lines (relative levels) and then assign each an appropriate isobaric spin number. Going over to the excited states of actual nuclei we lose this "guide line" and, not knowing the structure, are unable to predict the isobaric spins.

Deuterons

It can be shown that the isobaric spin can be determined from the usual basic quantum-mechanical parameters (total angular momentum and parity) only for the simplest system consisting of two nucleons. In S_0 states (spins of the nucleons opposed; total momentum equal to zero), T = 1 for even states and T = 0 for odd states. In S_1 states (spins of nucleons parallel, total momentum equal to unity),

T = 0 for even and T = 1 for odd states.

Thus, the ground state of the deuteron has spin 0; the singlet state of the deuteron, if it existed, would have an isobaric spin of 1.

α -Particles

The isobaric spin of α -particles cannot be calculated with certainty theoretically. Reasoning based on the chart of Fig. 1 would indicate that it should be 0. It would appear obvious that the tighest packing of two neutrons and two protons will obtain when they all occupy the lowest level and have antiparallel spins; in this situation T = 0. It is clear, however, that this situation cannot obtain in H^4 and Li^4.

We can, however, deduce that the isobaric spin of α-particles is zero from the experimental evidence that if two states A and B have different values of isobaric spin the reaction $A(d,\alpha)B$ does not occur. This is understandable if the isobaric spin of α -particles is zero. On the other hand, if the isobaric spin of the α -particle were 1, 2 or greater, the isobaric-spin selection rules would not forbid the reaction in all cases. For example, the $O^{16}(d,\alpha)$2.31Mev N^{14} reaction is not observed, i.e., is not allowed, since for O^{16} T = 0, while for the 2.31 Mev state of N^{14} T = 1 (see under Section 7, below).

More complex nuclei

The isobaric spin of more complex systems than the deuteron cannot be computed if only the energy, the orbital and total momenta and parity are known: more detailed information regarding the structure of the state is needed and this we do not have at present.

There are, however, three ways of deducing the isobaric spin from experimental data: the first is through observation of nuclear reactions, the second is through investigation of the value of ft characterizing the β-decay process and a third is by seeking similar states of atomic nuclei. We shall consider these in turn.

Nuclear reactions

In many cases we can determine the isobaric spin by applying the rules of isobaric spin addition in nuclear reactions. By applying this rule and invoking the fact that both deuterons and α -particles have T = 0, we can determine the isobaric spins of the ground states of all light nuclei and of many of the excited states of these nuclei.

Ground states of nuclei with $A \leq 20$. By way of illustration let us trace the procedure in determining the isobaric spins of the ground states of nuclei with $A \leq 20$. Let us start with nuclei of the type $_ZM^{2Z}$. Since the following reactions proceeding to the ground state have been observed:*

$$Li^6(d,\alpha)\alpha,\ Be^8 \rightarrow 2\alpha,\ B^{10}_5(d,\alpha)Be^8,\ C^{12}(d,\alpha)B^{10},\ N^{14}(d,\alpha)C^{12} \text{ and } O^{16}(d,\alpha)N^{14},$$

we deduce in turn that Li^6, Be^8, B^{10}, C^{12}, N^{14} and O^{16} all have T = 0. At O^{16} our series of (d,α) reactions breaks off, since the reaction $O^{16}(d,\alpha)F^{18}$ has not been investigated. However, the isobaric spin of F^{18} can be determined indirectly: the 5.61 Mev state of F^{18} is obtained at the resonance of $N^{14} + \alpha$ (E_α = 1.7 Mev) and hence has T = 0. On the other hand, this level is also obtained by the $_{10}Ne^{20}(d,\alpha)$ reaction whence it follows that for Ne^{20}, T = 0. Inasmuch as the ground level F^{18} is also obtained through the $Ne^{20}(d,\alpha)$ reaction, we conclude that for it, too, T = 0.

---

* Data regarding the nuclear reactions mentioned in the present section will be found in the survey by Ajzenberg and Lauritsen[52].

Turning next to $_ZM^{2Z+1}$ nuclei, we find that the following reactions proceeding to the ground level are observed:

$Li^6(d,p)Li^7$, $B^{10}(n,\alpha)Li^7$, $Li^7(d,t)Li^6$, $Li^6(d,n)Be^7$, $B^{10}(p,\alpha)Be^7$, $Be^9(d,\alpha)Li^7$, $B^{11}(d,\alpha)Be^9$, $N^{14}(n,\alpha)B^{11}$, $B^{10}(d,p)B^{11}$, $B^{10}(d,n)C^{11}$, $N^{14}(p,\alpha)C^{11}$, $C^{13}(d,\alpha)B^{11}$, $O^{16}(n,\alpha)C^{13}$, $B^{10}(\alpha,p)C^{13}$, $C^{12}(d,p)C^{13}$, $C^{12}(\alpha,p)N^{15}$, $C^{12}(\alpha,n)O^{15}$, $N^{14}(d,n)O^{15}$, $N^{14}(\alpha,p)O^{17}$, $F^{19}(d,\alpha)O^{17}$, $N^{14}(\alpha,n)F^{17}$, $O^{16}(d,n)F^{17}$, $O^{16}(\alpha,p)F^{19}$ & $O^{16}(\alpha,n)Ne^{19}$.

From these we determine step by step that the isobaric spins of Li^7, B^9, Be^9, B^{11}, C^{11}, C^{13}, N^{13}, N^{15}, O^{15}, O^{17}, F^{17}, F^{19} and Ne^{19} equal $\frac{1}{2}$.

The isobaric spins of the $_ZM^{2Z+2}$ nuclei, $_2He^6$, $_3Li^8$, $_4Be^{10}$, $_5B^{12}$, $_6C^{14}$, $_7N^{16}$, $_8O^{18}$ and $_9F^{20}$, can be deduced in the following manner. For all these nuclei $T_z = 1$ and, therefore, $T \geqslant 1$. On the other hand, investigators have observed the following reactions proceeding to the ground state:

$Be^9(n,\alpha)He^6$, $Li^6(n,p)He^6$, $Li^6(t,p)Li^8$, $B^{11}(n,\alpha)Li^8$, $Li^7(d,p)Li^8$, $B^{10}(n,p)Be^{10}$, $C^{13}(n,\alpha)Be^{10}$, $Be^9(d,p)Be^{10}$, $Be^9(\alpha,p)B^{12}$, $B^{11}(d,p)B^{12}$, $C^{14}(d,\alpha)B^{12}$, $C^{12}(t,p)C^{14}$, $B^{11}(\alpha,p)C^{14}$, $N^{14}(n,p)C^{14}$, $C^{13}(d,p)C^{14}$, $N^{15}(d,p)N^{16}$, $O^{18}(p,\alpha)N^{15}$, $O^{18}(p,n)F^{18}$ and $F^{19}(d,p)F^{20}$.

By quantum mechanical addition we could have $T = 0$ or $T = 1$, but since, as noted above, the zero value is inadmissable, we have $T = 1$.

Not much is known regarding light nuclei of the $_ZM^{2Z+3}$ group: Li^9, C^{15}, N^{17} and O^{19}. For these, $T_z = 3/2$ and, consequently, $T \geqslant 3/2$. However, from the fact that the reactions $Be^9(d,2p)Li^9$, $C^{14}(d,p)C^{15}$, $C^{14}(\alpha,p)N^{17}$, $O^{17}(n,p)N^{17}$ and $F^{19}(n,p)O^{19}$ have been observed, it follows that for all these nuclei T cannot be greater than 3/2 and, hence, must be equal to 3/2.

To summarize, it may be stated that for all light nuclei with $A \leqslant 20$ the ground state has the lowest possible isobaric spin: $T = T_z$.

There is, however, no reason to assume that this will also always be the case for nuclei with $A > 20$.

We can expect mirror nuclei of the first order to have $T = \frac{1}{2}$ in view of their symmetry. For the same reason mirror nuclei of the second order may be expected to have $T = 1$. All even-even nuclei in the ground state are closely packed; at any rate in all investigated cases these states belong to the +0 type. It may be assumed that for these nuclei the isobaric spin of the ground state will always be minimal. We have no analogous arguments where nuclei of other types are concerned.

It is possible that Cl^{34} is the first example of a nucleus for which $T = 1$, rather than 0 in the ground state, as might have been expected from the fact that this nucleus has an equal number of protons and neutrons ($T_z = 0$).

The currently accepted decay scheme for Cl^{34} is shown in Fig. 4.[53]

It was long considered an established fact that the ground state of Cl^{34} was a state having a half-life of 33.2 minutes and decaying by the emission of β^+-particles having components with end-point energies of 1.3, 2.58 and 4.55 Mev and γ-rays with energies of 0.145, 1.16, 2.10 and 3.22 Mev.[54] For Cl^{34}-S^{34} the displacement, $\Delta E_{Coul-n+p} = 5.13$ Mev; this value is close to the energy released in the decay of the above-mentioned 33-minute state of Cl^{34} ($4.55 + 2m_0c^2 \simeq 5.5$ Mev). However, the 33-minute state of Cl^{34} is not at all similar to the ground state of S^{34} since for $\tau = 33$ min and $E_{ep} = 4.55$ Mev, we find $f\tau = 3.3 \cdot 10^6$ sec; consequently the β-decay of 33-min $Cl^{34} \longrightarrow S^{34}$ is forbidden and the quantum characteristics of these two states are different. From this it had to be concluded that the +0 state of Cl^{34} similar to the ground state of S^{34} lies near the 33-min state of Cl^{34} but is not identical with it.

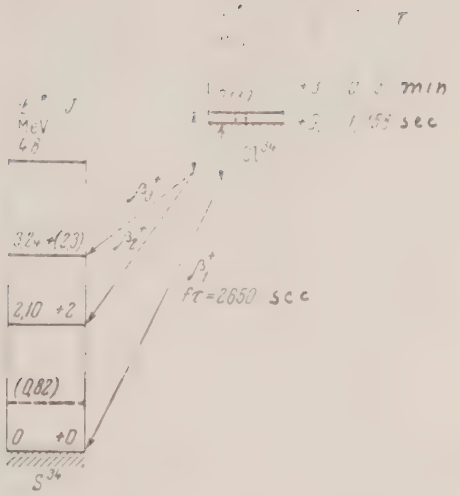

Fig. 4. Decay scheme for Cl^{34}. β^+_1: E_{ep} = 4.45 Mev (46%); β^+_2: E_{ep} = = 2.58 Mev (28%); β^+_3: E_{ep} = 1.3 Mev (26%). [E_{ep}= end-point energy]

In 1953 Arber and Stähelin[55] resolved the inconsistency. They discovered that in the Cl^{35} (γ,n) reaction there is produced, in addition to the 33-min state, another state with a half-life of 1.58 ± 0.05 sec and a positron spectrum end point energy E_{ep} = = 4.45 Mev.

The product $f\tau$ for the β-decay of this state equals 2650 sec, i.e., corresponds to a favored allowed β-disintegration.[40] This is the value of $f\tau$ that should be expected if the new state is of the +0 type and the β-transition decay of the +0 → +0 type.

In the new decay scheme for Cl^{34} the 33 Mev state is the first excited state, has an excitation energy of 139 kev and disintegrates partly directly to S^{34} and partly (about 50 per cent) by isomeric transition (γ and e^-) to the ground state of Cl^{34}. The conversion ratio of the isomeric transition was measured by Arber and Stähelin and proved to correspond to M3. This indicates that the 33-min state is an even state with spin 3. The great difference of momenta explains the high degree of forbiddenness for the 139 Kev transition and the comparatively long lifetime of the first excited state of Cl^{34}.

According to the new scheme the ground state of Cl^{34} is similar to the ground state of S^{34} and should have the same value of isobaric spin. This also follows from the selection rule for the β-decay (see Table 5), according to which +0 → +0 transitions can occur only between states with equal values of T. Since S^{34} has $T_z = 1$, for it $T \geqslant 1$. Whence it follows that for the ground state of Cl^{34} the isobaric spin, $T > 0$, is greater than the minimum possible value of T ($T = T_z$).

It is possible that there are cases even before Cl^{34}, in the interval $20 < A < 34$, where $T > T_z$ for the ground state of the nucleus. There is reason to think that this may be true in the case of Al^{26} for which the difference $Al^{26} - Mg^{26}$ is almost equal to the displacement ΔE and $f\tau$ = 2700 sec. It would seem likely that T = 1 for the ground state of Al^{26}.

Excited states of nuclei with A even. In many cases the isobaric spins of the excited states of nuclei can be determined from data on inelastic scattering of deuterons, α-particles, protons and neutrons. Inelastic scattering of deuterons and α-particles can result only in excited states which have the same isobaric spin as the initial nucleus, while inelastic scattering of protons and neutrons can lead to excited states with an isobaric spin equal to that of the parent nucleus as well as to states with an isobaric spin differing by unity.

By way of example, the analytic procedure for determining the isobaric spins of the excited states of B^{10} is illustrated in Fig. 5. All the excited states, except one, are attained through (d,d') scattering; hence, obviously for these states T = 0. The exception, i.e., the state with an excitation energy of 1.74 Mev, is not obtained by (d,d') scattering but only through (p,p') scattering. For this state, we find T = 1.

A similar analytic diagram for the excited states of N^{14} is shown in Fig. 6. The ground and the first two excited states (2.31 and 3.95 Mev) are obtained by the $N^{14}(p,p')N^{14*}$ reaction, but only the ground state and the second excited state are also attained through the $N^{14}(d,d')N^{14*}$ reaction. It follows that the 2.31 Mev state of N^{14} has T = 1.

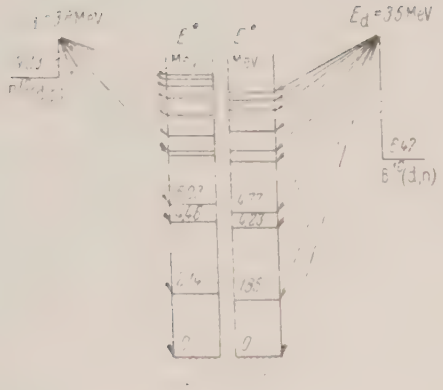

Fig. 8. Determination of the isobaric spins of excited states of the mirror nuclei B^{11} & C^{11}.

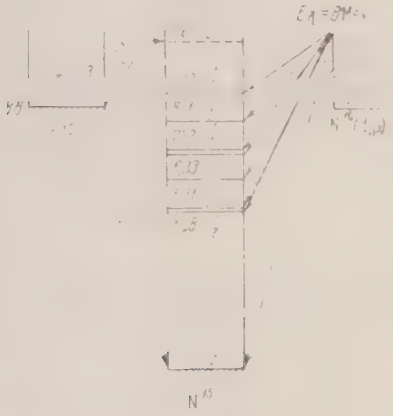

Fig.9. Analysis of isobaric spins of excited states of Ni^{15}.

If light nuclei should have states with high values of T, such states would not be produced as a result of the usual nuclear reactions. It might be thought that numerous excited states with high values of T exist but that we are simply unaware of them due to the fact that they are unattainable by conventional experimental reactions. This is, however, unlikely. As a result of (n,2n), (n,p), (p,n) and (p,2n) reactions there can be formed nuclear states with different degrees of excitation and values of isobaric spin differing by unity, for example, T and T + 1. Since the selection rule for γ-emission allows $\Delta T = 0, \pm 1$, the emission of γ-quanta could lead to states having isobaric spins of T - 1, T, T + 1 and T + 2, while γ-ray cascades could result in states with an even greater diversity of isobaric spins. Since such states have not been observed, it may be assumed that they do not exist.

Gamma-ray absorption reaction. Above we considered nuclear reactions involving only heavy particles. In some cases the isobaric spins of excited states can be determined through comparison of the (γ,n) and (γ,t) reactions. This will be discussed at greater length under Section 9.

The product ft

Wigner and Feenberg[59] and later Kofoed-Hansen[60] called attention to the following attribute of the matrix element of β-decay.

In "pure Fermi" β-transformations of the $+0 \rightarrow +0$ type, the matrix element does not depend on the variant of the β-decay theory or the nuclear model applied. If the charge independence of nuclear forces hypothesis is valid and we can neglect the Coulomb and magnetic forces and the difference (n - p), or, in other words, if the isobaric spin can be regarded as a "good quantum number", the square of the matrix element should be equal to

$$T(T + 1) - T_{z_1} T_{z_2},$$

where T is the isobaric spin common to the two states and T_{z1} and T_{z2} are its components in the respective states. Since T cannot be 0 for the two states of neighboring isobars between which the β-transformation occurs, the matrix element must always be greater than zero.

For all transitions between two states with T = 1, the matrix element squared equals 2; while for transitions between states with T = 2, the matrix element squared equals 6, if at least one of the nuclei has $T_z = 0$. This conclusion can be verified inasmuch as equality of the matrix elements means equality of the products ft.

Three β-disintegrations of the $+0 \rightarrow +0$ type are known: $C^{10} \rightarrow B^{10*}$, $O^{14} \rightarrow N^{14}$ and $Cl^{34} \rightarrow S^{34}$. It is known for certain that T = 1 for both states in the first two cases and there is good reason to assume that this also holds for the last case.

The values of the product ft for the three cases are 6000 ± 3000, 3300 ± 900

and 2650±200 sec, respectively[52].

While in view of the wide limits of error indicated it is impossible to assert positively that these values are equal, it can be seen that all the $f\tau$ values may be equal to 2400-2900 sec. In any case if Cl^{34} and S^{34} had T = 2, the value of $f\tau$ for Cl^{34} would be one half to one third that for the first two cases. Inasmuch as this is apparently not the case, it may be assumed that for both the states connected by the β-transformation T = 1.

Of course, this method of determining the isobaric spin will become of practical value only when the values of $f\tau$ are ascertained with greater precision and an appreciably larger number of +0 → +0 transformations has been studied. Although its practical usefulness lies in the future, it should be noted that this method has one advantage over the previously mentioned methods: it does not involve analysis of a consecutive series of reactions but permits determining T directly for an isolated pair of nuclei.

Investigation of decay processes of the type +0 → +0, T = 1 and $\Delta T = 0$ should prove of great interest. Although the nuclide A^{34} has not yet been observed, there can be little doubt that its ground state is similar to that of S^{34}, since these are mirror nuclei of the second order. This being the case, the $A^{34} \rightarrow Cl^{34}$ decay should be of the above type.

As mentioned above, it may be assumed that Al^{26} also undergoes this type of decay ($f\tau$ = 2700 sec).

It is possible that the newly discovered isotopes of the $_{Z}M^{2Z}$ type - $_{23}V^{46}$ (τ = 0.40 sec), $_{25}Mn^{50}$ (τ = 0.28 sec) and $_{27}Co^{54}$ (τ = 0.18 sec) - also exhibit +0 → +0 decay [61]; using equation (3) given above to compute ΔE and then the end-point energy of the β^+-spectra, we obtain values which in conjunction with the cited experimental values for τ yield a figure in the neighborhood of 2700 sec for the product $f\tau$.

Similar states

There are two ways in which the concept of similar states of isobaric nuclei can be utilized for deducing the isobaric spin.

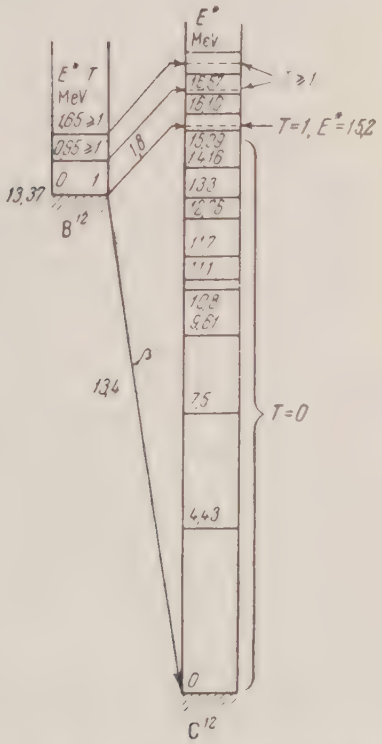

Fig. 10. Isobaric spins of excited states of C^{12}.

A) If for a given nucleus we know the position of the level similar to the ground state of a neighboring, less symmetrical isobar with isobaric spin T_1, we can make use of the fact that all lower-lying levels of the given nucleus have $T < T_1$.

Example: Consider the case of Fig. 10. The 15.09 Mev state of Cl^{12} is presumably similar to the ground state of B^{12} and has T = 1. Hence, all lower-lying states of C^{12} have T = 0, since there can be no states of B^{12} similar to them.

Table 6 lists the positions of the first level having an isobaric spin one unit greater than in the ground state for a number of light nuclides.

B) If neighboring isobars have similar states[34], i.e., levels displaced relative to each other by $\Delta E_{Coul} - (n - p)$ and characterized by the same angular momentum (spin) and parity, it may be assumed that these states have the same value of isobaric spin. In no known instance does experiment invalidate this assumption. Consequently, where the isobaric spin for any one of the states can be deduced in some way (for example, analysis of nuclear reactions), we immediately know the value of T for all other similar states.

Example 1: He^6 - Li^6. Consider the 3.572 Mev excited state of Li^6 (Fig. 11), which is formed in

Table 6

Excitation energy (Mev) of the first levels of light nuclei, having an isobaric spin one unit greater than in the ground state.

"Symmetric" nuclei - $_ZM^{2Z}$ (ground state, T = 0)		Mirror nuclei - $_ZM^{2Z+1}$ (ground state, T = ½)
"Deuteron" nuclei	"α-particle" nuclei	States with T = 3/2
States with T = 1	States with T = 1	
Li^6: 3.572 (5.28) B^{10}: 1.72, 5.11 or 5.17 N^{14}: 2.31, 8.06 F^{18}: (1.20)	Be^8 : 16.9 (19.18) C^{12} : 15.09, 16.10 O^{16} : 12.51, 13.09 Ne^{20}: (10.22, 10.9)	Be^9 & B^9 : 15.0 O^{15} & N^{15}: 10.9 O^{17} & F^{17}: 11.3

Note: The values in parenthesis are conjectural.

the $Be^9(p,\alpha)$ and $Li^7(p,d)$ reactions. Inasmuch as both Be^9 and Li^7 have T = ½, the excited state in question must have T = 0 or T = 1. Apparently this state is similar to the ground state of He^6. Addition of the equivalent of ΔE_{Coul} - (n - p) to the mass of He^6 leads to an excitation energy value of 4.04 Mev for Li^6. Although the difference between the computed and observed value of the excitation is appreciable, it can be ascribed to the error in computing the Coulomb energy and to the ever-present, but so far unexplained, relative downward shift of the similar state of the isobar with the larger atomic number. Inasmuch as Li^6 exhibits no other excited levels in the 3 to 5 Mev interval, there can be little doubt that the 3.572 Mev state of Li^6 is the one similar to the 0 Mev state of He^6. Since, as was shown above (in our discussion of isobaric spins of nuclei in the ground state) He^6 has T = 1, we conclude that the isobaric spin of the 3.572 Mev state of Li^6 is also 1.

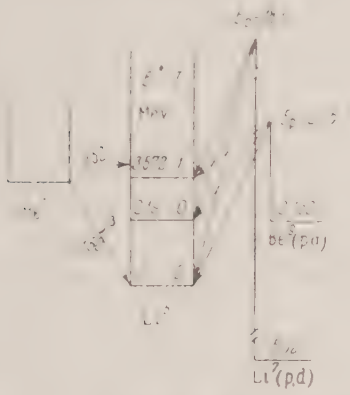

Fig. 11. Use of the similar states, 0 Mev of He^6 and 3.572 Mev of Li^6, to determine the isobaric spin of the latter.

Example 2 : States with T ⩾ 1. The 17.0 Mev and 19.28 Mev states of Be^8 should be similar to the ground and 2.28 Mev excited states of Li^8. In the above interval of excitation of Be^8 the levels are closely spaced; moreover, the nuclear reactions which could aid us in determining the isobaric spins have not been investigated. Hence in seeking to identify the states of Be^8 similar to states of Li^6 we must depend on comparison of the quantum characteristics of the corresponding levels.

The state similar to the 3.37 Mev state of Be^{10} is probably either the 5.11 or the 5.17 Mev state of B^{10}. The states of C^{12} similar to the 0, 0.947 and 1.65 Mev states of Be^{12} are probably the 15.09, 16.10 and 16.8 Mev excited states of this carbon isotope. The 8.06 Mev state of N^{14} is probably similar to the 6.10 Mev state of C^{14}; the 0 and 1.6 Mev states of N^{16} are probably similar to the 12.51 and 13.09 Mev states of O^{16}, etc.

Now Be^{10}, Be^{12}, C^{14} and N^{16} are all $_ZM^{2Z+2}$ nuclei, for all states of which T ⩾ 1. Consequently the designated state of the other nucleus of each of the above pairs must also have T ⩾ 1. Our determination is only tentative, for

definitive identification of similar states cannot be based exclusively on measurement of the mass differences, in view of the fact that the uncertainty of computing the Coulomb energy and the previously mentioned relative shift of the levels of nuclei with high values of Z can, in some cases, amount to several hundred kev while some of the more symmetrical nuclei have several levels within this energy interval. Hence to identify the similar levels and establish the isobaric spin of the excited states of Be^8, B^{10}, C^{12} and the other nuclides with a greater degree of certainty one must carry out a careful analysis and comparison of the corresponding angular momenta and parities.

Example 3: The mirror pair Li^7 & Be^7. As is known, the ground states and corresponding excited states of mirror nuclei are similar. It is probable that the isobaric spins of the corresponding state-pairs are also equal. In many cases this can be shown directly through analysis of nuclear reactions (see, for example, Fig. 8 for the B^{11} - C^{11} pair). In other cases, where experimental data is lacking, the unknown isobaric spin can be established by making use of the similarity principle. Thus we can readily show that the ground and 0.478, 4.61 and 7.46 Mev levels of Li^7 all have $T = \frac{1}{2}$ inasmuch as the first three are attained through the $Li^6(d,p)$ and $Li^7(d,d')$ reactions, while the last is produced by the $Li^6 + n$ and $Be^9(d,n)$ reactions. No similar nuclear-reaction data is available where the 6.56 Mev level of Li^7 is concerned.

We deduce that the 0 and 0.430 Mev states of Be^7 have $T = \frac{1}{2}$ since they are formed in the reaction $Li^6(d,n)$ and that the 6.4 and 7.16 Mev states of Be^7 also have $T = \frac{1}{2}$ since they are intermediate products in the $Li^6 + p \rightarrow Be^7 \rightarrow He^3$ reaction. Nothing is known regarding the 4.6 Mev state of Be^7. By combining all these data we can readily show that the isobaric spins of the paired states 0 Mev of Li^7 & 0 Mev of Be^7, 0.478 Mev of Li^7 & 0.430 Mev of Be^7 and 7.46 Mev of Li^7 & 7.16 of Be^7 are equal; in the light of this we are probably safe in assuming that the isobaric spin of the 4.6 Mev state of Be^7 and the 6.56 Mev state of Li^7 also equals $\frac{1}{2}$.

7. Uniqueness of the Isobaric Spin and Strictness of the Selection Rules

It follows from what has been said above that if the n-n, n-p and p-p forces are exactly equal and the n and p masses are identical the isobaric spin must be an integral of the motion or, to employ the expression used in quantum mechanics, is a "good quantum number". Under these conditions it is analogous to the total mechanical momentum J.

Actually, however, the forces of interaction between nucleons are probably only approximately equal, the neutron and proton masses are slightly different and the electrostatic and magnetic forces undoubtedly violate the ideal conditions.

In consequence the isobaric spin ceases being a "good quantum number" and components with different values of T (but, of course, with the same values of the ordinary spin and parity) appear in the wave equations of the system. That is, a similar situation obtains as in the case of the orbital momentum of the nucleus, where, in consequence of the fact that the nuclear forces are not precisely central, the orbital momentum is not a perfect quantum number and the wave functions of nuclei comprise components with different values of L, but with the same total momentum and parity. Thus the expression for the ground state of the deuteron, which has a spin 1, contains functions with $L = 0$ (S_1-state) and $L = 2$ (D_1-state) ($L = 1$ is excluded by the law of the conservation of parity): figuratively speaking, it may be said that the deuteron is in the S_1-state 96% of the time and in the D_1-state 4% of the time.

In light nuclei non-central forces play a relatively unimportant part and consequently the component of the wave function relating to one of the values of L is appreciably greater than others.

Analogously, in light nuclei the deviations from charge independence are minor and consequently one of the values of T is the principal one.

The fact that T does not have a unique value should lead to a certain "relaxation" of the strictness of the selection rules. That is, where the selection

rules cited in Table 5 forbid a certain reaction or transformation for the principal value of T, they may allow it for the admixture state or states having a different value of T. Thus a transformation, strictly forbidden for the principal value of T, may nevertheless occur.

In order to describe the admixture of different states quantitatively, the wave function may be expressed in the form

$$\psi = \psi(T) + \sum_{T'} \alpha(T')\psi(T'),$$

where $\psi(T)$ is the component relating to the principal value of the isobaric spin T, $\psi(T')$ is the component corresponding to the isobaric spin T' and $\alpha(T')$ is a coefficient characterizing the extent or amplitude of the admixture of the state with T'.

If some process is forbidden for the principal value of T, but allowed for T', the magnitude of $\alpha^2(T')$ determines the residual probability of the process.

The value of the coefficient $\alpha(T')$ can either be evaluated theoretically on the basis of certain assumptions regarding the nuclear forces and structure or derived from experimental data.

Theoretical evaluation

The admixture of functions relating to different values of T may be due to a certain dependence of the nuclear forces on the charge, to the effect of Coulomb forces or to inequality of the n and p masses.

The only theoretical evaluations of $\alpha(T')$ we know of are concerned solely with the effect of the Coulomb field and limited to two particular cases. In the first, Radicati[62] examined the possible admixtures to the ground state of a symmetrical nucleus with $T_z = 0$, in which there are two nucleons external to the closed shell (i.e., nuclei of the Li^6, N^{14}, F^{18} type).

The ground state of these nuclei has T = 0, J = 1, S = 1 and L = 0. Radicati determined the admixture of the state with T = 1, J = 1, S = 1 and L = 0, due to the effect of the Coulomb field of the shell on the two external nucleons (states with T = 1 and J = 1, but other values of S and L do not yield admixtures). The energy of the first excited state with T = J = S = 1 and L = 0 was computed assuming a square potential well; the value found for N^{14} was 40 Mev, which is probably too high. Having computed the matrix element connecting this excited state with the ground state, Radicati obtained $\alpha^2(1) = 2.5 \cdot 10^{-3}$.

The second evaluation was for the case where in addition to the closed shell there are four external nucleons (as in the Be^8 and Ne^{20} nuclei) or where the closed shell has four vacancies (as in the C^{12} and A^{36} nuclei). The ground states of these nuclei have T = J = S = L = 0; one may expect admixtures of the states with T = 1, J = 0, S = 0 and L = 0 and with T = 2, J = 0, S = 0 and L = 0. Radicati's rough approximations indicate that in C^{12} these levels should lie at about 15 Mev. This value yields

$$\alpha^2(1) \lesssim 5 \cdot 10^{-5} \text{ and } \alpha^2(2) \lesssim 4 \cdot 10^{-6}.$$

Obviously these are no more than very approximate evaluations and for particular cases at that.

Nevertheless it may be concluded that the Coulomb force of the nuclear shell on the nucleons external to it does not produce an appreciable displacement of the energy level.

Hence if it turns out that nuclear states are very "pure" as regards the isobaric spin, this may be taken as an indication that the other causes, too, do not produce energy-displacement of the nuclear states and that, consequently, nuclear forces are virtually independent of the charge.

The evaluations made by Radicati relate only to the ground states of nuclei. The values of $\alpha(T')$ increase as the distance between the T and T' levels decreases. The higher the excitation of a nucleus, the smaller the mean separation of the levels. Hence as the excitation increases, α tends to 1 and the uniqueness of the isobaric spin vanishes, i.e., its value becomes ambiguous.

Experimental determinations

Experimental determinations of the admixture of states can be made by observing cases of violation of the selection rules. The selection rules governing nuclear reactions are the most strict.

Thus, for example, the $O^{16}(d,\alpha)2.31$ Mev N^{14} reaction is entirely forbidden; if it should occur to any minor extent, its relative intensity is determined by the admixture of the state with T = 0 to the 2.31 Mev state of N^{14} having T = 1.

The most conclusive results to date have been obtained, for two particular cases, by Buechner and his associates who for many years have carried on studies of the spectra of the charged particles emitted in nuclear reactions. In the investigations of this group the protons or deuterons are accelerated by an electrostatic generator and a well collimated, monoenergetic portion of the beam is directed at a very thin target. The secondary particles knocked out at 90° to the direction of the incident beam are analyzed by means of a magnetic spectrometer.

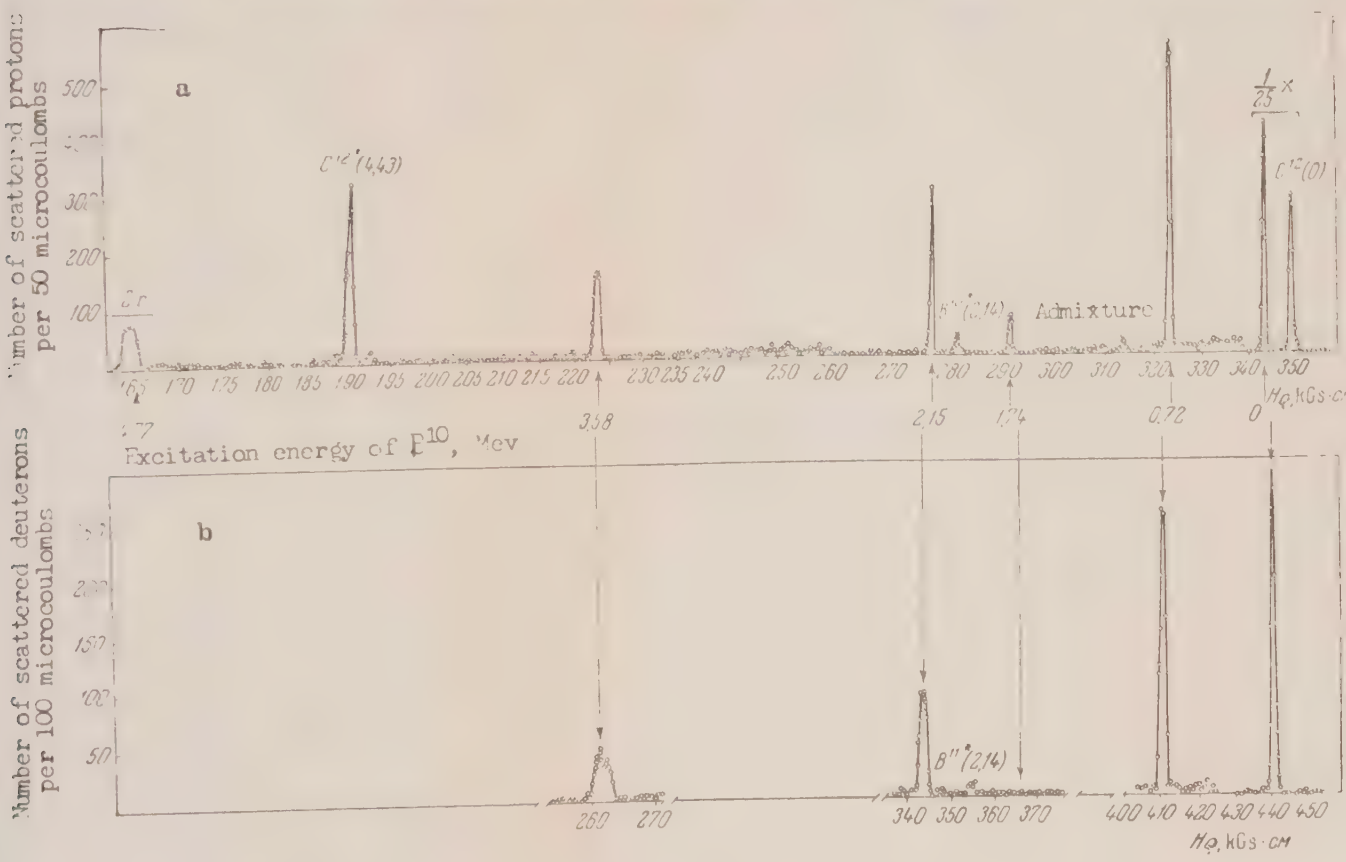

Fig. 12. Groups of protons (a) and deuterons (b) inelastically scattered by B^{10} at an angle $\theta = 90°$ (according to Ref. 63). Energy of the incident protons: 6.92 Mev; energy of the incident deuterons: 6.98 Mev. In proton scattering excited states of B^{10} having energies of 0.72, 1.74, 2.15, and 3.58 Mev are formed. With deuteron scattering the same states are obtained, with the exception of the 1.74 Mev state, the appearance of which is forbidden by the conservation of isobaric spin law.

Fig. 12 shows the results of the measurements of the spectrum of protons (a) and deuterons (b) inelastically scattered by B^{10} (Ref. 63). The ordinate scales have been selected to facilitate matching of lines pertaining to equal-energy levels. In the upper figure (a), the pronounced peaks correspond to elastic scattering (0 Mev) and inelastic scattering of protons at the 0.72, 1.74, 2.15, 3.58 and 4.77 Mev levels of B^{10}. In the lower curve (b) one can find deuteron scattering resonances corresponding to all the above levels with the exception of the one at 1.74 Mev, which we have already encountered in our discussion of Fig. 5 and which has T = 1. In the region of the lower curve corresponding to the 1.74 Mev peak we find only a weak scattered background showing little variation over a wide energy interval.

The values of the relative intensities are listed in Table 7.

Table 7

Relative intensity of groups of protons and deuterons inelastically scattered from B^{10} and N^{14} nuclei ($E_{p,d} \simeq 7$ Mev)

Level of B^{10}	Protons	Deuterons	Level of N^{14}	Protons	Deuterons
0	100	100	0	100	100
0.72	6	9	2.31	5	<0.5
1.74	1	<0.15	3.95	10	10
2.15	5	4			
3.58	5	4			

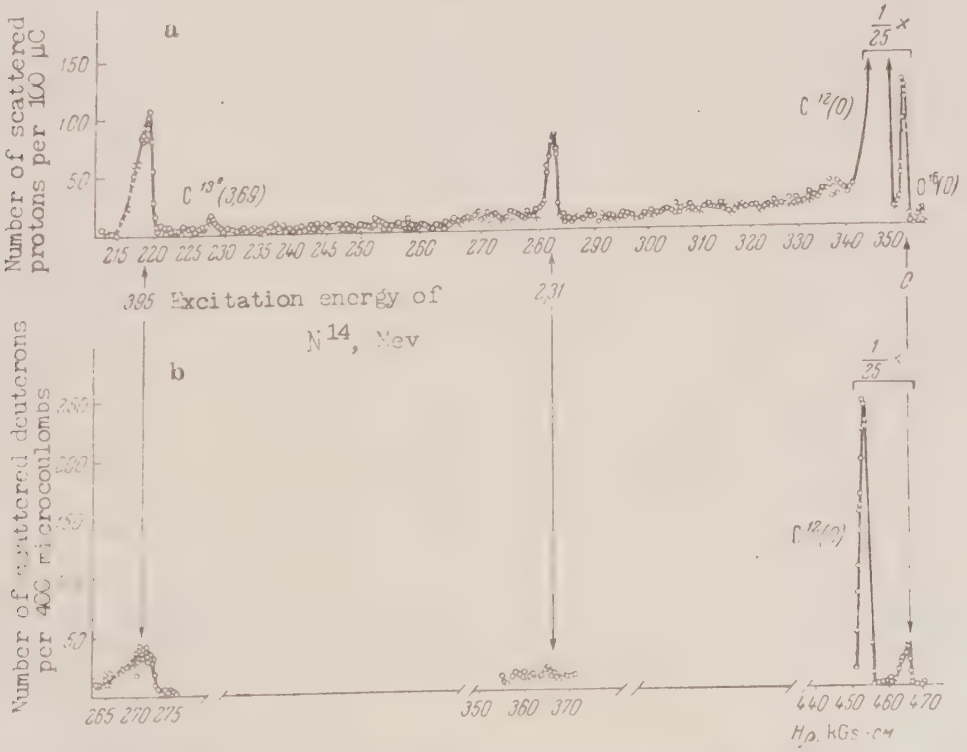

Fig. 13. Same as Fig. 12 but for scattering by N^{14}. In proton scattering excited states of N^{14} with energies of 2.31 and 3.95 Mev are formed; the 2.31 Mev state does not form in the case of deuteron scattering since it is forbidden by the conservation of isobaric spin.

The selection rules allow the $B^{10}(d,d')$ reaction only for the state with T = = 0. In order to determine the upper bound of $\alpha^2(0)$ from the data of Table 7 one would have to know to what extent the group corresponding to the 1.74 Mev level

of B^{10} is weakened compared to what it would be if the reaction were not forbidden by the isobaric spin selection rule. It is impossible to compute this since present-day theory is not sufficiently advanced to permit evaluating the relative intensity of individual lines from the scattering angle of the particles and energy and the spin and parity of the formed states.

We are, therefore, reduced to an approximation: assuming that the relative intensities of the groups produced by the (p,p') and (d,d') reactions vary in parallel and differ at no point by a factor of over 1.5, we conclude that the hypothetical group of deuterons, corresponding to the 1.74 Mev level of B^{10}, would have a relative intensity of 1 ± 0.5. From this we get $\alpha^2(0) < 0.15/0.5 = 0.3$ and $\alpha(0) < 0.55$.

Analogous results were obtained by Buechner and associates for the $N^{14}(p,p')$ and $N^{14}(d,d')$ reactions (Fig. 13). The relative yields of the particles are listed in Table 7. Reasoning as outlined above for B^{10}, we arrive at $\alpha^2(0) < 0.5/2.5$ and, hence, $\alpha(0) < 0.45$.

These values appear to be excessively high. Buechner et al indicate that the upper limits of $\alpha^2(0)$ may be reduced to <0.04 for the 1.74 Mev state of B^{10} and to <0.1 for the 2.31 state of N^{14}.

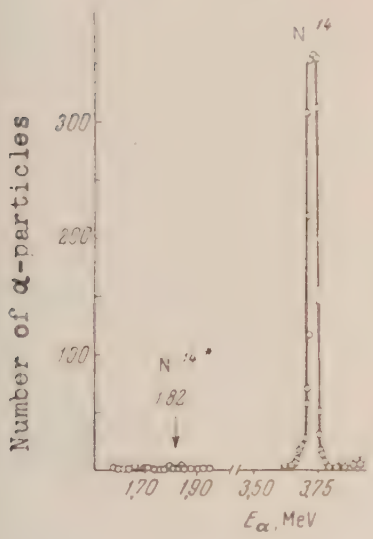

Fig. 14. Spectrum of α-particles emitted in the $O^{16}(d,\alpha)N^{14}$ reaction. The α-particle group associated with the 2.31 Mev state of N^{14} is missing; it should have an energy of 1.82 Mev.

The results of an investigation[58] of the α-particle spectrum obtained in the $O^{16}(d,\alpha)N^{14}$ reaction are shown in Fig. 14. While the group of α-particles emitted by N^{14} in the ground state is clearly discernible, no group associated with the 2.31 Mev state is observed; the group should have an energy of 1.82 Mev (or slightly less due to slowing-down in the target) and should appear at the point indicated by the arrow in the figure. The investigators note that their instrument was sensitive enough to detect a group having an intensity of only 1/50 that of the ground state group.

In addition to the above, a number of other attempts to evaluate the admixture of isobaric spin values for certain states of Be^{10}, B^{10}, C^{12} and O^{16} have been reported (Refs. 48, 64, 65 and 66), but in most cases the results are questionable due to the incompleteness of the experimental data.

8. Isobaric Spin and Gamma-Emission

The selection rule for γ-emission ($\Delta T = 0, \pm 1$) is so unrestrictive that it virtually forbids nothing, for so far no levels in any nucleus are known for which the isobaric spin differs by more than one unit from the isobaric spin of the ground state.

The rule concerning nuclei with equal numbers of protons and neutrons ($T_z = 0$) is more restrictive. Here only transitions with $\Delta T = \pm 1$ are allowed for electric dipole emission (E1 transitions).*

For $\Delta T = 0$ the probability is reduced by a factor of about $(\lambda/R)^4$ where λ is the wavelength of the γ-rays and R is the radius of the nucleus.[67] Thus in the case of A = 20 and $h\nu = 1$ Mev the probability is decreased about $300^4 \approx 8 \cdot 10^7$ times.

---

*We remind the reader that E1 (electric dipole) type transitions comprise transitions in which the total momentum changes by 0 or 1 and the parity is altered; $0 \rightarrow 0$ transitions are excluded.

A number of instances of the operation of this selection rule have been observed experimentally. The corresponding γ-lines are either greatly weakened or vanish altogether. It is not clear, however, whether any persisting intensity is connected with the fact that El transitions are not entirely forbidden or with the ambiguity ("non-uniqueness") of the isobaric spin values of the given states.

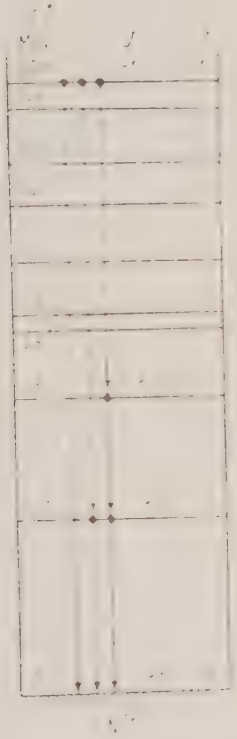

Fig. 15. Gamma-transitions from the 8.06 Mev state of N^{14}.

N^{14}

The 8.06 Mev state of N^{14} (Fig. 15) is apparently of the -1 type [spin one; parity odd]. It is formed as a result of radiative capture, by the $C^{13}(p,\gamma)N^{14}$ reaction, at a proton energy of 554 kev.[68] The great width of the proton resonance (32 kev)[69] and the isotropy of the γ-radiation[70] indicate capture of protons with zero orbital angular momentum and hence that the 8.06 Mev state of N^{14} is of the -0 or -1 type (the parity and spin assignment for the ground state of C^{13} is $-\frac{1}{2}$). Inasmuch as there is a definite if weak γ-transition to the 2.31 Mev level of N^{14} belonging to the +0 type, it follows that the -0 assignment for the 8.06 Mev level of N^{14} is excluded and only -1 remains.

This state of N^{14} is apparently similar to the 6.093 Mev excited state of C^{14}. The state should presumably lie at 2.31 + 6.093 = 8.40 Mev, but in nuclei with a large value of Z, similar levels, as a rule, have a reduced energy. In any case N^{14} exhibits no other states in the 8.14 to 7.69 Mev interval. If, therefore, the N^{14} 8.06 Mev and C^{14} 6.093 Mev states are similar states, the former should have T = 1 inasmuch as the latter undoubtedly has T = 1 (it has $T_z = 1$ and is obtained by the $C^{13}(d,p)C^{14}$ reaction).

The 8.06 Mev state of N^{14} decays by γ-emission; direct and cascade transitions to the ground level produce γ-rays with $h\nu_1 = 8.03\pm0.08$, $h\nu_2 = 5.81\pm0.25$, $h\nu_3 = 4.1$, $h\nu_4 = 2.3\pm0.4$ and $h\nu_5 = 1.6$ Mev (Refs. 68, 71 & 72) (see Fig. 15). The 8.06 Mev → 0 Mev, 8.06 Mev → 2.31 Mev and 8.06 Mev → 3.9 Mev transitions are all El, but the first and third occur between levels with T = 1 and T = 0 and hence are not forbidden; the second is between two levels with T = 1 and consequently is forbidden by the selection rules for isobaric spin.

Actually this transition is so weak that there is no mention of it in the last reference [72], although the $h\nu = 8.03$ and $h\nu = 4.1$ Mev lines were clearly distinguished in this investigation.

It may be noted that in the case of C^{14} there is known to be a transition between the 6.093 Mev state and the ground state of C^{14}, which states are similar, respectively, to the 8.06 and 2.31 Mev states of N^{14}. Here the transition is also between states with T = 1 and is an electric dipole transition; however, since the C^{14} nucleus has unequal numbers of protons and neutrons, the γ-emission, forbidden for the N^{14} nucleus, is not forbidden for the C^{14} nucleus. Both Thomas and Lauritsen[73] and Baggett and Bame[74] report observing this transition in C^{14}; the latter also observed the internal conversion positrons emitted in this transition and found that the number of these is consistent with an El transition, although the possibility of it being E2 or Ml is not wholly excluded.

O^{16}

The energies and quantum characteristics of the ground state and the first four excited states of O^{16} are indicated in Fig. 16. The values are taken from the survey by Ajzenberg and Lauritsen.[52] All these states have T = 0; the lowest

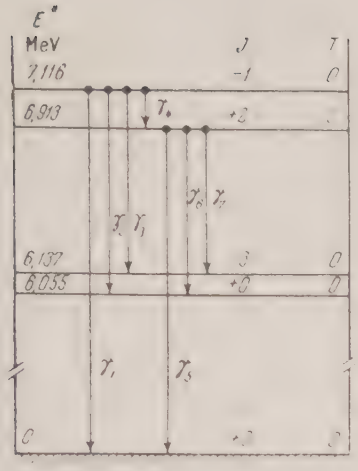

Fig. 16. -transitions between the lower excited states of O^{16}.

level of O^{16} having T = 1 lies at 12.51 Mev[18] (it is similar to the ground state of N^{16}). All the excited states can lose energy only by γ-emission or conversion.

Let us examine the highest state shown in Fig. 16: this familiar state, which has an excitation energy of 7.116 Mev, is obtained as a result of the $F^{19}(p,\alpha)O^{16}$ reaction[75] or through β^--decay of N^{16}(Refs. 76 & 77).

It is the source of four γ-lines:

γ_1: $h\nu_1$ = 7.116 Mev $-1 \rightarrow +0$ E1,
γ_2: $h\nu_2$ = 1.061 Mev $-1 \rightarrow +0$ E1.
γ_3: $h\nu_3$ = 0.979 Mev $-1 \rightarrow -3$ E2,
γ_4: $h\nu_4$ = 0.203 Mev $-1 \rightarrow +2$ E1.

The first line is well-known[78]; the last has a low energy and must be relatively weak.

Let us assume that we have O^{16} appropriately excited to the 7.116 Mev state. If the isobaric spin selection rule was strict, the three lines γ_1, γ_2 and γ_4 would be entirely forbidden and the whole discharge would take place through the cascade starting with γ_3. By measuring the intensity ratios γ_1/γ_3, γ_2/γ_3 and γ_4/γ_3 one can evaluate the degree of forbiddenness.

Wilkinson and Jones[79] excited the 7.116 Mev state of O^{16} by the resonance method, using the $F^{19}(p,\alpha)O^{16}$ reaction, and studied the resultant γ-ray spectrum by means of a luminescent NaI(Tl) crystal. Not only was the "forbidden" γ_1 line clearly visible, but the investigators could not detect the allowed γ_3 line. In view of the sensitivity of the detectors used they concluded that $\gamma_1/\gamma_3 > 120$.

Evaluating the relative probabilities of the γ_3 and γ_1 lines according to Weisskopf's equations for the single particle model, we get

$$\gamma_1/\gamma_3 = 2.4\cdot10^7.$$

It follows that the "forbidding" of the γ_1 line by the isobaric selection rule could not reduce its intensity by a factor exceeding $2.4\cdot10^7/120 = 2\cdot10^5$.

If the residual intensity of the γ_1 line is ascribed to an admixture of a state with T = 1 (transitions from which are not forbidden), the value of $\alpha(1)$ adequate to explain the above results equals $(2\cdot10^5)^{-\frac{1}{2}}$ ≈ 0.2%. It must be recalled however that the isobaric selection rule does not completely bar E1 transitions.

We turn next to the 6.913 Mev state of O^{16}. Transitions from this level can give rise to the following lines:

γ_5: $h\nu_5$ = 6.913 Mev $+2 \rightarrow +0$ E2,
γ_6: $h\nu_6$ = 0.858 Mev $+2 \rightarrow +0$ E2,
γ_7: $h\nu_7$ = 0.776 Mev $+2 \rightarrow -3$ E1.

The isobaric spin selection rule forbids only the γ_7 line transition. Experiments carried out by Wilkinson and Jones[79] indicate that $\gamma_5/\gamma_7 > 200$.

If not forbidden by isobaric spin considerations, the γ_5 line should show one sixth the intensity of the γ_7 line. Thus the isobaric "prohibition" weakens the intensity of the γ_5(E1) line by a factor of over 1200. This also means that the admixture of states with T = 1, for which corresponding transitions are not forbidden, does not exceed $1200^{-\frac{1}{2}} \approx 3\%$ in amplitude for both the discussed states of O^{16}.

9. Isobaric Spin and the Excitation of Nuclei by γ-Rays

The processes of γ-emission and excitation of nuclei by γ-rays are interrelated. Where a given γ-emission is forbidden, the corresponding excitation is also forbidden. Isobaric selection rules which do not restrict γ-emission from light nuclei, with the exception of $_{Z}M^{2Z}$ nuclei, naturally do not limit photoexcitation of all types of nuclei, except $_{Z}M^{2Z}$. Hence in this section we will consider only $_{Z}M^{2Z}$ nuclei, for which one may expect to find a number of "isobaric" anomalies.

The ground states of light ($A \leq 20$) nuclei of the $_{Z}M^{2Z}$ type all have $T = 0$.

By irradiating nuclei of this type with γ-rays with an energy $h\nu$ one can expect to excite states having an excitation energy inferior to $h\nu$. If a continuous spectrum is used for irradiation, the actual excitation is produced by a narrow spectral band, the width of which corresponds to the partial width of the γ-quanta emission of the same energy after excitation.

Electric dipole emission is the "fastest"; its emission time is the shortest, its radiation width, the greatest. Consequently the probability of excitation by a continuous γ-ray spectrum is the highest in the case when E1 transitions are possible. However, when in a $_{Z}M^{2Z}$ type nucleus there exist, among the levels with $T = 0$ and $E^* \leq h\nu$, one or more states for which the transition to the ground state belongs to the E1 type, the excitation of such states will be restricted by the operation of the isobaric selection rule (i.e., the probability of their excitation is decreased approximately in proportion to the ratio of the probabilities of E1 to M2 emissions).

Hence if the energy $h\nu$ is insufficient to excite the first level with $T = 1$, the excitations of the nucleus will occur in accordance with the probabilities of E2, M1, M2, etc. type transitions (depending on the specific quantum characteristics of the levels with $E^* \leq h\nu$.

If the upper bound of the γ-ray spectrum is raised, there comes a point where the first level with $T = 1$ is reached. If the spin and parity of this level are such that transitions from it to the ground level are of the E1 type, there should at this point be observed a sharp rise in the probability of excitation (in accordance with the shape of the continuous γ-spectrum near its end point).

On the other hand, if the spin and parity of the first state with $T = 1$ are such as to forbid E1 transitions, the excitations will be correspondingly less intense. This will continue as the spectrum limit is raised until a level with $T = 1$ to which E1 transitions from a lower level are allowed, when the intensity of excitations will increase sharply.

By way of example, let us examine the N^{14} nucleus. The ground state has $T = 0$ and $J = \pm 1$; the sought state that can be excited by electric dipole absorption must have $T = 1$ and $J = -0, -1$ or -2.

The numerous states of N^{14} with $T = 0$ and the well-known 2.31 Mev state having $T = 1$ and $J = +0$ do not meet these requirements. Apparently the first state to meet them is the 8.06 Mev state of N^{14} for which $T = 1$ and $J = -1$. Hence intensive excitation of N^{14} should begin with $h\nu > 8.06$ Mev.

It should be noted that in nuclei of the C^{12}, O^{16} and N^{20} type the first $T = 1$ level lies above 10 Mev (see Table 6), while in nuclei of the Li^6, Be^{10}, N^{14} and F^{18} type it lies appreciably below 10 Mev. Consequently excitation of nuclei of the latter type by hard γ-radiation (for example, 17.6 Mev γ-rays should be more intense.

(γ,n) and (γ,t) reactions

Peaslee and Telegdi[80] called attention to the fact that the isobaric spin of a number of states could be determined through comparison of the (γ,n) and (γ,t) reactions.

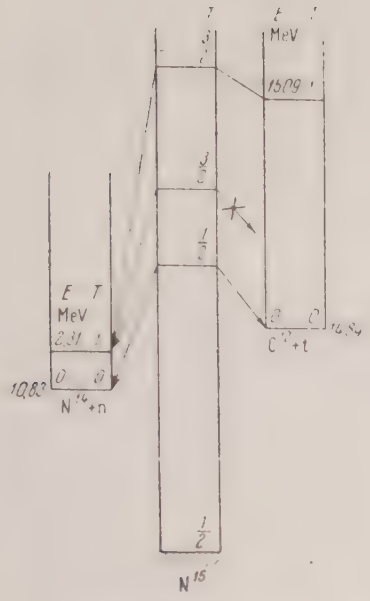

Fig. 17. $N^{15}(\gamma,n)$ and N^{15} (γ,t) reactions passing through excited states of N^{15} having $T=\frac{1}{2}$ and $T=3/2$. Level locations shown are tentative.

The case of N^{15} can serve as an example (see Fig. 17). In its ground state, as was noted above, the N^{15} nucleus has $T = \frac{1}{2}$.

Among the numerous excited levels of N^{15}, some have $T = 1/2$, others have $T = 3/2$; both the former and the latter can be excited by γ-radiation. In the case of resonance excitation of the former, both the $N^{15*} \rightarrow$ $\rightarrow N^{14} + n$ and $N^{15*} \rightarrow C^{12} + t$ processes may occur; the N^{14} and C^{12} nuclei are found to be in the ground state or in one of the excited states with $T = 0$ or $T = 1$. In the case of resonance excitation of N^{15*} to levels with $T = 3/2$, the above gamma-induced processes can take place only when the product nucleus arrives at a state with $T = 1$. In the case of N^{14}, the state with $T = 1$ is low-lying (2.31 Mev), while in the case of C^{12} it is a high-lying state (15.09 Mev).

Whence it may be concluded that if both the (γ,n) and the (γ,t) reactions occur at excitation energies under 30 Mev the initial level of N^{15*} has $T = 1/2$, while if only the (γ,n) reaction takes place, the level in question has $T = 3/2$.

A similar analysis can be carried out for the Li^7, B^{11} and F^{19} nuclei.

10. Isobaric Spin and Photodisintegration

The (γ,α) reaction with α-particle nuclei: C^{12}, O^{16}, Ne^{20}, etc.

Irradiation of nuclei of the C^{12}, O^{16} and Ne^{20} type by a continuous hard γ-ray spectrum results in the formation of various excited states of these nuclei. Many of these states in decaying are capable of emitting an α-particle. We must distinguish between the following (γ,α) reactions:

a) The "allowed" dipole reaction when the initial nucleus absorbs the electromagnetic wave as an electric dipole (E1 excitation) and then emits an α-particle without violating the isobaric selection rules.

b) The forbidden dipole reaction when the initial nucleus undergoes dipole excitation but cannot emit an α-particle without violating the isobaric selection rule.

c) Other reactions in which the nucleus absorbs a wave of higher multiplicity than E1 (for example, E2, M1, M2, etc.).

The (γ,α) reaction proceeds with particularly high intensity when the γ-ray energy is high enough to produce allowed dissociations of type a); it still occurs, however, when type a) dissociations are barred but the b) and c) reactions are possible.

In view of the fact that the nuclei in question have $T_z = 0$, the special rule of Table 5 is applicable: $T = \pm 1$ for E1 and $T = 0, \pm 1$ for other multipoles.

Inasmuch as the ground state of these nuclei has $T = 0$ and $J = \pm 0$, dipole excitation is possible only for states with $T = 1$ and $J = -1$. However, that a state with $T = 1$ and $J = -1$ be attainable is a necessary but in itself not sufficient condition for the dipole reaction to be "allowed": the formed state must also be able to disintegrate into an α-particle and a product nucleus with $T = 1$, since only this disintegration is allowed by the isobaric selection rules.

If there is excited such a state with $T = 1$ and $J = -1$ that after emission of the α-particle the product nucleus can reach only states with $T \neq 1$, the decay can occur only in violation of the isobaric selection rules.

By way of example, let us examine the $C^{12}(\gamma,\alpha)Be^8$ reaction. In recent years this reaction has been studied by a number of investigators[81-89] by means of nuclear emulsions; when the incident γ-radiation is sufficiently hard the tracks show the tracks of three α-particles, emitted in the (γ,α) reaction and the subsequent disintegration of Be^8.

The energy threshold of the reaction for the ground state of Be^8 is $h\nu = 7.4$ Mev.

The cross section of the reaction up to $h\nu = 15$ Mev is small ($\sigma = 30$ μbarns); the cross section shows a first maximum at 18 Mev ($\sigma \approx 130$ μbarns) and a second maximum at $h\nu \approx 27$-31 Mev ($\sigma \approx 200$ μbarns), after which the cross section falls off rapidly (Fig. 18).[87 & 88]

The initial section of the curve and the first peak relate to the excitation of the numerous levels of C^{12} lying in the 7.4 to 20 Mev interval (Fig. 19). Most of these levels have T = 1 and are excited by E2, M1 or M2 transitions, which are not forbidden by the isobaric selection rules. These states decay with the emission of an α-particle to the ground or first excited state (3.0 Mev) of Be^8 (for both states T = 0). The energy distribution of the α-particles indicates that at the first maximum the decay leads primarily to the 3.0 Mev state of Be^8.

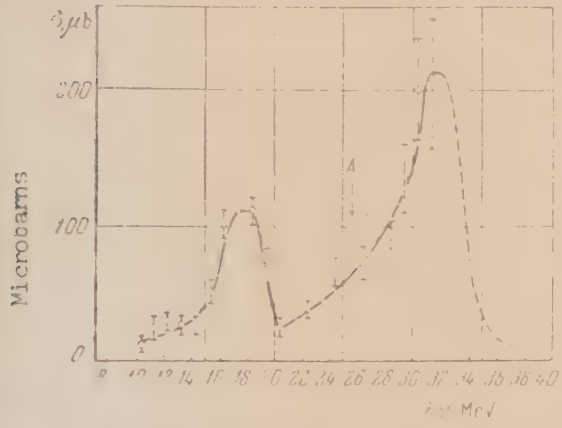

Fig. 18. Variation of $C^{12}(\gamma,\alpha)Be^8$ cross section with γ-ray energy.

The fact that C^{12} has a first level with T = 1 at 15.09 Mev is not reflected in the cross section curve for the reaction, since the dissociation of this state into $\alpha + Be^8$ is, in principle, forbidden; furthermore this level of C^{12} is probably +1 and hence is not excited by dipole transitions. The same argument applies to the next T = 1 level of C^{12}, having an energy of 16.1 Mev and a parity and spin of +2. However, higher up, in the 17 to 25 Mev excitation energy interval, there must be a number of states with T = 1 and at least one of them must be of the -1 type (i.e., attainable by dipole excitation), but as noted above, the $\alpha + Be^8$ dissociation (T = 0) can occur only due to ambiguity ("non-uniqueness") of the isobaric spin.

The situation should change radically at $h\nu > 24.4$ Mev when dipole excitation of T = 1 levels of C^{12} capable of decaying, by α-emission, to the first state of Be^8 with T = 1 (excitation energy: 17.0 Mev) becomes possible. The rapid rise of the cross section curve (Fig. 18) after the 24.4 Mev point is doubtless due to the inception of this "allowed" process.

Wilkins and Goward[87] showed that most of the disintegration at $h\nu = 26$ Mev do actually lead to the formation of the 16.9±0.3 Mev state of Be^{8*}. Gell-Mann and Telegdi[67] and Wilkinson[48] note that such disintegrations amount to 95% of the total number observed.

It should be noted that the isobaric spin rule forbids disintegration of the 16.9 Mev state of Be^8 (T = 1) with the emission of two α-particles (T = 0). This process does occur to some extent, apparently due to the ambiguity ("non-uniqueness") of the isobaric spin value for this state. Decay of this state by the ejection of a neutron or proton is energetically impossible. Hence, the only competing processes are γ-emission and α-decay; the level should be anomalously narrow.

Thus we see that the isobaric selection rule forbids all the stages of the $C^{12} + \gamma \rightarrow C^{12*} \rightarrow \alpha + Be^{8*} \rightarrow 3\alpha$ reaction, just as it bars the direct $C^{12} + \gamma \rightarrow C^{12*} \rightarrow 3\alpha$ reaction for dipole absorption.

Let us turn back, for a moment, to the first peak in the $C^{12}(\gamma,\alpha)$ cross section curve situated in the 15-19 Mev region. It is not known whether the reaction here comprises an α-decay forbidden by the isobaric selection rules or high multipolarity excitations of some levels of C^{12}. However, the fact that this maximum coincides with the energy levels of the first states of C^{12} with T = 1 suggests

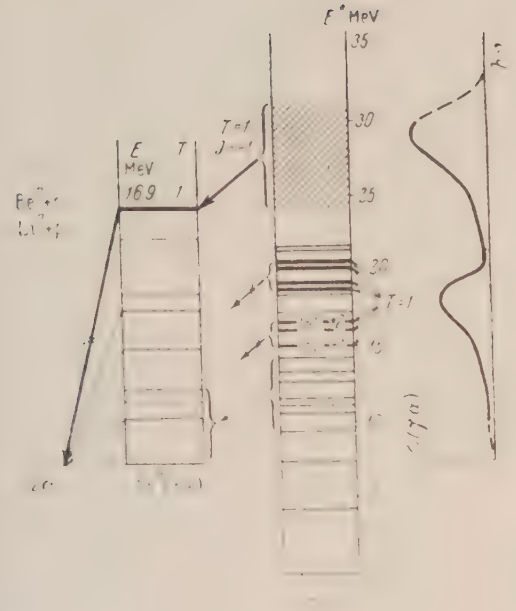

Fig.19. Scheme of $C^{12}(\gamma,\alpha)Be^8$—3α reaction. Light lines indicate states with T = 0; heavy lines, states with T = 1. The T = 0 states are excited with a multipolarity above E1 but can yield α + Be^8. States in the 15-20 Mev interval with T = 1 can be excited by E1 type absorption but cannot decay into α + Be^8. Only states of C^{12} with T = 1, J = -1 and E* > 24.4 Mev (hatched band) can be attained by E1 absorption and disintegrate into α + Be^8 (T = 1).

that the fact that dipole excitation is possible leads to the relatively frequent formation of these states and that their α-decay, although forbidden to some degree does compete successfully with the α-decay of the states of C^{12} excited by E2 and M1 type absorption. As the excitation energy is increased, states of C^{12} with T = 1 should be encountered with increasing frequency; at the same time, however, neutron and proton ejection processes should also begin to compete more successfully with α-particle emission.

The $O^{16}(\gamma,\alpha)$ reaction is in many respects similar to the one we have just discussed. The reaction threshold lies at 7.1 Mev, but the probability of the reaction at γ-quanta energies under 20 Mev is low. It does not increase to any noticeable extent even at the point where the first state of O^{16} with T = 1, located at 12.5-13.0 Mev (analogous to the ground state of N^{16}), might be excited.

The allowed (γ,α) reaction induced by electric dipole absorption is possible only for the state of O^{16} (T = 1) that can dissociate into an α-particle and C^{12*} in the lowest state with T = 1: the 15.2 Mev state. Thus the effective threshold of the allowed $O^{16}(\gamma,\alpha)$ reaction is 7.1 + 15.2 = 22.3 Mev. But the 15.2 Mev state of C^{12} forming in this case disintegrates into an α-particle and Be^8 only in violation of the isobaric selection rule.

In the case of irradiation of the heavier "α-particle" nuclei — Ne^{20}, Mg^{24}, Si^{28} and S^{32} — with sufficiently hard γ-rays one might venture to predict the emission of distinctive cascades of α-particles, leading to the appearance of α-stars in the nuclear emulsion.

A dipole absorption of a γ-quantum should be followed by a cascade of allowed α-disintegrations, terminating in the forbidden 16.9 Mev $Be^8 \rightarrow 2\alpha$ dissociation.

The (γ,α) reaction with "deuteron" nuclei: Li^6, B^{10} and N^{14}

In nuclei of the Li^6, B^{10} and N^{14} group electric dipole excitation can take place at comparatively weak γ-ray energies since the system of levels with T = 1 in these nuclei begins at lower energies. Here, too, however, realization of an allowed (γ,α) reaction is contingent upon the product nucleus attaining a level with T = 1. This condition leads to high threshold energy values for the all[illegible] reactions: about 8.0 Mev for B^{10} and 23.3 for N^{14}. In so highly excited a sta[illegible] these nuclei are capable of ejecting protons (N^{14} can also emit neutrons and even deuterons); these competing processes, of course, reduce the probability [illegible] (γ,α) reaction.

The case of Li^6 is of particular interest. Here the gamma-alpha reaction assumes the form $Li^6(\gamma,\alpha)d$. For an excited state of Li^6 to disintegrate into α+d it must have T = 0 (α and d do not have states with T = 1), but electric dipole excitation of such a state is forbidden by the isobaric selection ru[illegible]

Thus the $Li^6(\gamma,\alpha)d$ reaction must proceed either through E2, M1 or M2 excitations, by virtue of incomplete prohibition of the E1 excitation or due to an admixture of isobaric spin values ("non-uniqueness" of the isobaric spin). Actually the $Li^6(\gamma,\alpha)d$ reaction is observed, but has an abnormally small cross section: $\sigma \leq 8\pm2$ μbarns at $h\nu$ = 2.76 Mev, $\sigma \leq 6\pm3$ μbarns at $h\nu$ = 6.3 Mev and $\sigma \leq 5\pm3$ μbarns at $h\nu$ = = 17.6 Mev.[90] For purposes of comparison we note that the cross sections of the $Li^7(\gamma,\alpha)t$ reaction are 26 ± 1 μbarns at $h\nu$ = 6.1 Mev and 120 ± 60 μbarns at $h\nu$ = 17.6 Mev.[91] Thus the inhibiting effect of the isobaric spin selection rules is very clearly manifested in this case.

The (γ,d) reaction

The conditions necessary for the realization of electric dipole disintegrations in the case of the (γ,d) reaction are the same as in the case of the (γ,α) reaction, the difference being that the reaction thresholds are lower.

Thus for B^{10}, N^{14}, C^{12} and O^{16} the thresholds lie in the neighborhood of 22-27 Mev. There are virtually no experimental data on the (γ,d) reaction with these nuclides available.

The $He^4(\gamma,d)d$ reaction — the dissociation of alpha-particles into two deuterons — may occur with electric dipole absorption since in this case only states having T = 1 are formed which is in conformity with the isobaric selection rules.

11. Various Problems Connected with Isobaric Spin

The existence of di-neutrons

The problem of whether di-neutrons exist has long attracted the attention of physicists. Despite persistent efforts no one has yet succeeded in detecting these particles in nuclear reactions at low energies or in the fission of heavy nuclei.

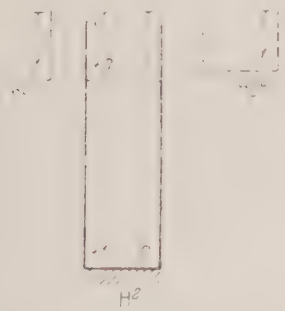

- Fig. 20 -

Zhdanov, Lukirski and Sokolova[92] found that two neutrons are emitted "as though together" from Be^9 in the capture of a negative meson. Panofsky, Aamodt and Hadley[46], studying the γ-ray spectrum from the $\pi^- + d = n + n + \gamma$ reaction, also found that two neutrons are often emitted as though together. Of course, these observations do not prove the existence of di-neutrons: there must necessarily be correlation of the directions of emergence of the neutrons even if the forces acting between them do not produce a coupled condition.

Hence the question of the existence of the di-neutron still remains open. The isobaric spin concept permits a new approach to the problem. Let us consider the diagram of Fig. 20.

The ground states of the di-neutron and di-proton must have $T_z = 1$ and, consequently, T = 1. In accordance with the Pauli principle they must have spin zero. Hence they cannot be similar to the ground state of the deuteron for which the assignment is J = +1 and T = 0. They should, rather, be similar to the singlet state of the deuteron, having J = +0 and T = 1, and form an isobaric triplet with it. However, the deuteron singlet state is not just unstable; it is non-existent, or what may be termed a virtual state. (The last term is used here in the sense characterizing the nature of the forces acting between neutrons and protons: n-p scattering and other properties of the n-p system can be accurately described with the aid of certain parameters, commonly ascribed to virtual levels.)

However, for the purposes of our argument, we need only accept that the singlet state of the deuteron is unstable. Granted equality of the n-n and n-p

forces and equality of the n and p masses, the properties of the di-neutron and of the singlet state of the deuteron should be identical. Hence, in the case of rigorous charge independence of nuclear forces the di-neutron must also be unstable.

Electrostatic energy does not come into the picture and any difference between the neutron and proton masses would only heighten the instability of the di-neutron.

The above argument also largely applies to the di-proton . However, Landau and Smorodinski point out that the instability of the hypothetical di-proton can be established directly from experimental data on proton-proton scattering.

"Isobaric isomerism"

The existence of isobaric selection rules for γ-emission can lead to what may be called "isobaric isomerism": in certain cases, the lifetime of an excited state may be extraordinarily long although the absolute values of the conversion coefficients (α_K, α_L, etc.) and of the relative coefficients (K/L or L/M) associated with the change of parity and ordinary spin may not indicate a high degree of forbiddenness for the transition. Such isomerism may occur a) in any nucleus when a low-lying excited level and the ground level have very dissimilar values of T or b) in nuclei with $T_z = 0$ if the low-lying level as well as the ground level has $T = 0$.

By way of illustration of the difficulties which may arise because of "isobaric isomerism", let us examine the case of the isomeric state of Cl^{34}. Judging from the energy of the transition ($h\nu = 0.139$ Mev) and the half-life (T = 33.2 minutes) in the case of ordinary isomerism this transition may be identified as M3. However, in view of the possibility of "isobaric isomerism" we cannot make an unambiguous identification solely on the basis of the above data: this can be a conventional M3 transition between states with near values of T, but it can also be an isobaric-isomeric transition of the type E1 between two states with $T = 0$. Unique assignment can be made only on the basis of careful measurements of the conversion coefficients. In the case of Cl^{34} this actually is an M3 transition.

On the (d,pn) reaction

The (d,pn) reaction can compete with the (d,d') reaction, leaving the target nucleus in the ground state as well as in the excited states.

Observation of the (d,pn) reaction is hampered by the fact that the product particles have a continuous spectrum: observations relating to the threshold energies for the excitation of a given level cannot be made with a convincing degree of accuracy, for the threshold of the A(d,d')A* reaction lies appreciably lower than the threshold of the A(d,pn)A* reaction and when the latter first becomes possible, the former already proceeds with high intensity. Actually at present we have no reliable information on the extent to which the (d,d') and (d,pn) reactions compete.

We can, however, invoke the isobaric selection rule to investigate the problem.

The B^{10}(d,d') 1.74 Mev B^{10} and N^{14}(d,d') 2.31 Mev N^{14} reactions, as we know, are forbidden, but the corresponding (d,pn) reactions are not.

Consider the following experiment. We have an N^{14} target bombarded with deuterons, the energy of which is gradually increased. Near the target we have a gamma-spectrometer adjusted to record γ-lines in the 1 to 4 Mev interval.

Until the deuteron energy is raised to 2.64 Mev, the 2.31 Mev level cannot be excited; hence the $h\nu = 2.31$ Mev line cannot appear and only the γ from the competing (d,p), (d,n) and (d,α) reactions will be observed. In the 2.64 to 4.51 Mev deuteron energy interval the $h\nu = 2.31$ Mev γ-line cannot because the (d,d') reaction is forbidden. It will show up only when

energy reaches 4.51 Mev and the 3.95 Mev level of N^{14} is excited. Up to 5.49 Mev, when the next (4.80 Mev) level of N^{14} begins to be excited, the relative intensities of the $h\nu$ = 1.6, 2.31 and 3.95 Mev lines should remain constant since they are all related to the decay of the 3.95 Mev state of N^{14}, excited by (d,d') scattering.

If the (d,pn) reaction does exist, then starting with a deuteron energy of 5.19 Mev, the 2.31 Mev level of N^{14} should be excited by this reaction and the intensity of the $h\nu$ = 2.31 Mev line should begin to increase relative to the intensities of the 1.6 and 3.95 Mev lines. Thus, observation of the relative intensities of the ν-lines should provide an index to the probability of (d,pn) processes. In practice the outlined experiment will be hampered by the fact that the experimental energy interval is rather narrow and by the not unlikely presence of a background due to competing reactions; to minimize the obscuring effect of the background the spectrometer used must have a high resolution.

It is possible that an experiment of this type can be carried out more easily with a target of Li^6: the 3.58 Mev level of Li^6 cannot be excited by the (d,d') reaction but can be excited by the (d,pn) reaction. However we have no information of the levels of Li^6 above 3.58 Mev, hence it is difficult to predict how the $h\nu$ = 3.58 Mev γ-line will be excited.

12. The Isobaric Spin of Mesons and Light Particles

The usefulness of the isobaric spin concept where nucleons and nuclei are concerned has prompted a number of attempts to generalize and extend it to include other particles. A detailed examination of the isobaric spins of mesons and light particles lies outside the scope of this survey, hence we will merely outline the present status of the problem.

Extension of the isobaric spin concept to π mesons appears to offer the greatest promise. Three kinds of mesons are known: π^+, π^0 and π^-.

All three have almost the same mass ($\pi^- = 276.1\pm1.3\ m_o$ 93&46, $\pi^0 = 265\pm3\ m_o$ 46 and $\pi^+ = 277.4\pm1.1\ m_o$ 93&94) and apparently all have spin zero; for the π^0 this follows from the fact that it disintegrates into two photons[95]; for the π^+, from the reaction $\pi^+ + d = p + p$[96].

Apparently all π mesons have odd wave functions ("pseudo-scalar particles").[97]

There are no known facts conflicting with the hypothesis that all three mesons are simply different-charged states of the same particle (just as neutrons and protons may be assumed to be different states of the same nucleon - see Section 4 above). All π mesons interact strongly with nuclei; at sufficiently high energies this interaction is not electromagnetic in character.

Experiments indicate that the probabilities of the formation of π mesons by hard γ-quanta and fast nucleons are nearly identical for all three mesons[98-100].

It may be assumed that the specifically meson forces in the interaction of all three π mesons with any given nucleon or nucleus are equal. This together with the equality of their masses is sufficient to permit assigning isobaric spins to the three mesons (essentially, we require no more in assigning definite values of isobaric spin to atomic nuclei).

It would seem logical to assign all π mesons an isobaric spin T = 1, and third components T_z = -1, 0 and +1, respectively, to the π^-, π^0 and π^+ mesons (the + and - sign assignments are a matter of convention). On the basis of this assumption the isobaric spin selection rules listed in Table 5 should be applicable to reactions involving only mesons and nuclei or nucleons.

There have also been a number of attempts to assign isobaric spin values to μ and τ mesons, electrons, positrons and the neutrino. However, we will not dwell on such speculations here, since so far they offer no promise of deductions of practical value.

Received
30 September 1954

Bibliographic References

1. E.Wigner, Phys. Rev., 51, 106 (1937).
2. D.Inglis, Rev. Mod. Phys., 25, 390 (1953).
3. I.Shapiro, Usp. fiz nauk, 53, 7 (1954).
4. G.Zel'tser, Usp. fiz. nauk, 53, 455 (1954).
5. D.Ivanenko, Nature, 129, 798 (1932).
6. V.Kravtsov, Usp. fiz. nauk, 47, 341 (1952).
7. W.Heisenberg, ZS Phys., 77, 1 (1932); 78, 156(1933); 80, 587 (1933).
8. L.Young, Phys. Rev., 47, 972 (1935); 48, 913 (1935).
9. E.Wigner, Phys. Rev., 56, 519 (1939).
10. G.Breit, E.Condon & R.Present, Phys. Rev., 50, 825 (1936).
11. E.Fermi, Iadrennaia fizika (Nuclear Physics), M. 1951.
12. L.Landau & Ia.Smorodinski, Journ. Phys. USSR, 8, 154 (1944).
13. Ia.Smorodinski, Journ. Phys. USSR, 8, 219 (1944); 11, 195 (1947).
14. J.Schwinger, Phys. Rev., 72, 742 (1947).
15. H.Bethe, Phys. Rev., 76, 38 (1949).
16. J.Blatt & J.Jackson, Phys. Rev., 76, 18 (1949).
17. F.Barker & R.Peierls, Phys. Rev., 75, 312 (1949).
18. R.Hatcher, G.Arfken & G.Breit, Phys. Rev., 75, 1389 (1949).
19. G.Chew & M.Goldhaber, Phys. Rev., 75, 1466 (1949); 75, 1637 (1949).
20. G.Squires, Progr. Nucl. Phys., 2, 115 (1952).
21. E.Hafner, W.Hornyak, C.Falk, G.Snow & T.Coor, Phys. Rev., 89, 204 (1953).
22. G.Snow, Phys. Rev., 87, 21 (1952).
23. E.Salpeter, Phys. Rev., 82, 60 (1951).
24. J. Jackson & J.Blatt, Rev. Mod. Phys., 22, 77, 109 (1950).
25. J.Schwinger, Phys. Rev., 78, 135 (1950).
26. D.Hamilton, W.Alford & L.Gross, Phys. Rev., 83, 215 (1951); 92, 1521 (1953).
27. L.Langer, & J.Moffat, Phys. Rev., 88, 689 (1952).
28. C.Wong, Phys. Rev., 92, 529 (1953).
29. T.Bonner & J.Butler, Phys. Rev., 83, 1091 (1951).
30. H.Willard, J.Bair, J.Kington, T.Hahn, C.Snyder & F.Green, Phys. Rev., 85, 849 (1952).
31. H.Willard, J.Kington & J.Bair, Phys. Rev., 86, 259 (1952).
32. H.Roderick & C.Wong, Phys. Rev., 92, 204 (1953).
33. B.Dzhelepov & L.Zyrianova, Usp. fiz. nauk, 48, 465 (1952).
34. L.Alvarez, Phys. Rev., 80, 519 (1951).
35. F.Ajzenberg & W.Franzen, NSA, 8, 2632 (1954).
36. J.Gow & L.Alvarez, Phys. Rev., 94, 365 (1954).
37. A.Birge, Phys. Rev., 85, 753 (1952).
38. N.Glass, L.Jensen & J.Richardson, Phys. Rev., 90, 320 (1953).
39. N.Glass & J.Richardson, Phys. Rev., 93, 942 (1954).
40. B.Dzhelepov, Izv. (Bulletin) AN USSR, Ser. fiz., 17, 391 (1953).
41. R.Hofstadter, H.Fechter & J.McIntyre, Phys. Rev., 92, 978 (1953); L.Schiff, Phys. Rev., 92, 988 (1953).
42. V.Fitch & J.Rainwater, Phys. Rev., 92, 789 (1953); L.Cooper & E.Henley, Phys. Rev., 92, 801 (1953).
43. B.Dzhelepov, Izv. (Bulletin) AN USSR, Ser. fiz., 15, 496 (1951).
44. R.Aamodt, W.Panofsky & R.Phillips, Phys. Rev., 83, 1057 (1951).
45. K.Watson & R.Stuart, Phys. Rev., 82, 738 (1951).
46. W.Panofsky, R.Aamodt & J.Hadley, Phys. Rev., 81, 565 (1951).
47. R.Adair, Phys. Rev., 87, 1041 (1952).
48. D.Wilkinson, Nature, 172, 576 (1953).

49. L.Trainor, Phys. Rev., 85, 962 (1952).
50. L.Radicati, Phys. Rev., 87, 521 (1952).
51. F.Hund, ZS, Phys., 105, 202 (1937).
52. F.Ajzenberg & T.Lauritsen, Rev. Mod. Phys., 24, 321 (1952).
53. P.Endt & J.Kluver, Rev. Mod. Phys., 26, 95 (1954).
54. J.Hollander, I.Perlman & G.Seaborg, Rev. Mod. Phys., 25, 469 (1953).
55. W.Arber & P.Stähelin, Helv. Phys. Acta, 26, 433 (1953).
56. H.Burrows, C.Powell & J.Rotblat, Proc. Roy. Soc., 209, 478 (1951).
57. A.Ashmore & J.Raffle, Proc. Phys. Soc., 64, 754 (1951).
58. R. Van de Graaff, A. Sperduto, W.Buechner & H.Enge, Phys. Rev., 86, 966 (1952).
59. E.Wigner & E.Feenberg, Rep. Progr. Phys., 8, 274 (1941).
60. Kofoed-Hansen, Phys. Rev., 92, 1075 (1953).
61. W.Martin, & S.Breckon, Canad.J.Phys., 30, 643 (1952).
62. L.Radicati, Proc. Phys. Soc., 66, 139 (1953).
63. C.Bockelman, C.Browne, W.Buechner & A.Sperduto, Phys. Rev., 92, 665 (1953).
64. G.Jones & D.Wilkinson, Phys. Rev., 90, 722 (1953).
65. D.Wilkinson & G.Jones, Phys. Rev., 91, 1575 (1953).
66. D.Wilkinson, Phys. Rev., 90, 721 (1953).
67. M.Gell-Mann & V.Telegdi, Phys. Rev., 91, 169 (1953).
68. W.Fowler & C.Lauritsen, Phys. Rev., 76, 314 (1949).
69. J.Seagrave, Phys. Rev., 85, 197 (1952).
70. S.Devons & M.Hine, Proc. Roy. Soc., 199, 56, 73 (1949).
71. C.Lauritsen & W.Fowler, Phys. Rev., 58, 193 (1940).
72. H.Woodbury, R.Day & A.Tollestrup, Phys. Rev., 85, 760 (1952).
73. R.Thomas & T.Lauritsen, Phys. Rev., 88, 969 (1952).
74. L.Baggett & S.Bame, Phys. Rev., 84, 154 (1951).
75. A.French & J.Seed (See No. 67).
76. E.Bleuler, P.Scherrer, Walter & W.Zunti, Helv. Phys. Acta, 20, 96 (1947).
77. H.Sommers & R.Sherr, Phys. Rev., 69, 21 (1946).
78. C.Millar, G.Bartholomew & B.Kinsey, Phys. Rev., 81, 150 (1951).
79. D.Wilkinson & G.Jones, Phil. Mag., 44, 542 (1953).
80. D.Peaslee & V.Telegdi, Phys. Rev., 92, 126 (1953).
81. V.Telegdi & W.Zünti, Helv. Phys. Acta, 23, 745 (1950).
82. M.Eder, & V. Telegdi, Helv. Phys. Acta, 25, 55 (1952).
83. J.Wilkins & F.Goward, Proc. Phys. Soc., 64, 201 (1951).
84. J.Wilkins & F.Goward, Proc. Phys. Soc., 63, 1173 (1950).
85. F.Goward & J.Wilkins, Proc. Phys. Soc., 64, 93 (1951).
86. V.Telegdi, Phys. Rev., 84, 600 (1951).
87. J.Wilkins & F.Goward, Proc. Phys. Soc., 64, 1056 (1951).
88. V.Telegdi, Phys. Rev., 87, 196 (1952).
89. F.Goward, V.Telegdi & J.Wilkins, Proc. Phys. Soc., 63, 402 (1950).
90. E.Titterton (See No. 52).
91. E.Titterton, Proc. Phys. Soc., 63, 915 (1950).
92. A.Zhdanov, P.Lukirski & Z.Sokolova, Doklady AN USSR, 80, 729 (1951).
93. W.Barkas, F.Smith & E.Gardner, Phys. Rev., 82, 102 (1951).
94. W.Cartwright, Phys. Rev., 82, 460 (1951).
95. D.Peaslee, Helv. Phys. Acta, 23, 845 (1950); 24, 298 (1951).
96. D.Clark, A.Roberts & R.Wilson, Phys. Rev., 83, 649 (1951).
97. R. Marshak, Rev. Mod. Phys., 23, 137 (1951).
98. R.Littauer & D.Walker, Bull. APS, 26, 3, 15 (1951).
99. H.Medicus, Phys. Rev., 83, 662 (1951).
100. A.Shapiro, Phys. Rev., 83, 874 (1951).

* * * * *

INVESTIGATION OF THE RADIATION OF Zr^{95} + Nb^{95}*

by P. P. Zarubin

1. Introduction

Investigations of the radiation of Zr^{95} and Nb^{95}, carried out earlier with Zr^{95} + Nb^{95} compound specimens as well as with Zr^{95} and Nb^{95} compounds separately, showed that Zr^{95} transforms into Nb^{95} by a complex β^--decay scheme. Nb^{95}, which in addition to the ground state has an isomer state, is also unstable and decays to Mo^{95}. The decay proceeds to one of the excited levels of Mo^{95}, with subsequent γ-emission and internal conversion leading to the ground level of Mo^{95}.

The most accurate values of the half-lives of Zr^{95} and Nb^{95} were obtained by Cork et al[2], who continued their measurements on Zr^{95} over a period of a full year and who separated the Nb^{95} chemically from the Zr^{95}. According to these authors, the half-lives of Zr^{95} and Nb^{95} are 65.2 ± 1 and 35 ± 0.5 days, respectively.

The half-life of Nb^{95}* was apparently best determined by Slätis and Zappa[3]. Their value of the half life (84 ± 2 hours) agrees well with the average of the value based on the work of earlier investigators.

The main outlines of the $Zr^{95} \rightarrow Nb^{95} \rightarrow Mo^{95}$ decay scheme were established about 1943 by Levinger, Nedzel, Brady, et al[4-6]. This scheme is shown in Fig. 1a. A somewhat more complex scheme was proposed by Shpinel[7] in 1951 (see Fig. 1b).

At the time we started our investigation of Zr^{95} and Nb^{95} the following points in connection with the decay scheme of these isotopes were still in need of clarification:

1) There was no information on the intensity of the 720-730 kev γ-radiation, and consequently, the characteristics of the corresponding excitation level of Nb^{95} could be deduced only from β^--decay data.

2) It was not clear in what way the 910-930 kev γ-rays discovered by Mandeville in 1948[8] and by Nedzel, who qualifies them as "doubtful", in 1944 (published in 1948[9]) are associated with the decay of Zr^{95} or Nb^{95}.

3) There existed a certain dispersion of the values of the end-point energies of all β^--transformations and, particularly, of the end-point energy of the hard β-spectrum of Zr^{95} (840-1100 kev) obtained in spectrographic measurements.

4) It was necessary to verify the existence of a partial β^--spectrum of Zr^{95} with an end point energy of about 650 kev, reported by Shpinel[7] (but by none of the preceding investigators) and, consequently, it was necessary to resolve the problem of which decay scheme was correct.

The program of our investigation was, therefore, planned primarily for the purpose of elucidating these doubtful points.

Our investigation was carried out on the "betron", a transverse magnetic field β-spectrometer with improved electron focusing, achieved by making the magnetic field inhomogeneous in one direction.

---

* The present article takes into account the data of ref. 1, which was published after the 1954 convention (i.e. subsequent to the initial presentation of this paper).

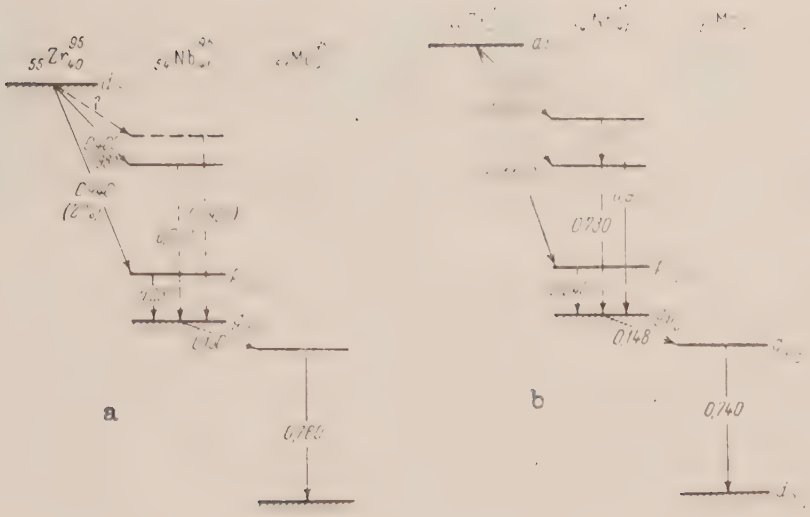

Fig. 1. Decay schemes for Zr^{95} and Nb^{95}: a) according to Levinger, Nedzel, Brady et al[4-6] and b) according to Snpinel[7].

2. Description of the Instrument

β-spectrometers of the type mentioned above have already been described[10,11]. The ketron, which we used for our investigation of Zr^{95} + Nb^{95}, was constructed and put into operation in 1951 at the Radium Institute and has the following basic parameters: the radius -ρ- of the principal trajectory, i.e., the path in a homogeneous field, is 11 cm; the angle of the horizontal divergence $\varphi = 30^{\circ}$ while the angle of vertical divergence $\varepsilon = \pm 3^{\circ}$.

To obtain the theoretically prescribed magnetic field distribution, pole pieces were made of No. 3 steel. Each pole piece consisted of two bars: one, with a rectangular cross section to produce a homogeneous field and the other an adjoining bar with trapezoidal cross section to produce the inhomogeneous component of the field.

The current in the magnet windings is regulated and kept constant by a balancing circuit employing a PPTV-1 potentiometer with an accuracy of within 0.01-0.001%.

An induction coil and a ballistic galvanometer with an accuracy of within 0.1% were used to make relative measurements of the magnetic field for the purpose of insuring the theoretically required field distribution, to study the topography of the field, and also to calibrate the instrument.

The required bevel of the trapezoidal steel bar producing the inhomogeneous component of the magnetic field was established semi-empirically by successive planing of the bar three times. Relative measurements of the magnetic field showed that the distribution of the inhomogeneous field coincided with the theoretical distribution to within 0.1-0.2% over the entire working area.

A study of the topography of the homogeneous magnetic field showed that homogeneity is maintained to within 0.1-0.2% over the entire working area.

The measuring chamber is made of brass and measures 332 x 282 x x 72 mm. Inside the measuring chamber are the main frame with the

3. Measurement Conditions and Sources

When measuring the radiation of Zr^{95} and Nb^{95}, the electrons were detected with a single counter. The entry slit of the counter chamber was sealed with an organic film having superficial density of about 0.3 mg/cm^2. This film transmitted electrons having energies from 13-14 kev.

The test material, received by us three months after its preparation, consisted of a solution of zirconium salt and contained radioactive Zr^{95} mixed with radioactive Nb^{95}. Here, naturally, only one isomer of Nb^{95} was in radioactive equilibrium with Zr^{95}.

The radiation source was prepared by evaporating the above solution on an aluminum foil with a superficial density of 1.5 mg/cm^2. Rectangular strips having the most uniform distribution of active matter were then cut out of the coated foil. The main series of measurements was made using a source measuring 12 x 0.6 mm and having a superficial density of 2-4 mg/cm^2; the dimensions of the source used in the control measurements were 0.4 x 9 mm and its superficial density was 0.5-0.8 mg/cm.

The nominal resolution (i.e. resolution with an infinitely thin source) for the main series of measurements was about 0.5%; the actual resolution was somewhat lower because of the finite thickness of the specimen. Thus, in the vicinity of 200 kev, the resolution was about 1%, while in the vicinity of 700 kev it was about 0.7%.

4. The β^--Spectrum of Zr^{95} and Nb^{95}

The β^--spectrum of Zr^{95} + Nb^{95}, plotted in terms of the values of $N/H\rho = f(H\rho)$, is shown in Fig. 2. Whether a particular portion of the spectrum is due to zirconium or niobium is determined from the half-lives of the isotopes. The rate of attenuation of the major part of the spectrum and most of the internal conversion lines corresponded to a half-life $T \sim 65$ days. Only the portion of the spectrum 14 to $\sim$120 kev interval and the internal conversion lines in the vicinity of 740 kev faded at a slower rate than the one consistent with T = 65 days. These parts of the spectrum must be attributed to the decay of Nb^{95} that has not yet reached radioactive equilibrium with the Zr^{95}.

The values of all points of the spectrum have been reduced to the same measurement interval (that for the 14-160 kev interval) and corrected for absorption in the source itself and in the entry slit of the counter chamber.

It will be noted from Fig. 2 that the β^--spectrum is complex and comprises at least three components, the third (hard) component being appreciably weaker than the two softer components.

Fig. 3 shows the Kurie plot by means of which the complex β^--spectrum was separated into its simple components.

The Kurie plot for the high-energy region is redrawn to a larger scale in the right upper corner of the figure. It is impossible to draw a single line through the experimental points in the 400-1050 kev range; a slight but definite break occurs near the 900 kev point.

Three possible explanations for the shape of the experimental curve in the indicated region suggest themselves:

1) There exists a spectrum component with an end-point energy of 1130 kev which is not of the Fermi type; the Kurie plots of spectra of this type display a downward bulge in the region near their end-point energy.

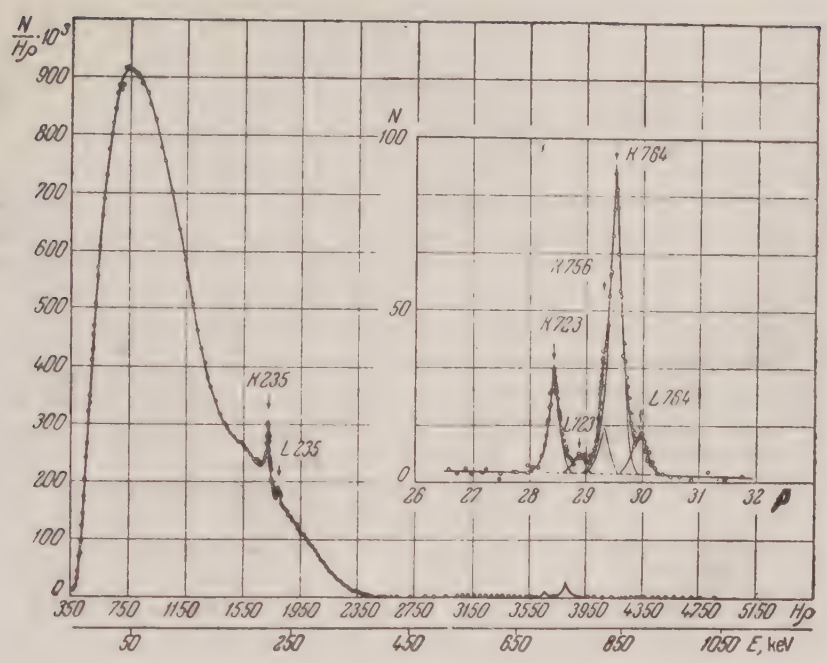

Fig. 2

β^--spectrum and internal conversion spectrum of Zr^{95} + + Nb^{95}. On the right is an enlarged scale plot of the conversion lines in the 700 kev region (horizontal scale graduated in potentiometer readings.

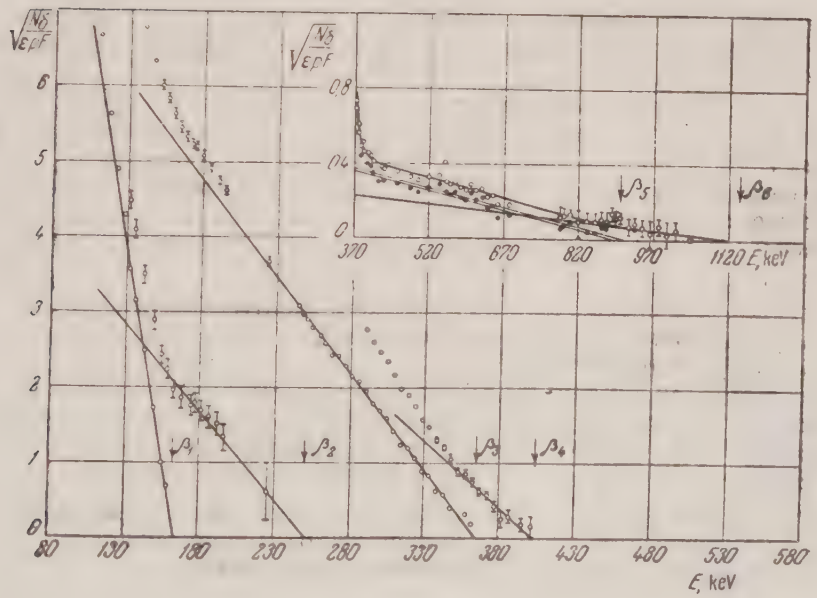

Fig. 3

Kurie plot for the β^--spectrum of Zr^{95} + + Nb^{95}. The diagram in the upper right corner shows a Kurie plot of the hard end of the β^--spectrum (the solid dots correspond to points of the Kurie plot of the spectrum obtained after subtraction of the β_6 component).

2) There are present a component with an end-point energy of 900 kev and one or more weak internal conversion lines in the 880-1050 kev interval; an approximate estimate of the possible intensity of a conversion line in this energy interval indicates that a pulse count of 2-3 pulses per minute above the background rate at its maximum corresponds to γ-radiation having a multipolarity of at least 4.

3) There are two components with end-point energies of 1130 kev and 900 kev.

In view of the low intensity of this part of the spectrum it is difficult to determine which of the suggested explanations is the true one; it may well be that two or all three of the possible factors operate simultaneously.

It must be noted that none of the possibilities conflicts with the decay scheme established on the basis of the more intense components, in the light of an analysis of the probable nuclear transformations. Each of the suggested possibilities directly or indirectly implies the existence of a spectrum component with an end-point energy of 900 kev. In analyzing the β^--spectrum by means of the Kurie plot we assumed that the existence of the 900 kev end-point energy component is definitely established and that a component with an 1130 end-point energy is probably present.

The results of our analysis are summarized in Table 1. It will be seen that as regards the intensity the total contribution of both the hard components amounts to only a little over 1%.

Table 1

Values of the end-point energy, relative intensity and log $f\tau$ of the components of the β^--spectrum of Zr^{95} and Nb^{95}.

Component	E_{ep}, kev	Relative intensity %	log $f\tau$
β_1	162 ± 5		5.08
β_2	250 ± 30	11	6.91
β_3	364 ± 8	53	6.74
β_4	404 ± 8	34	7.10
β_5	900 ± 30	0.9	9.89
β_6	1130 ± 40	0.4	10.55

The large value of log $f\tau$ for these components indicates that they correspond to highly forbidden transformations. We could not investigate the form of these relatively weak components and therefore subtracted them from the total spectrum as Fermi-type components.

It must be noted that in view of the low relative intensity of these hard components this introduced virtually no distortion into the remaining part of the total spectrum.

An outstanding feature of the Kurie plot of the spectrum remaining after subtraction of these hard components is the break in the vicinity of 360 kev. There can be no doubt that this break is due to the presence of two components with close end-point energies.

If we assume these are Fermi components, we find their end-point energies to be 404 ± 8 and 364 ± 8 kev and their relative intensities 34 and 53%, respectively.

In the Kurie plot for the spectrum remaining after subtraction of the β_4 component there is a noticeable deviation of the experimental points from a straight line, beginning at about 260 kev. A number of reasons may be suggested for this deviation:

1) The number of electrons in the low-energy region is increased by scattering, mainly in the source. However, comparison of the results of our measurements with those of measurements on

other materials, made both with our instrument and with the Leningrad State University ketron, operating under similar conditions (see, for example, the investigation of Lu^{177}, reported in Ref. 12), shows that in the energy range in question the excess of electrons due to scattering should not play an important part; the number of electrons produced by scattering in the given source becomes significant only at energies below about 150 kev.

2) One of the components (most probably β_3) is not of the Fermi type.

3) There exists another (β_2) component with an end-point energy of about 250 kev, which is emitted in a transformation leading to the 900 kev level of Nb^{95}.

4) There is a β^--transformation, with an end-point energy of 250 kev, from the isomeric level of Nb^{95} to an excited level of Mo^{95} at about 930 kev.

The characteristics of the excited levels of Nb^{95}, as determined from γ-radiation measurements, speak in favor of the last two alternatives. It is impossible, of course, to draw any definite conclusion regarding the form of any of these components, in view of the small number of experimental points available for this part of the spectrum (amounting to 10% of the overall length) as well as in view of the comparatively low intensity of the components. Consequently, we were forced to draw a straight line through such experimental points as are in alignment (after subtraction of the β_3 component). The relative intensity of the β_2 component (11%) must be regarded as the upper limit of the intensity 1) because distortion in the instrument is not fully eliminated, and 2) because the β^--transformation with the given end-point energy may partially, if not entirely, be attributed to the Nb^{95} isomer. Furtnermore, a slight (i.e. within the limits of the experimental error) change in the slope of the Kurie plot of the β_3 component results in a very appreciable (to 50%) change in the intensity of the β_2 component.

Finally, a straight line can be drawn through the points obtained after subtracting the β_2 component; this line gives an end-point energy of 162 ± 5 kev for the Nb^{95} spectrum. The experimental points lie on or close to this line down to about 130 kev; below this point there is some divergence which may well be explained by the presence of scattered electrons and may, therefore, be expected, under our conditions of measurement. The form of the spectrum resolved as described above is in agreement with the results of correlation experiments[13], the value of $\log ft$ (see Table 1), the characteristics of the ground state of Nb^{95} and of the excited state of Mo^{95} and, lastly, the results of other authors investigating the β^--spectrum of pure Nb^{95} with thin sources (for example, see Ref. 14).

5. Comparison of the Results of Measurement of the β^--spectrum of Zr^{95} and Nb^{95} with the Data of Other Investigators

A relatively large number of investigations has been devoted to the β^--spectra of Zr^{95} and Nb^{95}. The results of these investigations are summarized in Table 2.

From an inspection of the table, it will be seen that approximately one-third of the investigations were carried out either with a Wilson cloud chamber or by means of the absorption metnod. The

Table 2

Components of the β^--Spectra of Zr^{95} and Nb^{95} as Measured by Different Investigators

Investigators & Year	End-point energy E_{ep}, kev						Relative intensity of components	Method	Refs
	Nb	Zr							
	β_1	β_2	β_3	β_4	β_5	β_6			
Sarane, Kojima, Miyamoto & Ikawa (1940)		200 250		480	-		-	Wilson chamber	[15]
Goldschmidt & Perlman (1942)	150				--		—	Absorption Absorption in Al	[16]
Engelkemeier & Brady (1943)	150			420	1000		$\beta_4 : \beta_5 = 95 : 5$	Absorption in Al	[17]
Medzel & Sampson (1945)	154			394	1000	-	$\beta_4 : \beta_5 = 98 : 2$	Beta-spectrometer	[5]
Mitchell & Brown (1946)				400	880	-	—	Absorption ?	[18]
Levinger (1948)	156			400	887	-	$\beta_4 : \beta_5 = 98 : 2$ $\beta_4 : \beta_5 = 98{,}6 : 1{,}4 \div$ $\div 99{,}85 : 0{,}15$	Beta-spectrometer Beta-spectrometer	[19] [4]
ool & Edwards (1948) rummitt & Wilkinson (1948)	150 15			390 500	800	—	$\beta_4 : \beta_5 = 8 : 1$	Absorption ? Absorption	[20] [21]
	14			400				Absorption (accd. Feather	[8, 22, 23]
	140						$\beta_4 : \beta_5 = 98.6 : 1.4$	Magnetic lens	[24]
	148			400	1100		$\beta_3 : (\beta_4 + \beta_5) = 98 \div$ $\div 95 : 2 \div 5$	β-spectrometer - do -	[7]
	160							- do -	[14]
	147							- do -	[25]
			364	396			$\beta_3 : \beta_4 = 54 : 43$	Beta-spectrometer	[26]
			360 ± 10	405 ± 10	910 ± 50	-	$\beta_5 \sim 2\%$	Double focusing beta spectrometer	[2]
			--	371 ± 10	840 ± 80	-	$\beta_4 : \beta_5 = 99 : 1$	Magnetic lens -spectrometer	[3]
	162	150	364 ± 8	394 ± 8	900 ± 30	(1130±40)	$\beta_6 : \beta_5 : \beta_4 : \beta_3 : \beta_2 =$ $= 0.4 : 0.9 : 34 : 55 : 11$	β-spectrometer	

---

* [illegible] detected in Refs. 3, 4, 5, 7, 8, 11, [illegible] 17; consequently [illegible] references act only [illegible] the β_2, β_3 and β_4 components.

dispersion of the end-point energy values reported is very great (particularly for the β_4 and β_5 components), primarily owing to the inaccuracy inherent in the methods of determining these energies.

Approximately two-thirds of the investigations were carried out on β-spectrographs of different types. Prior to 1935 spectrometric measurements were made as a rule with instruments having a low resolution (5-8%) (Danish type spectrometers and magnetic lens spectrographs employing relatively thick sources). Only Fan[14] in 1952 used a twin lens β-spectrometer having a resolution of approximately 2% and employing a source with a superficial density of 0.05 mg/cm^2.

Unfortunately, analysis of the data of approximately half the investigations is rendered difficult by the fact that only the final results are given.

On the whole, the results of spectrometric investigations accomplished before 1953 are in agreement as regards the number of separated components and the values of the end-point energy, with the exception of the energy of the β_5 component and of some results reported by Shpinel[7].

Shpinel used a magnetic lens spectrometer with a resolution of 5.5% as determined for the half width of the F-line of ThB. The superficial density of the source was 5.8 mg/cm^2. Obviously the actual resolution with so thick a source was appreciably lower. Shpinel's separation of a weak Zr^{95} component with an end-point energy of 600 kev was apparently erroneous; its "presence" was presumably due to radioactive contamination of the source or distortion in the instrument, for this component was not observed in any of the subsequent investigations made under superior conditions. The component with an end-point energy of 365 kev separated by Shpinel corresponds as regards intensity with our β_4 component; however, in the light of the decay scheme proposed by Shpinel himself, we have tentatively placed this component in the β_3 column.

Four spectrometric investigations of the β^--spectra of Zr^{95} and Nb^{95} were published in 1953. In two of these (Refs. 25 and 3) magnetic lens spectrometers were employed. The instrument used in the investigation of Ref. 3 had annular focusing. However, due to a high transmission factor and greater specimen thickness (2-6 mg/cm^2) the resolution was reduced to 9-11%. Hence, the results of these two investigations are on a level with the results of spectrometric studies carried out prior to 1953.

In the other two investigations (Mittelman - Ref. 26 and Cork et al - Ref. 2) β-spectrometers with a high resolving power (1% or higher) were employed. This made it possible to separate the β_3 component of the Zr^{95} spectrum and to refine (Ref. 2) the values of the end-point energies of the other components. As previously noted, the investigation by Cork et al[2] is the most thorough and accurate to date. Our results, also obtained with a high resolving power, are in good agreement with the data of Cork et al, and in addition furnish evidence of the possible presence of β_2 and β_6 components.

6. Internal Conversion Electron Spectra of Zr^{95} and Nb^{95} and Nuclear Transformations in Nb^{95} and Mo^{95}

Conversion electron lines and the corresponding nuclear transformations

As may be seen from Fig. 2 the internal conversion spectrum was found to consist of seven lines, bunched in two groups: two fully resolved lines in the vicinity of 200 kev and 5 not completely resolved lines in the 700-740 kev interval. The individual lines of the latter group were separated in the following manner. The separation procedure was based on the half-width and the form of the almost fully resolved line at 704 kev. This line as obtained in several series of both the main and control (with thinner sources) measurements was carefully analyzed.

In veiw of their proximity to this line there was no danger of the other lines differing appreciably in form or width because of energy differences. The reference line was plotted in relative coordinates:

$$\frac{N}{N_0} = f\left(\frac{P}{P_0}\right)$$

where N is the number of pulses and P is the indication of the potentiometer (the subscript $_0$ in each case indicates the value for the line maximum). Using this plot and the known maxima for the lines we could readily determine N and P values for all the lines, i.e., carry out the desired separation (see Fig. 2).

The connection between individual internal conversion lines and specific nuclear transformations in Nb or Mo was established on the basis of the observed half-lives (decrease in line intensity with time), the data of other investigators studying Zr or Nb separately, and the values of the difference (K - L) for Zr, Nb and Mo listed in Table 3.

Table 4 lists part of the results of processing the conversion line data.

Table 3

Energy difference between the K- and L-lines for Zr, Nb and Mo

Atom	Binding energy (kev) in the:		Difference, kev	
	K-shell	L-shell	K - L	Δ(K - L)
Zr	18.00	2.53	15.47	0.82
Nb	18.99	2.70	16.29	0.84
Mo	20.00	2.87	17.13	

It should be noted that the lines in rows Nos. 2, 4 and 7 also comprise the unresolved M-lines; this is confirmed by analysis of the form of the lines of rows Nos. 2 and 7.

To determine the energy of the nuclear transformations, the binding energy of the electron in the corresponding shell was added to the energy of the conversion electron line.

Table 4

Energy, origin and intensity of conversion lines. Energy of nuclear transformations

Row No.	Electron energy, kev	Diff. (K-L) kev	Shell & nuclide involved	Value of hν determined for the line, kev	Probable energy of transition, kev	Intensity of the conversion line n_e
1	2		4	5	6	7
1	218,6	16,6	KNb	234,6	235 ± 1	$(5,2 \pm 0,5)\cdot 10^{-4}$
2	233,2		LNb	234,9		$(1,1 \pm 0,1)\cdot 10^{-3}$
3	706,3	16,1	KNb	723,3	723 ± 2	$(6,0 \pm 0,5)\cdot 10^{-4}$
4	720,4		LNb	723,1		$(1,0 \pm 0,2)\cdot 10^{-4}$
5	736,7		KNb	755,7	756 ± 2	$(2,4 \pm 0,3)\cdot 10^{-4}$
6	744,3	16,9	KMo	761,3	764 ± 2	$(1,8 \pm 0,2)\cdot 10^{-3}$
7	761,2		LMo	763,1		$(2,6 \pm 0,3)\cdot 10^{-4}$

As may be seen from Col. 6 of Table 4, we established four nuclear transformations: two of Nb and one of Mo. In Col. 7 we list the intensities of the electron lines, n_e, determined in the following manner: denoting the number of internal conversion electrons for the given line through N_e and the total number of β^--particles emitted by the nucleus through N_β, we get $n_e = N_e/N_\beta$. The value of n_e was determined as the ratio of the conversion line area to the area of the total β^--spectrum of the given nucleus. The values of n_e for the lines of rows Nos. 2 and 7 in Table 4 include the value of n_e for the corresponding M-lines.

Internal conversion coefficients α_K/α_L, types, multipolarity and intensity of γ-transitions

Table 5 shows the results of processing the conversion spectrum data for the purpose of determining the changes in angular momentum and parity in the corresponding nuclear transformations, which for γ-radiation is equivalent to determining their character, i.e., their type and multipolarity.

Column 2 of the table lists the experimental values of the conversion coefficients α_K for the K-shell, determined from the ratio of the areas of the conversion K-lines to the areas of the corresponding partial β-spectra.

Column 3 lists the theoretical values of α_K, obtained by interpolating the data of Rose et al[27] for the region of Z and E of interest to us. It must be noted that these interpolations, made on the basis of a small number of theoretical points, are necessarily approximate and may comprise errors of up to 10-15%.

Column 4 gives the ratios of the conversion coefficients on the K- and L-shells α_K/α_L. In this case the ratios serve to determine the character of γ-rays more accurately than is possible with reference to α_K alone. To this end we used the empirical curves of Goldhaber and Sunyar[28] showing the variation of α_K/α_L with the ratio Z^2/E, for transitions characterized by different changes of momentum and parity (here E is the transition energy and Z the nuclear charge).

Table 5

CHARACTER AND INTENSITY OF GAMMA-TRANSITONS

1	2	3								4	5	6
$h\nu$	E, kev	Experimental value of α_K	Theoretical value of α_K							$\frac{\gamma_K}{\gamma_L}$	Transition type	Intensity $n_\gamma = \frac{n_{eK}}{\alpha_K}$
			E1	E2	E3	E4	M1	M2	M3	M4		
$h\nu_1$	235	2,6 ±0,6	$9,12\cdot10^{-3}$	$4,68\cdot10^{-2}$	$2,14\cdot10^{-1}$	$9,04\cdot10^{-1}$	$2,12\cdot10^{-2}$	$1,12\cdot10^{-1}$	$5,25\cdot10^{-1}$	2,40	4,7 ± 0,3	$(2,0\pm0,5)\cdot10^{-3}$
$h\nu_2$	723	0,0018 ± 0,0002	$4,94\cdot10^{-4}$	$1,42\cdot10^{-3}$	$3,36\cdot10^{-3}$	$8,20\cdot10^{-3}$	$1,37\cdot10^{-3}$	$3,32\cdot10^{-3}$	$9,38\cdot10^{-3}$	$2,22\cdot10^{-2}$	5,7±0,6*	E2 or M1 $(3,4\pm0,3)\cdot10^{-3}$
$h\nu_3$	756	0,00046 ± 0,00004	$4,58\cdot10^{-4}$	$1,28\cdot10^{-3}$	$2,97\cdot10^{-3}$	$7,05\cdot10^{-3}$	$1,25\cdot10^{-3}$	$2,97\cdot10^{-3}$	$9,37\cdot10^{-3}$	$1,88\cdot10^{-2}$	—	E1 $(5,3\pm0,4)\cdot10^{-4}$
$h\nu_4$	764	0,0018 ± 0,0002	$1,79\cdot10^{-4}$	$1,33\cdot10^{-3}$	$3,08\cdot10^{-3}$	$7,20\cdot10^{-3}$	$1,34\cdot10^{-3}$	$3,16\cdot10^{-3}$	$8,56\cdot10^{-3}$	$1,98\cdot10^{-2}$	7,2 ± 0,4	E2 or M1 1,0±0,1

*This figure is for the ratio $\frac{\gamma_K}{\gamma_{L_1}+\gamma_M}$.

Unfortunately it is impossible to make use of these curves in the 700 kev region since for $Z^2/E < 5$ and $\alpha_K/\alpha_L > 5$ interpretation becomes ambiguous.

The ambiguity is explained, first, by the lack of reliable experimental points and the consequent highly approximate extrapolation of the curves in this region and, second, by the fact that in the region of small values of Z^2/E and large values of α_K/α_L, the latter ratio is not particularly sensitive to the character of the γ-transitions.

In our case, for transitions in the neighborhood of 700 kev, $\alpha_K/\alpha_L > 5$ and $Z^2/E \lesssim 2.2$-2.3, which corresponds to the above-mentioned ambiguity region.

It will be noted from the table that the $h\nu_1$ transition is closest to transitions of the M4 type as regards the values of both α_K and α_K/α_L.

The same value of α_K was obtained for the $h\nu_2$ and the $h\nu_4$ transitions. The theoretical value of α_K nearest to the experimental value is the one computed by Rose for E2 or M1 transitions.

Comparison of the experimental and theoretical values of α_K for the $h\nu_3$ transition indicates that it is of the E1 type.

7. Comparison of Our Conversion and γ-Ray Spectra Measurements with the Data of Other Investigators

The results of measurements of the conversion electron and γ-ray spectra of Zr^{95} and Nb^{95} reported by different investigators are listed in Table 6.

From an examination of the entries in the table it will be seen that the greatest number of investigations have been devoted to determination of the energy of the $h\nu_1$ and $h\nu_2$ transitions.

If we exclude the investigations by the method of absorption, which show a considerable dispersion

of energy values (to 200 kev), the results of most of the spectrometric investigation will be found to be in close agreement as regards the $h\nu_1$, $h\nu_2$ and $h\nu_4$ transition energies.

As was noted above, in almost all spectrometric investigations of Zr^{95} and Nb^{95} carried out prior to 1953 the resolution of the instrument was low. By virtue of the high resolution of our instrument, we succeeded in isolating another nuclear transition, one with an energy of 756 kev ($h\nu_3$).

In 1953 there appeared two articles [2, 26], whose authors also worked with high resolution spectrometers. Their reports confirm the existence of the $h\nu_3$ transition. In our investigation we established that this transition must be attributed to niobium on the basis of half-life measurements; the author of Ref. 26 established this by using enriched isotopes, while the authors of Ref. 2 used chemical separation of Nb and Zr. In addition, the authors of Ref. 2 established the existence of another transition ($h\nu_5$) in Mo, with an energy of 753 kev and suggest that there may be yet another transition with an energy $h\nu_4 - h\nu_5 = 16$ kev.

Very soft γ-quanta were detected in the investigation of Ref. 2 by absorption in aluminum. In our investigation, as in that of Ref. 26, the $h\nu_5$ transition was not detected.

As for the energies of the $h\nu_1$, $h\nu_2$, $h\nu_3$ and $h\nu_4$ transitions, the data of Refs. 2 and 26 virtually coincide with our results.

Two other groups of investigators [3, 5] note yet another ($h\nu_6$) transition in Nb, with an energy of 920 or 1070 kev. The authors of Ref. 5 even determined the total conversion coefficient of the γ-rays, although they themselves qualify them as "doubtful". In the investigation of Ref. 3 γ-rays with an energy of 1070 kev were detected both by means of conversion electrons and by means of photoelectrons; the half-life, determined from the rate of decrease of the intensity of these γ-rays, proved to be 65 days. However, the relative intensity of these γ-rays as compared with the intensity of the 720 kev γ-rays differed greatly for two different specimens (2% and 20%). The authors concluded that these γ-rays were due to radioactive contamination.

It may also be noted that a $h\nu_6$ transition detected by Mandeville and Sherb was first ascribed by them to Nb,[8] then later attributed to Mo (after disintegration of the Nb)[22, 37] and finally admitted to be non-existent[34]. According to our data a certain increase in the spectrum intensity in the vicinity of the energy of this transition is probably connected with a hard component of the β^--spectrum, although, of course, it is not impossible that there may be very weak conversion electron lines in this energy interval (see Sec. 4 above and Sec. 8 below).

As will be seen from Table 6, the values of the conversion coefficients and of α_K/α_L were determined in only a few of the spectrometric investigations, while the character of the γ-emissions was identified in even a lesser number, particularly where the $h\nu_2$ and $h\nu_3$ transitions are concerned.

Obviously, in measurements with a low resolution, the errors in determining α, α_K and α_K/α_L are necessarily appreciable. Hence, it is not surprising that the values obtained in the various studies employing low resolution instruments differ widely. Thus, in Ref. 5 the value of α_{total} for the $h\nu_1$ transition is far too low (by about

Table 1
(continued on next page)

Conversion electron and γ-ray spectra of Zr^{95} and Nb^{95} according to the data of different investigators

Ref. No.	$h\nu_1$/Nb	α_K	$\frac{\alpha_K}{\alpha_L}$	Trans.	$h\nu_2$/Nb	α_K	$\frac{\alpha_K}{\alpha_L}$	Trans.	$h\nu_3$/Nb	α_K	Trans.
(17)	240	Almost entirely convert.			880						
(5) (29) (19) (18) (30)	234	*0.002			730	*0,001					
	240	Almost entirely convert.			708 600						
(4) (20) (31)	242	Same			850						
(24)	216±10	Entirely convert.									
(32) (7)	240										
(33) (14)	232±2		*3,5±0,9	*M*4							
(34) (35)					730±20						
(3) (25)	231±10	∞			721±10	*0,0024 (<0,0021)		*E*2 или *M*1			
(26) (2)	235 235,2±0,5		4,5±0,6	*M*4	722 725±1,5	0,0014	5,0±1,0		754 758±1,5	0,0011	
(36)	220±2		4,3±0,1	*M*4							
Our data	235±1	2,6±0,6	4,7±0,3	*M*4	723±2	0,0018± ±0,0002	*5,7±0,6	*E*2 or *M*1	756±2	0,00046± ±0,00004	*E*1

Notes: 1) Single * in the α_K columns indicated that the designated value is for α_{total}; in some cases α_{total} and (α_K) as computed by the investigators in question are given. 2) Double ** in the α_K columns indicate that the $h\nu_2$ and $h\nu_4$ lines were merged. 3) * in the α_K/α_L columns denotes that the value is for $\frac{\alpha_K}{\alpha_L+\alpha_M}$. 4) All $h\nu$ transition energies are given in kev.

Table 6 (continued from preceding page)

Conversion electron and γ-ray spectra of Zr^{95} and Nb^{95} according to the data of different investigators

Ref. No.	$h\nu_\gamma$/Mo	α_K	$\frac{\alpha_K}{\alpha_L}$	Trans.	$h\nu_\gamma$/Mo	$h\nu_\gamma$/$\frac{\text{Mo?}}{\text{Nb?}}$	α_K	Method, Resolution of instrument & emission used.
(17)	820							Absorption
(5)	776	0,004	13,4			920	*0,0007	Spectrometer, e⁻
(29)	790							" , photoel.
(19)								"
(18)	580							Absorp. coincidence
(30)								Absorption
(4)	776							Spectrometer, e⁻
(20)	780							Absorption ?
(31)	750±15							Mag. lens spectr. e⁻ & photoe. R ≃ 4-6%
(24)	758±20	*0,0021						Mag. lens spect. e⁻ & photoe. R ∽ 5-8%
(32)	762							Spectrometer
(7)	730	*0,0021 **						Mag. lens spectrometer; e⁻ & photoe. R ∽ 6-7%
(33)								Spectrometer, e⁻
(14)	770±10	*0,0016± ±0,0016 ~0,0013	*4	E2 or M1				Twin-lens spectrometer; e⁻, R ∽ 2 %
(34)	760±20							Scintillation spectr.
(35)	774		*6,6±0,4					Solenoid spectrometer e⁻; R ≥ 1 %
(3)	745±10	*0,0024 (<0,0021)		E2 or M1		1070		Spectrometer; e⁻ and photoe;. R ∽ 9-11 %
(25)	771	*0,0018	*2,4					Magnetic lens spectrometer; e⁻ and recoil electrons
(26)	764							Spectrometer, e⁻; R — high.
(2)	768±1,5		7,6±0,6	M1	753±1,5			Spectrograph; e⁻ and photo el. R — high
(36)								"Danish" spectrometer, e⁻, R ∽ [illegible]
Our data	764±2	0,00187± ±0,0002	7,2±0,4	E2 or M1				Ketron, e⁻, R ∽ 0.7-1.0 %

[See Notes on preceding page]

three orders of magnitude!) while the value of α_K for the $h\nu_4$ transition is double what it should be. In Refs. 5 and 25 the values of α_K/α_L for the $h\nu_4$ transition differ by a factor of about 5.

In general with a low resolution instrument all that can be expected is a determination of α_{total} and at most a rough approximation of α_K. An example of this is furnished by the investigation of Ref. 14, where α_K is determined from α_{total} on the basis of a rough estimate of α_K/α_L.

On the other hand, the results of measurement of α_K and α_K/α_L and determinations of the character of the γ-radiation obtained in investigations where the resolution of the spectrometer was 1% or better are generally in agreement. Such investigations include those of Refs. 2, 26, 35 and 36 and our own.

In all these references the investigators reach the conclusion that the value of α_K/α_L for the $h\nu_1$ transition agrees well with the value of this ratio for M4 type transitions as determined from the Goldhaber and Sunyar curves. In our investigation this conclusion is also corroborated by the agreement of the experimental value of α_K with the theoretical value of α_K obtained by Rose and associates for M4 transitions. The lifetime of the isomeric state agrees well with the lifetime determined theoretically for the case of Nb and M4 type transition[28], and also with the empirical relationship between the lifetime and the energy of M4 isomeric transitions established by Goldhaber and Sunyar[28].

The experimental values of the conversion coefficient obtained by many investigators for the $h\nu_2$ transition indicate either an E2 or M1 transition, inasmuch as the theoretical values of α_K for these transitions are almost identical.

The same can be said of the $h\nu_4$ transition. It should be noted that the emphatic assertion made in Ref. 2 to the effect that the $h\nu_4$ transition is of the M1 type does not follow from the experimental data given in the same reference.

As for the $h\nu_3$ transition, we can compare our data with the result of only a single investigation: Ref. 26. The value of α_K for $h\nu_3$ reported in Ref. 26 differs from ours by a factor of 2.4. We hold to the opinion that the $h\nu_3$ transition is an E1 transition. The value of α_K in Ref. 26 is more in conformity with an E2 or M1 transition. Actually the author does not concern himself at all with the character of the transition; nor do we know the error in determining α_K in this investigation.

8. Decay scheme of $Zr^{95} \rightarrow Nb^{95} \rightarrow Mo^{95}$

As mentioned earlier, the main outlines of the decay scheme for Zr^{95} and Nb^{95} were established by Levinger, Nedzel, Brady, et al[4-6] around 1945. This scheme is shown in Fig. 1a. Figure 1b shows a decay scheme suggested by Shpinel in 1951[7]. By the middle of 1953 two other reports were published [3, 34] proving that a decay scheme essentially analogous with that proposed by Levinger et al is the correct one.

The results of our investigation permit construction of somewhat different decay scheme for Zr^{95} and Nb^{95}, although a few points still remain unclear even in this scheme.

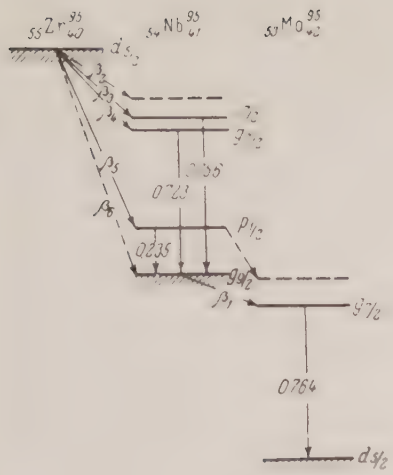

Fig. 4. Decay scheme for Zr^{95} and Nb^{95} according to our data (cf. also Ref. 2).

A similar decay scheme (although less complete with respect to the characteristics of the levels) is given by Cork and associates[2]. The Cork scheme contains no indication of the β_2 and β_6 components, tentatively introduces still another level in Mo^{95} (752 kev), and suggests the existence of a γ-transition of 16 kev energy between the 768 and 752 kev levels of Mo^{95}.

The decay scheme according to Cork's and our data is shown in Fig. 4.

According to the results of our measurements, this scheme is, in general, not inconsistent with intensity and energy balance considerations.

Let us review the principal characteristics of the ground states of Zr^{95}, Nb^{95}, Mo^{95}.

In our case these characteristics can be determined from the following data:

1) data on the character of the γ-transitions;
2) β^--decay and β-γ angular correlation data;
3) experimental determinations of the nuclear spin;
4) nuclear shell models.

Where the nuclear-shell model is concerned, the fiftieth neutron of $_{42}Mo^{95}_{53}$ in the ground state completes the filling of the fourth shell, and the remaining three neutrons should be at the $d_{3/2}$ level. The ground state of the Mo^{95} nucleus is thus characterized by even parity and has a total angular momentum J = 5/2. This value of the total momentum is confirmed by measurements of the spin of the Mo^{95} nucleus[38].

The characteristics of the ground state of $_{41}Nb^{95}_{54}$ are determined by the forty-first proton, which is relegated to the $g_{9/2}$ level, after the 3p level is filled by the fortieth proton. The value of the total momentum of this state is confirmed by the experimental value of the spin of the stable isotope $_{41}Nb^{93}_{52}$, which was found to equal 9/2. As a rule, addition of two neutrons when the number of neutrons is even does not change the value of J.

The characteristics of the ground state of $_{40}Zr^{95}_{55}$ are determined by the five neutrons, located at the $d_{5/2}$ level, after the fourth shell has been filled by the fiftieth neutron. The value of the total momentum of this state is identical with the total momentum of the ground state of $_{42}Mo^{95}_{53}$ since, as a rule, the addition of two protons when Z is even does not alter J.

Now let us examine the excited levels of Nb^{95} and Mo^{95}.

On the basis of both the character of the γ-radiation and the shape of the resolved soft component of the β^--spectrum, the excited 764 kev level of Mo^{95} can be either $g_{9/2}$ or $g_{7/2}$. Of the two, the nuclear shell model calls for the selection of the $g_{7/2}$ level as a level of successive excitation.

The isomeric transition of Nb^{95} is a transition of the M4 type. Consequently, the isomer state is a $p_{1/2}$ state; the β^--transition from the ground state of $Zr^{95}(d_{5/2})$ to the $p_{1/2}$ level is accompanied by a change of parity and a change of the total angular momentum by two. Consequently, the β^--spectrum component with an end-point energy of 900 kev should be that of a once forbidden transition and should belong in the category of α-type spectra. This is confirmed by the high value of $\log f\tau$ for this spectrum.

The next excited level of Nb^{95} (723 kev), to judge from the character of the γ-radiation ($h\nu_2$), may be either $g_{7/2}$ or $d_{5/2}$. Both alternatives are consistent with the nuclear shell model and it is impossible to make a definite selection by means of the shell model. This is explained by the fact that pairs of spin levels in a given shell (levels with different spin orientations relative to the orbital momentum), originating from neighboring levels of the rectangular potential well, have a tendency to approach each other and even to interchange positions, depending on the number of nucleons in the nucleus. Such level pairs are $f_{5/2}$ and $p_{3/2}$, $g_{9/2}$ and $g_{7/2}$, $d_{5/2}$ and $d_{5/2}$, etc. In such cases one must either determine the character of the γ-transition from the level more uniquely or make use of other information on the excitation of the level, i.e. such information as may be that gained by studying the β-decay or γ-ray cascade transitions (where these occur).

In our case, the 723 kev level is excited as the result of a β^--transition. In the case of a $d_{5/2} \rightarrow d_{5/2}$ transition, the corresponding β_4 component should be an allowed one. However, the high value of $\log f\tau$ for this component indicates the contrary. The value of $\log f\tau$ is more in accord with a $d_{5/2} \rightarrow d_{7/2}$ transition, assuming that we are dealing here with a so-called l-forbidden β^--spectrum. In this case, the transition, while allowed from the point of view of the change in parity and spin (the parity is unaltered and $\Delta J = 1$), is forbidden in accordance with the selection rules for orbital momentum. In our particular case (parity unaltered and $\Delta J = 1$) the l-prohibition means that $l = 2$, which is the case for a $d_{5/2}$ $d_{7/2}$ transition. The value of $\log f\tau$ for such spectra is high —experimental data indicate that it is between 6 and 8 - which is also in agreement with our data. The shape of the l-forbidden spectrum is that of a Fermi spectrum, as was assumed by us in separating the β_4 component by means of the Kurie plot. The 723 kev level of Nb^{95} is, therefore, a $g_{7/2}$ level.

Next, let us consider the 756 kev excited level of Nb^{95}. If the $h\nu_3$ transition is assumed to be an E1 type transition, the 756 kev level may be either an $f_{7/2}$ or an $h_{11/2}$ level. From the point of view of the nuclear shell model, the latter is acceptable as the next successive-excitation level. However, in this case the $d_{5/2} \rightarrow h_{11/2}$ β^--transition turns out to be a third-forbidden transition and the theoretical value of $\log f\tau$ for the spectrum (> 10) is greatly at variance with the experimental value.

The $f_{7/2}$ level is difficult to reconcile with the nuclear shell model, but agrees well with the β^--decay data. In fact, the $d_{5/2} \rightarrow f_{7/2}$ transition is a first forbidden one. The theoretical value of $\log f\tau$ for the β^--spectrum agrees with the experimental value.

If we assume that the $h\nu_3$ transition is of the E2 or M1 type (as apparently follows from Mittelman's investigation[26]), we run into the contradiction that while only a $d_{5/2}$ level is consistent with the nuclear shell model, the $d_{5/2} \rightarrow d_{5/2}$ β^--transition is an allowed one and the value of $\log ft$ corresponding to it is in disagreement with the experimental value. Only a $g_{7/2}$ level is consistent with the β^--spectrum; this indicates an M1 type transition.

Thus we arrive at the following conclusions regarding the characteristics of the 756 kev level:

1) It follows from our investigation and that of Mittelman[26] that the 756 kev level best in accord with the β^--spectrum data is one with $J = 7/2$.

2) A 756 kev level with this value of J does not fit into the arrangement of levels predicted by conventional shell model theory; apparently this level is reached in some way other than by ordinary successive or hole excitation.

3) According to our data, the parity of the 756 kev state is odd $(-7/2)$; on the other hand, analysis of Mittelman's results leads to even parity $(+7/2)$.

4) A $-7/2$ level is more consistent (than $+7/2$) with the experimental magnitude of $\log ft$ for the β_3 component, if no special assumptions are made regarding the decrease in the probability of β-transitions to this level in view of its unusual genesis. (Our conclusions regarding the characteristics and the exceptional nature of the 756 kev level are supported by the collective nuclear model, developed during the last 2-3 years. In the light of this model, the 756 kev level is a collective level and is not susceptible to description in terms of the simple nuclear-shell model.[1])

The still doubtful or obscure particulars of the decay scheme for Zr^{95} and Nb^{95} include the transitions and levels indicated by dash-lines in Fig. 4. The β_2 and β_6 transitions have been discussed above. We have no conclusive experimental proof of the existence of an excited level of Nb^{95} with an energy of 900 kev.

Regarding β^--transitions from the isomeric level of Nb^{95} it may be said that the characteristics of certain excited levels of Mo^{95} (for example, $s_{1/2}$ and $d_{3/2}$) indicate that such transitions are possible. In fact, they are not improbable for it is known, for instance, that excited levels of Mo^{95} are reached by transitions from the ground $(g_{9/2})$ state as well as from the isomeric $(p_{1/2})$ state of Tc^{95}.

Analogous transitions from the ground and isomeric states of Z - 1 and Z + 1 isobars to excited levels of the Z isobar have been observed, for instance, in the case $Kr^{85} \rightarrow Rb^{85} \leftarrow Sr^{85}$.

Lastly, we must note that another moot point in the above decay scheme is the matter of β^--transitions from the ground and isomeric states of Nb^{95} to the ground state of Mo^{95}, with end-point energies close to the end-point energies of the β_5 and β_6 components of the β-spectrum.

The writer wishes to express his deep gratitude to B. S. Dzhelepov for guidance in the investigation and discussion of the results, to N. A. Vlasov who supervised the construction of the kentron and to K. P. Artemov for his assistance in calibrating the kentron.

Received
26 August 1954

Bibliographic References

1. L.Sliv & L.Peker, Doklady AN SSSR, 94, 849 (1954).
2. J.Cork, J.Le Blank, D.Martin, W.Nester & M.Brice, Phys. Rev., 90, 579 (1953).
3. H.Slatis & L.Zappa, Ark. Fys., 6, 81 (1953).
4. J.Levinger, Rev. Mod. Phys., 20, 4 (1948).
5. V.Nedzel & M.Sampson, Rev. Mod. Phys., 20, 4 (1948).
6. E.Brady, D. Engelkemeier & E.Steinberg, Rev. Mod. Phys., 20, 4 (1948).
7. V.Spinel', Zhur. eksp. i teor. fiz., 21, 1370 (1951).
8. C.Mandeville & M.Sherb, Phys. Rev., 73, 1434 (1948).
9. G.Seaborg & S.Perlman, Rev. Mod. Phys., 20, 4 (1948).
10. M.Korsunski, V.Kel'man & B.Petrov, Zhur. eksp. i teor. fiz., 14, 394 (1944).
11. B.Dzhelepov & A.Bashilov, Izv. (Bulletin) AN SSSR, Ser. fiz., 14, 263 (1950).
12. N.Anton'eva, A.Bashilov, B.Dzhelepov & A.Zolotavin, Izv. (Bulletin) AN SSSR, Ser. fiz., 14, 299 (1950).
13. R.Stump & S.Frankel, Phys. Rev., 79, 243 (1950).
14. C.Fan, Phys. Rev., 87, 252 (1952).
15. R.Sagane, S.Kojima, G.Migamoto & M.Ikawa, Phys. Rev., 57, 1179 (1940).
16. B.Goldschmidt & I.Perlman, Rev. Mod. Phys., 20, 4 (1948).
17. D.Engelkemeier & E.Brady, Rev. Mod. Phys., 20, 4 (1948).
18. A.Mitchell & M.Brown, Ark. Fys., 6, 81 (1953).
19. W.Lyon & J.Hudgens, Nucl. Data, IX (1950); IV, XI (1951).
20. M.Pool & J.Edwards, Phys. Rev., 67, 60 (1945).
21. W.Grummitt & G.Wilkinson, Nature, 158, 163 (1946).
22. C.Mandeville & M.Sherb, Phys. Rev., 74, 1248, 1266 (1948).
23. C.Mandeville & M.Sherb, Phys. Rev., 74, 888 (1948).
24. J.Hudgens & W.Lyon, Phys. Rev., 75, 206 (1949).
25. E.Sturcken & A.Weber, Phys. Rev., 91, 484 (1953).
26. P.Mittelman, Phys. Rev., 91, 484 (1953).
27. M.Rose, G.Goertzel, B.Spinrard, J.Harr & P.Strong, Phys. Rev., 83, 79 (1951).
28. M.Goldhaber & A.Sunyar, Phys. Rev., 83, 906 (1951).
29. E.Jurney & E.Wollan, Rev. Mod. Phys., 20, 4 (1948).
30. E.Steinberg, Rev. Mod. Phys., 20, 4 (1948).
31. W.Rall & G.Wilkinson, Phys. Rev., 71, 321 (1947).
32. H.Medicus, P.Preiswerk & P.Scherrer, Helv. Phys. Acta, 23, 299 (1950).
33. P.Preiswerk & P.Staehlin, Helv. Phys. Acta, 24, 300 (1951).
34. C.Mandeville, E.Shapiro, R.Mendenhall, E.Zucker & G.Conklin, Phys. Rev., 89, 559 (1953).
35. R.Maerker & R.Birkoff, Phys. Rev., 89, 1159 (1953).
36. B.Dolishniuk, G.Drabkin, V.Orlov & L.Rusinov, Doklady AN SSSR, 92, 1141 (1953).
37. M.Sherb & C.Mandeville, Bull. Am. Phys. Soc., 23, 3, 56 (1948); 4, 19 (1948).
38. E.Feenberg, Phys. Rev., 77, 774 (1950).

* * * * * * * *

INVESTIGATION OF THE RADIATION OF Rb^{86}

- A. G. Dmitriev and P. P. Zarubin

1. Introduction

Radioactive Rb^{86}, first detected by Snell[1] in 1937 while bombarding rubidium with slow neutrons, has become the object of relatively many investigations.

The most accurately measured value of the half-life of Rb^{86} is 19 ± 1 days[2-4]. It has also been established that β^--decay transforms this isotope from its ground state to the ground state of Sr^{86} and also to a highly excited state of Sr^{86}, with subsequent emission of γ-quanta; internal conversion electrons have not been observed in this transition.

It is probable that the ground state of Rb^{86} also decays by β^+-emission or K-capture to Kr^{86}.

The main outlines of the decay scheme of Rb^{86} were established in 1948 by Zaffarano, Kern, and Mitchell[3]. This scheme is shown in Fig. 3 below. It was confirmed and refined in many subsequent investigations. At the time we began our investigation (November 1953) the following points in connection with the decay scheme of Rb^{86} were still in need of further clarification.

1) Although as a result of many investigations the hard component of the β^--spectrum has been classed among α-type spectra, there were conflicting opinions regarding the soft component and the degree of its forbiddenness. We also felt it would be of interest to verify the "uniqueness" of the hard component under the conditions obtaining in a high-resolution β-spectrometer.

2) Only three investigations, with a single spectrometric one among them[3], determined the ratio of the soft and hard components of the β^--spectrum; values of this ratio determined by the three investigations diverged considerably. Furthermore, the value obtained in the spectrometric investigation did not take into account the non-Fermi form of the hard component so that its intensity was underestimated.

3) The energy of the nuclear transformation to Sr^{86} was determined in only three investigations, two of which were made with low-resolution spectrometers; the character of the γ-transformation was unknown, and the momentum and parity of the excited state of Sr^{86} were not determined uniquely.

4) The conversion branch of Rb^{86} into Kr^{86} by β^+-decay or K-capture was not studied (only the upper limits of the ratios K/β (Ref. 5) and β^+/β^- (Refs. 6 and 7) were established.

In our study the radiation of Rb^{86} was investigated with a magnetic lens spectrometer with improved focusing, namely, the ketron, described in Ref. 8 [the preceding article in the present issue]. The results of this investigation throw light on some of the above-mentioned puzzling aspects of the decay scheme of Rb^{86}.

No definitive conclusions have been reached concerning certain questions because of the presence of radioactive impurities (S^{35} and probably other radioactive isotopes) in our specimen material. Some results of our investigation (particularly of the investigation

of the γ-radiation) still require verification; hence, the present report on the radiation of Rb^{86} must be considered as only a preliminary one.

2. Measurement Conditions in the Ketron

In our investigation of the β^--spectrum of Rb^{86} and the photoelectron spectrum, the electrons were detected with a single counter, operating with a quenching-gas mixture consisting of 70% argon and 30% methane. Use of the argon-methane mixture results in a counter plateau approximately 30% longer than that obtained with an Ar + C_2H_2 mixture[8].

The window of the counter chamber was covered with a ten-layer organic film having a total superficial density of about 0.02 mg/cm^2. Such a film is transparent to electrons having energies as low as 3.5-4.0 kev.

Our radioactive specimen containing Rb^{86} was obtained in the form of small rubidium chloride crystals, bombarded with slow neutrons. The product contained a considerable admixture of radioactive S^{35}. Analysis of the β^--spectrum and the rate of attenuation of its intensity indicated that there were no other radioactive admixtures, having a half-life and β^--spectra end-point energies differing appreciably from the half-life of Rb^{86} and the end-point energies reported for Rb^{86} in the literature, present in our specimen material. However, one cannot exclude the possible presence of other impurities, such as radioactive isotopes, decaying by positron emission or undergoing transformation by K-capture, with a half-life of ten days or longer.

As may be seen from the resultant β^- and photoelectron spectra, our specimen material contained virtually no radioactive Cs^{134} which is frequently formed as a co-product when Rb^{86} is produced by the (n,γ) reaction.

The source for studying the β^- and internal conversion electron spectra of Rb^{86} was prepared by evaporating an aqueous solution of rubidium chloride on an aluminum foil having a superficial density of about 1.5 mg/cm^2. A rectangular strip, measuring 0.9 x 19 mm was then cut from the coated foil. The superficial density of the active coating was approximately 0.2 mg/cm^2.

The theoretical resolution of our instrument was computed to be about 0.6%. In view of the thinness of the specimen we expected to obtain an experimental resolution approaching the theoretical from energies of the order of 200-250 kev. Unfortunately, it was impossible to verify this, since the observed β^--spectrum contained no internal conversion electron lines.

Two sources were prepared for investigating the γ-radiation of Rb^{86} by means of the photoelectron emission.

The first was a cylindrical copper container with lead foil, measuring 1.5 x 18 mm and having a superficial density of about 21 mg/cm^2, cemented to the cylindrical surface. The container was filled with the powder obtained by grinding up the active rubidium chloride crystals.

The second source was specially prepared to investigate the suspected low-energy γ-radiation of Rb^{86}. Here the active powder was placed in a container made of thin copper foil and covered with a layer of tin on the outside. The photoelectron radiator (tin) measured 2.8 x 20 mm and had an average superficial density of 10 mg/cm^2.

3. The β^--Spectrum of Rb^{86}

The general appearance of the β^--spectrum in conventional coordinates is shown in Fig. 1. As noted earlier, our material contained an admixture of radioactive S^{35}. Fig. 2 shows the β^--spectrum in the region above 175 kev, i.e., above the end-point energy of the β^--spectrum of S^{35}. The portion of the spectrum from 175 to 1800 kev, plotted from a large number of experimental points, will be the one analyzed below. The average statistical error of measurement was 1.5-2.5%. All experimental points of the spectrum are normalized to a single measurement interval. Check measurements, performed 85 days after the principal series of measurements showed that the intensity of the β^--spectrum fell off in conformity with a half-life T = 19 days.

Not a single internal conversion electron line was observed to stand out against the continuous spectrum background.

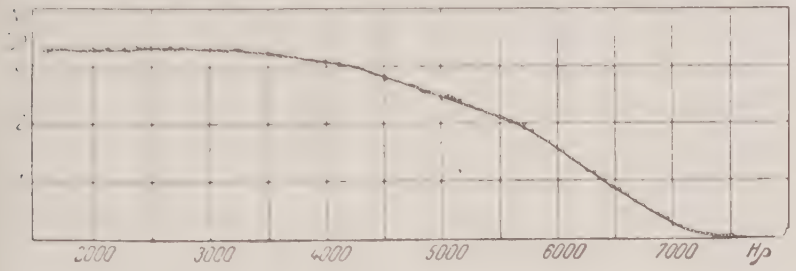

Fig. 1. β^--spectrum of Rb^{86}

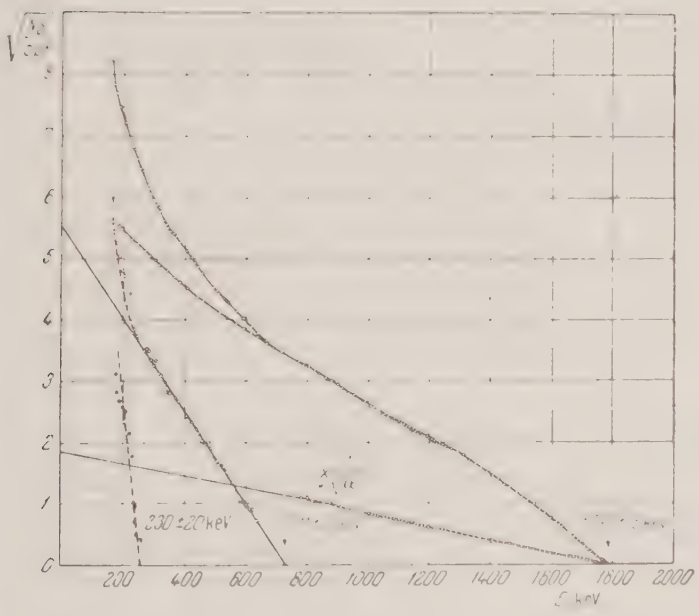

Fig. 2. Kurie plot of the β^--spectrum of Rb^{86}

Fig. 2 is the Kurie plot of the β^--spectrum. As can be seen from the figure, the plot of the hard component β_1 in the energy region above $E_{ep}/2$ shows the "bulge" characteristic of "unique" spectra.

It is known that the spectrum of a transformation involving a spin change of 2 and a change of parity ("unique" or α-type spectra) differs in form from the spectrum of an allowed transformation by a factor α which increases the fraction due to energy electrons and, when $E_{ep} > 2$, the fraction due to low-energy electrons as well.

An approximation of the α factor for "unique" spectra is given by

$$\alpha \approx (E_{ep} - E)^2 + E^2 - 1.$$

The approximation lies in neglecting the dependence of α on Z. However, when Z is small, taking this dependence into account makes only a minor difference in the value of α.

The Kurie plot for a "unique" spectrum differs from the plot for an allowed spectrum, i.e., from a straight line, by a constant factor of $1/\sqrt{\alpha}$.

Hence, multiplication of all the point-values of the experimental curve by $1/\sqrt{\alpha}$ should rectify the Kurie plot of a "unique" spectrum.

Accordingly, all the points of our experimental Kurie plot in the 780 to 1800 kev range were multiplied by $1/\sqrt{\alpha}$. As will be noted from the figure, this straightened out the Kurie plot satisfactorily, confirming the assumption that the hard component of the β^--spectrum of Rb^{86} is a "unique" spectrum. According to our measurements the end-point energy of this spectrum is 1795 ± 15 kev. The value of $\log f\tau$ is about 8.6, which is also in conformity with the values of α-type spectra.

Further analysis of the Kurie plot was carried out as follows: The straight-line of the rectified Kurie plot was extended from 780 to 175 kev. The points on the line corresponding to the experimental points in this energy region were multiplied by $\sqrt{\alpha}$. This operation permitted plotting the non-rectified Kurie plot of the hard spectrum for energies under 780 kev. As can be seen from the figure, the Kurie plot in the 780 kev region remains smooth. Moreover, an increase in the number of soft electrons over the number present in the case of an allowed spectrum becomes noticeable; this was to be expected, for in our case $E_{ep} = 4.51$ (in m_oc^2 units).

After subtracting the hard component from the overall spectrum, a new Kurie plot was drawn for the remaining soft component; this plot is rectilinear down to energies of 230-250 kev. The end-point energy of the soft component β_2 is 711 ± 15 kev.

The relative intensities of the β_1 and β_2 components were found to be 86 and 14%, respectively.

The deviations from a straight line in the Kurie plot of the soft spectrum component in the 175 - 230 kev energy region cannot be attributed to distortions in the instrument, in view of the relative thinness of the source.

As can be seen from our measurements and analysis of the isotope table, there is also little likelihood of these deviations being caused by a radioactive impurity having a soft β^--spectrum.

Two hypotheses can be advanced to explain the curvature in the Kurie plot below 23-250 kev:

1) The spectrum component β_2 is forbidden and, hence, its Kurie plot is not a straight line.

2) There exists a still softer β^--spectrum component (β_3) having an end-point energy near 230-250 kev and an intensity of only a few percent (1 - 5%).

It should be noted apropos the first hypothesis that experiments made by many investigators in 1950 and 1951[9 — 12] on the β-γ-angular correlation for Rb^{86} have shown that this correlation actually exists. Despite the low accuracy of these experiments, it has apparently been possible to establish that the form of the correlation function and the sign and magnitude of the correlation (i.e., the sign and magnitude of the coefficient ε in the correlation function $1 + \varepsilon \cos^2 \theta$) correspond to the first forbidden transition associated with the β_2 component and to the shape of this component which differs little from the shape of the allowed spectrum. The 7.7 value of $\log f\tau$ for the β_2 component also confirms this conclusion.

In this case, the first hypothesis alone cannot explain the observed curvature of the Kurie plot of the β_2 component of the spectrum.

The difficulty with the second hypothesis is that we lack convincing experimental proof of the existence of the β_3 component. The

Kurie plot, drawn with a small number of experimental points obtained after subtracting the β_2 component, assumed to be of the Fermi type, does form a straight line. However, only an insignificant portion of the spectrum has been subjected to this analysis (175 - 230 kev).

Thus, additional experiments are necessary to decide between the above two hypotheses. It is quite possible that both are true. In that case the end-point energy of the β_3 component will be lower.

4. Comparison of results with measurements made by other investigators

To date there have been quite a few investigations devoted to determination of the end-point energies and relative intensities of the individual components of the β^--spectrum of Rb^{86}.

The results of these investigations together with our own are listed in the table below.

As can be seen from the table, the absorption method was used in five of the investigations. In view of the large errors inherent in this method, the accuracy of the end-point energy and relative intensity determinations is open to question.

It is, therefore, not surprising that the values of the end-point energy, $E_{\beta 1}$, of the hard component of the spectrum, determined in Refs. 2 and 16, differ by approximately 440 kev, while the relative intensities of the soft component β_2, determined in Refs. 15 and 18, differ by a factor of nearly three.

Let us consider in somewhat greater detail the results of several of the spectrometric investigations, which yield much more accurate values of the end-point energies $E_{\beta 1}$ and $E_{\beta 2}$ and the relative intensities of the components, and which also permit of evaluating the degree of forbiddenness of the corresponding β^--transformations.

The first spectrometric investigation of the β^--spectrum of Rb^{86} was made in 1942 by Haagstrom[13]. The solenoid spectrometer he employed had a resolution of approximately 5%. The statistical accuracy of the β^--spectrum measurement was low. The great dispersion of the experimental points and their limited number (18 points over the entire spectrum) not only failed to yield reliable information concerning the form of the hard component of the spectrum, but also did not allow of separating out the soft component. The Kurie plot had a slight bend near 0.7 Mev, but no explanation of its presence was given.

In 1948 Zaffarano, Kern and Mitchell used a magnetic-lens spectrometer to investigate the radiation of Rb^{86}. This is one of the most complete and thorough spectrographic studies of Rb^{86} to date.

The superficial density of the sources used in that investigation ranged from 0.45 to 9 mg/cm^2. The resolution was low, amounting to only a few percent.

These investigators were the first to succeed in separating the soft component of the β^--spectrum of Rb^{86}, in determining the relative intensities of both components of the spectrum and in establishing, from a Kurie plot, that the hard component has the form of a forbidden spectrum. However, they subtracted this component from the total, taking this spectrum to be of the Fermi type, and tentatively drew a straight line through the experimental points of the Kurie plot. Starting with 250 kev, the Kurie plot of the β_2 component deviated from a straight line, to the side of an increase in the number of soft electrons. However, this deviation was not discussed by the investigators.

The next investigation was made by Muether and Ridgeway in 1950[17]. This investigation is valuable in that it is the first to employ β-γ-coincidence to separate the soft component of the β^--spectrum. The spectrometer used was of the magnetic lens type with a resolution from 3 to 15%, depending on the energy region studied. The sources were produced by evaporation under vacuum and had a superficial density of 0.4 and 1 mg/cm^2.

The resultant Kurie plot of the β_2 component was nearly a straight line, corresponding to an allowed spectrum with E_{ep} = 726 ± 10 kev or to a once forbidden spectrum with E_{ep} = 714 ± 10 kev. The authors are inclined to favor the second alternative.

It should be noted that, as in Ref. 3, the deviation in the Kurie plot of the β_2 component, corresponding to an increase in number of soft electrons, begins approximately at 200 kev. Ref. 17 also confirms the forbidden character of the β_1 component and is the first to note its "uniqueness" (α-type spectrum).

As will be noted from the above review and an examination of the table, all the spectrometric investigations, with the exception of those covered by Ref. 19 and 20, are in good agreement as regards the values of the end-point energies.

Our determinations differed from the others mentioned in that we used an instrument with a higher resolving power, which permits us to analyze the form of the component β^--spectra with greater assurance. In contrast to the case of Ref. 3, we took into account the forbiddenness of the β_1 component in determining the relative intensity of the spectrum components. In addition, our measurements permit advancing the hypothesis that there is a third, even softer component present in the spectrum of Rb^{86}. It will have been noted that the Kurie plots of the β_2 component drawn by other investigators on the basis of tests under different experimental conditions show deviations from the straight line in the energy interval under 250 kev. None of the investigators in question advance an explanation for this deviation.

If the β_3 component actually exists, the intensities of both the β_1 and β_2 components will be somewhat lower than those tabulated.

5. Gamma-Radiation of Rb^{86}

The γ-radiation of Rb^{86} was investigated by studying the photoelectron spectrum emitted by the radiators described above. The main series of measurements (with the lead target) covered the energy range from 4 to 1200 kev.

We succeeded in detecting in this region five photoelectron lines, standing out against the recoil electron continuum and, in the hard region, against the background of the hard β^--radiation which partially penetrated the walls of the copper container.

As a result of three series of measurements, we detected in the 420-440 kev electron-energy region two almost fully resolved photoelectron lines. The half width of these lines was approximately 2 - 2.2%, which is in good agreement with the results of experiments on other radioactive materials under comparable conditions. The most probable values of the γ-ray energies corresponding to these photoelectron lines are $h\nu_2$ = 509 ± 3 kev and $h\nu_3$ = 526 ± 3 kev.

The intensity of the $h\nu_3$ γ-rays is approximately 20% higher than that of the $h\nu_2$ gamma rays.

In the 1000 kev energy region, also as a result of three series of measurements, we observed three photoelectron lines, of which two

are almost entirely merged. It must be noted here that the presence of the harder of the unresolved lines is manifested as a change in the slope on the side of the softer-line peak and also results in an abnormally large half-width of the soft line (~2%). The half-width of the line in this energy region and under the given measurement conditions should be approximately 1.5%.

The most probable values of the γ-ray energy, corresponding to these photoelectron lines, are $h\nu_4 = 1065 \pm 4$ kev and $h\nu_5 = 1079 \pm 4$ kev.

The third photoelectric line in this group consists apparently of two L-shell photoelectrons, ejected by $h\nu_4$ and $h\nu_5$ gamma rays. Adding the binding energy of the L-level electrons in lead to the energy of the third photoelectron line yields a γ-ray energy of approximately 1067 kev.

An approximate evaluation of the gamma-ray intensities shows that

$$\frac{I_{h\nu_4}}{I_{h\nu_5}} \approx 1.2 \qquad \text{and} \qquad \frac{I_{h\nu_5}}{I_{h\nu_3}} \approx 2.5.$$

The last ratio takes into account the fact that under the measurement conditions in our spectroscope, a relatively higher intensity is obtained for hard γ-rays as compared with soft γ-rays.

In view of the detection of two pairs of γ-lines with close energy values, we went on to investigate the photoelectron and recoil electron spectra under conditions favorable to the observation of soft γ-quanta. The emission of these could be associated with transitions between two neighboring energy levels.

The radiator with the tin target described above was used for this purpose. With it we investigated the energy region from 3.5 to 35 kev.

As a result of three series of measurements we detected a weak photoelectron line at 5.3 kev.

If this line is assumed to be due to photoelectrons ejected from the K-level of Sn, there should also be evident a line of at least comparable intensity at about 30 kev, associated with photoelectrons ejected from the L-shell. However, no other lines in the 3.5 to 35 kev interval were observed. Hence, it may be concluded that the detected line is due to photoelectrons ejected by γ-rays from the L-level rather than from the K-level of Sn. In this case the energy of the corresponding $h\nu_1$ γ-rays is 10 ± 1 kev.

The connection between the observed γ-radiation and the decay of Rb^{86} has not been definitively established since no measurements of the rate of decrease in the intensity of the photoelectron lines in question have been made and no control experiments with chemically pure Rb^{86} were carried out.

It should be noted that the $h\nu_4$ and $h\nu_5$ γ-ray energies are very close to the energies of γ-rays from Rb^{86} determined by Zaffarano, Kern and Mitchell[33] and Muether and Ridgeway[17].

6. Decay scheme for Rb^{86}

The decay scheme for Rb^{86}, whose principal features were established by Zarrarano, Kern and Mitchell, is shown in Fig. 3 (we have supplemented this scheme by indicating the possible K-capture decay and the suspected β_3 component in the β^--spectrum).

Table

Rb^{86} β^--Spectrum Components as Determined by Various Investigators

No.	Investigators, year	$E_{\beta 1}$ Mev	I,%	$E_{\beta 2}$ Mev	I,%	Method	Ref
1	Helmholz, Piecner, Stout (1941)	1.56±0.05	-	-	-	Absorption with analysis by Feather's rule	2
2	Haagstrom (1942)	1.6±0.3	-	-	-	Solenoidal spectrometer, R ~ 5%	13
3	Feidman, Giendenning (1946)	1.80	-	-	-	Absorption	14
4	Zaffarano, Kern, Mitchell (1948)	1.822.0.014	80	0.716±0.020	20	Magnetic lens spectrometer	3
5	Jurney (1948)	1.82	67	0.56	33	Absorption in Al with analysis after Bleier and Zünti	15
6	Goeckerman, Perlman (1949)	2.0	-	-	-	Absorption	16
7	Muetner, Ridgeway (1950)	1.80±0.01	-	0.714±0.010	-	Magnetic lens spectrometer with β-γ coincidence R ~ 3 - 15%	17
8	Mandeville, Shapiro (1950)	-	-	-	12±2	β-γ coincidence	18
9	Maklin, Lidofsky, Wu (1951)	1.760±0.010	-	0.670±0.005	-	Solenoidal spectrometer with β-γ coincidence, R ~ 10%	19
10	Palmer, Laslett (1951)	-	-	0.67	-	Scintillation spectrometer	20
11	Moreau, Perez (1952)	1.79	-	-	-	Spectrometer	21
12	Our data (1953)	1.795±0.015	86	0.711±0.015 E_3 0.230(?)	14 1-5	Ketron, R ~ 0.6 - 0.8%	

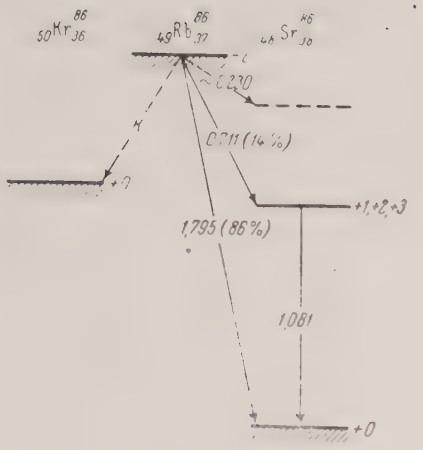

Fig. 3. Decay scheme for Rb^{86} (Energies and relative intensities of the β^--transformations shown are from our data).

The momenta and parities of the ground states of Rb^{86} and Sr^{86} and of the excited state of Sr^{86} were established in Refs. 9, 12, 17, and 22. Our own results confirm these conclusions concerning the angular momenta and parities. In fact, the ground state of the even-even nucleus $_{38}Sr^{86}_{48}$ has spin 0 and, apparently, even parity. In this case, in view of the "uniqueness" of the hard spectrum of Rb^{86} and the absence of β-γ coincidences for this spectrum[17] it may be deduced that the ground state of Rb^{86} has spin 2 and odd parity. This conclusion agrees with the results of Bellamy and Smith[22] who measured the spin and magnetic momentum of Rb^{86} by the magnetic-resonance method. According to their data the spin of Rb^{86} is 2, and $\mu = -1.09$. The value of μ is in conformity with the configuration of the odd-odd nucleus $_{37}Rb^{86}_{49}$, predicted by the nuclear-shell model.

This configuration (protons -- $f_{5/2}$, neutrons -- $g_{9/2}$) actually has odd parity.

The ground state of the even-even nucleus $_{36}Kr^{86}_{50}$ has a zero momentum and, apparently, even parity. In this case the $Rb^{86} \rightarrow Kr^{86}$ transition (ground state) will be forbidden to the same degree as the transition $Rb^{86} \rightarrow Sr^{86}$ (ground state).

Next, let us consider the excited state of Sr^{86}.

Analysis of the shape of the 0.711 Mev β^--spectrum, the value of $\log ft$ and the results of the β-γ angular correlation experiments, all support the hypothesis that this β^--spectrum is that of a first forbidden transformation and exclude the α-type spectrum hypothesis. In this case the angular momentum of the excited state can be 1, 2, or 3, and the parity is even.

Analysis of the first excited levels of the even-even nuclei (Refs. 23 and 24) shows, first, that the energy of the first excited level of Sr^{86} should lie between 1 and 1.5 mev, which is in agreement with experimental results; and, second, that 2 is the most probable value of the angular momentum for the first excited level.

If the existence of the β_3 component is proven more rigorously and a connection is established between the γ-radiation detected by us and the disintegration of Rb^{86}, the decay scheme of this isotope will become more complex. In refining the decay scheme it will be necessary to take into account that $h\nu_2 \approx h\nu_3 \approx E_{\beta 2} - E_{\beta 3}$ and $h\nu_1 \approx \approx h\nu_5 - h\nu_4$.

The authors express deep gratitude to B. S. Dzhelepov for his guidance and helpful discussion of the results of this investigation.

Received
26 August 1954

Bibliographic References

1. A.Snell, Phys. Rev., 52, 1007 (1937).
2. A.Helmholz, C.Plecher & P.Stout, Phys. Rev., 59, 902 (1941).
3. D.Zaffarano, B.Kern & A.Mitchell, Phys. Rev., 74, 682 (1948).
4. H.Waeffler & O.Hirzel, Helv. Phys. Acta, 21, 200 (1948).
5. R.Schwartz, M.Perlman & W.Bernstein, Phys. Rev., 91, 883 (1953).
6. W.Barber, Phys. Rev., 72, 1156 (1947).
7. W.Mims & H.Halban, Proc. Phys. Soc., 64A, 311 (1951).
8. P.Zarubin, preceding article of this issue of the Bulletin.
9. S.Frankel, Phys. Rev., 77, 747 (1950); 79, 243 (1950).
10. S.Ridgeway, Phys. Rev., 79, 243 (1950).
11. T.Novey, Phys. Rev., 78, 66 (1950).
12. D.Stevenson & M.Deutsch, Phys. Rev., 83, 1202 (1951).
13. E.Haagstrom, Phys. Rev., 62, 144 (1942).
14. M.Feldman & L.Glendenin, Rev. Mod. Phys., 20, 4 (1948).
15. E.Jurney, Phys. Rev., 74, 1049 (1948).
16. R.Goeckerman & I.Perlman, Phys. Rev., 76, 628 (1949).
17. H.Muether & S.Ridgeway, Phys. Rev., 80, 750 (1950).
18. C.Mandeville & E.Shapiro, Phys. Rev., 77, 439 (1950).
19. P.Maklin, L.Lidofsky & C.Wu, Phys. Rev., 82, 334 (1951).
20. J.Palmer & L.Laslett, Rev. Mod. Phys., 25, 469 (1953).
21. J.Moreau & J.Perez, C. R., 235, 38 (1952).
22. E.Bellamy & K.Smith, Phil. Mag., 7(44), 33 (1953).
23. M.Goldhaber & A.Sunyar, Phys. Rev., 83, 906 (1951).
24. G.Sharff-Goldhaber, Phys. Rev., 90, 587 (1953).

* * * * * * * *

A HIGH-TRANSMISSION WEDGE-TYPE SPECTROMETER WITH IMPROVED FOCUSING

- E. E. Berlovich

1. Introduction

Recent scientific advances in the field of nuclear spectroscopy have led to the development of new types of high resolution spectrometers: the ketron designed by Dzhelepov and Bashilov[1] can resolve lines with a half-width (width at half-maximum) of only 0.15%; the highest resolution of the Siday and Silverston[2] instrument is 0.13%; while that of the instrument developed by Kel'man et al[3] is less than one-tenth of one percent. Instruments of this kind are very useful for studying weak γ-lines, separating close-energy lines, and assigning internal conversion lines to different electron shells and, particularly, to specific subgroups of a given shell (for example, the subgroups of the L-shell). These investigations are important in establishing the multiplicity of nuclear transitions.

However, the resolution of the diverse spectrometers used in different nuclear experiments varies greatly, ranging from under one-tenth of a percent to well over ten percent (see list in the survey by Persico and Geoffrion[4]). An example of a case requiring a spectrometer with a large line half-width (low resolution) is furnished by β-γ angular correlation studies, in which the instrument must encompass a fairly wide energy interval in order to bring the β-γ coincidence counting rate to an acceptable level. In β-decay investigations there is no need for a very high resolution to obtain the correct shape of the spectrum; however, going to the other extreme - too large a minimal half-width - may result in distortion of the spectrum. A half-width (resolution) of 2-3% is entirely satisfactory for correct rendering of the shape of β-spectra.

Many spectrometrometric investigations require not so much a high resolution as a high intensity (transmission factor) of the instrument. This applies, for example, to the investigation of emission spectra from low specific activity sources as well as to experiments in which spectrometric measurements are employed in conjunction with coincidence counts.

High intensity and high resolving power are, in a sense, contradictory requirements: simply increasing the angle of acceptance in order to increase the intensity involves a reduction of the resolution of the instrument.

There are ways of overcoming this difficulty. In spectrometers with transverse focusing the angle of acceptance is increased without undue sacrifice of resolution by appropriate modification of the magnetic field distribution (Korsunski, Kel'man and Petrov[5], and Langier and Cook[6]); in high intensity spectrometers with longitudinal focusing compensating coils are used to the same end.

Below we describe a method of focusing widely divergent beams in wedge-type spectrometers. Using this method it proved possible to realize a spectrometer with transverse focusing, combining a resolution adequate for many experiments (2%) with the high intensity common to instruments with longitudinal focusing (transmission = 1% of the 4π solid angle). The focusing procedure for the spectrometer in question is much simpler than that for such instruments as the ketron. Another advantage of our instrument is that both the source and the detector are located outside the magnetic field.

2. Focusing Characteristics of Wedge-Shaped Magnetic Fields

The focusing properties of a wedge-shaped magnetic field, analyzed by Stephens[7] and Barber[8], are illustrated in Fig. 1 for the case of symmetric location of the source and "image".

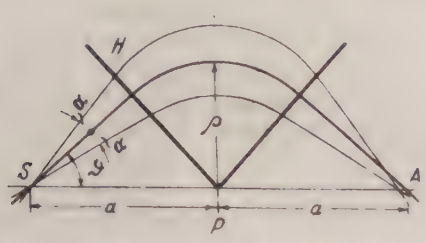

Fig. 1. Focusing effect of a wedge-shaped magnetic field with symmetrically located source S and image A.

Particles emitted from the point source S, in passing through the magnetic field H, converge to a band of finite width. The width of this image (i.e. the aberration) is given by

$$S = a\alpha^2 \sin\vartheta, \qquad (1)$$

where 2α is the angle of divergence, a is the distance of the wedge apex from the source and from the image and ϑ is the angle between the central ray of the beam at the point of emergence and the line passing through the source, image and apex of the wedge.

It will be seen from equation (1) that in this case, just as in the case of semicircular focusing, the width of the image is proportional to the square of the angle of divergence (angle of emission).

A number of investigators have examined the feasibility of modifying the shape of the wedge sides in order to correct this aberration (i.e., to reduce the width of the image). Kerwin[9] computes the optical properties of such systems; in his analysis Kerwin approximates the geometry of the wedge sides by sections of circular arcs and straight lines. Such approximations are, naturally, allowable only when the divergence angle is relatively small. Moreover, in Kerwin's analysis the wedge-shaped field is assumed to be ideal, i.e., homogeneous in the gap with no fringing (abrupt transition to zero at the edges). These assumptions detract from the practical value of Kerwin's calculations.

Lastly, Judd[10] and Rosenblum[11] examine the case of a wedge-shaped field falling off radially according to the law

$$H = H_0(\rho_0/\rho)^{1/2}$$

and providing focusing in two directions, as in the Svartholm-Siegbahn spectrometer[12]. This method should yield an increase in transmission, but fringing at both the entry and exit sides of the wedge may have an adverse effect.

3. Methods of Improving Focusing of Wide-Angle Beams in Wedge-Type Spectrometers

Assume we have a strongly divergent beam of charged particles emerging from the point S (Fig. 2) and entering a homogeneous magnetic field H, initially having a square cross section (dash line). Let us locate point A on the extension of the line SP, symmetrically with S with respect to P (the symmetry is not a necessary condition). Now from this point, let us draw a family of straight lines tangent to the circular paths of the particles in the field H. The locus of the points of tangency gives us the curve defining the shape the exit face of the pole piece should have for all the particle paths to intersect at A. The final shape of the pole piece profile so determined is shown in Fig.

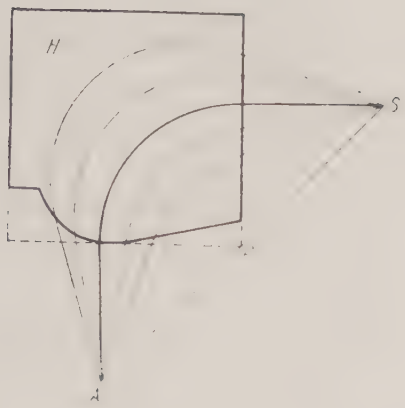

Fig. 2. Improving focusing by shaping the exit edge of the pole piece.

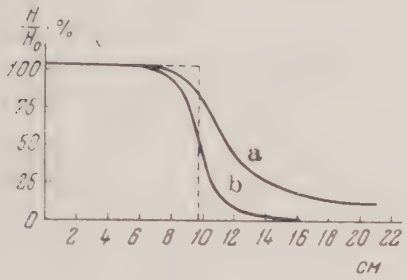

Fig. 3. Improving focusing by modifying the field distribution at the edges: a) actual field distribution, b) corrected distribution. Dash line indicates ideal field distribution.

by the solid line. Actually, the location of the focal point A can be selected arbitrarily: Moving the point will simply change the shape of the exit edge of the pole piece and the total angle through which the central ray is deflected.

With this method of shaping the pole piece, only particles having a certain momentum ($H\rho$) and, consequently, a certain radius of path in the given field (the path radius for which the pole piece is shaped) will be brought to a focus. Particles having other values of momentum (and, hence, other path radii) will be defocused, since the shape of the pole piece profile is arbitrary where they are concerned. Such "selective" focusing is a characteristic common to all systems corrected for aberration. As we know, in an ordinary (un-corrected) wedge-shaped field, just as in a semicircular field, particles having different momenta are focused at different points, lying along a straight line.

The described procedure would lead to accurate focusing of widely divergent beams if the field in the gap were homogeneous and cut off sharply at the edges (dash line in Fig. 3). The actual field distribution in the gap and immediately outside it, as plotted for the central path passing through point A and the apex of the exit edge, is shown by a) in Fig. 3.

The field distribution can be improved by the use of compensating plates in the gap (near the edges) and shielding windows outside the gap to attenuate the fringing field. It is obvious, however, that there is no way of converting the actual field distribution a) to the ideal (dash line). Thus, bringing a shielding window up to the gap in order to cut off the leakage field has the effect of changing the flux distribution in the magnetic core material and increasing the inhomogeneity of the field in the gap. Instead of attempting to obtain an ideal field, it is preferable, through appropriate choice of compensating baffles and shielding windows, to provide a field configuration such that the fringing field outside the gap will compensate for the deficiencies in field strength inside the gap, i.e., to provide a field distribution satisfying the equation

$$H_0 l = \int H dl, \qquad (2)$$

where H_0 is the field intensity in the region of homogeneity, l is the length of the central path (ray) in the region of the gap and H is the actual varying field.

The integration is carried out over the entire path, both inside and outside the gap. The field distribution corrected according to this principle is represented by the lower curve, b), in Fig. 3.

However, it is difficult to apply this principle in practice not just to the central path but to all the trajectories, particularly when the angle of divergence is large. Because of this and also due to the effect of various technical factors (inaccuracies in shaping the pole faces, misalignment of the two pole pieces, deviation from parallelism of the magnet surfaces, etc.) the actual focus is shifted from the theoretical design point.

We constructed two variants of an instrument embodying the above described principle. The instruments were twin spectrometers intended for separating partial β-spectra by the coincidence method. A twin spectrometer of a similar type is briefly described in our earlier article[13] on the investigation of the complex spectrum of RaB, which also shows the spectra and internal conversion lines recorded with that instrument.

The following procedure was employed to determine the actual location of the focus: we investigated narrow beams oriented in different directions within the confines of the entire acceptance angle of the instrument in the horizontal plane (30°). Using electrons of known energy (the internal conversion electrons of one of the lines observed in the β-decay of RaB), we determined, from the readings of a ballistic galvanometer connected to a coil in the magnetic field, the field intensity - in arbitrary galvanometer scale units - yielding the maximum count for each beam direction. With the counter (detector) in the initial position, the readings for the different individual narrow beams were different. This indicated that the electrons having the same energy were not all focused on the detector slit. From the difference in the indications for the different beams we could determine in what direction the counter slit had to be displaced to reduce the dispersion of readings for the maximum counts. After a series of consecutive displacements we succeeded in bringing the readings of the galvanometer to the same value - within the limits of the reading error - for all investigated orientations of the electron beams. This meant that the electrons having the given energy entered the detector slit with the same value of the field intensity for all beam angles, i.e., that the detector slit was at the focus of the instrument.

The parameters of the first version of our instrument were the following: angle of divergence in the horizontal plane: $2\alpha = 30^{\circ}$, angle of divergence in the vertical plane: $2\varepsilon = 5^{\circ}$; radius of curvature: $\rho = 12$ cm. The line half-width ratio (resolution) was brought down to 1.8% (see Fig. 4 in Ref. 13).

The theoretical transmission of the instrument computed on the basis of the above angles is 0.36%. The actual transmission was determined experimentally from the coincidence count, with one branch of the twin spectrometer recording the number of internal conversion electrons while the other branch registered the continuous spectrum electrons. The transmission was computed by means of the following relationship:

$$kC_g = N_k \omega_\beta \varepsilon_\beta \frac{F_i(H\rho)\, d(H\rho)}{\int F_i(H\rho)\, d(H\rho)}, \qquad (3)$$

where C_g is the number of coincidences per unit time, N_k is the number of internal conversion electrons detected in one branch of the twin spectrometer, ω_β is the solid angle accepted by the branch recording

the β-decay electrons (i.e., the transmission), ε_β is the efficiency of the electron detector and k is an experimentally determined correction factor taking into account absorption of electrons by the counter window. The fraction $\frac{F_i(H\rho)\,d(H\rho)}{\int F_i(H\rho)\,d(H\rho)}$ is the ratio of the number of electrons of the partial spectrum in question recorded with the given field intensity to the total number of electrons of the said spectrum and is determined from the known line half-width for the particular branch of the spectrometer detecting the β-decay electrons and from the recorded coincidence spectrum.

The experimentally determined transmission of the instrument proved to be $\omega_\beta = 0.3\%$ (a somewhat lower value - 0.25% - was indicated in Ref. 13). The experimentally determined transmission is somewhat lower than the theoretical value (0.36%); the reason for this will be explained below. It is worth noting that the described method of finding the transmission experimentally does not require a source of accurately known activity; the error in determining the transmission should not exceed 3-5%.

In order to evaluate the effectiveness of the method of focusing employed one might compare the resolution obtained by us (1.8%) with the resolution which would be obtained with a conventional spectrometer with the same angle of beam divergence.

Using equation (1) and the relationship $f = a \sin\vartheta$ (self-evident from Fig. 1), the width of the image of a point source with angles of divergence of 2α in the horizontal plane and 2ε in the vertical plane can be described by

$$S = \rho(\alpha^2 + \varepsilon^2), \tag{4}$$

which is identical with the corresponding expression for semicircular focusing. If the width of the slit is taken equal to the width of the image, the relative half-width of the line (width at half-maximum for a line having an approximately triangular shape) will be

$$\frac{\Delta(H\rho)}{H\rho} = \frac{S}{\rho} = \alpha^2 + \varepsilon^2. \tag{5}$$

With our conditions ($2\alpha = 30^\circ$ and $2\varepsilon = 5^\circ$) this gives a value for the half-width equal to 7% as against the value of 1.8% obtained by us.

The design of the instrument just described does not take into account the effect of vertical focusing in the region of the field edges. This effect is connected with the fact that due to fringing (barrel-like "bulging" of the field at the gap edges) the field vector acquires a horizontal component which deflects electrons moving in the horizontal plane towards the vertical. As Khurgin[14] showed, the focal distance of a cylindrical lens equivalent to the "bulging" boundaries of the magnetic field is given by

$$F = \rho \operatorname{ctg}\varphi. \tag{6}$$

where ρ is the radius of the path and φ is the angle between the direction of motion of the particle outside the field and the normal to the field boundary. Depending on the sign of φ the particle is deflected either towards the central plane between the pole pieces (focusing) or away from it (defocusing). This is the reason for the small discrepancy

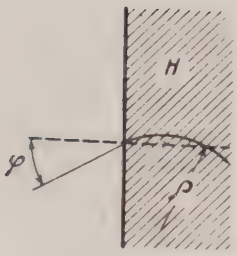

Fig. 4. Vertical focusing effect. Path of rays in the horizontal symmetry plane.

between the theoretical and experimental values of the transmission mentioned above. In their passage through the deflecting field of the instrument the particles encounter two such cylindrical lenses, corresponding to the two boundaries of the magnetic field.

In the second version of our instrument the transmission was raised further by increasing the angles in the horizontal and vertical planes (to $2\alpha = 45^\circ$ and $2\varepsilon = 10^\circ$) and by taking into account the vertical focusing effect.

It will be seen from equation (6) that the focal distance varies with the angle φ. One could try to bring both focal points (horizontal and vertical) for the first lense into coincidence by shaping the entry face so that the angle φ for all rays emitted from the source would be the same. However, without reducing the desired large angle of divergence in the horizontal plane this would lead to an excessive increase in the dimensions of the pole pieces and, consequently, of the entire magnet. Moreover, the shape of an exit edge designed according to the above-described method proves to be extremely complicated and results in a great diversity of values of φ for the exit edge and, hence, in an appreciable dispersion of the focal distances for the second cylindrical lens. It must also be noted that equation (6) is approximate and yields somewhat distorted values of the focal distance particularly for large angles φ. For all these reasons it was deemed preferable to allow for the vertical effect only to the extent of enlarging the counter slit to insure detection of all the electrons, including those "defocused" by the vertical effect.

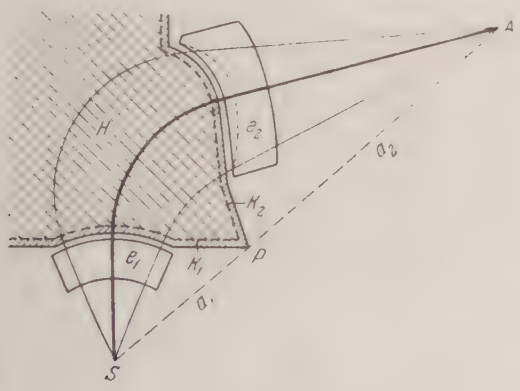

Fig. 5. Shape of pole piece and location of the correcting components in the high transmission spectrometer.

Fig. 5 shows the shape of the pole piece and the location of the source S, the focus A, the shielding windows of Armco iron e_1 and e_2 and the compensating plates K_1 and K_2 attached to the pole pieces inside the gap. The entry edge of the pole pieces is a circular arc and the paths of the particles arriving from the source are normal to it; consequently, the particles are not subject to vertical deflection (according to equation (6), the focal distance in this case is infinite, i.e., the first lens is absent). The focus is located on the straight line passing through the source and the apex P at a distance AP equal to twice SP; this distance is sufficiently great to insure the reasonable smoothness and low curvature of the exit edge necessary to minimize the variation in φ for the exit lens. We computed the focal distances and locations of the image for the various paths (according to the thin lens formula) and plotted the trajectories in the vertical plane. The width of the detector slit was determined on the basis of the path subject to the greatest deflection away from the horizontal plane of symmetry.

Displacement of the counter, which is wholly enclosed in the counter chamber in this version of the instrument, is accomplished by means of a special worm-gear mechanism, controlled from the outside through a Wilson seal and designed to move the counter carriage in two mutually perpendicular directions. The displacements are indicated on two suitable scales.

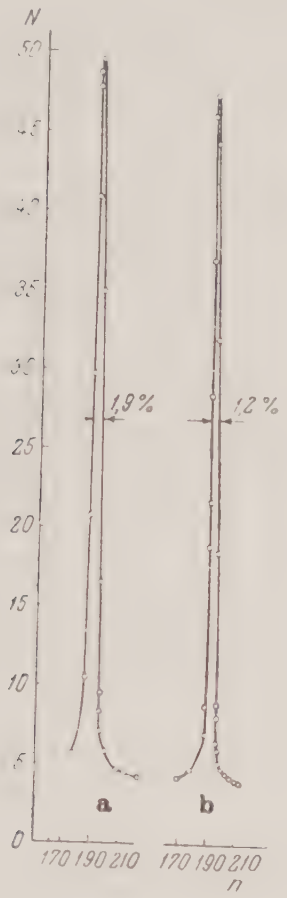

Fig. 6. F line of radioactive thorium precipitate, obtained a) with entry slit fully open; b) with only middle third of slit length open.

For the final focusing, in addition to shifting the counter, we also used the procedure described below, based on modifying the section of the fringing field at the exit face, between the face itself and the shielding window. Satisfactory focusing could not be achieved by displacement of the counter alone (as described above) in view of the increased angles of beam divergence in both planes and the increased path length of the beam after leaving the magnet (distance AP, Fig. 5). Inaccuracies in the fabrication and assembly of the magnet and departures from the conditions prescribed by equation (2) have a much more appreciable effect in the second version of the instrument (as compared with the first) because of the increased divergence angles and extended path length. By carefully following the variation of the intensity (counting rate) for the selected conversion line with the readings of the ballistic galvanometer with different narrow beams we were able to adjust the configuration of the fringing field by gradual filing of the edge of the shielding window next to the gap so as to bring all the narrow beams to the slit with the requisite precision. Hence, in the case of the second version of the instrument the focusing procedure comprised two stages: 1) determining the optimum position of the counter (as with the first version) and 2) refining the distribution of the fringing field. The instrument is designed so that the shielding window can easily be demounted for filing after disconnecting the counter chamber which is fastened to the main chamber of the instrument by means of bolts and rubber gaskets. How much easier the adjustment is in the case of our instrument - as compared with other improved-focusing spectrometers which require complete disassembly of the entire magnet and repeated grinding of all the surfaces of both pole pieces - is evinced by the fact that our readily demounted shielding box weighs only one and a half kilograms and can easily be clamped in a vise; the edge can be cut down with an ordinary file.

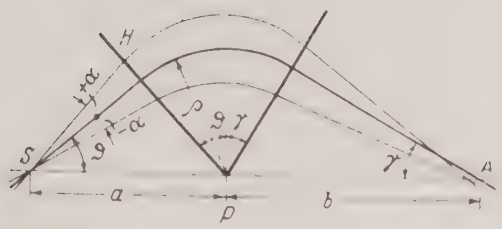

Fig. 7. Diagram pertaining to the spherical aberration equation for asymmetrically located source and image.

The line half-width separated without difficulty in several instruments of this type amounts to 1.9 - 2.0%. Fig. 6a shows one of the internal conversion lines of a radioactive precipitate of thorium (the F line) recorded using the full angles of divergence. The transmission, determined as before using the coincidence method with a twin spectrometer, consisting of two instruments of this type, was found to be 1.08%, which is in good agreement with the value computed on the basis of the two divergence angles.

In order to calculate the half-width of the line resolved by a wedge spectrometer without correction for aberration, for the given values of the divergence angles, one should use the following equation for the general case of asymmetrical transmission through a wedge-shaped field, derived from the theory of wedge-field spectrometers[7] (see Fig. 7):

$$S = \frac{a\alpha^2}{2}\left(\frac{\sin^2\vartheta}{\sin\gamma} + \frac{\sin^2\gamma}{\sin\vartheta}\right). \tag{7}$$

In our case, where AP = 2PS = $2a$ (Fig. 5), it is evident that

$$\rho = a\sin\vartheta = 2a\sin\gamma \tag{8}$$

and

$$\sin\gamma = \frac{\sin\vartheta}{2}. \tag{9}$$

Taking (8) and (9) into account the expression for the dispersion

$$D = a\frac{\sin\theta}{\sin\gamma}(\sin\theta + \sin\gamma), \tag{10}$$

can be simplified to

$$D = \frac{S}{3\rho}. \tag{11}$$

Finally, invoking the following expression from electron optics

$$\frac{\Delta(H\rho)}{H\rho} = \frac{S}{D}, \tag{12}$$

we obtain for a slit width equal to the image width

$$\frac{\Delta(H\rho)}{H\rho} = \frac{2S}{D} = \frac{3}{4}(\alpha^2 + \varepsilon^2). \tag{13}$$

For the angles used in the described version of the instrument this expression yields a line half-width of about 13% [1.3% ?].

Thus it will be seen that the procedure and methods employed made it possible to bring the transmission of the instrument with transverse focusing to the level characteristic of spectrometers with longitudinal focusing and yet retain a resolution appreciably better than obtaining in ordinary wedge spectrometers with uncorrected aberration.

Examination of the data on spectrometers summarized in Ref. 4, which lists most instruments described in scientific literature up to 1951, shows that as regards intensity our instrument is superior by at least one-two orders of magnitude to all fourteen of the transverse focusing instruments listed in the table and that only seven of the twenty-five spectrometers with longitudinal focusing have a higher transmission; five of these seven have lower resolution.

We venture to introduce another quantity which may be useful in characterizing spectrometers: the ratio of the transmission to the resolved line half-width, $\zeta = \omega/\eta$, which one might call the "quality" or Q-value of the spectrometer. Obviously this ratio cannot be used alone to characterize a spectrometer in every case since, as was pointed out in the introduction to the present article, the actual values of the transmission or of the resolution may be of paramount importance in different investigations. However, the ratio is indicative in the sense that it characterizes conjunction of the two conflicting properties of beta-spectrometers: the intensity and the resolution. Of the thirty-nine spectrometers listed in the table of Ref. 4, only six have a higher Q-value than our instrument.

4. Possibilities of Further Improvement in Focusing

The parameters obtained in our instrument are by no means the limiting values. With the attained transmission (1.08%), an appreciable reduction in the resolvable line half-width is still possible. The width of the entry slit of the counter, on which the beam was focused, was 6 mm. Obviously, with more careful and painstaking adjustment the beam can be focused on a narrower slit. The focusing procedure can be made more accurate where the galvanometer readings are concerned by increasing the sensitivity of the counter or using a higher energy line so that the field corresponding to the maximum intensity of the line (with the given narrow beam orientation) will produce a full-scale deflection of the galvanometer.

Furthermore, it is known that even in spectrometers with semicircular focusing in a nomogeneous field the image of a line source is curved. The curvature should be even greater in our case where the field distribution in the different horizontal planes is obviously non-uniform (in the region of the magnet edges). Hence, in using a rectilinear detector slit, which in our case is 120 mm long, we clearly fail to obtain the best focusing. Actually, the focal line may be curved in a complicated manner; from certain considerations it follows that the focal line does not lie in a plane normal to the central ray. However, it should be possible to improve the focusing considerably even by taking into account the curvature of the focal line only in this normal plane. Fig. 6b shows the same line as in Fig. 6a but obtained with only the central third of the entire counter slit length uncovered. It will be seen that the half-width of the line is reduced to 1.2%, which is consistent with the considerations educed above. The shape of the focus line can be investigated either photographically or by means of a fluorescent screen (if the source is sufficiently intense) or, finally, by making electron counts for individual sections of the slit area.

5. Construction of the Spectrometer

The spectrometer chamber is diagrammed in Fig. 8. It comprises three parts: a) the source chamber, b) the beam-deflection chamber, and c) the counter chamber.

The source in the form of a layer of active material deposited on a strip of aluminum foil or zapon film is mounted in a special frame, which is positioned by means of a cylindrical stub, entering a mating opening in the center of the source chamber. The emitter frame is surrounded by two coaxial cylinders of plexiglass. The outer cylinder has a wide slit - wide enough to pass the entire beam, while the inner cylinder, friction fitted into the outer one, has two slits: a wide and a narrow one. When the instrument is being adjusted (focused) by the method described above, the narrow slit of the inner cylinder is set in line with the middle of the wide slit in the outer cylinder. A crank operated gear train connects to the outer cylinder; thus by turning the crank both cylinders can be revolved to set the narrow slit in various positions and obtain the variously oriented narrow beams. The angles of rotation are indicated by a pointer moving over an appropriate scale on the cover of the source chamber. In making measurements with the full-width beam, both wide slits are aligned at the middle setting. The first shielding window of Armco iron is also located in the source chamber. The chamber design has provision for changing emitters without loss of vacuum.

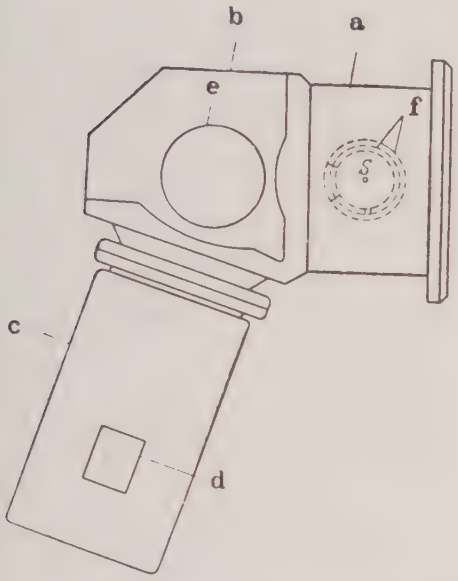

Fig. 8. Diagram of the spectrometer: a) source chamber, b) deflection chamber, c) counter chamber, d) detector carriage, e) magnet core, f) plexiglass cylinders, S - source.

After passing through the shielding window and the "aperture diaphragm" (first defining slit) the beam enters the deflection chamber where there are a number of auxiliary diaphragms (baffles) whose location and dimensions are determined by the geometry of the beam. In order to keep the vertical angle sufficiently great without increasing the air gap the bottom and top of the chamber are formed by the inner sections of the Armco-iron pole pieces, which are attached directly to the sidewalls of the chamber. A seal is provided by rubber gaskets. The height of the deflection chamber at the center (between the poles) is 52 mm; in the section of the compensating plates, the height is 48 mm.

From the deflection chamber, the beam enters the counter chamber; as already noted the chamber is bolted to the spectrometer, with a rubber gasket joint, and can readily be detached from the deflection chamber. The second shielding window, although located in the counter chamber, is actually mounted in a groove machined in a brass flange, attached to the magnet and protruding from the deflection chamber. The counter carriage, which is operated from outside the chamber, has provision for mounting either a slit-type gas-discharge (G-M) counter or

a diaphragm with an entry slit backed by a thin layer of scintillating material coated on a light-conductor bearing against a quartz window.

The photomultiplier tube, which is set with its cathode against the outside of the quartz window, is mounted in a magnetic shield consisting of three coaxial cylinders of Armco iron. The carriage control mechanism is mounted on a side wall of the counter chamber. The C-shaped magnet core is assembled of Armco iron. The weight of the iron in the core is 260 kg; the weight of the copper, 200 kg. The winding consists of 35,000 turns of 2 mm diameter wire. The winding was designed to permit using a low-current power supply. This made it possible to use a vacuum-tube current stabilizer instead of bulky storage batteries which have to be connected through a buffer in order to stabilize the current. For example, with this winding a current of only 100 ma is required to focus 2 Mev electrons.

The writer wishes to express his gratitude to I. M. Belousov and G. M. Obraturov, graduate students at the "M. I. Kalinin" Leningrad Polytechnical Institute, for their assistance in adjusting the instruments.

Received
30 August 1954

Bibliographic References

1. B.S.Dzhelepov & A.A.Bashilov, Izv. (Bulletin) AN SSSR, Ser. fiz., 14, 263 (1950).
2. R.E.Siday & D.A.Silverston, Proc. Phys. Soc., Sec. A, 65, 328 (1952).
3. D.L.Kaminski, Beta-spektrometr postroennyi po analogii s opticheskim spektrometrom (A beta-spectrometer analogous in design with optical spectrometers). Thesis, Leningrad Physico-Technical Institute, 1953.
4. E.Persico & C.Geoffrion, Rev. Sci. Instr., 21, 945 (1950).
5. M.Korsunski, V.Kel'man & B.Petrov, Zhur. eksp. i teor. fiz.,14,394 (1944).
6. L. Langer & C.Cook, Rev. Sci. Instr., 19, 257 (1948).
7. W.E.Stephens, Phys. Rev., 45, 513 (1934).
8. N.F.Barber, Proc. Leeds Phil. Soc., 2, 427 (1933).
9. L.Kerwin, Rev. Sci. Instr., 20, 36 (1949); L.Kerwin & C.Geoffrion, Rev. Sci. Instr., 20, 381 (1949).
10. D.L.Judd, Rev. Sci. Instr., 21, 213 (1950).
11. E.S.Rosenblum, Rev. Sci. Instr., 21, 586 (1950).
12. N.Svartholm & K.Siegbahn, Ark. Mat. Astr. o Fys., 33, 21 (1947).
13. E.E.Berlovich, Izv. (Bulletin) AN SSSR, Ser.fiz., 16, 3, 314 (1952).
14. Ya.L. Khurgin, Zhur. eksp. i teor. fiz., 9, 824 (1939).

THE RITRON - A GAMMA-SPECTROMETER UTILIZING RECOIL ELECTRONS*

- B. S. Dzhelepov, N. N. Zhukovski and Iu. V. Khol'nov

1. Introduction

Gamma-spectroscopy must be based on one of the following forms of interaction of gamma-rays with matter: classical scattering of the γ-rays, Compton scattering, the photoeffect, pair formation or photodisintegration of nuclei. All these effects or processes are utilized to some extent for spectrometric purposes, but their fields of application differ inasmuch as the probability of each varies markedly but in different ways with the energy of the gamma-quanta.

Classical scattering and the photoeffect can be utilized only in the low energy region - principally below 0.5 Mev; pair formation and photodisintegration (nuclear photoeffect) are used only at high energies - in practice, above 3 Mev. In the intermediate region (0.4-3.0 Mev) the predominant form of the interaction of gamma-radiation with matter is the Compton effect. More than half of all the known lines characteristic of radioactive substances lie in this intermediate region. Hence, the importance of developing spectrometric methods based on the Compton effect is evident.

It may be noted that the theory of Compton scattering is more fully developed than the theories of the other interaction processes. This facilitates the design of spectrometers for this region of the gamma-spectrum and creates a climate favorable to the solution of the most difficult problem in spectrometry, namely, accurate determination of the relative intensities of the spectral lines.

The first investigation of gamma-spectra utilizing recoil electrons was carried out back in 1927 by Skobel'tsyn[1] who measured the energies of recoil electrons ejected by the gamma-rays of RaC in a Wilson chamber located in a magnetic field. In 1940-41 Latishev and his co-workers[2] measured the energies of recoil electrons using a conventional magnetic spectrometer with a homogeneous transverse field. The target was a small strip of styrol (C_2H_8), having a superficial density of 23 mg/cm^2. The instrument had a low intensity and consequently only the gamma-spectra of RaC and Th(C+C'') were investigated. Subsequently, a number of other investigators[3&4] used the same method with some modification of the field distribution.

In 1948 Dzhelepov and Orbeli[5] developed a new method of focusing recoil electrons and constructed an instrument by means of which the spectra of Co^{60}, Ag^{110}, Fe^{59}, Sb^{124}, Br^{82}, Cs^{134} and Cu^{64} (Refs. 6 through 12) were later measured. However, to date, no full description of the instrument and its properties has been published. The present communication is intended to fill the gap.

In addition to the above, there have been many investigations[13] in which the energy distribution of recoil electrons from thick emitters

---

* The present paper is based on reports presented as sessions of the Academy of Sciences of the USSR.

was studied. While certain conclusions regarding the gamma-lines can be drawn on the basis of such distribution curves, these investigations cannot properly be regarded as spectrometric. For the sake of completeness, we should also mention here gamma-spectrometers consisting of two scintillation counters, one of which detects recoil electrons, the other scattered photons[14]. A positive feature of such spectrometers is their high transmission; a shortcoming is their low resolution.

2. Principle of Operation of the Ritron

Assume we have a parallel beam of monoenergetic gamma-rays impinging on a very thin target of light material (Fig. 1). Let us first consider the case of recoil electrons ejected in the plane of the drawing; in the absence of a magnetic field they will form parallel beams of particles having different energies. The fastest electrons will be those ejected forward in the direction of the incident photons.

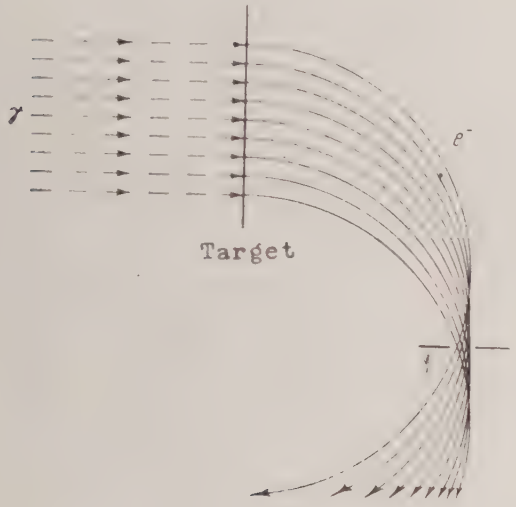

Fig. 1. Focusing of recoil electrons ejected directly forward.

Now if a homogeneous magnetic field perpendicular to the plane of drawing is applied, the parallel beams of recoil electrons will be focused, not at points but at certain focal lines or segments which we will term "foci".

The width of the focus [i.e., the length of the focal line] will depend on the radius of curvature of the electron paths, the width of the target (radiator), and angle of emission of the recoil electrons. The narrowest focus will be that for the electrons ejected directly forward. Let us locate a slit with a suitable electron detector(counter) behind it at this focus. Then let us vary the intensity of the magnetic field and at the same time count the number of pulses of the detector; as a result we will obtain a peak, i.e., a "spectral line" of the form shown in Fig. 2. Let H_o be the intensity of the field at which electrons ejected directly forward (i.e., in line with the incident photons) enter the slit along a path normal to its surface and just grazing its outer edge.

Some of the recoil electrons ejected at other angles may enter the slit even with fields slightly exceeding H_o. However, the major part of the recoil electrons will enter the slit only at fields weaker than H_o; this major group will comprise electrons ejected in the plane of the figure in the direction of the slit as well as most electrons ejected at some angle to the plane of the drawing. Our line will, therefore, have a "tail" in the region of lower field intensities.

Although by means of such a simple instrument it is feasible to determine the energy of the recoil electrons and, hence, of the photon energies from the peak or break in the line, it is obvious that the

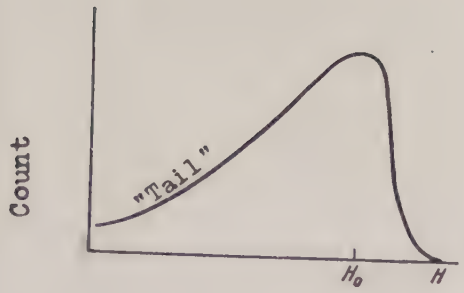

Fig. 2. Shape of spectral line obtained in recording recoil electrons with one counter. H_o is the field at which an electron ejected along the normal to the center of the target is brought to the outer edge of the slit.

spectroscopic qualities of such an instrument are poor: the long "tails" will hamper the investigation of more complex gamma-spectra. Every tail will include electrons of diverse energies and will extend down to very low values of the field intensity.

The intensity of the "tail" portion of the line can be reduced considerably by refocusing the electron beams 180° after the first focusing (see Fig. 3). To this end we locate a second slit at the second focus and move the counter to behind this slit. The shape of the line we now obtain will be more favorable for detailed investigations; it will resemble the experimental curves shown in Fig. 8 below.

Use of the second slit does not reduce the transmission of the instrument where the electrons ejected directly forward are concerned, but does diminish the transmission of electrons emitted at other angles. It will be noted that all the electrons entering the second slit do so after passing through the first. Hence, if we leave the (first) counter behind the first slit in place, but make it transparent to electrons, all the electrons detected by the second counter will also be detected by the first (but, naturally, not vice versa).

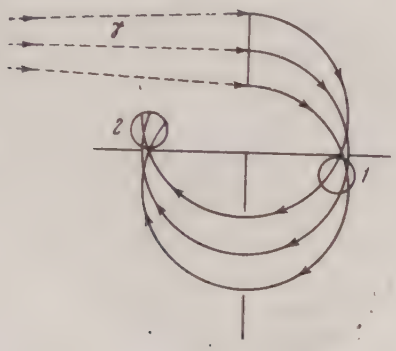

Fig. 3. Diagram of double focusing instrument: 1) first counter; 2) second counter.

By recording the coincidences in the two counters we can virtually eliminate background counts, since the coincidence background is very weak for two widely separated counters.

3. Description of the Gamma-Spectrometer

Chamber

The chamber of the spectrometer consists of a brass box measuring 20 x 20 x 8 cm. The front wall of the chamber has a window 1 (see Fig. 4) over which a copper foil 50μ thick is soldered. The gamma-rays enter the chamber through this window, strike the thin cellophane target 2 and eject recoil electrons from it.

The target is cemented over an aluminum frame larger than the cross section of the collimated gamma-ray beam. The frame is mounted on a sliding support 3 passing through the side wall of the chamber. By means of this support the target can be moved to the bottom of the chamber, out of the path of the beam; this is necessary for measuring the background.

Gamma-rays passing through the target emerge to the outside through the back wall 10 of the instrument (made of 0.1 mm thick brass). The

top cover of the instrument is removable; it fits into [illegible] groove and is fastened by screws. The diaphragms (defining slits 4 and 5 and the counters 6 and 7 are mounted on this cover. The diaphragms and counters can be demounted and replaced without removing the top cover. The latter has to be taken off only for changing the target.

The central shielding block 11 of lead-clad tungsten, an auxiliary block 12 of lead and the baffles 8 are attached to the floor of the chamber.

The inside surface of the instrument is lined with celluloid to minimize electron scattering.

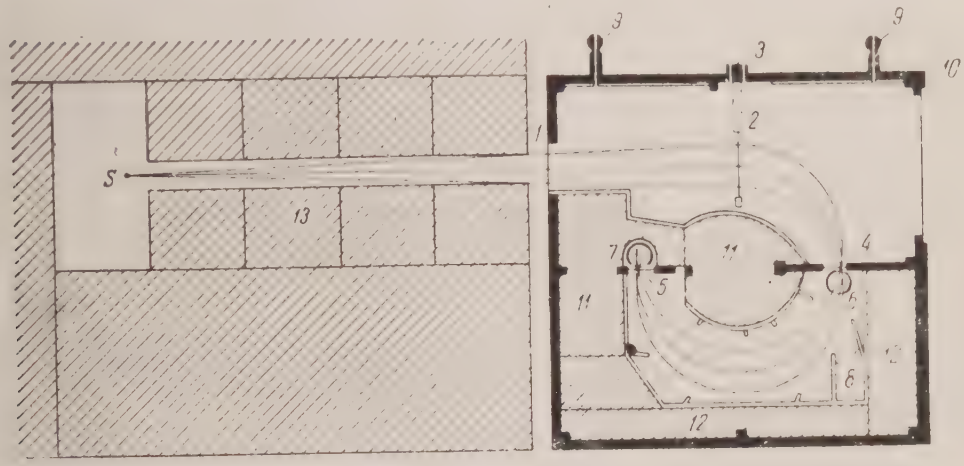

Fig. 4. Horizontal section diagram of the Nitron: S) Source of gamma-rays, 1) window, 2) target, 3) sliding support, 4 and 5) main diaphragms (slits), 6 and 7) counters, 8) auxiliary defining baffles, 9) gas-line nipples, 10) back wall of instrument, 11 and 12) shielding blocks, 13) collimator.

Size and location of slits

With the main slits covering the counters set at their normal width (2 mm) the electron beam is defined by these slits. The outer edges of the slits are parallel and 11 cm distant from each other. Half this distance - 5.5 cm - is termed the design radius of the instrument; this parameter will be encountered below in our calculations of the line shape and the transmission of the instrument.

The width of the main (counter) slits can be varied between 1 and 8 mm, while their height may be either 46 or 54 mm. In addition to the main defining slits in front of the counters the instrument also has a number of aluminum baffles which do not limit the beam when the main slits are set at 2 mm, but serve only to trap electrons straying from the beam, thereby minimizing scattering. When the main slits are opened much wider than the normal setting, these baffles do partially limit the beam section.

Counters

The counters employed in the instrument (6 and 7, Fig. 4) are ordinary cylindrical Geiger-Müller counters, 1.2 cm in diameter and

6 cm in length. Prior to the summer of 1953 the counter windows were made of 17 μ thick cellophane, with the [illegible] with atomized bismuth. In more recent experiments the cellophane has been reduced in thickness to 1-2 μ.

When the instrument is in operation the pressure in the chamber and in the counters is the same, hence the cylindrical envelopes of the counters are not deformed. The counter filaments (anodes) are made of tungsten wire 80 μ in diameter. The background count of the counters is about 40 pulses per min.

When the counters are filled with air at 11.2 cm Hg the counter threshold lies at about 1480 volts and the width of the plateau is about 100 volts. When filled with helium at a pressure of 32 cm Hg the threshold voltage was found to be around 1250 volts and the plateau width about 200 volts. (It is possible that the helium used in these tests was contaminated by organic gas liberated from the cellophane and the cement used to attach the cellophane. When the counters were filled with a mixture of He (31 cm Hg) and CH_4 (1.2 cm Hg), the threshold voltage was 1500-1550 volts and the plateau had a width of about 200 volts with a slope of 1% per 100 volts at a pulsing rate of 500 per min.

In working with counters filled with "pure" helium it was found that the threshold voltage is very sensitive to even minute admixtures of air. Even an air leak too slow to show on the manometer over a period of 24 hours is capable of raising the threshold voltage appreciably and render a counter operating near the threshold inoperative.

Vacuum system

The chamber is sealed off from the atmosphere by gaskets and packings of "plastilin" and picein (the latter was used only for the leads from the counter filaments). The vacuum system permits filling the chamber with two gases; it comprises a "vacuum fan" - a small blower - which can be rotated by an external alternating magnetic field, thus inducing a slow circulation of the gaseous mixture filling the chamber.

Composition of gas in the chamber and counters

In the first experiments[5] both the instrument and the counters were filled with ordinary air at a pressure of 11.2 cm Hg. The efficiency of the two counters, connected in a coincidence circuit, attained 95% (assuming the specific ionization of air for relativistic electrons to be 21 ion pairs per centimeter of path)[15]. With air at 11.2 cm Hg filling the system, the electrons were subject to appreciable scattering in travelling through the chamber.

In the next series of experiments [6-12] the air was replaced by helium at 32 cm Hg. The efficiency of the counters in detecting relativistic electrons was reduced only slightly - to 81% (it being assumed that relativistic electrons produce 5.02 primary ion pairs per centimeter of path in helium at standard atmospheric pressure)[16]. However, electron scattering was appreciably reduced. As a result, the number of pulses at the peak of the Co^{60} line, other conditions remaining equal, was doubled.

In the latest series of tests a new mixture, consisting of helium at a partial pressure of 31 cm Hg and methane at 1.2 cm Hg, was used

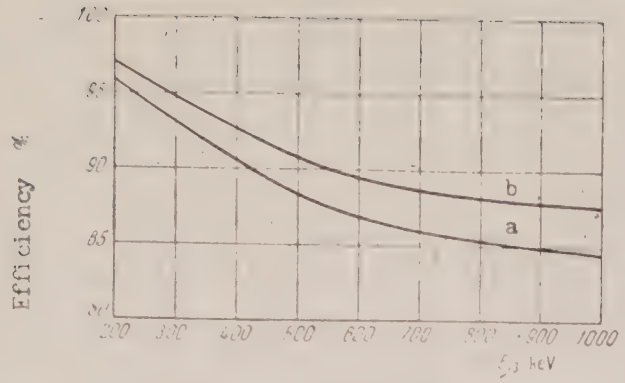

Fig. 5. Variation of coincidence counter efficiency with electron energy: a) counters filled with pure helium at 32 cm Hg; b) counters filled with mixture of helium (31 cm Hg) and methane (1.2 cm Hg).

to enhance the stability of the counters. This mixture insured stable counter operation and yielded a counter efficiency of 88% for relativistic electrons; as regards electron scattering, it is equivalent to pure helium at 32 cm Hg pressure.

The efficiency of the counters when connected in a coincidence circuit depends to a considerable extent on the energy of the electrons being detected. This factor must be taken into account when determining the relative intensities of gamma-lines. Fig. 5 shows the variation of the efficiency with electron energy in the 200 to 1000 kev range (above 1000 kev the efficiency levels off and remains virtually constant) as computed according to Ref. 16 for two of the above media: a) for pure helium at 32 cm Hg and b) for the mixture of helium (31 cm Hg) and methane (1.2 cm Hg).

Curves similar to those shown in Fig. 5 were also plotted for other gas pressures. Lowering the gas pressure in the instrument reduces the efficiency of the counters.

Coincidence circuit

Pulses from the G-M tubes are fed into a coincidence amplifier circuit having a resolution time of $1.2 \cdot 10^{-6}$ sec.

Thus when the counter load is around 1000 pulses/min, the random coincidence background is 0.04 coincidences/min. The above load is obtained when a 0.4 curie source of radium and its decay products are placed in the collimator. The normal rate in observing gamma-radiation amounts to tens or hundreds of coincidences per minute.

In working with weak specimens it is essential to reduce false coincidences due to extraneous electric factors to an absolute minimum. In order to eliminate such false counts a) the amplifier and its power supply were thoroughly shielded, and b) a third counter unit, coupled to a small antenna, was connected to the coincidence circuit in anti-coincidence; thus only events where both G-M counters are triggered, but an antenna pulse is absent, are recorded.

As a result of these measures accidental coincidences were virtually obviated: in the absence of a gamma-ray source the count is nearly constant at 1-2 coincidences per hour. This feeble background is presumably due to cosmic rays and, of course, is only a few thousandths, or at most hundredths, of the coincidence rate for gamma-lines.

Collimator

As may be seen in Fig. 4, the source is located outside the instrument proper. To prevent stray gamma-rays from reaching the counters

and producing accidental coincidences, the source is placed in a special collimator[13] which permits only a narrow beam of gamma-rays to pass through the instrument.

Under the standard conditions, under which the gamma-spectra of Co^{60}, Ag^{110}, Fe^{59}, Sb^{124}, Br^{82}, Cs^{134} and Cu^{64} (Refs. 6, 7, 8, 9, 10, 11 and 12, resp.) were investigated the source is located at a distance of 31-32 cm from the target.

The collimator consists of a large block of lead-clad tungsten with a central channel 1.5 cm in diameter and 20 cm in length. The source is placed at 1 cm from the entrance to the channel, in a small well measuring 5 x 10 x 10 cm. The well is surrounded on all sides by a considerable thickness of lead.

This collimator and the shielding blocks located inside the instrument provide the equivalent of more than 27 cm of lead in the way of shielding along the direct line from source to counters (actually the equivalent of 38.5 for the first counter and 27.4 for the second). With this thickness of shielding the most penetrating rays from ThC" (2.62 Mev) should be attenuated by a factor of 10^4.

Table 1

Load on Counters Due to Gamma-Rays (Discharges per Minute)

Material	E_γ, Mev	Activity of mat.	First counter		Second counter	
			Calc.	Exper.	Calc.	Exper.
Co^{60}	1.2	1 curie	3	1080	365	440
ThC"	2.6	1 curie	27	3700	1300	1020

The expected counting rates of the first and second counters with ThC" ($h\nu$ = 2.62 Mev) and Co^{60} ($h\nu$ = 1.17 Mev and 1.31 Mev) are shown in Table 1. The listed values were calculated on the basis of the values of τ_a, σ_a and π_a taken from Davisson and Evans[17], using approximate evaluations of the efficiency of the counters. The observed values are shown in the adjacent columns. It will be seen that the second counter records the direct rays within 25% of the computed value. On the other hand the first counter yields a count several hundredfold greater than the calculated. This shows that a major portion of its load is due to gamma-rays and electrons scattered from the edges of the collimator, the gas in the instrument, the back wall of the spectrometer, etc.

Size and shape of the source

Gamma-ray sources of various forms were used, depending on the amount of radioactive material available, the hardness of the gamma-radiation and absorption coefficient of source material.

In the case of materials with a high specific activity (for example, ThC" and Cs^{134}) the source was prepared in the shape of a cylinder 4-5 mm in diameter. Experiments showed that in such cases precise positioning of the source is not essential (see Table 5 below).

In the case of low-activity materials, large amounts had to be used; in these cases the material (for example, Fe^{59}, Cu^{64} and Br^{82}) was packed in a soldered tube, 15 mm in outside diameter (along the line of the collimator channel) and 6-7 cm in length. Larger dimensions of the source led to broadening of the spectral lines and a reduction of the intensity.

If the thickness of the specimen in the direction of propagation of the gamma-rays is such that 200 kev rays are absorbed in the specimen to the extent of more than 1%, an appropriate correction (different for different gamma-ray energies) must be introduced. The correction factor is taken from tables of primary gamma-ray absorption coefficients.

Magnetic field distribution

The principle of operation of the described spectrometer is founded on the assumption that the magnetic field is homogeneous. Actually the vertical component of the magnetic field set up between the poles of the C-shaped magnet (i.e., in the region of the spectrometer) decreased slightly in the x direction (see Fig. 6). The topography of the field was surveyed with a long and narrow (5 mm) search coil and fluxmeter. The results are shown in Fig. 7: the cross-hatched circle on the left (2) is the target spot while the rectangle on the right indicates the cross section of the widest part of the beam.

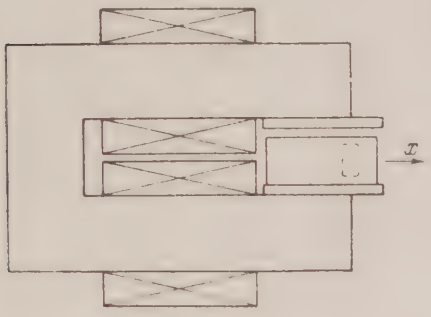

Fig. 6. Magnet and chamber

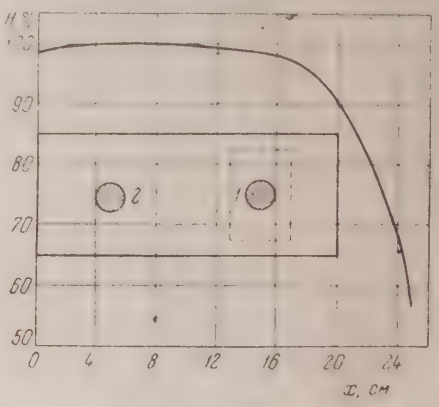

Fig. 7. Variation of field intensity with distance from the back wall of the chamber. 1) position of widest part of electron beam after first slit relative to magnetic field distribution.

In the region of the extreme paths utilized (extreme outer point of target) the field intensity is 1.5% less than in the main part of the instrument.

Measurements of the magnetic field

Conventional measurements of the field intensity were made with a slip coil and fluxmeter to gain a general idea of the field strength.

For the actual experimental work the instrument was calibrated with reference to gamma-lines of accurately known energies, i.e., a calibration curve of potentiometer readings at the observed maxima (peak coincidence counts) against the photon energies was plotted. This method eliminated most of the systematic errors; it is discussed in more detail below under Section 5.

Magnet power supply

Storage batteries were used to supply current for the magnet. A compensating circuit with a KMS-6 resistance box and a galvanometer made it possible to maintain the current constant within ±0.002 amperes; a 0.01 ampere change in the current produced a deflection of 5 graduations on the galvanometer scale.

In the main operating range ($h\nu$ = 0.5 to 2.0 Mev) the field intensity varies linearly with the current. Above 2 Mev some deviation from linearity is observed and at 3 Mev the field is 5% weaker than it should be according to the linear law. Actually, this is of little import since, as noted above, the instrument was calibrated with reference to known gamma-lines.

To obtain the identical field strength at the same current setting, one must, of course, reach the given point via the same particular hysteresis loop. Hence, the following cycle was always adhered to in regulating the current during the experiments:

$$0 \rightarrow I_{oper} \rightarrow I_{max} \ (h = 3.2 \text{ Mev}) \rightarrow 0 \rightarrow I_{oper} \rightarrow \ldots$$

As a general practice, the cycle was repeated 3-4 times before starting measurements. This procedure insured reproducibility of the magnetic field to within 0.1%. Greater accuracy is not required when the half-width of the spectral lines exceeds 4%.

4. Shape of the Spectral Lines

A spectral line produced in our instrument by monoenergetic gamma-rays has a "tail" on the low energy side, theoretically extending down to $H\rho = 0$. In the case of complex spectra, it is important to know the shape of the gamma-lines at different energies in order to be able to separate the individual peaks. The requisite data can be obtained either experimentally or by computation.

Experimental data on line shapes

For experimental investigation of line shapes it is most convenient to use substances yielding either a single line (Zn^{65} and positron emitters having no nuclear gamma-rays) or widely separated lines (Na^{24} and Au^{198}).

Inasmuch as gamma-spectrum studies have been carried out on the Ritron over several years and the experimental conditions have been changed during this period, the curves given below are arranged in accordance with the experimental conditions obtaining at the time of observation.

Shape of lines obtained in the 1950-1952 experiments

The gamma-spectra of Co^{66}, Ag^{110}, Fe^{59}, Sb^{124}, Br^{82}, Cs^{134}, and Cu^{64}, already described in earlier communications, were investigated under the following conditions: round target of cellophane, about 50 μ thick and 22 mm in diameter; cellphane windows over counters about 17 μ thick; instrument filled with helium at a pressure of 32 cm Hg; dimensions of both slits 2 x 54 mm.

The following lines were investigated in order to ascertain the line shape:

$h\nu_1$ = 411.77 kev — Au^{198},
$h\nu_2$ = 510.98 kev — annihilation,
$h\nu_3$ = 1118 kev — Zn^{65},
$h\nu_4$ = 1367.9 kev — Na^{24},
$h\nu_5$ = 2614.3 kev — ThC'',
$h\nu_6$ = 2753.5 kev — Na^{24}.

These lines are shown in Fig. 8 (solid lines) as obtained in the experiments (background substracted). The abscissa scales are graduated in terms of $H\rho_o$, where H is the value of the magnetic field

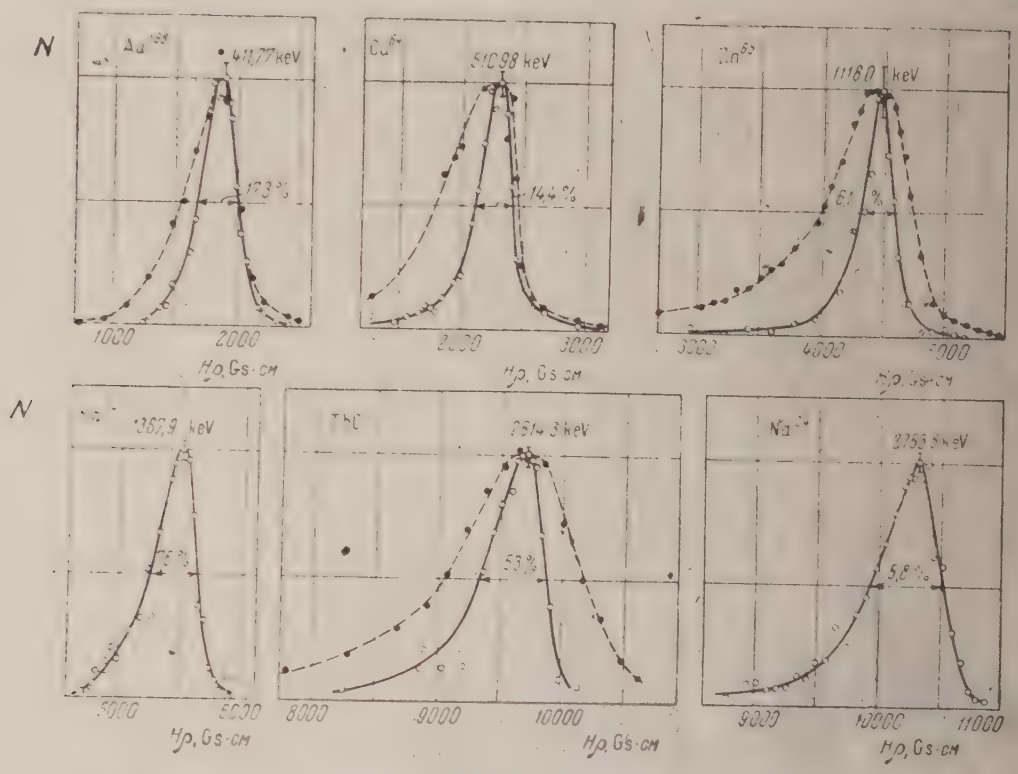

Fig. 8. Shape of some experimental lines obtained with the Ritron. Solid lines obtained with cellophane target 50 μ thick and slits 2 mm side. Dash lines obtained with beryllium target 0.4 mm thick and slits 7 mm wide.

and ρ_o is the design radius of the spectrometer. Inasmuch as the Ritron was calibrated directly with reference to known gamma-lines, there was no need to measure the field accurately, hence the $H\rho$ scale values are only indicative. Fig. 9 shows the same lines replotted to a uniform gamma-energy scale. To facilitate comparison

the peaks have been brought into line and shifted along the ordinate to separate the curves.

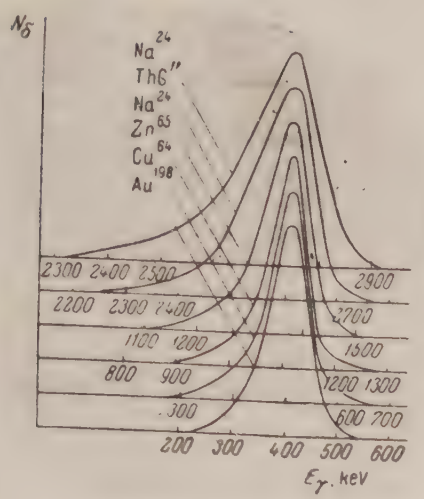

Fig. 9. Gamma-lines replotted to a uniform energy scale; heights of all lines made equal.

The variation of the relative half-width of lines, $\Delta H\rho/H\rho$, with $H\rho$ is shown by the solid line in Fig. 10. For plotting this curve, in addition to the lines of Figs. 8 and 9, we used the lines of Ac^{228}, Ag^{110}, Co^{60}, Fe^{59}, Sb^{124}, Cs^{134}, and La^{140} the half-widths of which can be accurately determined. It will be noted that the relative half-width reaches 34% at $h\nu$ = 338 kev, falls off sharply to 7% at 1 Mev, continues to diminish slowly to 5.5% at 1.7 Mev and then remains constant.

In magnetic beta-spectrometers the relative line half-width $\Delta H\rho/H\rho$ [i.e., the resolution] is independent of the energy provided the source is sufficiently thin. In gamma-spectrometers this is not the case in general; however, above 1 Mev the energy-dependence does become almost negligible. A few remarks concerning the individual points in Fig. 10 are in order. The resolved half-width of the lines depends to some extent on the width of the

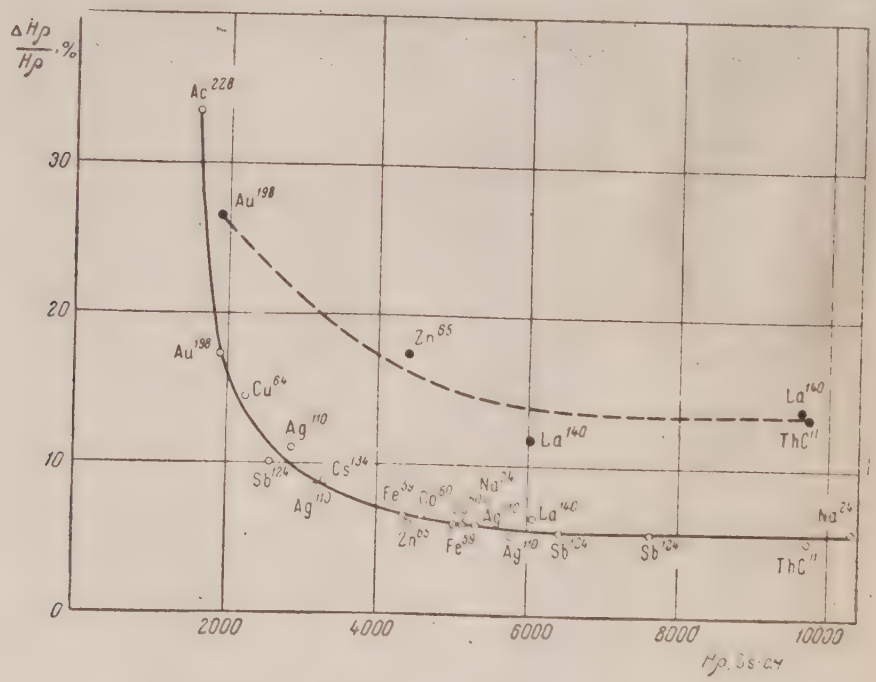

Fig. 10. Dependence of $\Delta H\rho/H\rho$ on $H\rho$. Solid lines for "standard" conditions: 50 μ thick cellophane target; 2 mm wide slits. Dash line for 0.4 mm beryllium target and 7 mm wide slits.

source and this differed for different specimens. The dimensions of the Na^{24} and Cu^{64} specimens were particularly large: in view of the low specific activity of these materials it was necessary to prepare the source by packing them into a tube 14 mm in diameter. Consequently, the points for these sources lie somewhat above the solid curve in Fig. 10. The sources of the other substances were about 5 mm in diameter. It is possible that the observed line for Ac^{228} is exaggerated in width due to the presence of neighboring lines of radioactive admixtures.

By interpolation of the smoothed out curves of Fig. 9 one can plot the shape of the line for any intermediate photon energies. Such interpolated curves were plotted whenever it was necessary to separate the components of a complex gamma-spectrum.

Shape of lines obtained with the beryllium target

A number of gamma-spectra comprise lines too weak to allow of investigation under the standard conditions that obtained in the main series of experiments. The transmission of the instrument had to be increased to permit observation of these lines.

To this end the following experimental conditions were selected: beryllium target 400 μ thick; cellophane films 17 μ thick over the counters, instrument filled with helium at 32 cm Hg, dimensions of both slots - 7 x 54 mm.

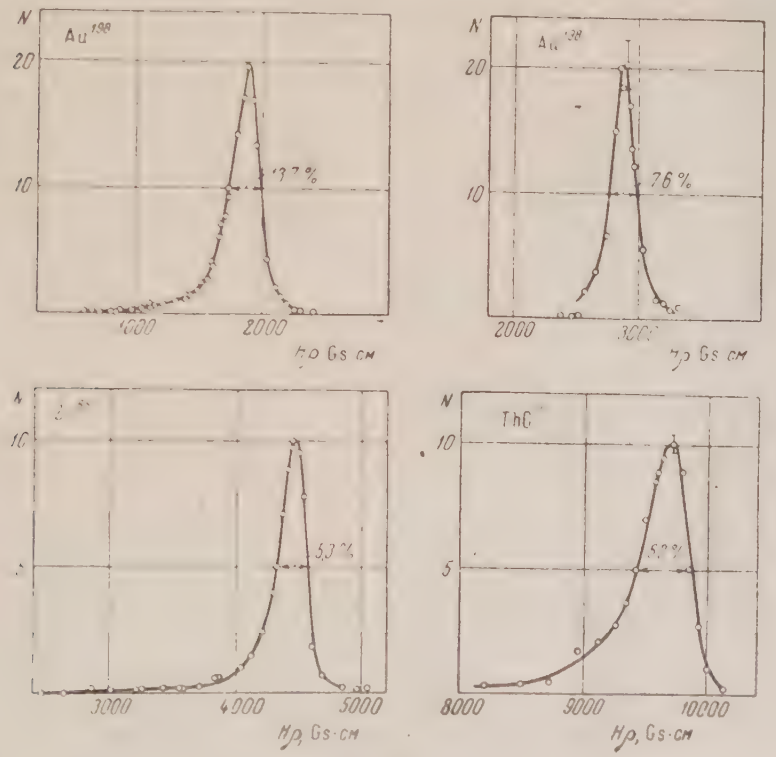

Fig. 11. Single lines of Au^{198}, Zn^{65} and ThC'' obtained under the new (1953) conditions (thinner counter windows and shorter slits).

The gamma-lines of Au^{198}, annihilation, Zn^{65} and ThC'' were investigated under these conditions. The results are represented by the dash-lines in Fig. 8. The observed lines are, naturally, much wider; however, it should be borne in mind that at this sacrifice in the sharpness we obtained a much higher counting rate: for example, in the case of Au^{198} the counting rate at the peak was increased 25 times. The ratio of the relative half-width to Hρ under these experimental conditions is shown by the dash-lines in Fig. 10.

Shape of lines obtained in the 1953 series of experiments

A number of modifications of the set-up were introduced in 1953 in order to improve the spectral characteristics of the instrument in the region of low gamma-ray energies: a) the thickness of the cellophane over the counter

windows was reduced from .7 to about 1 mg/cm², which [illegible] down the electron scattering in the counters; b) the pure helium at 32 cm Hg filling the instrument was replaced by a mixture of 96% helium and 4% methane at the same total pressure. This stabilized the operation of the counters with only a minor (about 15%) increase in the electron scattering by the gas; c) the height (length) of the slits was reduced from 54 to 46 mm since high slits tend to increase the line "tails".

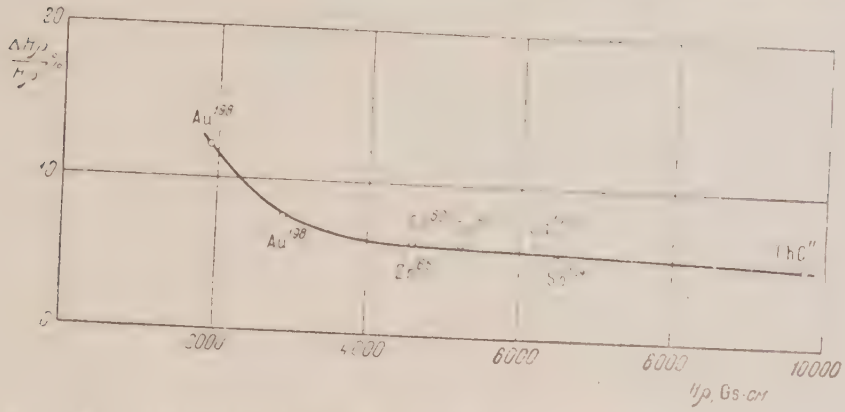

Fig. 12. Variation of $\Delta H\rho/H\rho$ with $H\rho$ under the new conditions.

The gamma-spectra of La^{140}, Au^{198}, Ir^{192}, Eu^{152}, Eu^{154}, W^{187}, and As^{76} were investigated under the new conditions. The single lines of Au^{198}, Zn^{65} and ThC" observed under these conditions are reproduced in Fig. 11. It will be seen that in the $h\nu$ = 400 - 500 kev region the line widths were appreciably reduced while in the region of higher energies no substantial change occurred. The dependence of the relative half-width on $H\rho$ is shown in Fig. 12.

The 411.77 kev line of Au^{198} and the 1118 kev line of Zn^{65} were studied with particular thoroughness: it was established that the "tails" of these lines actually extend quite far out but have so low an intensity that their presence does not seriously interfere with the separation of gamma-spectra into components.

Calculated line shapes

The shape of spectral lines is determined by the following factors:

1) the energy of the gamma-quanta,

2) the relative location and dimensions of the target and defining slits (i.e., the geometry of the instrument),

3) the scattering and slowing-down of the recoil electrons in the target, [Translator's note: Re: "slowing down": in view of the repeated use of the term below it seems easier to translate it thus than by the round-about "energy loss due to radiation".],

4) the size of the source, and

5) the scattering and slowing-down of the recoil electrons in the gas filling the instrument and in the film forming the window of the first counter.

Rigorous calculation of the line shape taking into account the simultaneous effect of all the above factors is unduly complicated. At present, we only have data on the individual effect of these factors acting separately.

The spectral line shapes were calculated by Khol'nov, without taking account of factors 3) and 4) for the following specific geometry

and dimensions of the source, target and slits: a) point source located at 32 cm from the target on a line normal to the center of the target, b) circular target 22 mm in diameter, c) radius of curvature of the central path (path through center of target) 55 mm, d) dimensions of first and second slits 2 x 54 mm.

The calculations were made for photon energies of $h\nu$ = 0.5, 1, 2, 4 and 7 m_0c^2 (255, 511, 1022, 2044 and 3577 kev). The target was subdivided into 112 sections, each of which was replaced by a point situated at the center of the section. The number of recoil electrons ejected from each point-section and passing through both slits was computed for 14 different values of the magnetic field, taking into account the angular and energetic distribution of the electrons and the angle of incidence of the gamma-photons on the given section. The data for the different sections were then summed to obtain a spectral line defined by fourteen points.

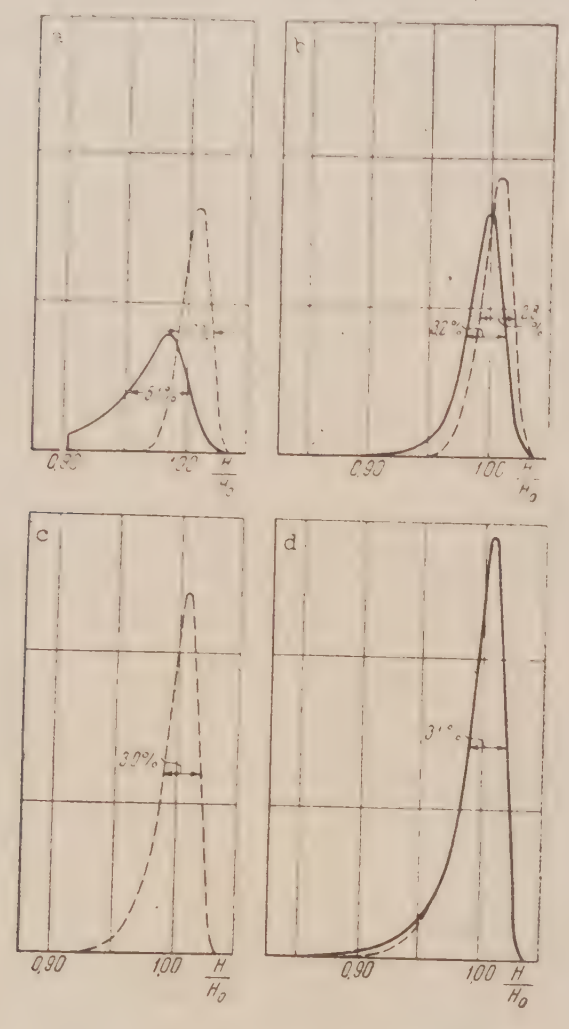

Fig. 13. Calculated gamma-line shapes: a) 511 kev, b) 1122 kev, c) 2044 kev, d) 3577 kev. Dashes indicate the "geometric" line shapes; the solid curves were obtained taking account of the scattering and slowing-down of recoil electrons in the target.

The resultant "geometric" line shapes are shown by the dash-lines in Fig. 13; taking into account the slowing-down and scattering of recoil electrons in the target modifies the lines to the shape given by the solid lines. Examination of the curves of Fig. 13 leads to the following deductions:

a) All the lines exhibit a rather slow rise on the low-energies side and a sharp drop on the side of high energies; this asymmetry is greater for higher gamma-quanta energies.

b) The geometric half-width of the lines increases from 2.7% at 511 kev to 3.1% at 3577 kev.

c) The investigated lines comprise no electrons with $H\rho < 0.90\ H\rho_{max}$ at any gamma-ray energy.

d) The peaks of all the lines occur at values of the magnetic field somewhat greater than H_0 (the field at which an electron ejected directly forward from the center of the target moves along a circle of radius ρ_0 and just grazes the outer edges of both slits. The maximum intensity is observed with a field H, exceeding H_0 by about 1%, when the above-described electron path passes at a distance of 0.5 mm in from the outer edge of the slit.

The "geometric" shape of the line is of interest in that it represents the "ultimate" shape; that is, if all the factors producing diffusion of the lines (thickness of the target, gas pressure in the instrument, thickness of the counter-window film and size of the source) are decreased the actual line obtained should approach the "geometric" shape.

Effect of multiple scattering and slowing-down of the recoil electrons in the target

In 1954 Khol'nov, Prokhodtseva, Ivanov and Nedovesov calculated the line shapes for the same geometric conditions but taking into account factor 3), i.e., the multiple scattering and slowing-down of the recoil electrons in the target (approximately 50 μ thick cellophane, having a superficial density of 6.15 mg/cm^2).

In allowing for the energy loss due to slowing-down [radiation] it was assumed that the recoil electrons are generated with equal probability in any layer of the target and that they then pass through the remaining thickness of the target along the normal to its surface. The multiple scattering effect was computed according to the method described in Ref. 19, based on Williams' theory of multiple scattering, without taking into account the loss due to "bremsstrahlung". This separate consideration of the two effects is, of course, an approximation: actually recoil electrons ejected at appreciable angles have a lower energy, undergo larger ionization losses and are subject to greater scattering that would be indicated by the calculations; on the other hand, multiple scattering increases the electron path length in the target and the actual losses increase accordingly.

Separate consideration of the two effects should not involve an appreciable error, provided both effects are relatively weak. As may be seen from the data of Table 2, this is the case under the conditions of interest to us.

Table 2

Data on scattering and slowing-down of recoil electrons in a cellophane film 50 μ thick (σ = 6.15 mg/cm^2)

γ-ray energy in m_0c^2 units	Energy of electron ejected forward, kev	α_0 - mean scattering angle in film (Ref. 19)	Widening of line due to scattering for $\theta = 0$, %	dE/dx for the given energy, Mev g^{-1}cm^2	ΔE - mean loss in film, kev	$\Delta E/E$, %	Line widening due to slowing-down %	Total widening due to scattering and to slowing-down, %
0,75	229,9	15°3	2,0	3,05	18,8	8,18	1,8	4,8
	340,6	9°7	1,1	2,65	16,3	4,8	1,8	5,8
	817,6	4°8	0,17	2,15	13,2	1,6	0,16	0,2
	3339,6	1°4	0,06	2,10	12,9	0,39	0,1	0,16

The detailed calculations will be published later. The line shapes determined as a result of the calculations are shown by the solid curves in Fig. 13. The 511 kev line was broken off on the side of low energies at the electron energy corresponding to a Compton scattering angle of 20°; the other lines end of themselves (drop to zero) earlier. Williams' theory of multiple scattering cannot be applied to electrons knocked out at large angles and returned to the direction of the incident photons by subsequent collisions (see below).

Comparison of the solid and dash lines of Fig. 13 leads to the following conclusions:

a) Taking account of the scattering and slowing-down results in an appreciable widening of the soft gamma-lines ($h\nu \leq 1.02$ Mev).

b) Virtually no change results in the shape and width of the hard gamma-line ($h\nu = 3580$ kev).

Comparing the calculated and experimental line shapes we come to the following conclusions.

Allowing for the effect of factors 2) and 3) (the size and thickness of the target and the size and location of the slits; and the scattering and slowing-down of recoil electrons in the target) leads to a lesser line width than is actually observed; i.e., the experimental widening of the line cannot be wholly explained by these two factors.

The additional widening cannot be due to electron scattering in the gas and in the film window of the first counter, for the effect is observed even at $h\nu = 2760$ kev, i.e., in the region where such scattering cannot play a significant part. Tests at reduced gas pressures confirm that the influence of scattering in the gas is minor. Hence, it must be assumed that the observed widening of the line is due either to the influence of the source size (factor 4), to inaccuracies in positioning and aligning the target, slits and collimator, or to some other as yet unidentified factors.

The use of Williams' theory of multiple scattering is permissible only in the cases where the ejection angles do not exceed 20 degrees[20]. Yet the angular distribution of recoil electrons is such that whereas at $h\nu = 3500$ almost half the electrons are comprised in the $\theta = 0$ to 20° interval, at $h\nu = 383$ only 19% are ejected within this angular range (see Table 3).

Table 3

Data on recoil electrons

hν, kev	Energy, kev		Hρ, Gs·cm		$\frac{(H\rho)_{20°}}{(H\rho)_{0°}}$	Recoil electrons scattered within 20° angle, %
	θ = 0°	θ = 20°	θ = 0°	θ = 20°		
383	229,9	197,9	1790	1639	0,9156	19
511	340,6	289,5	2273	2056	0,9045	21
1022	817,6	660,2	4092	3516	0,8592	28,7
2044	1818	1326	6813	5141	0,7546	43,1
3577	3340	2134	12730	8656	0,6800	49,5

The other electrons can eventually emerge from the target in the direction of the incident photons provided they are again scattered through an angle exceeding 20°. Obviously, Williams' theory is not applicable to such electrons. Undoubtedly a certain number of these electrons are detected by the instrument; thus in the case of the very carefully investigated lines of Au^{198} ($h\nu$ = 411 kev) and Zn^{65} ($h\nu$ = 1118 kev) the "tails" extend down to $H\rho \approx 0.5\ H\rho_{max}$, or much beyond the value corresponding to $\theta = 20°$. These long "tails" are surely due to electrons initially scattered at angles exceeding 20°. In calculating the intensity due to such electrons it would be necessary to employ a multiple scattering theory applicable to a wider range of angles than is Williams' theory.

The intensity of the more remote points of the "tail" is low although the number of electrons, having the corresponding kinetic energies, produced is large. This is explained by the fact that the angular distribution of slow electrons approaches the isotropic so that only a small fraction enters the relatively narrow solid angle of acceptance of the instrument.

5. Energy Calibration of the Ritron

It will be clear from the preceding section that in many cases the spectral lines observed with the Ritron are complex. Having observed and recorded the lines we are faced with the problem: how can we determine the energy of the corresponding photons? If we could readily compute the line shapes for different photon energies, taking into due account all the experimental conditions, and the resultant lines fitted the observed one, the problem would be virtually solved: it would merely be necessary to select the calculated curve (or the interpolated curve for intermediate energy values) coinciding with the observed line and identify the photon energy from the said curve.

Unfortunately, at present we do not have calculated curves which fit the experimental ones with a satisfactory degree of accuracy. Hence, the above method is not practical at this stage and we must use a special calibration method instead.

The energy of certain gamma-lines is already known with a high degree of precision, for the energy of the more intense gamma-lines can now be measured with an error of less than 0.01% by means of DuMont curved-crystal spectrometers and beta-spectrometers detecting internal conversion electrons. The Ritron cannot compete with the above-mentioned instruments where energy determinations are concerned if only because the lines obtained with it have a much greater width than the conversion electron lines resolved by modern beta-spectrometers.

Our spectrometer is intended primarily for measurement of the relative intensity of gamma-lines rather than for energy determinations. In view of this, there can be no objection to graduating the instrument with reference to lines of known intensity. Obviously, such calibration will hold good only provided the gamma-spectra are subsequently investigated under the same conditions (i.e., with the same geometry).

The calibration measurements were made with reference to the line peaks. The location of the maximum E_{max} on the energy scale was identified as the abscissa of the point of intersection of straight

lines drawn tangent to the steepest sections of the line, plotted in terms of $N = f(E_\gamma)$, where N is the coincidence count rate and E_γ is the energy of the photons as computed according to the following equations

$$E_\gamma = \frac{1}{2} m_o c^2 \left(E_{el} - \sqrt{E_{el}^2 - 2E_{el}} \right)$$

and

$$E_{el} = m_o c^2 \left[\sqrt{1 + \left(\frac{e}{m_o c^2} \right)^2 (H\rho_o)^2} - 1 \right]$$

where H is the measured magnetic field and ρ_o is the design radius of the instrument, equal, in our case, to 55 mm. Essentially the calibration consisted in plotting an experimental curve correlating the true photon energy E_{true} with peak-position energy E_{max}.

The following gamma-lines were used in calibrating the instrument:

$h\nu_1$ = 411.77 kev -- Au^{198}	$h\nu_7$ = 1331.6 kev -- Co^{60}
$h\nu_2$ = 510.98 kev -- annihl.	$h\nu_8$ = 1761.0 kev -- RaC
$h\nu_3$ = 609.37 kev -- RaC	$h\nu_9$ = 2200.0 kev -- RaC
$h\nu_4$ = 1118.0 kev -- Zn^{65}	$h\nu_{10}$ = 2450.0 kev -- RaC
$h\nu_5$ = 1122.0 kev -- RaC	$h\nu_{11}$ = 2614.3 kev -- ThC''
$h\nu_6$ = 1171.5 kev -- Co^{60}	$h\nu_{12}$ = 2753.5 kev -- Na^{24}

The calibration curves are reproduced in Fig. 14. As may be seen, values of the photon energy, E_{max}, computed according to the above equations, for the spectral peak are laid off along the abscissa while the ordinates are the corresponding values of the ratio E_{true}/E_{max}, where E_{true} is the "true" (actual) value of the photon energy as listed in the above table.

The points obtained under the standard conditions of 1952 (Fig. 14a) fall approximately on the $E_{true}/E_{max} = 0.95$ horizontal line, with a mean-square dispersion of ~1%. The points for measurements with the beryllium target are shown in Fig. 14b, while those for the conditions obtaining in the 1953-4 experiments are plotted in Fig. 14c. After separation of the observed line into components, the photon energy for the lines is found by multiplying the experimental value of E_{max} by the appropriate coefficient (i.e., the value of the ratio E_{true}/E_{max} taken from the calibration curves).

6. Spectral Sensitivity of the Instrument

Definition of "spectral sensitivity"

The initial experimental curve for the variation of the coincidence count with the magnet current must be processed: the background substracted, the values replotted to a uniform energy scale and corrections introduced to compensate for the differences in attenuation of the gamma-rays before they strike the target and the dependence of the counter efficiency on the electron energies. As a result of this processing there is obtained a curve comprising a series of peaks representing the gamma-lines. The area under each

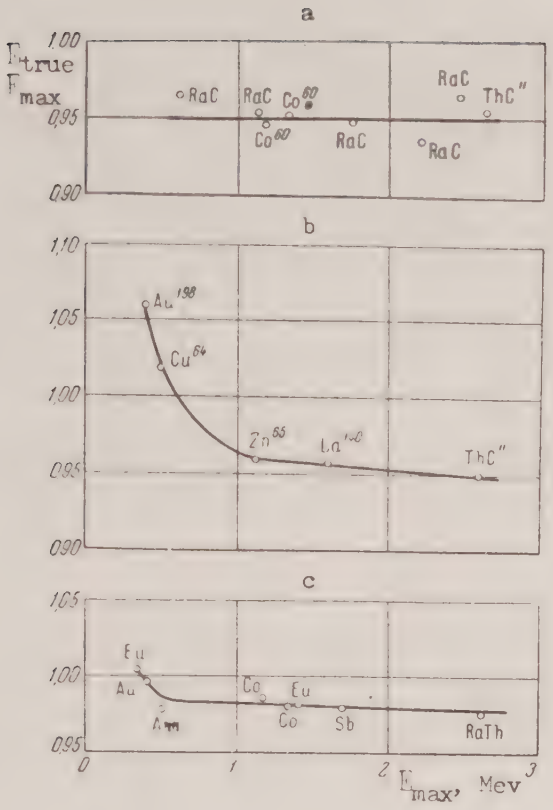

Fig. 14. Ritron energy calibration curves: a) under standard 1952 conditions; b) under beryllium target conditons; c) under standard 1953-4 conditions.

peak is proportional to the number of photons of the given energy emitted by the source; however, equal numbers of photons of different energies produce different areas. Thus, assuming the source emits a series of groups of photons of different energies but with each energy group comprised of the same number of photons, our processed curve will show a corresponding series of peaks, which, by making use of our data on line shapes, we can separate; the areas under the individual peaks will be different.

Let us arbitrarily take the unit area to be the area under the $h\nu$ = 1 Mev peak and let us designate the area under other peaks through S_γ. We shall hereinafter term the $S_\gamma = f(h\nu)$ curve the spectral sensitivity of the instrument.

The spectral sensitivity of the instrument is its most important characteristic: knowing the spectral sensitivity we can readily determine the relative intensity of the individual lines from the observed spectrum.

The spectral sensitivity of an instrument can be determined experimentally and by computation. If tnere were available a set of specimen materials emitting an accurately known number of gamma-quanta of different but known energies, determination of the spectral sensitivity would be reduced to straightforward measurement of the areas under the peaks and relating the results to the unit 1 Mev area. However, in practice absolute measurements of the number of photons emitted by a given source are so inaccurate that satisfactory determination of S_γ by this direct method is virtually impossible. It is necessary to resort to relative measurements.

Source materials suitable for experimental determinations of the spectral sensitivity

For experimental investigation of the spectral sensitivity, it is essential to use sources emitting gamma-rays of different energies in a known ratio of intensities. At first glance it might appear that any radioactive isotopes whose gamma-spectrum has been carefully measured could serve as a source. It must be remembered, however, that there are no wholly satisfactory methods for determining the relative intensities of photons of different energies in a complex gamma-spectrum. In attempting to develop such a method - a method

more accurate than any now extant - we obviously cannot base our calibration on data of inferior accuracy. Hence we must use source materials for which the intensity ratios can be determined with sufficiently high accuracy from indirect data.

Such suitable materials include, first, nuclides with a clearly-determined decay scheme in which ejection of the β^--particle is followed by the emission of photons in cascade and, hence, in the ratio of exactly 1:1. Examples of such nuclides are Na^{24} (1.38 and 2.76 Mev gamma-rays produced in almost 100% of the decays) and Co^{60} (1.17 and 1.33 Mev gamma-rays emitted following 100% of the decays). Second, one can use isotopes in which a β^+-decay is followed by the emission of one gamma-ray, for in such cases the ratio of the annihilation and nuclear photons equals equals exactly 2:1. An example of a source in this group is Na^{22} (1.277 Mev photon emitted after every positron-decay).

The nuclides in which the difference in photon energies is appreciable are particularly suitable for spectral sensitivity determinations.

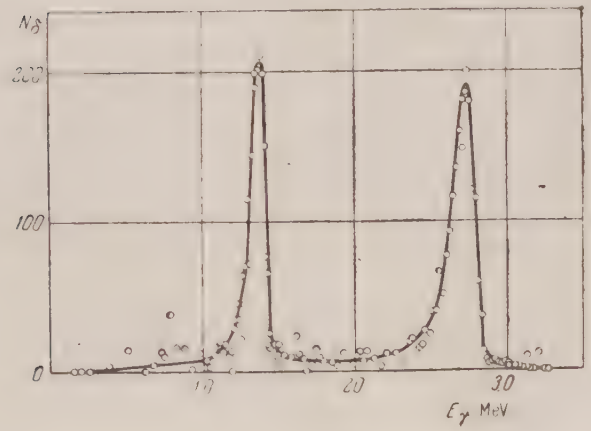

Fig. 15. γ-spectrum of Na^{24} plotted to a uniform energy scale.

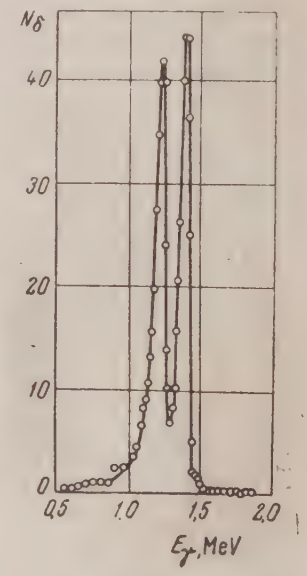

Fig. 16. Same as Fig. 15 but for Co^{60}.

Experiments with Na^{24}

Fig. 15 shows the curve obtained for Na^{24} after subtracting the background, converting to a uniform energy scale and introducing the correction for gamma-ray absorption in the source. The ratio of the areas under the lines is $S_{2.7}/S_{1.38} = 1.44$. The ratio of the spectral sensitivities at these energies $S_{2.76}/S_{1.38}$ should, therefore, also be 1.44.

Experiments with Co^{60}

The experimental curve for Co^{60} after introduction of all the above-mentioned corrections, but before allowing for the sensitivity of the instrument, is shown in Fig. 16. Separating the total curve

into two similar peaks, we find $S_{1.33}/S_{1.17} = 1.074$, whence it follows that $S_{1.33}/S_{1.17}$ should equal 1.074.

Spectral sensitivity with an infinitely thin target

The spectral sensitivity can also be evaluated from data obtained in studying the line shapes, provided the appropriate intensity scale is used. Curve 1 of Fig. 17 shows the spectral intensity of the Ritron as computed by Khol'nov[18] for a point source (L = 31 cm; target 22 mm in diameter, slits 2 mm wide), taking into account the angular and energy distribution of Compton electrons but not allowing for the scattering and slowing-down of the electrons in the target. As was noted under Section 4 above, the calculated "geometric" lines (Fig. 13) are narrower than the experimental ones. Hence, direct comparison of the calculated spectral sensitivity with experimental data is justified only on the assumption that the factors causing diffusion of the lines do not alter the area under the peaks.

If the point for the 1.38 Mev gamma-rays of Na^{24} is located on the curve of Fig. 17, the second, $h\nu$ = 2.76 Mev point for Na^{24} falls exactly on the line. The same is true of the two energy points for Co^{60}, although here the accuracy of the fit is harder to evaluate since the two points are close together.

The fact that the experimental data for Na^{24} and Co^{60} fit the calculated curve confirms the above assumption. Comparison of the calculated values for an infinitely thin target with the experimental data obtained with a 50 μ thick cellophane target is justified only for hard gamma-rays (E > 1 Mev), as is evinced by the curves of Fig. 13.

Calculation of the spectral sensitivity taking into account the slowing-down and multiple scattering of recoil electrons in the target

The method of calculating the spectra of electrons ejected at different angles has already been described in Section 4 above and the resultant calculated line shapes are shown in Fig. 13. The same calculations yield the information required to plot the spectral sensitivity curve.

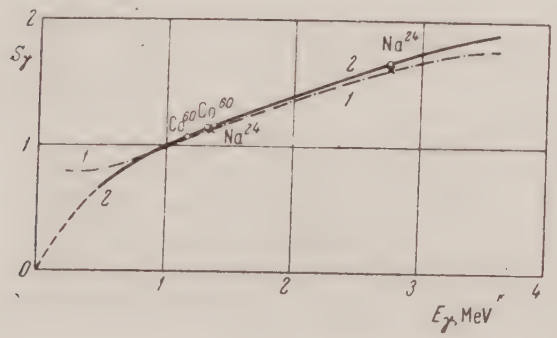

Fig. 17. Calculated spectral sensitivity curves for the Ritron: 1) "geometric", 2) taking into account slowing-down and scattering of electrons in the target. The calibration points for Na^{24} and Co^{60} are shown as circles on Curve 1 and as crosses on Curve 2.

The scattering and slowing down of electrons in the target are virtually negligible in the energy region above 1 Mev. Hence, in this energy region not only the line shapes but also the spectral sensitivity curves calculated taking account of and ignoring the scattering and energy loss by radiation practically coincide. The situation is more complicated in the region below 1 Mev, where the scattering and slowing-down are more pronounced; here the experimental curves develop "tails" which do not lend themselves to theoretical analysis.

The fact that Williams' theory of multiple scattering is not applicable to large scattering angles makes it necessary to subdivide the recoil electrons into two groups: those ejected forward at angles $\Theta = 0$ to 20^o and those scattered at $\Theta = 20$ to 90^o. In our analysis, we apply Williams' theory to the electrons of the first group and entirely disregard those in the second group. Hence, in comparing the experimental and calculated lines we shall use only the sections corresponding to scattering angles between 0 and 20^o.

Having determined a complex spectrum and resolved it into components with the aid of the experimental curves of Fig. 8 or 11, we must separate out from each resolved component the portion corresponding to $\Theta = 0$-20^o and only then determine the relative intensities of the gamma-rays.

However, direct comparison of calculated and experimental lines cut-off at $E_{\Theta=20^o}$ involves a certain error. Electrons ejected at angles between 0 and 20^o and initially having an energy between E_{max} and E_Θ will be recorded even at lower magnetic field intensities because of some slowing-down (energy loss due to radiation) and due to the actual width of the slits. On the other hand, some portion of the electrons corresponding to $\Theta > 20^o$ will enter the $E > E_O$ region because of the width of the slits. While the ensuing errors are negligible for hard gamma-lines, they apparently may attain several percent for the soft gamma-lines. Nevertheless we have so far neglected them. We have accordingly calculated a theoretical curve of the spectral sensitivity for the $E = 0.383$ to 1 Mev region (Curve 2 in Fig. 17). It will be seen that the spectral sensitivity falls off at an increasing rate with decreasing gamma-ray energies.

Comparison of our data with those of other investigators

The gamma-spectra of La^{140} and Au^{198} investigated by us comprise lines whose relative intensities have been determined by other authors. Making use of these data and our measurements of the ratios of the areas under the line shapes, we plotted the corresponding points on our spectral sensitivity curve with the results shown in Fig. 18. It should be borne in mindthat the accuracy of most of the intensity determinations was relatively low (within 10-20%). This serves to explain the appreciable dispersion of the individual points; nevertheless the agreement with the general form of the curve is satisfactory.

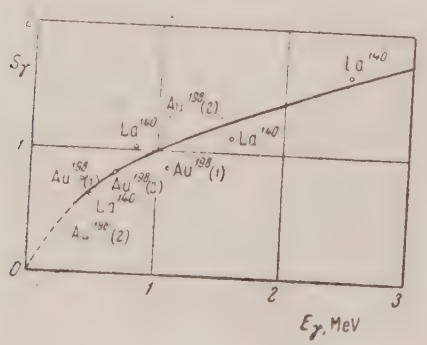

Fig. 18. Comparison of our calculated Ritron spectral sensitivity curve with data reported by other investigators (La - Ref. 25; Au - Refs. 26 and 27): (1) designates the soft, (2) the hard gamma-line of Au.

7. Transmission of the Ritron. Determination of the Number of Photons of a Given Energy Emitted from a Source

The Ritron can obviously be used to determine the number of photons of given energy emitted by a source. Having the appropriate calibration, the number of emitted photons can be determined either from the counting rate at the peak or from the area under the line. The calibration can be experimental or based on theoretical calculations.

In view of the difficulties of effecting calculations taking into account all the experimental factors, we elected to use experimental calibration with reference to the peak counting rate. We define the transmission of the instrument as the number of coincidence counts per second at the line peak (with the background subtracted) per curie, i.e., per 3.70×10^{10} photons of the given energy emitted per second.

Table 4

Transmission of the Ritron under different conditions

Source	Photon energy kev	Dimensions of source, cm dia.	length	Transmission*, counts/sec/cu	Remarks
		Standard conditions of 1951			
Cu^{64}	411.77	1.4	6	0.60	Strong absorption
Na^{24}	1380	1.4	8	3.3	
Na^{24}	2753	1.4	8	6.6	
Co^{60}	1171.5	0.4	0.6	3.8	
Zn^{65}	1118	1.4		2.9	
		Experiments with beryllium target			
Au^{198}	411.77	0.8		10	
Zn^{65}	1118	1.4		73	
		Standard conditions of 1953-54			
Au^{198}	411.77	0.4		1.0	
Zn^{65}	1118	1.0		4.5	
Co^{60}	1171.5	0.4	0.6	8.0	

* In the case of a source having an activity of 1 curie, 3.27×10^{6} photons per second are incident on each cm^2 of target (assuming one photon per disintegration).

The transmission of the instrument naturally depends on the energy of the photons, the size of the source and the experimental conditions.

The results obtained in experiments carried out under different conditions are summarized in Table 4. To determine the transmission one must know both the counting rate and the activity of the source. The latter was determined in the Dosimetric Laboratory by conventional procedures[23]. The dispersion of the listed values is due partly to errors in these activity measurements and partly to the size of the source and absorption in it.

8. Effect of Varying the Experimental Conditions on the Line Shape and the Spectral Sensitivity

Influence of target thickness

As was noted above, most of the experimental investigations and the basic calculations were carried out with a cellophane target 50 μ thick. It was of interest to determine how the line shape and the area under it are affected by changes in the thickness of the target.

Experiments with a target less than 50 μ thick

The gamma-spectrum of Sb^{124} was recorded with both a 50 μ and a 17 μ thick target. The results are shown in Fig. 19. Curves 1 represent the spectrum obtained with the 50 μ thick target; the plotted points and curve 2 are for the 17 μ target spectrum. The intensity values were adjusted to obtain coincidence of the respective hard gamma-lines (1697 kev) whose shape should not be affected by the thickness of the target inasmuch as electron scattering and energy loss due to radiation are minimal at this energy (see Table 2). It will be seen that the hν = 597 kev line (with a possible admixture of the weaker 650 kev line) obtained with the thinner target (dash curve 2) is some 13% higher and slightly narrower than the line shape obtained with the 50 μ target; as a result the net area is increased by 2 ± 5%. It may, therefore, be concluded that

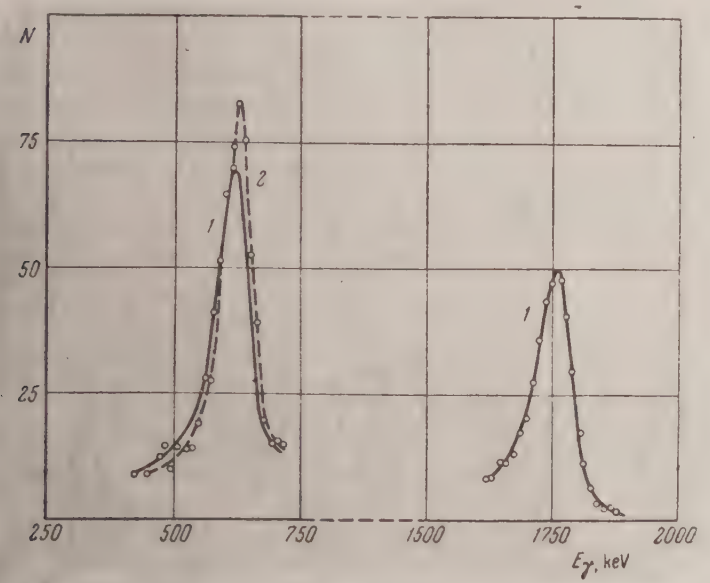

Fig. 19. Principal gamma-lines of Sb^{124}. Curve 1 for 50 μ thick target; points and curve 2 for 17 μ target.

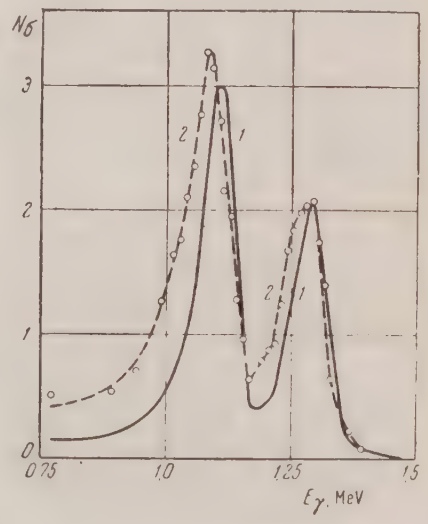

Fig. 20. Gamma-lines of Fe^{59}. Curve 1 for 50 μ target; points and curve 2 for 200 μ target.

in the 600-1700 kev interval increasing the target thickness from 17 to 50 μ does not result in any appreciable error in determining the relative line intensities, provided the latter are determined from the area under the peak. This justifies the use of the 50 μ target in this higher-energy interval.

Experiments with a target more than 50 μ thick

The gamma-spectrum of Fe^{59} which consists of a 1100 kev and a 1278 kev line was investigated using the 50 μ and a 200 μ thick target. The results are shown in Fig. 20, where for convenience in comparison the values have been adjusted to bring the hard-line peaks into coincidence (actually, the coincidence count at the hard-line peak with the 200 μ target is twice the rate with the 50 μ target). It will be seen that both peaks (Curve 2) obtained with the 200 μ target have become somewhat wider (the relative half-width of the hard-gamma peak is 9.6% with the 200 μ target as against 7.2% with the 50 μ target), that the peak points have shifted some 2-3% to the side of lower energies and that the "tails" have augmented. However, the ratio of the areas under the lines has changed little, from 1.39:1 with the 50 μ target to 1.35:1 with the 200 μ target. It follows that one can safely use a cellophane target 200 μ thick for investigating the portions of gamma-spectra above 1 Mev without fear of distortion of the relative intensities due to scattering and slowing down of recoil electrons in the target. In fact, the above tests indicate that we can class scattering and energy loss due to radiation in the target with the factors that produce diffusion and shifting of the lines but do affect the relative area under the peaks.

Influence of lateral dimensions of the source

In order to bring out the effect of the lateral dimensions of the target on the line width and the transmission of the instrument we carried out a series of tests with a small specimen of Au^{198}, moving it successively to different points in the collimator at equal distances from the center of the target. The $h\nu$ = 411.77 kev line was recorded for each position of the small source. The positions of the points are shown in Fig. 21a; the results of measurements, in Fig. 21b and in Table 5.

Table 5

Changes in line shape incident to moving the source (Au^{198}) at right angles to the collimator axis

Curve	Location of source	Position of peak kev	Half-width %	Height peak %	Area under line,%
1	At center of collimator	411.2±2	12.2	100	100
2	0.6 cm above center	408.5±2	14.4	66±5	71
3	Up 0.6 cm (ref. Fig. 4)	411.2±2	12.4	75±5	73
4	Down 0.6 cm (ref. Fig.4)	410.3±2	13.8	90±5	97
A	Averaged line	411.8±2	14.1	80±5	82

The location of the peak on the energy scale does not shift by more than 1% for any of the 6 mm lateral displacements of the source; the relative width of the spectral line likewise changes very little. However, the height of the peak and what is more important the area under the line are altered to a very appreciable extent - the area,

as much as 29%. If we compute the change in transmission resulting from going over from a virtual point source to one extending over the entire section of the collimator, on the basis of the values in Table 5, we find that the transmission is reduced by 18%. This is, of course, a substantial amount and an appropriate correction should be introduced in determining the transmission when using a wide source.

Similar but less extensive tests were made with Co^{60}. They showed that the coincidence count with the small source at positions 2, 3 and 4 (Fig. 21) is about 10% lower than with the source at the center.

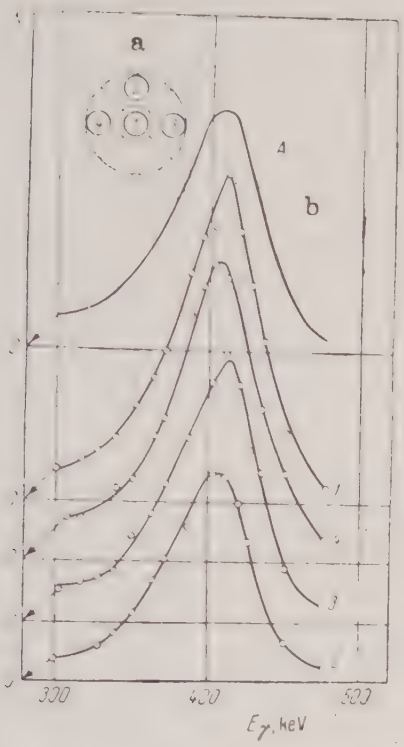

Fig. 21. The 411.77 kev line of Au^{198} recorded with the source at different locations in the collimator: a) positions of source, b) corresponding recorded lines, A) averaged line, weighted as per a).

Influence of the gas filling the instrument

The main series of experiments were carried out with the instrument filled with pure helium (initial, 1950-2 series) or with a mixture of 96.3% helium and 3.7% methane (new, 1953 series), in both cases at a total pressure of 32 cm Hg.

Recoil electrons having an energy above 1 Mev cannot be appreciably scattered or slowed-down in traversing this medium. But it was feared that these effects might make themselves felt on the width of the line and the transmission of the instrument at lower gamma-ray energies. Accordingly, we investigated the gamma-spectrum of Au^{198} ($h\nu$ = 411.77 kev) at gas pressures of 32 and 16 cm Hg and the spectrum of Ir^{192} ($h\nu$ = 314, 466, 898 and 1053 kev) at 32, 17 and 8 cm Hg, maintaining other conditions equal.

The results are shown in Figs. 22 and 23. They indicate that 1) the relative half-width of the 411.77 kev line increases only slightly when the pressure is raised from 16 to 32 cm Hg - from 12.3 to 13.4%, 2) the counting rate at the peak remains virtually unchanged.

Conclusions

The magnetic γ-spectrometer described in the present article can be used to investigate the γ-spectra of radioactive sources in the 300 to 4000 kev energy range. Under our standard conditions (target 50 μ thick, slits 2 mm wide) the relative half-width of the lines (resolution) in the 1 to 3 Mev interval is about 5.5%; at lower values of E_γ the line shapes are wider. Under these conditions sources having an activity in excess of 1 millicurie (where the investigated line is concerned) can be studied.

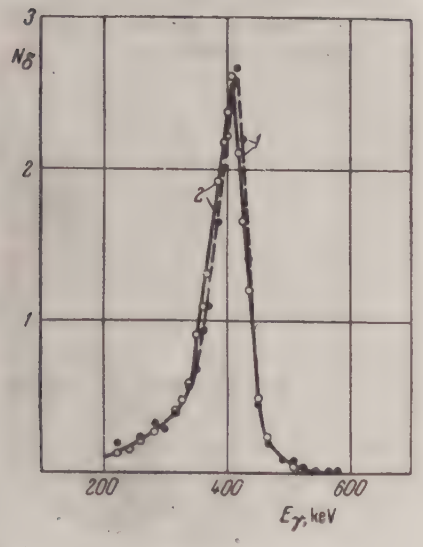

Fig. 22. 412 kev line of Au^{198} obtained at a gas pressure of 16 (1) and 32 (2) cm Hg.

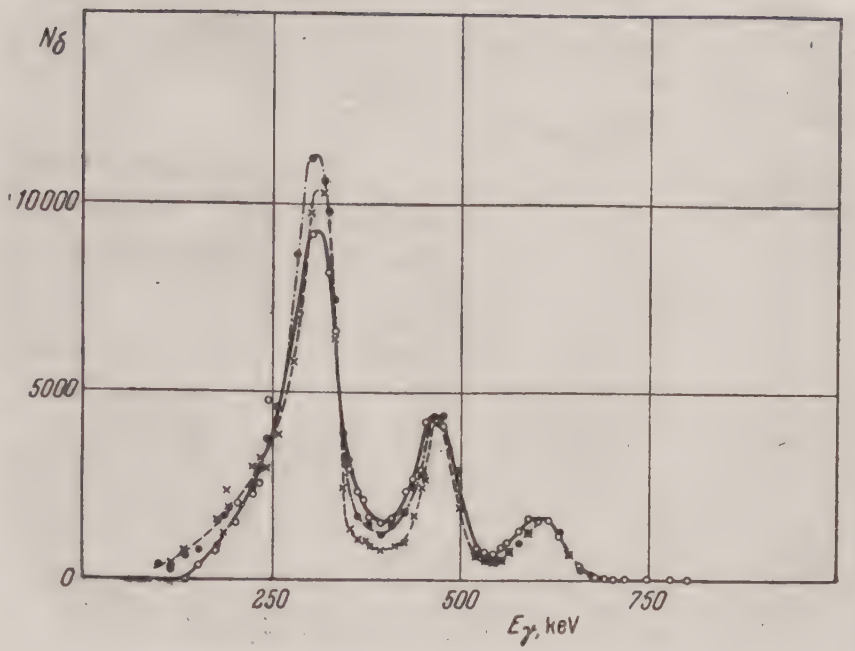

Fig. 23. Soft part of gamma-spectrum of Ir^{192} obtained at different gas pressures: • - 8 cm Hg, x - 17 cm Hg and o - 32 cm Hg.

For the investigation of weaker sources a beryllium target 0.4 mm thick may be employed. With the beryllium target the transmission of the instrument is increased by a factor of 10-30.

As regards resolution the Ritron is at a disadvantage compared with the Elotron, a magnetic γ-spectrometer with improved focusing[24]. However, it has the advantage of employing only a homogeneous magnetic field, which makes it feasible to calculate the line shapes, the spectral sensitivity, transmission and other characteristics of the instrument.

This investigation was started in 1946 by M. L. Orbeli and one of the authors of the present article. Subsequently, V. P. Prikhodtseva, V. G. Chumin, and A. Feoktisov participated in studies of the characteristics of the instrument. The authors wish to express their indebtedness to these comrades.

Radium Institute of the
Academy of Sciences of the USSR

Received
4 November 1954

Bibliographic References

1. D.Skobel'tsyn, ZS. Phys., 43, 354 (1927).
2. G.Latyshev, A.Kompaneev, N.Borisov, I.Gusak, Journ.Phys.USSR, 3, 251 (1940); A.Kul'chitski & G.Latyshev, Journ. Phys. USSR, 4, 515 (1941); G.Latyshev, Rev. Mod. Phys., 19, 132 (1947).
3. M.Mladjenovic & A.Hedgran, Ark. fur Fys., 8, 49 (1954).
4. J.Motz, W.Miller, H.Wyckoff, H.Gibson & F.Kirn, Rev.Sci.Inst.,24,929 (1953).
5. B.Dzhelepov & M.Orbeli, Doklady AN SSSR, 62, 615 (1948).
6. B.Dzhelepov, Zhukovski & Khol'nov, Dolady AN SSSR, 77, 233 (1951)

7. B.Dzhelepov, Zhukovski & Khol'nov, Doklady AN SSSR, 77, 597 (1951).
8. B.Dzhelepov, Zhukovski & Khol'nov, Doklady AN SSSR, 86, 497 (1952).
9. K.Gromov, B.Dzhelepov, N.Zhukovski, A.Silant'ev & Iu.Khol'nov, Doklady AN SSSR, 86, 522 (1952).
10. B.Dzhelepov & A.Silant'ev, Doklady AN SSSR, 85, 533 (1952).
11. K.Gromov & B.Dzhelepov, Doklady AN SSSR, 85, 299 (1952).
12. B.Dzhelepov, N.Zhukovski, V.Prikhodtseva & Iu.Khol'nov, Izv. (Bulletin) AN SSSR, Ser. fiz., 17, 511 (1953).
13. S.Curran, P.Dec & J.Strothers, Proc. Royal Soc., 174, 546 (1940); C.Mandeville, Phys. Rev., 62, 309 (1942).
14. R.Hofstadter & J.McIntyre, Phys. Rev., 78, 619 (1950).
15. S.Korff, Schetchiki elektronov i iadrenykh chastits (Counters for electrons and nuclear particles) p.88, IL, Moscow 1947 /Electron and Nuclear Counters, N.Y.1946/.
16. G.Clure, Phys. Rev., 90, 796 (1953).
17. C.Davisson & R.Evans, Rev. Mod. Phys., 24 79 (1952).
18. Iu.Khol'nov, Thesis. Radium Institute AN SSSR, 1952.
19. B.Dzhelepov, Izv. (Bulletin)AN SSSR, Ser. fiz., 18, 95 (1954).
20. E.Williams, Proc.Royal Soc., A 169, 531 (1939);Phys.Rev., 58, 292 (1940).
21. D.Muller, H.Hoyt, D.Klein & J.DuMont, Phys. Rev., 88, 775 (1952).
22. J.Cork, Branyan, Stoddard, Keller, LeBlanc & Childs, Phys.Rev.,83, 681 (1951).
23. V.Bochkarev, I. Keirim-Markus, M.L'vova & Ia.Prislin, Ismerenie aktivnosti beta- i gamma-izluchenii (Measurement of beta and gamma activity), M.-L. 1953
24. B.Dzhelepov, N.Zhukovski, A.Karamian & S.Shestopalova, Izv. (Bulletin) AN SSSR, Ser. fiz., 17, 518 (1953).
25. R.Bannerman, G.Lewis & S.Curran, Phil. Mag., 42, 1097 (1951).
26. P.Cavanagh, Phys. Rev., 82, 791 (1951).
27. L.Elliot, M.Preston & J.Wolfson, Canad. Journ. Phys., 32, 153 (1954).

* * * * * * * * *
* * * * * *

BULLETIN of the Academy of Sciences of the USSR - Physical Series
Vol. 18, No. 5, 1954 - Conference on Beta & Gamma Spectroscopy

TABLE OF CONTENTS

	Page Orig.	Trans.
Isobaric spins and similar states of atomic nuclei - B.S.Dzhelepov	523	208
Investigation of the radiation of Zr^{95} + Nb^{95} - P.P.Zarubin	563	244
Investigation of the radiation of Rb^{86} - A.G.Dmitrev & P.P.Zarubin	580	264
A high-transmission wedge-type spectrometer with improved focusing - E.E.Berlovich	589	274
The Ritron - A gamma-spectrometer utilizing recoil electrons - B.S.Dzhelepov, N.N.Zhukovski & Iu.V.Khol'nov	599	285

Translated in 1955 by
Columbia Technical Translations
5 Vermont Ave., White Plains, N.Y.

TRANSACTIONS OF THE NINTH ALL-UNION CONFERENCE ON SPECTROSCOPY
(Tartu, Estonian SSR, 5 - 11 July 1954)

****

The transactions of the Ninth All-Union Conference on Spectroscopy will be published in the following order: a) papers read at the plenary sessions and reports presented to Section I of the Conference, concerned with problems of molecular spectroscopy and its applications, appear in the present issue of the Bulletin, b) reports to Section II of the Conference, devoted to atomic spectroscopy and spectroscopic equipment, as well as part of the transactions of Section III, concerned with emission spectral analysis, will be published in issue No. 1 of Vol. 19 (1955), c) the remaining reports of Section III will appear in subsequent issues for 1955.

Reports presented at plenary sessions are printed either in full or in condensed form; the other reports will be condensed or only the title given when the paper in question has been published earlier.

COMMISSION ON SPECTROSCOPY

/Translation editor's note: The only two "papers" in the last category (i.e. titles only) appearing in the present issue are:

1) "Calculation and interpretation of the vibrational spectra of certain monoalkyl- and polymethylbenzenes" by M.A.Kovner, published in Doklady AN USSR, 97, 2, 229 (1954) & Zhur. eksp. i teor. fiz., 26, 6, 704 (1954);

2) "The temperature dependence of the intensity of the first order Stokes line in Raman spectra" by Ia. S. Bobovich, Doklady AN USSR, 97, 5, 801 & 98, 1, 39 (1954).

The last sentence in the Commission's note above is somewhat ambiguous. Except for the footnotes there are no indications in the journal to show which papers have been condensed or to what extent; it will be obvious from the texts, however, that some have been severely dehydrated./

* *

OPENING ADDRESS by S. E. Frish

Comrades: All-Union Conferences on spectroscopy have become a tradition: we meet approximately every two years to report on work done, exchange views and discuss our achievements and the current scientific problems. We met in Moscow, the capital of our Fatherland, in Leningrad, in Sverdlovsk, and in Kiev, the capital of Ukraine. We are now gathered in the Estonian SSR, in Tartu, a city famous for its old university that has trained such great scientists as Lenz, Struve, Pirogov, and many others.

True to the principle of indissoluble friendship and brotherhood between all the republics of the Soviet Union, we strive toward unity in our endeavors for the benefit of the entire Soviet people.

In the past our conferences were highly successful and not only contributed to the general development of spectroscopy, but helped establish friendly relations between Soviet scientists working in various centers of the Union and stimulated research in our many universities and institutes. I am certain you share my confidence that this conference will prove just as fruitful.

We are starting our Conference under very favorable conditions. The state and party organizations of the Estonian SSR and of the city of Tartu, as well as the administration of Tartu University, have made every possible effort to facilitate our work. Permit me to convey on behalf of the Arrangements Committee of the Commission on Spectroscopy and of all the participants our profound gratitude for the preparations made and the generous hospitality shown us.

The scope of the conferences and the number of people attending them have increased steadily over the years. As of today 750 delegates have already registered and the number is still growing. The program of the Conference lists 190 papers which will be presented at three Sections of the Conference; in some cases it will be necessary for two Sections to hold sessions simultaneously. As you can see our program is an extensive one. This is not surprising, for the interaction between light and matter manifests itself in a tremendous number of physical phenomena; the range of problems to be discussed here extends far beyond the narrow boundaries of "spectroscopy" as the term was defined in physics not long ago. Present-day spectroscopy helps the physicist investigate the structure of matter in all its states: gaseous, liquid and solid. Spectroscopy throws light on the constitution of molecules and atoms, revealing their "inmost" properties (for example, the hyperfine structure of spectrum lines furnishes a clue to certain properties of atomic nuclei). Spectroscopic methods have proven to be exceedingly fruitful in studying highly complex processes, such as the processes occurring in gas, flash and spark discharges, investigation of which is virtually impossible by other methods. Raman spectroscopy yields most valuable information on the nature of chemical bonds. Methods new in principle are being devised, methods such as radio-spectroscopy, papers on which are included for the first time in the agenda of this Conference. We are also glad to note that reports will be delivered on related sciences, such as astrophysics.

There is no need to emphasize the tremendous practical value of spectroscopic investigations. The value of spectroscopic methods in the field of metallurgy is universally known. Intensive work is continuing in this field, work aimed at developing new, improved methods, and increasing the sensitivity, accuracy, speed and scope of spectrum analysis. Because of the recurring need for materials of exceedingly high purity, the requirements as regards sensitivity are higher than ever before. New problems are constantly arising: many papers to be presented are devoted to methods of spectroscopic analysis of slags, ores and minerals, and to the new applications of quantitative spectrum analysis in geology.

Certainly no less numerous and diverse are the problems involved in the application and extension of spectroscopic procedures in the field of chemistry. Much has been accomplished here, but a great deal still remains to be done. Spectroscopy is being successfully used in various types of chemical production, in pharmacology, in medicine, and in many branches of the food industry. We are faced with the problem of furthering the development of agriculture by means of spectroscopy. It is evident that spectrum analysis of soils can supply the key to the solution of many agronomic problems.

These necessary scientific advances in the field of spectroscopy are inconceivable without further development of experimental techniques. In recent years Soviet industry has made great advances in the commercial production of many new, modern spectroscopic instruments. Soviet diffraction gratings are now being produced. The first steps have been taken towards the general introduction of photoelectric methods of recording spectra and measuring line intensities. It is, therefore, natural for many of the papers to deal with spectroscopic instruments and the development of photoelectric methods for recording spectra.

The work of the Commission is not restricted to the time of the conferences. The Commission on Spectroscopy at the USSR Academy of Sciences is also quite active between conferences. Permit me to remind you briefly of the accomplishments of the Commission since the last conference in 1952.

Much work has been done to coordinate the investigations being carried out in the academies of the independent soviet republics, the various branches of the Academy of Sciences of the USSR and other affiliated institutions. Programs and plans for continuing spectroscopic research have been elaborated. An annotated bibliography on spectrum analysis and Raman spectroscopy has been compiled and is now in process of being printed. Regulations for the operation of industrial spectroscopic laboratories have been established and approved. Steps have been taken to arrange for the production of the special photographic materials required for spectroscopy. The transactions of the previous conference on spectroscopy have been made available: the papers dealing with molecular spectroscopy were published in the Bulletin of the Academy of Sciences - Physical Series; the papers on atomic spectroscopy are being brought out in abridged form. There have been lamentable delays in this connection which should not be allowed to recur: abstracts of the reports to be presented at this Conference should be published promptly.

We shall also have occasion to discuss organizational problems. The opinions expressed by participants in this Conference on such problems will doubtless prove of benefit to our future work.

In conclusion permit me to reiterate my confidence in the success of our work here and my conviction that it will contribute to the advance of spectroscopy in general and to its increasing usefulness in all branches of the national economy.

I declare the Ninth All-Union Conference on Spectroscopy open.

* * * * *

THE PRESENT STATE OF RADIO-FREQUENCY SPECTROSCOPY*

- M. A. El'iashevich

Radio-frequency spectroscopy is concerned with the study of transitions between energy levels, as evinced in the radio-frequency portion of the electromagnetic spectrum. As regards experimental procedures, which are based on modern radio engineering techniques, radio spectroscopy differs markedly from conventional "optical" spectroscopy which deals with radiation in the ultraviolet, visible and infrared portions of the spectrum. However, where theoretical principles and methods of interpreting and analyzing experimental data are concerned, radio spectroscopy is a typical branch of conventional spectroscopy with all the characteristic features of the latter. Despite this, radio spectroscopy offers new possibilities for investigating the structure of matter, in that it permits direct determination of small differences between the energy levels of atomic systems. These energy differences are associated with or correspond to the fine and hyperfine structure of electronic spectra, the rotational structure of spectra, diverse interaction processes inside atoms and molecules and the splitting of spectrum lines of atoms, molecules and crystals in external electric and magnetic fields.

The accuracy with which frequencies corresponding to transitions can be measured is very high, attaining one part in several million (10^{-4}-10^{-5}%). At present, radio-spectroscopic techniques are being successfully used to investigate transition frequencies ranging from

---

* Pub. in expanded form in Usp. fiz. nauk, 54, 513 (1954).

hundreds of kilocycles to 300,000 megacycles (10^5 to $3 \cdot 10^{11}$ cps), i.e., from $3 \cdot 10^{-6}$ to 10 cm^{-1} or in terms of wavelengths, from 3 km to 1 mm. Microwave spectroscopy has become particularly important; this covers the region of decimeter, centimeter and millimeter wavelengths, corresponding to ultra-high frequencies from 300 to 300,000 megacycles, i.e., 0.01 to 10 cm^{-1}.

Radio-spectroscopic methods are employed to study the following types of transitions, corresponding to small differences between energy levels of atoms, molecules and concentrated systems.

Transitions between energy levels in the absence of external fields:

1. Electronic transitions associated with the fine structure of the hydrogen atom and other light atoms.
2. Purely rotational transitions in molecules and various transitions associated with interaction in molecules (inversion splitting, spin splitting of the rotational levels of diatomic molecules and l-doubling of the rotational levels of linear polyatomic molecules.
3. Transitions connected with nuclear spin: with magnetic interaction between the nuclear magnetic dipole moment and the electron magnetic moments of atoms and molecules and with the electric interaction of the nuclear electric quadrupole moment with inhomogeneities of the internal electric field produced by electrons.

Transitions between neighboring energy levels in an external magnetic field (Zeeman effect) - magnetic resonance:

1. Transitions connected with electron magnetic moments (spin and orbital) of atoms and molecules.
2. Transitions associated with the magnetic moments of nuclei.
3. Transitions associated with the rotational magnetic moments of molecules.

Transitions between neighboring energy levels in an external electric field (Stark effect) - electric resonance.

A noteworthy characteristic of the transitions between near levels commonly investigated by the methods of radio spectroscopy is that, aside from absorption, the predominant energy changes are due to forced emission, while spontaneous emission is rarely encountered except in the case of extra-terrestrial (i.e., astronomic) sources of radio waves.

The virtual absence of spontaneous emission under ordinary laboratory conditions is due to the fact that the probability of such emission is proportional to the frequency to the third power (ν^3); hence, the probability of spontaneous emission at radio frequencies is much lower than at optical frequencies. Consequently in radio spectroscopic investigations of terrestrial sources spontaneous emission need not be taken into account. Forced emission, on the other hand, plays a very important role, since the populations of close-lying levels at low as well as at ordinary temperatures are nearly the same and the number of emissions (i.e., transitions from the higher to the lower level) differs little from the number of absorption events (i.e., transitions from the lower to the higher level).

Calculations indicate that the resultant absorption coefficient is inversely proportional to the temperature and directly proportional to the magnitude of the ratio $h\nu/kT$, which is small under the conditions

commonly prevailing in radio spectroscopic investigations ($h\nu$, the value of a quantum, in the radio-frequency region, is much smaller than the value of the mean thermal energy, kT).

We distinguish between two groups of radio spectroscopic methods:

1. Methods based on the absorption of radio waves in some given volume of matter, comprising a) investigation of absorption in gases by means of microwave spectrographs incorporating waveguides, b) investigation of magnetic resonance in liquids and solids placed in a homogeneous constant magnetic field and a superimposed radio-frequency field (nuclear resonance and nuclear induction; paramagnetic resonance; ferromagnetic resonance), c) investigation of purely quadrupole transitions in solids in an applied r-f field.

2. Molecular and atomic beam methods, comprising a) investigation of magnetic resonance in molecular and atomic beams and b) investigation of electric resonance in molecular beams.

Molecular and atomic beam methods differ from absorption methods in that in the former the variation in the intensity of the beam in the presence of an r-f field is determined by the sum total of absorption and emission transitions, whereas in absorption methods the absorption coefficient depends on the small difference between the numbers of these transitions.

In spite of the fact that radio spectroscopy is comparatively new, much valuable information bearing on the structure and constitution of matter has already been obtained with its aid. There can be no doubt that the scope of applications of radio spectroscopy will continue to expand rapidly.

Radio-spectroscopic methods are now basic in evaluating nuclear spins and the magnetic (magnetic dipole) and quadrupole (electric quadrupole) moments associated with nuclear spins. The magnetic moments are determined with high accuracy by the method of magnetic resonance in atomic beams. Measurement of purely rotational spectra in the microwave regions offers the most direct approach to determining molecular moments of inertia and, consequently, inter-atomic distances. The dipole moments of molecules can be determined with considerable accuracy (within a fraction of one percent) from data on the Stark splitting of rotational levels.

Data obtained specifically by radio-spectroscopic methods include information on intra-molecular fields derived from determinations of the magnitude of quadrupole interaction and data on the rotational magnetic moments of molecules, obtained by investigating the Zeeman effect in rotational spectra. In addition to data on the relative locations of molecular energy levels derived from the observed frequencies of spectrum lines in the radiowave region, much valuable information can be obtained by measuring the intensities and widths of the spectrum lines. Many deductions concerning the properties of solids and liquids can be drawn from the experimental results obtained in the investigation of nuclear resonance and paramagnetic and ferromagnetic resonance.

Although the use of radio spectroscopy for purposes of analysis is still in its initial stages, there can be no doubt of its potentialities and future importance in this field.

"A. I. Gertsen" Leningrad
State Pedogogical Institute

* * * * * *

ON THE OPTICAL PROPERTIES OF METALS

- V. L. Ginzburg and G. P. Motulevich

Despite the fact that the optical properties of metals have been investigated for a long time now, much in this branch of physics still remains obscure where both theory and experimental data are concerned. This may, in part, be explained by the widespread misapprehension regarding the contribution metal optics can make in obtaining information of value to the development of the electron theory of metals. Investigations in the field are commonly limited to finding the coefficient of reflection r = 1 - A from the metal surface at normal incidence. Yet it is both possible and essential to determine the two parameters n_{ef} and $\varkappa_{ef}$ (see below). Actually data on these two parameters, characterizing metals, are available (in the requisite frequency range) only for Ag, Au and Cu and these date back to 1913[1] and are, therefore, obviously in need of revision and refinement. Difficulties encountered in using what data are available stem from the failure of the early investigators to take into account the anomalous character of the skin effect in metals. This factor was analyzed only recently in Ref. 2, and even here in verifying the developed theory against experiment the conduction electrons were assumed to be entirely free (effective electron mass taken equal to $9.1\cdot10^{-28}$) and the electron concentration N instead of being derived from experimental data was taken equal to N_a, the concentration of atoms. Yet the principal value of optical investigations of metals stems precisely from the fact that the value of N can be determined experimentally. The purpose of this contribution is to elucidate the problems and potentialities of metal optics in the light of the above observations.

Where in considering the propagation of light in a metal it is permissible to make use of the complex dielectric constant

$$\varepsilon' = \varepsilon - i\frac{4\pi\sigma}{\omega} \equiv n - i\varkappa,$$

- and this is permissible when the length of the free path l_0 in the metal is much less than δ, the depth of the skin layer - the familiar equations for A, n and $\varkappa$ are applicable[3]. When l_0 is commensurate with or greater than δ, the skin effect becomes anomalous[2,4-7] and the concept of $\varepsilon'(\omega)$ cannot, in general, be used in calculating the field and the loss in the metal. However, even in this case the reflection of light from the metal is determined by one complex quantity, namely the surface impedance Z, characterized by

$$Z = \frac{4\pi}{c}\left[\frac{E_x}{H_y}\right]_0 = \frac{4\pi}{c\sqrt{\varepsilon'_{ef}}},$$

where components of the electric and magnetic fields **E** and **H** are taken on the surface of the metal and the effective dielectric constant

$$\varepsilon'_{ef} = \varepsilon_{ef} - i\frac{4\pi\sigma_{ef}}{\omega} \equiv (n_{ef} - i\varkappa_{ef})^2$$

(we can restrict ourselves to the introduction of the quantity Z only if the usual condition $|\varepsilon'_{ef}| \gg 1$) is satisfied).

To compute ε' or ε'_{ef} one must resort to electron theory. We analyzed the problem on the assumption that the Fermi surface is spherical and derived equations relating n and $\varkappa$ as well as n_{ef} and $\varkappa_{ef}$ with the concentration N of free electrons, the velocity v_0 on the Fermi surface and the number of collisions ν_0. (For more details see Refs. 2 and 8.)

It must be noted that if there exists a frequency interval satisfying the condition

$$\omega_0^2 \gg \omega^2 \gg \nu_0^2, \qquad (1)$$

where ω_0 is the frequency corresponding to the boundary of the internal photoeffect, we can assume with satisfactory accuracy, regardless of whether the skin effect is normal or anomalous, that

$$N = \frac{|\varepsilon| m\omega^2}{4\pi e^2} \approx \frac{m\omega^2 \sin^2\varphi_0 \operatorname{tg}^2\varphi_0}{4\pi e^2} = 1{,}12\cdot 10^{21}\,\frac{\sin^2\varphi_0 \operatorname{tg}^2\varphi_0}{\lambda^2}, \qquad (2)$$

where λ is the wavelength in microns and φ_0 is the principal angle of incidence. Thus in the region where the variation of N with $1/\lambda$ is quadratic, N can be determined by measuring φ_0. This appears to be the most reliable method of determining the concentration.

A second parameter which should be measured experimentally is ν_0. To this end one can make use of measurements of the electronic part of the specific heat, inasmuch as

$$\nu_0 = \pi k \sqrt{\frac{N}{\gamma}} = 1{,}44\cdot 10^{-2}\sqrt{\frac{N}{\gamma}},$$

where $\gamma = C^{(e)}/T$; $C^{(e)}$ here being the electronic portion of the specific heat of the metal, which can be measured in the region of low temperatures. Knowing the values of the parameters N and ν_0, we can compare theory with experiment.

Examination of experimental data on the optical properties of metals reported in the literature shows that most investigations are concerned with measurements of the absorption coefficient A for normal incidence at different temperatures[2,9,10]. Such measurements yield only one equation relating n and $\varkappa$, which is insufficient for determining N. The only deduction that can be made from the results of these investigations is that normal skin effect theory gives values of A that are too low, the divergence between theory and experiment increasing rapidly with decreasing temperature. Taking the skin effect into account, assuming diffuse scattering of the electrons from the surface of the metal, leads to closer agreement with experiment.

A smaller group of investigations is devoted to determinations of n and $\varkappa$. In the visible and ultraviolet regions of the spectrum these parameters are determined by means of a polarizer, analyzer and compensator. The phase difference Δ of light polarized parallel and perpendicular to the plane of incidence is measured for the given angle of incidence φ and the direction of the restored polarization is determined[11,12]. In the infrared region either the principal angle φ_0 or the principal azimuth ψ_0 is measured[1] or the ratio of the reflection coefficients for light polarized parallel and perpendicular to the plane of incidence is determined[13,14]. Since the frequency ω_0 commonly lies either in the visible or near infrared region, it is necessary to have data on n and $\varkappa$ in the infrared region; further, in investigating the dependence of $\sin\varphi_0 \tan\varphi_0$ on λ or on T, one should make certain that the measurements are made in the region of frequencies where inequality (1) holds. In actual fact, however, there is very little data on η and $\varkappa$ in the infrared region available. The most detailed investigation of the optical constants of a number of metals in the region to 4-4.5 microns was made by Försterling and Freedericks[1]. Unfortunately these investigators worked with metallic mirrors obtained by electroplating and cathode spattering. There is no assurance that the properties of the metals in thick layers will necessarily be the same as those of films formed in the above manner.

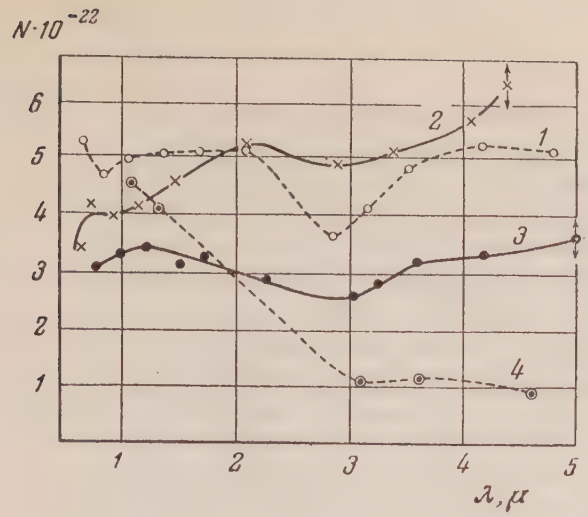

Variation of the free electron concentration with the wavelength for some metals: 1) gold, 2) silver, 3) copper, deposited by cathode spattering, 4) copper, electrically plated.

The results of our processing of the data of the last mentioned investigation are given in the accompanying table and figure, where the ordinates represent values of N computed according to equation (2). It will be seen from the figure that it is desirable to carry out measurements in a wide range of wavelengths (particularly, further into the region of longer wavelengths) in order to be sure of obtaining a measurement interval in which N, as determined according to (2), will be independent of λ. The data in the table for Au, Ag and Cu are taken from Ref. 1 (the values of N shown are the mean values for the three longest wavelengths). The data for Sn are taken from Ref. 11 and pertain to the visible region of the spectrum; for a number of reasons they are not particularly suitable for use with equation (2).

Constants of Some Metals Derived from Optical Measurements

Element	N_a	N, calc. acc. (2)	γ, erg cm^{-3} deg^{-2} (Ref. 16)	v_0, cm/sec
Au	$5.9\cdot10^{22}$	$5.2\cdot10^{22}$	-	-
Ag	$5.9\cdot10^{22}$	$5.7\cdot10^{22}$	$6.3\cdot10^{2}$	$1.4\cdot10^{8}$
Cu	$8.4\cdot10^{22}$	$3.3\cdot10^{22}$	$1.0\cdot10^{3}$	$8.3\cdot10^{7}$
Sn	$3.7\cdot10^{22}$	$6.2\cdot10^{22}$	$9.0\cdot10^{2}$	$1.2\cdot10^{8}$

We note in passing that the value of N - highly important for the theory of superconductivity[5,15] - is not known reliably for any superconductor.

It will be clear from the above that there is virtually no modern experimental data on n and $\varkappa$, which means that the field here is wide open for experimental investigation. As for theoretical problems, the most pressing are to take account of the quantum effects (important when $\hbar\omega \geq kT$, where T is the temperature of the metal) and the anisotropy and influence of mixed conduction, i.e., essentially an evaluation of the possibility of extending the quantitative theory to polyvalent metals.

"P. N. Lebedev" Physical Institute of the
Academy of Sciences of the U.S.S.R.

References

1. K.Försterling & V.Freedericks, Ann. de Phys., 40, 201 (1913).
2. R.B.Dingle, Physica, 19, 311, 348, 729, 1187 (1953).

3. M.V.Vol'kenshtein, Molekuliarnaia optika (Molecular Optics).M.-L. 1951.
4. G.Reuter & E.H.Sondheimer, Proc. Roy. Soc., 195, 336 (1948).
5. V.L.Ginzburg, Usp. fiz. nauk, 42, 333 (1950).
6. E.H.Sondheimer, Adv. in Physics, 1, 1 (1952).
7. T.Holstein, Phys. Rev., 88, 1427 (1952).
8. V.L.Ginzburg, Doklady AN SSSR, 97, 999 (1954).
9. K.Weiss, Ann. d. Phys., 2, 1 (1948).
10. K.G.Ramanathan, Proc. Phys. Soc., A65, 532 (1952).
11. P.Erokhin, Ann. d. Phys., 39, 213 (1912).
12. C.V.Kent, Phys. Rev., 14, 459 (1919).
13. D.G.Avery, Proc. Phys. Soc., 65B, 425 (1952).
14. J.N.Hodgson, Proc. Phys. Soc., 67B, 269 (1954).
15. V.L.Ginzburg, Zhur. eksp. i teor. fiz., 21, 979 (1951).
16. E.F.Burton et al, Phenomena at the Temperatures of Liquid Helium. 1940.

* * * *

ON PHOTOELECTRIC METHODS IN SPECTRUM ANALYSIS

- I. S. Abramson and S. L. Mandel'shtam

In recent years there has been a rapid development of photoelectric methods of spectroscopic analysis. The advantages of photoelectric methods of analysis are common knowledge; their application speeds up the analysis, increases its accuracy and automatizes the analytic process. It is frequently assumed that only speed and automation are gained by the introduction of photoelectric procedures; this is erroneous: higher accuracy is also of great practical import. Present photographic methods which are characterized by a quantitative accuracy on the order of 3-5% (the accuracy of visual methods is even lower, of course) cannot provide the accuracy of determination commonly required in practice when the concentration of the investigated element or component exceeds 10%. Photoelectric methods which insure an accuracy of within 0.5% of the total content of the measured component provide a way out of this difficulty and thus substantially widen the scope of application of spectrum analysis.

Photoelectric methods of analysis, as we noted, are currently in process of intense development. It would be erroneous to assume that all the problems connected with their use and application have been solved. However, their development has reached the stage where it is expedient to take stock and to formulate, in the light of experience gained, the problems arising incident to the operation and development of photoelectric equipment.

Every photoelectric spectrum-recording system consists of four basic components: a spectrum-exciting source, a spectroscopic instrument, a photoelectric radiation receiver and a unit for recording the photoelectric current. In photoelectric systems the components are generally more closely integrated than in systems of other types.

1. Spectroscopic sources

The spectroscopic sources used in photoelectric systems must satisfy particularly exacting requirements as regards reproducibility of the excitation conditions. In photographic methods, where the photometry error σ_{phot} may amount to 3-4%, the error in analysis due to the source σ_{sou} can go as high as 2-3% without seriously impairing the overall accuracy of the analysis, for if $\sigma_{phot} = 3\%$ and $\sigma_{sou} = 2\%$, $\sigma_{an} = \sqrt{\sigma^2_{phot} + \sigma^2_{sou}} \approx 3.5\%$. (The corresponding percentages are even higher in the case of visual methods.) On the other hand, when the requisite accuracy is 0.5%, obviously the error introduced by the source must not exceed 0.3-0.4%.

It has been established that modern spectroscopic sources assure excellent reproducibility as regards the conditions of excitation of atoms and that the main cause of instability is variation of the conditions of introduction of the analyzed material into the discharge. The best reproducibility as regards conditions of introduction of the material is obtained in spark sources; the worst is encountered in arcs, due to the turbulent nature of the processes occurring at the electrodes.

Unfortunately, the use of spark sources is hampered by the fact that this form of discharge produces strong electric interference, impairing operation of the electronic recording circuits. Moreover, sparks yield less total light. The actual duration of a spark discharge amounts to only a small fraction of the total exposure time:

$$\tau \approx 2\pi\sqrt{CL}\ nfT,$$

where C is the capacitance and L the self-inductance of the spark circuit, n is the effective number of oscillations per discharge train, f is the number of trains per second and T is the exposure time. For example, if C = 0.01 μf, L = 25 microhenries, n = 3 and f = 100, τ equals only about 10^{-3} T.

To some extent the short duration is compensated for by the greater brightness of the spark discharge. The brightness of a discharge may be evaluated on the basis of the magnitude of $I \approx e^{-E/kT}$. For $T_{arc} = 5000^{\circ}$, $T_{spa} = 10{,}000^{\circ}$ and $E \approx 4$ ev, we get $I_{spa}/I_{arc} \approx 10^2$. Thus with a given exposure time, a spark yields about one-tenth the light of an arc. As tests at the Physical Institute of the USSR Academy of Sciences and in the laboratory of the Commission on Spectroscopy have shown, it is possible to accelerate the processes at the electrodes of an arc by using an intermittent arc, i.e., by interrupting the arc discharge for more or less prolonged intervals, or, in some cases, by operating the arc in an atmosphere of nitrogen (for the purpose of reducing the intensity of oxidation processes).

Sources of this type are apparently the most suitable for photoelectric spectrum analysis. Electronically controlled generator circuits for supplying arcs were originated in the laboratory of the Commission on Spectroscopy (by I. S. Abramson) and subsequently improved and developed for producing intermittent arcs at the Physical Institute of the Academy (by L. S. Shelkov and A. I. Shurygin). Over five years of experience with such arcs has confirmed their suitability for spectrum analysis.

A block diagram of the latest version of the arc generator, developed in the laboratory of the Commission, is shown in Fig. 1.

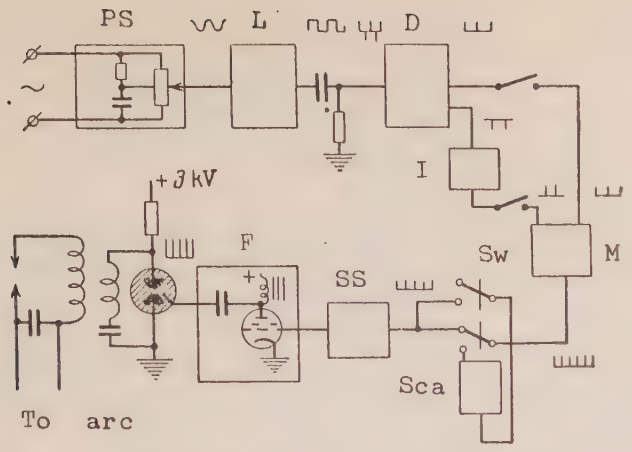

Fig. 1. Block diagram of generator with electronic control.

The pictured circuit operates as follows: the voltage from the regular a-c supply line is applied to the rotary phase shifter PS which energizes the limiter stage L, converting the sinusoidal oscillations into rectangular waves. These waves are differentiated by a RC network and the resultant positive and negative pulses are sorted by the divider D: the positive pulses go directly to the mixer M while the negative pulses are inverted by the stage I before reaching the mixer. The pulses then go through the selector switch Sw to the shaping stage SS, either directly or via the scaling circuit Sca. The shaping stage SS forms negative pulses with a steep leading edge. Next we have the stage F which generates the pulses firing the thyratron. The F stage is a normally conducting G-807 tetrode with a large inductance (1 henry) in its plate circuit. When a negative pulse (from the shaping stage) is applied to the grid, the plate current is suddenly cut off and an overvoltage attaining 5-7 kv is induced in the plate circuit inductance; this pulse infallibly fires the thyratron.

The described circuit can be used for different types of source operation: a-c discharge, pulsating d-c discharge of either polarity or intermittent operation with an adjustable duty cycle ranging from 1:2 to 1:16. The phase of the discharge can be regulated smoothly over 180° relative to the phase of the supply circuit. New circuit components introduced in this latest version of the generator - specifically, the rotary phase shifter and the thyratron firing circuit incorporating the inductive load trigger (replacing the previously used thyratron trigger) - make for more reliable operation of the unit. Experience has shown that the new generator has good dielectric and spectral stability.

Special tests carried out by Raiski and Shelkov at the Physical Institute showed that when the discharge regime (current strength, duty cycle, polarity, material and shape of the counter-electrode, etc.) is properly selected for the specimen in question, highly satisfactory results can be obtained as regards accuracy of analysis.

2. Spectroscopic instruments

The energetic characteristics of spectroscopic instruments employed in conjunction with photoelectric procedures differ from those of instruments used in photographic and visual recording of the spectrum. This is explained by the fact that photoelectric receivers react to the light flux rather than to the illumination, as do photographic plates and the human eye (provided the image area is not too small). Hence the transmission of an instrument used for photoelectric measurements is determined by other parameters than the transmission of conventional spectrographs and spectroscopes (see table in Fig. 2).

The transmission of a photoelectric spectrometer depends on the

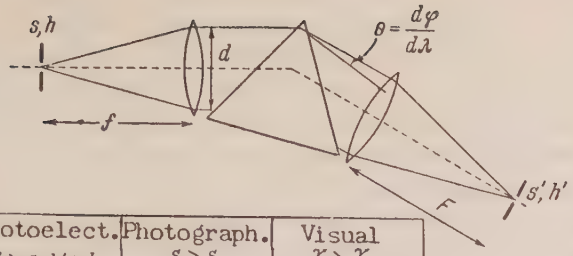

Photoelect. $s' \geq s,\ h' \geq h$	Photograph. $s > s_H$	Visual $\gamma > \gamma_H$
$d\Phi = \frac{\pi}{4} Bsh \left(\frac{d}{f}\right)^2$ $d\Phi = \frac{\pi}{4} Bh \frac{d^2}{f} \theta \Delta\lambda$	$E' = \frac{\pi}{4} B \left(\frac{d}{F}\right)^2$	$E' = \frac{\pi}{4} B \left(\frac{d}{F}\right)^2 \frac{1}{\gamma^2}$

Fig. 2. Comparison of the energetic characteristics of spectroscopic instruments used with photoelectric, photographic and visual methods of recording spectra.

area of the entry slit and the aperture of the collimator, whereas in the case of photographic and visual recording the slit area is not a determining factor and only the aperture of the tube is important. Where dispersion is concerned, we note that whereas in the case of photographic and visual recording (of line spectra) dispersion does not affect the transmission factor of the instrument, in photoelectric recording the dispersion determines the width of the entry slit s (Fig. 2).

Thus, assume that the nearest interfering line is situated at a distance $\Delta\lambda$ (in angstroms) from the observed line; then for separation, the slit image s' must be $\leq \Delta\lambda\theta F$, but $s' = sF/f$. Consequently,

$$d\Phi = \frac{\pi}{4} Bh \frac{d^2}{f} \theta \Delta\lambda,$$

where θ is the angular dispersion (in radians per angstrom); i.e., it is advantageous to use instruments with a large angular dispersion. We arrive at the same conclusion without the need for calculation: increasing the angular dispersion, resulting in an increase in the separation of the lines, permits using a wider entrance slit; on the other hand, increasing the linear dispersion at the expense of F is of no advantage since in this case the width of the line images increases in proportion to the increase in the distance between lines and, therefore, the slit width cannot be increased. The reason for the transmission being a function of f rather than of f^2 is obvious: increasing f by a factor of m reduces the flux by a factor of m^2; if at the same time F remains constant, the width of the slit image s' is decreased by m; consequently the slit width s can be increased m times. In the case of an equal-arm instrument, an increase in f is accompanied by an equal increase in F with s' remaining constant, i.e., in this case the slit width can also be increased by virtue of an increase in the linear dispersion.

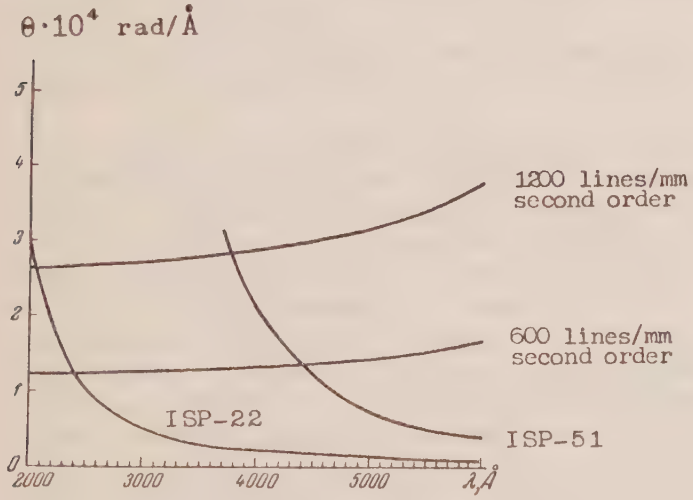

Fig. 3. Comparison of the angular dispersion of diffraction gratings having 1200 and 600 lines/mm, a 60° quartz prism (ISP-22 spectrograph) and a three-prism glass system (ISP-51 spectrograph).

The question arises: what type of dispersing element - grating or prisms - is more advantageous from the point of view of obtaining the maximum angular dispersion? The angular dispersions produced by diffraction gratings having 600 and 1200 lines/mm in the second order spectrum (acc. to Igl), a 60° quartz prism (ISP-22 spectrograph) and a three-prism glass system (ISP-51 spectrograph) are compared in Fig. 3. It will be seen from thefigure that the 1200 lines/mm grating is superior to the prism systems inthe entire region from 2000 to 6000 A, while the 600 lines/mm grating yields to the prism systems only in the 2000-2400 and 3700-4300 A intervals. Thus it will be seen that a grating assures a higher degree of angular dispersion in virtually all cases of interest in practical spectrum analysis. Moreover, use of gratings as a rule permits realizing a greater effective aperture (particularly in the ultraviolet region) than is feasible with prism instruments.

Regarding illumination of the instrument slit, it may be remarked that whereas in using photographic and visual methods the slit illumination must be uniform along its length (so that sharp focusing of the source image on the slit is usually impractical) this requirement does not apply in the case of photoelectric recording. A system of illumination of the slit and light receiver, having a number of merits, is illustrated in Fig. 4.

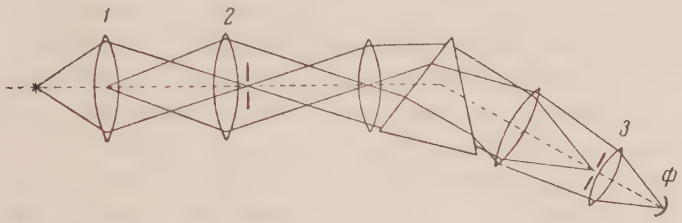

Fig. 4. System of illumination of the spectrograph slit when photoelectric recording is employed: 1 and 2) first and second condensing lenses, 3) lens, ф) photocathode.

The first condensing lens (1) focuses a sharp image of the source on the slit; the second condensing lens (2) forms an image of the plane of the first condensing lens on the entry element of the instrument (usually the objective of the collimator or the face of the prism) and serves to prevent vignetting incident to displacement of the source image along the slit. The last lens (3) produces an image of the entry element of the instrument (or essentially, of the uniformly illuminated surface of the first condensing lens) on the surface of the photocathode of the receiver. This arrangement insures uniform illumination of the same section of the photocathode throughout the series of measurements, which is very important, because the surface of most photocathodes is not uniform as regards sensitivity, and any displacement of the area illuminated by the beam incident to shifting of the source has an adverse effect on the accuracy of results obtained. Inasmuch as the brightness of the source image on the slit does not depend on the source-to-image ratio, it is advantageous to throw an enlarged image of the source on the slit. However, the size of the image must be smaller than the length of the slit to allow of some displacement of the image incident to wandering and other shifting of the discharge over the electrodes.

Where such shifting occurs, the described system has certain advantages over a conventional three-lens condenser. It must be noted, however, that any appreciable displacement of the discharge point (source) leads to serious complications in the operation of photoelectric recording systems; consequently, proper selection of the conditions of illumination of the slit and photocathode is of paramount importance.

3. Photoelectric receivers

At present three types of receivers are used: photon counters, photocells and photomultipliers. Their suitability for the purposes of photoelectric spectrum analysis is determined by their sensitivity [threshold], spectral range of sensitivity, and linearity and by the method of recording the photocurrent employed.

The sensitivity [threshold] is determined by the requirement that the signal (radiant power) must exceed the noise level, i.e., the background count N_b in a counter or the dark current I_d in a photomultiplier or cell. Obviously what is most important is not the absolute value of N_b or I_d but the amplitude of fluctuation of the parameter, for if N_b or I_d remained constant, one could simply subtract the appropriate value from the recorded measurements. In view of the presence of fluctuation, the criterion for a detectable signal must be $N_s \geq 3\sigma(N_{s+b} - N_b)$ for counters and $I_c \geq 3\sigma(I_{s+d} - I_d)$ for photocells and multipliers, where σ is the mean square deviation of the quantity in the parentheses. For counters

$$3(N_{s+b} - N_b) = 3\sqrt{\sigma^2(N_s + N_b) + \sigma^2(N_b)} \approx 5\sigma(N_b)$$

Since $(\sigma)N = \sqrt{N}$, the sensitivity of a counter is determined by the condition that $N_s \geq 5\sqrt{N_b}$. Let us introduce the observation time τ and the counting rate (pulses per minute for the signal and background - n_s and n_b, respectively; then $N_s = \tau n_s$ and $N_b = \tau n_b$, and the sensitivity threshold becomes $n_s \geq 5(n_b/\tau)^{1/2}$.

Assuming that in practical measurements n_b equals about 5 pulses per min., $\tau \approx 1$ min and the quantum yield of a cathode counter $\alpha \approx 10^{-3}$, we find the sensitivity (threshold) $S_{co} = 2 \cdot 10^2$ quanta/sec $\approx 10^{-9}$ ergs/sec.

For photomultipliers we have

$$I_s \geq 5\sigma I_d \quad \text{and} \quad \sigma I_d = \sqrt{2e\,(2B + 1)M\,\Delta f\,I_d}.$$

Assuming $M = 10^5$, $I_d = 10^{-9}$ amp and $\Delta f = 1/\tau = 1/50$, we obtain $I_s \geq 5 \cdot 10^{-12}$ amp. If the response of the photomultiplier is 5 amp/lumen, $S_{phm} \approx 2 \cdot 10^3$ quanta/sec $\approx 10^{-8}$ ergs/sec. That is, under the usual technical testing laboratory conditions the sensitivity of a counter is higher than that of a photomultiplier. (It must be emphasized here that we are comparing the thresholds of counters and multipliers under ordinary technical laboratory conditions; the sensitivity of both types of detectors can be raised - i.e., threshold lowered - by reducing the noise level by refrigeration, prolonging the counting period, etc. As a rule, however, such measures are feasible only in research laboratories.)

In photoelectric spectrum analysis it is important not only to detect the signal but also to measure it accurately. If we re-examine the question of counters vs photomultipliers in the light of this last requirement, we arrive at somewhat different results.

The accuracy of measurement inthe case of counters can be characterized by the magnitude of the quantity $R = \sigma(N)/N$; in the case of multipliers, by $R = \sigma(I)/I$, where N and I are the mean values of the measured quantity (count or current) and $\sigma(N)$ and $\sigma(I)$ are the mean fluctuations of N and I. For a counter $\sigma(N) = \sqrt{N}$ and $R = 1/\sqrt{N}$. For the error in measurement not to exceed 1%, N must come up to about 10^4

pulses. Assuming a quantum yield $\alpha = 10^{-3}$, we find that we must record 10^7 quanta during the observation interval; at 3000 A this corresponds to an energy of $6 \cdot 10^{-5}$ ergs.

For a photomultiplier, $\sigma(I) = \sqrt{2e(2B + 1)M \Delta f I}$. Assuming $\Delta f = 1/\tau$, we obtain $R = \sqrt{eM/\tau I}$; but $I = eMn$, where n is the number of electrons ejected by the light per second. Consequently,

$$R = \sqrt{\frac{1}{\tau n}} = \frac{1}{\sqrt{N}}$$

where $N = \tau n$, the number of electrons ejected from the photocathode during the exposure time; i.e., the expression for R has the same form as in the case of counters. However, in the case of a photomultiplier the quantum yield of the cathode is approximately 100 times greater than in a counter, i.e., $\alpha = 10^{-1}$. Consequently for the error not to exceed 1%, the minimal energy need only be $E \approx 6 \cdot 10^{-7}$ ergs. With an observation time of about 50 sec, this corresponds to a light flux of about 10^{-12} lumens. Under the usual spectrum analysis conditions (flux = 10^{-8}-10^{-10} lumens) the statistical error introduced by the photomultiplier can be neglected. In the case of counters under like conditions (flux on the order of 10^{-10} lumens) the statistical error already becomes significant, i.e., amounts to an appreciable proportion of the total error. In practice this counter-error, apparently, cannot be reduced to any appreciable extent by increasing the light flux. Thus, in the equipment developed by the Physical Institute of the Academy of Sciences, the actual "exposure" time (taking into account the "off-time" or duty cycle of the source) amounts to about 3 seconds; consequently the counting rate to obtain R = 1% should be about $3 \cdot 10^3$ pulses/sec. At such high counting rates, as Shelkov has shown, counter operation tends to become unstable; moreover, in view of the necessity of resolving the close pulses, more complicated scaling circuits must be used.

For the above reason the use of counters must at present be limited to measurements of low concentrations of the investigated elements, i.e., to cases where the requirements as regards accuracy of determination are not too exacting. Another shortcoming of counters is that their range of spectral sensitivity is comparatively limited.

The most commonly used receivers at present are photomultipliers. However, their use is fraught with certain difficulties; they often show evidences of "fatigue" even in recording relatively moderate values of the flux and in general have a fairly high dark current. Photocells are somewhat more stable than multiplier tubes and have a somewhat more favorable signal to dark current ratio. However, their sensitivity is rather low and their use imposes rather exacting requirements as regards insulation of the input circuit.

4. Photocurrent recording systems

A great variety of recording and registering systems is used in photoelectric spectrometers thanks to the wide choice afforded by modern electronics. All the systems, however, are designed to measure not the instantaneous value of the flux from a given spectrum line but the value averaged over some more or less protracted interval (usually between 30 and 100 seconds). Such averaging over a certain time interval is essential in order to minimize dispersion of the measured data due to variation of the instantaneous value of

the flux from the source and fluctuation of the photocurrent. In photoelectric recording systems the averaging is usually accomplished by means of a RC integrating circuit, having a time constant much greater than the observation time. Two alternatives are possible: either the storage capacitor can be charged directly with the current from the photocell or photomultiplier (Fig. 5a) or the photocurrent can be preamplified (Fig. 5b). Both alternatives have their specific advantages and shortcomings. The principal drawback of the former is that when a photocell is employed the capacitor charge is very small; with the values of the light flux usually obtaining, the accumulated charge is about $5 \cdot 10^{-12}$ - $1 \cdot 10^{-10}$ coulombs. In order to measure such small charges it is necessary to resort to special electrometric circuits. Electromagnetic d-c amplifiers have been commonly used for this purpose, despite their operational shortcomings: they have a tendency to drift, and require a set of carefully matched tubes and an accurately stabilized power supply. When a photomultiplier is used, the charge on the capacitor is higher - 10^{-7} - 10^{-5} coulombs, - and, hence, easier to measure. On the other hand, photomultipliers have a comparatively heavy dark current, which must be compensated for. Since the dark current is not steady, compensation with the requisite accuracy is difficult to achieve.

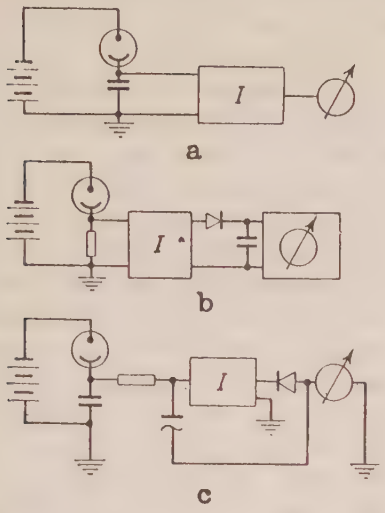

Fig. 5. Photocurrent recording circuits: a) with direct charge accumulation in a capacitor with subsequent amplification, b) with preamplification, c) with a dynamic capacitor.

Both these difficulties are eliminated when preamplification is used. Inasmuch as the radiation from the source is usually modulated, a-c amplification can be employed. Amplification stability in this case is very high and there is no need to compensate for the dark current since its constant (d-c) component is blocked by the amplifier.* The charge on the capacitor can be brought up to as much as 10^{-6}-10^{-4} coulombs; hence, its measurement presents no difficulty.

However, as noted, systems based on preamplification have their own shortcomings: in the case of instruments used for simultaneous determination of several elements, it is necessary to connect in several amplifiers which obviously complicates the installation. It is impossible in such systems to vary the frequency of the source in accordance with the analytic requirements. Moreover, such systems are more sensitive to electric noises from the generator.

Direct charging systems do not have these shortcomings: they have but one measuring channel which can be switched in turn to a number of capacitors. As used in our laboratory the most noise-sensitive section of the system had a small a-c impedance (relatively large capacitance) at the input and the charge could be measured with the generator disconnected. This means that the direct charging system was less sensitive to electrical noise than the preamplification

---

*The fluctuations of the dark current, as was shown above, in the case of spectrum lines having a flux of 10^{-6}-10^{-8} lumens are relatively small and can be disregarded.

circuit.*

To some extent the various advantages of the systems described above have been reunited in the so-called dynamic capacitor circuit whose operation is based on the principle of parametric modulation formulated by Mandel'shtam and Papalekis. Some results of an investigation of this system will be given in a paper by Abramson and Maliavkin; here we shall only note that use of the dynamic capacitor permits designing an electrometric circuit of the type pictured in Fig. 5c, having the following interesting features: a) It does not consume current and can be used for measuring very small charges, thus facilitating the use of photocells as light receivers and thereby eliminating the difficulties associated with compensating the dark current of photomultipliers. b) The dynamic capacitor converts the measured d-c voltage on the integrating capacitor to an a-c voltage which is then amplified by a resonant amplifier. This feature obviates drift of the amplifying circuit, the need for accurate stabilization of the power supply, etc. At the same time the dynamic capacitor system retains all the advantages of the direct charging circuit: the use of only one measuring channel, comparative insensitivity to noise, etc. It promises, therefore, to be eminently suitable for use with photoelectric instruments.

We have been able to touch upon only a few of the problems involved in the application of photoelectric methods to spectrum analysis. There are naturally many other important and complex problems relating not only to the mentioned fields of optics, electronics and spectroscopy, but also to other scientific fields, such as metallurgy, physical chemistry, etc. For example, there is need for a rapid method of bringing the lines of the investigated element into alignment with the exit slit of the instrument, for better and more convenient reference standards, for a method of obtaining more uniform samples, for ways of eliminating the influence of extraneous elements, etc. Further development of photoelectric methods of spectrum analysis requires the close cooperation of scientists in the various fields; only the joint efforts of many investigators can insure the success of our endeavors. But tne full development and widespread introduction of photoelectric methods of analysis is so worthwhile a goal that its achievement will repay all the effort expended on attaining it.

Physical Institute of the
Academy of Sciences of the USSR
and the
Commission on Spectroscopy at the
OFMN of the Academy of Sciences of the USSR

---

*There exist systems in which direct measurement of the charge built up on an integrating capacitor is replaced by measurement of the difference in the discharging times (to a certain voltage) of capacitors in the "analyzed line" circuit and in a "reference line" circuit. This time difference is proportional to the logarithm of the ratio of the line intensities. Consequently the system operates more directly with the quantities familiar in spectrum analysis. Measurement of small charges is replaced by measurement of short time intervals. While ostensibly these recording systems are free of some of the shortcomings peculiar to the systems described above, they are characterized by other sources of errors inherent in the time-measurement circuit and furthermore they require very close voltage control.

NEW SPECTROSCOPIC INSTRUMENTS

- V. K. Prokof'ev

During the past three years a large group of new spectroscopic instruments has been produced in the USSR. They comprise instruments intended for scientific research and equipment for use in industrial laboratories. Some are prototypes, others have already been produced in limited numbers. The first instruments of each type have been installed in the laboratories of the new building of Moscow State University.

This new group of instruments is distinguished from the spectroscopic equipment manufactured hitherto by the following features:

1. Extensive use of diffraction gratings. During the past few years the production of diffraction gratings of different types was organized in the Soviet Union and we now have available domestic gratings of the following types: concave gratings with a radius of curvature of 1 meter, ruled on glass with spacings of 600 or 1200 lines/mm and different rulings to provide maximum intensity in the desired spectrum order; plane gratings with 600 or 1200 lines/mm in different sizes. The 600 lines/mm plane gratings come as large as 150 x 150 mm. The plane gratings are available with different rulings to throw the maximum of light into the desired order. We also now have available the necessary echelette gratings for infrared spectroscopic instruments.

2. Provision of photocells and photomultipliers as receivers of radiation, together with the appropriate electronic equipment for recording the spectra.

In developing and producing these new instruments the optical instrument industry worked in close contact and cooperation with the personnel of scientific research institutes and the Commission on Spectroscopy of the Academy of Sciences of the USSR.

The newly developed instruments may be divided into ten main groups: 1) instruments for the vacuum ultraviolet region, 2) high transmission spectroscopic instruments, 3) high dispersion and high resolution instruments, 4) interferometric instruments, 5) spectroscopic instruments for visual observation, 6) spectrophotometers, 7) instruments for the infrared region, 8) spectrum source generators, 9) instruments for studying spectrograms, and 10) demonstration instruments, i.e., instruments used for instruction purposes.

This short listing suffices to indicate the extensive range and variety of the new spectroscopic instruments and equipment. We shall now describe briefly the instruments in each group.

1. Spectroscopic Instruments for the Vacuum Ultraviolet

1) DFS-6 diffraction-grating spectrograph with a grazing incidence glass grating having a radius of curvature of 1 meter (Fig. 1). This instrument is intended for spectroscopic research in the 60 to 2000 A region. The availability of this new instrument makes it possible to extend the investigation of atomic and ionic spectra into the extreme ultraviolet. The instrument comes complete with all the necessary vacuum equipment which is housed in the special stand mounting the spectrograph. For convenience of operation all the main parts of the instrument are mounted on a vertical panel; the main body

of the spectrograph, carried on rollers, is clamped against this panel for operation. Different types of sources can be readily attached to the main flange of the instrument.

2) Fluorite spectrograph (Fig. 2). This is a relatively small instrument with a prism and lenses made of natural fluorite[1]. The spectrum is thrown on a curved surface. In order to insure high spectral purity the objectives (simple fluorite lenses) are made with parabolic surfaces. The instrument produces a high purity spectrum and is intended for photographing spectra up to 1300 A. A hitherto unknown group of lines of ionized molybdenum and a unique second order collision effect in the glow of a discharge in argon have been recorded by means of this instrument used in conjunction with a hollow cathode source. The spectra were photographed on a film sensitized with transformer oil. In addition I. R. Protas has developed a special emulsion for the vacuum ultraviolet which is much faster than the familiar Schumann emulsion. As compared with the latter, this emulsion requires only 1/4 to 1/5th the exposure in the 1400 A region to obtain the same blackening.

3) Fluorite monochromator, designed as a simple or double monochromator[2]. In view of the fact that natural fluorite contains many inclusions which increase scattering, it was deemed expedient in designing the instrument to provide for the possibility of double monochromatization. An external view of the double monochromator is shown in Fig. 3. The use of a Wadsworth mounting with lens optics permits arranging the optical elements of the double monochromator in one line.

The instrument consists of two parts. The first or main part comprises the system of the first monochromator. With a radiation receiver placed at the exit slit, this part of the instrument operates as a simple monochromator. When necessary the second part of the instrument, containing the second monochromator, is mounted in place of the radiation receiver. The joint is tight enough to insure maintenance of an adequately high vacuum. The radiation receiver is then mounted at the exit of the second part and the entire system operates as a double monochromator. It should be noted that the double monochromator gives somewhat less light in the extreme region. Hence, the useful transmission limit of the instrument used as a double monochromator lies at about 1400 A.

Either a photomultiplier with a fluorescent screen (FEU-19) or a photon counter with a fluorite window may be used as the radiation receiver with this instrument. The use of counters is more advantageous, inasmuch as they permit detection of weaker radiation. On the other hand, the photomultiplier with fluorescent screen can be used to make spectral energy measurements. For example, the instrument with a photomultiplier was successfully used to refine the energy distribution in the emission spectrum of a hydrogen tube, previously obtained by photographic photometry. This instrument greatly simplifies the investigation of transmission and reflection spectra in the short wave region.

2. High Transmission Instruments

Until recently the only high transmission spectrograph produced by our Soviet industry was the glass optics ISP-51 spectrograph, which was satisfactory for many purposes. However, scientific research laboratories have long felt the need for high-transmission

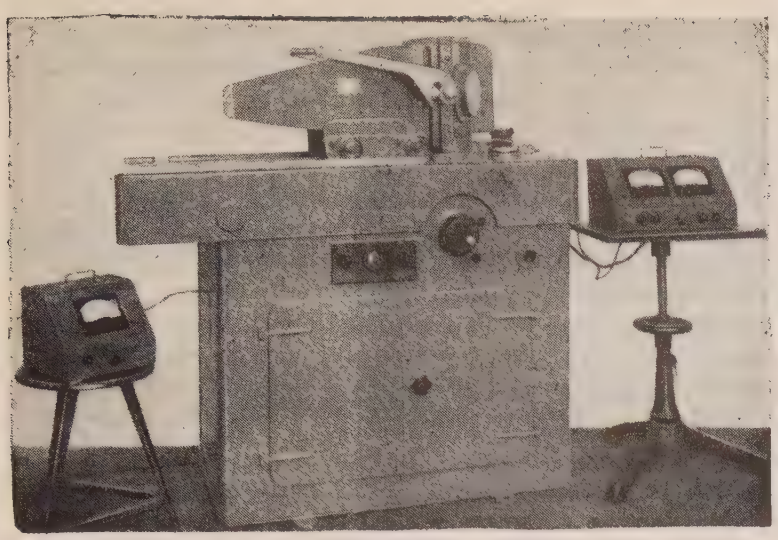

Fig. 1. DFS-6 Diffraction spectrograph.

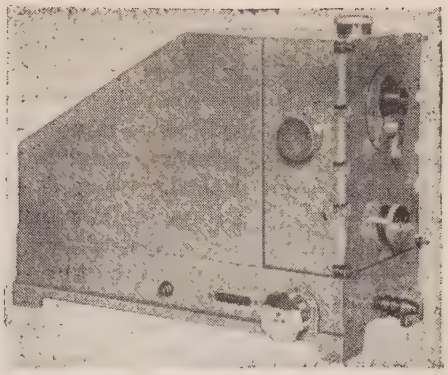

Fig. 2. Fluorite spectrograph.

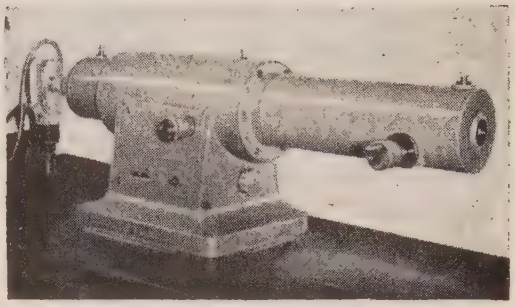

Fig. 3. Double fluorite monochromator.

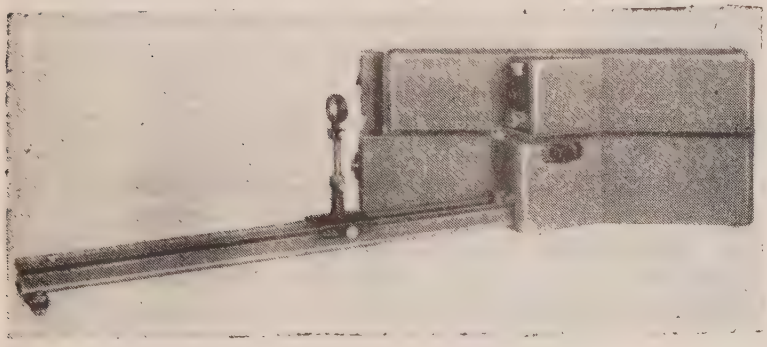

Fig. 4. ISP-66 Quartz spectrograph.

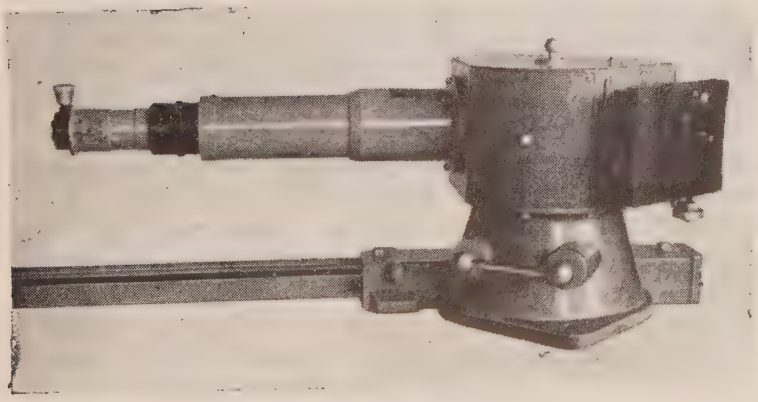

Fig.5. ISP-26 High-transmission spectrograph (laboratory model).

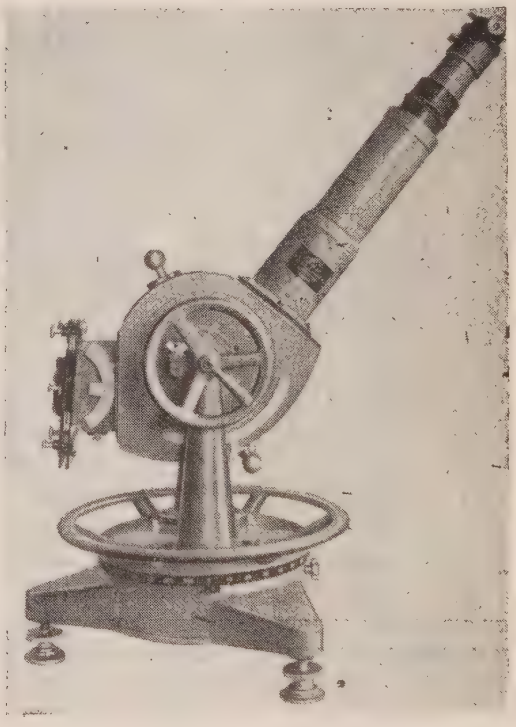

Fig. 6. ISP-26 High-transmission spectrograph (field model).

quartz spectrographs. Among the new instruments we now have the ISP-66 quartz spectrograph which has an aperture ratio of 1:4.6 with a spectrum length of 90 mm (Fig. 4). This instrument utilizes the proven optical system of the ISP-22 spectrograph; however, in view of the appreciably shortened focal distances the spherical collimating mirror used in the ISP-22 had to be replaced by a unique off-axis parabolic mirror. The production of the ISP-66 spectrograph, characterized by high spectral purity, is evidence of the fact that the workers of the instrument industry have succeeded in solving the difficult technological problems connected with the production of high grade off-axis-focus parabolic mirrors, insuring excellent quality spectra in the ultraviolet region. The availability of this new instrument permits carrying out investigations of low-emission sources in the ultraviolet (fluorescent emitters) as well as of corresponding absorption spectra; a special set of accessories (KPS-4) is produced for absorption work.

Another noteworthy instrument in this category is the new super-high-transmission glass spectrograph with a lens system, having an aperture ratio of 1:0.7. This instrument can be used for studying very weak fluorescence in the visible range of the spectrum as well as the glow of the night sky. The instrument is made in two versions: a laboratory model, designated ISP-26 (Fig. 5) and having the characteristics of a conventional spectrograph and a portable field model, designated ISP-63 (Fig. 6), mounted on an azimuth circle and having provision for sighting the instrument at any desired region of the sky. This instrument has a very large glass prism (base over 100 mm) and a compound, micro-type glass objective. Despite the large size of the optical elements the instrument produces a high quality spectrum.

This group also includes a very high transmission (aperture ratio 1:7.3) spectroscopic instrument of original design, utilizing a plane diffraction grating. This is the DFS-4 instrument pictured in Fig. 7. The spectrum can either be photographed on a flat plate or recorded by means of a FEU-17 photomultiplier equipped with a suitable amplifying system. After amplification the spectrum is recorded by a mirror galvanometer on a strip of photographic paper. To permit recording of weak spectra (such as Raman spectra), the instrument design incorporates all possible provisions for insuring a maximum flux transmission, including long entrance and exit slits (to 40 mm) and provision for mounting a 150 x 150 mm plane grating, ruled with 600 lines/mm to concentrate the light in the desired orders in the visible range of the spectrum. The focal length of the instrument lens is 1200 mm. The reciprocal dispersion is 13.5 A/mm. The optical design of the instrument permits recording a Raman spectrum in about 15 minutes (photographing a like spectrum takes upwards of an hour).

The 600 lines/mm grating is interchangeable with a 1200 lines/mm plane grating. With the latter the aperture ratio is reduced to 1:10.4 while the reciprocal dispersion is 6.5 A/mm.

Tests with the instrument and with mock-ups assembled in the course of its design have shown[3] that the instrument can be used to record the Raman spectra of constituents of hydrocarbon mixtures present in amounts down to about 1%. Satisfactory results are also obtained in recording the Raman spectra of different types of glass, which are difficult to study by means of photographic procedures. The availability of this instrument will greatly facilitate the investigation of fluorescence and phosphorescence spectra, the line and band spectra of luminescent molecules, various types of absorption spectra, the intensity distribution in certain emission spectra, etc.

A special attachment developed for the ISP-51 spectrograph may also be classed in this group of instruments. This attachment is essentially an exit collimator with a focal length of 300 mm, equipped with a photomultiplier, suitable amplifier and recorder in the form of a mirror galvanometer recording on a strip of photographic paper. The attachment (PS-381 - see Fig. 8) can be used with any production model ISP-51 spectrograph to record Raman spectra, luminescence and similar spectra. The attachment has a high transmission factor; its dispersion, however,is not particularly high.

The PS-382 instrument, so far existing only as a prototype, also belongs in this group: this is an exit collimator with a focal length of 800 mm, designed to serve as an attachment ot the ISP-51 spectrograph (Fig. 9). This instrument comes with two photomultipliers: a FEU-17 and a photomultiplier with a cesium oxide cathode, which is still in the experimental model stage. Tests with the model indicate that the instrument should prove particularly useful in investigating spectra in the near infrared - to 10,000 A[4].

There can be little doubt that the introduction of the PS-381 and PS-382 attachments on the one hand and of instruments of the DFS-4 type on the other marks the beginning of widespread use of photoelectric recording methods in spectroscopy, with an effective saving of many spectroscopist man-hours. In fact, even the relatively few investigations so far carried out with such instruments have clearly proved their advantages.

3. High Dispersion and High Resolution Instruments

1) ISP-67 multiple prism spectrograph with interchangeable cameras (Fig. 10). The instrument employs three large glass prisms (150 mm faces) mounted in a unique system which permits using either conventional direct transmission or autocollimation. The instrument is supplied with three interchangeable cameras with appropriate collimators. The two short-focus cameras are intended for investigations requiring higher speeds; the long-focus camera (focal length 3 meters) is intended for use with the spectrograph optical system in the autocollimation setting and when so used permits obtaining a resolving power of 200,000 or more with high dispersion. Thus it can be used for direct photography of the hyperfine structure of individual spectrum lines. For example, in the 4000 A region with a reciprocal dispersion of 0.88 A/mm, lines only 0.04 A apart are readily distinguished[5]. Fig. 10 shows the instrument with the large camera in place.

2) DFS-2 two-meter diffraction grating spectrograph (Fig. 11). This is the first Soviet made spectroscopic instrument with a concave diffraction grating, employing the classic Paschen-Runge mounting[6]. The instrument has two gratings with 2 meter radii of curvature - one with 600, the other with 1200 lines/mm - mounted one above the other and can be used for photographing the spectrum on one long strip of film over the entire range from 2000 to 10,000 A. The overall length of the spectrum is 1 meter with the 600 lines/mm grating and 2 meters with the 1200 lines/mm grating. The instrument is equipped with special film holders permitting photography of 0.5 meters of spectrum in one exposure. The purity of the spectra obtained, testifying of the high quality of Soviet made diffraction grating[7], puts this instrument in the class of top grade spectrographs, suitable for studying complex spectra. This instrument will doubtless find wide application both in scientific research laboratories and in industrial spectroscopic

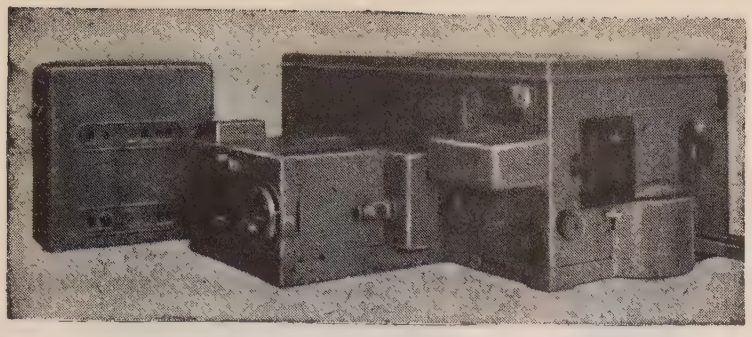

Fig. 7. DFS-4 High-transmission spectrograph with plane diffraction grating.

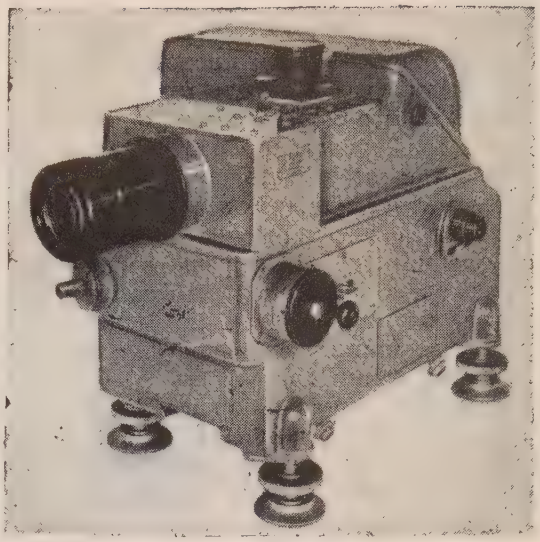

Fig. 8. PS-381 Attachment for spectrograph (exit collimator).

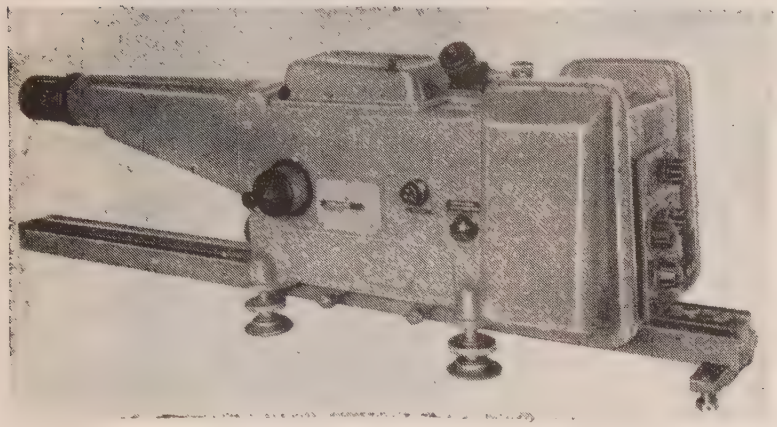

Fig. 9. PS-382 Attachment.

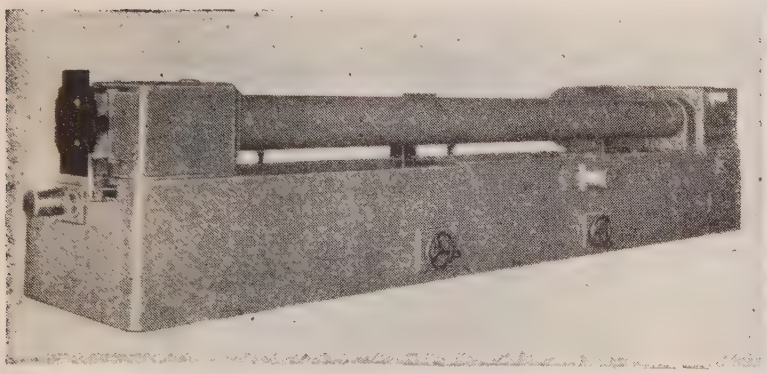

Fig. 10. ISP-67 Multiple prism spectrograph with interchangeable cameras.

laboratories where materials characterized by complex spectra must by analyzed.

3) DFS-3 large diffraction grating spectrograph (Fig. 12). This instrument, which is even better suited for the investigation of some complex spectra than the preceding spectrograph, has a plane grating and a 4 meter focal length spherical mirror. It takes flat photographic plates up to 24 cm in length[6]. The spectrum is photographed in small sections but with very high dispersion: the plate factor with the 600 lines/mm grating is 4 A/mm and 2 A/mm when the 1200 lines/mm grating is used. Hence, the instrument permits of direct photography of the hyperfine structure of mercury lines. The use of a plane grating, assuring a spectrum free of astigmatism, permits combining this spectrograph with other interferometric

Russian designations:

DFS = ДФС	SL = СЛ	IG = ИГ
ISP = ИСП	ST = СТ	OSK = ОСК
STL = СТЛ	SF = СФ	IKS = ИКС
PS = ПС	MF = МФ	
SP = СП	DG = ДГ	

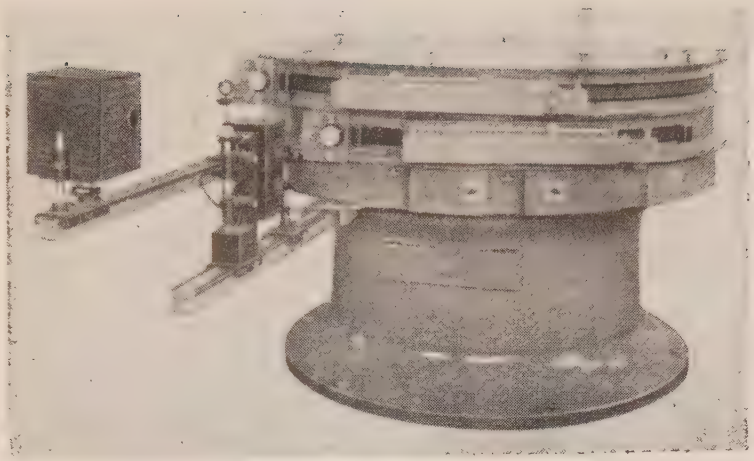

Fig. 11. DFS-2 Diffraction spectrograph with concave grating.

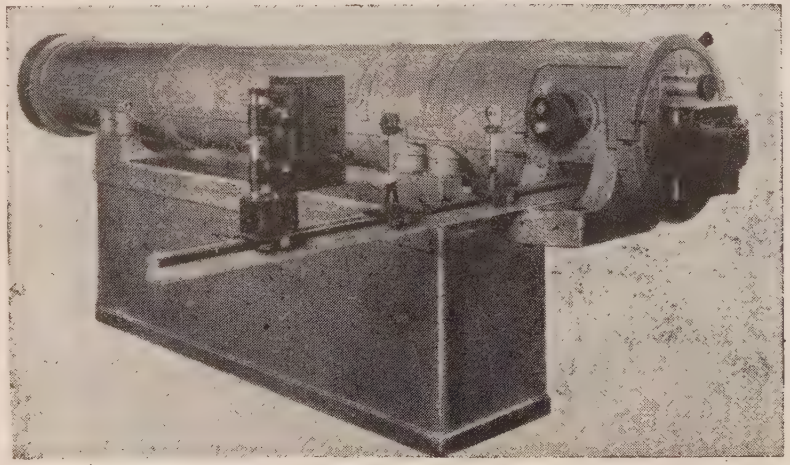

Fig. 12. DFS-3 Large diffraction spectrograph with plane grating.

Fig. 13. Section of iron arc spectrum obtained with DFS-3 instrument using 1200 lines/mm grating.

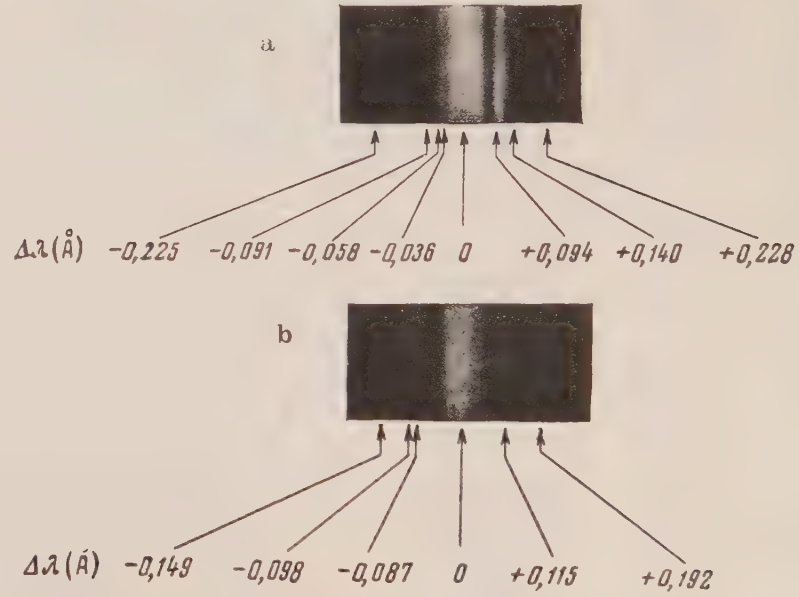

Hyperfine structure of the 5461 and 4358 A lines of mercury obtained with a 150 mm wide, 600 lines/mm grating in an autocollimating spectrograph (f = 3 m): a) 5461 A line, 8th order; b) 4358 A line, 10th order.

See next article.

instruments for special studies of a complex spectra. Thus, this instrument may be crossed with a Fabry-Perot etalon for investigating the shape and structure of individual lines of complex spectra. It can also be crossed with a Rozhdestvenski interferometer (a limited number of these has also been produced for Moscow State University) to study the fine detail of anomalous dispersion phenomena and investigate dispersion anomalies in the vicinity of individual spectrum lines.

By way of illustration a portion of the arc spectrum of iron in the 3100 A region obtained by means of the instrument with the 1200 lines/mm grating is shown in Fig. 13. It should be noted that the two diffraction grating instruments (DFS-2 and DFS-3) yield a higher quality spectrum than the KS-55 and UF-85 prism instruments with the same dispersion and resolution.

4. Interferometric Instruments

In this group we have Fabry-Perot etalons, permitting observation of interference with a path length difference $(2t)$ of up to 300 mm. The etalons are supplied with a large assortment of plate spacers ranging from 0.3 to 150 mm in thickness. This assortment of spacers allows the etalons to be used for a variety of spectroscopic purposes, from investigation of Raman spectra to studying the structure of separate lines of the heavy elements. The Fabry etalons are made in two variants: 1) for work in thevisible range of the spectrum with the etalon installed inside the ISP-51 spectrograph (Fig. 14) and 2) for investigations in the ultraviolet range with the etalon mounted outside the ISP-22 spectrograph (Fig. 15). Special accessories have been developed for mounting the etalons in and on the said spectrographs; however, these etalons can also be used in conjunction with other spectroscopic instruments. To illustrate the high quality of these etalons, it may be noted that with the 300 mm path difference (150 mm spacer) one can observe the interference pattern for the green krypton line emitted by a krypton tube operated at the temperature of liquid air.

In addition to the Fabry etalons, a few small glass Lummer plates have been produced for use with ISP-51 spectrograph. These Lummer plates are intended exclusively for student laboratory work and have a resolving power of 20,000.

5. Spectroscopic Instruments for Visual Observation

Worthy of first mention in this group is the SP3e portable spectroscope which is issued in two models: a hand model (Fig. 16) and a stand mounted one (Fig. 17). The SP3e is a direct vision instrument with three prisms intended for visual observation of emission and absorption spectra. A special attachment fitting over the entry slit permits direct observation of the absorption spectra of solutions, which makes the spectroscope a very convenient instrument for the selection of suitable absorbing materials, rapid visual inspection and comparison of the absorption of different substances, and numerous other purposes. This instrument is virtually indispensable for any spectroscopic laboratory using different light sources and particularly gas discharge tubes.

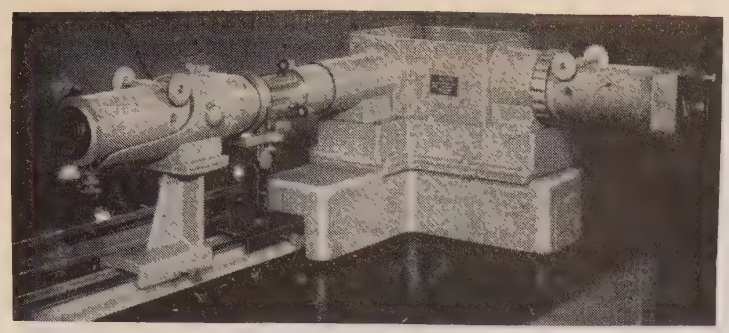

Fig. 14. ISP-51 Spectrograph with Fabry etalon mounted inside the instrument.

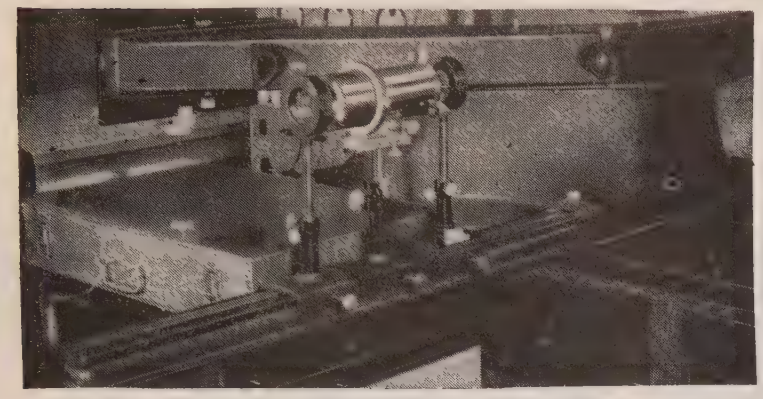

Fig. 15. Fabry etalon for the ultraviolet and its installation outside the ISP-22.

Fig. 16. SP3e Hand spectroscope.

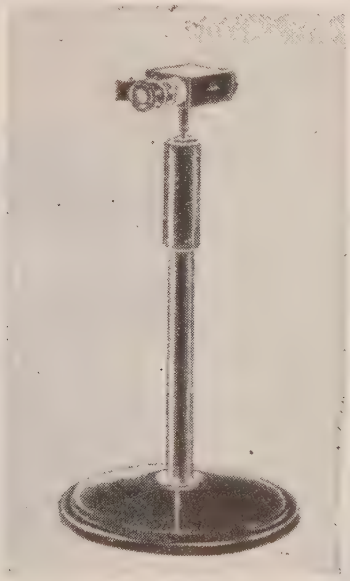

Fig. 17. SP3e Hand spectroscope mounted on stand.

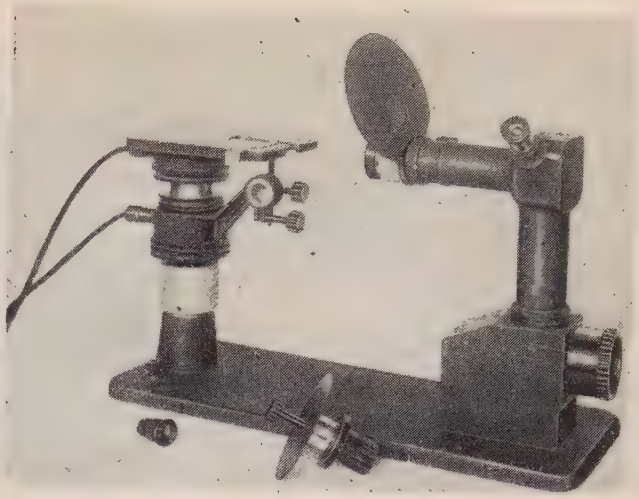

Fig. 18. SL-10 Styloscope.

For a period of years no "styloscopes" and "stylometers" [visual comparators] were manufactured in the USSR. Recently production of the SL-10 styloscope (Fig. 18) was started; this is a small autocollimating spectroscopic instrument, designed for rapid sorting and classification of spectrum lines. The new ST-7 stylometer has an interesting and original optical system. Instead of the polarizing optical system employed in earlier Soviet stylometers, this instrument uses photographic wedges for comparative photometry of spectrum lines. The unique optical system employed permits locating the spectrum lines compared almost next to each other. This obviously increases the accuracy of analysis. The instrument is regularly supplied with the production model IG-2 spark generator[8].

b. Spectrophotometers

The SF-4 spectrophotometer with quartz optics for the visible and ultraviolet regions of the spectrum is

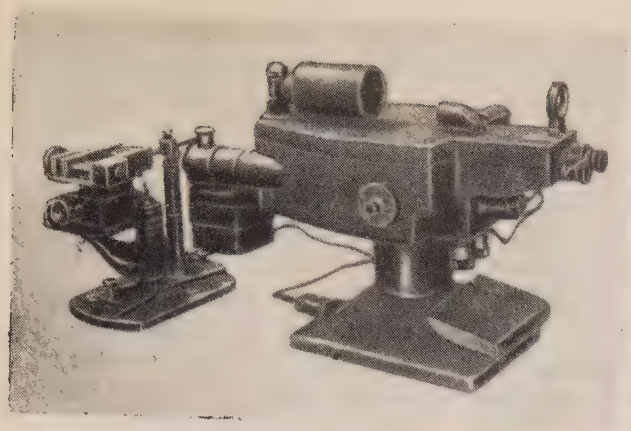

Fig. 19. ST-7 Stylometer.

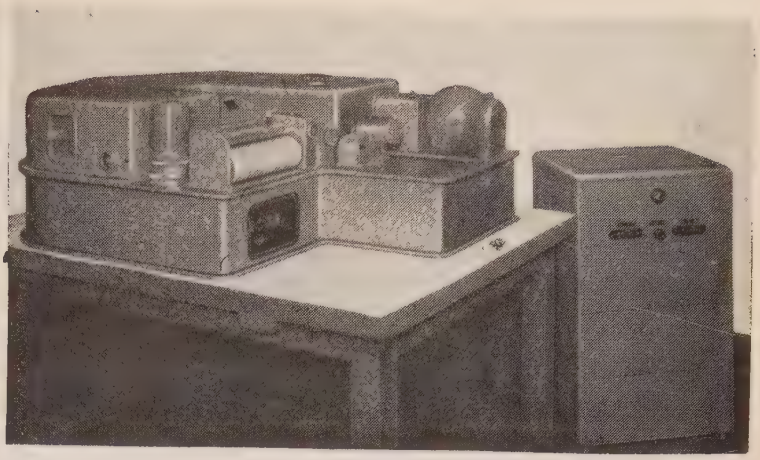

Fig. 20. SF-2 Automatic spectrophotometer.

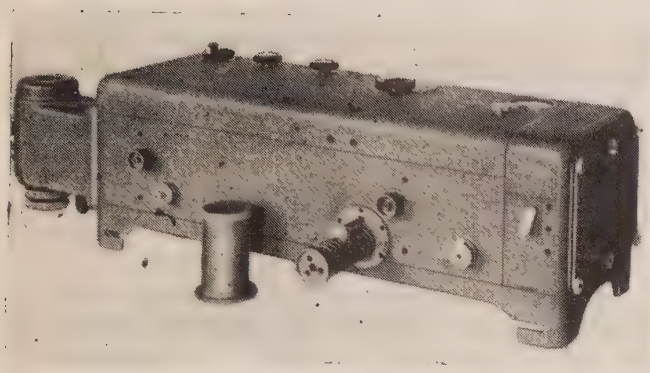

Fig. 21. Simplified spectrophotometer.

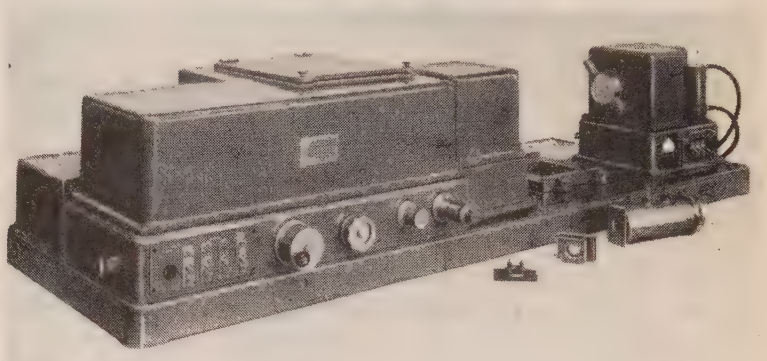

Fig. 22. IKS-6 Infrared spectrometer with high resolving power.

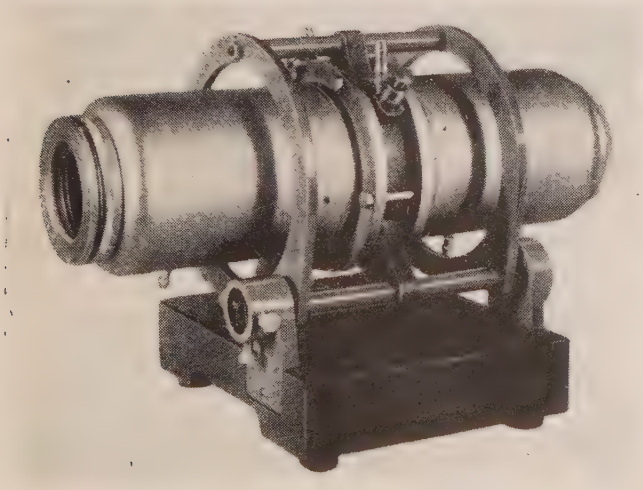

Fig. 23. Gas cell for IKS-6 spectrometer.

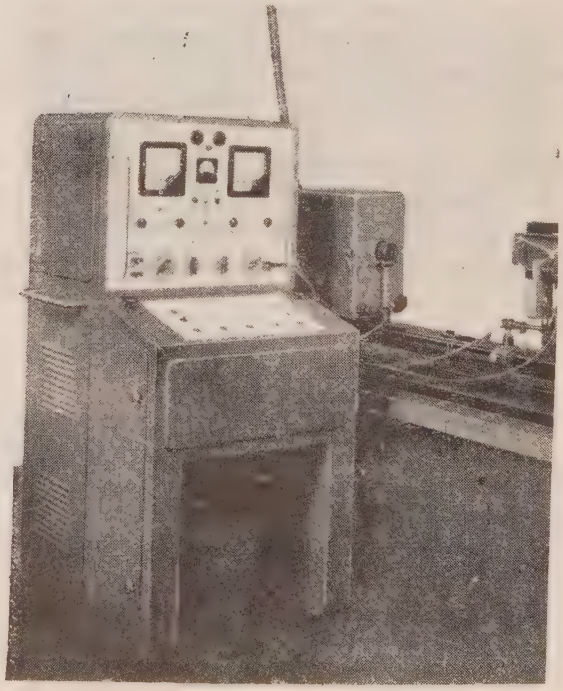

Fig. 24. Special generator with electronic control.

already familiar to many spectroscopists; this instrument is equipped with cesium-antimony and cesium oxide photocells, operating in a single-beam system, with electric compensation by means of a calibrated measuring potentiometer.

A recent addition to this group of instruments is the SF-2 automatic, glass optics spectrophotometer (Fig. 20) designed to record absorption spectra in the visible region directly on paper. For this purpose the instrument employs a special electronic amplification and comparison circuit which automatically gives the absorption in terms of percent of transmission. The instrument will be widely used to measure the reflection and absorption spectra of many substances, particularly dye solutions.

However, the production of such complex precision instruments does not necessarily preclude the manufacture of simpler spectrophotometers which are both cheaper and more versatile. Among the advantages of such simpler instruments as compared with most precision spectrophotometers is that they can be used with high light fluxes and, therefore, permit investigation of more opaque objects. In recent years several types of such simplified spectrophotometers have been developed in the Soviet Union.

One type, based on a focal monochromator[10], is intended for work in the visible and ultraviolet regions of the spectrum. It permits separating out narrow sections of the spectrum (10-15 mμ). The instrument is used with radiation receiving, amplifying and measuring systems similar to those employed with the SF-4 spectrometer. An external view of the instrument is shown in Fig. 21.

Another simplified instrument uses interferometric filters for the visible and near infrared regions and can be employed for the investigation of both transparent and opaque objects. Here, too, the radiation receiving, amplifying and measuring system is analogous to that employed in the SF-4 spectrophotometer. Although at any setting this instrument shows a rather wide section of the spectrum, in view of its simplicity it should find wide application in those branches of the national economy where light absorption methods of analysis are commonly employed, particularly for the inspection and control analysis of mass-produced materials. It may be noted that our instrument industry is aware of the need for the development and production of simplified spectrophotometers.

Finally we might mention the potential usefulness in spectroscopy of the special absorption filters for the ultraviolet suggested by a number of Soviet scientists. The availability of such filters will further the development of special spectroscopic instruments for analytic work in the ultraviolet region[11].

7. Instruments for the Infrared Region

The IKS-11 is an infrared prism spectrograph consisting of a multiple component installation, intended for obtaining the absorption curves of various substances in the spectral region extending to 25 μ. The spectrum is recorded in the form of a trace on photographic paper; the recording unit employs a system of photoelectric-optic amplification developed by Kozyrev[12&13].

In order to be able to produce this instrument it was necessary to solve a series of technological problems connected with grinding off-axis-focus parabolic mirrors and growing large artificial crystals.

These problems were solved and our laboratories now have excellent infrared spectrometers capable of recording the spectra of diverse organic substances. The availability of these instruments facilitates detailed investigation of molecular spectra and the study of the structure of molecules and make it possible to solve many technological control problems encountered in the production of fuels, polymers, synthetic rubber, etc.

In addition to the above instrument, a number of IKS-6 two prism infrared spectrometers with a high resolving power have been produced (Fig. 22). This infrared instrument differs from the IKS-11 as regards its optical system: it employs two prisms with a common base of 200 mm instead of the single 70 mm face prism used in the IKS-11. The highest resolving power is 1.4 cm^{-1} as against 3 cm^{-1} in the IKS-11. The aperture ratio is 1:5.5, i.e., somewhat inferior to that of the IKS-11 (1:4.5).

To meet the needs of infrared spectroscopy and analysis thermostatic absorption cells for liquids and gases have been developed and are now available as prototypes. The cell for liquids is of the expansion type and can be adjusted to provide layers of different thickness, down to some hundredths of a millimeter. The gas absorption cell is to be made in two sizes: one with an overall gas column length of 150 mm, the other with a 300 mm column. The cells will be thermostatically controlled to maintain constant temperatures in the -60^{o} to $+150^{o}C$ range, and are intended primarily for use with the IKS-6 spectrometer. Fig. 23 shows the 300 mm column gas absorption cell.

8. Spectrum Source Generators

Two source generators - the IG-2 spark generator and the DG-1 arc generator - both of which have proved to be reliable units, are now in series production. It may be noted that the DG-1 arc generator, incorporating the original circuit proposed by N. S. Sventitski, is finding ever wider application in spectrum analysis, thanks to the potentialities of its design. This versatile generator can be used for producing different types of arcs, sparks and high-frequency discharges. The spark regime is often used in the analysis for elements whose spectra are difficult to excite; the high-frequency regime is now used in determining the thickness of coatings and for the analysis of materials available only in very small quantities. However, this generator employs a high-frequency ignition system which does not insure sufficiently stable excitation. Accordingly, a number of electronically controlled generators, free of this shortcoming, have recently been developed.

One such special generator, developed at the request of Moscow State University, is shown in Fig. 24. An experimental model has been assembled and is now being tested[13]. This is a universal type generator designed to meet the needs of both research spectroscopists and industrial spectroscopic laboratories. It provides power for different discharge regimes between metallic electrodes, from low intensity arcs to extremely bright flashes of high power. The instrument has a wide range of capacitance and inductance adjustments. The high power (brightest) flashes yield spectra duplicating some of the features of the solar spectrum. For example, a 400 ampere arc flash discharge between copper electrodes gives a well-developed absorption spectrum of neutral and metastable copper atoms as well as of copper ions. This

spectrum stands out clearly against a rather intense continuum.

The generator has provision for flexible control of the instant of discharge; a special circuit permits varying the ignition phase over a wide range. An appropriate scaling circuit makes it possible to obtain uni-directional discharges every cycle, or, if desired, only every second, fourth, eighth, sixteenth, etc. cycle. The experimental model generator is housed in a special air-tight cabinet which meets all the current requirements for modern spectroscopic laboratory equipment. The cabinet both deadens the noise of the discharges and permits exhausting the gaseous discharge products to maintain an atmosphere of constant composition in the discharge region. The high-voltage and high-frequency components of the generator are enclosed in a metal shield inside the cabinet to insure suppression of the high-frequency oscillations of the discharges and eliminate external static and interference. Tests on the model have shown that the generator can provide stable discharge characteristics necessary for high precision quantitative spectrum analysis.

9. Instruments for Studying Spectrograms

1) STL Spectrogram viewing stand. A number of different stands for examining and comparing spectrograms have been produced in the past, but all of them suffered from more or less serious defects. These shortcomings have been largely eliminated in the new STL stand, which can be used for examining plates up to 9 x 24 cm in size. Illumination is provided either by an electric lamp or by daylight. The possibility of using daylight is very important where geological field laboratories are concerned. This stand is illustrated in Fig. 25.

2) MF-4 recording microphotometer. This comparator of original design is based on the production model MF-2 photometer. The designers have skillfully added the recording part to the basic comparator, so that the MF-4 can be used at will either as a recording instrument or as a direct reading comparator (i.e. as a standard MF-2). The recording is accomplished by means of the illuminating lamp and mirror galvanometer used in the standard MF-2. The regular selenium photocell used in the MF-2 was also successfully utilized in the new recording instrument. At first it was feared that the selenium cell would not assure a sufficiently accurate record for measurement purposes. Tests showed, however, that these fears were groundless. It was thought that the selenium cell would cause the null to wander. In fact, a special device was developed to reset the null value at the instant of recording. However, experiments showed that the null matching circuit is sufficiently stable so that no re-setting is necessary. The instrument records microphotograms quite rapidly and produces a satisfactory and accurate trace. Extensive tests of the instrument indicate that it is simple to use and dependable in operation and there can be little doubt that it will find wide acceptance in spectroscopic, x-ray and electron diffraction laboratories[14]. Fig. 26 shows the microphotometer proper, without the motor and lamp voltage stabilizer.

3) A special projection viewer for the detailed study of spectra has also been produced. The instrument is designed to permit widening narrow spectra (for example, star spectra) and minimizing graininess of the image due to the photographic grain of the emulsion. Some time ago Linnik suggested the use of an oscillating objective in spectrum viewing microscopes in order to obviate graininess of the examined

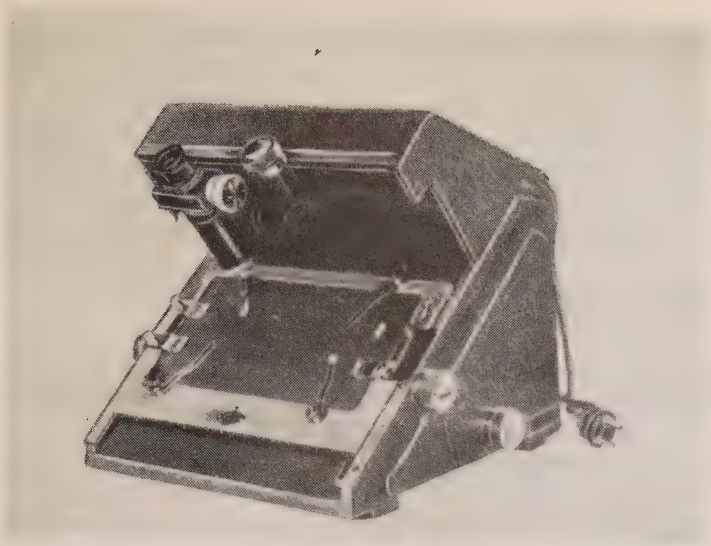

Fig. 25. STL Viewing stand.

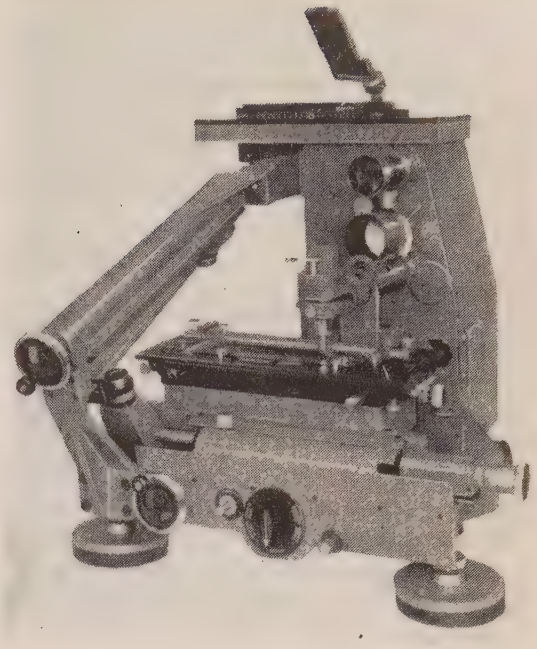

Fig. 26. MF-4 Recording microphotometer (view without motor and voltage stabilizer).

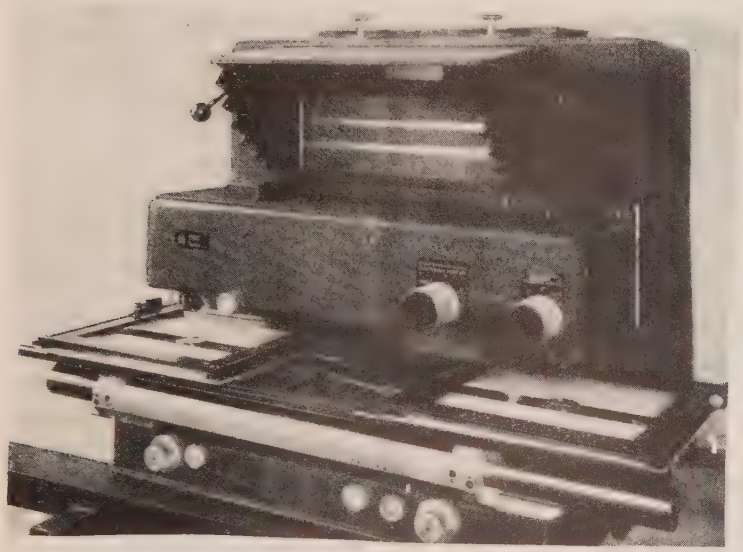

Fig. 27. Projection viewer

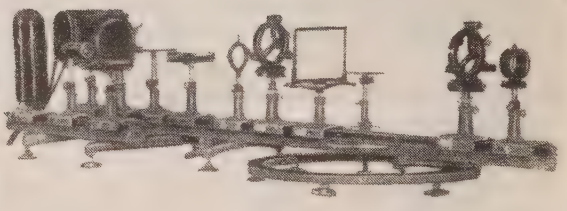

Fig. 29. OSK-1 Spectroscopic bench

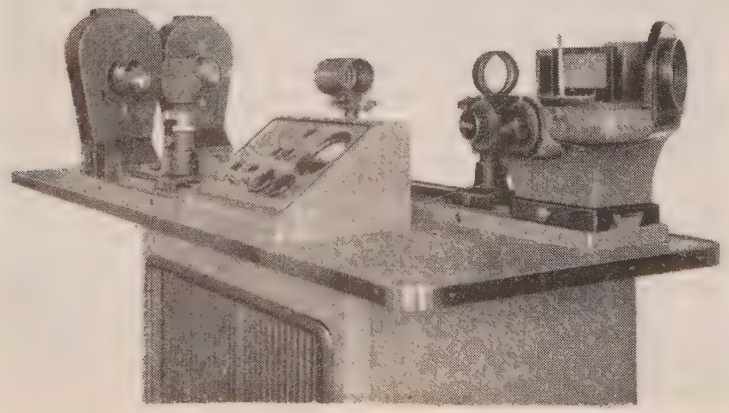

Fig. 28. ISP-74 Spectrum projector

image. Instead of the oscillating objective, however, the designers of this projector introduced a special system of cylindrical lenses which by eliminating the graininess permits greater enlargement and makes it possible to distinguish finer detail in complex spectrophotographs. The optical system also provides for comparison of two different spectrograms (i.e., consists of a dual projection system). An external view of the projection viewer appears in Fig. 27.

10. Demonstration Instruments

It may be objected that the equipment in this group does not belong to the category of true spectroscopic instruments. However, in view of the necessity of training students no one can deny the need for demonstration instruments. Among the instruments in this group we must mention the ISP-74 lecturer's spectrum projector (Fig. 28). This instrument can be used for projecting spectra of different types on a suitable screen from the lecturer's stand. This is a prism instrument employing a modified Wadsworth mounting. The objective lens has a focal length of about 4 meters so that the spectrum is thrown onto a screen at some distance from the instrument. The instrument is the only one of its kind for it can show a continuous spectrum from an incandescent filament and line spectra from an arc between metal electrodes, both in the visible and in the ultraviolet regions. For demonstrating the latter the screen is coated with a fluorescent paint. To permit showing ultraviolet spectra, the entire optical system is made of fused quartz.

Another interesting instrument is the OSK-1 spectroscopic bench, with an assortment of different optical components which can be arranged to illustrate the systems of different spectroscopic instruments: single and multiple prism spectroscopes, diffraction grating spectrometers, etc. This demonstration bench is an innovation in our student laboratories and should prove to be a valuable teaching aid. In addition it can be used to assemble set-ups for testing and experimental purposes. The bench with its accessories arranged at random is shown in Fig. 29.

It is impossible in so brief a report to describe any of the instruments in detail. The purpose of this communication was to summarize systematically the achievements of our Soviet industry during the past three years. It will be noted that our optical instrument industry is now capable of producing a large number of new spectroscopic instruments. Whereas only a few years ago we produced only a few types of instruments which just barely satisfied the basic needs of industrial spectroscopic laboratories and could not at all meet the more exacting requirements of research and scientific institutions, now our Soviet industry has mastered the production of all necessary types of spectroscopic equipment and has, furthermore, gained the experience and know-how that will serve it in good stead in developing and producing even better and more advanced instruments in the future.

It should be noted that during the past three years our Soviet optical industry has designed and produced five times as many new instruments as in its entire history prior to 1952. Such productive growth is truly phenomenal. It bears evidence to the high degree of technological organization attained in the industry as the result of

close collaboration between the workers of science and industry. It is evidence, too, of the great qualitative improvement of its cadres, to the growing skill of the designers, technicians and workers, who have mastered a new field of production in so short a time. We can be certain that this group of new spectroscopic instruments will be supplemented by more improved instruments, instruments which will assure the successful solution of many of the complex and difficult problems facing our country in putting into effect the decisions of the Nineteenth Congress of the Communist Party of the Soviet Union.

Bibliographic References

1. A.V.Iakovleva, I.I.Gromova & I.R.Protas, Izv. (Bulletin) AN SSR, Ser. fiz., 19, 1 (1955).*
2. S.A.Kulikov & A.V.Iakovleva, ibid., 19, 1 (1955).*
3. Ia.S.Bobovich & D.B.Gurevich, ibid., 19, 1 (1955).*
4. T.K.Fal'k, ibid., 19, 1 (1955).*
5. A.I.Ryskin, ibid., 19, 1 (1955).*
6. R.I.Tveriankina, ibid., 19, 1 (1955).*
7. F.M.Gerasimov (this issue, next article).
8. E.L.Berman, Izv. (Bulletin) AN SSR, Ser. fiz., 19, 1 (1955).*
9. V.N.Osipova, ibid., 19, 1 (1955).*
10. A.S.Toporets, Usp. fiz. nauk, 40, 2, 255 (1950).
11. S.N.Andreiev, Zhur. prikl. khim., 25, 2, 205 (1952).
12. S.A.Khrshanovskii, Vestnik (Review), Leningrad State University, 3 (1950).
13. M.I.Demidov, N.N.Ogurtsova & I.V.Podmoshenskii, Izv. (Bulletin) AN SSR, Ser. fiz., 19, 1 (1955).*
14. G.Ia.Kossov, ibid., 19, 1 (1955).*

---

* The next issue of the Bulletin.

* * * * *

SPECTRAL CHARACTERISTICS OF SOVIET DIFFRACTION GRATINGS

- F. M. Gerasimov

At present almost all the types of diffraction gratings used in modern spectroscopy are being produced in the Soviet Union. Gratings are being made with 200, 300, 600 and 1200 lines/mm, with ruled areas ranging from 50 x 50 to 150 x 150 mm. Concave gratings are being made with 1, 1.5, 2, 3, 4 and 6 meter radii of curvature. The gratings are ruled on aluminum over glass and directly on glass.

The present report is concerned with the principal spectral characteristics of domestic (Soviet) gratings. The data cited represent averaged results obtained by different testing methods.

Most of the gratings having 200, 300 and 600 lines/mm produce virtually perfect spectrum lines with truly symmetrical contours in the first and second orders and have a resolving power closely approaching the ideal. The first order spectra of a considerable proportion of the 1200 lines/mm gratings and the second and higher order spectra

of most of the larger size 600 lines/mm gratings show a weak background and false lines in the vicinity of the spectrum lines. Although this does not reduce the resolving power of such gratings, it does make them unsuitable for the investigation of complex structure spectrum lines. The best gratings produce an excellent spectrum in the high orders and have a resolving power of up to 400,000.

A spectrogram of the green and blue (5461 and 4358 A) mercury lines obtained by means of a 150 x 150 mm grating with 600 lines/mm is reproduced under Fig. 13 of the preceding article (see page 336). On the original photograph one can readily distinguish lines only 0.01 A apart.

Reflection coefficients of diffraction gratings

Lines per mm	Spectrum order	Reflection factor at max.	
		Mean	Maximum
600	I	70	80
600	II	55	65
600	III	45	55
1200	I	50	70

The intensity of the Rowland ghosts produced by the 600 lines/mm gratings amounts on the average to 0.1% of the parent line intensity; in the best gratings the intensity may be as little as 0.02%. No Lyman ghosts are observed. The 1200 lines/mm gratings, in addition to the principal spectrum, show very weak secondary peaks located at the same diffraction angles as the odd-order maxima thrown by the 600 lines/mm gratings.

The gratings scatter less light than equivalent prism systems.

Reflection gratings ruled on aluminum coatings yield high concentrations. The direction in which the maximum concentration is thrown varies over a wide range. Data on the mean and maximum reflection factors of the 600 and 1200 lines/mm gratings are summarized in the accompanying table.

The intensity distribution in the regions of high concentration is in reasonably close agreement with the theoretical formulas.

Both the plane and the concave gratings sometimes show focal deviations due to ruling errors. In the case of plane gratings the deviations are usually small and of a random character and can generally be compensated for by adjustment of the focusing system of the spectrograph. In the case of concave gratings the ruling error is usually systematic. The spectrum lines obtained by means of such gratings are focused along a curve deviating somewhat from the Rowland circle. The shift of focus can be eliminated by mounting the grating so that it is tangent to the Rowland circle not at its geometric center but at some other point, selected in accordance with the magnitude of the deviation.

* * * * *

RADIOSPECTROSCOPIC INVESTIGATION OF MOLECULES

- N. A. Irisova

The /full/ report gives data on the equipment for radiospectroscopic investigation of the rotational spectra of molecules, designed and constructed by a group, headed by A. M. Prokhorov, in the Vibration Laboratory of the Physical Institute of the USSR Academy of

Sciences. A brief description of the constructed radiospectroscopes having a sensitivity of $2 \cdot 10^{-8}$ cm^{-1} with a 2 cps pass-band detector is given. By means of these spectroscopes the frequency of absorption lines can be determined with an accuracy of 1 part in 10^6 and the absolute values of the absorption coefficients measured to within 5-10%.

The report also gives results of frequency and intensity measurements of the hyperfine-structure line associated with the $J = 0 \rightarrow 1$ transition of $C^{12}H_3I^{127}$ and $C^{13}H_3I^{127}$ molecules.

Currently the group is studying the structure of a series of organic molecules.

Physical Institute of the
Academy of Sciences of the USSR

* * * * *

ON THE OPTICAL-ACOUSTICAL EFFECT IN THE MICROWAVE REGION

- G. G. Neuimin and O. I. Chernyshevski

The first report on the existence of an acoustical effect in the microwave region, analogous to the optical-acoustical effect in the infrared investigated earlier by Veingerov[1] was published in 1946 by Herschberger[2]. However, no practical application for the effect was found until 1953 when Vasil'ev and Zhabotinski[3] proposed utilizing the optical-acoustical effect to measure microwave power. In the receiver suggested by these investigators a metallized collodion film was to serve as the power absorber. As far as we know the acoustical effect in the centimeter wave region has not been studied until now.

We attempted to observe the effect and to utilize it for the purpose of determining the lifetime of excited states by means of a method similar to that successfully employed by Slobodskaia and Stepanov[4] in the infrared region.

Our set-up consisted of a 3-cm, 10 mw output oscillator and a resonant cavity filled with the absorbing gas (ammonia). The cavity communicated with a second chamber containing a microphone. The high-frequency radiation was modulated at a frequency of about 1.5 kc. The amplified signal from the microphone was applied to a phase detector, designed to compare the phase of the signal with that of the voltage modulating the klystron. We measured the variation of the phase shift of the signal with the pressure of the ammonia and with its concentration in ammonia-air mixtures.

It was found that a phase shift occurs only at certain modulation frequencies and with definite concentrations of ammonia on the ammonia-air mixture. Additional tests established that the observed phase shift is due to purely acoustic factors (i.e. is connected with a phase shift near the acoustic resonance frequency of the cavity) and is not associated with phase displacement due to the finite lifetime of the excited NH_3 molecules. Thus, under the experimental conditions (i.e. $P_{NH_3} \geq 100$ mm Hg) the lifetime of the excited state

associated with the inversion transition of NH_3 molecules must be shorter than 10^{-5} sec, inasmuch as higher lifetime values would have been detected by our set-up. From data in the literature on the breadth of the NH_3 lines under the conditions of our experiment, we deduce that the lifetime of the excited state in question is of the order of 10^{-9} - 10^{-10} sec.

Hence, we conclude that to utilize the proposed method one must either resort to lower ammonia pressures or greatly increase the modulation frequency. At lower ammonia pressures it will be necessary to effect the excitation at exactly the wavelength of the peak of the NH_3 absorption line ($\lambda \simeq 1.25$ cm) since at low pressures the absorption is too low at even slightly lower and higher frequencies. The use of a much higher modulation frequency, on the other hand, will necessitate recording weak ultrasonic oscillations. Hence, both expedients involve considerable experimental difficulties.

References

1. M.L.Veingerov, Doklady AN SSSR, 19, 687 (1938).
2. Herschberger, RCA Review, 7, 422 (1946).
3. G.A.Vasil'ev & M.E.Zhabotinski, Zhur.eksp. i teor.fiz.,24,571 (1953).
4. P.V.Slobodskaia & B.I.Stepanov, Izv. (Bulletin) AN SSSR, Ser. fiz., 12, 565 (1948).

* * * * *

BOND FORCE CONSTANTS AND THE CONFIGURATION OF MOLECULES

- A. I. Kitaigorodski

As we know the values of valence bond angles for coupled atoms can be predicted from general quantum-chemical considerations. While in some cases the observed values for the angles differ very appreciably from the theoretical values, in general the predictions of quantum-chemical theory are fulfilled: the character of the spatial arrangement of atoms (i.e., trigonal, tetrahedral, pyramidal, etc.) is in conformity with the demands of theory. This circumstance suggests a "natural" method of treating the distribution of atoms in a molecule: to regard as "normal" the valence angles predicted by quantum-chemical theory and to attribute deviations from the "normal" values to the interaction between atoms not linked by valence bonds.

Analysis of experimental data on the crystal structure of organic compounds yields sufficiently accurate information on the external form of the molecules, enabling us to assign an effective radius to each constituent atom.

It can also be shown that deviation of the configuration of a molecule from the "normal" is always a consequence of equilibrium of the elastic forces of valence angles and the forces of repulsion between atoms not joined by valence bonds.

The value of the atomic radii and information on the structure of complex molecules can be obtained through x-ray analysis, while

the elastic (bond force) constants can be determined spectroscopically. Assuming that intermolecular forces vary linearly with the deformation of the atoms, we can characterize each atom by a specific coefficient of coercibility.

Thus the successive application of the methods of spectrum and x-ray analysis makes it possible to determine the molecular configuration.

Numerous illustrative examples are available. For instance, let us determine the configuration of the orthodichlorobenzene. Making the simplifying assumption that the Cl-H interaction is very weak as compared to the Cl-Cl interaction, we can write the following equation for bond energy of the chlorine atoms:

$$U = \frac{1}{2}k(\Delta d)^2 + k_1(\Delta\varphi)^2 + k_2(\Delta\theta)^2,$$

where Δd is the reduction of the Cl-Cl distance and $\Delta\varphi$ and $\Delta\theta$ are the angles of deviation of the C-Cl valence bond in the plane of the nucleus and in the plane perpendicular to the nucleus, respectively. Inasmuch as d can readily be expressed in terms of φ and θ, we obtain the condition for the minimum of U in the form of two equations:

$$2\frac{k_1}{k}\varphi - \Delta d\,\frac{\partial d}{\partial\varphi} = 0 \text{ and } 2\frac{k_2}{k}\theta - \Delta d\,\frac{\partial d}{\partial\theta} = 0;$$

from these equations we can easily determine φ and θ and, consequently, Δd when the constants for the molecule are known.

Institute of Elemento-organic Compounds
of the Academy of Sciences of the USSR

* * * * *

ABSORPTION ANISOTROPY OF GYPSUM CRYSTALS IN THE INFRARED

- G. A. Zaitsev and B. S. Neporent

We investigated the anisotropy of infrared absorption of gypsum crystals in the 2 to 10 μ region. The absorption spectra of thin sections of the crystals were obtained by means of a spectrometer with a magnifying attachment in the form of two specular objectives having an aperture of 0.45. The minimal area of the specimens as determined by the characteristics of the spectrometer was 0.2 x 1.5 mm. A selenium-film polarizer was used. We also studied the spectra of reflection from polished sections with an aperture not exceeding 0.1 and an angle of incidence of 4°.

The general form of the absorption spectrum obtained is in agreement with the data of other investigators. The strong absorption band between about 3600 and 3200 cm^{-1} is associated with the valence vibrations of the water of crystallization molecules and overtones of a

number of other vibrations. This band is broadened to some extent, presumably due to the influence of the hydrogen bonds. The absorption is clearly anisotropic (see figure); however, it was impossible to resolve the band into separate components even in the case of a section only 2 μ thick. The bands in the 2300-2100 cm^{-1} interval represent an overtone (2130 cm^{-1}) due to vibration of the SO_4^{--} group and a combination tone (2220 cm^{-1}) of H_2O. The bands near 1675-1615 cm^{-1} are associated with the deformational vibrations of molecules of the crystallization water. The absorption at 1100-1200 cm^{-1} is due to the triply degenerate vibration of the SO_4^{--} ion. The last absorption band also cannot be resolved.

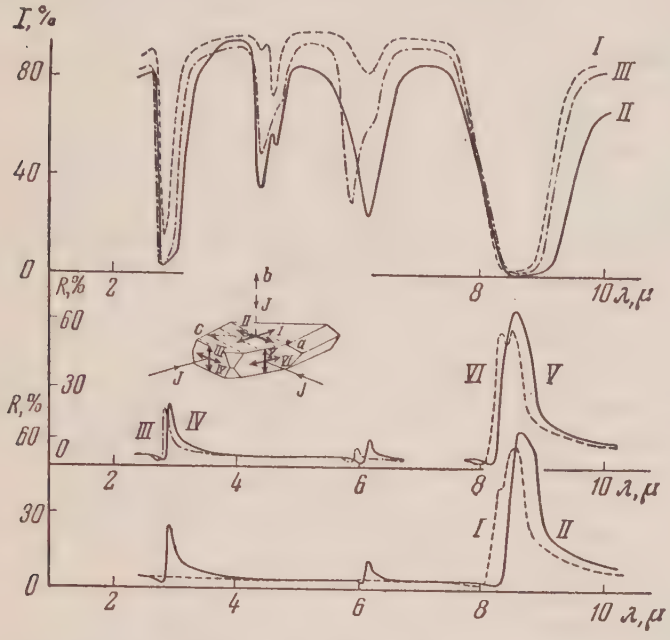

Absorption (I,%) and reflection (R,%) spectra of gypsum crystals.

The reflection spectra of gypsum crystals in polarized light are shown in the lower part of the figure. The distinct bands near 3510 and 3400 cm^{-1}) in the reflection spectra are associated asymmetrical and symmetrical vibrations of the water molecules, polarized at right angles to each other. The band corresponding to the deformational vibrations of water molecules separates into two mutually perpendicular components (1675 and 1615 cm^{-1}). No splitting of the 3510 and 3400 cm^{-1} bands was observed. Further investigation and analysis of the spectrum in this region are indicated. The degenerate valence vibrations of the SO_4^{--} ion in the vicinity of 1100-1200 cm^{-1} split into three components under the influence of the crystal field (1180, 1150 and 1120 cm^{-1}). The observed deviation of these components from strict mutual perpendicularity is apparently due to the asymmetry of the crystal field acting on the ion. The orientation of all the investigated vibrations, as established by polarization measurements, is in good agreement with the generally accepted crystal model proposed by Wooster.

* * * * *

DETERMINATION OF THE OPTICAL ANISOTROPY AND THE FORM OF SOME AROMATIC HYDROCARBON MOLECULES FROM LIGHT SCATTERING IN SOLUTIONS

- M. F. Vuks and I. A. Bogdanov

The purpose of the present investigation, which was essentially a continuation of an earlier study[1 & 2], was to determine, by means of the developed methods, the optical anisotropy and the polarizability tensor of a number of aromatic hydrocarbons, containing two benzene rings, with a view to establishing the form of these molecules and the relative orientation of the benzene rings.

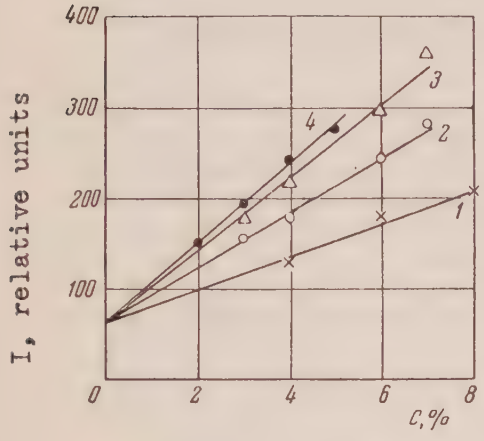

Intensity of anisotropic light scattering of solutions in CCl_4: 1) diphenyl ether, 2) benzophenone, 3) diphenyl, 4)diphenylamine.

The hydrocarbons chosen for investigation were diphenyl, dibenzyl, diphenyl methane, dibenzyl, diphenyl ether, diphenylamine and benzophenone. These compounds were dissolved in carbon tetrachloride, cyclohexane, heptane and benzene in concentrations of 1-8% (up to 15% in benzene); the intensity of the parallel component of the scattered light was measured in each case. The results of measurement for four of the six mentioned compounds in CCl_4 solutions are shown in the accompanying figure, where the horizontal scale is laid off in percent volumetric concentration and the vertical scale is graduated in relative intensities of anisotropic scattering with irradiation by the D-line of Na, the unit intensity being that of the anisotropic scattering by benzene. To convert to the scattering constant R_{an}, the above intensity values must be multiplied by $5.5 \cdot 10^{-6}$. The values of the optical anisotropy γ^2 of the solute molecules were computed by means of the following equation

$$R_{an} = \frac{8\pi^4}{\lambda^4} \cdot \frac{13}{45}\left(\frac{n^2+2}{3}\right)^2 (N'\gamma^2 + N''\gamma_{ef}^2),$$

where n is the index of refraction of the solution, N' is the number of molecules of the solute and N'' the number of molecules of the solvent per cubic centimeter of solution and γ_{ef}^2 is the effective optical anisotropy of the solvent molecules.

It is known that in many cases the molecular polarizability tensor can be calculated by the simple addition of the tensors pertaining to the individual bonds or structural groups. The following data are available for the benzene ring and individual bonds[3 & 4]: Benzene: $\alpha_1 = \alpha_2 = 123.1 \cdot 10^{-25}$; $\alpha_3 = 63.5 \cdot 10^{-25}$; C--H bond: $\alpha_{\parallel} = 7.9 \cdot 10^{-25}$ and $\alpha_{\perp} = 5.8 \cdot 10^{-25}$; C—C bond: $\alpha_{\parallel} = 18.8 \cdot 10^{-25}$ and $\alpha_{\perp} = 0.2 \cdot 10^{-25}$; C=O bond: $\alpha_{\parallel} = 19.9 \cdot 10^{-25}$ and $\alpha_{\perp} = 7.5 \cdot 10^{-25}$. The values indicated for the C—C bond were also assumed for the C—O and C—N bonds. The N—H bond may be assumed to be isotropic: $\alpha = 7.5 \cdot 10^{-25}$.

Results of measurements and calculations of the optical anisotropy, form and principal polarizabilities of molecules

Substance	Mean polarizability from refraction $\alpha \cdot 10^{25}$	Measured optical anisotropy $\gamma^2 \cdot 10^{48}$	Form of molecule	Angle θ between benzene rings	Principal polarizabilities α_X	α_Y	α_Z
Diphenyl	208	160	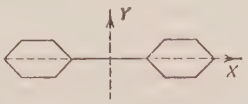	0°	257,3	242,9	123,7
Diphenylmethane	219,5	61	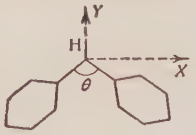	119°	240,5	167,9	249,4
Dibenzyl	238	210		0°	295,4	275,2	144,8
Diphenyl ether	210,5	80	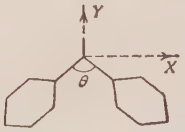	126°	241,0	151,6	239,4
Diphenylamine	226	195	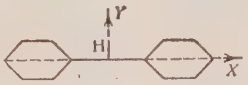	180°	286,8	136,7	253,8
Benzophenone	226	130	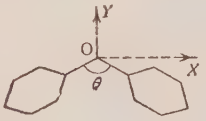	155°	276,7	151,2	250,9

The results of our measurements and computations are summarized in the accompanying table.

"A. A. Zhdanov" Leningrad State University
and
L. M. Kaganovich Military-Transport Academy

References

1. M.F.Vuks, I.A.Bogdanov & V.I.Elfimov, Izv. (Bulletin) AN SSSR, Ser. fiz., 17, 531 (1953).
2. M.F.Vuks & V.I.Elfimov, Doklady AN SSSR, 92, 29 (1952).
3. G. Stewart, Struktura molekul (Molecular Structure), Khar'kov-Kiev, 1937.
4. K. Denbigh, Trans. Faraday Soc., 36, 939 (1940).

* * * * *

THE VIBRATIONAL SPECTRA OF DIPHENYL AND DECA-DEUTERO-DIPHENYL

- G. S. Landsberg, A. I. Shatenshtein, G. V. Peregudov, E. A. Izrailevich and L. A. Novikova

The importance of the investigation of the molecular spectra of deuterium-substituted compounds for the theoretical interpretation and analysis of spectra is generally acknowledged. Until recently, however, the preparation of deuterium-substituted substance was beset with difficulties. Now the results of investigations of the isotope exchange reaction in liquid deutero-ammonia with potassium amide as the catalyst[1 & 2] have opened new possibilities for obtaining deuterium-substituted aromatic hydrocarbons.

Three samples of deca-deutero-diphenyl were prepared by two- and threefold treatment of chemically pure diphenyl with fresh batches of a solution of potassium amide in liquid deutero-ammonia, obtained in a special reactor through the reaction between magnesium nitride and heavy water (99.6% D). The product was purified by solution in benzene, evaporation and twofold vacuum distillation.

A check on the degree of deuterogenation by measuring the ratio of the intensities of the infrared absorption lines of the CH- and CD-vibrations indicated that the deca-deutero-diphenyl content of the samples was not less than 95%.

For obtaining the Raman spectra we developed a special cell, having a volume of 0.5-1.0 cm^3, and a three-lens condenser assuring uniform illumination of the 1 mm high slit with the collimator filled with light[3]. The exposures were made for a period of 12-18 hours, using a spectrograph having an aperture ratio of 4.7 and a plate factor of 18 A/mm[4].

Table 1

Vibrations of diphenyl and deca-deutero-diphenyl molecules.

Vibration class	No. vibr. in given class	Polarization	Selection rules	
			IR	Raman
A_g	11	p	—	+
A_u	4	—	—	—
B_{1g}	10	dp	—	+
B_{1u}	6	p_x	+	—
B_{2g}	6	dp	—	+
B_{2u}	10	p_y	+	—
B_{3g}	3	dp	—	+
B_{3u}	10	p_z	+	—

The infrared absorption spectra in the 2-15 μ region were obtained by means of the two-beam automatic recording spectrometer of the Physical Institute of the USSR Academy[5], equipped with an IKS-11 monochromator. The thickness of the absorption cells was 0.05 to 0.1 mm. In obtaining the infrared spectra as in photographing the Raman spectra the specimens were kept in the liquid state (70°C).

Both the $C_{12}H_{10}$ and the $C_{12}D_{10}$ molecules belong in the $V_h = D_{2h}$ symmetry class. The number and possible types of vibration of diphenyl and deca-deutero-diphenyl molecules are listed in Table 1. The plus sign (+) indicates active (allowed) frequencies in the given spectrum; the minus sign (-) indicates forbidden frequencies.

It will be seen that of the 60 possible modes of vibration, 30 are active in the Raman spectrum (of these 11 are polarized and 19 are depolarized); 26 are active in the absorption spectrum and 4 are forbidden in both spectra.

Table 2

INFRARED AND RAMAN SPECTRA OF $C_{12}H_{10}$ AND $C_{12}D_{10}$

No.	ν, cm⁻¹	Type band	Interpretation	No.	ν, cm⁻¹	Type band	Interpretation
1	2	3	4	1	2	3	4
1	168(1/2)	Raman	Fundmental	1	122(1 1/2)	Raman	Fundamental
2	267(2, d)	"	»	2	248(2, d)	"	»
3	(270)	infrd	»	3	(250)	infrd	»
4	315(1 1/2)	Raman	»	4	300(1 1/2)	Raman	»
5	(370)	infrd	»	5	(300)	infrd	»
6	407(3, d)	Raman	»	6	355(2, d)	Raman	»
7	540(0)	"	»	7	(450)	infrd	»
8	(590)	infrd	»	8	540(0)?	Raman	»
9	612(2 1/2)	Raman	»	9	(560)	infrd	»
10	(670)	infrd	»	10	589(2 1/2)	Raman	»
11	700(vs)	"	»	11	652(4)	"	»
12	740(vs)	"	»	12	(680)	Infrd	»
13	742(4)	Raman	»	13	692(3)	Raman	»
14	780 (1, d)	"	»	14	710(vw)	infrd	250+450
15	780(s)	infrd	»	15	713(0)?	Raman	Fundamental
16	838(1 1/2)	Raman	»	16	750(md)	infrd	»
17	840(md)	infrd	»	17	780(1/2)	Raman	»
18	897(0)?	Raman	»	18	790(md)	infrd	»
19	910(md)	infrd	»	19	820(vs)	"	»
20	965(1/2)	Raman	»	20	835(1/2)	Raman	»
21	970(w)	infrd	»	21	840(1/2)	"	»
22	990(md)	"	267+700	22	840(s)	infrd	»
23	1010(s)	"	Fundmental	23	870(4)	Raman	»
24	1003(8)	Raman	»	24	880(w)	infrd	240+680
25	1032(4)	Raman	»	25	920(md)	"	Fundamental
26	1040(md)	infrd	»	26	948(w)	"	652+300
27	1070(c.)	"	»	27	960(10)	Raman	Fundamental
28	1092(0)	Raman	»	28	960(w)	infrd	650+300
29	1100(vw)	infrd	652+450	29	980(s)	"	Fundamental
30	1120(vw)	infrd	355+750	30	1010(w)	"	352+680
31	1156(2, d)	Raman	Fundmntl	31	1070(0)?	Raman	Fundamental
32	1160(md.)	infrd	»	32	1100(vw)	infrd	652+450
33	1185(1 1/2)	Raman	»	33	1120(vw)	"	352+750
34	1180(md)	infrd	»	34	1188(8)	Raman	Fundamental
35	1125(1, d)	Raman	2×612	35	1200(w)	infrd	»
36	1270(w)	infrd	612+670	36	1260(md)	"	»
37	1280(10, d)	Raman	Fundmentl	37	1320(s)	"	»
38	1287(w)	infrd	1003+270	38	1345(0)	Raman	»
39	1326(0)?	Raman	Fundmentl	39	1350(vs)	infrd	»
40	1310(cp.)	infrd	»	40	1380(s)	"	»
41	1330(cp.)	infrd	»	41	1410(md)	"	960+450
42	1380(md)	infrd	»	42	1412(6)	Raman	Fundamental
43	1430(vw)	"	»	43	1440(md)	infrd	»
44	1452(0)	Raman	»	44	1530(md)	"	»
45	1480(vs)	infrd	»	45	1540(md)	"	»
46	1504(4)	Raman	»	46	1566(8, d)	Raman	»
47	1560(s)	infrd	»	47	1574(10)	"	»
48	1580(s)	"	»	48	1580(s)	infrd	»
49	1592(6)	Raman	»	49	1610(md)	infrd	»
50	1611(8)	"	»	50	1640(vw)	"	960+680
51	1655(w)	infrd	1003+670	51	1690(vw)	"	960+750
52	1748(md)	"	1003+740	52	1870(vw)	"	1190+680
53	1795(md)	"	1003+780	53	2220(vs)	"	Fundamental
54	1886(md)	"	1280+590	54	2260(vs)	"	»
55	1953(md)	"	1280+670	55	2270(vs)	"	»
56	2617(vs)	"	1611+1010	56	2272(3)	Raman	»
57	3000(vs)	"	Fundmentl	57	2280(2)	"	»
58	3020(vs)	"	Fundmentl	58	2297(3)	"	Fundamental
59	3060(3.dbl)	Raman	»	59	2400(vw)	infrd	1570+820
60	3900(vw)	infrd	3060+840	60	2840(vw)	"	1412+1440
61	4590(w)	"	3060+1560	61	3020(vw)	"	2270+560
				62	3300(vw)	"	1570+1580
				63	4380(vw)	"	2270+2260

Note:

The frequency values given in parentheses in the "ν, cm⁻¹" column are computed from the component tones. The figures in parentheses following Raman spectra frequencies are intensities evaluated visually in the ten point scale; d = diffuse band, dbl = double line. In the case of infrared spectra vs = very strong, s = strong, md = median, w = weak, vw = very weak.

We observed 26 frequencies in the Raman spectrum of diphenyl and 23 frequencies in that of deca-deutero-diphenyl.

In the absorption spectrum in the 2 to 15 μ interval we detected 37 frequencies for $C_{12}H_{10}$ and 40 frequencies for $C_{12}D_{10}$.

For preliminary separation of the fundamental frequencies it was assumed that all Raman spectrum lines are associated with fundamentals and only the infrared bands comprise component frequencies.

In view of the fact that the $C_{12}H_{10}$ and $C_{12}D_{10}$ molecules have centers of symmetry, only component frequencies of the type ($\nu_{Raman} + \nu_{i.r.}$) and even tones of the absorption spectrum can be active in the infrared absorption spectrum. This circumstance facilitated identifying the fundamental infrared frequencies (see Table 2). It must be admitted that this method of identifying the fundamentals is not entirely free of error; hence our classification must be regarded as only tentative.

We are extending our investigation of the spectra of $C_{12}H_{10}$ and $C_{12}D_{10}$ into the 15-25 μ region and are studying the degree of depolarization of the Raman spectrum lines. The additional information will enable us to verify and refine the above results.

"P. N. Lebedev" Physical Institute of
the Academy of Sciences of the USSR
and
"L. Ia. Karpov" Physico-Chemical Institute

References

1. A.I.Shatenshtein, Doklady AN SSSR, 40, 1029 (1950).
2. A.I.Shatenshtein & E.A.Izrailevich, Doklady AN SSSR, 94, 941 (1954).
3. S.G.Rautian, Zhur. eksp. i teor. fiz., 27, 5(II), 625 (1954).
4. M.L.Sosinski, Izv. (Bulletin) AN SSSR,Ser.fiz., 17, 621 (1953).
5. V.I.Malyshev, M.N.Markov & A.A.Shubin, Izv. (Bulletin) AN SSSR, Ser. fiz., 17, 654 (1953).

* * * * *

THE VIBRATIONAL SPECTRA AND STRUCTURE OF DIBORANE (B_2H_6)

- L. M. Sverdlov and I. N. Zaitseva

A number of authors have proposed an ethene-like model for diborane [boroethane] B_2H_6: two boron atoms and four hydrogen atoms in one plane and the remaining two hydrogen atoms at equal distances from this plane on a line perpendicular to it and passing through the center of the B—B bond.

We calculated the normal vibration frequencies and the potential (bond) energy constants for diborane, using El'iashevich's method. In the case of diborane there are 18 normal vibrations. In computing the kinematic coefficients we used the following geometric parameters: r(B—H) = 1.18 A, r(B—H') = 1.39 A, ∠HBH = 120° and ∠HBH' = 100°. We made use of the frequencies of the isotopic molecules $B_2^{11}H_6$, $B_2^{10}H_6$

Interpretation of the vibrational spectra of diborane and its isotope-substituted analogues

Coordinates	Symmetry	$B_2^{11}H_6$		$B_2^{10}H_6$		$B_2^{10}D_6$		$B_2^{10}D_2H_4$	$B_2^{10}H_2D_4$
		Obs.	Comp.	Obs.	Comp.	Obs.	Comp.	Obs.	Comp.
q	A_g	2524	2518		2524	1860	1859	2524	1842
q'	A_g	2104	2078		2083	1511	1525	1543	2093
α	A_g	1180	1181		1188	929	937	1188	951
Q	A_g	794	791	820	820	726	702	791	715
α'	A_u	829	829	829	829	592	593	829	593
q'	B_{2g}	1747	1742	—	1746	1273	1284	1300	1730
α'	B_{2g}	1035	1035	1044	1054	870	871	1053	876
q	B_{2u}	2612	2609	2625	2626	1999	2003	2626	2003
β	B_{2u}	950	953	—	954	705	694	953	695
α'	B_{2u}	368	372	368	373	262	273	276	369
q	B_{1g}	2591	2582	—	2608	1980	2000	2608	2000
α'	B_{1g}	920	918	930	943	740	755	943	755
q'	B_{1u}	1915	1929	1920	1938	1465	1455	1456	1938
α'	B_{1u}	973	965	977	972	728	736	961	747
α'	B_{3g}	1012	1015		1015	730	726	839	924
q	B_{3u}	2525	2526	2528	2531	1845	1844	2531	1853
q'	B_{3u}	1602	1607	1606	1613	1205	1195	1200	1607
α	B_{3u}	1177	1171	1181	1178	881	883	1176	888

and $B_2^{10}D_2$ for determining the 33 independent force coefficients by the method of the variation of constants. The roots of the secular equations were computed by the iteration method of L. Maiants [Mainz?]. The results of our calculations are given in the accompanying table; it will be seen that the resultant interpretation of the vibrational spectra is correct. It may, therefore, be concluded that the ethene model on which the analysis was based is validated. In addition to the force coefficients we also evaluated the system of the "effect" coefficients of diborane, which characterize the force field of the molecule more fully. The force field of the diborane molecule has certain distinctive features: a comparison of the "effect" coefficients of the BH bonds shows that the internal B---H linkage is only half as strong as the external B-H bond. In contrast to the relatively great strength of the H'BB and BH'B angles, that of the HBH' angles is low; there also appears to be very strong interaction between the angles of the latter type.

"I. G. Chernyshevski" Saratov State University

* * * * *

THE FINE STRUCTURE OF FLUORESCENCE SPECTRA OF AROMATIC HYDROCARBONS IN FROZEN SOLUTIONS

- E. V. Shpol'ski and L. A. Klimova

It was shown in an earlier communication[1] that the aromatic hydrocarbon coronene, consisting of seven condensed rings, exhibits in hexane and heptane solutions frozen at 70°C a striking fine structure whose characteristics ($\Delta\nu$ and intensity distribution) depend on the solvent. In the present investigation the earlier results were confirmed and the observations extended to include 3,4-benzopyrene and pyrene in addition to coronene as the solutes and normal saturated hydrocarbons ranging from hexane through nonane as the solvents.

Coronene. Three groups of lines are observed in all the solvents used:

a) Intense, sharp doublets with a rather stable value of $\Delta\nu$: in going from the light to the heavier solvents, $\Delta\nu$ consistently decreases from 86 cm^{-1} in the case of hexane to 44 cm^{-1} in the case of nonone; the short-wave components of the doublets remain stationary while the long-wave components shift towards them.

b) A large number of weak, close lines, with a separation on the order of 20 cm^{-1}.

c) A region of persistent emission at 19,000 cm^{-1} and lower frequencies. In this region the spectrum in oil solutions shows pronounced triplets; in normal saturated hydrocarbons - hexane and heptane - each of the narrow bands of the triplet is clearly separated into three components spaced 60 cm^{-1} apart; in octane and nonane only two components - the same $\Delta\nu$ apart - are observed.

3,4-Benzopyrene. The fluorescence spectrum of solutions in mineral oil and in benzene consists of two systems of double bands of alternating intensity and some 100-150 cm^{-1} broad each[2]. In normal saturated paraffins these bands split into components some 20-40 cm^{-1} distant from each other.

An analogous picture is observed in the case of pyrene.

Inasmuch as in the case of coronene the position of the short-wave components of the bright doublets does not change for different solvents, while the long-wave component is displaced towards the short-wave one (i.e., the separation decreases) as the weight of the solvent molecule increases, it may be assumed that these long-wave components are produced as the result of the excitation of slow vibrations of the solvent lattice (Grossov's frequencies) at the expense of part of the energy of the emitted photon. If this is the case, the intensity distribution between the components of the multiplet should serve as measure of the probability of transfer of part of the photon energy to the lattice of the solvent.

V. I. Lenin Moscow Pedagogical Institute

References

1. E.V.Shpol'ski, A.A.Il'ina & L.A.Klimova, Doklady AN SSSR,87, 935 (1952).
2. E.V.Shpol'ski & A.A.Il'ina, Izv.(Bulletin) AN SSSR,Ser.fiz.,15,585 (1951).

* * * * *

INFLUENCE OF THE SURROUNDING MEDIUM AND THE VIBRATIONAL ENERGY LEVEL OF THE MOLECULES ON THE CONTINUOUS SPECTRA OF ORGANIC COMPOUNDS

- B. S. Neporent, N. A. Borisevich, V. P. Klotchkov and O. A. Motovilov

In recent investigations[1], devoted to elucidation of the mechanism of the formation of continuous spectra of complex aromatic compounds and the effect of various factors on such spectra, the authors established that the effect of the solvent does not extend to altering molecular interactions but is limited to displacement of the spectra of the investigated molecules. The purpose of the present investigation was to trace the changes in the spectra incident to the addition of an extraneous gas or vapor to the vapor of the investigated substance and the gradual increase in the concentration of the former through the critical point to the liquid state.

The investigated substances were 3-aminophthalimide and 3,6-tertamethyl-diaminophthalimide. The former is characterized by modulation spectra; the latter, by attenutation spectra. Ethyl ether and hexane were selected as the extraneous substances for the experiments.

We investigated the effect of the reserve of vibrational energy on the shape of the spectra of the investigated molecules and determined the limiting conditions of fluorescence spectrum excitation (i.e., conditions under which no excitation occurs).

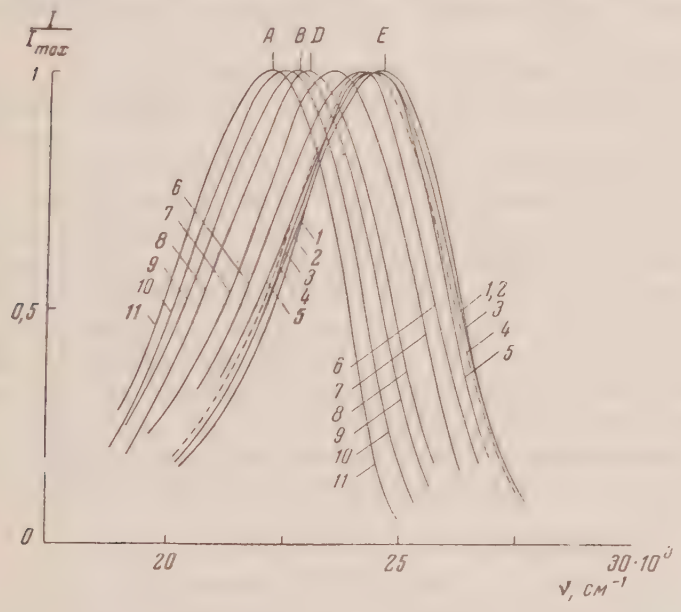

Variation of the position of the peak of the continuous fluorescence spectrum of 3-aminophthalimide in mixtures with ethyl ether with the concentration of the ether (see accompanying table).

We found that the fluorescence spectra of the investigated compounds shift gradually to the side of lower frequencies as the concentration of the extraneous substance increases and the substance undergoes transformation from the gaseous to the liquid phase. (See accompanying figure and table for the behavior of the 3-aminophthalimide-ethyl ether system.)

The displacement of the levels depends solely on the concentration of the extraneous substance and is independent of its state of aggregation. Change in the spectrum begin to be apparent at ethyl ether concentrations of only a few hundred millimeters Hg. The spectrum shifts without noticeable alteration of the relative band widths, except for minor broadening in two transition regions: 1) at very low concentrations of the extraneous gas and 2) near the critical point of the ether.

Characteristics of the continuous fluorescence spectra of 3-aminophthanimide in mixtures with ethyl ether

No. of curve in figure	Aggregate state of ether	t, °C	Concentrat. of ether 10^{20} mol/cm³	Width of band $\Delta\nu$, cm^{-1}	Location of peak ν_{max}, cm^{-1}
1(E)	—	220	0,00	4100	24650
2	Vapor	220	0,08	4200	24600
3	»	220	0,15	4200	24450
4	»	220	0,20	4300	24300
5	»	220	0,48	4200	24500
6	»	220	1,20	4250	24150
7	»	220	4,75	4250	23600
8(D)	Critical state	220	16,5	4200	23050
			21,5	—	—
		194			
9(B)	Liquid	190	28,5	4300	22850
10	»	100	49,6	4050	22600
11(A)	»	20	58,0	4000	22300

In the first case the broadening is due to the fact that at low concentrations the investigated molecules are in various states of interaction with the ether molecules. The effect is neutralized at ether concentrations of only $3.5 \cdot 10^{19}$ molecules per cm^3 (1000 mm Hg). Thus collisions between the molecules of the investigated substance and the molecules of the extraneous substance produce an appreciable effect and, apparently, occur over some more or less prolonged interval.

In the second case the band broadening is presumably due to fluctuations of the ether density in the vicinity of the critical state.

The results obtained confirm our observation that the addition of extraneous substances primarily affects the location of the electron energy levels of the investigated molecules. Interaction between molecules, causing displacement of the levels, is due mainly to dispersional forces. We have elucidated the nature of these interactions. The noted absence of a sudden change in the spectra incident to passing through the critical point is in conformity with the results reported by other investigators. Comparison of our results with those of other authors indicates that the influence of extraneous molecules on the molecules of aromatic compounds is enhanced by the introduction of substituent groups into such compounds.

References

1. B.S.Neporent, Zhur. eksp. i teor. fiz., 21, 172 (1951).
2. B.S.Neporent, Izv. (Bulletin) AN SSSR, Ser.fiz., 15, 533 (1951)
3. B.S.Neporent, V.V.Zelinski & V.P.Klochkov, Doklady AN SSSR,92, 927 (1953).

* * * * *

ANOMALOUS LIGHT DISPERSION IN SOLUTIONS OF COMPLEX ORGANIC COMPOUNDS *

- I.S.Gorban' & A.A.Shishlovski

To investigate dispersion in the region of absorption the present authors used the method employed by Rozhdestvenski in studying dispersion in metal vapors, consisting of crossing the dispersion of a Rayleigh type interferometer with that of a spectroscope. The objects of the investigation were solutions of complex organic compounds of the dyestuff group comprising fluorescein, erythrosin, fuchsine, cyanine, rhodamine-B, etc., all having "simple" absorption bands in the visible region of the spectrum.

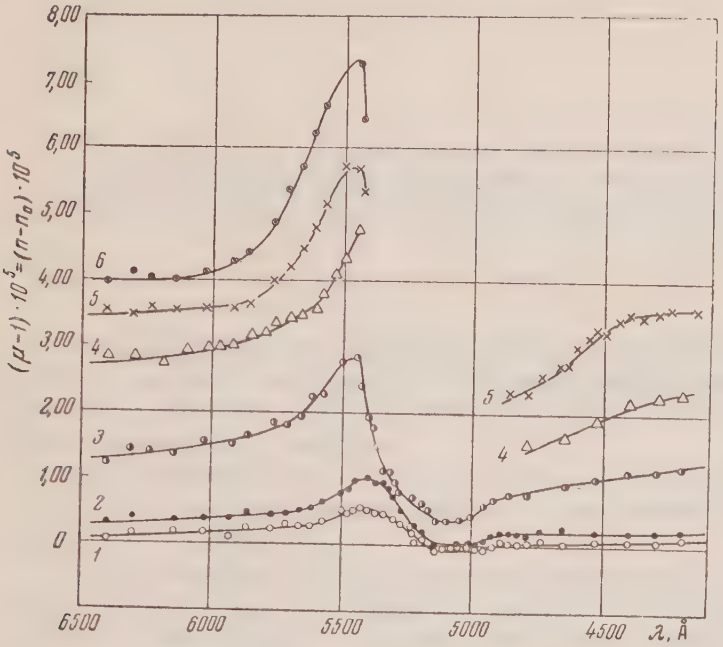

System of dispersion curves for a series of aqueous solutions of erythrosin (iodeosin): 1) $5\cdot10^{-6}$ gm/cm^3, 2) $1\cdot10^{-5}$gm/cm^3, 3) $2.5\cdot10^{-5}$ gm/cm^3, 4) $5\cdot10^{-5}$ gm/cm^3, 5) $6.67\cdot10^{-5}$ gm/cm^3 and 6) $8.11\cdot10^{-5}$ gm/cm^3

It developed that in contrast to the case of vapors, characterized by line absorption spectra, the dispersion curves of the investigated solutions of complex organic compounds exhibit asymmetry of the "simple" absorption bands (see figure), in that the maxima of the dispersion lines are sharper and more pronounced than the corresponding minima. This is intimately connected with the asymmetry of the absorption curves in which the curve falls off more slowly on the shortwave side of the peak than on the side of long waves. In cases where there is a more or less pronounced subsidiary maximum on the shortwave side of the main peak, the minimum of the dispersion curve becomes even less pronounced and in some instances is entirely absent.

Comparison of the experimental results with the theory of Davydov[1] showed that shape of the dispersion curves of the investigated solutions on the long-wave side of the absorption peak - from the peak out to the maximum of the dispersion curve - is described with good accuracy by a hyperbolic function. This, according to Davydov, is indicative of weak interaction between the molecules of the solute with the solvent. Attempts to fit the experimental curve to the Gaussian type error curve derived by Davydov for the case of strong interaction of the solute molecules with the solvent in a relatively wide wavelength interval, proved vain.

Investigation of the concentration-dependence of the indices of refraction showed that at low concentrations (just as in vapors) the variation is approximately linear, which is in accord with Davydov's theory.

The authors succeeded in developing a new procedure for quantitative dispersion analysis of multiple-component liquid solutions on the basis of their investigation of the concentration-dependence of the dispersion curves (which

---

*For the full report see Trudy fiz. fakul'teta (Proceedings of the Physics Department) of Kiev State University, 10 (1955).

within the bounds of certain spectral regions have a different shape peculiar to each substance) and direct experimental proof that the concentration-dependence is little affected by a number of solvents.

Tests of the developed procedure in the visible range of the spectrum, involving analysis of three-components solutions of certain hydrocarbons (artificially prepared benzine fractions), yielded promising results.

Physics Department of Kiev State University

Reference

1. A.S.Davydov, Izv. (Bulletin) AN SSSR, Ser. fiz.,17,523 (1953).

* * * * * * *

THE METHOD OF CONCENTRATIONAL OPTICAL FUNCTIONS AS A PHYSICO-CHEMICAL ANALYTIC METHOD IN THE PRESENCE OF REVERSIBLE CHEMICAL REACTIONS*

- A.A.Shishlovski

The systematic investigation of solutions of luminescent electrolyte salts of heavy metals carried out by the author and his colleagues led to the development of a simple optical procedure for the determination of the composition of ion association products.

In principle the method is based on analysis of the functional dependence of certain optical properties of the solution on the concentration of its formative components.

For purposes of analysis we must select optical properties such as luminescence, absorption, refraction and the like that are specific to the forming chemical compounds. In addition these optical properties must vary linearly with the concentration, i.e., must be additive quantities.

Analysis is carried out on the assumption that the relation between the concentration of the formative components of the solution, A and B, and the concentration of the product of their reaction AB in the case of reversible reactions of the type $nA \pm mB \rightleftarrows A_nB_m$ is given by an expression of the form

$$C_A^n \, C_B^m = \alpha \, C_{A_nB_m}$$

(familiar for binary solutions).

Obviously given the appropriate experimental data one can readily compute the proportions n and m of the components A and B from the above expression. To obtain the requisite data we provide conditions under which the concentration of one of the components remains constant while that of the other varies and vice versa. From the nature of the concentrational function obtained as a result one can evaluate the number of elements /parts?/ of the given component, entering into the composition of the compounds formed.

The method of concentrational optical functions is applicable in cases where the optical properties utilized vary only quantitatively but remain qualitatively unaltered.

Our full report also gives examples of the application of the method to other cases, for instance, in the presence of photochemical reactions and where

---

*For the full report see Trudy fiz. fakul'teta (Proceedings of the Physical Department) of Kiev State University, 8 (1954).

the equilibrium of the system is disturbed by changes in the temperature of the solution.

Physics Department of Kiev State University

References

1. B.E.Gordon & A.A.Shishlovski, Zhur. fiz. khim., 14, 1419 (1940).
2. M.U.Belyi, I.I.Kondilenko & A.A.Shishlovski in "Sbornik" (Symposium) dedicated to the memory of S.I.Vavilov, Pub. AN SSSR, M.-L. 1952.
3. I.I.Kondilenko & A.A.Shishlovski, Doklady AN SSSR, 35, 8 (1942).

* * * * * * *

METHODS OF INVESTIGATING THE BREADTH OF RAMAN SPECTRUM LINES

- P.A.Bazhulin, S.G.Rautian, A.I.Sokolovskaia & M.M.Sushchinski

In the present report we summarize the results of our investigation of methods of determining the breadth and shape of Raman spectrum lines and give some specific data obtained for certain lines by means of a spectograph.

It is common knowledge that in studying spectrum lines one must take into account a number of factors that may influence the breadth and shape of the lines. Such distorting factors include diffraction at the diaphragm aperture, defects in the optical system, the finite width of the slit and the resolving power of the photographic emulsion. In the case of Raman scattering an added factor is the breadth of the exciting line.

The distorting effect of each of the above mentioned factors depends not only on the width but also on the form of the corresponding instrumental functions as well as on the shape of the observed line. In investigating the breadth and shape of Raman lines it is difficult to allow for the influence of each of these factors individually. However, in practice it is not necessary to take account of these factors separately: in order to eliminate the influence of the distorting factors and determine the true shape of a Raman spectrum line from its observed shape it is sufficient to have data characterizing the observed shape of the exciting line.[1] Hence in our investigation in addition to measuring the breadth and shape of the Raman spectrum lines we also studied the observed shape of the exciting lines. The resultant data was used to determine the true breadths and shapes of the Raman lines from their observed shapes.

The measurements were made with a V-III three-prism spectrograph having a linear /reciprocal/ dispersion of about 56 A/mm in the vicinity of the 4358 A line. The results of measurement for a number of Raman spectrum lines are summarized in the accompanying table. Analysis of the line shapes showed that, within the limits of the experimental error, all the lines are described by the dispersion curve.

The data on the breadth of Raman spectrum lines obtained for a wide range of values was used to verify the validity of the effective line breadth method proposed in an earlier communication.[2]

In order to establish the correlation between the values obtained by the method of effective line breadths (using values of I_0 from Ref. 3) and the results of direct measurements of δ, we compared the corresponding values for a number of lines. We found that the relationship between δ_{eff} and δ (when $\delta_{eff} > 2$) is described by the equation

$$\delta = 3.4(\delta_{eff} - 1.4).$$

Breadth of Raman Spectrum Lines

Substance	$\Delta\nu, cm^{-1}$	I_∞	δ, cm^{-1}	I_o ISP-51	δ_{eff}, cm^{-1}	δ_{comp}, cm^{-1}
Toluene	521	210	3,2	100	2,1	2,3
	1031	230	2,0	130	1,8	1,8
	1211	260	3,4	120	2,2	2,7
	1605	310	6,5	85	3,6	7,5
Cyclohexane	802	500	2,0	250	2,0	2,0
	1029	480	10	105	4,6	11
	1267	440	11	90	4,9	12
	1445	470	12	85	5,5	14
Cyclopentane	889	550	9	150	3,7	8
	1031	270	20	44	6,2	16
	1449	300	17	42	7,2	19
Cyclopentene	900	350	5,2	140	2,5	3,7
	1108	460	6,6	130	3,5	7,0
	1614	380	3,2	150	2,5	3,7
Methylcyclohexane	770	300	3,2	115	2,6	4,0

The values of the line breadth computed using this equation are shown in the last column of the table (δ_{comp}). As may be seen the divergence between the directly measured line breadths and the values obtained indirectly by calculation through δ_{eff} does not exceed the limits of the measurement error.

"P.N.Lebedev" Physics Institute
of the Academy of Sciences

References

1. M.M.Sushchinski, Zhur. eksp. i teor. fiz., 25, 87 (1953).
2. M.M.Sushchinski, Izv. (Bulletin) AN SSSR, Ser. fiz., 14, 387 (1950) & 17, 608 (1953); Zhur. eksp. i teor. fiz., 22, 765 (1952).
3. P.A.Bazhulin et al. Izv. AN SSSR, Otd. khim. nauk, 1, 14 (1941); 2, 198 (1943); 1, 7 (1946); 6, 480 (1949); 5, 501 (1950); P.A.Bazhurin & Kh.E.Sterin, Izv. (Bulletin) AN SSSR, Ser. fiz., 11, 456 (1947).

* * * * * * *

ALLOWING FOR THE DISTORTING EFFECT OF THE OPTICAL SYSTEM OF THE MONOCHROMATOR ON THE OBSERVED SHAPE OF THE SPECTRUM LINE

- I.V.Peisakhson

The finite width of the monochromator slit, diffraction at the edges of the light beam and aberration in the optical system all contribute to distortion of the results of spectrophotometric measurements. Hence the experimentally observed line contours do not represent the true spectral distribution of the energy entering the instrument.

Let $F(x)$ be the function describing the observed line (where x is the measured distance, in wave numbers, from some fixed reference point on the line contour). The problem of finding the function $f(x)$ describing the true line contour is reduced to the successive solution of two integral equations. When

the widths of the entry and exit slits of the monochromator are equal, the solution may be obtained in the form of an infinite series:

$$f(x) = F(x) - F^{(II)}(x)\frac{(\Delta\nu)^2}{12} + F^{(IV)}(x)\frac{(\Delta\nu)^4}{240} - \ldots, \qquad (1)$$

where $\Delta\nu$ is the effective spectral width of the slits.

When the slit width is greater than normal and exceeds the size of the aberrational diffusion spot in a point image, the value of $\Delta\nu$ can be found from the relationship:

$$(\Delta\nu)^2 = s^2 + s_0^2, \qquad (2)$$

where s is the width of the monochromator slits and s_0 is the normal width of the slits (both expressed in wave numbers).

The series (1) converges in the same interval as the power series of the function F(x). Calculations show that when the effective spectral width of the slits is of the same order of magnitude as the true half-breadth (breadth at half-height) of the spectrum line it is sufficient to take only the first three terms to obtain the value of f(x) within the limits of accuracy of conventional photometric measurements.

Thus knowing the analytic expression F(x) for the observed contour of a spectrum line and computing its even derivatives $F^{II}(x)$, $F^{IV}(x)$, etc. (or differentiating the F(x) curve graphically), we can readily find the true contour f(x) of the spectrum line with an accuracy sufficient for practical purposes. The above method is equally applicable to both emission and absorption lines and bands. It is both simple and practical since the function F(x), whether given in analytic or graphic form, is easily differentiated.

The present investigation was undertaken at the suggestion of the Division of Scientific and Applied Spectroscopy, headed by V.M.Chulanovski, of the Physics Department of Leningrad State University. A more detailed description of the method and its use in calculating the true contour of absorption bands will be published elsewhere.

"A.A.Zhdanov" Leningrad State University

* * * * * * *

THE RAMAN EFFECT AND ITS FREQUENCY DEPENDENCE*

- P.P.Shorigin & L.Z.Ositianskaia

In most cases the intensity I of Raman spectrum lines increases rapidly with increasing frequency of the incident (exciting) light. According to Placzek, I is approximately proportional to ν^4 and is also roughly proportional to the square of the derivative of the polarization factor α of the molecules with respect to the normal nuclear coordinate Q_n, $(\partial\alpha/\partial Q_n$ or $\alpha')$. Placzek's theory was developed for the conditions where the frequencies ν are remote from the electron transition frequencies ν_e of the substance. Under these conditions α' is virtually independent of ν and hence I is actually proportional to ν^4. When the difference $(\nu_e - \nu)$ is not great, again according to Placzek, I should be proportional to $\nu^4(\nu_e - \nu)^{-2}$. According to quasiclassical theory, in a region where the influence of a near electron level is dominant, the intensity of a valence vibration line

---

*For the full report see Doklady AN SSSR, 98, 51 (1954).

$$I = \text{const} \cdot \nu^4 (\nu_e^2 + \nu^2)^2 (\nu_e^2 - \nu^2)^{-4},$$

or, with some approximation,

$$I = \text{const} \cdot \nu^4 (\nu_e - \nu)^{-4}.$$

In the present investigation we determined the variation of I as a function of ν for a number of compounds with conjugate and non-conjugate multiple bonds: C=C, C=O, C≡N and NO_2. The integral intensity of the valence vibration lines for these bonds was measured by the method of photographic photometry with the use of an internal standard (solutions in cyclohexane were used). The ratio of the intensity of the investigated line to the intensity of the standard line - the 1440 cm^{-1} Raman line of cyclohexane - was measured for each of the exciting frequencies (18,307, 22,938, 24,705, and 27,388 cm^{-1}). The intensity of the standard line approximately satisfies the relationship $I = \text{const} \cdot \nu^4$.

Our measurements showed that the intensity of the Raman lines increases 1½ to 2 times faster than it should according to the $\text{const} \cdot \nu^4$ relationship, presumably due to an increase in α'. The intensity of lines associated with conjugate multiple bonds rises more rapidly than that of lines associated with non-conjugate bonds. The relationship $I = \text{const} \cdot \nu^4$ should hold rigorously only in the case where the absorption bands are extremely remote (which is never the case in practice). In fact it may be said that the presence of Raman scattering is connected with the fact that the transition frequencies ν_e are not too far removed from ν and, hence, with the deviation from $I = \text{const} \cdot \nu^4$.

An approximate evaluation of the probable electron transition frequency ν_e, determining the intensity of the observed Raman line, may be made on the basis of the experimental data for $I = f(\nu)$. Using the equations of quasiclassical theory (see above) we obtain plausible values for ν_e, i.e. frequencies in the region where there actually are strong absorption bands. On the other hand, the commonly accepted expression, based on Placzek's theory, yields lower values of ν_e, (i.e., frequencies in the region below the strong absorption bands). Other available data also indicate that the latter expression is unsatisfactory and does not properly take into account the factors producing changes in the polarizability of molecules incident to nuclear vibration and, hence, giving rise to Raman spectra.

Comparison of the rates of increase of I as well as the intensity of the absorption bands for monoolefines and diolefines shows that the great proximity and high intensity of the first absorption band of diolefines are about equally responsible for the high intensity of the line associated with the C=C conjugate double bond in the Raman spectra of diolefines.

"L.Ia.Karpov" Physico-Chemical Institute

* * * * * * *

RAMAN SPECTRA IN THE REGION OF ABSORPTION BANDS

- L.M.Kutsyna & P.P.Shorygin

Raman spectra in the region of an absorption band can be observed in the absence of fluorescence in the given part of the spectrum; in practice this is the case when the mean life of the molecules in the excited state is very short (less than 10^{-11} sec). A short mean lifetime results in a great breadth of the vibrational-structure components of the absorption and, given a sufficient breadth, these components merge and the vibrational structure disappears.

In the light of quasiclassical and quantum theory treatment of Raman scattering it may be assumed that as the frequency of the incident light approaches that of the absorption band the greatest increase in intensity will be exhibited by the Raman lines associated with the normal coordinates whose equilibrium values change appreciably at the given electron excitation. At the same time such normal vibrations may be present in the vibrational structure of the absorption band. It may also be assumed that the broader the system of the vibrational-structure components, corresponding to the given normal vibration, the more effective should be the electron excitation level for the corresponding Raman spectrum line.

In order to determine experimentally which attributes of absorption spectra are important as regards the possibility of observing Raman spectra in the absorption band, we investigated the Raman spectra of a number of suitable colored solutions of different organic compounds. The 4358 A mercury line was used for exciting the Raman effect; in the case of most of the compounds investigated this line lies on the long wave side of the peak in the absorption band of the compound.

We failed to obtain Raman spectra of the solutions of diphenylene ketone, anthraquinone, anthrone, azobenzene and 3-nitrodimethylaniline; the failure was due not only to fluorescence but also to the fact that the intensity of the Raman line was insufficient to make up for the great light loss due to absorption.

In contrast, Raman spectra of nitroso- and nitro-compounds were observed with no difficulty. 4-Nitrosodiethylaniline has a very strong absorption band with a maximum near 4200 A and a weaker band in the region of 7600 A (with methanol as the solvent); with excitation by the 4358 A Hg line, six sharp lines of nitrosodiethylaniline are clearly visible in the Raman spectrum of the solution. In the spectrum of a solution of nitrosobenzene, whose strong absorption band lies much higher, approximately the same number of lines appear, among them are the 1004 and 1594 cm^{-1} lines of the benzene ring and a line presumably attributable to the nitroso group (1448 or 1510 cm^{-1}).

Investigation of the absorption spectrum of 4-nitrosodiethylaniline in the 3000-4500 A region showed that no fine structure is discernible in the first intense absorption band with the material in solution, in the vapor state or in the form of crystals at low temperature (temperature of liquid nitrogen). In all probability the lifetime of the excited state of the molecules is extremely short, possibly because of internal conversion of the excitation energy. We conclude that Raman spectra can be more readily obtained in the region of strong and broad absorption bands than in the region of weaker (except, of course, very weak) and narrower bands.

"N.D.Zelinski" Institute of Organic Chemistry

* * * * * * *

RESONANCE RAMAN SCATTERING

- L.N.Ovander

Our theoretical investigation of the process of scattering was carried out using the model of an admixture in a crystal. The energy levels and the eigenfunctions were determined in the adiabatic approximation. The degree of nonadiabaticity determines the possibility of radiationless transitions. For the sake of simplicity we assumed that the admixed molecule has only three levels.

We solved the problem by the methods of quantum electrodynamics which has the advantage that the scattering spectrum is obtainable from the resultant equations with any given form of the incident spectrum.

The final results are considered separately for the following two cases:

1) The case of irradiation by a broad beam (continuous spectrum) whose breadth exceeds that of the absorption spectrum; in this case the shape of the Raman line will coincide with the shape of the absorption spectrum.

2) The case when the breadth of the incident line is less than the breadth of the absorption spectrum but exceeds the so-called natural breadth of the Raman line in solution; in this case the shape of the scattering spectrum will coincide with the shape of the incident line. The natural breadth of the Raman line does not become manifest in this case. The intensity of the scattered line depends to an appreciable degree on the frequency of the excitation spectrum; it is proportional to the ordinate of the absorption spectrum, taken at the frequency of the incident line.

Inasmuch as the excitation is effected by light with a frequency lying in the region of the absorption band, it is essential to distinguish between luminescence and resonance scattering. In our calculations we assumed that emission always occurs from the same levels to which the transition under the influence of the light quanta took place. A state of statistical equilibrium is not attained because of the short lifetimes, due to appreciable quenching. It should be noted that resonance Raman scattering is observed in substances characterized by considerable quenching. Resonance Raman scattering may be subject to quenching by admixtures and to concentrational quenching.

"T.G.Shevchenko" Kiev State University

* * * * * * *

CONNECTION BETWEEN RAMAN SPECTRA AND THE ELECTRONIC SPECTRA OF MOLECULES

- M.D.Zepe

In their derivation of Placzek's equation

$$(a_{\sigma\sigma})_{00}^{01} = \left[\frac{\partial (a_{\sigma\sigma})}{\partial q}\right]_{q_0} q^{01}, \qquad (1)$$

where $a_{\sigma\sigma}$ are components of the polarization tensor and q is the vibration coordinate, Vol'kenshtein and El'iashevich limited themselves to the linear term relative to q in the approximate expression for the wave function:

$$\Psi_e^r(\xi, q) = \left\{\Psi_e(\xi, q_0) + \left[\frac{\partial \Psi_e(\xi, q)}{\partial q}\right]_{q_0} q + \cdots\right\} U_e^r(q), \qquad (2)$$

where Ψ_e is the electronic part of the function and U_e^r is the vibrational part.

In our analysis we show that in computing (1) the calculations can actually be restricted to the linear approximation, but that in calculating $(a_{\sigma\sigma})_{00}^{02}$, $(a_{\sigma\sigma})_{00}^{03}$, ... it is necessary to continue the expansion through the quadratic, cubic, etc., terms. In calculations by the method of Vol'kenshtein and El'iashevich the discrete function

$$F(\nu_{0e}^{0r}) = \frac{2\nu_{0e}^{0r} - \nu_{vib}}{(\nu_{0e}^{0r})^2 - \nu^2 - \nu_{vib}(\nu_{0e}^{0r} - \nu)} \qquad (3)$$

is differentiated with respect to q, which is permissible only provided F is replaced by a continuous function of q. The possibility of such replacement can be proved by means of the method of Van Vleck, according to which

$$(a_{\sigma\sigma})_{00}^{01} = \sum_e{}' \sum_r \left(\frac{1}{A + w_e^r} + \frac{1}{B + w_e^r}\right) (p_\sigma)_{0e}^{0r} (p_\sigma)_{e0}^{r1}, \qquad (4)$$

where w_e^r is the vibrational energy of the excited electron state, while A and B depend on ν_{0e}, ν, w_0^0 and w_0^1. Expanding the frequency term into a binomial series in w_e^r and expressing the Hamiltonian of the vibrational motion of the excited electronic state H_e through the Hamiltonian of the ground state, with the potential energy represented in the form of a Morse function, we obtain, taking only the linear term,

$$\left.\begin{aligned} F(\nu_{0e}) &= A^{-1} + B^{-1} - (A^{-2} + B^{-2})(D_e\beta_e^2 q'^2_0 - 2D_e\beta_e^2 q'_0 q), \\ \left[\frac{\partial F(\nu_{0e})}{\partial q}\right]_{q=0} &= 2\ (A^{-2} + B^{-2})\, D_e\beta_e^2 q'_0, \end{aligned}\right\} \qquad (5)$$

where D_e and β_e are parameters of the Morse function of the excited state and q'_0 is the variation of the equilibrium state with electron excitation. Calculations prove the validity of the method of Vol'kenshtein and El'iashev for the case when

$$\nu_{0e}^{0r} - \nu \gg \nu_{vib}. \qquad (6)$$

It can be shown that (1) is also valid when $\nu_{0e}^{0r} - \nu \sim \nu_{vib}$.

Lastly, when $\nu_{0e}^{0r} - \nu \sim \gamma_e^r$, where γ_e^r is the attenuation constant of the vibrations, two cases are possible:

1) the incident photon $h\nu$ approaches one of the higher Franck-Condon levels and a transition to resonance fluorescence takes place or 2) $h\nu$ approaches the zero vibrational level of the excited electronic state. In the latter case for small values of q'_0 and relatively flat potential curves, $(p_\sigma)_{0e}^{00}(p_\sigma)_{e0}^{01}$ has a finite value and the term, corresponding to the zero vibrational level in the scattering equation, may predominate due to the smallness of the denominator, in which the attenuation should be taken into account. Thus, we get

$$(a_{\sigma\sigma})_{00}^{01} = \frac{1}{h} \cdot \frac{(p_\sigma)_{0e}^{00}(p_\sigma)_{e0}^{01}}{\nu_{0e}^{00} - \nu + i\gamma_e^r}. \qquad (7)$$

When the numerator in (7) is very small, one should also take into consideration the next 2-3 vibrational levels. When q'_0 is large and the potential curves are steep, (1) once more obtains approximately.

Institute of Physics of the
Academy of Sciences of the Latvian SSR

* * * * * * *

THE ABSORPTION SPECTRA OF SOLID SOLUTIONS OF LEAD IN CADMIUM HALIDES

- A.F.Malysheva

Investigation of the absorption spectra of activated crystalline phosphors presents a twofold interest: 1) comparison of the absorption bands of the host material and the activator with the excitation bands of the phosphor permits drawing certain deductions regarding the character of the processes occuring in the phosphor and aids in classifying the phosphor as to type and 2) comparison of the absorption bands of the pure host material and of the pure activator with the absorption bands of the phosphor offers a clue to the influence of the field of the crystal lattice of the host on the energy levels of the activator and vice versa to the effect of the introduced activator on the energy states of the base substance lattice.

Measurement of the absorption spectra of crystal phosphors in the usual form

of fine-crystal powders is commonly hampered by strong scattering of the light. On the other hand, it is sometimes impossible and always technically difficult to grow large single crystals of phosphors. However, phosphor sublimates prepared in the form of thin, dense layers by evaporative deposition on a suitable support under vacuum[1 & 2] are convenient for the purpose of spectroscopic absorption studies.

In the present investigation we studied the absorption spectra of phosphor sublimates with halide salts of cadmium as the hosts and halide salts of lead as the activators.

The absorption spectrum measurements were carried out by means of an SF-4 photoelectric spectrometer and extended over the region from 220 to 450 mμ. To simplify comparison and facilitate measurement of the spectra partially overlapping layers of the host and activator salts were deposited successively on the same support; thus the specimens comprised sections of pure host material, pure activator and phosphor.

The absorption spectra of the pure host materials ($CdCl_2$, $CdBr_2$ and CdI_2) consist of a system of maxima which are displaced to the side of longer wavelengths in going from the chloride to the iodide. The observed positions of the maxima were in agreement with Fesenfeldt's data[3].

The absorption spectra of the pure activators ($PbCl_2$, $PbBr_2$ and PbI_2) are located at longer wavelengths than the spectra of the corresponding host materials. This circumstance is apparently an important condition where formation of the phosphor is concerned (where the phosphor is not formed by recombination). The pure activator spectra also show some displacement towards longer wavelengths in going from the chloride to the iodide. At the same time the sharp structure exhibited by the spectrum of lead chloride becomes increasingly more diffused in the bromide and iodide.

The two-layer system as initially prepared turned into a phosphor only after appropriate heating, insuring diffusion of the activator substance into the host lattice and formation of a solid solution. Accordingly, the spectrum of the $CdI_2 \cdot PbI_2$ system prior to heating roughly duplicates the absorption curve of pure CdI_2, except that the absorption is intensified at certain points where the tail of the activator absorption curve is superimposed on the host curve. After heating there appears a new narrow band with a maximum at 390 mμ, which can be interpreted only as an absorption band of lead (incorporated in the host lattice) shifted by the field of the host material lattice. Compared with the absorption band of pure lead iodide, the band of the lead in the cadmium iodide lattice is considerably narrower, which may be explained by the weaker interaction between ions in the pure PbI_2 lattice.

In contrast to the case of $CdI_2 \cdot PbI_2$, heating of the $CdCl_2 \cdot PbCl_2$ and $CdBr_2 \cdot PbBr_2$ systems does not lead to the appearance of a new line; the absorption band characteristic of the pure activator remains virtually unaltered. The difference in the behavior of the systems is probably connected with the different conditions under which the activator enters the host lattice.

The emission spectra of the above systems are wide bands in the 500-700 mμ region[2]; the breadth of the emission band is much greater than that of the absorption band. The difference in band breadths can be explained with the aid of a scheme of energy levels in the form of potential curves in configurational coordinates, if one takes account of the displacement of the potential curve of the excited state with respect to the minimum of the normal state curve and the extreme flatness of the former.

The writer wishes to thank F. D. Klement under whose guidance this investigation was carried out.

Institute of Physics and Astronomy of the
Academy of Sciences of the Estonian SSR

References

1. F.D.Klement, Doklady AN SSSR, 46, 295 (1945).
2. F.D.Klement & A.F.Malysheva, Doklady AN SSSR, 96, 465 (1954).
3. H.Fesefeldt, ZS. Phys. 64, 741 (1930).

* * * * * * *

SPECTRA OF ELECTRON CAPTURE LEVELS IN ALKALI-HALIDE CRYSTAL PHOSPHORS

- Ch. B. Lushchik

The spectrum of the electron capture levels is one of the most important characteristics of crystal phosphors, for it determines all the inertial properties of the phosphor.

In the present investigation we studied the spectra of the thermal energy of activation of capture centers of 15 crystal phosphors: NaCl·AgCl, NaCl·CuCl, NaCl·TlCl, NaBr·AgBr, NaBr·CuBr, NaBr·TlBr, KCl·AgCl, KCl·CuCl, KCl·TlCl, KBr·AgBr, KBr·CuBr, KBr·TlBr, KI·AgI, KI·CuI and KI·TlI. We employed the method of thermal luminescence in the 130-500°K temperature interval with a rigorously constant rate of heating (0.15 degrees/sec). The measurements were made with a photoelectric photometer based on the design by S. F. Rodionov.

The observed shape of the thermoluminescence peaks and the fact that their positions and half-widths are characteristically independent of the amount of stored up energy indicate that these are elementary peaks. Hence the thermal activation energy spectrum consists of a series of discrete levels. The energy of these levels was calculated from the thermoluminescence data by several different methods.

We determined that the great majority of the capture centers are actually thermal microdefects of the host material lattice and are not connected with the presence of activator ions in the crystal. However in crystals activated by thallium we also detected activator capture centers.

We established a connection between certain additional absorption bands of pure alkali-halide crystals (F,M,R and F') and definite thermoluminescence peaks, which permitted us to compare the optical and thermal activation energies of the corresponding capture centers.

The thermal energies of activation of centers of the same type in the homologous series NaCl, BaBr, KCl, KBr and KI vary in parallel with the melting point of the host substance; in some cases parallelism with the variation in the magnitude of the lattice constant breaks down, however. Hence, the familiar Mol'vo ratio is not applicable to the thermal activation energies of capture centers. We further established that the anions of the host material have an appreciably stronger influence on the thermal energy of activation that do the cations.

The spectrum of the electron capture levels becomes considerably more complex when the host material is a mixed crystal. It was established that individual thermoluminescence peaks of KCl·KBr·TlCl, corresponding to the activator capture centers, are constituted by several superposed elementary thermoluminescence peaks. This is evinced by the complicated shape of these peaks and their abnormally great half-width (the half-width maximum for equal KCl and KBr content). Particularly indicative is the fact that after extinction of the KCl·KBr·TlCl phosphor, for some time before the thermoluminescence curve is obtained, the maximum of the thermoluminescence peak is shifted to the side of higher temperatures [wavelengths?] while the half-width of the peak is reduced. The complex character of the thermoluminescence peaks of mixed crystals may be explained by the presence in these phosphors of "isostructures of capture centers"; the question of the existence of such "isostructures" has been examined in a number of

crystallo-chemical papers (Ref. 2 and others).

Institute of Physics and Astronomy of the
Academy of Sciences of the Estonian SSR

References

1. S.F.Rodionov & A.L.Osherovich, Zhur. eksp. i teor. fiz., 19, 184 (1949).
2. Y.Durham & J.Hawkins, J. Chem. Phys., 19, 149 (1951).

* * * * * * *

SPATIAL DISTRIBUTION OF THE RADIATION FROM COLOR CENTERS AND THE NATURE OF SUCH CENTERS IN IONIC CRYSTALS*

- P. P. Feofilov

Perfect symmetry of cubic ionic crystals does not preclude anisotropy of the spatial distribution of the radiation from anisotropic color centers, oriented along the crystal axes of symmetry.

The luminescence of centers that form in the process of photochemical or additive coloring of single crystals of CaF_2, NaF and LiF, excited by linearly polarized light, is found to be partially polarized. The degree of polarization is greatly dependent on the wavelength of the exciting light and on the orientation of the electric vector of the exciting light relative to the crystallographic axes. The dependence of the degree of polarization on the wavelength of the exciting light (polarization spectrum) can be satisfactorily explained with the aid of the classical oscillator model of an anisotropic luminescent center, comprising a certain combination of linear and circular oscillators. The dependence of the degree of polarization on the relative orientations of the crystal axes and the electric vector (azimuthal dependence) is indicative of an ordered orientation of the anisotropic centers relative to the crystal axes of symmetry.

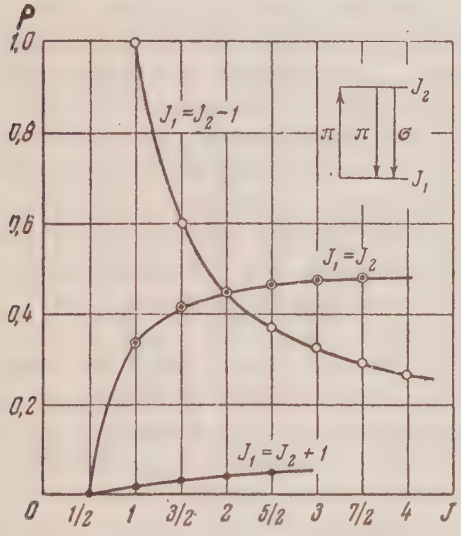

Degree of polarization of resonance radiation for different values of J in the ground and excited states.

Analysis of the azimuthal relationships shows that in CaF_2 crystals the linear oscillators of the centers are oriented along the fourth order axes, while in crystals of LiF and NaF they are aligned with the crystallographic axes of the second order.

The experimentally observed absolute values of the degree of polarization may be taken to indicate extreme anisotropy of the elementary emitters of the color centers. Analysis of the polarization of the resonance radiation,

---

*For a more complete account of the investigation see Doklady AN SSSR, 92, 545 & 743 (1953) & Zhur. eksp. i teor. fiz., 26, 609 (1954).

which has a certain similarity with the luminescence of the color centers under excitation in the long-wave absorption band, shows that the high absolute degrees of polarization observed can be attained only when the inner quantum number J equals zero in the ground state or unity in the first excited state (see the accompanying figure in which the results of calculations of the degree of polarization of the resonance emission for different values of J in the ground and excited states are indicated). The fact that J is always an integer shows that color centers cannot be treated as one-electron systems like, for example, ordinary F-centers or superstoichiometric metal atoms (in the case of LiF and NaF). It may be assumed that the color centers in this case are so-called F_2-centers, i.e., electron pairs localized at neighboring anion sites. Examination of the crystallochemical structure of the compounds in question indicates that the F_2-centers should align with the fourth order axes in CaF_2 crystals and along the second order axes in LiF and NaF crystals, which, of course, is in agreement with the results obtained in our analysis of the azimuthal dependence of the polarization of luminescence.

* * * * * * *

APPLICATION OF A SPECTROPHOTOMETRIC METHOD TO THE INVESTIGATION OF CHEMICAL SENSITIZATION OF A PHOTOGRAPHIC EMULSION

- E.A.Kirillov, Zh.L.Broun & K.V.Chibisov

The authors used the differential spectrophotometric method developed by Kirillov[1] to observe the process of center formation in the course of chemical (reduction) sensitization. The study was carried out on a Lippman type silver bromide emulsion which was sensitized by immersion in hydrazine solutions of different concentrations ($0.23 \cdot 10^{-4}$ to $7.5 \cdot 10^{-4}$ mol/liter). The affect of the hydrazine was compared with that of accelerated aging of an air-dry layer in a thermostatic chamber, maintained at 52°C. In addition to the spectrophotometric measurements, the sensitization and aging effects were compared by photographic determination of the sensitivity.

The spectrophotometric measurements showed that the absorption spectrum obtained as the result of treatment with hydrazine or accelerated aging is characterized by the same clearly defined fine structure as is observed in the case of photochemically dyed silver halides and atomized silver coatings applied under vacuum. Whence it may be concluded that the silver centers formed as the result of photolysis, chemical reduction and accelerated aging are identical as regards structure. Further we determined that when a Lippman emulsion is processed in alkaline (pH = 10.17) hydrazine solutions, increase in the hydrazine concentration is accompanied not only by an increase in absorption but also by broadening of the spectrum into the long wavelength region. Increasing the hydrazine concentration from $0.23 \cdot 10^{-4}$ mol/liter to $7.5 \cdot 10^{-4}$ mol/liter also resulted in 14-fold increase in the speed of the processed emulsion. A certain increase in sensitivity (speed) is also observed in the case of accelerated aging which may be regarded as a type of chemical (second) ripening.

It follows from the experimental data that the physical process occurring in sensitization with hydrazine and in chemical ripening (i.e., in accelerated aging) consists of a supplementary formation of silver centers, the number and size of which increase with increasing concentration of hydrazine or the length of time the emulsion is held in the thermostatic chamber. We may add that the

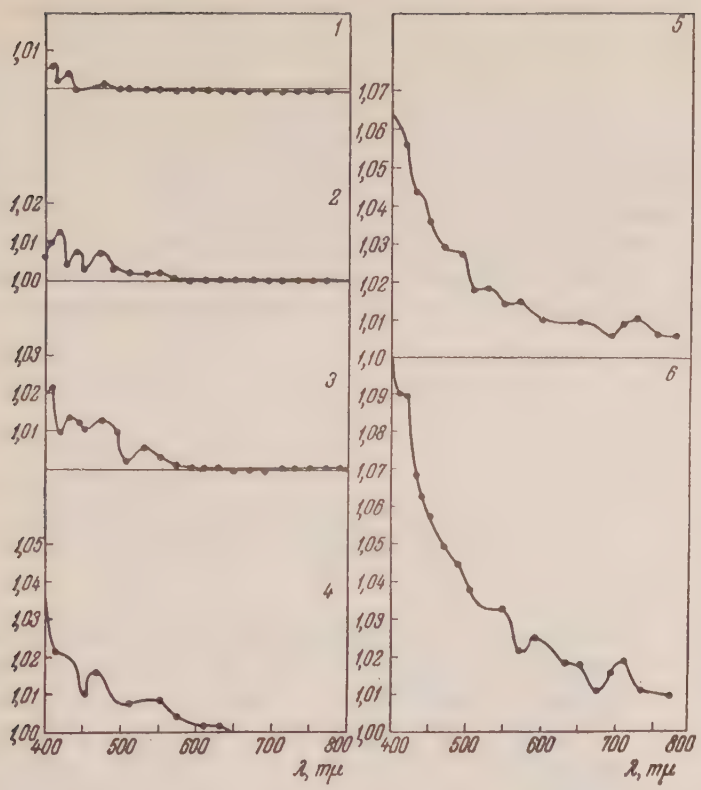

Dependence of the absorption spectrum of the silver bromide emulsion on the hydrazine concentration in alkaline solutions: 1) buffer solution only (pH = 10.17); in hydrazine solutions (pH = 10.17); 2) 0.23, 3) 0.47, 4) 0.95, 5) 1.9, 6) 7.5 — all x 10^{-4} mol/liter.

emulsion layers processed as described above did not show even a trace of fog upon development, for the silver centers formed under our experimental conditions did not attain the size or characteristics of fog centers. It was, however, possible to detect certain changes in the emulsion by means of the spectrophotometric method which goes to prove that this method is more sensitive than the photographic one. Comparing the results obtained for emulsions sensitized with hydrazine with those for emulsions chemically ripened in the process of accelerated aging we tentatively conclude that the increase in sensitivity (speed) occurring in treatment with hydrazine is connected primarily with the growth and accumulation of centers in the size range conducive to light-absorption in the shorter wavelength region of the visible spectrum.

Institute of Physics of
Odessa State University

* * * * * * *

INFRARED BOUNDARY OF BLEACHING OF THE FINE STRUCTURE IN THE SPECTRUM OF PHOTOCHEMICALLY COLORED SILVER HALIDE*

- E. A. Nesterovskaia

The question of the long-wavelength boundary of the disintegration of latent-image centers by light has been investigated by Terenin[1], Bartelt and Krug[2] and others. In these studies it was established that the infrared boundary of the Herschel effect for pure silver chloride and silver bromide emulsions lies near 1000 mμ. Discovery of the fine structure in the absorption spectrum of photochemically dyed silver halide[3 & 4] and of the destruction of the centers associated with it under the influence of light[5] brought up the problem of determining the bleaching boundary of the fine structure and comparing the location of this boundary with that of the Herschel effect.

The fact that the positions of the spectral maxima of bleaching and of absorption coincide, established by us in an earlier investigation, suggests that the corresponding centers play a significant part in the processes connected

* The complete report appeared in Doklady AN SSSR, 96, 6, 997 (1954).

with bleaching. From a comparison of the spectral curves for absorption, bleaching and the internal photoeffect[5, 6 & 7] it may be concluded that centers associated with the fine structure are active not only photochemically but also photoelectrically: a possible mechanism of their destruction is the ejection of an electron from the silver particle with its subsequent emergence into the conductivity zone of the crystal. By analogy with the Herschel effect one might expect the fine-structure bleaching process to have a spectral boundary in the red region at a point where the energy absorbed by the particles is just sufficient to cause ejection of the electrons. To determine the location of this boundary we extended our investigation of bleaching in fine grain silver chloride and bromide emulsions into the infrared region.

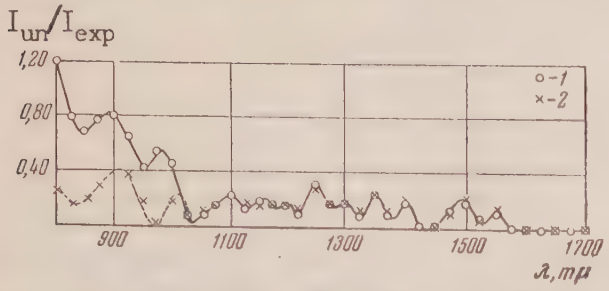

Absorption spectra of AgCl: 1) after the first exposure of the emulsion to light from a mercury lamp for 15 min; 2) after a second exposure through a red (650-3000 mμ) filter for 15 hours. Ordinate scale graduated in ratios of the intensity of light passing through the unexposed section to the intensity of light passing through the exposed section of the emulsion.

Our measurements were carried out by the differential method described by Kirillov[3 & 4]. We employed a double quartz-prism monochromator equipped with a thermopile and a photorelay with a silver sulfate photocell. The spectral boundary was determined by two methods, both previously employed in our preceding investigation[5]. The first consisted of comparing the absorption spectra obtained after the first coloring exposure of the emulsion and after the second bleaching exposure. The boundary wavelength of the bleaching effect is given by the point of intersection of the two spectral absorption curves (see figure). The second method consists of measuring the bleaching spectrum; the boundary is given by the point of intersection of the inverted curve with the X-axis.

As may be seen from the accompanying figure, bleaching of the fine structure is limited on the long wave side, with the boundary lying at about 1000 mμ. A certain decrease in absorption is observed in the region of shorter wavelengths; beyond the boundary there is no appreciable change in the form of the absorption curve after the second exposure.

The mean position of the fine-structure bleaching boundary for AgCl and AgBr (at about 1000 mμ) is in close agreement with the boundary of the Herschel effect as determined by photographic methods[1 & 2]. This coincidence confirms that the Herschel effect is due primarily to destruction of centers of the same type as those associated with the fine structure.

From the experimental results we can also draw the conclusion - important where fine structure theory is concerned - that only bands lying in the 1000 mμ region correspond to the absorption causing the destruction of the centers in question.

Institute of Physics of Odessa State University

References

1. A.N.Terenin, ZS. F. Phys., 29, 294 (1925).
2. O.Bartelt & H.Klug, ZS. f. Phys., 89, 779 (1934).
3. E.A.Kirillov, Izv. (Bulletin) AN SSSR, Ser. fiz., 12, 533 (1948).
4. E.A.Kirillov, Trudy (Proceedings) of Odessa State Univ., 13, 69 (1951).
5. E.A.Nesterovskaia, Doklady AN SSSR, 90, 4, 587 (1953).
6. E.A.Kirillov, & A.S.Fomenko, Trudy (Proc.) Odessa State Univ., 13, 69(1951).
7. N.M.Zaidman, Zhur. fiz. khem., 26, 1791 (1952).

* * * * * * *

SPECTROSCOPIC INVESTIGATION OF THE MECHANISM OF CONDENSATION OF β-IONONE WITH ETHYL γ-BROMOCROTONIC ACID

- N.A.Slovokhotova, G.I.Samokhvalov, M.A.Miropol'skaia, L.A.Bakulova, L.P.Zhukova & N.A.Preobrazhenski

We investigated the condensation products of β-ionone with ethyl γ-bromocrotonic acid in a benzene solution in the presence of metallic zinc. The reaction is accompanied by dehydration and leads to an unsaturated ether. Saponification of the ether results in a viscous oily mixture of acids from which trans-β-ionolidene-crotonic acid (I, R = H):

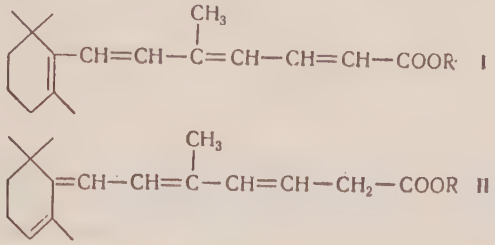

crystallizes out (the yield is 7-20%, referred to β-ionone).

By fractional saponification we succeeded in separating out an acid (II) from the readily saponifiable part of the ethers. Both acids were then reconverted to methyl ethers through the action of diazomethane. The absorption band in the vicinity of 1700 cm^{-1} in the infrared spectrum of methyl β-ionolidene-crotonic acid (see Fig. 1, a) is characteristic of the group in aliphatic ethers. The frequency of vibration of the C=C bond is also reduced (to 1595 cm^{-1}) because of the linkage. The maximum of the absorption band in the ultraviolet region for this ether lies at about 325 mμ (ε = 1025).

The absorption band of the carbonyl group in the infrared spectrum of the methyl acid separated out of the easily saponified part of the ether lies at about 1730 cm^{-1}, while the band associated with the C=C bond appears at 1600 cm^{-1} (Fig. 1, b). The absorption peak in the ultraviolet for this ether is located at 315 mμ. This justifies assigning the acid obtained from the readily saponified ether the structure II (see above), wherein the C=O group is not linked with the polyene chain.

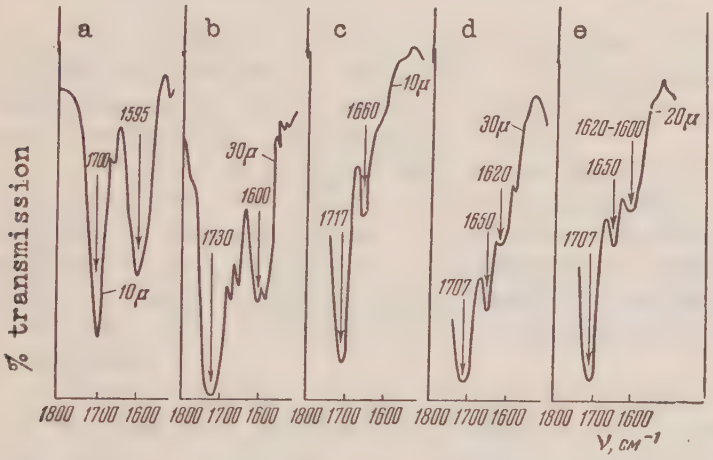

Fig. 1. Absorption spectra: a) methyl β-ionolidene-crotonic acid; b) methyl acid separated from the easily saponified part of the ether; c, d and e) fractions 17, 19 and 21, respectively, obtained as the result of fractionation of the interaction product of β-ionone with ethyl γ-bromocrotonic acid.

The product of the reaction of β-ionone with ethyl γ-bromocrotonic acid was fractionated under vacuum, 22 fractions being separated. The first 14 fractions consisted primarily of β-ionone. The remaining 8 fractions (constituting 40% of the distillate by weight) differ markedly from the ethers of β-ionolidene-crotonic acid (I, R = CH_3) and have ultraviolet absorption maxima of different intensities at 285 mμ. Introduction of a base simultaneously with saponification results in isomerization with the formation of acids having the structures I and II (R = H). The process is accompanied by displacement of the absorption peak

in the ultraviolet by some 30-40 mμ to the side of longer wavelengths, which is indicative of the lengthening of the system of conjugate double bonds. Thus the principal product of condensation is the alkali-unstable ether V (see below), formed as the result of the anionotropic rearrangement and dehydration of the intermediate hydroxy-ether III:

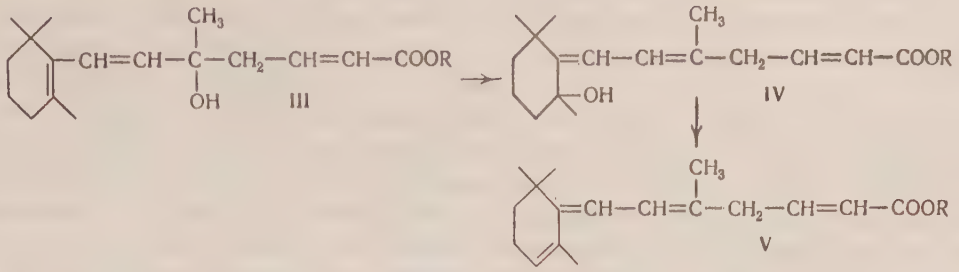

Slower rearrangements also occur under the influence of heat in the process of distillation. Analysis of the infrared spectra of fractions 17, 19 and 21 (Fig. 1, c, d & e) indicates the presence of products of step-by-step prototropic rearrangement of the condensate V.

"L. Ia. Karpov" Physico-Chemical Institute

* * * * * * *

THE CHEMILUMINESCENCE OF 3-AMINOPHTHALHYDRAZIDE (LUMINOL)

- K.L.Klimovskaia, V.N.Vishnevski & V.E.Shmaevski

The authors studied the variation of the chemiluminescence of white and yellow 3-aminophthalhydrazide in the process of oxidation by hydrogen peroxide and potassium ferricyanide in an alkaline medium. The variation in intensity was recorded on photographic film.

It was found that increasing the hydrogen peroxide concentration (within the range of $76 \cdot 10^{-6}$ to $70 \cdot 10^{-3}$ mol/liter) with the concentrations of the white hydrazide and the alkali - sodium hydroxide - being held constant at $118 \cdot 10^{-5}$ and $20.3 \cdot 10^{-3}$ mol/liter, respectively, shifts the peak of the I(t) curve to the side of larger values of t [time]. The maximum intensity of the luminescence of the solution is observed at a hydrogen peroxide concentration of about $3 \cdot 10^{-3}$ mol/liter.

The existence of an optimum hydrogen peroxide concentration was also noted in the case of solutions of the yellow 3-aminophthalhydrazide. Furthermore it was established that the variation in the intensity of luminescence of the yellow hydrazide with increasing concentrations of sodium hydroxide (from $12.5 \cdot 10^{-3}$ to $43.8 \cdot 10^{-3}$ mol/liter) and potassium ferricyanide (from $21 \cdot 10^{-5}$ to $171 \cdot 10^{-5}$ mol/liter) with oxidation of the hydrazide ($80 \cdot 10$ mol/liter) by hydrogen peroxide ($2 \cdot 10^{-5}$ mol/liter) is almost linear.

With the concentrations of the yellow hydrazide and hydrogen peroxide constant (at $80 \cdot 10^{-5}$ and $2 \cdot 10^{-5}$ mol/liter, respectively) the effects of changing the concentrations of the alkali and of the potassium ferricyanide are qualitatively equivalent where the effective luminescence time is concerned. In both cases there is an optimum concentration at which the effective luminescence time is greatest; for the NaOH this optimum concentration is $25 \cdot 10^{-3}$ mol/liter (with the potassium ferricyanide concentration held at $6 \cdot 10^{-5}$ mol/liter) while the optimum for the potassium ferricyanide is $8.34 \cdot 10^{-4}$ mol/liter (NaOH concentration - $18 \cdot 10^{-3}$ mol/liter).

It was established that the luminescence intensity curve for white hydrazide can have one or more (2-3) intensity peaks. The relative locations of the peaks and their height were found to depend on the instant of introduction of the potassium ferricyanide solution ($20.3 \cdot 10^{-5}$ mol/liter) and on the concentration of hydrogen peroxide employed (varied between $34 \cdot 10^{-5}$ and $26.6 \cdot 10^{-3}$ mol/liter). Potassium ferricyanide increases the intensity of the first peak in the case of hydrogen peroxide concentrations under the optimum intensity one and, on the contrary, reduces the intensity in the case of peroxide concentrations exceeding the optimum intensity level.

The luminescence of white hydrazide solutions ($118 \cdot 10^{-5}$ mol/liter white hydrazide, $20.3 \cdot 10^{-3}$ mol/liter NaOH, and $106 \cdot 10^{-5}$ mol/liter H_2O_2) was investigated at different temperatures between +10 and +30°C. The record showed that the luminescence reaches its maximum intensity more quickly as the temperature of the solution is increased; moreover increasing the temperature shortens the effective luminescence time and changes the shape of the curve.

The following effect was noted in studying the luminescence of yellow hydrazide. At a NaOH concentration of $25 \cdot 10^{-3}$ mol/liter, the concentration corresponding to the maximum effective luminescence time, the blackening of the film did not change gradually (smoothly) during the entire luminescence period (as in all other cases); instead, the curve shows a slowing down of the rate of decrease in intensity at uniform intervals of about 2 sec (the galvanometer period was 1.1 sec). We obtained this stepped curve only with the indicated concentration; the effect quickly vanishes with any appreciable increase or decrease in the NaOH concentration. Thus at alkali concentrations of $18.75 \cdot 10^{-3}$ and $31.25 \cdot 10^{-3}$ mol/liter the effect was no longer apparent. The concentrations of the other solution components remained constant during the test (hydrazide - $80 \cdot 10^{-5}$, hydrogen peroxide - $2 \cdot 10^{-5}$ and potassium ferricyanide - $0.6 \cdot 10^{-4}$ mol/liter).

The authors wish to thank B. Ia. Sveshnikov for making available the white hydrazide used in the experiments.

"Ivan Franko" L'vov State University

* * * * * * *

THE ULTRAVIOLET AND VISIBLE ABSORPTION SPECTRA OF CERTAIN NITRO DERIVATIVES OF DIPHENYLAMINE

- P. M. Bugai & V. N. Konel'skaia

In connection with our study of the structure and chromaticity of intermediate dye compounds, we undertook the investigation of the absorption spectra of a number of nitro derivatives of diphenylamine (4-nitrodiphenylamine, 4, 4'-dinitrodiphenylamine, 2-nitrodiphenylamine, 2, 2'-dinitrodiphenylamine and 2-methoxy-2'-nitrodiphenylamine) in ethyl alcohol, in a 2 molar alcohol solution of sodium alcoholate and in concentrated sulfuric acid.

The observed absorption curves are reproduced in the accompanying figure.

Where the solvent is ethyl alcohol the color of the substance is not altered and the influence of only the nitro and methoxy groups on the character of the diphenylamine absorption spectrum can be observed.

In contrast the 2 molar solution of sodium alcoholate has a strong effect on the absorption spectrum and chromaticity of the compounds:

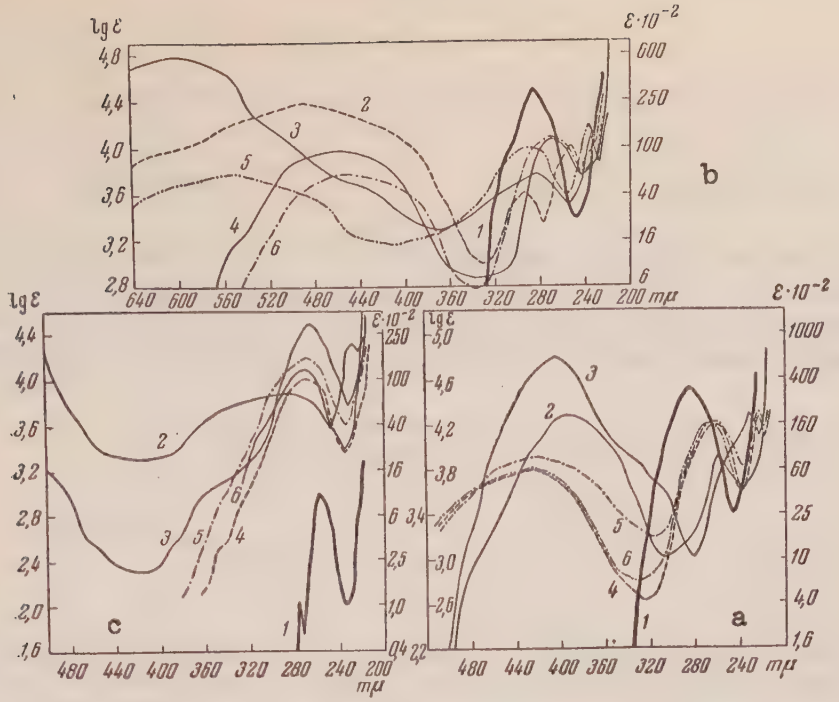

Absorption curves of nitro-derivatives of diphenylamine:
a) in ethyl alcohol, b) in 2 molar alcohol solution of sodium alcoholate, c) in concentrated sulfuric acid. In all figures: 1 - diphenylamine, 2 - 4-nitrophenylamine, 3 - 4, 4'-dinitrodiphenylamine, 4 - 2-nitrophenylamine, 5 - 2, 2'-dinitrodiphenylamine, 6 - 2-methoxy-2'-nitrodiphenylamine.

ABSORPTION OF SOLUTIONS OF DIPHENYLAMINE AND ITS DERIVATIVES

Curve No. in figure	Substance	Solutions					
		in ethyl alcohol (a)		in 2-molar Na alcoholate (b)		in concentrated H_2SO_4 (c)	
		lg ε	λ, mμ	lg ε	λ, mμ	lg ε	λ, mμ
1	Diphenylamine*,**	— 4,49	— 285	— 4,49	— 287	2,96 2,0	259 276
2	4-Nitrodiphenyl-amine*	4,26 3,89	392 258	4,38 3,60 4,00	490 294 253	4,38 3,89	580 282
3	4,4'-Dinitrodi-phenylamine	4,78 4,26	403 231	4,78 3,78 4,08	600 282 234	4,49	266
4	2-Nitrodiphenyl-amine*	3,78 4,19 4,26	425 260 222	4,00 4,08	460 270	4,00	270
5	2,2'-Dinitrodi-phenylamine*	3,89 4,19 4,26	423 265 224	3,78 4,00 4,19	550 290 236	4,19	270
6	2-Methoxy-2'-nitro-diphenylamine	3,78 4,19 4,26	423 265 223	3,78 4,08	435 270	4,08 4,30	270 227

* Solutions of these substances in ethyl alcohol have also been studied by other investigators. (Refs. 1 & 2).

** The spectra of diphenylamine in concentrated sulfuric acid have been obtained by a number of investigators. (Ref. 3).

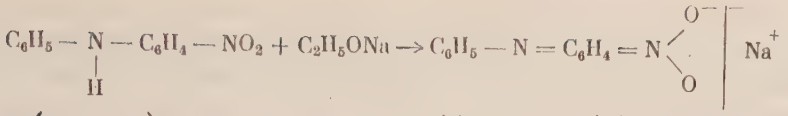

(yellow) (orange-red)

Analogous reactions occur with the dinitro derivatives of diphenylamine, accompanied in each case by the appearance of a characteristic color (see table).

Concentrated sulfuric acid first acts on the investigated nitro derivatives of diphenylamine as an oxidizing agent and then forms ionoid type [quinoid structure?] salts:

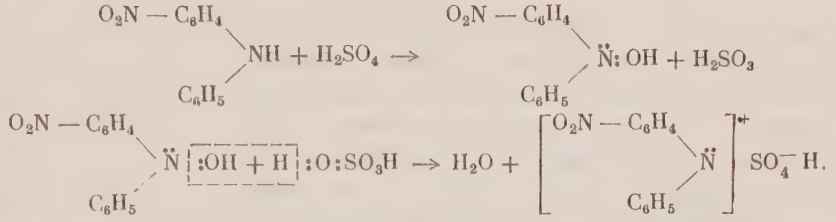

All ortho- and para-nitro derivatives of diphenylamine also react with sulfuric acid. The occurrence of the reaction is evinced by the change in the nature of the absorption spectrum and the deepening of the color characteristic of such substances in azo salts of the ionoid [quinoid?] type.

Conclusions

1. The nitro group as an auxochrome group affects the character of the absorption curve.

2. The reaction of 2 molar sodium alcoholate solution with nitro derivatives of diphenylamine leads to the formation of molecules of the quinoid type which in turn yield deeply colored ionic salts.

3. Concentrated sulfuric acid reacting with the nitro derivatives of diphenylamine forms compounds of the ionic azo type; the initial reaction here is oxidation and this is followed by the formation of an azo sulfate which greatly intensifies the color.

"V. I. Lenin" Khar'kov Polytechnical Institute

References

1. W.Shroeder, Wilcox, Trueblad & Dekker, Anal. Chem., 23, 1740 (1951).

2. P.Ramart-Lucas & M.Grumez, C.R., 211, 120 (1940).

3. A.Hantsck, ZS. phys. Chem., 61, 278 (1907); N.A.Valiashko & G.M.Druzhinin, ZhRKhO (Journ. Russian Chem. Soc.) 45, 2021 (1913).

4. R.Witsinger, Organicheskie krasiteli (Organic dyestuffs) pp. 21-2, ONTI, L. 1936.

* * * * * * *

SPECTROSCOPIC INVESTIGATION OF SOLUTIONS OF ANTIMONY CHLORIDES

- R. A. Dashkovskaia & I. I. Kondilenko

We investigated the absorption spectra and Raman spectra of solutions of antimony tri- and pentachloride in parallel. The absorption spectrum of the solution of $SbCl_3$ in saturated hydrochloric acid is located at 230 mμ (Curve 1

in the accompanying figure.) Reducing the HCl concentration lowers the absorption curve and displaces the peak to the side of shorter wavelengths. At an HCl concentration on the order of 0.5 mol/liter only the long-wave edge of the band can be observed. The main part of the spectrum of the pure-water solution of $SbCl_3$ ($2.8 \cdot 10^{-5}$ mol/liter) lies in the region below 200 mμ. Under the influence of short ultraviolet radiation, the absorption band of $SbCl_3$ in saturated hydrochloric acid solution at 230 mμ gradually fades and instead there develops a new maximum at 270 mμ (Curves 2 & 3). This photochemical transformation proceeds more slowly at lower HCl concentrations and ceases entirely in pure water. Special experiments showed that the photochemical process is irreversible.

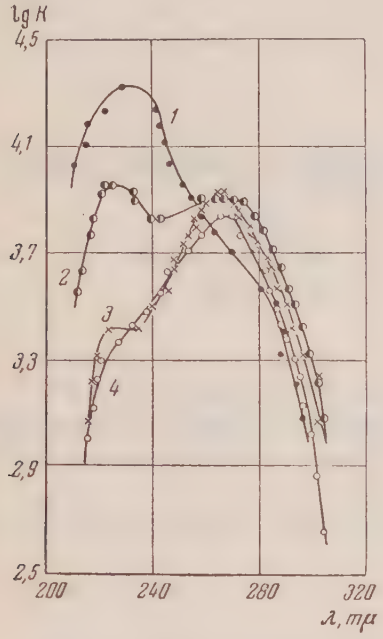

Absorption spectra of antimony chloride solutions (all concentrations in mol/liter): 1) $SbCl_3$ - $2.3 \cdot 10^{-4}$ & HCl - 11.5; before irradiation with short ultraviolet; 2) same solution but after irradiation for 10 min; 3) same solution but after 3 hours irradiation; 4) $SbCl_5$ - $5.96 \cdot 10^{-4}$ & HCl - 11.5.

As regards shape and location on the wavelength scale, the absorption curve of the irradiated solution of $SbCl_3$ in saturated HCl virtually coincides with the absorption curve of $SbCl_5$ in saturated HCl (Curve 4). The latter curve is lowered without being shifted as the hydrochloric acid concentration is decreased.

The spectroscopic samples were purified by repeated vacuum distillation. The Raman spectra were obtained using conventional equipment for this purpose. It may be noted that the Raman lines of $SbCl_3$ solutions proved to be rather diffuse.

The results of measurement are given in Tables 1 and 2, together with frequencies of the Raman spectra of molten $SbCl_3$ and $SbCl_5$ reported by other investigators[1-3]. It will be seen from Table 1 that the Raman spectrum of $SbCl_3$ in solution exhibits no new lines, but as compared with the molten state spectrum, the lines are shifted to the side of the exciting line, the shift being greater for higher concentrations of HCl. The shortest frequency (134 cm^{-1}) line was not observed; presumably it was obscured by the halo around the greatly overexposed 4358 A line.

The following conclusions may be drawn from the experimental results:

1. The Raman spectra of the aqueous solutions of $SbCl_3$, as well as the spectra of the molten salt and its non-aqueous solutions, indicate that the nucleus of the absorption "centers" is constituted by a $SbCl_3$ formation in the shape of a trihedral pyramid; this pyramidal formation is surrounded by ions and molecules of the solvent which exert a deforming influence - primarily electrostatic in character - on the $SbCl_3$ bonds. This leads to the weakening of the bonds and a reduction of the vibrational frequencies as the HCl concentration is increased.

2. In consequence of the appreciable influence of the hydrogen ions on the pyramidal $SbCl_3$ formation there appears a new absorption maximum at a wavelength of 232 m at high concentrations of HCl.

Irradiation with short ultraviolet causes breaking away of an electron (whose bonds have been weakened through the influence of the hydrogen ions) from the Sb^{+++} ion. The Sb^{+++} ion is thus "oxidized" to a four valent one and then undergoes a rapid transition to five valent antimony. Hence after irradiation of a solution of $SbCl_3$ in saturated hydrochloric acid with short ultraviolet, the absorption (at 270 mμ) occurs in the newly formed complex comprising Sb^{5+}.

Table 1

Raman spectra of solutions of $SbCl_3$ and of the molten salt

Molten $SbCl_3$	Solutions of $SbCl_3$ in different concentrations of HCl (mol/liter):				Solutions in:	
	11.5	6.5	3.8	2.3	H_2O	$LiCl-H_2O$
360 cm^{-1}	321 cm^{-1}	321 cm^{-1}	332 cm^{-1}	337 cm^{-1}	348 cm^{-1}	332 cm^{-1}
320 "	276 "	276 "	285 "	285 "	292 "	285 "
165 "	146 "	147 "	147 "	147 "	146 "	147 "
134 "						

Table 2

Raman spectra of $SbCl_5$ solutions in saturated HCl and of the molten salt

$SbCl_5$	400	356	309	177	72 cm^{-1}
$SbCl_5$+HCl	321	281	208	178	136 cm^{-1}

That hydrogen ions play an essential part in the above-described process is confirmed by the fact that no analogous process is observed in the case of aqueous solutions with KCl or LiCl.

"T. G. Shevchenko" Kiev State University

References

1. P. Daure, Ann. de phys., 12, 375 (1929).
2. P. Krishnamurti, Ind. Journ. Phys., 5, 116 (1930).
3. H. Mouren, M. Magat & G. Wetroff, Proc.Ind.Acad.Sci., 8, 356 (1938).

* * * * * * *

RAMAN SPECTRA OF SOME HYDROCARBONS OF THE CYCLOBUTANE SERIES

- V.T.Aleksanian, M.Iu.Lukina, Kh.E.Sterin & B.A.Kazanski

The present investigation, which forms part of a series of studies carried out under the joint auspices of the Institute of Organic Chemistry and the Physical Institute of the Academy of Sciences of the USSR, concerned the Raman spectra of nine hydrocarbons of the cyclobutane series. The results follow:

[Translator's note: d = double, w = wide, p = polarized, bkgd = background; the figures in parentheses are presumably relative intensities.]

METHYLCYCLOBUTANE. t_{boil} = 37.4° (760 mm); n_D^{20} = 1.3870; d_4^{20} = 0.6990; MR_D = 23.58; MR_D (calc. for C_5H_{10}) = 23.09; increment MR_D = 0.49.

$\Delta\nu cm^{-1}$: 319 (9,d), 374 (1), 417 (7), 605 (16,p), 775 (3,w), 864 (15,w),

881 (23,w), 914 (60), 922 (60), 965 (70,p), 1064 (10,p), 1082 (3), 1104 (23,p), 1124 (0), 1160 (7,p), 1181 (5,p), 1199 (1), 1223 (11,w), 1233 (4), 1260 (5,w), 1285 (1,w), 1341 (7,w), 1379 (3,w), 1445 (35,w), 1456 (20,w), 1463 (5,?), 2859 (100, p, bkgd), 2867 (130, p, bkgd), 2906 (140,p, bkgd), 2920 (130,p), 2951 (150, bkgd.), 2961 (160, bkgd).

TRANS-1, 3-DIMETHYLCYCLOBUTANE. t_{boil} = 57.4-57.6° (760 mm); n_D^{20} = 1.3896; d_4^{20} = 0.7016; MR_D = 28.39; MR_D (calc. for C_6H_{12}) = 27.71; increment MR_D = 0.68.

$\Delta\nu cm^{-1}$: 333 (3), 357 (15,w), 366 (3), 433 (23,p), 463 (1), 472 (0), 565 (40,p), 586 (2), 622 (1), 644 (3), 745 (3), 763 (5), 854 (4), 877 (30,w), 887 (88,w,p), 946 (18,p), 975 (5), 1001 (1), 1035 (2), 1060 (13), 1083 (1), 1103 (20,w), 1130 (26,w,p), 1150 (3), 1175 (10), 1198 (5), 1234 (16,w), 1273 (7,w), 1293 (5), 1352 (21), 1376 (3), 1458 (49,w), 2852 (50,p,p), 2869 (120, p,p), 2890 (150,p), 2910 (50, bkgd), 2928 (190, w, bkgd, p), 2957 (190,w,d).

CIS-1, 3-DIMETHYLCYCLOBUTANE. t_{boil} = 60.5-60.6° (760 mm); n_D^{20} = 1.3933; d_4^{20} = 0.7106; MR_D = 28.26; MR_D (calc. for C_6H_{12}) = 27.71; increment MR_D = 0.55.

$\Delta\nu cm^{-1}$: 276 (4,w), 333 (24,w,p), 380 (14,w), 433 (2,w), 565 (1,w), 617 (0), 644 (33,p), 664 (3, bkgd), 704 (2,w), 756 (0,w), 797 (14,w), 855 (69,p), 891 (63,w), 935 (11,p), 962 (1), 974 (1), 988 (1), 1004 (1), 1031 (11,w), 1110 (48,w), 1130 (0), 1158 (7), 1169 (7), 1189 (5), 1219 (11,w), 1245 (12,w), 1348 (17,w), 1377 (5), 1456 (57,w), 2847 (20,p), 2869 (120, p, bkgd, p), 2893 (90, bkgd), 2922 (250,bkgd,p), 2936 (250, bkgd, p), 2956 (250, bkgd).

TRANS-1-METHYL-3-ETHYLCYCLOBUTANE. t_{boil} = 87.9-88.1° 760 mm); n_D^{20} = 1.4005; d_4^{20} = 0.7224; MR_D = 32.96; MR_D (calc. for C_7H_{14}) = 32.32; increment MR_D = 0.64.

$\Delta\nu cm^{-1}$: 236 (1), 249 (1), 284 (1), 325 (3), 380 (0), 409 (54,w,p), 434 (8, w, bkgd), 557 (1), 583 (23,w), 609 (3), 751 (4,w), 804 (1), 882 (52), 894 (63,w,p), 928 (36,w), 939 (15,w), 959 (5,w), 1066 (17,w), 1096 (19,w), 1118 (20, w,p), 1135 (18,w), 1175 (8,w), 1233 (16,w), 1260 (9,w), 1309 (10,w), 1338 (3), 1362 (16,w), 1380 (3), 1445 (10, bkgd), 1458 (56,w), 2855 (80), 2868 (60, bkgd), 2890 (160, bkgd), 2901 (60, bkgd), 2925 (50, bkgd), 2943 (140, bkgd), 2959 (170, bkgd).

CIS-1-METHYL-3-ETHYLCYCLOBUTANE. t_{boil} = 91.0-91.1° (760 mm); n_D^{20} = 1.4043; d_4^{20} = 0.7316; MR_D = 32.81; MR_D (calc. for C_7H_{14}) = 32.32; increment MR_D = 0.49.

$\Delta\nu cm^{-1}$: 284 (0), 321 (25,w,p), 349 (1), 425 (10,w,p), 438 (15,w), 505 (0), 556 (0), 621 (0), 651 (18,p), 673 (0), 704 (1), 725 (1), 750 (3,w), 789 (4), 807 (21,w,p), 858 (10,w) 868 (38,p,p), 887 (28), 925 (34,w), 958 (5), 990 (5), 1008 (5), 1043 (10), 1096 (30,p), 1116 (26,p), 1141 (1), 1176 (3), 1194 (5), 1214 (3), 1240 (7), 1252 (3), 1271 (4), 1308 (6), 1333 (4), 1357 (12), 1376 (2), 1455 (56,w), 2853 (60), 2871 (100, w, bkgd, p), 2893 (140,w), 2914 (100,w), 2933 (255,w,p), 2955 (150,w).

TRANS-1-METHYL-3-n-PROPYLCYCLOBUTANE. t_{boil} = 116.1-116.3° (760 mm); n_D^{20} = =1.4088; d_4^{20} = 0.7370; MR_D = 37.60; MR_D (calc. for C_8H_{16}) = 36.94; increment MR_D = 0.66; aniline point = 60.4°.

$\Delta\nu cm^{-1}$: 286 (2), 293 (2), 320 (20,p), 346 (3), 392 (21,p), 423 (6,w), 454 (6,w), 495 (0), 531 (1?), 584 (8,w), 603 (11,w), 705 (1), 740 (2), 803 (6,w), 851 (10,w), 886 (42,d, one component p), 913 (21,p), 947 (30,w), 996 (0), 1026 (9,w), 1039 (9,w), 1072 (17,w), 1109 (15), 1123 (21), 1174 (4), 1204 (1), 1231 (7,w), 1270 (1), 1303 (5), 1317 (2),1341 (7,w), 1366 (4), 1441 (25,w), 1457 (46, w), 1488 (0), 2398 (0), 2441 (5), 2452 (10), 2489 (20,w), 2847 (80,w,p), 2864 (120, w, bkgd, p), 2887 (170, bkgd), 2910 (80, bkgd), 2919 (120, w, bkgd), 2934 (80, bkgd), 2958 (150, w, bkgd).

CIS-1-METHYL-3-n-PROPYLCYCLOBUTANE. t_{boil} = 118.5-118.7°; n_D^{20} = 1.4128; d_4^{20} = 0.7453; MR_D = 37.49; MR_D (calc. for C_8H_{16}) = 36.94; increment MR_D = 0.55; analine point = 57.2°.

$\Delta\nu$ cm^{-1}: 201 (0) (the intensities here are visual evaluations on the ten-point scale), 230 (1), 242 (1), 257 (1), 293 (3), 317 (3,w), 386 (1,w), 416 (3), 425 (2,w), 463 (1), 516 (0), 538 (0), 589 (1), 627 (1), 679 (1,w), 707 (1), 737 (0), 794 (3), 808 (3), 827 (3,w), 845 (5), 888 (7,w), 943 (5,w), 976 (1,w), 1001 (2), 1033 (3,w), 1056 (2,w), 1080 (1,w), 1110 (7,w), 1127 (2), 1153 (1), 1195 (2, bkgd), 1208 (2, bkgd), 1239 (3,w), 1276 (2), 1301 (3), 1315 (1), 1342 (3,w), 1370 (0,w), 1442 (5,w), 1455 (8,w), 1481 (1), 1502 (0), 2839 (5), 2869 (7,w), 2887 (5,w), 2916 (5, bkgd), 2933 (8,w), 2956 (5,w).

TRANS-1, 2-DIMETHYL (Ref. 1). t_{boil} = 56.8-56.92° (760 mm); n_D^{20} = 1.3893; d_4^{20} = 0.7029; MR_D = 28.33; MR_D (calc. for C_6H_{12}) = 27.71; increment MR_D = 0.62; aniline point = 52.0°.

$\Delta\nu$ cm^{-1}: 201 (2), 248 (12,w), 295 (1,w), 308 (1), 343 (0), 374 (7,w), 483 (29,p), 568 (0), 592 (10,w), 756 (66,p), 800 (4), 877 (60,w), 900 (18), 933 (60, p), 1073 (3), 1096 (15,w), 1117 (24,p), 1165 (12,p), 1199 (10), 1222 (7,p), 1252 (7), 1289 (1), 1307 (0), 1325 (9), 1378 (5,w), 1442 (34,w), 1456 (51,w), 2864 (180,w,p), 2886 (160,w), 2901 (50, bkgd), 2923 (160, bkgd, p), 2956 (220,w).

1-METHYL-2-ETHYLCYCLOBUTANE (with an appreciable preponderance of the trans-form). t_{boil} = 90.1° (760 mm); n_D^{20} = 1.4030; d_4^{20} = 0.7284; MR_D = 32.86; MR_D (calc. for C_7H_{14}) = 32.32; increment MR_D = 0.54.

$\Delta\nu$ cm^{-1}: 265 (15,w), 322 (2,w), 349 (2), 373 (3), 411 (11), 432 (16), 475 (21,p), 502 (0), 526 (1), 550 (1), 590 (8,w), 607 (4), 677 (3), 735 (22,p), 756 (13,p), 784 (27,p), 797 (15,w,p), 880 (17,w), 910 (48,w), 930 (43,w,p), 954 (12), 985 (2), 1020 (5), 1088 (28, w, bkgd), 1116 (30, w, bkgd), 1144 (2), 1170 (12), 1192 (10,p), 1220 (7), 1235 (5), 1243 (5), 1276 (1), 1305 (10), 1337 (8,w), 1360 (2), 1381 (4), 1445 (66,w), 1456 (40,w), 2862 (100, w, bkgd), 2876 (170,w,p,bkgd), 2902 (130, p, bkgd), 2935 (140, p, bkgd), 2960 (170, w, bkgd).

The investigated spectra exhibit a number of distinctive features:

1. All the spectra have a group of three-four intense, partially polarized lines in the region of 850-950 cm^{-1}, one or two lines in the 1090-1120 cm^{-1} region and a polarized line in the 300-450 cm^{-1} interval. Despite the comparatively limited number of compounds studied, it may be safely assumed that the above mentioned lines are characteristic of hydrocarbons containing a cyclobutane ring.

The stereoisomers, characterized by the same type of ring substitution, have the following common frequencies:

Trans-1, 3-substituted: 392-433, 877-886, 886-894, 930-945, 1096-1110, 1123-1135 and 1230-1233.

Cis-1, 3-substituted: 317-333, 644-650, 790-810, 845-865, 887-891, 925-943, 1096-1110, 1240-1245.

Trans-1, 2-substituted: 475-483, 756, 877-888, 900-910, 930-933, 1038-1096, 1117.

3. The frequencies of the cis- form, as in the case of most homologues of cyclopentane and cyclohexane, are generally lower than the corresponding frequencies of the trans- form.

In the accompanying table our experimental results are juxtaposed with the interpretation of the ring frequencies of cyclobutane given in Ref. 2.

It will be noted that the frequency of pulsation of the ring goes down from 1010 cm^{-1} in cyclobutane to 850-900 cm^{-1} in the spectra of its di-derivatives. It may be assumed that this is connected with a decrease in ring strain, which is in conformity with the lower value of the refraction increment in cis-1,

3-compounds as compared with trans- compounds in accordance with the lower value of the totally symmetrical ring frequency in the 850-900 cm^{-1} region. Lastly, we note that in contrast to the case in the spectra of paraffins, naphthenes (5- and 6-membered), alkenes and many aromatic series compounds, the C—H valence vibration lines are very sharp in the spectra of most of the investigated compounds. An analogous effect was observed in the spectra of ethylcyclopropane and 1, 1, 2-trimethylcyclopropane.

Tentative interpretation of the frequencies of the investigated hydrocarbons

Frequency in cyclobutane spectrum (Ref.2), cm^{-1}	Type of symmetry	Frequency in spectra of monoderivatives, cm^{-1}	Approx. type of symmetry	Frequency in spectra of di-derivatives, cm^{-1}	Remarks
1010(p, Rmn)	A_{1g}	930-967 (p)	A	850-900 (p)	
940(d, Rmn)	B_{1g}	910-930 (d)	B	900-954 (dp)	
627(i.r., ⊥)	E_u	?	A+B	?	A number of frequencies present in this region; exact assignment difficult.
595 (very weak, Raman)	B_{2g}	?	A	?	
145 (forbidden)	B_{1g}	??	A	??	So low a value appears doubtful. May correspond to the polarized line at 300-450 cm^{-1} observed in all spectra.

Commission on Spectroscopy at the
OFMN of the Academy of Sciences
and the
Institute of Organic Chemistry of the
Academy of Sciences of the USSR

References

1. B.A.Kazanski & M.Iu.Lukina, Doklady AN SSSR, 94, 887 (1954).
2. T.P.Wilson, Journ. Chem. Phys., 11, 369 (1943).

* * * * * * *

INVESTIGATION OF THE MOLECULAR SPECTRA OF ORGANO-SILICON COMPOUNDS BY THE METHODS OF RAMAN AND INFRARED SPECTROSCOPY

- Iu. P. Egorov

In order to study the molecular spectra of organo-silicon compounds and refine the assignment of C—H group vibration frequencies to the various paraffin isomers, we investigated a series of unsaturated silanes - $(CH_3)_kSi(CH_2CHCH_2)_{4-k}$ [k - 0, 1, 2 or 3] - and five branched-dodecanes. We ob-

tained the Raman spectra, measuring the polarization, integral intensity and breadths of the characteristic lines[1] and the infrared absorption spectra.

A definite proportional relationship was found to obtain between the integral intensity of each of the characteristic Raman lines and the number of $CH_2CH{=}CH_2$ groups about the Si atom , with the values of the line width and polarization remaining constant. The magnitude of the molecular absorption coefficient for the corresponding infrared bands is characterized by a like proportionality. It was also established that the contour and breadth of the 3.25 and 6.16 μ bands remain constant. A similar relationship characterizing the intensity of these bands has been observed in molecules of the type $R_3Si{-}(CH_2CH{=}CH_2)$ where R = CH_3, C_2H_5, etc.[2]

The results indicate that interaction between neighboring groups linked to the Si atom is very weak and that the effect of the groups is additive, i.e., that the manifestation of these groups in silane molecules is rigorously characteristic of the coordinate group as a whole, which is in agreement with theory[3].

These attributes are particularly apparent in the frequency region of C—H vibrations. In silanes of the form $Si(CH_3)_4$ (Ref. 4), $(CH_3)_3Si{-}C{\equiv}C{-}C_6H_5$ (Ref. 5) and others, there are only two lines in this region — at 290 and 2963 cm^{-1} — and, in conformity with theory, the first of these is polarized, the second, depolarized. In contrast, the simplest analogous molecule not containing silicon, i.e., $C(CH_3)_4$, has five lines in the CH vibration region.[4] Three-four frequencies — 2880, 2900-2915 and 2965 cm^{-1} — are reported in Refs. 5 and 6 for silanes having the formulas $(C_2H_5)_3Si{-}C{\equiv}C{-}C_6H_5$ and $(C_2H_5)_4Si$. From comparison of these data it follows that the frequencies associated with the CH_2 group are 2880 and 2915 cm^{-1}, while the frequencies belonging to the CH_3 group are 2900 and 2963 cm^{-1}. The results indicate that it is expedient to assign frequencies on the basis of the spectra of molecules with non-interacting functional groups. This is particularly important in the case of branched paraffins, for which C—H vibration frequency assignments in the literature are conflicting.

Assuming the multiplicity of lines in this region to be a consequence of interaction between neighboring groups and comparing the spectra of silanes and diverse paraffins, we arrived at the interpretation given in the accompanying table.

Assignment of CH vibration frequencies to different molecular groups

Investigators	Frequencies, cm^{-1}				
	2856	2875	2905	2936	2965
Iu.P.Egorov	CH_2 **CH_3**	CH, CH_2 **CH_3**	**CH_2, CH_3**	CH_2 **CH_3**	**CH_3**
M.V.Vol'kenshtein et al [4]	**CH_2, CH_3**	**CH_3**	**CH_2, CH_3**	**CH_3**	**CH_3**

The lines do not have unique assignments; the predominant groups in each case are indicated in heavy type. The principal differences between our interpretation and that of other investigators are the assignment of the 2875 cm^{-1} frequency to the CH and CH_2 groups instead of to CH_3 and of the 2936 cm^{-1} frequency to CH_2 instead of to CH_3.

To verify our attributions, we obtained the Raman and infrared spectra of three isoparaffins differing radically in structure: (I) — n-dodecane, (II) — 2, 5, 8-trimethylnonane and (III) — 2, 2, 4, 6, 6-pentamethylheptane. Measurements showed that the intensity of the 2875 cm^{-1} line is 70 in (I), 60 in (II) and 35 in (III), although (I) has only two CH_3 groups while (II) and (III) have

2.5 and 3.5 times that number, respectively. The intensity of the 2936 cm^{-1} line decreases in a like manner, being 45 in (I), 40 in (II) and 5 in (III). This variation in intensity is explained by the decrease in the number of CH_2 groups present as we go from (I) to (III) and by the numerous CH groups present in (II). The variation in the intensity of the other lines and bands in the spectra confirms our interpretation.

In closing the writer wishes to express his gratitude to P.A.Bazhulin for his help and advice in the preparation of this report.

Physics Department of
Moscow State University

References

1. P.A.Bazhulin, Iu.P.Egorov & V.F.Mironov, Doklady AN SSSR, 92,515 (1953).
2. Iu.P.Egorov & P.A.Bazhulin, Doklady AN SSSR, 88, 647 (1953).
3. M.V.Bol'kenshtein, Molekuliarnaia optika (Molecular optics), M.1951.
4. D.H.Rank & others, Disc. Far. Soc., 9, 187 (1950).
5. A.D.Petrov, Shchukovski & Egorov, Doklady AN SSSR, 93, 293 (1953).
6. V.A.Kolesova & others, Izv. AN SSSR, Otd. khim. nauk, 2, 294 (1953).
7. M.V.Vol'kenshtein, M.A.El'iashevich & B.I.Stepanov, Kolebaniia molekul (Molecular vibrations), Vol. I, GITTL, Moscow 1949.

* * * * * * *

ANALYSIS OF THE AROMATIC COMPONENTS OF LIGROIN BY RAMAN SPECTROSCOPY

- B.A.Kazanski, G.S.Landsberg, V.T.Aleksanian, T.F.Bulanova, A.L.Liberman, E.A.Mikhailova, A.F.Plate, KH.E.Sterin & S.A.Ukholin

As is known, spectroscopic determination of the hydrocarbon composition of gasolines becomes increasingly difficult as the boiling point goes up. When we get into the ligroins the difficulties mount with the increase in the number of hydrocarbon isomers present, particularly since their spectra are still largely unknown. We attempted to obviate the difficulties to some extent by taking advantage of the fact that the Raman spectra of mono-, di- and tri-substituted benzenes contain lines that are characteristic of the type of substitution in the benzene ring[1,2]. We felt that these properties of benzene homologues could be made use of for determining the composition of the natural (primary) aromatic hydrocarbons of ligroin as well as of its cyclohexane constituents converted to aromatic compounds (secondary aromatics). The present report is devoted to a description of our procedure and a summary of the results of individual and narrow-group analyses of the primary and secondary aromatic compounds of ligroin.

1. The preparatory phase of the investigation consisted of studying the characteristic lines of aromatic hydrocarbon spectra. The most suitable for our purpose, of course, were spectra whose line intensities had been measured with reference to the scale used in our (Soviet) laboratories; unfortunately there are few such spectra. Most of the spectra used were taken from the literature; many of these were investigated under uniform conditions by the method of photoelectric recording[2] while the remainder were obtained photographically by different investigators, with the intensity being evaluated visually in most cases. All the pertinent data reported in spectroscopic literature, although of varying value, was utilized to some extent in our study. Subsequently we added to our list the spectra of a number of hydrocarbons specially synthesized

for the purposes of this investigation.

From the material so assembled we carefully selected the lines characterizing each type of substitution in the benzene ring. It was found that the intensity of the lines associated with a given type of replacement was not markedly dependent on the substituted radical. Hence the intensity of a line averaged for different compounds may also be said to characterize, to some extent, the given type of substitution in the experimental temperature interval (around 50°C). The characteristic lines and their "typical" average intensities are listed in Table 1. The number of spectra of each type studied may be taken as an index to the reliability of the indications. Obviously, the frequency values in Table 1 are far more reliable than the intensity values.

2. A ligroin sample of Emba petroleum (Koschagyl' deposit), boiling between 150 and 250°C, was subjected to Raman spectro-analysis by the methods adopted for gasolines[3]. The special procedures employed for ligroin in such analyses will be described elsewhere. Here we will only note that the spectrum of the fractions boiling at above 200° has a strong background.

Primary aromatic hydrocarbons. First the individual composition of the first six fractions, boiling at under 179°C, was established rather fully. Then, using the data of Table 1 we carried out a group analysis for the different benzene homologues of five of these fractions. As will be seen from Table 2, there are only minor divergences between the results of the individual and narrow-group analyses, which promises well for the proposed method.

By extrapolation of the narrow-group indications we also evaluated the content of the various benzene homologues in the higher-boiling fractions (179-255°C). A number of individual hydrocarbons were also identified in these fractions: the simplest tetra-alkylbenzenes and very minor amounts of indan and tetralin and naphthalene.

Table 1

Characteristic lines in the spectra of aromatic hydrocarbons and their average intensities

Hydrocarbons, type substitution & number of given type spectra analyzed	Frequency cm^{-1}	Intensity *1	Hydrocarbons, type substitution & number of given type spectra analyzed	Frequency cm^{-1}	Intensity *1
Monoalkylbenzenes	621±2*2	40	1, 2, 3-Trialkyl-benzenes	482±2	75
17	1002±2	350		532±3	55
	1031±1	75	3	652±3	450
	1156±1	30		994±1	50
	1182±1*3	15		1097±5	100
	1205±5	65			
1, 2-Dialkylben-zenes	586±4	35	1, 2, 4-Trialkyl-benzenes	458—485*5	75
	714±3	130		548±6	120
6	1039±6	200	4	738±5	150
	1220±5	150		1245±2	120
1, 3-Dialkylben-zenes	525±6*4	80	1, 3, 5-Trialkyl-benzenes	513±2	120
	716±8	140		574±3	240
6	1002±1	400	2	999±2	350
	1247±3	65		1297±3	100
			Naphthalene & its homologues	510—525	~250
1, 4-Dialkylben-zenes	642±2	50		1368—1385	~2500
	780—810	250		1570—1585	300—500
8	1204±4	100			
			Diphenyl homologues	1270—1285	

*1. Intensities referred to cyclohexane.
*2. Possible range of frequency variation for different spectra.
*3. In five of the seventeen spectra this line was not observed.
*4. This line is absent in one of the six spectra.
*5. One or two lines.

Table 2

Comparison of results of individual and group analyses

Individual hydrocarbons & types of alkyl-substituted benzenes	Content, % Fraction No. and boiling points				
	II 155-161°	III 161-165°	IV 165-169°	V 169-175°	VI 175-179°C
n-Propylbenzene	15	3	-	-	-
tert-Butylbenzene	-	5	10	1-2	-
Isobutylbenzene	-	-	10	2	-
n-Butylbenzene	-	-	-	5	25
Monoalkylbenzenes*	15	5	10	20	20
1-Methyl-2-ethylbenzene	5	10	-	-	-
1,2-Diakylbenzenes*	5	?	-	2	-
1-Methyl-3-ethylbenzene	40	5	-	-	-
1-Methyl-3-n-propylbenzene	-	-	-	-	20
1,3-Dialkylbenzenes*	35	2	10	5	15
1-Methyl-4-ethylbenzene	15	5	-	-	-
1-Methyl-4-isopropylbenzene	-	-	-	10	20
1,4-Dialkylbenzenes*	15	3	5	10	20
1,2,3-Trimethylbenzene	-	-	5	65	5
1,2,3-Trialkylbenzenes*	-	-	3	45	3
1,2,4-Trimethylbenzene	-	25	65	10	-
1,3-Dimethyl-4-ethylbenzene	-	-	-	-	10
1,2,4-Trialkylbenzenes*	2	20	60	10	15
1,3,5-Trimethylbenzene	15	45	2	-	-
1,3-Dimethyl-5-ethylbenzene	-	-	-	-	10
1,3,5-Trialkylbenzenes	20	60	2	-	20

*Group analysis data

Secondary aromatic hydrocarbons (153-271°C). The fractions here were taken in a rather wide temperature interval and hence we were forced to restrict the analysis to the determination of a few individual hydrocarbons. In contrast to the case of the lighter fractions, we detected diphenyls in the higher boiling fractions, while alkylbenzenes were identified only from group indications.

Comparison of the results for the primary and secondary aromatic hydrocarbons indicates that the original ligroin contained alkyl-substituted benzenes and cyclohexane, primarily with short replacement radicals.

"N.D.Zelinski" Institute of Organic Chemistry
of the Academy of Sciences of the USSR
and the
Commission on Spectroscopy at the
OFMN of the Academy of Sciences of the USSR

References

1. M.M.Sushchinski, Izv. (Bulletin) AN SSSR, Ser. Fiz., 17, 608 (1953).
2. D.H.Rank, M.R.Fenske, et al, Anal. Chem., 19, 700 (1947); W.G.Braun, D.F.Spooner & M.R.Fenske, Anal. Chem., 22, 1074 (1950).
3. G.S.Landsberg & B.A.Kazanski, Izv. AN SSSR, Otd. Khim. nauk, 2, 100 (1951).

* * * * * * *

APPLICATION OF INFRARED SPECTROSCOPY TO THE INVESTIGATION OF PETROLEUM PRODUCTS

- K.I.Zimina, A.V. Iogansen & A.G.Sigriuk

We applied the methods of infrared absorption spectroscopy to group structural analysis of petroleum products: gasolines, kerosenes, oils and tarry residues.

1. Characteristic bands in the 800 to 1000 cm^{-1} region, associated with non-plane, distortional vibrations of hydrogen atoms at double bonds, were used to establish the content of the following types of unsaturated hydrocarbons: I - $RCH{=}CH_2$ (909 and 993 cm^{-1}); II - $RR'C{=}CH_2$ (about 890 cm^{-1}); III - trans-$RCH{=}CHR'$ (about 970 cm^{-1}); IV - $RR'C{=}CHR''$ (about 820 cm^{-1}). In motor vehicle and aviation gasolines produced by catalytic cracking, compounds of types IV and II predominate, those of type III are present in small amounts, while type I is absent. Hydrocarbons of all four types are found in gasolines and kerosenes produced by heat cracking.

2. The presence of isoparaffin hydrocarbons in normal paraffins, separated from straight-run kerosene in deparaffination with carbamide, was determined according to the integral intensity of the band at 1380 cm^{-1} (distortional vibration of CH_3 groups). In the analysis of oil fractions, increase in branching or in the number of side chains of aromatic hydrocarbon molecules with increasing molecular weight of the fraction was determined in an analogous manner.

3. We also investigated the region of the characteristic frequencies (1300-4000 cm^{-1}) in the spectra of tarry residues from different crudes. Bands at about 3400, 2900, 1700, 1610, 1500, 1460 and 1380 cm^{-1} are characteristic of almost all the tars. The most intense bands are the ones at 2900, 1460 and 1380 cm^{-1} (valence and distortional vibrations of the C—H groups). The high intensity of the 1460 and 1380 cm^{-1} bands indicates an appreciable content of CH_2 and CH_3 groups; very intense bands at 1610 and 1500 cm^{-1} are evidence of the presence of benzene rings in large numbers. The presence of C=O groups was established in all tar fractions, however the intensity of the 1700 cm^{-1} band associated with this group, varied in the spectra of different samples and different adsorption-separated tar fractions. The broad bands at 3200-3400 cm^{-1} observed in the tar spectra may be attributed to O—H or N—H groups, forming hydrogen bonds. Tars from different crudes exhibit qualitatively similar spectra, differing mainly as regards the intensity of individual lines.

4. Our experiments indicated that group structural analysis with the aid of infrared absorption spectra can be successfully used for the investigation of petroleum products in a wide range of molecular weights. It has greater potentialities than quantitative analysis of simple mixtures of hydrocarbons, such as narrow fractions of benzenes, alkylates and similar compounds.

Central Institute of Aviation Fuels and Oils

* * * * * * *

A LOW-PRESSURE MERCURY TUBE AND ITS USE IN STUDYING RAMAN SPECTRA

- M.L.Sosinski

We have succeeded in making further improvements in the low-pressure mercury tube with narrow lines and a weak continuous background, described in Ref. 1. Specifically we eliminated the rapid darkening of the tube walls from which the early version suffered, enhanced the stability of the emission and developed a tube design suitable for use in studying Raman spectra. Of the

domestic (Soviet) types of glass, the best as regards technological and thermoelectrical properties proved to be "pireks" [Pyrex]. As a result of our development work, we now have a stable tube capable of prolonged operation.

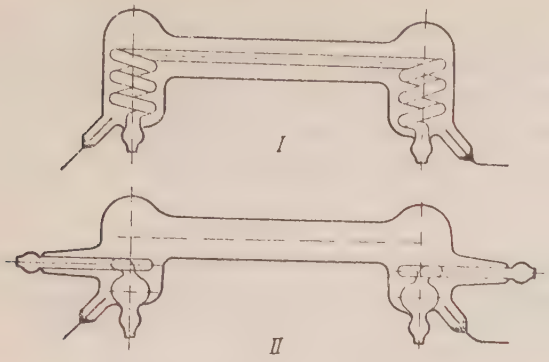

Low-pressure mercury tube: I - with cooling of the liquid electrodes and of the entire length of the discharge; II - with cooling of the electrodes and the region in their vicinity.

The accompanying figure shows two versions of the tube, I with cooling of the liquid electrodes and the entire length of the discharge, and II with cooling of the electrodes and the region of the discharge adjacent to them. We investigated the variation of the intensity and breadth of the lines in the visible region of the spectrum with the current strength, the pressure of an extraneous gas (helium) in the tube and the temperature of the cooling water. The intensity of the emission of tube II proved to be independent of the cooling unit temperature. The intensity of the background of both tube versions is of the same order. The half-breadth of the 4358 A line changes from 0.014 to 0.021 A in the case of tube I and from 0.023 to 0.025 A in the case of tube II when the current is varied between 5 and 15 amps. We also developed a simple and dependable circuit for operating the tube. Tube II is fully adequate for Raman spectroscopy; tube I gives narrower lines.

We also constructed helical tubes: a tube with two turns which cuts down the exposure time by a factor of 2.5 and operates from a 120 volt source and a tube with three turns which requires a 220 volt supply.

The new tubes permit extending the range of applications of Raman spectroscopy. Purity checks on a number of hydrocarbon standards showed that the admixture of halide derivatives in them does not exceed 0.5%. The new tube was used in investigating the concentration-dependence of the intensity and shift of the lines of 1,2-dichlorethane in various solvents at concentrations ranging down to 1/5 to 1/8th of those previously studied[2]. It was also established that the spectra of 1,2-dichlorethane in different neutral solvents are identical. Extrapolation of zero concentrations and comparison with the data of Mizushima et al[3] and Mazumder[4] showed that when 1,2-dichlorethane is mixed with a neutral solvent the spectrum of dilute solutions approaches that of the vapor (see table).

Ratio of line intensities and frequency shifts of 1,2-dichlorethane in dilute solutions and in vapor form

	Solution	Vapor	
	our data	Mazumder 150°C	Mizushima 170°
I_{753}/I_{653}	7	4.5	5
ν_{301}, cm^{-1}	0	0	+1
ν_{653}, cm^{-1}	+11	+14	+12
ν_{753}, cm^{-1}	+8.5	+7	+13

Moscow Physico-Technical Institute

References

1. M.L.Sosinski, Izv. (Bulletin) AN SSSR, Ser. fiz., 17, 621 (1953).
2. A.M.Aronov, V.M.Tatevski & A.V.Frost, Vestnik MGU (Moscow State University Review) 1, 125; 2, 45 & 50 (1948).
3. Mizushima & others, Journ. Chem. Phys., 17, 592 (1949).
4. M.Mazumder, Ind. Journ. Phys., 27, 8, 406 (1953).

* * *

SOME GENERALIZATIONS OF THE "METALLIC" MODEL IN THE THEORY OF COMPLEX MOLECULES

- M.G.Veselov and T.N.Rekasheva

In the present paper we propose certain elaborations of the "metallic" model of molecules with conjugate bonds: 1) for systems having incompletely equalized [aligned?] simple and double bonds and 2) for taking account of the inductive effect in conjugate systems.

In both cases we consider a one-dimensional potential box with infinitely high walls and a length equal to the length of the molecule.

Table I

Comparison of the calculated frequency and strength of the oscillators of butadiene and hexatriene and thiophene molecules with experimental data

Molecule	Frequency, cm^{-1}		Oscillator strength	
	computed	experiment.	computed	experiment.
C_4H_6 trans	48,900	48,000	0.98	0.53
C_4H_6 cis			0.64	
C_6H_8	32,200	39,750	1.60	0.62-0.70
C_4H_4S	40,100	42,000	0.32	0.084

We take account of the incomplete equalization of the simple and double bonds in conjugate systems by introducing barriers into the potential box at locations corresponding to the simple bonds. Using this elaboration we calculated the frequencies and strengths of the oscillators corresponding to the principal absorption transition of butadiene, hexatriene and thiophene molecules. The height V_o of the barrier corresponding to the simple carbon bond was selected so as to make the computed frequency of the long-wave absorption band of butadiene approximately equal to the experimental frequency. The same value was then used for the barriers corresponding to the simple carbon bonds in the two other molecules. The results are shown in Table 1.

Table 2

Results of calculation of the dipole moments of vinyl chloride, bromide and iodide and acrolein molecules compared with experimental data

Molecule	Dipole moment	
	Computed	Experiment.
C_2H_3Cl	0.67	0.65
C_2H_3Br	0.62	0.58
C_2H_3I	0.47	0.50
C_3H_4O	0.80	1.19

The inductive effect of the electronegative atom in conjugate systems was taken into account by introducing a "pit" into the potential box at the point corresponding to this atom. The pit depth V_o was taken equal to approximately half the electronegativity of the substituent atom, replacing the carbon atom. Proceeding in this manner we calculated the states of the π-electrons in the molecules of vinyl chloride, vinyl bromide, vinyl iodide, acrolein and chlorobenzene. The computed values for the principal electronic transitions are in good agreement with experiment. The dipole moments of the conjugate bond systems were also calculated for these molecules. We assumed uniform distribution of the positive charge over the entire length of the molecule in each case and took into account the uncompensated dipole moment of the CH linkages. The results are summarized in Table 2.

Physics Institute of
Leningrad State University

* * * * * * *

THE SHAPE AND TEMPERATURE-DEPENDENCE OF IMPURITY-ACTIVATED LUMINESCENCE AND ABSORPTION BANDS OF SOLID AND LIQUID DIELECTRICS AND SEMICONDUCTORS

- S.I.Pekar

Our theory of the shape of bands has been set forth in Refs. 1, 2, 4 and 5. It was developed without reference to a specific impurity-center model and without explicit expression of the electron part of the wave function of the system. Hence the results obtained are wholly general and applicable to centers of any type, to crystals of any structure and to liquid solutions.

In the case of phototransitions with a high thermal emission[4] the half-width $\delta\omega$ of the band at any arbitrary temperature and in the absence of dispersion of the normal atomic vibration frequencies is given by

$$\delta\omega = 2\sqrt{2\ln 2}\sqrt{\omega_0\Delta\omega\left(\bar{n}_0+\frac{1}{2}\right)}, \quad \bar{n}_0=\frac{1}{e^{\hbar\omega_0/kT}-1}, \tag{1}$$

where ω_0 is the vibration frequency of the atoms and $\Delta\omega$ is the Stokes shift.

With arbitrary dispersion of the atomic vibration frequencies, but at high temperatures

$$\delta\omega = 2\sqrt{2\ln 2}\sqrt{\frac{\Delta\omega kT}{\hbar}}. \tag{2}$$

Equations (1) and (2) contain no unknown parameters and agree well with experiment. The shape and temperature-dependence of absorption bands are characterized by the general equations in Refs. 2 and 4. The mean thermal emission incident to a phototransition is $\hbar\Delta\omega/2$. The expression relating the energies of optical transitions and the thermal excitation energy of the corresponding W_{12} transition is

$$W_{12}=\hbar\left(\omega_{\max}^{\text{abs}}-\frac{\Delta\omega}{2}\right)=\hbar\left(\omega_{\max}^{\text{emi}}+\frac{\Delta\omega}{2}\right). \tag{3}$$

In the case of low heat evolution when the electronic transition interacts primarily with one branch of the normal vibrations and the spectrum has the form of a "progression" of uniformly spaced bands, the dependence of the integral intensity of an absorption band on its ordinal number q in the "progression" is given by

$$T(q)=\text{const}\,\frac{[\sigma(T)]^q}{q!}, \quad q=0,1,2,3,\ldots \tag{4}$$

Comparisons of the results of our theory with numerous experimental results in the case of high values of heat evolution have appeared in Refs. 2 (Sections 5 & 7) and 7 (Chapter VI). The calculated luminescence and absorption band shapes, the half-width and its temperature dependence, the relation between the half-width and the Stokes shift (1) & (2) and the relationship between the phototransition energy and the thermal excitation energy (3) have proved to be in good quantitative agreement with experiment. In addition to the earlier published data we might cite the verification of the validity of equation (1) in the case of M-centers in LiF crystals carried out by Krivoglaz. According to experimental data[8 &9], the luminescence peak lies at 1.74 ev, while the corresponding half-width is 0.43 ev. The maximum of the absorption spectrum occurs at 2.69 ev and the half-width of the peak is 0.42 ev. Hence the Stokes shift $\hbar\delta\omega$ = 0.95 ev. If for the mean effective frequency ω_0 in equation (1) we take the end-point frequency of the optical vibrations of ions, equal to 0.082 ev, the calculated half-width $\hbar\Delta\omega$ proves to be 0.46 ev, which is in good agreement with the experimental value. Krivoglaz also obtained excellent quantitative agreement of theory with experiment for the shape and temperature-dependence of the luminescence bands of Zn_2SiO_4 with Mn_2SiO_4 as the activating impurity[10].

Band No. (q)	Band area arbit.units	
	Comput.	Measured
0	100	100
1	88	88
2	39	38
3	12	12
4	2,5	3

Good agreement with theory was also reported by Grechushnikov who investigated experimentally the shape and temperature of the absorption band of ruby with an admixture of chromium.

Of particular interest is investigation of the absorption band of ammine solutions which, as has now been firmly established, is due to the absorption of light by polarons. Here, too, the theory has proved to be in full quantitative agreement with experiment. A special report on this subject will be presented by M.F.Deigen (see below).

The electron-vibration progression of impurity-activated absorption bands observed for a CdS crystal[12] indicates that here we are dealing with low thermal evolution. The variation of the integral intensity of the bands with their ordinal numbers is satisfactorily described by equation (4), as may be seen from the accompanying table[10]. The computed area of the first two bands has been made to fit the experimental data by appropriate selection of the theoretical parameters: const = 100 and $\sigma = 0.88$. Verification of the theory is provided by the close agreement of the areas for the remaining three bands.

Institute of Physics of the
Academy of Sciences of the Ukranian SSR

References

1. S.I.Pekar, Zhur. eksp. i teor. fiz., 22, 641 (1952).
2. S.I.Pekar, Usp. fiz. nauk, 50, 2, 197 (1953).
3. V.L.Levshin, ZS. f. Phys., 72, 368, 382 (1931); Acta Phys.-chem. URSS, 1, 685 (1935) & 6, 213 (1937).
4. S.I.Pekar & M.A.Krivoglaz, Trudy Instituta fiziki (Proc. of the Institute of Physics) of the Ukranian SSR Academy of Sc., 4, 37 (1953).
5. S.I.Pekar, Zhur. eksp. i teor. fiz., 20, 510 (1950).
6. Huang & Rays, Proc. Royal Soc., (A) 204, 406 (1950).
7. S.I.Pekar, Issledovaniia po elektronnoi teorii kristallov (Investigations relating to the electron theory of crystals), GTTI, Moscow 1951.
8. C.C.Klick, Phys. Rev., 79, 894 (1950).
9. P.P.Feofilov, Doklady AN SSSR, 92, 743 (1953).
10. M.A.Krivoglaz, Thesis. - Kiev 1954.
11. B.N.Grechushnikov, Thesis, Inst. of Crystallography of the Academy of Sciences of the USSR, Moscow 1953.
12. C.C.Klick, JOS, A41, 816 (1951).
13. M.F.Deigen - below in present issue of the Bulletin.

* * * * * * *

LUMINESCENCE OF MOLECULAR CRYSTALS CONTAINING IMPURITY MOLECULES

M.D.Borisov & A.C.Davydov

We investigated naphthalene crystals containing various concentrations of anthracene, grown from melted naphthalene and anthracene. The anthracene concentration in the crystals was determined according to the absorption spectrum of anthracene, for which purpose control crystals were dissolved in alcohol.

We determined whether the anthracene had entered the naphthalene lattice in

the form of individual molecules or of crystal formations from photographs of the luminescence spectra. Only the crystals into which the anthracene had been incorporated in the form of individual molecules were subjected to further studies.

The sphere method was used to measure the absolute luminescent energy yield of the anthracene impurity activated naphthalene crystals. In this method the investigated crystal and alternately a screen coated with a layer of MgO are mounted in the center of the sphere, the inside walls of which are covered with a layer of MgO. The exciting light (λ = 2950 A) is beamed on the crystal (or screen) through an opening in the sphere. In the first case a light flux of energy E_i - or in the second case, a light flux of energy E_e - emerges from a second aperture in the sphere. In both cases the emergent flux was measured by means of a CdS crystal connected to a linear amplifier.

After introduction of the appropriate corrections, we obtained the energy yields of both pure crystals as well as crystals containing impurities. In the latter case, of course, the emergent flux E_l consisted of the total light emitted by the naphthalene and by the anthracene ($E_l = E_{ln}+E_{la}$).

Knowing the total flux E_l one can readily determine the values of E_{ln} and E_{la} by means of the following equations:

$$E_{ln}=\frac{E_l - 0.09\ E_e}{1+\gamma} \quad \text{and} \quad E_{la}=\frac{(E_l - 0.09\ E_e)}{1+\gamma},$$

where 0.09 is the value of the coefficient of reflection of 2950 A light from the naphthalene crystal and $\gamma = E_{la}/E_{ln}$. The value of γ is found by supplementary measurements.

Two types of excitations may be produced in a molecular crystal by incident electromagnetic radiation (photons)[1]: a) excitations which spread rapidly through the crystal in the form of excitation waves (excitons) and b) "localized excitations" which are propagated very slowly through the crystal.

In moving through the crystal the exciton can transfer its energy to the lattice vibrations. The annihilation of excitons in connection with luminescence competes with this energy transfer process. If we denote the probability of the two competing processes through P_{te} and P_{le}, (probable number of events of each kind per sec), the luminescence yield due to excitons will be given by

$$W_{1K} = \frac{kP_{le}}{P_{le} + P_{te}} \qquad (1)$$

where k is a factor indicating what fraction of the absorbed quanta produce exciton excitations.

Analogously the quantum yield due to "localized excitations" will be given by

$$W_{2K} = \frac{(1 - k)P_{ll}}{P_{ll} + P_{tl}} \qquad (2)$$

where P_{ll} and P_{tl} are the respective probabilities of dissipation of the "localized excitation" energy through emission and of transfer of the excitation energy to vibrations of the lattice. The total quantum yield of a pure crystal will, therefore, be equal to the sum of equations (1) and (2).

If, however, the crystal contains impurity molecules, the exciton produced in the host substance as a result of absorption may, in its passage through the crystal, transfer its energy to an impurity molecule which may then in turn emit the absorbed energy. It can be shown that in this case the quantum yield of the

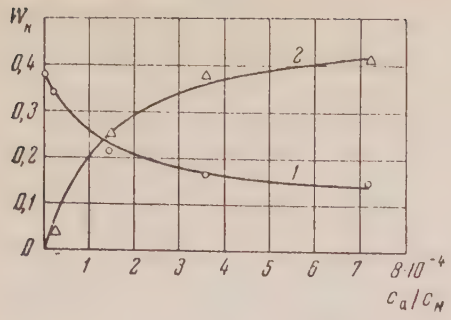

Variation of the luminescence yield of naphthalene (1) and anthracene (2) with the concentration of anthracene. Curves computed according to (3) and (4); the points are experimental values.

main component of the crystal (the host substance) containing the impurities will be

$$W_K(C) = \frac{W_{1K}}{1+\frac{P_i C}{P_{1e}+P_{te}}} + \frac{(1-k)\,P_{1l}}{P_{1l}+P_{tl}}, \quad (3)$$

where C is the concentration of the impurity (i.e., ratio of the number of impurity molecules to the number of host molecules per unit volume. The quantum yield of the impurity will be

$$W_{Ki}(C) = \frac{kP_{il}}{P_{1e}+P_{te}} \cdot \frac{C}{1+\frac{P_i C}{P_{1e}+P_{te}}}. \quad (4)$$

$W_K(C)$ and $W_{Ki}(C)$ computed according to equations (3) and (4) are in good agreement with the experimental values, if the following values are assumed for the variables in these equations:
$W_{1K} = 0.30$; $W_{2K} = 0.08$; $P_i/(P_{1e} + P_{te}) = 6.70 \cdot 10^3$; $kP_{il}/(P_{1e} + P_{te}) = 3.4 \cdot 10^3$.

Curves computed by means of these equations are reproduced in the accompanying figure, where the experimental values of $W_K(C)$ and $W_{Ki}(C)$ are indicated by points.

Institute of Physics of the
Academy of Sciences of the Ukranian SSR

References

A.S.Davydov, Zhur. eksp. i teor. fiz., 18, 210 (1948) & 19, 168 (1949); Trudy Institua fiz. AN UkSSR (Proc. of the Inst. of Phys. of the Ukranian SSR Academy of Sciences) 1 (1951).

* * * * * * *

THE PROPERTIES OF LOCAL ELECTRONIC CENTERS IN SOLID AND LIQUID IONIC DIELECTRICS

- M.F.Deigen

The theory of light absorption by polarons as well as by two types of color centers - F- and F'-centers - was developed in Refs. 1 through 6; many deductions based on this theory are in agreement with experiment.

However, the theory has not until recently been verified for the case of the polaron absorption band, the parameters of which have been calculated by the author in Ref. 7.

1. In addition to the above-mentioned local electronic centers, we have examined, in Ref. 8, the case of a quantum mechanical system consisting of two strongly interacting color centers in close proximity, i.e., of a so-called double color center or F_2-center.

We computed the parameters of the ground and excited states and the thermal dissociation energy of an F_2-center, the frequency of the peak of the F_2-absorption band as well as the half-width of this band. Comparison of the results of these calculations with experimental data led us to conclude (Ref. 9) that as regards its characteristics the F_2-absorption band is similar to the absorption band located to the "red" side of the F-band, i.e., to the so-called R-absorption band.

This conclusion has recently been confirmed by the results of measurements of the magnetic susceptibility in the course of investigations of the paramagnetic resonance of color centers in alkali halide crystals (Ref. 10) as well as by the results obtained by Shatalov (Ref. 11).

2. Davydov (Ref. 12) was the first to suggest that the polaron theory might be extended to the interesting group of liquid ionic dielectrics, constituted by ammine ["metal-ammoniacal"] solutions.

We have shown (Ref. 13) that in ammine solutions, in addition to polarons, there must exist F- and F_2-centers and have explored the possibility of extending the theory of local electron states to this class of liquid dielectrics. In Ref. 13 we determined the equilibrium concentrations of polarons, F- and F_2-centers as a function of the concentration of the dissolved metal and the temperature. It turned out that in dilute solutions, such as those with which the light absorption measurements were made, the electrons are mainly in the polaron state.

In view of the fact that the oscillators associated with the optical transitions of an electron in a polaron and in an F-center differ little as regards strength, it may be assumed that the above-mentioned absorption band is due to polaron absorption.

Thus the direct polaron absorption of light has been demonstrated for the first time.

At higher concentrations of the dissolved metal light absorption by the F- and F_2- centers becomes appreciable. Calculations indicated that the maximum of F-band absorption in ammine solutions should occur at 0.83 ev.

The absorption band predicted by theory has recently been observed experimentally (the peak was recorded at 0.80 ev; Ref. 14); the temperature dependence of the band's intensity is also in close agreement with the predictions of theory.

At sufficiently high concentrations (on the order of 10^{21} cm^{-3}) the radius of the electron state in the F-center $r_F \simeq 2.5$ Å, while the mean separation between centers $r_0 \simeq 10^{-7}$ cm. In view of this the solution becomes a quasi-metal with a metallic conductivity and a characteristic metallic color.

3. In addition to explaining the optical properties and color characteristics of ammine solutions, the theory of local electron states provides a consistent explanation of the magnetic properties of these solutions as well as of the anomaly in the concentration-dependence of their conductivity.

It has been established that highly dilute ammine solutions are paramagnetic (Ref. 15). As the concentration of the dissolved metal is increased the paramagnetism decreases; at a metal atom concentration of about 10^{20} cm^{-3} and a sufficiently low temperature (- 75°C) the coefficient of magnetic susceptibility changes sign.

At still higher concentrations the solution again becomes paramagnetic. This singular variation of the magnetic susceptibility coefficient with the metal concentration may be explained as follows. At low concentrations, polarons predominate in the solution and the solution owes it paramagnetic properties to these quasi-atomic formations. With increasing concentration the number of F_2-centers, which are quasi-molecular formations, grows and consequently the paramagnetism of the solution diminishes. At concentrations on the order of 10^{20} cm^{-3} an overwhelming majority of the electrons is in the F_2-centers, which leads to diamagnetism of the solution. Finally, at still higher concentrations the solution turns into a quasi-metal with the paramagnetism characteristic of a "free" electron gas.

The results following from our theory are in good quantitative agreement with experiment (Ref. 13). The constancy of the equivalent electrical conductivity at low concentrations, its decrease at medium concentrations and subsequent increase at high concentrations (Ref. 17) can readily be explained within the framework of our theory. The expression for the dependence of the number of current carriers (polarons) on the temperature and the number of metal atoms, derived in Ref. 13, permits determining the temperature coefficient of the conductivity (Ref. 7); the value so determined proves to be in close agreement with the experimental one ($\beta_{theo} \simeq 1.7 \cdot 10^{-2}$; $\beta_{exp} \simeq 1.5 \cdot 10^{-2}$). The value of the thermal dissociation energy of an F_2-center calculated on the basis of theory also proved to be in agreement with experiment: $I_{theo} \simeq 0.195$ ev (Ref. 13); $I_{exp} \simeq 0.2$ ev (Refs. 15 & 16).

Physical Institute of the
Academy of Sciences of the Ukranian SSR

References

1. S.I.Pekar & M.F.Deigen, Zhur. eksp. i teor. fiz., 18, 481 (1948).
2. M.F.Deigen, Zhur. eksp. i teor. fiz., 18, 818 (1948); Trudy fiz. fak. KGU (Proc. Phys. Dept. of Kiev State University) 5, 21 (1950).
3. G.E.Zil'berman, Zhur. eksp. i teor. fiz., 19, 135 (1949).
4. S.I.Pekar, Zhur. eksp. i teor. fiz., 20, 510 (1950); ibid. 17, 879 (1947).
5. S.I.Pekar & M.A.Krivoglaz, Trudy Instituta fiz. (Proc. of the Physical Institute) of the Ukranian SSR Academy of Sciences), 4, 37 (1953).
6. S.I.Pekar & S.F.Tomasevich, Zhur. eksp. i teor. fiz., 21, 1218 (1951).
7. M.F.Deigen, Zhur. eksp. i teor. fiz., 26, 300 (1954); Trudy Instituta fiz. (Proc. of the Physical Institute of the Ukranian SSR Academy) 5, 119 (1954).
8. M.F.Deigen, Zhur. eksp. i teor. fiz., 21, 992 (1951).
9. M.F.Deigen, Zhur. eksp. i teor. fiz., 24, 631 (1953).
10. C.A.Hutchinson & G.A.Noble, Phys. Rev., 87, 1125 (1952); C.V.Heer & C.Rauch, Phys. Rev., 90, 530 (1953).
11. A.A.Shatalov, Doklady AN SSSR, 92, 549 (1953).
12. A.S.Davydov, Zhur. eksp. i teor. fiz., 18, 913 (1948).
13. M.F.Deigen, Zhur. eksp. i teor. fiz., 26, 293 (1954) Trudy Instituta fiz. (Proc. Physical Institute) of the Ukranian SSR Academy, 5, 105 (1954).
14. J. Kaplan & C.Kittel, Journ. Chem. Phys., 21, 1429 (1953).
15. E.Huster, Ann. de Phys., 33, 447 (1938); S.Freed & N.Sugarman, J. Chem. Phys., 11, 354 (1943); C.A.Hutchinson & R.C.Pastor, J. Chem.Phys.,21, 1959 (1953).
16. Coulter, Wolsky, Zdanuk & Monchick, Abstract, 101, p. 50, P, 119th Meeting of the Amer. Chem. Soc.

* * * * * * *

THE INFLUENCE OF SOLVENTS ON THE ABSORPTION AND LUMINESCENCE SPECTRA OF MOLECULES

- A.F.Lubchenko

With a view to elucidating the effect of the medium on molecular absorption and luminescence spectra we undertook to extend certain concepts of quantum electrodynamics for a vacuum to anisotropic media. The electromagnetic field in the dielectric, in this case, is described by a wave function in requantized form; the wave function for the system molecule + solvent + radiation field (in the absence of interaction of the field with the impurity molecule) is evaluated in the adiabatic approximation.[1]

The probability of transition of the system from one quantum state to another

during the unit time interval with emission (or absorption) of a quantum of light of a given frequency in the direction $d\Omega$ is computed by means of the following equation:

$$w\,d\Omega = \frac{2\pi}{\hbar}\rho_E |H'|^2 d\Omega,$$

where $\rho_E dE$ is the energy of the end states in the energy interval E to E + dE and $|H'|^2$ is the square of the matrix element of the energy of interaction between the field and the impurity molecules. The derived equations permit writing expressions for the ratio of the radiation energy components whose electric vectors are directed along the axes of Cauchy's ellipsoid[2]:

$$\Lambda_1 = \frac{I_{1p}^{xr}}{I_{1p}^{zr}} = \frac{n_x(\nu_{p1})\cos^2\alpha}{n_z(\nu_{p1})\cos^2\gamma}, \quad \Lambda_2 = \frac{I_{1p}^{yr}}{I_{1p}^{zr}} = \frac{n_y(\nu_{p1})\cos^2\beta}{n_z(\nu_{p1})\cos^2\gamma}, \tag{1}$$

where $n_{xi}(\nu_{p1})$ are the components of the index of refraction tensor, for the frequency ν_{p1}, along the axis $0X_i$ (i = 1, 2, 3), and $\cos\alpha$, $\cos\beta$ and $\cos\gamma$ are the directional cosines of the average orientation of the dipole moment associated with the transition.

When the orientations of the impurity molecules are purely random (probability of orientation in any given direction equal to that in any other direction), the cosines in (1) cancel out and only constants, dependent on the solvent and susceptible of experimental verification, remain in the right hand members of the proportions (1).

Analogous expressions are obtained for the energy absorbed per unit time:

$$\Lambda_1' = \frac{I_{1p}^{xa}}{I_{1p}^{za}} = \frac{n_z(\nu_{p1}')\cos^2\alpha}{n_x(\nu_{p1}')\cos^2\gamma}, \quad \Lambda_2' = \frac{I_{1p}^{ya}}{I_{1p}^{za}} = \frac{n_z(\nu_{pi}')\cos^2\beta}{n_y(\nu_{p1}')\cos^2\gamma}. \tag{2}$$

From (1) and (2), we find

$$\frac{\Lambda_1}{\Lambda_1'} = \frac{n_x(\nu_{p1})\,n_x(\nu_{p1}')}{n_z(\nu_{p1})\,n_z(\nu_{p1}')}, \quad \frac{\Lambda_2}{\Lambda_2'} = \frac{n_y(\nu_{p1})\,n_y(\nu_{pi}')}{n_z(\nu_{p1})\,n_z(\nu_{p1}')}. \tag{3}$$

The relationships of (3) remain valid for any orientation of the impurity molecules and for any solvent.

For determining the shape of the absorption and luminescence bands we used the method of Weisskopt and Wigner[3]; the integral equation for the band shape obtained by this method differs from that derived earlier by Davydov[4] only in that in it account is taken of the dependence of the crystal and local[5] vibration frequencies on the electronic state of the impurity center and that local vibrations are explicitly separated from the crystal oscillations. It appears impossible to integrate this equation in the general case. However, the expressions obtained for the limiting cases permit drawing the following conclusions:

In the case of strong coupling between the electronic excitation and the vibrations of the lattice[4], the emission and absorption bands exhibit the shape of the emission curve of a free molecule when the Doppler effect is taken into account. At high temperatures the band shape approaches a purely Gaussian curve. As the temperature is reduced, the band shape becomes somewhat asymmetric relative to the normal to the frequency axis, passing through the peak.

The temperature dependence of the half-widths of the bands is described by

$$\Delta\Omega_i = c_i \sqrt{\sum_s \frac{1}{e^{\frac{l_i \hbar\omega_s}{kT}} - 1} + \frac{1}{2}}, \tag{4}$$

where c_i is a quantity independent of the temperature (different for absorption and emission). This expression is similar in form to the expressions deduced

earlier by Davydov[4] and Pekar[6]; however (4) differs from the latter expressions in that in it the frequency ω_s of the crystal vibrations is dependent on the electronic state l_i of the impurity; hence the half-widths of the bands and their temperature dependence in general are different for absorption and emission.

In consequence of the dependence of the crystal and local vibrations on the electronic state of the impurity, the mirror symmetry of the absorption and emission spectra is distorted to some extent.

On the other hand, when the interaction between the vibrations of the lattice and the electronic excitation is weak, the absorption and emission spectra consist of a system of lines similar to those of atomic spectra, with the half-width of each line being equal to 2Γ. When there is interaction between the electronic excitation and the acoustic vibrations as well, the lines broaden and, at high temperatures, overlap. Both in the case of strong and in the case of weak interaction between the electronic excitation and the vibrations of the lattice, the location of the band maxima is dependent on the temperature.

Our calculations indicate that the intra-molecular vibrations whose frequencies fall into the allowed vibration intervals of the solvent do not show up in the spectrum in the form of separate electron-vibration bands.

It can also be readily shown that when the transition is accompanied by a change in the number of local vibrations, the absorption and luminescence spectra in some cases will consist of a system of wide bands, formed by the superposition of a number of individual bell-shaped lines having a half-width (4). As the temperature is reduced there will occur a redistribution of the spectral energy: in the case of absorption the intensity peak will be shifted to the violet side; in the case of emission, it will be displaced to the red side.

The mathematical treatment developed can be utilized to compute the value of Γ, the reciprocal of the mean life of the impurity molecule in the excited state. The temperature dependence of Γ in the case of strong coupling between the electronic excitation and the vibrations of the lattice is characterized by

$$\Gamma = c_1 + c_2 \sum_s (\omega_s^{l_0})^2 \left[\frac{1}{e^{\frac{h\omega_s^{l_0}}{kT}} - 1} + \frac{1}{2} \right], \qquad (5)$$

where c_1 and c_2 are quantities independent of T. The functional variation of $\tau(T) = 1/\Gamma$ as defined by the above equation (5) is in agreement with the experimental data given by Galanin, Gavioli and Rau.

In the case of weak interaction of the electronic excitation with the vibrations of the lattice, the functional dependence of Γ on the temperature may be written as

$$\Gamma = c_3 e^{-g(T)},$$

where

$$g(T) = c_4 \sum_s \left(\frac{1}{e^{\frac{h\omega_s^{l_0}}{kT}} - 1} + \frac{1}{2} \right);$$

here c_3 and c_4 are temperature independent quantities. This form of the temperature dependence of Γ is observed in the case of solutions of anthracene and naphthalene[7].

In conclusion the writer wishes to thank A.S.Davydov for suggesting the subject of the investigation and his guidance in carrying it out.

Physical Institute of the
Academy of Sciences of the Ukranian SSR.

References

1. M.Born & J.Oppenheimer, Ann. de Phys., 84, 457 (1927).
2. K.Shefer, Teoreticheskaia fizika (Theoretical Physics), M.-L. 1938.
3. W.Weisskopf & E.Wigner, ZS. f. Phys., 63, 54 (1930).
4. A.S.Davydov, Zhur eksp. i teor. fiz., 24, 197 (1953).
5. N.M.Lifshits, Zhur. eksp. i teor. fiz., 24, 197 (1953).
6. S.I.Pekar, Zhur. eksp. i teor. fiz., 22, 641 (1952).
7. S.H.Liebson & J.O.Elliott, Phys. Rev. 78, 65 (1950).

* * * * * * *

THE VIBRATIONAL SPECTRUM OF THE VINYL GROUP AND ITS QUANTITATIVE DETERMINATION IN COMPLEX HYDROCARBON MIXTURES

- A.V.Iogansen

We investigated the infrared absorption spectra of 1-alkenes from C_5 to C_{13}, as well as C_{16}. Utilizing methods of taking into account the resolving power of the monochromator developed earlier[1], we determined the intensities, shape and width of the 909 and 993 cm^{-1} bands of these hydrocarbons and evaluated, on the basis of published data[2], the characteristics of the analogous bands of liquid 1-butene and 1, 3-butadiene. The 909 cm^{-1} band characteristic of the-Ch=Ch_2 group was studied in detail. The position of the band maximum remains constant for the 1-alkene series and for 1, 3-butadiene. The value of the integral molar absorption [= molecular extinction] coefficient ($\varepsilon = \int \bar{\varepsilon}(\nu)\, d\nu$) remains virtually constant in the 1-alkene series at $2.00 \cdot 10^3$ liter mol^{-1} cm^{-1} and is but little different for 1, 3-butadiene ($2.1 \cdot 10^3$). The band width varies in an orderly fashion from 19 cm^{-1} for 1-butene to 7.8 cm^{-1} for 1-hexadecene (the width is 30 cm^{-1} for 1, 3-butadiene). The absorption coefficient at the peak (ε_{max}) shows a corresponding variation - from 72 to 160 liter mol^{-1} cm^{-1} (45 liter mol^{-1} cm^{-1} for 1, 3-butadiene). All investigated bands have a dispersional shape.

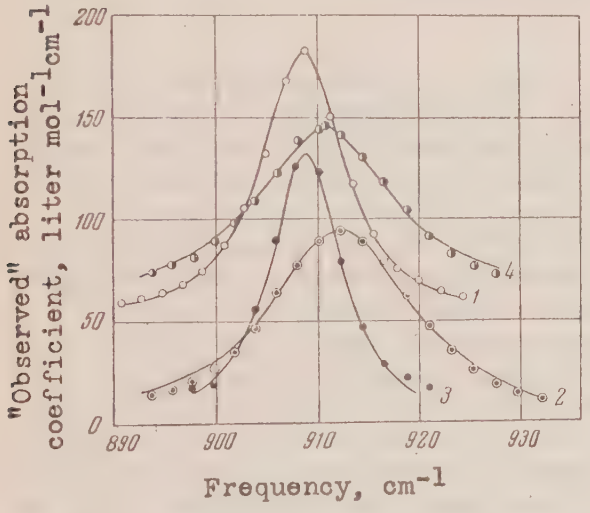

Shape of 909 cm^{-1} absorption band of 1-tridecene: 1) the undissolved hydrocarbon: 2 - 4) C ≈ 0.6 mol/liter solutions: 2) in bromoform, 3) in n-hexane, 4)in benzene. Curves 1 and 4 have been raised 50 units, i.e., 50 = 0 on the coef. scale. The points are measured values; curves are the "observed" shapes calculated for the experimental conditions on the assumption that the true shape is dispersional.

When dissolved in different solvents (n-hexane, n-hexadecane, benzene, carbon tetrachloride and bromoform) the characteristic bands of the hydrocarbons change: the frequency by 0.4%; ε by ±15% and the band width by a factor of 2-3. The shape of the bands remains dispersional (minor deviations are observed in the case of bromoform solutions - see accompanying figure). Both the shape and width of the bands is determined by intermolecular interaction; unsaturated structures (C=C, C=C—C=C,) have an appreciably stronger disturbing influence than paraffin structures (CH_2 and CH_3). This explains the regular, orderly variation in band width in the homologous series and

its great increase in the case of 1, 3-butadiene. The virtual equality of the values of $\tilde{\varepsilon}$ for the 1-alkenes and 1, 3-butadiene indicates that the dipole moments of the =C—H bonds are nearly equal in the two cases.

The data obtained can be utilized, by means of the developed procedure[1], for quantitative analysis without the need for preliminary "calibration" of the instrument with reference to standards. A valuable application may be determination of the total —CH=CH_2 group content. A practical method of such analysis (according to the value of the integral absorption) has been developed for petroleum products ranging from gasolines to lubricating oils; the accuracy of the developed method attains 5%; the sensitivity, 0.05%.

The developed method can be extended to other products, particularly to high-molecular compounds (synthetic rubbers, etc.) where preparation of suitable standards is difficult.

We also evaluated the intensity and width of two other characteristic bands (993 cm^{-1} and 1642 cm^{-1}) of the above named hydrocarbons.

Central Institute of Aviation Fuels and Oils.

References

1. A.V.Iogansen, Doklady AN SSSR, 87, 527 (1952); 92, 919 (1953).
2. E.C.Greitz & G.F.Smith, J. Research Nat. Bur. Stand., 43, 365 (1949).

* * * * * * *

INTERMOLECULAR BONDS OF THE (OH)...(OH) AND (OH)...(OCR) TYPE IN OXYGEN-CONTAINING SUBSTANCES

- V.M.Chulanovski & Kim Den Dok

The hydrogen bond in oxygen-containing substances is commonly represented by the general formula O-H...O, in which no distinction is made between the case where both the joined substances contain a hydroxyl group and the case where one of the coupled molecules has only an oxygen atom.

The interpretation of the absorption spectra of pure and mixed substances containing associated OH groups or an OH and say an OC group is also commonly based on the assumption that both types of H-bonds are approximately equivalent.

One of the present authors has shown in an earlier article* that this treatment leads to obvious inconsistencies.

The present investigation was devoted to determining the influence of the intermolecular bond in pure acetone and acetone solutions on the position and shape of the band associated with the C=O group of acetone as well as of the band associated with the C—O group of methyl alcohol. We assumed that the shift of the absorption band associated with a given group under the influence of an external field (for example, neighboring molecules) may be taken as a measure of the magnitude of this influence, i.e., of the extent to which the external field (factor) affects the investigated group. This shift in this case is to the side of lower frequencies.

On the other hand, if the intermolecular bond is formed with a neighboring group rather than with the investigated group, the distortion of the electronic shell caused by it may lead to strengthening of the linkage in the investigated group, i.e., to displacement of the characteristic spectrum band to the side of higher values of ν .

The first effect occurs in the case of the active C=O group. When acetone

---

*V.M.Chulanovski, Doklady AN SSSR, 93, 25 (1953).

is dissolved in CCl_4 the band at 1713.5 cm^{-1} observed in the spectrum of pure liquid acetone is shifted to 1716.5 cm^{-1}. When the acetone is dissolved in hexane the shift is even greater (to 1722.6 cm^{-1}). From this it may be concluded that intermolecular bonding is fairly strong in pure acetone.

When acetone is dissolved in methyl alcohol the band is displaced to 1707.2 cm^{-1}; in chloroform - to 1709.8 cm^{-1}. In both cases the shifts of the band relative to its position with the acetone in a neutral solvent (hexane) - corresponding roughly to the case of the absence of intermolecular interaction - are nearly equal in magnitude, although, according to commonly accepted concepts, a hydrogen bond is present in the first case and absent in the second.

From this we conclude that although the intermolecular bond does become stronger when acetone is dissolved in hydroxyl-containing substances, it does not reach the exceptionally high strength which normally distinguishes the hydrogen bond from other types of bonds.

In pure methyl alcohol the formation of a hydrogen bridge should weaken the OH bond (as is evinced by the spectrum of this group) and strengthen the CO bond. Actually, two bands appear in the vicinity of 10 μ in the spectrum of pure methyl alcohol: a stronger one at 1030 cm^{-1}, which shifts different distances in different solvents, and a weaker band at 1118 cm^{-1} which fades out in solutions and in the vapor spectrum. We ascribe the first band to alcohol molecules not joined by a hydrogen bridge and the second band to associated molecules.

When methyl alcohol is dissolved in CCl_4 the frequency of the monomeric band is reduced to 1024 cm^{-1} (i.e., the shift is in the opposite direction to that for acetone). When methyl alcohol is dissolved in acetone, the frequency increases to 1035.5 cm^{-1} (i.e., the band shifts in the same direction as the band of the associated molecules relative to the monomeric band). Hence the formation of a hydrogen bridge between the alcohol molecules displaces the band by 88 cm^{-1} while solution of the alcohol in acetone results in a shift of only 5.5 cm^{-1}, i.e., in a shift one order lower in magnitude.

It may be concluded, therefore, that an (OH···(OCR) type bond is much weaker than an (OH)···(OH) bond and that all hydrogen bond schemes based on the assumption that the two types of bonds are about equally strong must be characterized as doubtful.

Physical Institute of Leningrad State University

* * * * * * *

THE HYDROGEN BOND AND THE STRUCTURE OF AROMATIC COMPOUNDS

- V.V.Perekalin

The intramolecular hydrogen bond, forming an additional ring, i.e., a hydrogen ring, exerts an appreciable effect on the electron density distribution in aromatic compounds, as is evinced by their absorption spectra and their chemical behavior.

In ortho-oxyazo dyes, the hydrogen bond by furthering coupling alters the electronic structure of the molecule in such a manner that the excitation energy is reduced and the long-wave band in the electronic absorption spectrum (as compared with the absorption of the para-isomers) is displaced into the visible region[1-4] (see accompanying table).

The lability of the hydrogen atoms of the hydroxyl group in ortho- and para-oxyazo dyes is reduced due to the formation of additional linkages with the nitrogen of the azo group[1,3 & 4]. The positions of the long-wave bands in the absorp-

tion spectra of ortho- and para-oxyazo dyes (I, II and III) were found to remain unchanged as the pH of the medium was increased; the hydroxyl groups of the dyes did not react with caustic soda.

Shift of the long-wave absorption band in oxyazo dyes under the influence of the hydrogen bond

	Dye	λ, mμ	
		Ethyl alcohol	NaOH+ethyl alcohol
I	2-Benzeneazo-1-naphthol	490	490
II	8-Benzeneazo-1-naphthol	460	460
III	1-Benzeneazo-2,8-aminonaphthol	500	500
IV	2-Benzeneazo-1-methoxynaphthol	380	--
V	4-Benzeneazo-1-naphthol	470	490
VI	5-Benzeneazo-2,8-aminonaphthol	505	520

In a number of other, similar cases the intramolecular hydrogen bond acts to stabilize the hydrogen atom[5]. While the presence of intramolecular hydrogen bonds does not entirely prevent chemical reactions involving the hydrogen atom, it does render such reactions slow or difficult due to the necessity of overcoming the blocking influence of the hydrogen bonds.

The hydrogen ring hinders coupling of substitute groups with the aromatic kernel; where such coupling occurs, the activating or stabilizing influence of such groups on the benzene nucleus is reduced and the equilibrium of the ring forces is disturbed. The aromatic kernel imparts a greater degree of stability to the molecule than the ring comprising the H-bond. Hence the presence of an intramolecular hydrogen bond produces only a partial disturbance of the normal alignment of the benzene ring bonds. An indicative example is furnished by the chemical behavior of a number of ortho- and para-oxyazo dyes of the napthalene series[3,4 & 6] and oxy-derivatives of acetophenone[7]. The monoazo dyes form diazo dyes only with great difficulty, while acetophenone derivatives do not react at all with ethyl acetoacetate.

In some cases, although structural considerations may admit of the formation of an H-bond, the actual bond if formed is very weak. For example, in 2-benzeneazo-1-naphthol-4-sulfonic acid[8] the H-bond tends to stabilize the hydrogen atom while the coupling of the hydroxyl with the electronegative substituent group tends to increase its lability; in this case the effect of the coupling is predominant, so that the hydrogen atom of the hydroxyl group in the azo dye is as labile as in 1-naphthol-4-sulfonic acid.

The matter of the association of the hydrogen atom is very important, i.e., whether it retains its covalent bond with the parent group (for example, with the hydroxyl group in ortho-oxyazo dyes) or whether the character of the bond is altered. In the case of an intramolecular hydrogen bond, equalization of the hydrogen and covalent bonds occurs: it is less pronounced when the hydrogen joins atoms differing in their affinity for electrons (in 1-benzeneazo-2-naphthol, for example) and more complete in the case of identical atoms (in naphthazarine).

The exact mechanism of the formation of intramolecular hydrogen bonds is not clear. Thus 2-benzeneazo-1-naphthol may be prepared in two ways: azo-coupling with 1-naphthol or the condensation of 1,2-naphthoquinone with phenylhydrazine. In one of these syntheses the covalent bond is transformed into a hydrogen bond.

The ability of many substances to form internal complex lake salts may hinge on a qualitative reaction involving the formation of intramolecular hydrogen bonds. However, the inverse does not necessarily hold: not every compound having

an H-bond can form lakes.

"A.I.Gertsen" Leningrad State Pedagogical Institute

References

1. V.V.Perekalin & M.V.Savost'ianova, Zhur. ob. khim., 21, 1329 (1951).
2. R.Kuhn, Lieb. Ann., 516, 2, 143 (1935).
3. V.V.Perekalin & N.M.Slavachevskaia, Zhur. ob. khim., 21, 837 (1951).
4. Errera, Helv. Chem. Acta, 20, 1373 (1937).
5. G.Branch & D.Jabroff, J. Am. Chem. Soc., 56, 2658 (1934).
6. E. Nölting, Ber., 24, 1592 (1891).
7. V.V.Perekalin, Zhur. ob. khim., 21, 1057 (1951).
8. V.V.Perekalin, Zhur. ob. Khim., 21, 129 (1951).

* * * * * * *

THE HYDROGEN BOND AND ITS EFFECT ON THE ENERGY DISTRIBUTION IN THE VIBRATIONAL AND ELECTRONIC SPECTRA OF MOLECULES

- D.N.Shigorin

We investigated the infrared absorption spectra of a number of amino- and oxy-derivatives of anthraquinone (see figure below) as well as of certain oxy- and amino-azo compounds[1-3]. The bands of the valence vibrations of the α-hydroxyl groups participating in the formation of intramolecular hydrogen bonds (in the crystalline as well as in the vapor state of the substance) are noticeably shifted to the side of longer wavelengths (3000-3150 cm^{-1}) and greatly diffused. In the crystalline state of the investigated substance the intensity of the α-OH group bands is 10-12 times less than the intensity of the bands of the β-OH groups; the β O-H bonds are more polar in character than the α bonds. The half-width of the α-group (in the vapor state) is 5-6 times greater than the half-width of the β-group band (also in the vapor state). The valence vibration band associated with the NH group of indanthrone (3165 cm^{-1}, wide) is greatly diffused and has one-tenth to one-twelfth the intensity of the NH group in 1-methylamino-anthraquinone (3300 cm^{-1}, sharp). This difference in the behavior of the NH groups is explained by their different stereo-orientations relative to the plane of the molecules. In α-oxy- and amino-derivatives of anthraquinone the absorption peaks in the electronic spectra and the fluorescence maxima are shifted to the side of long-waves as compared with their positions in the spectra of β-derivatives. Furthermore, α-derivatives do not exhibit fluorescence quenching by oxygen, whereas β-derivatives are subject to strong quenching[4]. We explain these differences in behavior by the fact that an intramolecular H-bond is present in the α-derivatives and not in the β-derivatives. The peculiar nature of this type of H-bond stems from the fact that the electron of the hydrogen atom (or in the case of intra-complex compounds, the electrons of the metal atom) enters directly into the interaction with the π-electron (or the π-electrons, in the presence of a metal) and thus participates in extending the effects of this interaction through the entire system of conjugate bonds. In the case of such interaction the electron cloud of the hydrogen atom undergoes a corresponding deformation, resulting in a broadening of the potential well of the hydrogen atom participating in the formation of the H-bond. Intramolecular hydrogen bonds included in molecules with conjugate bonds and formed over comparatively short distances belong to this type of H-bonds.

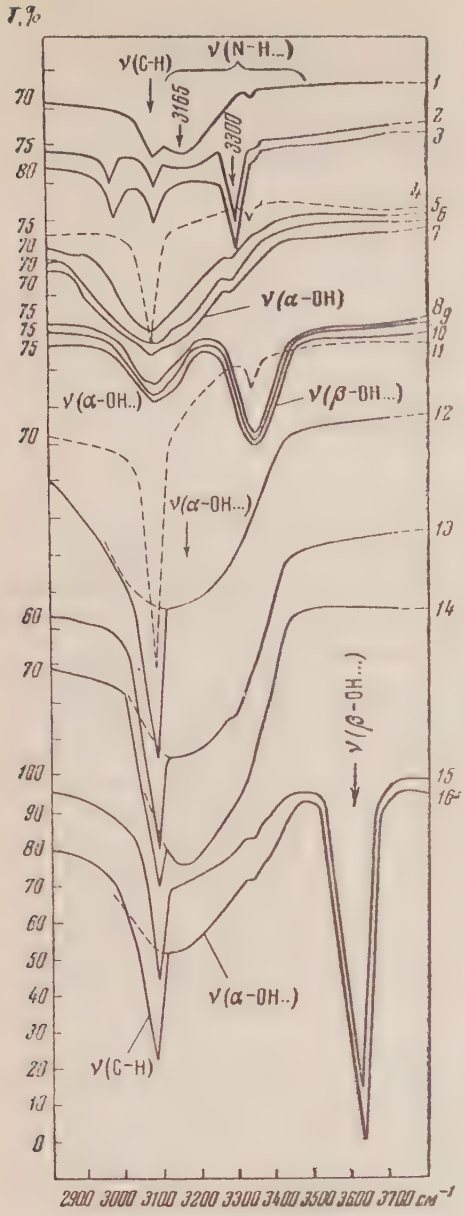

Infrared absorption spectra of amino- and oxy-derivatives of anthraquinone. The curves have been shifted to avoid overlapping, but the vertical scale for all curves is the same. The figures at the left for curves 1 through 14 indicate the percent transmission at the point of intersection of the given curve with the y-axis. The substances characterized by curves 1, 4 and 7 were prepared of 50 gm of the material + 0.6 gm of oil; those characterized by curves 2, 3 and 8-10 consisted of 50 gm of the material + 1.2 gm oil.

1) Indanthrone, d = 0.5 mm; 2) 1-to-2 molar mixture of indanthrone + 1-methylaminoanthraquinone; d=0.25 mm; 3) 1-methylaminoanthraquinone, d=0.25mm; 4) anthraquinone, d = 0.5 mm; 5) 1, 5-dioxyanthraquinone, d = 0.5 mm; 6) 1, 8-dioxyanthraquinone, d = o.5 mm; 7) 1, 4-dioxyanthraquinone, d = 0.5 mm; 8) 1-to-3 molar mixture of 2-oxyanthraquinone + 1, 5-dioxyanthraquinone, d = 0.25 mm; 1-to-3 molar mixture of 2-oxyanthraquinone + 1, 8-dioxyanthraquinone; 10) 1-to-3 molar mixture of 2-oxyanthraquinone + 1, 4-dioxyanthraquinone; 11) anthraquinone vapor, t = 290°C, d = 180 mm; 12) 1, 4-dioxyanthraquinone vapor, t = 260°C, d = 180 mm; 13) 1, 5-dioxyanthraquinone vapor, t = 300°C, d = 180 mm; 14) 1, 8-dioxyanthraquinone vapor, t=300°C, d = 180 mm; 15) 1, 3, 4-trioxyanthraquinone (purpurin) vapor, t = 320°C, d = 180 mm; 16) 1, 2-dioxyanthraquinone (alazarin) vapor, t = 290°C, d = 180 mm.

No great diffusion of the absorption bands or marked reduction of their intensity is observed in the case of intramolecular hydrogen bonds without π-electron interaction. The presence of π-electron interaction in the investigated molecules and the participation in it of the hydrogen atom (or of the metal atoms in the case of intra-complex compounds) favors migration (transfer) of the absorbed energy to the O-H··· and N-H··· (or O-Me··· and N-Me···) bonds inside the molecule, which should lead to shortening of the lifetime of the molecule in the excited vibrational state and, consequently, to diffusion of the band ($\tau \Delta E = h$). The hydrogen (and metal) atoms in intramolecular bonds are comprised in the conjugate system of bonds and in a sense may be said to form junctions which play an important part in determining the character of energy transfer in the molecule. Consequently all changes in the valence state of these atoms (under the influence of light, the solvent, other reagents, etc.) due to π-electron interaction will be reflected in the electron density distribution of the entire molecule. Hence substantial changes in the molecular system can occur without transition of the molecule from the singlet to the triplet state. These considerations should help explain the familiar peculiarities of the absorption and fluorescence spectra of chlorophyll and similar compounds.

"L.Ia.Karpov" Physico-Chemical Institute

References

1. D.N.Shigorin, Zhur. fiz. Khim., 27, 554 (1953).
2. D.N.Shigorin, Izv. (Bulletin) AN SSR, Ser. fiz., 27, 596 (1953).
3. G.D.Bagratishvili, Doklady AN SSSR, 96, 753 (1954).
4. A.V.Kariakin, Zhur. fiz. khim., 23, 1332, 1345 (1949).

* * * * * * *

INFRARED SPECTRA AND ASSOCIATION IN SOLUTIONS

- E.N.Vasenko

In studying the solubility in ternary systems it is desirable to have at least approximate data on the state of the molecules of the associated liquid in the presence of the third component - the homogenizing agent. To this end we obtained the infrared absorption spectra in the vicinity of 1700 and 3400 cm^{-1} of pure water, formamide $HCONH_2$ (the associated components) and diethylformamide $HCON(C_2H_5)_2$ (the homogenizer) as well as of 10% solutions of these liquids in acetone. In addition, we obtained the spectra of a solution of 2.5% water + 2.5% diethylformamide in acetone and of a solution of 5% formamide + 5% diethylformamide in acetone.

Comparison of the spectrum of a highly dilute (0.01%) solution of formamide in CCl_4, which we also observed, with the spectrum of pure liquid formamide confirmed the evidence of Raman spectroscopy[1-4] that formamide is highly associated by means of N-H···O bonds and indicated that monomeric formamine molecules are present in the solution. Davies and Evans[5] reached the same conclusion on the basis of spectroscopic observations in the region of the valence vibrations of the NH_2 group.

In order to bring out more clearly the changes taking place during the mixing of formamide or water with diethylformamide in equimolecular proportions, spectra of superposed separate layers of water and diethylformamide and of formamide and diethylformamide were obtained and compared with the spectra of the corresponding equimolecular mixtures dissolved in acetone (see accompanying figure).

We also recorded the spectra of two ternary solutions - 35.8% water + 30.9% CCl_4 + 33.3% diethylformamide and 36.0% formamide + + 35.4% CCl_4 + 28.6% diethylformamide; these closely duplicate the spectra of the corresponding equimolecular solutions as regards the position, shape and intensity of the absorption lines.

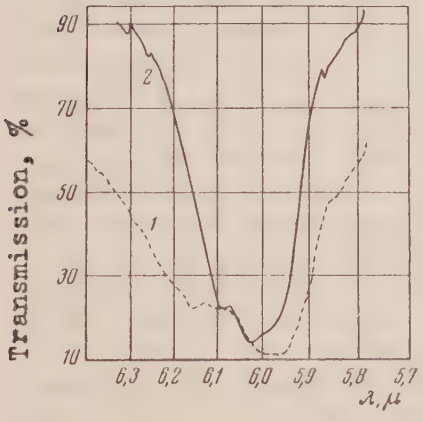

1) Absorption spectrum of water and diethylformamide 2) spectrum of an equimolecular mixture of these.

The measurements were made on an IKS-11 spectrometer with a rock salt prism. All compositions given above are in molar percent.

Analysis of the experimental results leads to the following deductions:

1. The interaction between the molecules of diethylformamide and water apparently consists of the formation of O-H···O=C type hydrogen bonds of such great strength that they persist not only in carbon tetrachloride solutions (facilitating the solution of appreciable amounts of water in the CCl_4) but also in acetone solutions.

2. The spectrum of the equimolecular solution of diethylformamide and water in the region of

deformational vibrations is characterized only by the band associated with the formation of hydrogen bonds between the C=O groups of diethylformamide; neither the monomeric water molecule bands nor the band characteristic of associated water appear in the spectrum of this solution. It may be assumed that the complex systems of water in the liquid state have an effect on the deformational vibrations of water molecules differing from that of the systems formed by water molecules with the molecules of diethylformamide.

3. Pure liquid formamide is strongly associated by N-H···O hydrogen bonds, which is evinced by the broadening and the marked shift - to the long wave side - of its NH_2 and C=O bands.

4. The interaction between formamide and diethylformamide consists of the formation of N-H···O bonds, which persist not only in the ternary solution of formamide + diethylformamide + carbon tetrachloride but also to some extent in the formamide + diethylformamide + acetone solution.

In conclusion I wish to thank G.S.Landsberg for his guidance and valuable advice and express my gratitude to V.M.Chulanovski for his help in carrying out the investigation and discussing the results.

L'vov Polythechnical Institute

References

1. K.Kohlrausch & A.Pongratz, ZS. phys. Chemie, B27, 176 (1934).
2. V.N.Thatte & M.S.Joglekar, Phil. Mag. 19, 116 (1935).
3. L.Kahovec & H.Wassmuth, ZS. phys. Chemie, B48, 70 (1940).
4. B.D.Saksena, Proc. Ind. Acad. Sci., 11, 53 (1940).
5. M.Davies & J.C.Evans, J. Chem. Phys., 20, 342 (1952).

* * * * * * *

ON HYDROGEN BONDS IN SILICOLS

- V.I.Kastochkin, M.F.Shostakovski, O.I.Zil'berbran & D.A.Kochkin

The characteristic chemical properties of silicols R_3SiOH (R = an alkyl or aryl group) are determined in many respects by the peculiarities of the hydroxyl group in their structure. The unique behavior of the OH group in silicols is due to the intramolecular influence of the silicon atom in this group. Some of the properties of silicols apparently also depend on the association of their molecules, i.e., on the formation of hydrogen bonds. For the purpose of investigating the nature of the molecular association of silicols and the influence of the silicon atom on the OH group, we obtained and analyzed the infrared absorption spectra in the 2-4 μ interval of tert-butyl alcohol $(CH_3)_3COH$ and of five silicols: $(CH_3)_3SiOH$, $(CH_3)_2C_2H_5SiOH$, $CH_3(C_2H_5)_2SiOH$, $(C_2H_5)_3SiOH$ and $C_6H_5(C_2H_5)_2SiOH$. In order to determine the effect of solvents on the molecular association we also studied the absorption spectra of various concentrations of the silicols and tert-butyl alcohol in carbon tetrachloride, cyclohexane and benzene.

Most of our curves were based on experimental points obtained with an IKS-11 spectrometer equipped with an LiF prism. For a few of the specimens the absorption curves were obtained by means of the two-beam automatic recording spectrograph of the Physical Institute of the Academy of Sciences (see figure).

Only the valence vibration bands of CH and OH (near 3600 cm^{-1}) appear in the spectra of 0.5% solutions of the silicols and tert-butyl alcohol in CCl_4. The absence of a wide band at 3100-3500 cm^{-1} is evidence of the predominance of monomolecules in the solutions. As compared with the tert-butyl alcohol, the silicols show a 25% greater absorption in the hydroxyl band and a displacement of about

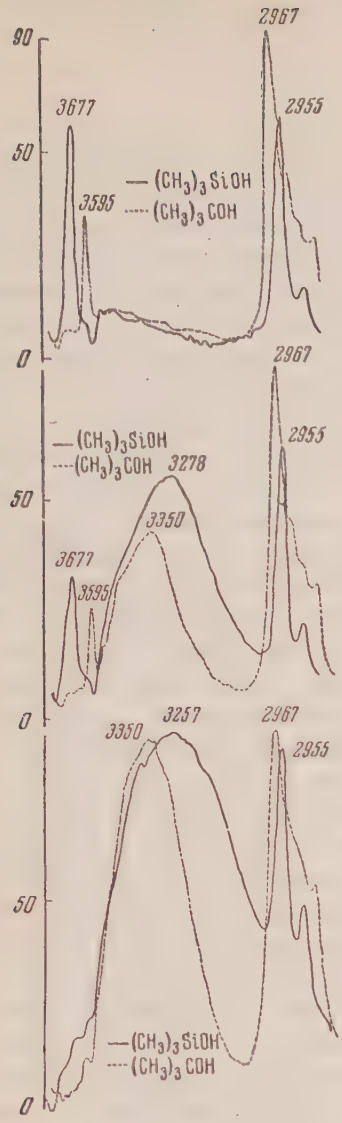

Infrared absorption spectra of different silicol and tert-butyl alcohol solutions in carbon tetrachloride.

82 cm^{-1} of the band in the direction of higher frequencies. This effect can be explained by an increase in ionic dipole polarizability and the strengthening of the O-H bond in the silicols, owing to the replacement of the carbon atom by the less electronegative silicon atom. At higher concentrations the wide and intense band characteristic of the hydroxyl group participating on a hydrogen bond appears in the spectra. As compared with the tert-butyl alcohol spectrum, the band in silicol solutions has an appreciably greater intensity and width and its peak is displaced further to the side of low frequencies relative to the band of the non-coupled hydroxyl groups, which is indicative of stronger interaction between the hydroxyl groups in the silicols. The displacement of the band peak in tert-butyl alcohol is 245 cm^{-1} whereas in trimethylsilicol $\Delta\lambda$ = 325 cm^{-1}. The degree of association of the molecules increases with increasing concentration of the solutions. This is clearly evinced by the increase in the intensity of the O-H···O band and the decrease in the intensity of the OH band. Finally, in the spectra of pure silicols and tert-butyl alcohol only the O-H···O band remains. The absence of the non-coupled hydroxyl band (which, it will be recalled, is characterized by a high intensity when "free" hydroxyl groups are present) indicates that most of the molecules are associated in ring-like systems, with virtually all the hydroxyl groups participating in hydrogen bonds. According to cryoscopic studies of some silicol and butyl alcohol solutions in cyclohexane, the associated systems consist of four molecules. The formation of closed groups of four molecules joined by H-bonds is in accord with the tetrahedral valence angles in silicon and carbon.

The nature of the solvent has an appreciable effect on the dissociation process. Thus, dissociation is greater in benzene than in CCl_4. Silicol solutions in cyclohexane occupy an intermediate position as regards the extent of dissociation. The C-H bonds are also affected by substitution of a silicon atom for carbon. Thus, as compared with tert-butyl alcohol, in silicols the band at about 2955 cm^{-1} associated with the C-H group is reduced in intensity and shifted some 12 cm^{-1} to the side of lower frequencies (see figure).

The distinctive chemical properties of silicols, particularly their amphoteric characteristics, may justifiably be attributed to the strengthening of the O-H bond and the strong interaction between the oxygen and hydrogen atoms of neighboring molecules due to the heightened polar character of O-H bonds.

Institute of Mineral Fuels of the
Academy of Sciences of the USSR

* * * * * * *

DETERMINATION OF THE TRUE ABSORPTION SPECTRUM OF LIGHT-DISPERSING COLORED OBJECTS FROM THEIR DIFFUSE REFLECTION SPECTRUM

- O.P.Girin, Z.V.Zhidkova, B.I.Stepanov, A.P.Ivanov & A.S.Toporets

Determining the true absorption spectrum of the substance of particles comprising a dispersing system constitutes a difficult and complex problem which until now could be solved only roughly, mainly by guess-work. The quantity susceptible of measurement - the diffuse reflection coefficient - is dependent on a number of factors connected both with the properties of the reflecting layer (internal factors) and the conditions of illumination and observation (external factors). The aim of the present study was experimental and theoretical investigation of the influence of these factors.

1. In addition to the true absorption coefficient k_λ, the internal factors include the particle size l and the index of refraction for the particles and the medium n_1/n_2. In our theoretical evaluation of the influence of these factors on the diffuse reflection spectrum we analyzed the path of a light ray through a simplified model consisting of a scattering and absorbing layer. We assumed that the layer is made up of an infinite number of lamina having a thickness l. The derived expression for R_λ the coefficient of diffuse reflection of the light-scattering layer, as a function of the product $k_\lambda l$ and the reflection coefficient r_λ of the particles shows that the spectral dependence of log R_λ may differ appreciably from the dependence of k_λ.

Theoretical analysis and experimental studies showed that in the case of weak absorption the variation of log R_λ with the wavelength parallels the variation of k_λ, the agreement being closer for smaller values of l and higher values of n_1/n_2. The variations become wholly dissimilar, however, when the value of n_1/n_2 changes over the spectrum.

The derived equations were used to determine the true absorption of different types of colored glass having known values of R_λ, l and r_λ. The values of R_λ were obtained by measuring the diffuse reflection of glass in powdered form with different values of l and in different binding media. The computed values of k_λ are in satisfactory agreement with the experimental values obtained with transparent plates, which justifies our selection of the light-scattering layer model for the theoretical analysis.

2. The diffusely reflected flux is comprised of two components: an external or superficial one, reflected from the surface, and an internal component, reflected from inside the specimen. We used a new method which allows measuring the two components separately to study the variation of the two components with changes in the illumination conditions. The new method is based on the difference between the two components as regards polarization: under certain conditions the external component retains the polarization of the incident flux, while the internal component is depolarized. This difference makes separate determination of the components feasible.

Analysis of the spatial distributions of the internal and external components shows that

1) the internal and external components vary in a different manner with changes in the angle of incidence; consequently, the ratio of the intensities of the components and the value of the reflection coefficient depend on the angle of incidence;

2) the shape of the dispersion curves, particularly that for the external component, also depends on the character of the surface of the light-scattering object;

3) the characteristic curve of the internal component depends on the value of the absorption; reducing the absorption extends (flattens) the curve.

It is important to bear the above facts in mind when investigating the spectral properties of light-scattering colored objects.

* * * * * * *

ABSORPTION SPECTRA OF COMPLEX COMPOUNDS [AMMINES] IN CRYSTAL FORM

- A.V.Babaeva & R.I.Rudyi

The electronic spectra of complex compounds provide valuable information on the characteristics and attributes of such compounds. For the most part experimental data on the absorption spectra of complex compounds apply solely to compounds in solution. Yet many such compounds react to a certain extent with the solvent, while for others it is difficult to find a suitable solvent. These considerations impelled us to go over to obtaining the spectroscopic characteristics of complex substances in the crystal state by the method of reflection from crystalline powders, proposed in 1934 by Karl[1] and subsequently developed by French investigators[2].

We studied the spectra of the absorption of the crystalline powders of aminates, amino-acido- and acido-compounds of various metals, primarily of the platinum group, in the ultraviolet and visible regions of the spectrum at room temperature.

Comparison of the spectra of these compounds in crystals and in solutions showed that in the case of amino-compounds (Table 1) with a purely covalent bond between the central atom and the substituent the positions of the absorption peaks are virtually identical in both cases.

Table 1

Location of absorption peaks in amino-compounds, mμ

$[Co(NH_3)_6]Cl_3$	Crystals	470	344				
	Solution	472	340				
$[Rh(NH_3)_6]Cl_3$	Crystals				300		254
	Solution				303		254
$[Pd(NH_3)_4]Cl_2.H_2O$ . . .	Crystals					294	
	Solution					295	
$[Pt(NH_3)_4]Cl_2.H_2O$ . . .	Crystals					282	
	Solution					282	
$[Co(NH_3)_5Cl]Cl_2$	Crystals	488	370				
	Solution	480	363				
$[Rh(NH_3)_5Cl]Cl_2$	Crystals			330			
	Solution			327			

In the case of mono-acido-compounds - $[Co(NH_3)_5Cl]Cl_2$ and $[Rh(NH_3)_5Cl]Cl_2$ - the spectrum of the solution is shifted slightly to the side of higher frequencies relative to the spectrum of the crystal powder. In trans-diamine and acido-compounds (Table 2) the shift becomes appreciable; this may be explained by the effect of mutual labilization of the substituent groups, located trans to each other. Replacement of these by water molecules leads to a hypsochromic effect, which is the greater, the more trans-active the substituents.

Investigation of the absorption spectra of a number of different chloroplatinites in the crystalline state showed that the location of the absorption peaks is somewhat dependent on the nature of the cation not absorbing light in the given spectral region; this is not the case in solutions.

The spectra of isomeric amino-acido-compounds in the crystalline state constitute a reversal of the pattern exhibited in solutions. Thus in the spectra of solutions of di- and tetravalent platinum diamines having a cis-configuration the band peaks and long-wave absorption end-points are situated at shorter wavelengths than the corresponding peaks and end-points of the trans-isomers[3]. In crystals, on the contrary, the peaks and absorption end-points of the trans-

isomers lie at shorter wavelengths. This reversal of the spectral pattern of isomers incident to solution is doubtless connected with the trans-influence phenomenon[4], which is often relatively strong in solutions of complex compounds.

Table 2

Location of absorption peaks in trans-diamines and acido-compounds, mμ

$[Pd(NH_3)_2Cl_2]$	Crystals					380	356			256
	Solution									
$[Pt(NH_3)_2Cl_2]$	Crystals					376		317	295 273	
	Solution									
$(NH_4)_3[RhCl_6].H_2O$ . . .	Crystals	506		416						
	Solution	499			390					[240]
$(NH_4)_2[PdCl_4]$	Crystals		464			374				
	Solution			427				302		
$(NH_4)_2[IrCl_6]$	Crystals	500		428						
	Solution	490		418						
$K_2[PtCl_4]$	Crystals	500			396		356			
	Solution		470		392			328		

"N.S.Kurnakov" Institute of General
and Inorganic Chemistry of the
Academy of Sciences of the USSR

References

1. M.A.Karl, Bull. Soc. Chem., 5, 1453 (1934).
2. M.Amy, C.R., 207, 329 (1938); M.Billy & A.Berton, C.R., 206, 1958 (1938); T.Guilmart, Bull. Soc. Chem., 5, 54, 209 (1938); Rev. Scien. Inst., 17, 199 (1938).
3. A.V.Babaeva, Doklady AN SSSR, 40, 4 (1943); 65, 4(1949); 64, 5 (1949).
4. I.I.Cherniaev, Izv. Sektora platiny (Bulletin, Sector of Platinum, Inst. of General & Inorganic Chemistry) 4, 213 (1926); 5, 118 (1927).

* * * * * * *

THE ABSORPTION SPECTRA OF LEUCO BASES IN THE SOLID STATE

- A.T.Vartanian

The absorption spectra of solid leuco bases have not been investigated hitherto. We established that in the presence of gaseous hydrogen sulfide many dyes in the solid state are transformed into a colorless compound. The rate of the reaction increases rapidly with increasing temperature of the dye. At temperatures above 50°C these colorless compounds sublimate at a rather high rate. Hence, under vacuum one can readily obtain a uniform transparent layer of the compound on any suitable surface, as, for example, the surface of a quartz plate.

The absorption spectrum of the colorless compound formed when methylene blue (MB) is exposed to the action of hydrogen sulfide is shown in the accompanying figure (Curve 1). It consists of two bands peaking at 262 and 335 mμ; these bands coincide with two of the three bands observed by Holst in the spectrum of leuco-MB dissolved in 0.1 N HCl. In view of the fact that leuco-MB oxidizes slowly in 0.1 N HCl solution and turns into the dye, it may be assumed that the third peak

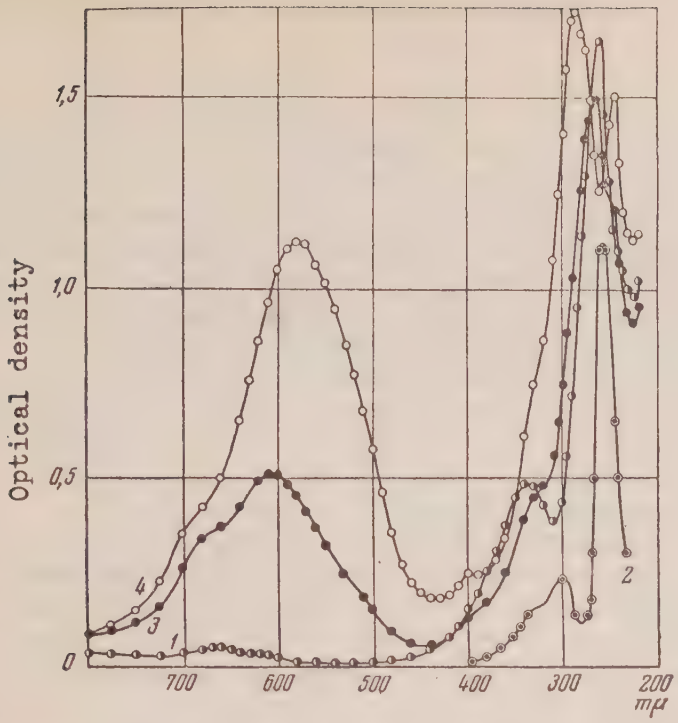

Absorption spectra of leuco-methylene blue: 1) in the solid state, 2) in 0.1 N HCl; 3) of leuco-MB film after 3 hours exposure to air, 4) of leuco-MB film after 20 hours exposure to air.

at 295 mμ belongs to MB, which is known to have a strong absorption band in this region of the spectrum. The absorption spectrum of a solution of the colorless compound we obtained by treating MB with H_2S is virtually identical with the spectrum of the leuco-MB solution; hence, it may be safely assumed that the product of the reaction of MB in the solid state with hydrogen sulfide is leuco-MB. Using the same method (i.e., treatment with H_2S) we obtained the leuco bases of thionine (Lauth's violet), thionine blue, Capri blue, malachite (Victoria) green, crystalline violet and a number of other dyes available in the solid state. The absorption spectra of these leuco bases also consist of two bands; they are located at about 255 and 335 mμ in leuco-thionine; 265 and 338 mμ in leuco-thionine blue; 245 and 340 mμ in leuco-Capri blue; and 265 and 310 mμ in leuco-malachite green and leuco-crystalline violet.

The solid leuco base films deposited under vacuum acquire the color of the initial dye on exposure to air. The absorption spectra of the colored products formed indicate that the original dyes are restored (Curves 3 & 4). In fact the two weak bands discernible in the visible region of the spectrum of the newly deposited leuco base (Curve 1 at 665 and 610 mμ) are doubtless due to first traces of the regenerated dye. The position and relative height of the peaks of these two bands, which coincide with the position and height of the band peaks in weak aqueous solutions of MB, are evidence that the monomeric form of the dye predominates in the initial stage of oxidation of leuco-MB in the solid state. As the concentration of restored dye increases (Curves 3 and 4), the spectrum becomes increasingly similar to that of a high-concentration aqueous solution of MB - as well as to the spectrum of a solid film of MB - which is indicative of the formation of dimers and polymers.

In dry oxygen the regeneration of MB proceeds slowly and the film retains its pale blue color indefinitely. In a moist atmosphere the solid leuco-MB film first turns blue and then acquires a violet coloration similar to that developed by a solid film of MB after long exposure to moist air. Apparently water facilitates the formation of high-order polymers.

Water solutions of leuco-MB prepared by the above described method gradually assume a blue color. The absorption spectra of such solutions are identical with the spectra of equal-concentration solutions of the dye.

* * * * * * *

MOLECULAR ADDITION AND THE ELECTRONIC ABSORPTION SPECTRA OF QUINONE AND PHENOL IN DIFFERENT STATES OF AGGREGATION

- V.E.Zuev

Quinone and phenol react in the solid state to form a complex - phenoquinone - which is one of the simpler complex compounds of quinone, known as quinhydrones. Although numerous attempts have been made to elucidate the structure of hydroquinones and the nature of the addition bonds in them, so far these remain obscure. Hence it appeared of interest to determine the dissociation energy of phenoquinone and to find out whether the complex persists in the molten state, in solutions and in the vapor state or whether it decomposes into quinone and phenol.

We investigated the electronic absorption spectra, in the visible and ultraviolet regions, of quinone, phenol and their mixtures in various relative concentrations, and of phenoquinone in the solid, liquid and vapor states and in solutions.

The following results were obtained:

1. The electronic absorption spectrum of solid phenoquinone differs substantially from the spectra of both components: in the visible region phenoquinone is characterized by stronger absorption than quinone (phenol does not absorb light in the visible region); in the ultraviolet, on the contrary, both quinone and phenol have an appreciably higher absorption coefficient than phenoquinone. This indicates that the formation of phenoquinone is accompanied by considerable deformation of the electron shells of the quinone and phenol molecules.

2. Analysis of the spectrum of the liquid material shows that phenoquinone does not dissociate to any great extent in melting, which indicates that the bond between the phenol and quinone molecules is relatively strong.

3. Some dissociation of phenoquinone is observed in solutions in n-hexane, carbon tetrachloride and benzene; the degree of dissociation increases with rising temperature and decreases with increasing concentration.

4. In the vapor state at temperatures above 100°C there is virtually complete dissociation into phenol and quinone.

5. We determined the dissociation energy of phenoquinone dissolved in CCl_4. On the basis of the law of reacting masses and Buger's [Lambert-Beer] law for a narrow temperature interval and a low degree of dissociation, we derived the following approximate expression for the strength of the intermolecular bond:

$$U = 3k \frac{T_1 T_2}{T_1 - T_2} \ln \left[\left(\frac{T_1}{T_2} \right)^2 \frac{\ln I_1 - \ln I_a}{\ln I_2 - \ln I_a} \right],$$

where k is Boltzmann's constant, I_1 and I_2 are the intensities of the light passing through the solution at temperatures T_1 and T_2, respectively, and I_a is the intensity corresponding to complete association of phenoquinone. (By running a series of three experiments at different temperatures we eliminated I_a from the equations and could thus determine U.) The numerical value of the energy of dissociation of phenoquinone was found to be equal to about 13.4 Kcal mol^{-1} per bond. This rather high value of the intermolecular bond energy is in accord with the other experimental results.

The suggested method of calculating the bond strength can be applied in other cases as well. The dissociation energy of the quinone-phenol complex was computed on the basis of Iaroslavski's data[1] on the temperature-dependence of the infrared absorption spectrum of phenol in carbon tetrachloride; its value was found to be approximately 3.5 Kcal mol^{-1}.

Siberian Physico-Technical Institute
at Tomsk State University

Reference

1. N.G.Iaroslavski, Zhur. fiz. khim., 22, 3, (1948).

* * * * * * *

QUANTITATIVE ANALYSIS BY MEANS OF ULTRAVIOLET ABSORPTION SPECTRA OF THE VAPOR

- A.N.Shabadash & L.A.Igonin

The ultraviolet absorption spectra of the vapor of many organic compounds (particularly, of aromatic compounds) are more selective than the spectra of the substances in solution. Despite this the method of quantitative analysis by means of the ultraviolet absorption of the vapor has been little used, primarily because of experimental difficulties. The procedures suggested by a number of authors[1-3] are based on analysis at room temperatures; at such temperatures the gas cell has to be made at least 4-5 meters in length in order to achieve the requisite sensitivity and accuracy[3].

To obtain high analytic sensitivity with an absorption length of only 40-50 cm, we developed a special absorption chamber which allows of using more elevated temperatures.

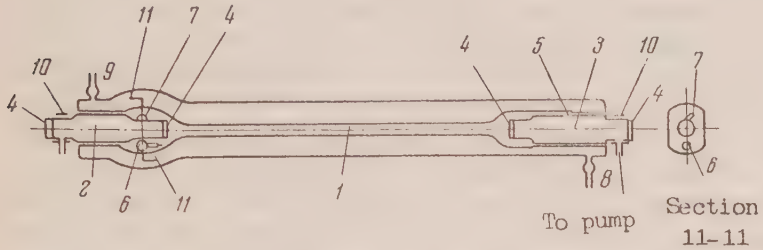

Absorption chamber

The absorption tube 1 (see figure) is surrounded by a water jacket and has tapered openings at both ends, ground to receive the conical plugs 2 and 3 with sealed in quartz windows 4. The air is evacuated from the chamber through a channel in plug 3, which, when the plug is turned to the appropriate position, communicates with the opening 5. The ampoule containing the investigated substance is placed in the other end of the chamber; after the air has been exhausted, the ampoule is crushed by projection 7, forced against it by rotating the plug 2. Sleeves 8 and 9 in the water jacket provide connection to an ultra-thermostat. The ends of the conical plugs are warmed by means of small electric heaters 10.

To facilitate vapor analysis by means of the SF-4 spectrophotometer, we constructed a movable carriage for the absorption chamber which was installed between the hydrogen tube source and the entry slit of the spectrophotometer.

By means of the described set-up it is possible to analyze not only substances which volatilize completely in the chamber but also vapors in equilibrium with the condensed phase.

By way of illustration, we may cite two successful applications of the described method: 1) the amount of styrene, from 0.2%, in polystyrene was determined by analysis of the vapor in equilibrium with a solution of the polystyrene in CCl_4; the relative concentration of styrene was determined according to a calibration curve plotted beforehand with reference to the optical density of the 2880 A absorption line of styrene; 2) the amount of free phenol, from 0.5%, in phenol-formaldehyde resins was determined in a similar manner with reference to the 2751 A absorption line of phenol. The relative error of analyses was less than 15%.

State Scientific Research and Design
Institute for Plastics

References

1. P.A.Cole & D.W.Armstrong, J. Opt. Soc. of Amer. 31, 740 (1941).
2. W.W.Robertson, N.Ginsburg & F.A.Matsen, Ind. Eng. Chem. (Anal.Ed.) 18, 746 (1946).
3. A.Berton, Annales de Chemie, 19, 394 (1944).

* * * * * * *

THE USE OF INFRARED ABSORPTION SPECTRA FOR DETERMINING THE CRYSTALLINITY AND MELTING-TEMPERATURE INTERVAL IN POLYETHYLENE

- V.I.Nikitin & E.I.Pokrovski

It has been established in recent years that the nascence of crystals in a number of polymers is accompanied by changes in their infrared spectrum. It may be accepted as a fact that the transition of a polymer to the crystalline state is evinced in the infrared spectrum by the appearance of new absorption bands[1-4]. These bands are characteristic of the crystalline state and vanish upon transition to the amorphous state.

In the present report we give the data obtained as a result of our investigation of the temperature dependence of the intensity of the infrared absorption bands of polyethylene in the range from 20 to 250°C. The measurements were made on the spectrometer with a rock salt prism described earlier by Nikitin[5]. The thickness of the polyethylene films was 0.006 to 0.010 cm. The film was clamped between rock salt plates which were warmed by a special heater. Crystallinity in polyethylene is characterized by a band at 730 cm^{-1}; however, determination of the percent crystallinity from the intensity of this band is difficult[6]. In studying the 1308 cm^{-1} absorption band in the spectrum of polyethylene we established that the intensity of this band varies with the temperature. We found that in the process of melting the absorption at 1308 cm^{-1} increases to the point of complete transition of the polyethylene to the amorphous state. This led us to assume that the band at 1308 cm^{-1} characterizes the amorphous phase in polyethylene. This assumption was confirmed by an investigation of the normal hydrocarbons, $C_{16}H_{34}$, $C_{20}H_{42}$, $C_{32}H_{66}$ and $C_{36}H_{74}$. We found that in the melted state these straight-chain hydrocarbons have an absorption band at 1308 cm^{-1} which disappears upon crystallization. The absorption spectra of eicosane in the liquified and crystalline states are shown in Fig. 1. Inasmuch as polyethylene at room temperature is partially in the amorphous state, the 1308 cm^{-1} band also appears in its spectrum at this temperature. In a certain temperature interval t_1-t_2 the crystals melt with a consequent increase in the proportion of the amorphous phase, which leads to an increase in the intensity of the band at 1308 cm^{-1}. At and above t_2 the polyethylene is wholly in the amorphous state, so that the intensity of the 1308 cm^{-1} band is not affected by a further temperature rise. Thus the curve reproduced in Fig. 2 permits determining the initial and final temperatures, t_1 and t_2, of the transition. The temperatures obtained in this manner are virtually identical with the temperature values determined by the dilatrometric method.

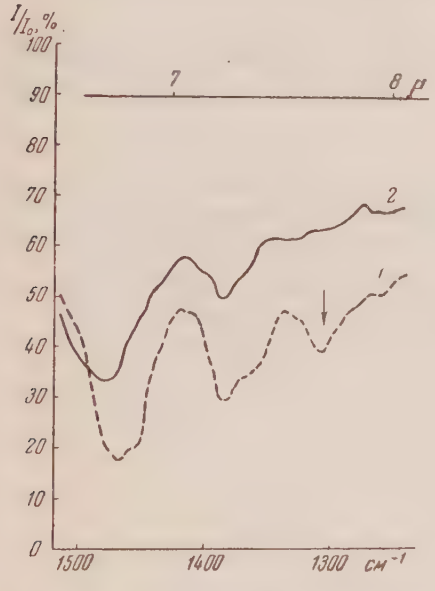

Fig. 1. Infrared absorption spectra of eicosane in the melted (1) and in the crystalline state (2).

We propose the following method for determining the crystallinity of polyethylene. Inasmuch as at t_2 the concentration of the amorphous phase $C_a = 1$, according to the Buger-Lambert-Beer law we have

$$D_1 = KC_a d, \qquad (1)$$

where D_1 is the optical density of the 1308 cm^{-1} band at a temperature $t > t_2$, K is the absorption coefficient and d is the thickness of the layer.

Then at temperatures below t_2,

$$D_2 = KC'_a d, \qquad (2)$$

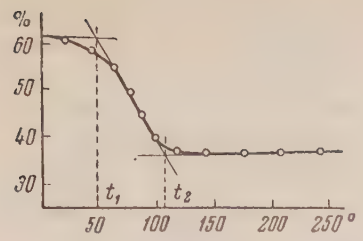

Fig. 2. Variation of the percent transmission with the temperature for the 1308 cm^{-1} band of polyethylene.

where C'_a is the concentration of the amorphous phase at the given temperature. Then, putting $C_a = 1$, we obtain from (1) and (2):

$$C'_a = D_2/D_1.$$

Thus by measuring the optical density at two temperatures we can readily obtain the percent crystallinity $C_c = (1 - C'_a) \cdot 100$ at any temperature.

Measurements on five samples of polyethylene yielded the following average values: $t_1 = 52°C$, $t_2 = 115°C$ and 56% for the percent crystallinity at 20°C. The reproducibility of the crystallinity percentage is within 5% of the measured value.

We also investigated samples of polyethylene stretched to 4-5 times their initial length at room temperature and at 100°C. It might be assumed that the percent crystallinity would increase with stretching; however, our measurements show that it actually remains constant within the limits of the experimental error.

An X-ray determination of the crystallinity carried out in our laboratory by L.A.Volkova on one of the polyethylene specimens gave a value of 55%. It may be assumed that the band at 1308 cm^{-1} is associated with the deformational vibration of the CH_2 group. The absence of this 1308 cm^{-1} band in the spectra of the solid hydrocarbons and its appearance in the spectra of these hydrocarbons in the liquified state, together with the increase in the intensity of the band in the spectrum of polyethylene with increasing temperature in the melting interval leads us to believe that this band should be attributed to the bent rotational isomer.

Institute of High-Molecular Compounds
of the Academy of Sciences of the USSR.

References

1. R.G.Stein & G.B.Sutherland, J. Chem. Phys., 21, 370 (1950).
2. W.E.Mochel & M.B.Hell, J. Amer. Chem. Soc., 71, 4082 (1949).
3. B.L.Burton, Cobbs & Haskell, J. Polymer Sci., 7, 569 (1951).
4. M.Rugg, J.Smith & J.Wartman, J. Polymer Sci., 11, 1 (1951).
5. V.N.Nikitin, Izv. (Bulletin) AN SSSR, Ser. fiz., 17, 644 (1953).
6. V.N.Nikitin & E.I.Pokrovski, Doklady AN SSSR, 95, 109 (1954).

* * * * * * *

THE EFFECT OF POLYMERIZATION TEMPERATURE ON THE STRUCTURE OF BUTADIENE-STYRENE COPOLYMERS

- A.P.Sheinker & S.S.Medvedev

The addition of monomer molecules to a growing polymer chain in the polymerization of diene compounds may occur in different ways. In the case of polymerization of butadiene coupling occurs at the 1, 2 and 1,4 positions; in the latter case there are formed polymer chains differing from each other as regards the spatial arrangement of the CH_2 at the double bonds (i.e., cis- and trans-configurations). That is, polymer chains having different configurations are formed. It is obviously of interest to know how the proportions of these configurations vary with the conditions of polymerization.

We used infrared spectroscopy (2-15 μ) to investigate the composition of copolymers of butadiene with styrene, obtained in emulsions at different temperatures (-15 to +38°C); we also determined the content of different butadiene links in the polymer chains. Glycerol was used as the antifreeze in carrying out polymerization at temperatures below 0°C.

The spectra were obtained in carbon disulfide solutions. The concentrations of the polymers varied between 16.6 and 40.9 gm/liter. The thickness of the solution layer was 0.2 mm.

The number of styrene links in the polymer was determined according to the optical density of the band at 700 cm^{-1} which is characteristic of the benzene ring, while the content of the different configurations of the butadiene links was determined by measuring the optical density of the bands at 967 and 909 cm^{-1}, which are associated with the trans- and 1,2-configurations, respectively. These bands correspond to the deformational vibration of the C=C-H groups. The cis-configuration content was determined as the difference between the trans- and 1,2-configuration contents and the total butadiene content. In computing the relative amounts of the configurations present it was assumed that the attenuation of radiation conforms to the Buger-Lambert-Beer law.

The specific absorption coefficient k_{700} for the 700 cm^{-1} band was evaluated from the intensity of this band in the spectrum of polystyrene, prepared by emulsion polymerization.

For calculating the amounts of the trans- and 1,2-configurations we used the specific absorption coefficients given in chemical literature. The results obtained are accurate to within 2.5% on the average. Our data indicate that as the temperature of polymerization is increased from 0 to 38°C, the trans-configuration content goes down from 56 to 39%, while the amount of 1,2-configuration groups and styrene links remains constant at 12% and 16%, respectively.

In the case of polymerization in the presence of glycerol the composition appears to be independent of the temperature (in the -15 to +20°C interval); however, in this case the polymers contain a higher proportion of styrene (32%). This is confirmed by measurements of the degree of unsaturation of the polymers: the number of unsaturated linkages present per gram of polymer is appreciably lower in the case of polymers obtained with glycerol, while the unsaturation calculated only for the butadiene links (taking into account the styrene content in the polymer) is the same in both cases (polymers formed with and without glycerol). This indicates that our data on the styrene contents are trustworthy.

The relatively small variation of the proportions of the different configurations in polymers formed at different temperatures leads us to believe that the effect of the polymerization temperature on the properties of the copolymer product cannot be due entirely to changes in the relative content of these configurations, as has been suggested by some authors.

"L.Ia.Karpov" Physico-Chemical Institute

* * * * * * *

THE INFRARED SPECTRA AND TAUTOMERISM OF HETEROCYCLIC COMPOUNDS

- Iu.N.Sheinker & S.G.Bogomolov

Until recently the dual reactivity exhibited by many compounds was explained on the grounds of tautomerism or the specific type of tautomerism known as pseudomerism.

A different interpretation of the phenomenon has been suggested by A.N. Nesmeianov, M.I.Kabachnikov and others: according to the data of these investi-

gators the formation of two series of derivatives is often connected with the migration or transfer of an activity center in the process of the reaction, rather than with tautomerism (or pseudomerism).

The present study was devoted to an investigation of tautomerism and dual reactivity in a series of heterocyclic compounds, using the methods of infrared absorption spectroscopy.

We observed the infrared spectra (2.5-13 μ) of a number of oxy-derivatives [hydroxy-derivatives] of heterocyclic compounds (derivatives of pyridine, pyridazine, pyrimidine, pyrazine, triazine, thiazole, etc.) and the sodium and silver salts of these derivatives obtained as intermediate products of the reactions. We also studied the spectra of some mercapto- and amino-derivatives of these compounds.

The spectra were obtained with the substances in the crystalline state and in solutions; particular attention was given to the absorption bands characteristic of the C=O, C=C, C=N, N-H, S-H and O-H bonds.

Intense bands in the 1680-1740 cm^{-1} region, which indicate the presence of C=O groups, and bands in the 3000-3300 cm^{-1} region, which may be assigned to N-H vibrations, were observed in the spectra of all the investigated oxy-derivatives. Hence all the investigated derivatives presumably have an oxo-type rather than an oxy-type structure. The only exception to the above is n-dioxypyridazine, whose spectrum is indicative of an oxy-structure and the presence of strong intermolecular hydrogen bonds.

According to our spectroscopic data, the metallic derivatives of the investigated heterocyclic oxy-compounds (sodium and silver salts), which are intermediate products obtained in the reactions leading to the formation of different series of derivatives, all have a similar structure. Their formation is connected with enolization of the molecules (the C=O group bands disappear from the spectra and new bands characteristic of unsaturated heterocyclic systems appear in 1500-1550 cm^{-1} region).

The molecules of the investigated mercapto-derivatives of imidazole, thiazole and pyrimidine have a structure similar to that of the corresponding oxygen derivatives, i.e., have a thiono- rather than a thiol arrangement (S-H bands at 2560 cm^{-1} absent; N-H bands at 3000-3300 cm^{-1} and C=S bands at 1530-1480 cm^{-1} in evidence). In contrast, analysis of the band frequencies indicates that the amino- rather than the imino-grouping is characteristic of most of the amino-derivatives.

On the basis of the observed data it may be concluded that the investigated oxy-derivatives of heterocyclic compounds in the non-reacting, free state (i.e., in solutions in inert solvents and in the crystalline state) are characterized by an oxo-type structure and that the dual reactivity of these compounds is not connected with differences in the structure of the metallic salts formed as intermediate products in the reactions. Analogous deductions can be drawn regarding the mercapto-derivatives (characterized by a thiono-structure) and the amino-derivatives (having an amino-structure) of the heterocyclic compounds.

The tautomeric relationship observed in the case of some of the investigated substances (specifically, n-dioxypyridazine) apparently has no direct connection with the reactivity of these substances.

"S.Ordzhokikidze" All-Union Chemico-Pharmaceutical
Scientific Research Institute

* * * * * * *

THE VIBRATIONAL SPECTRA AND BASICITY OF CYCLIC IMINES

- Iu.N.Sheinker & E.M.Peresleni

The purpose of our investigation was to evaluate the influence of ring strain on the optical and electrochemical properties of cyclic compounds through a study of the vibrational spectra and the basicity constants of cyclic imines.

We obtained the infrared absorption spectra (2.5-13 μ) and Raman spectra of cyclic imines containing three to seven atoms per ring and of their simple derivatives.

The transition from unstrained molecules (multiple-membered rings) to strained molecules (three- and four-membered rings) is accompanied by a noticeable change in the vibration frequencies of the bonds external to the ring. Thus the frequency of the H-C bonds increases with increasing ring strain (from 2919 cm^{-1} in hexamethylenimine to 3062 cm^{-1} in ethylenimine), while the frequency of vibration of the N-H bonds decreases (from 3368 cm^{-1} in hexamethylenimine to 3327 cm^{-1} in ethylenimine - all measured in dilute solutions). In dimethylamine, a non-cyclic analogue of ethylenimine, $\nu_{N-H} = 3360$ cm^{-1}.

If we assume that this effect is at least partially connected with changes in the magnitude of the force constant of the C-H and N-H bonds, we can expect the basicity of cyclic amines to decrease with increasing ring strain. And in fact measurements showed that the basicity constant for highly strained ethylenimine (three-membered ring) is only about one thousandth its value for pyrrolidine, piperidine and hexamethylenimine (multiple-membered rings).

However more extensive investigation indicates that the parallelism does not always obtain: thus the basicity constant for trimethylenimine is of the same order of magnitude as that for higher compounds, although ring strain is undoubtedly present and the N-H frequency is anomalously low (3334 cm^{-1}).

The formation of intermolecular hydrogen bonds is characteristic of cyclic iminies in the liquid state; in consequence, two lines, having frequencies corresponding to the N-H···N (3243-3310 cm^{-1}) and N-H (3316-3343 cm^{-1}) groups, appear in the Raman spectra.

From a comparison with the data for non-cyclic secondary amines (dimethyl-, diethyl- and dipropylamine) it follows that the formation of closed rings favors intermolecular interaction. At the same time, an increase in the number of members constituting the ring weakens this interaction.

These facts can be explained by taking into account steric hinderance to the interaction of chain rings.

Classification of the observed frequencies through comparison with data in spectroscopic literature permits establishing the character of the frequency shift of the symmetric and asymmetric vibrations of rings with increase in ring size. In general the frequency of the symmetric vibrations decreases, while the frequency of the asymmetric vibrations increases. Molecular refractivity does not appear to be affected by ring closure or ring strain.

"S.Ordzhonikidze" All-Union Chemico-Pharmaceutical
Scientific Research Institute

* * * * * * *

ASCERTAINING THE STRUCTURE OF THE SULFONIC ACIDS OF 2-AMINO-4-METHYLTHIAZOLE WITH THE AID OF INFRARED SPECTRA

- S.G.Bogomolov, Iu.N.Sheinker & I.Ia.Postovski

Two isomeric sulfo acids are obtained as a result of sulfonation of 2-amino-4-methylthiazole - one with a low, the other with a high melting point - depending on the reaction conditions. In heating with sulfuric acid the low melting point acid is transformed into the high melting point compound.

The question of the structure of these acids and their respective derivatives was until recently a matter of controversy. Most investigators tended to the conclusion that the low melting point acid was 4-methylthiazole-2-sulfamic acid while the high melting point one was 2-amino-4-methylthiazole-5-sulfonic acid.

In the present investigation the structure of these two acids has been determined and the above conclusion shown to be erroneous through analysis of the infrared spectra of the 2-amino-4-methylthiazole sulfonic acids as well as of a number of 2-aminothiazole derivatives.

To this end we studied the absorption of these substances in the 3000-3700 cm^{-1} region (the region of the characteristic bands of the OH, NH and NH_2 radicals). Through analysis of a number of substances whose structure is known, it was established that compounds with an NH group at the 2-position of the thiazole ring have an absorption band at 3155 cm^{-1}, while those with an NH_2 group are characterized by a series of bands at 3115, 3270 and 3400 cm^{-1} (all data pertain to the crystalline state).

Spectra of the isomeric acids in question show that the low melting point acid contains the NH_2 group and hence must have the structure 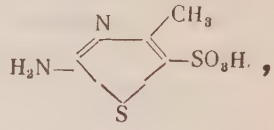 , while the high melting point acid contains an NH group and has the structure 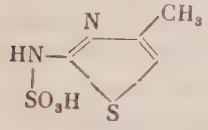

In the light of the above, the transformation of the low into the high melting point acid consists of a hitherto unobserved rearrangement of a sulfonic acid into a sulfamic acid.

"S.Ordzhenikidze" Chemico-Pharmaceutical
Scientific Research Institute

* * * * * *

LOW TEMPERATURE ABSORPTION SPECTRA OF SOME NITROGEN-CONTAINING HETEROCYCLIC COMPOUNDS

- A.N.Nikitina & G.C.Ter-Sarkisian

We obtained and investigated electronic absorption spectra of pyridine, 4-picoline (4-methylpyridine), quinoline, 4-methylquinoline (lepidine), 4-methyl-5,6-benzoquinoline, 4-methyl-7,8-benzoquinoline, acridine, 9-methylacridine, 9-methyl-1,2-benzacridine and 9-methyl-3,4-benzacridine, at room temperature and at -195°C and, in addition, the spectra of 4-methyl-7,8-benzoquinoline and 9-methyl-1,2-benzacridine at the above temperatures and at -259°C.

Lowering the temperature from 20°C to the temperature of liquid nitrogen and

particularly to that of liquid hydrogen results in an appreciable change in the absorption spectra of 4-methyl-7,8- and 4-methyl-5,6-benzoquinolines, 9-methyl-1,2-benzacridine and pyridine. Thus, whereas at room temperature the absorption spectrum of 4-methyl-7,8-benzoquinoline has only 5 broad lines, at the temperature of liquid nitrogen, 24 lines are distinguishable, while at the temperature of liquid hydrogen 30 lines can be seen. Moreover, the new lines are considerably narrower and sharper.

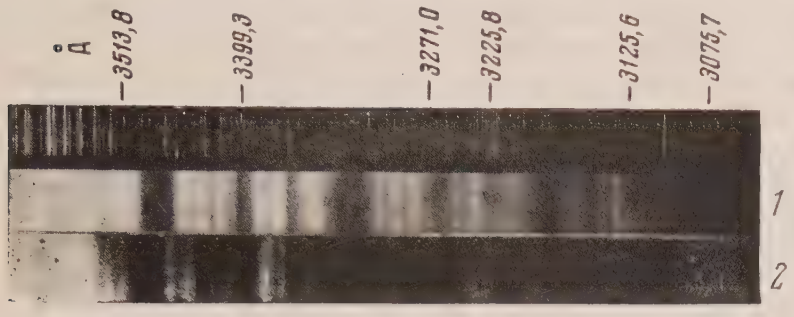

Absorption spectra (at -259°C): 1) 4-methyl-7,8-benzoquinoline; 2) phenanthrene.

In the spectra of 9-methyl-1,2-benzacridine, instead of 4 broad absorption lines at room temperature, there are 15 much narrower and sharper lines at the temperature of liquid nitrogen and 22 lines at the temperature of liquid hydrogen. In the case of pyridine, 5 absorption lines are observed at the temperature of liquid nitrogen instead of the continuous spectrum seen at room temperature.

The absorption spectra of quinoline, 4-methylquinoline, acridine, 9-methylacridine, 9-methyl-3,4-benzacridine and 4-picoline change little when the temperature is lowered.

In comparing the low-temperature absorption spectra of the investigated nitrogen-containing heterocyclic compounds with the spectra of compounds similar in structure but not containing nitrogen (benzene, naphthalene, anthracene and phenanthrene)[1] certain resemblances were observed between the corresponding spectra. The resemblance is particularly noticeable in the case of the absorption spectra of phenanthrene and 4-methyl-7,8-benzoquinoline at the temperature of liquid hydrogen: the two spectra are very similar in overall appearance and almost identical in some respects (see accompanying figure); the electronic transition bands coincide and the vibrational frequencies are very close.

Some analogies can also be traced between the absorption spectra of acridine and anthracene, quinoline and naphthalene.

These data indicate that replacement of a C atom in the rings of the investigated aromatic compounds by an N atom does not produce an appreciable change in the molecular electron clouds.

"N.D.Zelinski" Institute of Organic Chemistry
of the Academy of Sciences of the USSR

Reference

1. I.V.Obreimov & A.F.Prokhot'ko in "Sbornik" (Symposium) dedicated to the memory of S.I.Vavilov, Pub. AN SSSR Moscow 1952.

* * * * * * *

INFRARED ANALYSIS OF THE MICROSTRUCTURE OF SYNTHETIC RUBBERS

- K.V.Nel'son

The methods proposed hitherto for determining the structure of butadiene[1-3] and isoprene rubbers[4] require a large number of standards and involve an onerous procedure for finding the absorption coefficients.

In the present report we describe a simple procedure, requiring a minimum number of standards, developed for the quantitative determination of the 1,2,

trans-1,4 and cis-1,4 groups in butadiene and the 1,2,3,4, trans-1,4 and cis-1,4 groups in isoprene rubbers from their spectra in the 800-1000 cm^{-1} region.

The selection of reference substances (standards) having band contours similar to those of the absorption spectra of the analyzed rubbers makes it possible to use differential coefficients of absorption for purposes of analysis. In our opinion this procedure is more rigorous than that proposed by Richardson & Sacher[4].

The following substances, modeled after the corresponding groups in the polymers were synthetized: heptene-1 (band at 909 cm^{-1}) for determination of the 1,2 groups in butadiene and isoprene rubbers; 2,3,3-trimethylbutene-1 (band at 888 cm^{-1}) for 3,4 groups in isoprene rubbers; trans-octene-3 and trans-decene-5 (band at 967 cm^{-1}) for the trans-1,4 groups in butadiene rubbers. In addition, we made use of natural rubber and gutta-percha, consisting almost entirely (96-98%) of cis-1,4 and trans-1,4 groups, respectively, as standards in the analysis of isoprene synthetics. The spectra of natural rubber and gutta-percha differ only as regards the intensity and width of the bands near 840 cm^{-1}. These overlapping bands intersect at 857 and 815 cm^{-1}; the absorption coefficients obtained at these points can be used for determining the 1,4-group content. Using the values of the absorption coefficients at the peak (at 843 cm^{-1}) one can determine the amount of the cis-1,4 and trans-1,4 components in isoprene rubber separately. The effect of superposition of the bands is allowed for (i.e., the individual intensities and corresponding coefficients are determined) by calculating the theoretical contours according to the conventional dispersion equation.

The analysis of isoprene rubbers is carried out with reference to the absorption at the peaks of the bands at 909, 888 and 843 cm^{-1} and the absorption at 857 and 815 cm^{-1}. The results of the spectrometric measurements permit writing five simultaneous equations, solution of which gives the concentrations of the 1,2,3,4, cis-1,4 and trans-1,4 components. Since only four equations are necessary, one equation (that for the 857 or the 815 cm^{-1} frequency) is used for checking the results.

Butadiene rubbers are analyzed by measuring the intensities of the bands at 909 and 967 cm^{-1} to determine the 1,2 and trans-1,4 components; the cis-1,4 group content is then found by subtraction.

The validity of the Buger-Lambert-Beer law for the range of concentrations employed (not over 1 mol/liter) was verified experimentally.

A large number of butadiene and isoprene rubber specimens has been analyzed. All measurements were made in CS_2 solutions on a VIKS-M3 spectrometer with a rock salt prism. The accuracy of the infrared analysis of isoprene rubbers may be evaluated on the basis of the divergence between the analytically determined total concentration and the computed known value; in no case did the divergence exceed 10%. Comparison of the results obtained by the described procedure with the data on the external C=C bonds obtained by chemical analysis and with the results of spectroscopic analysis with reference to the first overtone of the C-H group vibrations shows satisfactory agreement.

A similar procedure for the analysis of isoprene rubbers is described in a recently published article by Pokrovski and Vol'kenshtein[5].

Z.D.Stepanova, graduate student of Leningrad State University, participated in the present investigation.

"S.V.Lebedev" Synthetic Rubber Scientific Research Institute

References

1. J.E.Field, D.E.Woodford & S.D.Gehman, Appl.Phys., 17, 386 (1946).
2. E.J.Hart & A.W.Mayer, J. Am. Chem. Soc., 71, 1980 (1949).
3. R.R.Hampton, Anal. Chem, 21, 8, 923 (1949).
4. W.S.Richardson & A.Sacher, J. Polymer Sci., 10, 4, 353 (1953).
5. E.I.Pokrovski & M.V.Vol'kenshtein, Doklady AN SSSR, 95, 2, 301 (1954).

* * * * * * *

BULLETIN of the Academy of Sciences of the USSR - Physical Series

Vol. 18, No. 6, 1954 - Conference on Spectroscopy (Tartu, 1954)

TABLE OF CONTENTS

	Page Orig.	Trans.
Opening address - S.E.Frish	627	313
The present state of radio-frequency spectroscopy - M.A.El'iashevich	629	315
On the optical properties of metals - V.L.Ginzburg & G.P.Motulevich	631	318
On photoelectric methods in spectrum analysis - I.S.Abramson & S.L.Mandel'shtam	635	321
New spectroscopic instruments - V.K.Prokof'ev	643	330
Spectral characteristics of Soviet diffraction gratings - F.M.Gerasimov	662	345
Radiospectroscopic investigation of molecules - N.A.Irisova	663	346
On the optical-acoustical effect in the microwave region - G.G.Neuimin & O.I.Chernyshevski	663	347
Bond force constants and the configuration of molecules - A.I.Kitaigorodski	664	348
Absorption anisotropy of gypsum crystals in the infrared - G.A.Zaitsev & B.S.Neporent	665	349
Determination of the optical anisotropy and the form of some aromatic hydrocarbon molecules from light scattering in solutions - M.F.Vuks & I.A.Bogdanov	667	351
The vibrational spectra of diphenyl and deca-deutero-diphenyl - G.S.Landsberg, A.I.Shatenshtein, G.V.Peregudov, E.A.Izrailevich & L.A.Novikova	669	353
The vibrational spectra and structure of diborane (B_2H_6) - L.M.Sverdlov & I.N.Zaitseva	672	355
The fine structure of fluorescence spectra of aromatic hydrocarbons in frozen solutions - E.V.Shpol'ski & L.A.Klimova	673	357
Influence of the surrounding medium and the vibrational energy level of the molecules on the continuous spectra of organic compounds - B.S.Neporent, N.A.Borisevich, V.P.Klotchkov & O.A.Motovilov	674	358
Anomalous light dispersion in solutions of complex organic compounds - I.S.Gorban' & A.A.Shishlovski	676	360
The method of concentrational optical functions as a physico-chemical analytic method in the presence of reversible chemical reactions - A.A.Shishlovski	677	361
Methods of investigating the breadth of Raman spectrum lines - P.A.Bazhulin, S.G.Rautian, A.I.Sokolovskaia & M.M.Sushchinski	678	362
Allowing for the distorting effect of the optical system of the monochromator on the observed shape of the spectrum line - I.V.Peisakhson	680	363
The Raman effect and its frequency dependence - P.P.Shorigin & L.Z.Ositianskaia	681	364
Raman spectra in the region of absorption bands - L.M.Kutsyna & P.P.Shorygin	682	365
Resonance Raman scattering - L.N.Ovander	683	366
Connection between Raman spectra and the electronic spectra of molecules - M.D.Zepe	684	367
The absorption spectra of solid solutions of lead in cadmium halides - A.F.Malysheva	685	368
Spectra of electron capture levels in alkali-halide crystal phosphors - Ch.B.Lushchik	687	370
Spatial distribution of the radiation from color centers and the nature of such centers in ionic crystals - P.P.Feofilov	688	371

	Page Orig.	Trans.
Application of a spectrophotometric method to the investigation of chemical sensitization of a photographic emulsion - E.A.Kirillov, Zh.L.Broun & K.V.Chibisov	689	372
Infrared boundary of bleaching of the fine structure in the spectrum of photochemically colored silver halide - E.A.Nesterovskaia	690	373
Spectroscopic investigation of the mechanism of condensation of β-ionone with ethyl γ-bromocrotonic acid - N.A.Slovokhotova, G.I.Samokhvalov, M.A.Miropol'skaia, L.A.Bakulova, L.P.Zhukova & N.A.Preobrazhenski	692	375
The chemiluminescence of 3-aminophthalhydrazide (luminol) - K.L.Klimovskaia, V.N.Vishnevski & V.E.Shmaevski	694	376
The ultraviolet and visible absorption spectra of certain nitro derivatives of diphenylamine - P.M.Bugai & V.N.Konel'skaia	695	377
Spectroscopic investigation of solutions of antimony chlorides - R.A.Dashkovskaia & I.I.Kondilenko	697	379
Raman spectra of some hydrocarbons of the cyclobutane series - V.T.Aleksanian, M.Iu.Lukina, Kh.E.Sterin & B.A.Kazanski	699	381
Investigation of the molecular spectra of organo-silicon compounds by the methods of Raman and infrared spectroscopy - Iu.P.Egorov	702	384
Analysis of the aromatic components of ligroin by Raman spectroscopy - B.A.Kazanski, G.S.Landsberg, V.T.Aleksanian, T.F.Bulanova, A.L.Liberman, E.A.Mikhailova, A.F.Plate, Kh.E.Sterin & S.A.Ukholin	704	386
Application of infrared spectroscopy to the investigation of petroleum products - K.I.Zimina, A.V.Iogansen & A.G.Sigriuk	707	389
A low-pressure mercury tube and its use in studying Raman spectra - M.L.Sosinski	709	389
Some generalizations of the "metallic" model in the theory of complex molecules - M.G.Veselov & T.N.Rekasheva	711	391
The shape and temperature-dependence of impurity-activated luminescence and absorption bands of solid and liquid dielectrics and semi-conductors - S.I.Pekar	712	392
Luminescence of molecular crystals containing impurity molecules - M.D.Borisov & A.C.Davydov	714	393
The properties of local electronic centers in solid and liquid ionic dielectrics - M.F.Deigen	716	395
The influence of solvents on the absorption and luminescence spectra of molecules - A.F.Lubchenko	718	397
The vibrational spectrum of the vinyl group and its quantitative determination in complex hydrocarbon mixtures - A.V.Iogansen	708	400
Intermolecular bonds of the (OH)•••(OH) and (OH)•••(OCR) type in oxygen-containing substances - V.M.Chulanovski & Kim Den Dok	720	401
The hydrogen bond and the structure of aromatic compounds - V.V.Perekalin	721	402
The hydrogen bond and its effect on the energy distribution in the vibrational and electronic spectra of molecules - D.N.Shigorin	723	404
Infrared spectra and association in solutions - E.N.Vasenko	725	406
On hydrogen bonds in silicols - V.I.Kastochkin, M.F.Shostakovski, - O.I.Zil'berbran & D.A.Kochkin	726	407
Determination of the true absorption spectrum of light-dispersing colored objects from their diffuse reflection spectrum - O.P.Girin, Z.V.Zhidkova, B.I.Stepanov, A.P.Ivanov & A.S.Toporets	728	409
Absorption spectra of complex compounds (ammines) in crystal form - A.V.Babaeva & R.I.Rudyi	729	410
The absorption spectra of leuco bases in the solid state - A.T.Vartanian	731	411

	Page Orig.	Trans.
Molecular addition and the electronic absorption spectra of quinone and phenol in different states of aggregation - V.E.Zuev	732	413
Quantitative analysis by means of ultraviolet absorption spectra of the vapor - A.N.Shabadash & L.A.Igonin	733	414
The use of infrared absorption spectra for determining the crystallinity and melting-temperature interval in polyethylene - V.I.Nikitin & E.I.Pokrovski	735	415
The effect of polymerization temperature on the structure of butadiene-styrene copolymers - A.P.Sheinker & S.S.Medvedev	736	416
The infrared spectra and tautomerism of heterocyclic compounds - Iu.N.Sheinker & S.G.Bogomolov	738	417
The vibrational spectra and basicity of cyclic imines - Iu.N.Sheinker & E.M.Peresleni	739	419
Ascertaining the structure of the sulfonic acids of 2-amino-4-methylthiazole with the aid of infrared spectra - S.G.Bogomolov, Iu.N.Sheinker & I.Ia.Postovski	740	420
Low temperature absorption spectra of some nitrogen-containing heterocyclic compounds - A.N.Nikitina & G.C.Ter-Sarkisian	740	420
Infrared analysis of the microstructure of synthetic rubbers - K.V.Nel'son	741	421

Translated in 1955 by
Columbia Technical Translations
5 Vermont Ave., White Plains, N. Y.